



PROCEEDINGS
OF THE
THIRD TECHNICAL SYMPOSIUM

HELD IN
GREAT GORGE, NEW JERSEY
OCTOBER 2-4, 1974



1974
Wild Goose Association
3rd Annual Convention

ROBERT L. FRANK
16500 N. 48075

1974

Schedule of Events
(Great Orange NJ)

Wednesday, October 2, 1974

10:00am to 5:00pm Golf Tournament
4:00pm to 8:00pm Registration
7:00pm to 8:00pm Reception and Golf Tournament Awards

Thursday, October 3, 1974

SESSION I: APPLICATIONS

- ✓ 9:00am 10 Predicted Performance of an Optimally Integrated LORAN/Inertial Aircraft Navigation System
Authors: Joseph F. Kasper, Jr./Daniel E. Gentry/Joseph A. D'Appolito
592
- ✓ 20 LORAN-C for Emergency Communications
Author: Walter W. Dean MAGNUS
- ✓ 30 Operational LORAN-C Experience in an Automobile Environment
Author: Willie Vogeler TELCOM NOT Available
- 10:15am Coffee Break
- 10:30am 40 LORAN-C AVM Urban Repeatability
Authors: Richard Stapleton/F.J. Chambers TELETYPE
- 50 Low Cost Navigation Processing for LORAN-C
Authors: A. Tuppin/Delarin 177
- 60 U.S. Coast Guard Workshop
Author: L. Fehlner APL see Proc. of Loran-C Work-
shop NTIS AC05909
June 5-7, 1984
- 12:00 noon Lunch
- 1:30pm 70 LORAN-C Spectrum: Navigation and Communications
Authors: C. Matthews/H. Englert
- 80 Simplified Algorithm for Accurate Airborne Computation of LORAN Secondary Phase
Author: Dr. R.J. Fredericks LORAN-SIEGLER

SESSION II: TRANSMITTERS & GRID CHARACTERISTICS

- 90 Semi-Automated LORAN Stations
Author: James T. Doherty, Jr. WCC *
- 100 Real Time Compensation of LORAN C/D Propagation Variations
Authors: Robert L. Frank/David L. McGrew COMM-TIME/SAFETY Copy HERE
- 3:15pm Coffee Break
- 3:30pm 110 LORAN-C Phase Code & Rate Modulation for Reduced Cross Chain Interference
Author: CDR. William F. Roland WCC
- 120 Spatial & Temporal Electrical Properties Derived from LF Pulse Ground Wave Propagation Measurements
Author: Robert L. Doherty 175
- 130 Propagation of a LORAN Pulse Over Irregular, Inhomogeneous Ground
Authors: J. Balch-Johnson/Samuel Horowitz

COCKTAIL PARTY & DINNER DANCE

7:30pm to 8:30pm Cocktail Party

9:00pm to 1:00am Dinner Dance

Guest Speaker: Hon. John M. Murphy

Friday, October 4, 1974

SESSION III: RECEIVERS & GENERAL INTEREST

✓ 9:00am ⁶⁰⁶14 • Performance Optimization of Linear LORAN Receivers Operating
in a Non-Gaussian Atmospheric Noise Environment

Author: Larry Postema LEAR-SIEGLER

✓ ⁶⁰⁶15 • U.S. Coast Guard Testing at Wildwood

Author: LT. CDR. William Schorr USCG

✓ ⁶⁰⁷16 • Progress Report on Group/Phase Test

Authors: R. Smith/J. A. Perschy APL

10:30am Coffee Break

10:45am PANEL DISCUSSION

Moderator: E. Durbin TELETYPE

Theme: "Impact of the Coastal Confluence Decision of
LORAN Activities"

SPECIAL FOR THE LADIES

Thursday, October 3, 1974

10:30am to 2:30pm Bus Tour to Brotherhood Winery
and Local Scenic Beauty

Bread and Cheese Treat Included

PREDICTED PERFORMANCE OF
AN OPTIMALLY INTEGRATED
LORAN/INERTIAL AIRCRAFT NAVIGATION SYSTEM*

Joseph F. Kasper, Jr., Daniel E. Gentry and Joseph A. D'Appolito

The Analytic Sciences Corporation
Reading, Massachusetts 01867

Com #3

1974

#1

See E

Presented at the
3rd Annual Convention
of the
Wild Goose Association

* Analyses described herein were supported in part under Contract No. F33615-72-C-1787 with the Air Force Avionics Laboratory.

FÄHLNER
REF 592
PP 25
1974 Vol 3-1
800412

ABSTRACT

Statistical models for the errors affecting an integrated Loran/Inertial navigation set are given, including Loran receiver noise and propagation anomalies, inertial system sensor errors and gravitational uncertainties. Based on these models and the assumption of optimal Kalman integration, predictions of rms system position, velocity and heading errors are obtained for a flight scenario typical of tactical aircraft operations. These predictions can serve as a lower bound on the performance of any Loran/Inertial navigation set. Results are given in terms of a system error budget to facilitate identification of dominant error contributors. Analyses which treat the question of sensitivity to proper error modeling are also included.

Introduction

The Kalman filter is a relatively new data processing algorithm which provides a logical systematic method for weighting various sources of information to produce a best estimate of the quantities of interest (Ref. 1). Only recently have Kalman filters been applied to aircraft inertial navigation systems, and in particular, to the multisensor configuration of current interest, the Loran/Inertial system.

As illustrated in Figure 1, the basic elements of this system are an inertial navigation system, a Loran receiver, and a computer which implements a Kalman filtering algorithm. The difference between the inertial system indication of position and the Loran measurement of position* is operated on by the Kalman filter to produce estimates of the inertial system position, velocity, and attitude errors and generally also to supply corrective signals to inertial platform and navigation algorithms. Properly designed, this configuration will combine the short-term stability of the inertial system with the bounded nature of Loran errors to produce the required navigation accuracy.

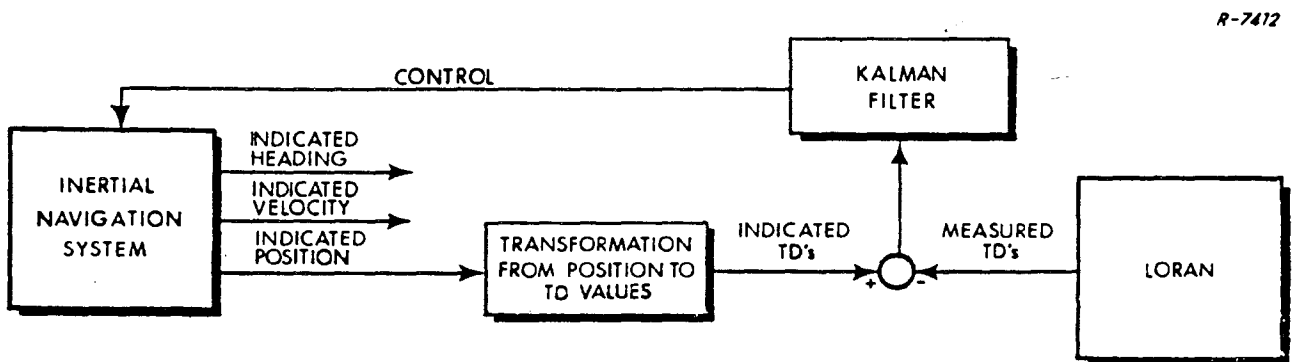


Figure 1 Typical Loran/Inertial Configuration

* As shown in Figure 1, this "position difference" is usually computed at the TDA, TDB level.

Clearly, the performance of a Loran/Inertial system is dependent both upon the hardware and the Kalman filtering algorithm. Kalman filtering theory is such that the filter structure is based upon assumed statistical and dynamic models of the true system. These models are always somewhat inaccurate, due both to lack of exact knowledge of the true system characteristics and to deliberate simplifications.

A covariance analysis simulation is used to predict optimal integrated Loran/Inertial system performance. This simulation requires a reference or real-world system model. This reference system is, in general, more complex than that assumed in the design of typical operational Kalman filters. It is in fact possible to design a more complicated and typically impractical "optimal" filter based on the reference or real-world model. Our interest herein involves estimating the performance of the optimal filter operating in the "real-world"; these performance predictions represent a baseline against which any practical filter can be compared.

In this paper the reference "real-world" error model is presented and described. The statistical nature of each error source is also defined. Since many parameters are trajectory-dependent, a complete description of the simulated flight path is also included. Evaluations of predicted system performance and error sensitivities are presented.

Flight Profile

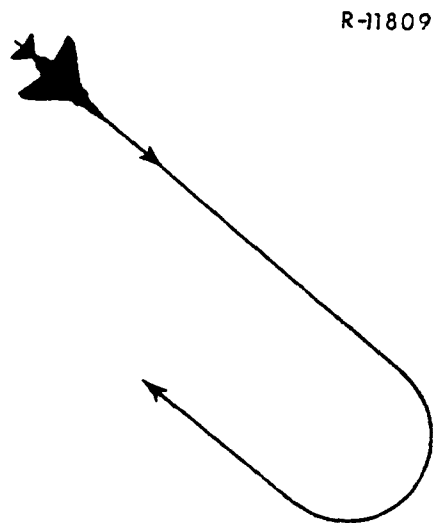
Extensive experience has been obtained with operation of Loran in a tactical environment in the vicinity of Eglin AFB, Florida. It is reasonable then to select simulation parameters to reflect the geometry and environment of this area. In addition, since most of the error sources which affect the

actual system are dependent on geometry, velocity, and acceleration, it is necessary to specify the flight profile for the simulations.

The flight profile used in the initial covariance analysis simulations consist of three segments and is shown in Fig. 2. Flight parameters are presented in Table 1 and the location of the aircraft relative to the East Coast Loran chain is shown in Fig. 3. The first segment is a straight and level flight lasting for approximately 10 minutes with no vehicle accelerations. During this period it is assumed that Loran fixes are being processed by the Kalman filter every 5 to 10 seconds using signals from the transmitters at Cape Fear, Jupiter, and Dana (Master, Slave A, and Slave B, respectively). With no lateral acceleration, good station geometry, and an assumed high signal-to-noise ratio, this represents an ideal situation during which the baseline accuracies of the system can be observed.

The second part of the flight path consists of a short high-speed turn lasting approximately 30 seconds. Since most inertial system errors are velocity- and acceleration-dependent, this turn will excite errors not observed during the first segment of the flight. In a sense, this represents a worst-case situation for the inertial system since all the errors are driving the system; thus, it is expected that the navigation errors will increase during this turn. The vehicle velocity is assumed to be maintained at a constant 800 fps as in the first segment, and the radius of the turn is selected such that the lateral acceleration is a constant 3 g's. It is assumed that Loran TD's are being processed during the turn.

The third and final segment of the flight is straight and level lasting approximately 5 minutes. Since it is expected that the navigation errors will increase during the turn, it is important to determine the recovery ability of the system after the turn. Again, it is assumed that Loran signals are



NOTE: NOT DRAWN TO SCALE

Figure 2 Flight Path for Covariance Simulations

Table 1

FLIGHT PARAMETERS FOR SIMULATION

Latitude	30.5 ° N (midflight)
Longitude	85° W (midflight)
Velocity	800 fps
Duration of flight	15 min { 10 min straight, level (about 80 nm) 30 sec turn 5 min straight, level
Turn radius	6667 ft
Acceleration in turn	3 g's
Altitude	5000 ft
Heading (initial)	135°
Bearings to transmitters:	
Master (Cape Fear)	45°
Slave A (Jupiter)	135°
Slave B (Dana)	350°

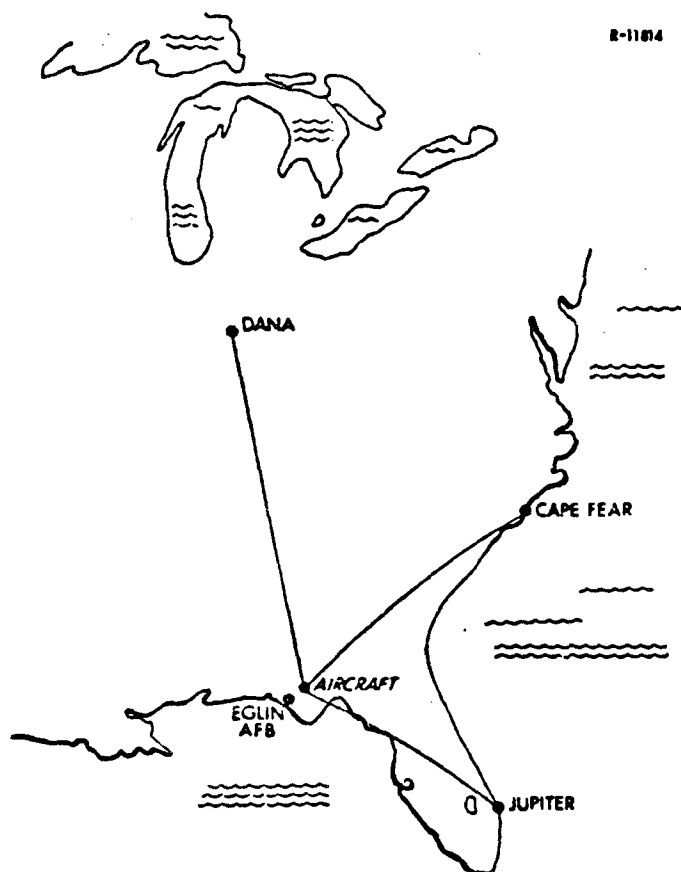


Figure 3 Location of Aircraft Relative to Loran Transmitters

continually being processed, the velocity is constant and lateral accelerations are zero. Also, the system dynamics are assumed to be constant.

Although the altitude of the aircraft does not explicitly appear in any of the error equations (except to influence the baroaltimeter errors), it is tacitly assumed that the vehicle is at a constant altitude throughout the flight somewhere between 5 and 10 thousand feet. This is a typical altitude and sufficiently low to insure that the received Loran signals will not be significantly attenuated. The simulated flight described here represents an actual elapsed time of approximately 15 minutes. Although short, it is sufficient to determine statistically the important effects and behavior of the Loran/Inertial system.

Reference System Error Model

In this section, the Loran/Inertial reference system error model is described based on TASC's experience with analysis of multisensor navigation systems and a set of computer simulations the reference system error model given in Table 2 has been determined to be appropriate for the Loran/Inertial navigation systems. It consists of 35 error quantities or states, grouped into 5 major categories.

The first category (states 1-7) provides the means for a mathematical description of inertial system error dynamics. Errors due to uncertainty in knowledge of the gravity vector are described by states 8 and 9. Inertial system accelerometer error quantities are described by states 10-21, and those corresponding to gyro error quantities by states 22-29. Loran-related errors are modeled by states 30-35.

The magnitudes of the inertial system errors have been selected such that the overall unaided inertial system error growth is approximately 1-2 nm per hour. The performance of existing airborne inertial platforms is consistent with this selection.

It is assumed that the operational area will be a highly-surveyed Loran area. In addition, the Loran/Inertial system is assumed to contain some form of correction scheme for the Loran propagation errors. Thus every effort is made to reduce Loran errors. Since it is impossible to completely remove all propagation errors, the reference error model includes two random processes, one for each time difference (TD). The magnitude and correlation distance of each error is relatively small, reflecting the highly-surveyed environment.

TABLE 2
REFERENCE SYSTEM ERROR MODEL

State	Description	Model	Initial RMS Error
1, 2	Level position errors	—	1000 ft/axis
3, 4	Level velocity errors	—	4 fps
5, 6, 7	Platform-to-computer misalignments	—	3, 3, 20 min
8, 9	Vertical deflections	Markov	5 sec
10, 11	Accelerometer bias errors	Bias	316 μ g
12, 13	Accelerometer random errors	Markov	10 μ g
14, 15	Accelerometer scale factor errors	Bias	170 ppm
16, 17	Accelerometer (2nd-order scale factor errors)	Bias	28.2 μ g/g ²
18, 19, 20, 21	Accelerometer misalignments	Bias	33.3 sec
22, 23, 24	Gyro bias errors	Bias	0.03 deg/hr
25, 26, 27	Gyro random errors	Markov	0.003 deg/hr
28, 29	Mass unbalance gyro errors	Bias	0.017 deg/hr/g
30, 31	Loran phase lock loop states for TDA	—	1.0 μ sec
32, 33	Loran phase lock loop states for TDB	—	1.0 μ sec
34, 35	Residual Loran propagation errors	Markov	0.150 μ sec

Reference System Results

The rms navigation errors for the reference system error model and the flight profile described previously are shown in Figs. 4, 5 and 6, and are summarized in Table 3. The Loran measurement interval is 10 seconds for the nonmaneuvering portions of the flight and 5 seconds during the turn. The covariance values given in Table 2 were used to initialize the system. The equations used to generate these results are standard and can be found, for example, in Refs. 2 and 3.

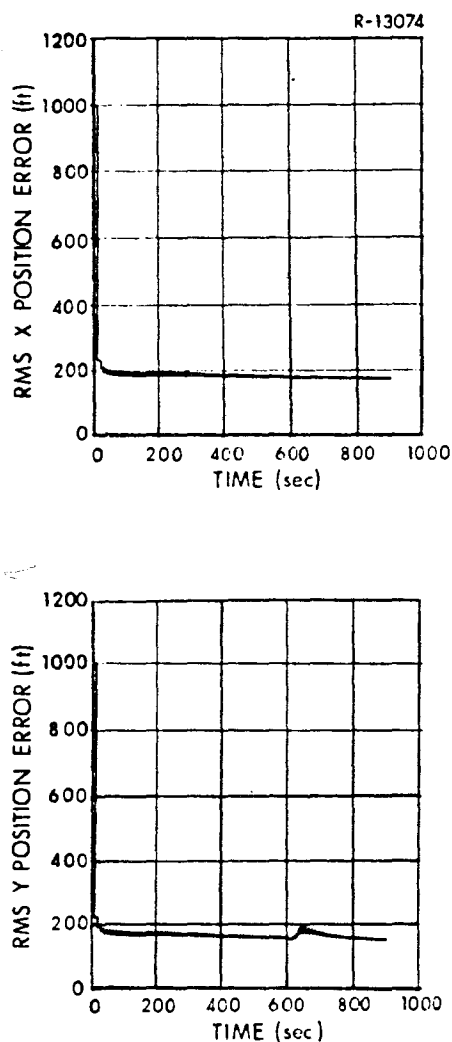


Figure 4 Optimal rms Position Errors (10 second fix interval, 5 second interval in turn)

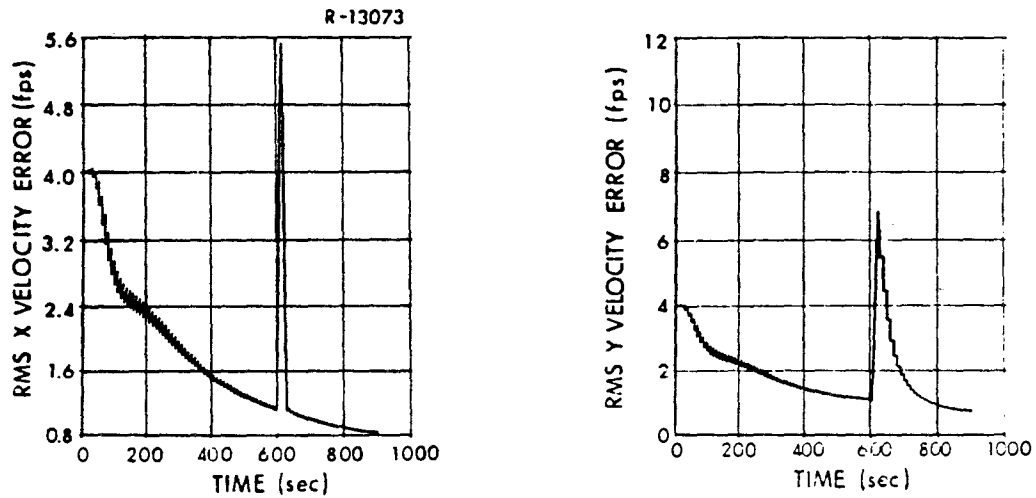


Figure 5 Optimal rms Velocity Errors (10 second fix interval, 5 second interval in turn)

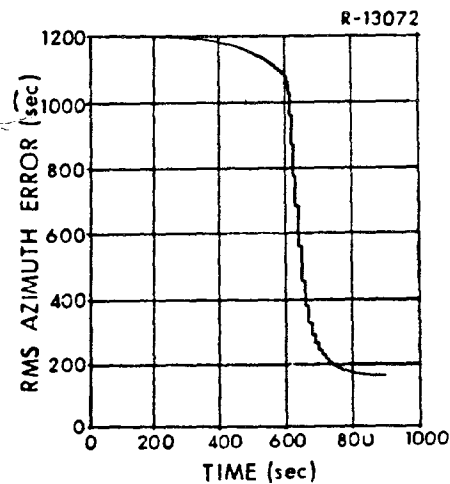


Figure 6 Optimal rms Azimuth Error (10 second fix interval, 5 second interval in turn)

TABLE 3
BASELINE OPTIMAL RMS NAVIGATION ERRORS

<div>Time (just after fix)</div> RMS Error	End of Straight/Level (10 min)	Mid Turn (10 min 15 sec)	End of Turn (10 min 30 sec)	End of Flight (15 min)
X-Position (ft)	175.6	174.0	174.7	171.2
Y-Position (ft)	155.3	152.0	159.7	150.6
X-Velocity (fps)	1.10	5.11	1.10	0.82
Y-Velocity (fps)	1.08	3.89	5.46	0.74
Azimuth Error ϕ_z (sec)	1078.0	957.3	678.2	159.8

The rms position error results shown in Fig. 4 clearly reflect the quality of the available Loran signals. Within the first few fixes the initial rms position uncertainty of 1,000 ft per axis is reduced to less than 200 ft rms. The position accuracy is seen to gradually improve as more measurements are processed until, as shown in Table 3, the final position uncertainties are slightly higher than the residual Loran markov propagation anomalies of 150 ft. rms per TD. Essentially the effect of the measurement white noise (200 ft rms per TD) has been "smoothed out."

Note also that the turn which occurs from 600 to 630 seconds into the simulation has very little effect on the position errors. Thus although the dynamics of the inertial system are rapidly changing, they do not significantly impact the position accuracy as long as Loran measurements are processed. As will be shown subsequently the time interval between fixes does have a noticeable effect. This is one reason the measurement interval is reduced to 5 seconds during the turn.

The turn, however, has a very large effect on the system velocity errors. This effect can be explained with two reasons. First, the Loran

measurements are essentially position measurements, thus there is a "delay" before velocity information is obtained. (Heuristically, from two position measurements at two different times, velocity and hence velocity errors can be estimated.) Secondly, the accelerations in the turn directly affect the velocity errors through the inertial system dynamics equations and since position is the integral of velocity, the effects of the accelerations on position errors are not as immediate.

The final navigation error is the azimuth error on ϕ_z . This quantity is directly related to heading error; for the system under study, heading error and azimuth error are nearly identical.

Although the description of the baseline simulations given above provides an understanding of the basic system behavior and accuracies, additional insight can be obtained through an examination of the optimal error budget. The error budget -- as shown in Figs. 7, 8 and 9 -- quantitatively identifies the relative effects of the system error sources. (The figures are for the y-component of position and velocity errors; the x-component error budgets are nearly identical.)

As shown in the error budgets, Loran-related errors dominate the output navigation errors. The measurement errors together with the uncompensated Loran propagation anomalies constitute nearly 99% of the mean-squared position errors. These figures can be used to determine the effect of a shift in error levels. If the Loran propagation corrections are improved to the point at which the remaining uncorrected anomalies had an rms magnitude of half that used in the simulation, then this would reduce the final rms position error level by nearly 40% (half of the 79.7% in Fig. 7). Thus, the figures identify the key error sources and quantitatively determine their relative effects.

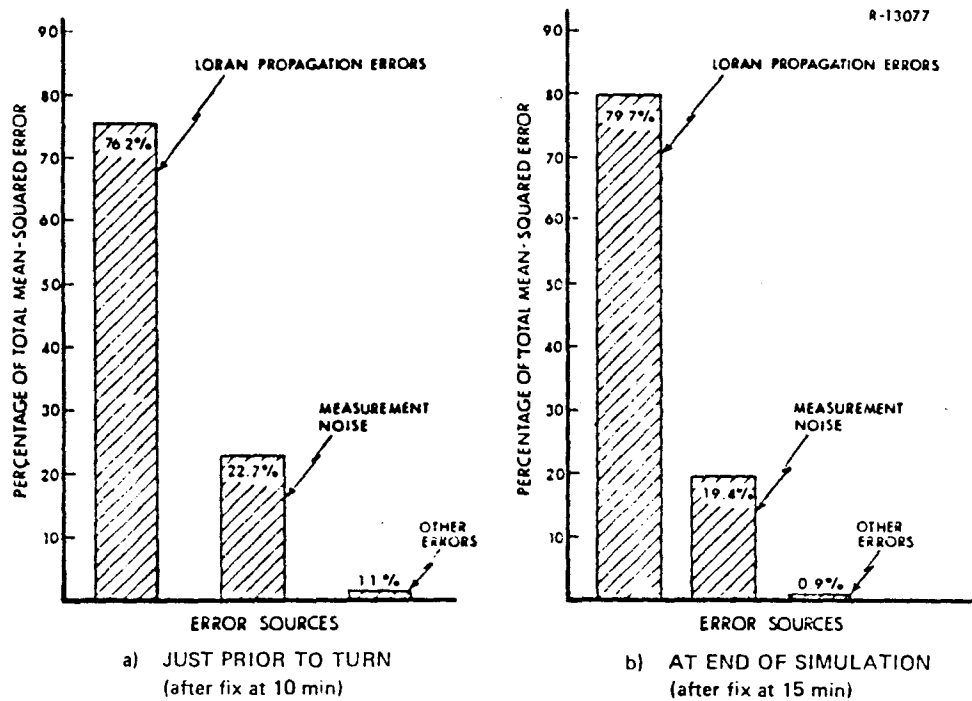


Figure 7 Optimal System - Y Position Error Budget

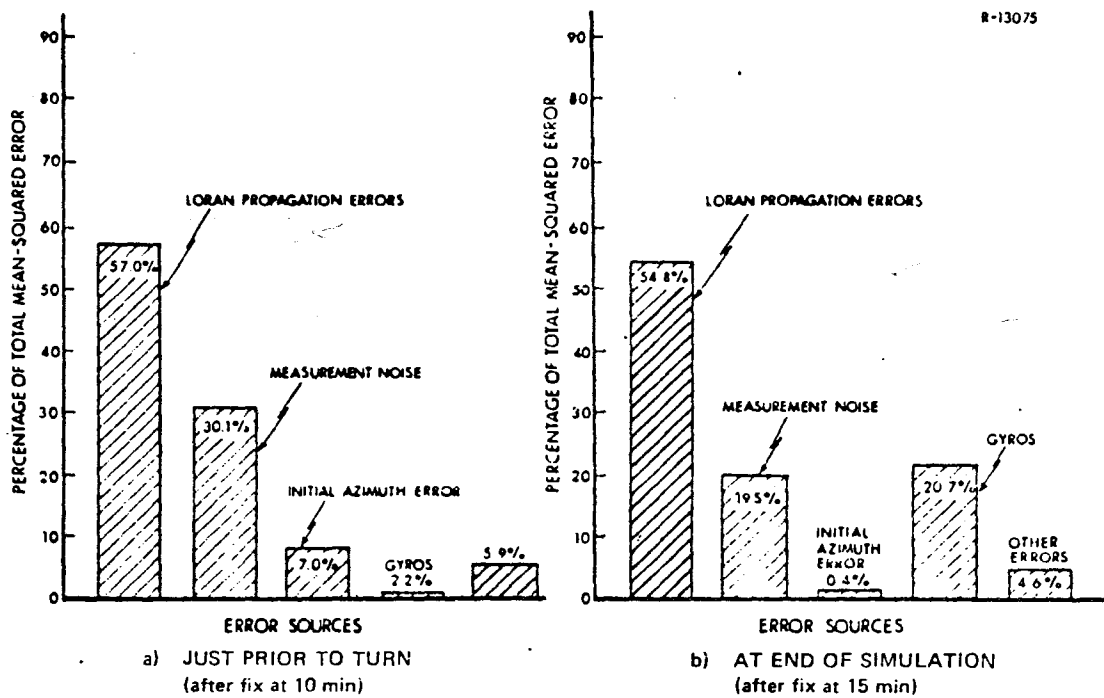


Figure 8 Optimal System - Y Velocity Error Budget

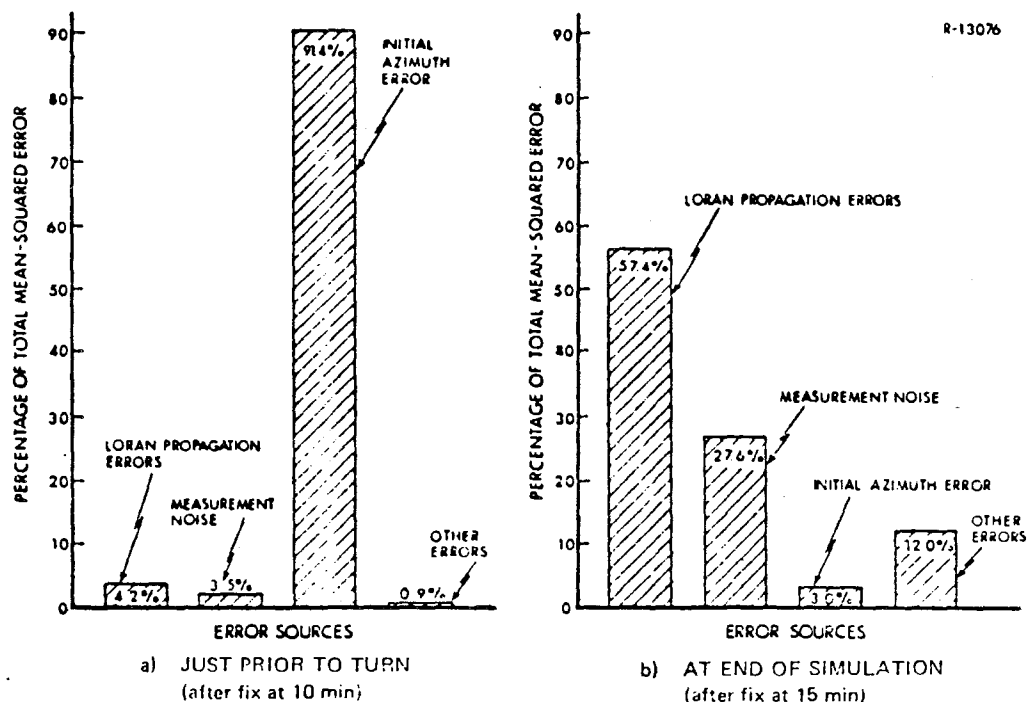


Figure 9 Optimal System - Azimuth Error Budget

Although Loran-related effects (propagation errors and measurement noise) clearly dominate the velocity error budget shown in Fig. 8, other errors are shown to have a significant effect. Prior to the turn, the large initial azimuth error (20 min) produces about 7% of the total velocity error. Since the azimuth error is highly observable in the turn (see Fig. 6), its effect at the end of the simulation is negligible, and the gyro errors which are not significantly affected by the turn become relatively more important by the end of the simulation.

The azimuth error budget is considerably different from the others. The Loran-related errors constitute less than 8% of the error budget prior to the turn; azimuth error is almost totally due to the initial alignment error. Since ψ_z is highly observable in the turn, its effects are easily identified and removed. As a result, the azimuth error budget at the end of the simulation is very similar to those for velocity and position.

Sensitivity Analyses

Additional understanding of the Loran/Inertial system is obtained by examining the results of special simulations. These simulations differ from the baseline in two ways: the error model correlation time and measurement interval sensitivities are examined, and next the behavior of the system in non-nominal conditions (free inertial, two station operation, etc.) is investigated.

The baseline optimal results presented above are only as accurate as the reference system error model. Although the "real-world" model is based upon past experience and analysis of extensive test results, it is nonetheless important to determine the sensitivity of the optimal covariance analysis to parameter variations.

The effect of the Loran fix interval on position accuracy is examined by simulating the 10 minute straight and level flight with various measurement intervals. The resulting effects on position and velocity errors are shown in Table 4. It can be seen that there is an expected degradation in accuracy at the time between fixes increases, and likewise an improvement as the fix interval decreases from 10 seconds. Note also that velocity errors are slightly more sensitive to the changes than are position errors. The results are similar for the other navigation error components, as shown in Table 4. There it can be seen that azimuth error is least affected, varying by only about 5% as the fix interval changes by a factor of 4.

Although the curves vary almost linearly with the fix interval, the overall impact on navigation accuracy is not very critical over the intervals considered. It is likely that the sensitivities would be noticeably reduced if the system initial conditions were more optimistic or if the comparison was made after the turn when all of the error cross-covariances were generated.

TABLE 4
SENSITIVITY OF NAVIGATION ERRORS TO
MEASUREMENT INTERVAL

<div>RMS Error after 600 sec</div> <div>Fix Interval</div>	5 Seconds	10 Seconds (Baseline)	20 Seconds
X-Position (ft)	168.5	175.6	185.6
Y-Position (ft)	146.8	155.3	167.8
X-Velocity (fps)	1.04	1.10	1.20
Y-Velocity (fps)	1.00	1.08	1.19
Azimuth (sec)	1052.	1078.	1104.

Nevertheless, it would appear that there is some advantage to implementing as short a fix interval as possible. Practical systems, however, are limited by a minimum cycle time for executing the filtering algorithms and by other hardware and software constraints.

Another important parameter in the reference system model is the Loran propagation anomaly correlation distance. A correlation distance of approximately 40 nm is used in the baseline simulations which corresponds to a correlation time of 300 seconds for a vehicle traveling 800 fps. This correlation distance is based upon available Loran data and the anticipated accuracy of the surveyed Loran operations area. Since the precise nature and magnitudes of Loran errors are not well known, it is important to determine the sensitivity of the navigation errors to Loran variations.

The error budget presented earlier qualitatively identifies the effects of the Loran error magnitudes on system errors. In Fig. 10, the effect of variations in Loran correlation distance is shown. Unlike fix interval sensitivity,

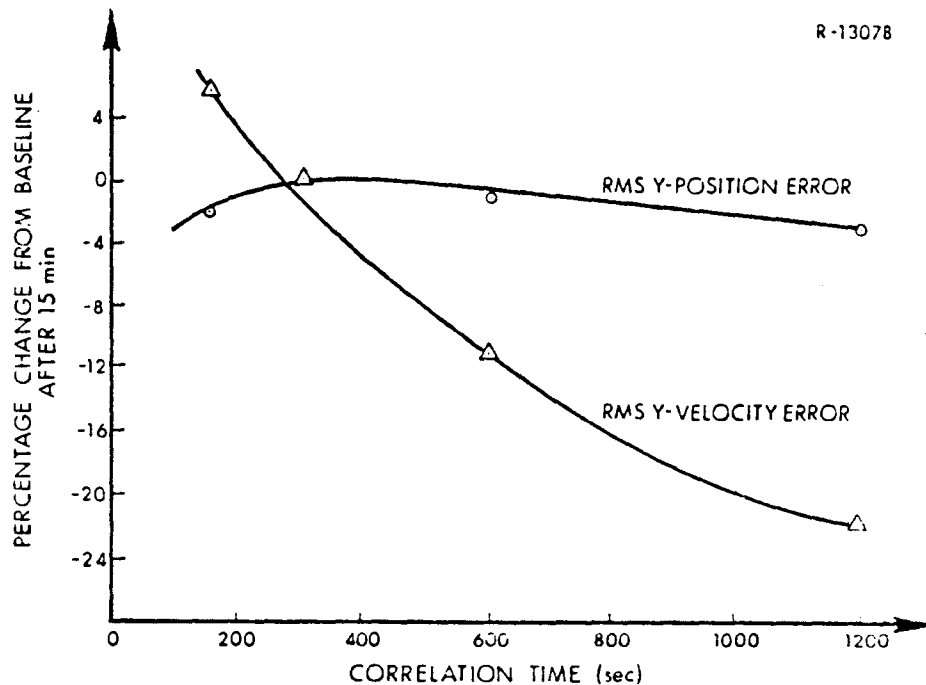


Figure 10 Effects of Loran Correlations on System Errors

Fig. 10 indicates very little position error sensitivity over the range considered. Although the velocity errors appear to be somewhat more sensitive to the correlation time, it should be noted that the actual velocity error differences are still less than 0.5 fps as shown in Table 5. Thus it appears that the magnitude of Loran errors is far more critical than the correlation distance.

The effect of a second turn on system dynamics is investigated next. The large error growth in velocity in the baseline results is not present in the second turn as shown in Fig. 11. In fact, the effect on all of the navigation errors is not as pronounced as in the first turn. This is because the initial error covariances, in particular the initial azimuth error, were larger than those which would be obtained after a thorough ground alignment. The initial straight and level segment and the first turn are sufficient to remove initial transient effects and bring the system into a relatively insensitive "steady state."

TABLE 5
SENSITIVITY OF NAVIGATION ERRORS TO
LORAN ERROR CORRELATION TIME

Correlation Time RMS Error After 15 min	150 Seconds	300 Seconds (Baseline)	600 Seconds	1200 Seconds
X-Position (ft)	165.8	171.2	170.4	167.9
Y-Position (ft)	147.8	150.6	149.2	146.8
X-Velocity (fps)	0.87	0.82	0.72	0.61
Y-Velocity (fps)	0.78	0.74	0.66	0.58
Azimuth ($\widehat{\text{sec}}$)	180.6	159.8	137.5	121.6

This is verified by noting that the error levels after the second turn are nearly identical to those obtained a few minutes after the first turn.

The sensitivity to initial conditions is now considered. The initial rms error levels used in the baseline analyses are perhaps somewhat pessimistic; hence, rms error values which correspond to levels attainable after a more lengthy period of ground alignment are examined. These initial conditions and results after a 15 minute simulation are compared with the baseline results in Table 6. Except for the parameters noted, all other error levels are unchanged. It can be seen that although there is considerable difference initially, there is no significant difference after the 15 minute flight simulation. The optimal system, therefore, is fairly insensitive to initial conditions.

Performance of the system in the free-inertial navigation mode is shown in Fig. 12. The straight and level segment of the flight with Loran fixes every 10 seconds was simulated for 10 minutes to obtain steady-state accuracies. Then, no measurements were processed and flight for an

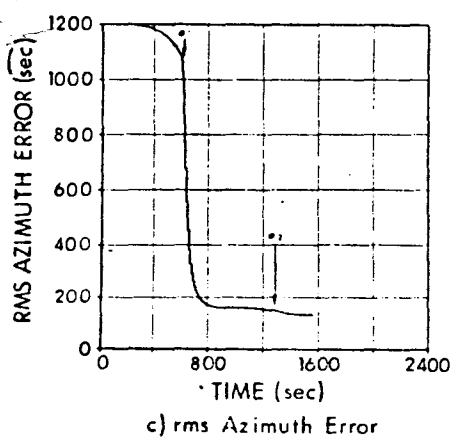
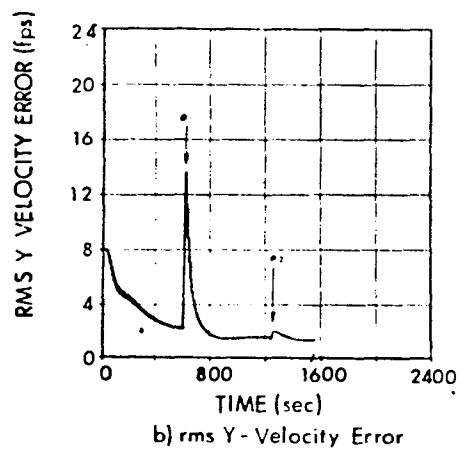
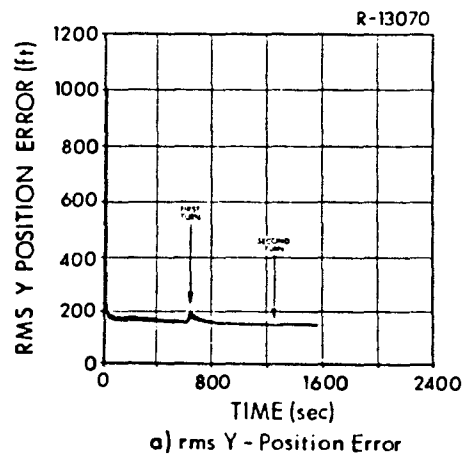


Figure 11 Effects of a Second Turn - Optimal System

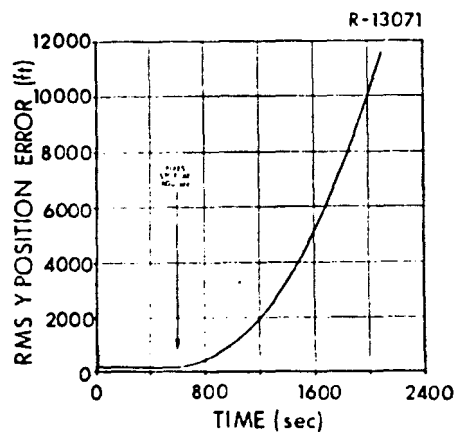
TABLE 6
REFERENCE SYSTEM SENSITIVITY
TO INITIAL CONDITIONS

	RMS Initial Conditions		RMS Error Level After 15 Minutes	
	Baseline	Improved	Baseline	Improved
X-position (ft)	1000.	500.	171.2	170.1
Y-position (ft)	1000.	500.	150.6	150.1
X-velocity (fps)	4.0	1.0	0.82	0.77
Y-velocity (fps)	4.0	1.0	0.74	0.71
X- } platform mis-	180.0	20.0	70.8	30.6
Y- } alignments (sec)	180.0	20.0	70.1	30.8
Z- }	1200.0	600.0	159.8	142.2

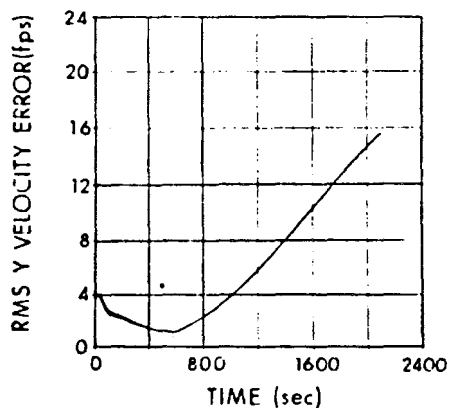
additional 25 minutes was simulated. As shown in the figure, the position and velocity errors begin to grow immediately after the fixes cease. Within a few minutes the position errors are beyond the acceptable range for accurate navigation. Although it is not clearly apparent in Fig. 12(b), the velocity errors do oscillate (as well as ramp) with a Schuler period of 84 minutes. Without Loran fixes the azimuth error oscillates at approximately earth rate.

Another mode of operation to consider is the behavior of the system when only two transmitters are on the air. Clearly if the Master is down, the Loran system cannot function, since the time differences are all referenced to the Master. Also, since this is a time difference rather than a direct ranging system at least two stations must be transmitting for Loran signals to be processed.

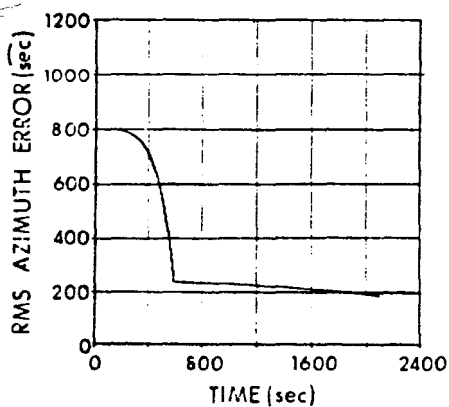
One time difference measurement is not sufficient for determining vehicle position; however, the information in the measurement may be useful



a) rms Y- Position Error



b) rms Y- Velocity Error



c) rms Azimuth Error

Figure 12 Free Inertial System Performance

in limiting the rate of navigation error growth. The results of two station operation are summarized in Table 7. As expected, the results for a single transmitting slave are considerably poorer than when all stations are operating. There is, however, about a 50% or more improvement over free inertial performance. Thus, although system performance is seriously degraded by the loss of even one transmitter, there may be some advantages to processing a single time difference for at least a short period of time. The magnitude of the navigation errors shown in Table 7 is due mainly to the large azimuth error in the system. That is, since the turn has not been simulated a large heading error remains which causes a misresolution of velocity and hence, the large rms position errors.

TABLE 7
NAVIGATION ERRORS AS A FUNCTION OF
NUMBER OF LORAN TRANSMITTERS

Loran Transmitters RMS Navigation Error (after 20 min) Operating	All Three Stations	No Slave A	No Slave B	Free Inertial
x-Position (ft)	169.2	841.3	818.2	1576.
y-Position (ft)	150.4	478.0	821.9	1959.
x-Velocity (fps)	0.79	2.43	1.94	4.09
y-Velocity (fps)	0.81	1.85	2.08	5.83
Azimuth ($\widehat{\text{sec}}$)	442.1	645.7	460.5	1084.

Summary

Based on the models and results given above, the following conclusions can be made regarding an optimally integrated airborne Loran/Inertial system:

- The overall accuracy of the system is limited by the accuracy of the available Loran data. Inertial instrument errors are not nearly as significant as are Loran errors under nominal conditions.
- Unless initial azimuth errors are very small, velocity errors are excited by level accelerations, but position is not significantly degraded as long as Loran data are available. A short high-speed turn is sufficient to appreciably reduce the large initial rms azimuth errors.
- Shorter Loran measurement intervals will yield slightly improved rms navigation accuracy.
- The residual Loran error correlation distance is not a significant factor in system performance over the range of values considered (20 nm to 160 nm).
- Two station Loran operation is considerably better than free inertial, but nonetheless is still sufficiently poor that advantages of operating in this mode for any length of time are questionable.

REFERENCES

1. Gelb, A. , ed. , Applied Optimal Estimation, M.I.T. Press, Cambridge, 1974.
2. "Platform Model for the A-7 D/E Inertial Measurement Set," Kearfott Systems Division, Doc. No. 6K0320025C, 29 March 1968.
3. D'Appolito, J. A. , "The Evaluation of Kalman Filter Designs for Multisensor Integrated Navigation Systems," The Analytic Sciences Corp. , AFAL-TR-70-271, January 1971 (AD-881-286).

FILE COPY

3-2

LORAN-C FOR EMERGENCY COMMUNICATIONS

WALTER N. DEAN

THE MAGNAVOX COMPANY

FORT WAYNE, IND.

FEHLNER
REF 594
PAPER 3-2
PP 25 (23+2)

2890112

ABSTRACT

The U.S. Department of Transportation plans to install a total of 13 Loran-C transmitters around the continental U.S. A new emergency communication system, DIDS, has been proposed by OCD. Loran-C could be used for emergency communications in three ways:

- (1) A low data rate system, which can use extremely simple receivers.
- (2) A teletype system similar to Clarinet Pilgrim.
- (3) Broadcast of voice utilizing Loran-C transmitting antennas.

It is concluded that the Loran-C chains could provide the necessary emergency communications in a cost-effective manner.

1. LORAN-C SYSTEM

Loran-C is a low frequency (100 KHz) pulse radio navigation system which is used for navigation over large areas of the north Atlantic and north Pacific oceans. It consists of a number of large high-powered transmitting stations with large antenna systems situated some 400 to 700 miles apart and providing a means of accurate position fixing over large areas of the ocean and over land.

The U.S. Department of Transportation announced in May of 1974 that the Loran-C system was being adopted to provide navigation in the coastal confluence of the United States which consists of all those areas along the Atlantic, Gulf and Pacific coasts including Alaska and also the Great Lakes. Accordingly, the U.S. Coast Guard is planning an expansion of the existing Loran-C coverage to include all of these areas. The projected coverage is shown in Figure 1. It will be seen that the completion of these installations will result in having a total of 13 Loran-C stations within the Continental U.S. These stations, operating as they do in the low frequency 100 KHz band, will be capable of being received almost anywhere within the continental U.S. with a good signal to noise ratio. At present the only reason for existence is to provide precise navigation information for surface vehicles.

2. EMERGENCY COMMUNICATIONS

There is an obvious need for a system with emergency communications within the United States to provide advance warning and communications in case of disasters, both natural and manmade. Such a system is already in existence as a combination of Federal, State and local networks. The Federal portion of this system, the National Warning System (NAWAS) connects three national warning centers with approximately 1,000 full time state and local warning points. Warning officers at the warning center initiate a voice warning message. See Figure 2. State and local personnel at the 1,000 warning points sound sirens or initiate action to sound sirens at these locations. NAWAS is a two-way party line telephone system. It is leased from ATT at an annual cost of well over a million dollars. State and local networks then have the responsibility of further dissemination of warning information. It is estimated that the present system could provide warning to approximately 60% of the urban population.

2.1 DIDS

The Office of Civil Defense is planning a new warning system, called the Decision Information Distribution System (DIDS), which is to include two 61 kHz control stations and ten 200 kHz distribution stations (see Figure 3). They are to transmit voice, teletype or siren switching signals via the LF transmissions, to nearly all the continental U.S. Figure 4 shows the proposed

coverage. The 200 KW 61 kHz stations will have 1260 ft. guyed tower antennas, while the antennas for the 50 KW 200 kHz stations will have towers only 700 ft. high.

The OCD is moving ahead with implementation of DIDS. An experimental transmitter was set up near Aberdeen, Md. in 1971-72. Money is now being spent on receiver design and production engineering-including a \$424,000 contract to Bendix in June.

3. LORAN-C COMMUNICATION

The Loran-C system, which is being installed in continental U.S. has the capability of use for communications in a number of ways, which could meet the OCD requirements. This includes ability to transmit Loran-C signals to a simple receiver for alert or siren control, a Loran-C teletype communication system capable of 60 WPM, and the facility to transmit voice over a separate transmitter using the Loran-C transmitting antenna.

3.1 Alert System

A method of transmitting low speed data from a Loran-C transmitter to a simple receiver was demonstrated by the Coast Guard ten years ago. The technique consists of shutting off alternate pulses in the Loran-C group to signal a change of state. As Figure 5 shows, the 1000 Hz component generated when all eight pulses are transmitted becomes a 500 Hz modulation when alternate

pulses are dropped. A receiver is shown in block form in Figure 6. No timing is required. The 100 kHz amplifier is less than 2 kHz bandwidth, feeding an ordinary diode detector. The detected output is then filtered at 1000 and 500 Hz, detected again, and the outputs compared.

The output of the comparator goes "on" when the 500 Hz input becomes larger than the 1000 Hz, which can only happen when the pulses are dropped. A breadboard receiver of this type was built and tested.

The tests indicate that reliable operation can be achieved at approximately +3 db signal to noise ratio. Conservatively, a +6 db SNR should be adequate.

The effect of this modulation on a tracking navigation receiver is to decrease the SNR by 3 db while half the pulses are off. Some of the more sophisticated receivers might interpret this as synchronous interference, and adjust their strobing to the odd pulses only. In any case, the modulation would be on only a small percentage of the time, even during an emergency.

3.2 Teletype System

A teletype system using Loran-C, Clarinet Pilgrim, has been in operation in the Northwest Pacific for five years. It operates by pulse-position modulation of six of the eight pulses in each transmitted pulse group. A balancing technique eliminates navigation errors. The same message is sent from all stations in the chain, and a receiver receiving three stations improves his error rate by "majority vote" technique. The teletype receiver

is more complex than the "alert" receiver, since it must synchronize with the Loran-C signals and decode each bit from the modulation of each pulse. Figure 7 is a simplified block diagram of a Clarinet Pilgrim receiver built for the U.S. Navy.

For operation within 250 miles of a Loran-C transmitter, a much simpler receiver, which uses only a single station could be used, as the strong local signal will provide satisfactory communication.

3.3 Voice Transmission

It is not feasible to voice modulate the Loran-C transmission; however, a simple experiment has shown that it should be feasible to use the Loran-C transmitting antenna to radiate voice modulated transmissions at about 82 kHz.

There are two basic questions to be answered, First, is it possible to radiate 50 KW CW at 80 kHz and 1 MW Loran-C pulses from the same antenna? Second, can a 50 KW voice transmission be received without interference from the 1 MW Loran-C? Figure 8 shows the impedance characteristics of a 625 foot Loran-C antenna. It is resonant at about 106 kHz, and has a reactance of $-j75$ ohms at 80 kHz.

Figure 9 shows how an 80 kHz transmitter could be coupled into the Loran-C antenna system. The combination L_1C_1 is parallel resonant at 100 kHz, so that the 80 kHz transmitter does not load the Loran-C transmission and the Loran-C pulses are blocked from the 80 kHz transmitter. The values of L_1 and C_1 are also selected so that the circuit from the voice transmitter to the antenna is tuned to 80 kHz. This requires L and C values of approximately 52 microhenries and .048 microfarads.

In order to determine whether sidebands of the Loran-C transmission would interfere with voice transmissions at 82 kHz, a simple experiment was performed. Simulated Loran-C signals were mixed with an 80 kHz voice modulated signal and fed to a communications receiver. The levels were set so that the 80 kHz signal was 30 db weaker than the Loran-C. The 80 kHz signal was then evaluated and found to be free of interference.

3.4 Loran-C Coverage

The amplitude of the received Loran-C signal depends on the distance and in, the case of the groundwave, the conductivity of the earth over which it passes. Skywave amplitude vary greatly from day to night. Figure 10 illustrates all of these.

The coverage available depends on the noise level and the bandwidth characteristics of the data transmitted. In the case of the "alert" system, the signal to noise ratio required for reliable operation is +6 db. This can be obtained out to a distance of over 400 miles from a Loran-C transmitter under summer day noise conditions. This covers all but seven states, as seen in Figure 11.

The teletype system has a different error rate with noise, and is also affected by other Loran stations. Figure 12 shows how the error rate varies with signal-to-noise ratio. Figure 13 relates bit errors to crossing rate interference, which is interference from other Loran-C chains. This problem occurs principally at night, as can be seen by reference to Figure 10. Nighttime skywaves from stations as distant as 1500 miles can have significant amplitude. Therefore, to have an error rate of 10^{-3} , the signal to interference ratio must be +6 db, which means the distance to a single transmitter must be less than 250 nautical miles.

Even so, the coverage of the country by Loran-C chains will be such that 23 out of the 24 largest cities will be within 250 miles of Loran-C stations. See Figure 14. The area includes approximately 170 million people. To reach remaining 35 million people would require a more complex data receiver.

At distances beyond 250 miles, the teletype receiver would derive its data from three stations, and perform a "majority vote" on the data to improve the data error rate.

The effectiveness of the "majority vote" technique is illustrated in Figure 15. Since the errors due to either atmospheric noise or crossing rates are uncorrelated from one station to another, the probability of error of the majority vote is easily calculated from the individual error rates.

A bit error rate of 2 per thousand is equivalent to one error in 140 characters, which is better than usually found in the ordinary telegram.

4. CONCLUSIONS

The expansion of the Loran-C system in the continental U.S. will result in nearly 90% of the population being within 250 miles of a Loran-C transmitter. The capability to transmit information using the Loran-C has been demonstrated. It seems obvious that use of the Loran-C facilities for emergency communication, a service which hopefully will see infrequent use, would be an economical utilization of resources.

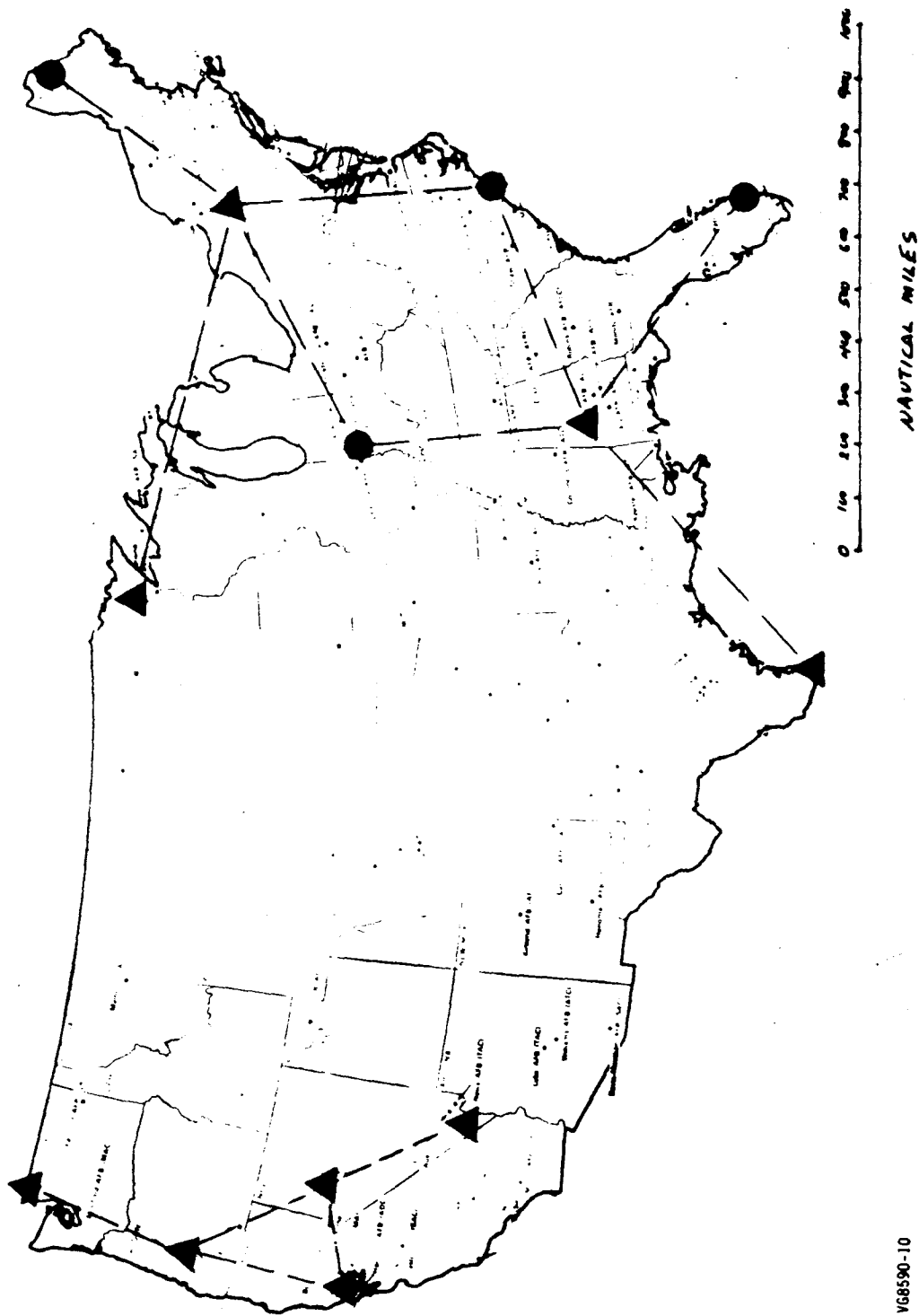
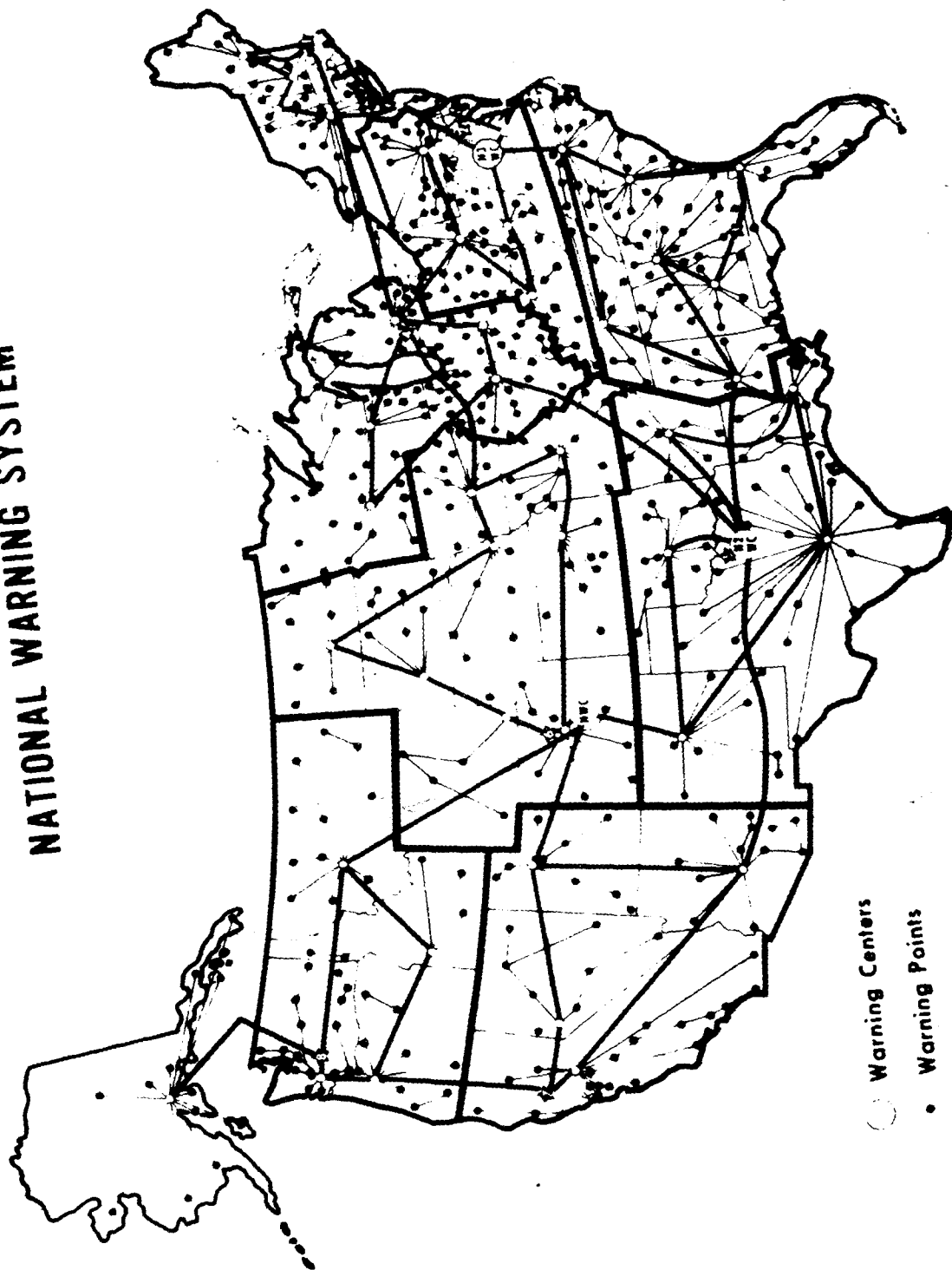


Figure 1 LORAN-C STATIONS

V68590-10

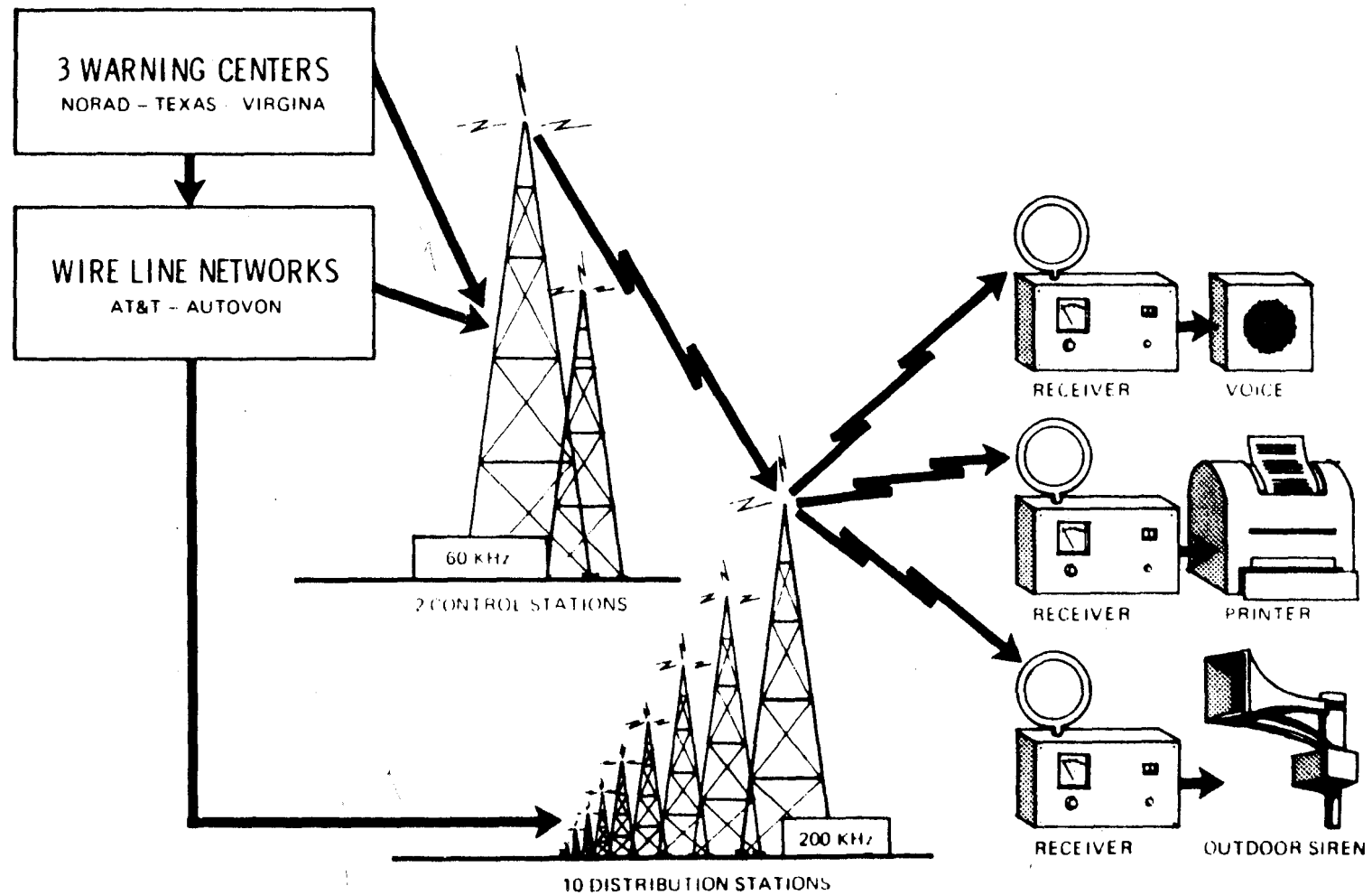
NATIONAL WARNING SYSTEM



VG8590-1

Figure 2

SYSTEM PLAN FOR DIDS

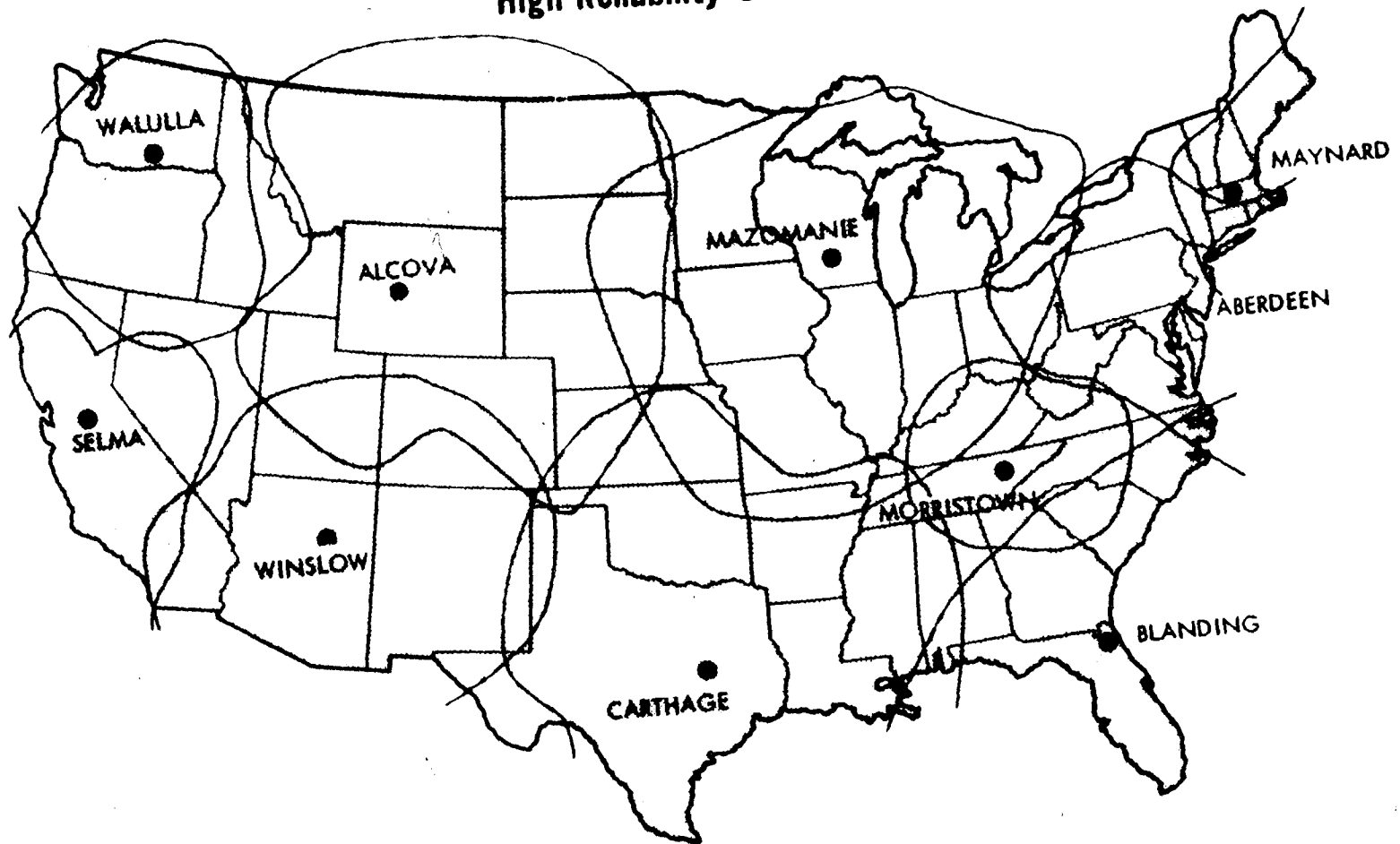


VG8590-2

Figure 3

DIDS TRANSMISSION COVERAGE

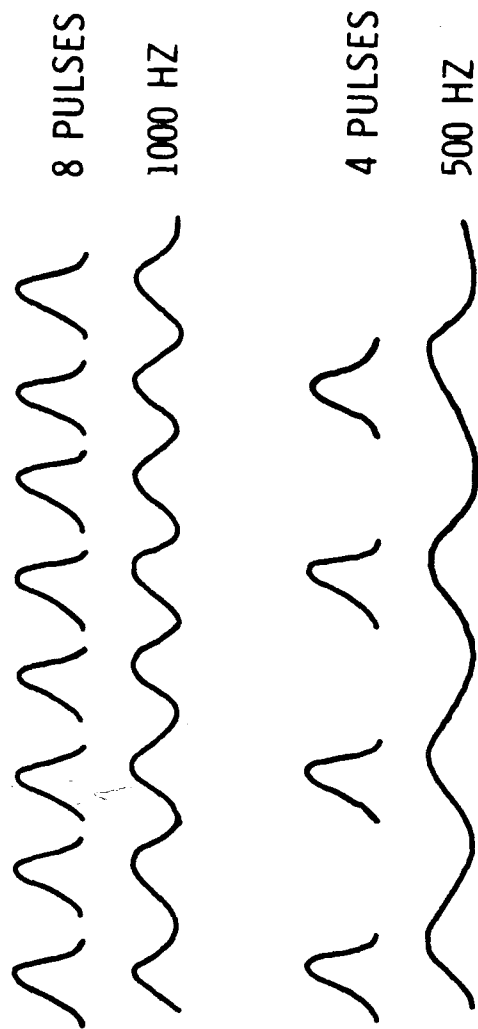
High Reliability Service



VG8590-3

Figure 4

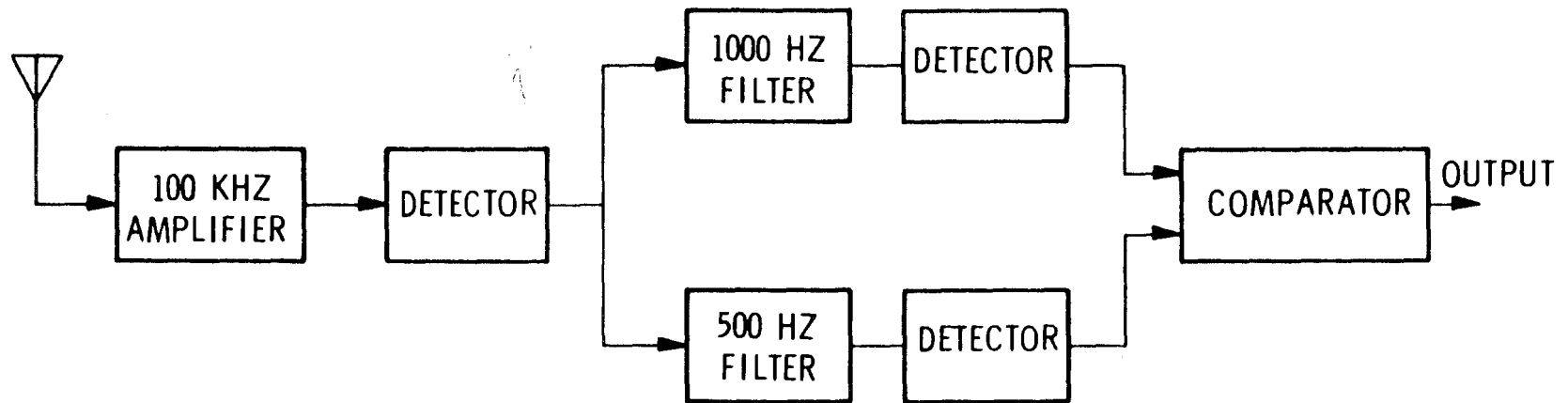
PULSE DROPPING TECHNIQUE



VG8590-6

Figure 5

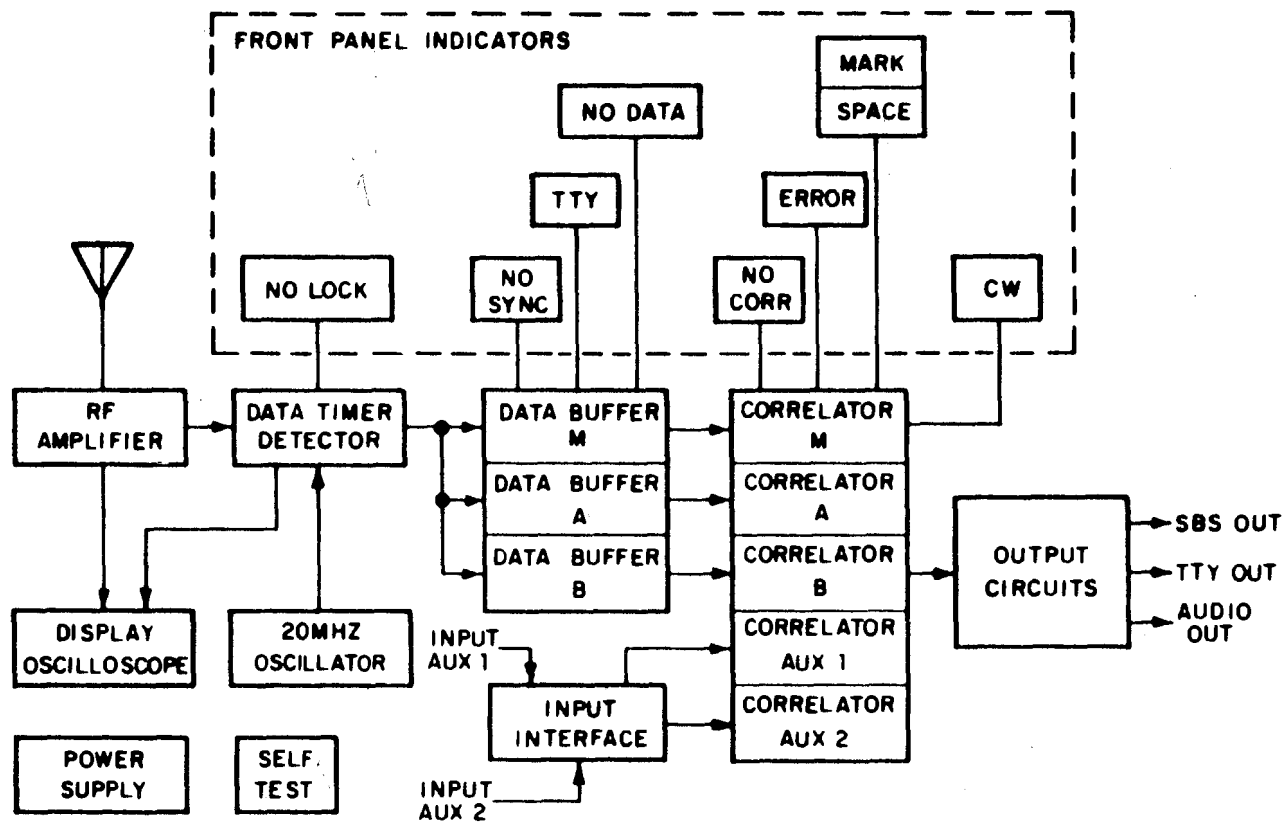
ALERT RECEIVER



VG8590-4

Figure 6

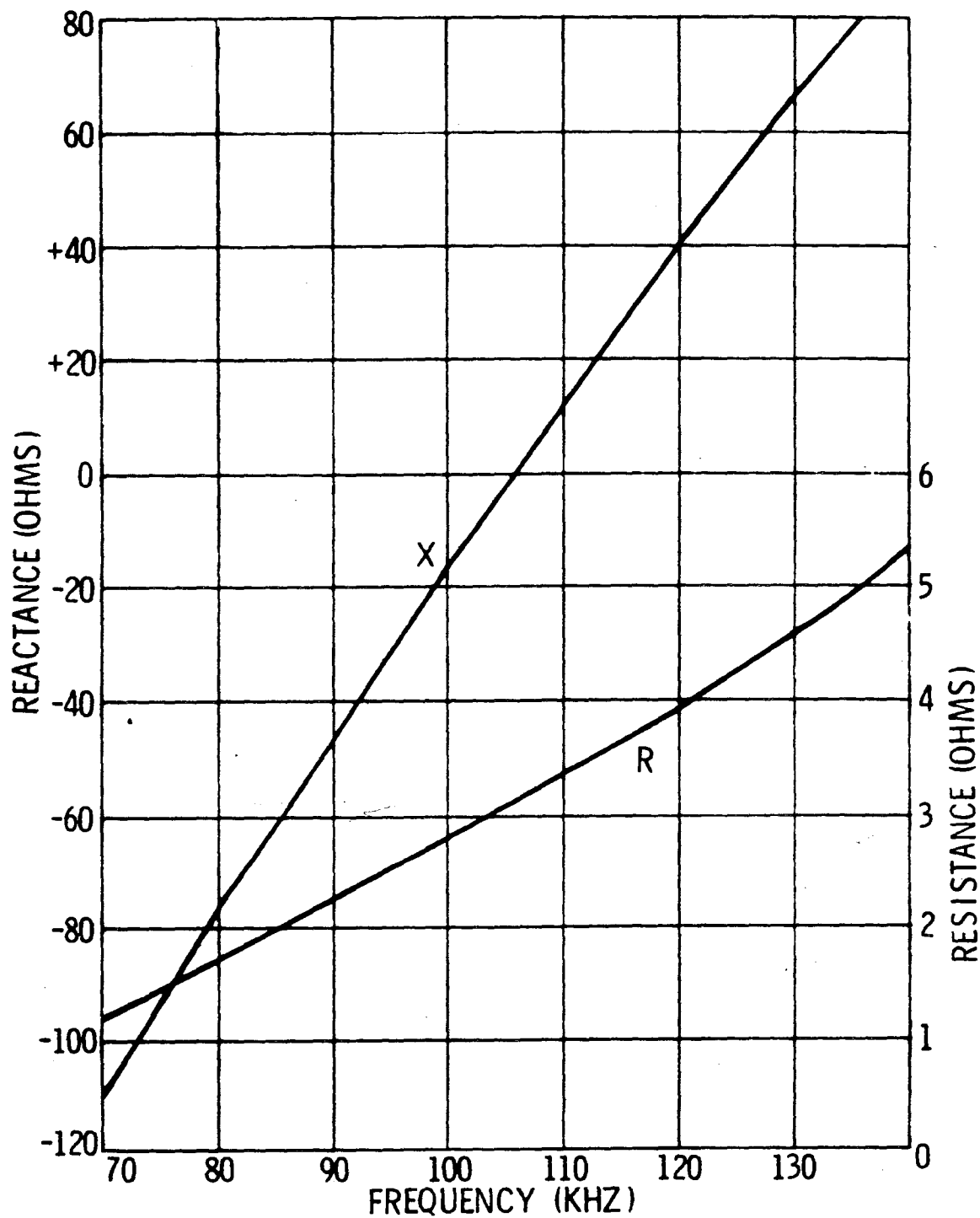
DIGITAL DATA RECEIVER R-1663(XN-1)/UR BLOCK DIAGRAM



VG8168

Figure 7

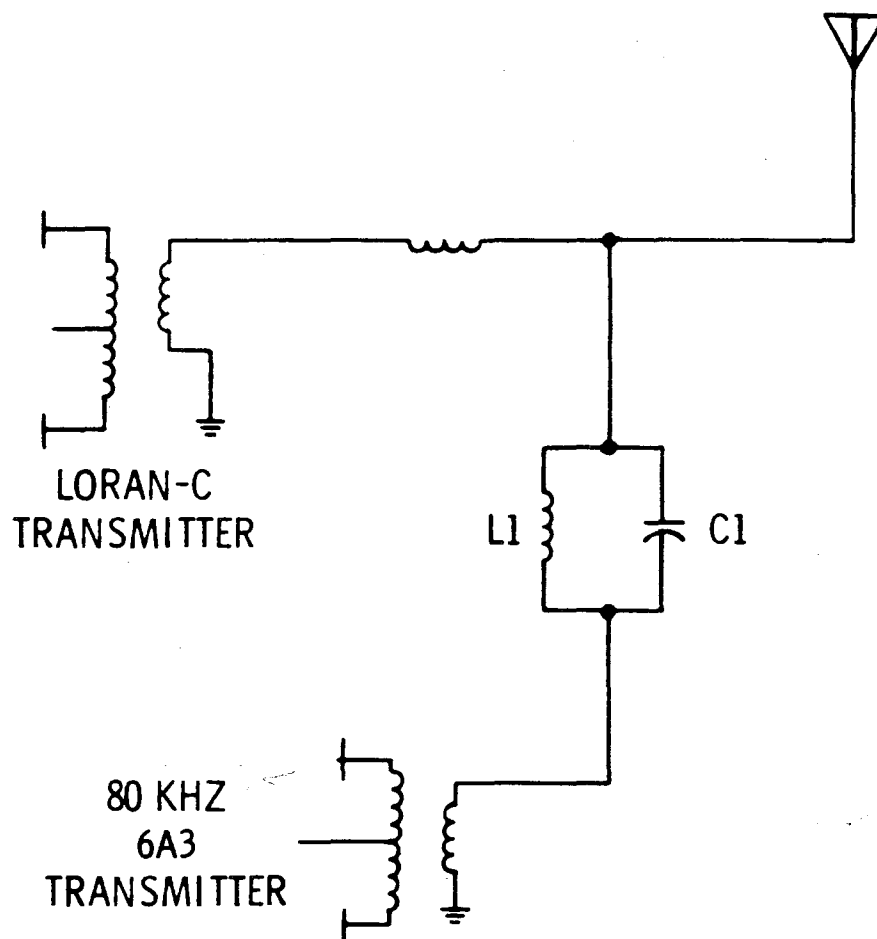
IMPEDANCE CHARACTERISTICS 625-FT LORAN-C ANTENNA



VG8590-7

Figure 8

COUPLING TO LORAN-C ANTENNA



VG8590-8

Figure 9

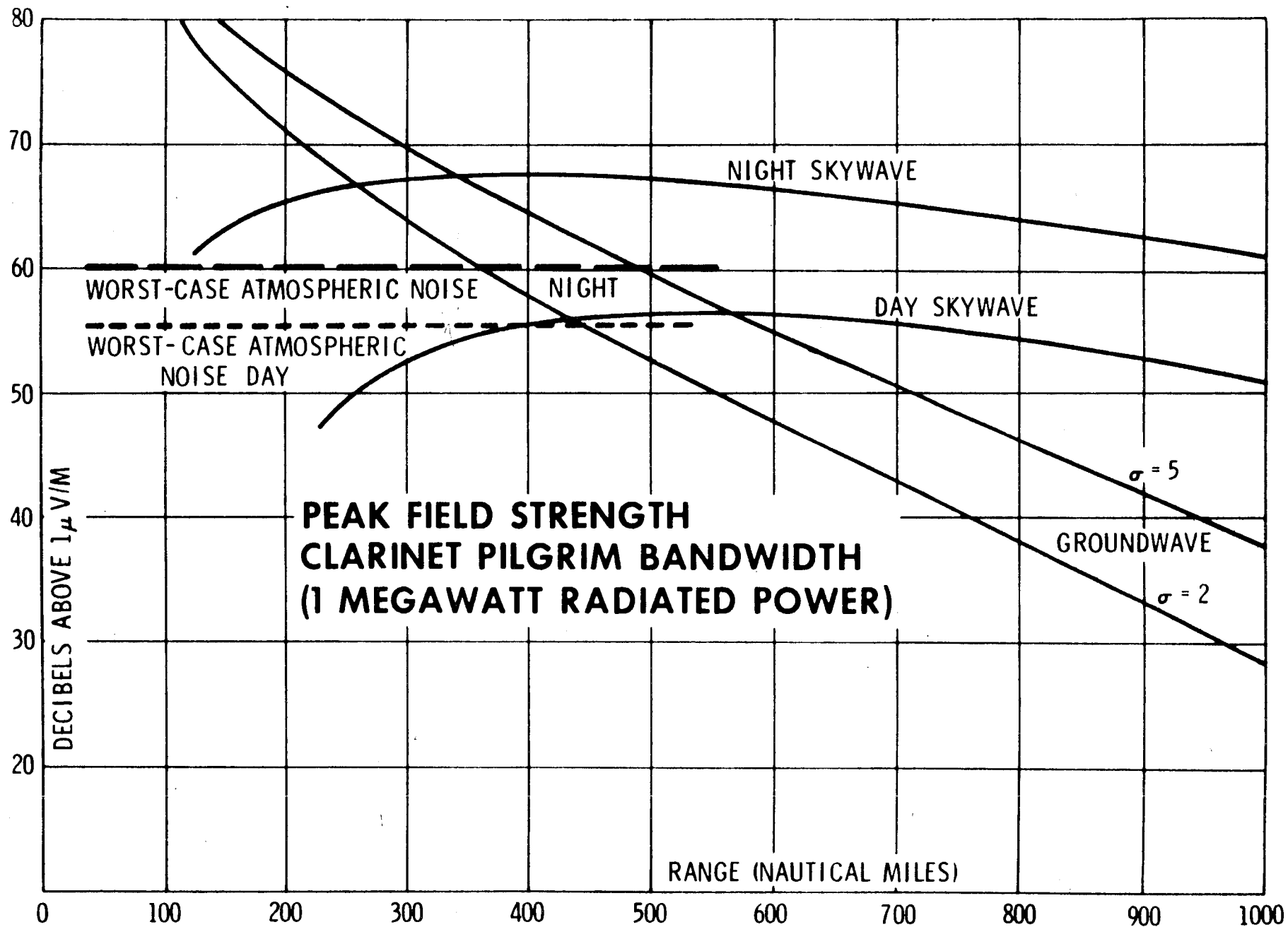
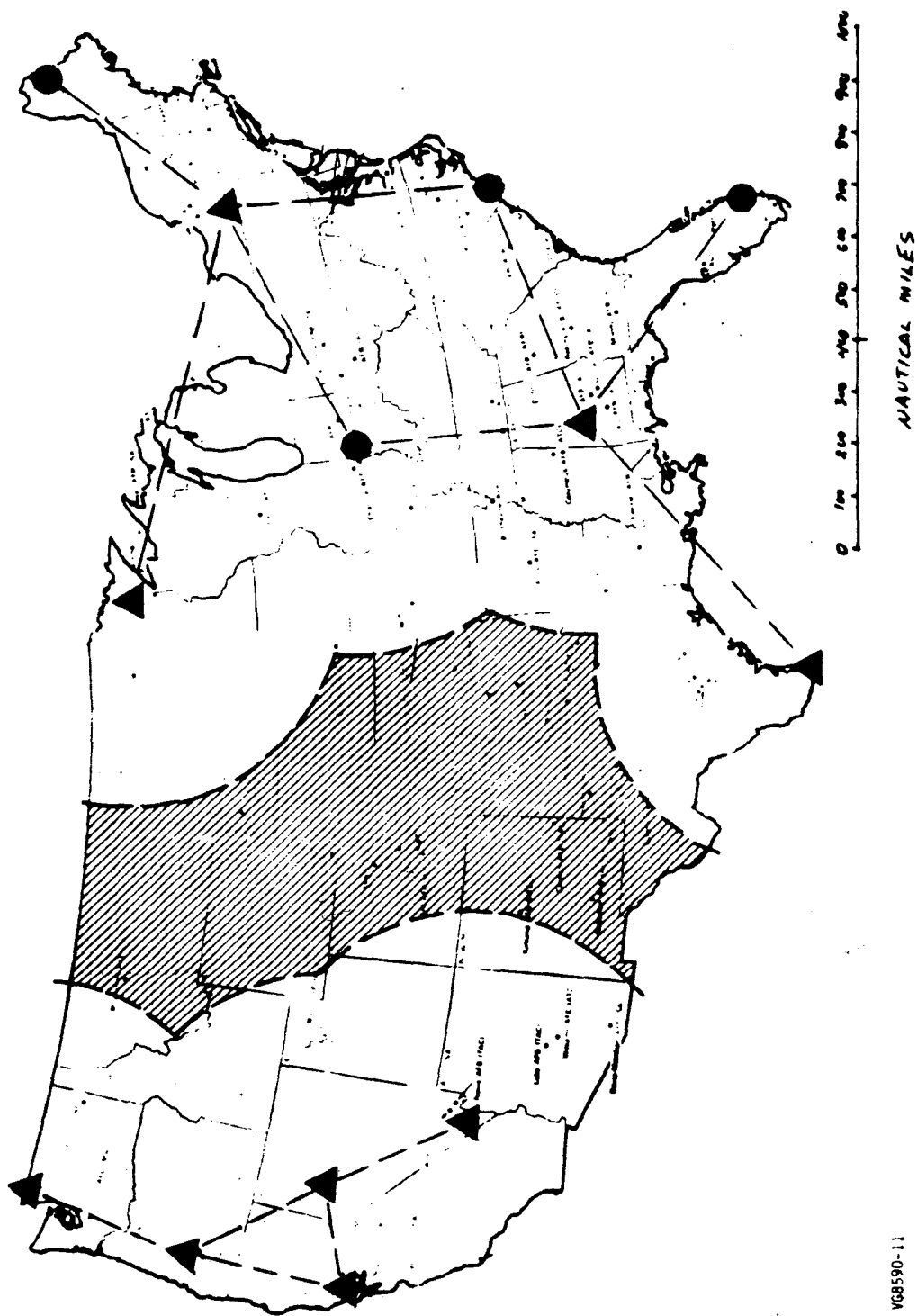


Figure 10

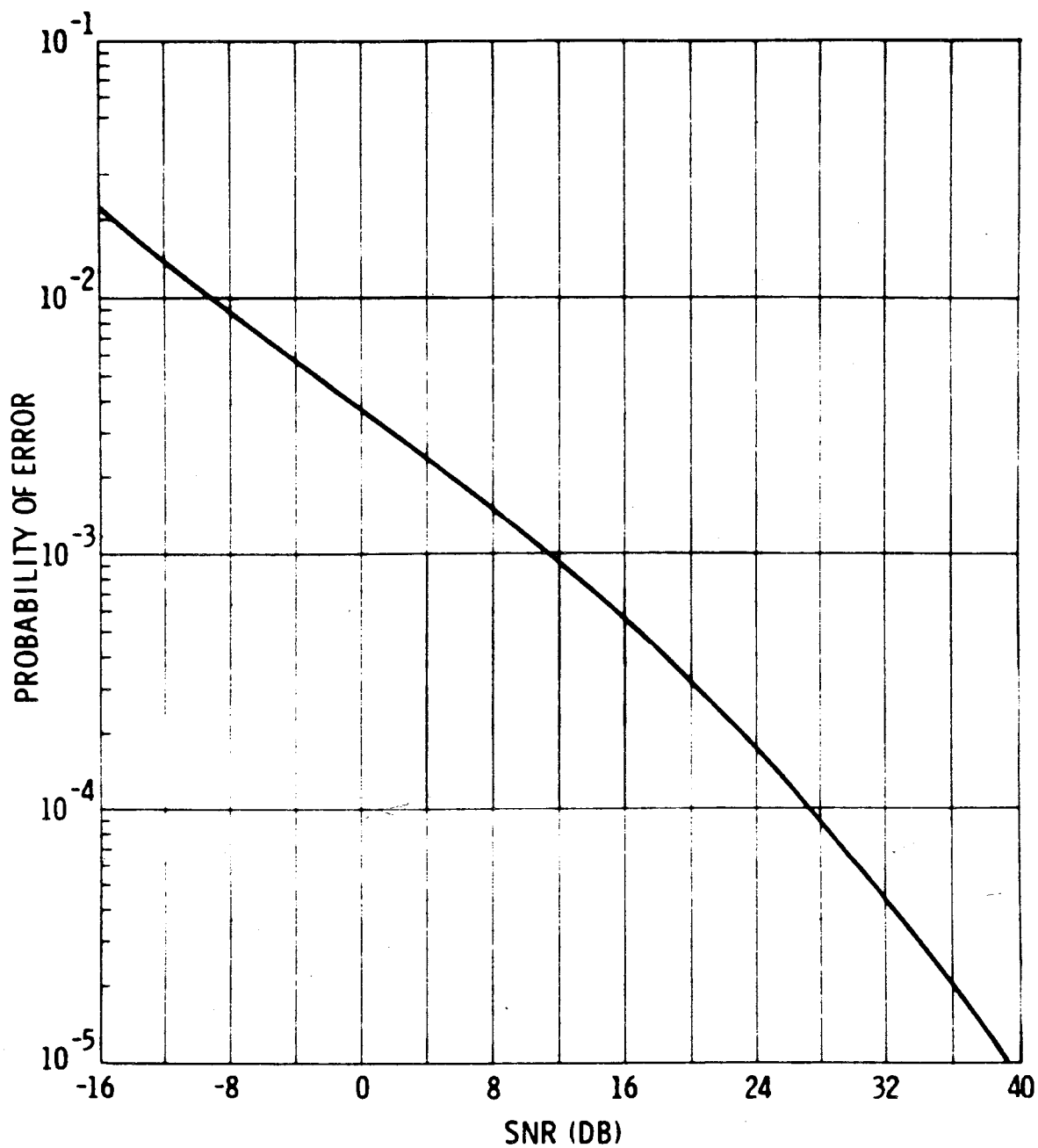


VG8590-11

Figure 11

ALERT RECEIVER COVERAGE

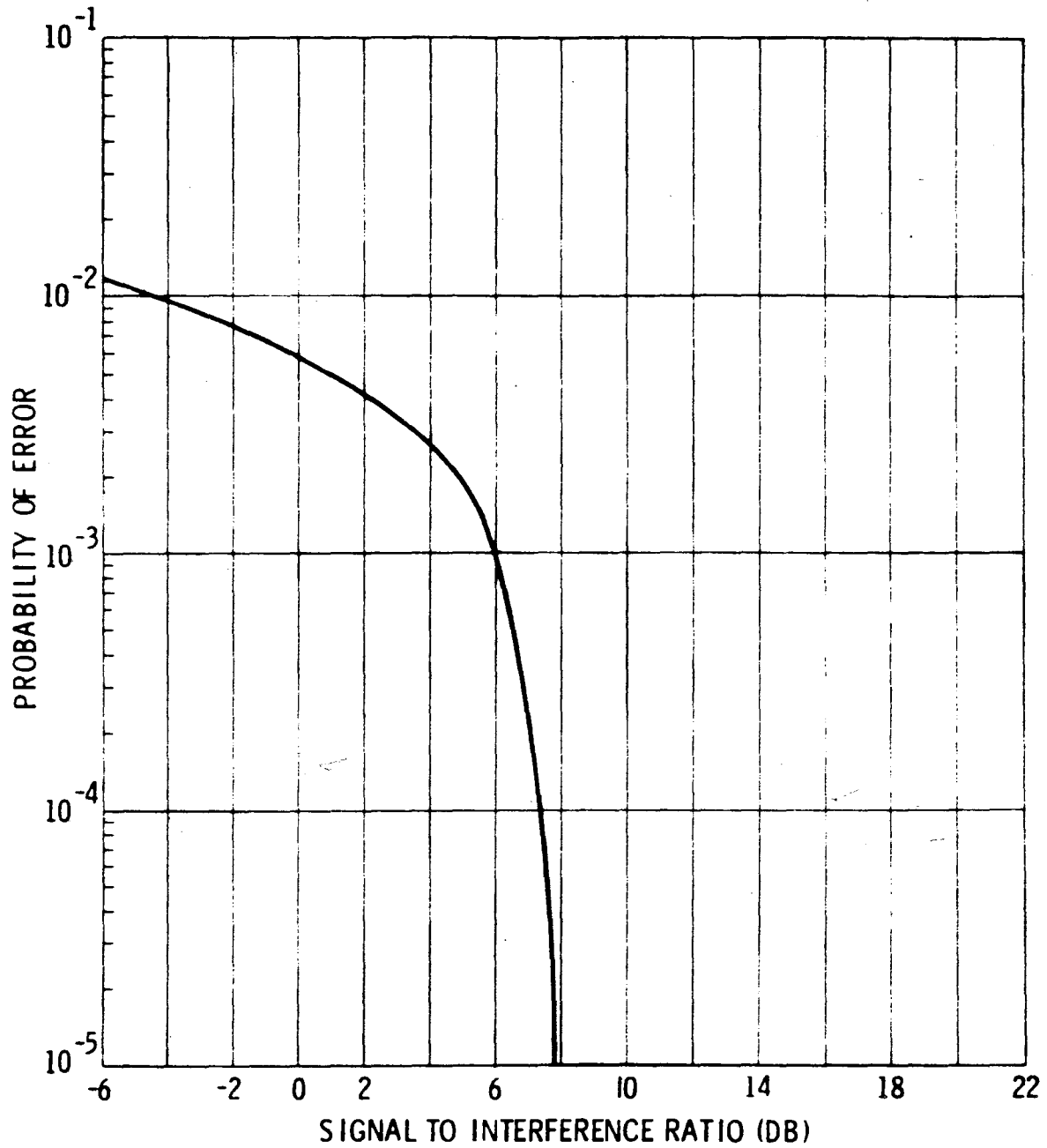
CLARINET-PILGRIM BIT ERROR PROBABILITY (ATMOSPHERIC NOISE)



VG8504-3A

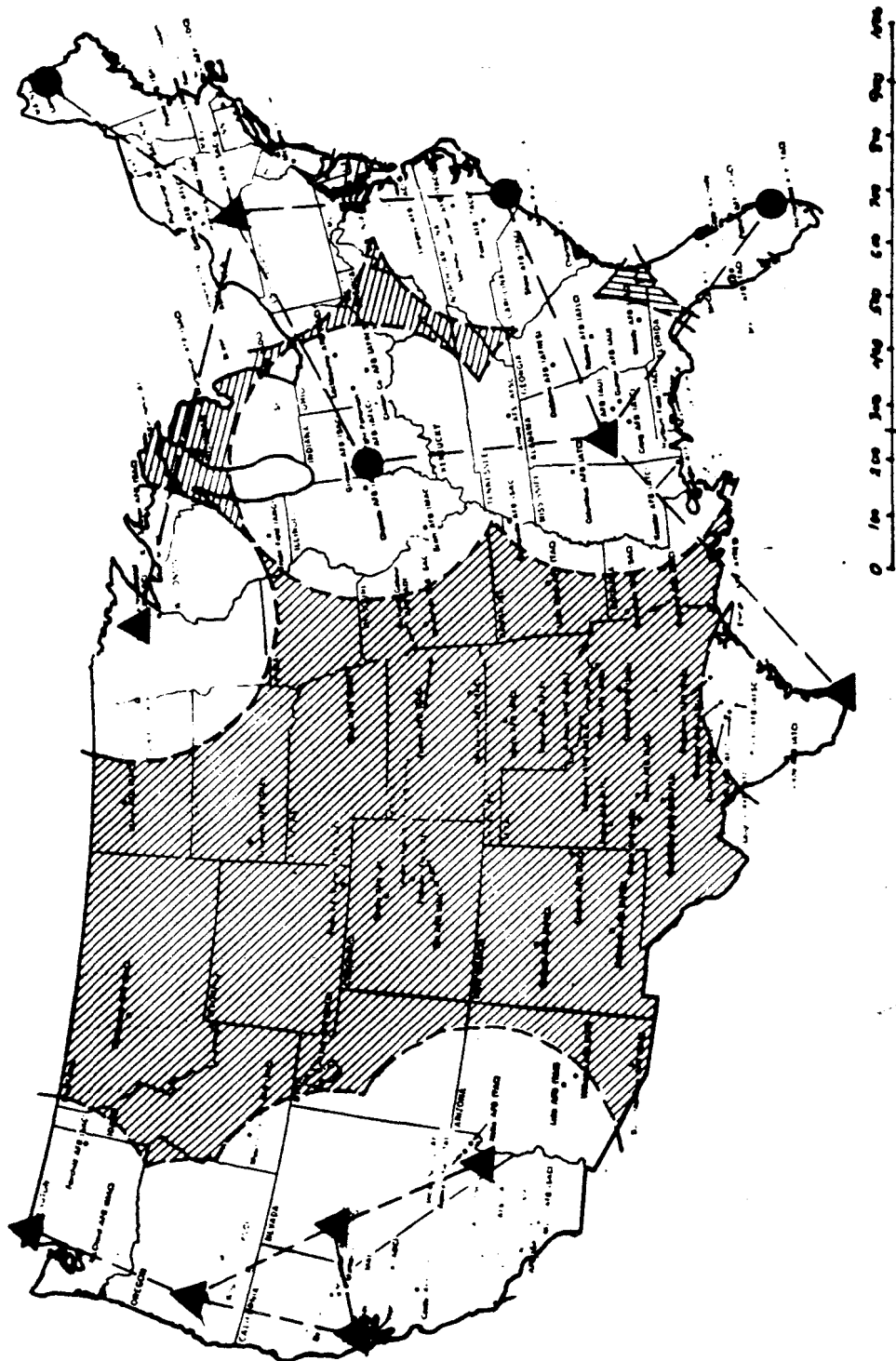
Figure 12

CLARINET-PILGRIM BIT ERROR PROBABILITY (CROSSING RATE INTERFERENCE)



VG8504-4A

Figure 13



VG8590-12

SINGLE STATION TELETYPE COVERAGE

Figure 14

RESULTS OF MAJORITY VOTE

<u>STATION</u>	<u>ERROR RATE</u>
A	.05
B	.02
C	.01

$$P_e = (P_A P_B + P_A P_C + P_B P_C - P_A P_B P_C)$$

$$= .001 + .0005 + .0001 - .00001$$

$$P_e = .00159$$

VG8590-9

Figure 15



FILE COPY

3-3

OPERATIONAL LORAN-C
EXPERIENCE IN AN AUTOMOBILE
ENVIRONMENT

Willi Vogeler
Senior Engineer
Telcom, Incorporated
McLean, Virginia

A paper presented at the
Third Annual Convention of
The Wild Goose Association,
McAfee, New Jersey, Oct. 2-4,
1974.

S. FEHLNER.

REF 594

PAPER 3-3

RP 22x1 = 23

12890412

OPERATIONAL LORAN-C EXPERIENCE IN AN AUTOMOBILE ENVIRONMENT

INTRODUCTION

Over the past several years, the application of the Loran-C grid to the task of locating land vehicles has generated some interest in the Loran community. This interest has been demonstrated in published papers, discussions at Loran-C meetings, and in at least one government sponsored investigative effort. The development of a low-cost receiver at Telcom, Inc., McLean, Virginia, included 100% usage of real-world signals from the East Coast Loran-C network. No simulator tests have been made. After bench-testing in the laboratory had been completed, field trials were conducted. Because Telcom does not have ready access to water or airborne platforms, it was decided to perform movable platform testing in an automobile. On only two occasions has the receiver/processor been operated in a boat environment. Both of these tests yielded excellent results. The purpose of this paper is to report the experiences and observations of the vehicle test program, including the recognition and definition of problems peculiar to an automobile Loran-C installation.

REQUIREMENTS OF THE USER COMMUNITY

The "navigation" concept of the potential user community for a vehicle location system is different than that of the present Loran-C users. Since automobiles and trucks always travel on prepared surfaces, such as highways and streets, the concept of determining "Where am I?" has no meaning. The prepared surfaces are generally marked with arterial and route identifiers, street signs, and geographical markers. Also the technique of driving an automobile under "instrument conditions" does not exist. Therefore the personnel in the vehicle always are aware of their location and do not need a navigation system. The vehicle's location is only of interest to dispatch and control centers. Perhaps the generation of a permanent record of the vehicle's travels may be a requirement. This paper does not address the problem of relaying or recording positional information. It is restricted to the problems of operating Loran-C in an automobile.

Conversations with potential users have generated the following list of desires for a Loran-C installation:

1. Should consume minimum power.
2. The smaller the size, the better.

3. Should have automatic start-up and self-correcting capability.
4. The antenna should be as small and inconspicuous as possible.
5. Provide accuracies ranging from one mile for one user to a one-quarter city block resolution for another.

INITIAL ATTEMPTS

The first automobile trial by Telcom was conducted on 26 March 1974. The equipment was carried in a station wagon. The power source was a 12 volt storage battery connected to a 12 volt to 110 volt A.C. inverter. The receiver/processor used its normal 110 volt input power configuration. The antenna was an 18 foot whip with a passive coupler strapped to the rear bumper. The tracking loop of the processor was in the first order or "bang-bang" mode. Acquisition in the McLean, Virginia, parking lot was successful but very slow compared to laboratory bench acquisition using the roof-top antenna. Two excursions in the Virginia suburbs and downtown Washington, D. C., areas were made. Frequent cycle slippage on all stations and occasional lost signal indication on the most distant transmitter (Dana) were observed. Oscilloscope observations indicated that the signal being received in the vehicle was one-fortieth of that received with the roof-top antenna.

Three changes were then made prior to the next attempt. The signal tracking loop response was changed and some signal sampling integration was incorporated. The cycle selection network was the target of major redesign. In order to enhance the received signal presented to the RF front end, an active coupler was designed and built. Vehicle operations in the station wagon were conducted on 21 May 1974. Excellent tracking was achieved, and the frequent cycle slippages noted on the previous trip did not reoccur. However, cycle selection was unreliable, and the observations indicated that the cycle selection network was being over-driven by the new antenna coupler.

The third try was made on 15 July 1974, again in the Washington, D. C., area. In addition to modifying the cycle selection network, the active coupler was altered to accept a five foot whip. The antenna was moved to the roof of the car. The 12 volt/110 volt inverter was eliminated. The power source for vehicle operation now consisted of a 6 volt storage battery. Experience has shown that eight hours of continuous operation can be obtained before battery recharging is necessary. Acquisition, cycle selection, and tracking performance were excellent.

All vehicle operations subsequent to the 15 July trip have not required any redesign or modification of the installation.

OPERATIONAL PROCEDURE

The installation which was used on 15 July consists of a five foot whip antenna with an active coupler (15 dB gain) at its base. A coaxial cable connects the coupler to the receiver. A 6 volt storage battery serves as the power source. A series dropping resistor is used to provide the +5 volt potential for the processor. A 6 volt to ± 12 volt DC/DC converter provides the voltages for the receiver. Loran-C positional data is observed by the operator and dictated into a cassette tape recorder. For some operations two people made up the crew - a driver and an operator. Most of the long distance runs were made by a one-man crew - the driver glancing at the unit and dictating Loran-C grid coordinates while he was underway. A block diagram of the vehicle set-up appears on Figure 1. In addition to the station wagon, a two-door sedan and a small pickup truck have been used to gather operational data.

Unfortunately, detailed charts do not exist for any of the areas in which automobile operations were carried out. Therefore, two styles of testing were used. One consisted of acquiring and locking to the signals, making passes throughout the area with hands-off the set, and returning to the starting point. If the same time differences were observed upon return, it was concluded that successful tracking had been achieved during the trip. The longest successful "hands-off" operation was achieved on 16 July 1974 during a 4½ hour trip in an area enclosed by the Beltway around Washington, D. C. The other test method is the comparison of time differences at identifiable landmarks and check repeatability for trips on separate days and different weather conditions.

OPERATING AREAS

Operations have been carried out in parts of the area serviced by the Cape Fear-Nantucket-Dana triad. Telcom has successfully operated in the following sections:

1. The corridor from the George Washington Bridge in New Jersey to Washington, D. C.
2. The entire Washington, D. C., metropolitan area.
3. The corridor between Washington, D. C., and Richmond, Virginia, including downtown Richmond.

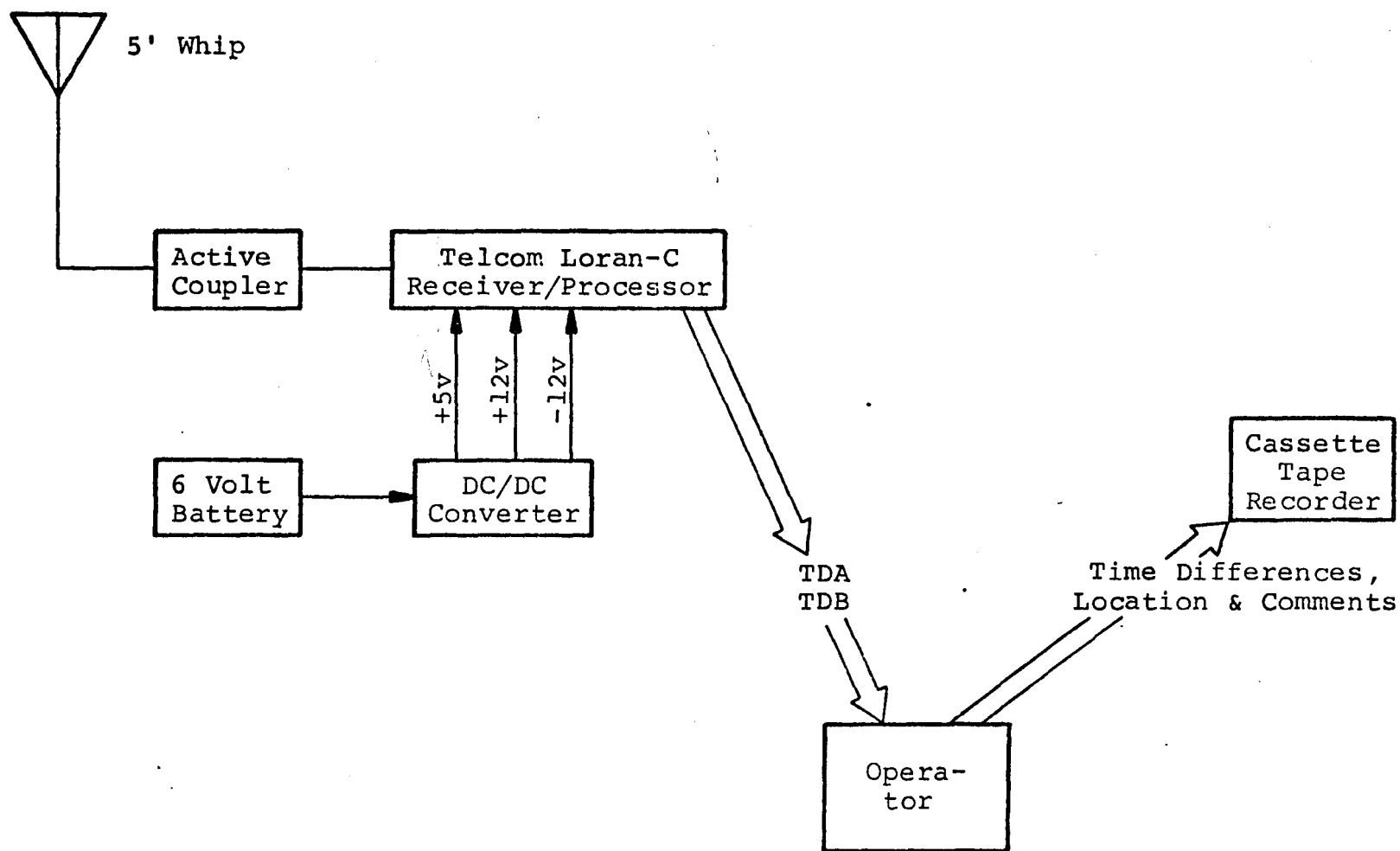


FIGURE 1
VEHICLE LORAN-C INSTALLATION

4. A corridor existing between Washington, D. C., and Toledo, Ohio (Interstate 70, Pennsylvania Turnpike, and Ohio Turnpike).

In the New England area between Newport, Rhode Island, and New York City good operation on the Nantucket leg was observed. However, periodic loss of the Dana signal rules that area as marginal. It may have been better to switch to the Cape Race signal but this was not done. In the upper New York City area (Cross Bronx Expressway), loss of all three signals was experienced. Heavy traffic and considerable bumper-to-bumper wait times in Upper Manhattan required a complete reacquisition. This was started on the George Washington Bridge and the receiver/processor was locked and tracking prior to entering the New Jersey Turnpike.

The excursion into the Middle West was started from McLean, Virginia, at 10 p.m. on 9 August 1974. This was a one-man operation. The battery exhausted approximately eight hours after start. The location at that time was 30 miles east of Toledo. It was planned to have the battery charged somewhere in Toledo or lower Michigan, but this was not accomplished. Therefore, no operations were conducted in the lower Michigan area. Late on Saturday afternoon, it was possible to charge the battery just north of the Straits of MacKinac (between upper and lower Michigan). Acquisition and lock were achieved while driving approximately 65 miles per hour. However, signal alarms appeared frequently (mostly on the master signal from Cape Fear) and several reacquisitions were achieved with the same results as before. The unit was shut down about 80 miles west of the MacKinac Bridge. Stationary operations on the Keweenaw Peninsula (260 miles west of the Straits of MacKinac) were attempted. Oscilloscope observations showed no sign of the Cape Fear or Nantucket signals - only Dana was visible. It was concluded after three days of trials, that insufficient signals existed in the Lake Superior area for vehicle operations. On the return trip (20 August 1974) the unit was operated from Cleveland to Washington, D. C.

OPERATIONAL DATA

The time differences which have been observed in the various operating areas appear on Tables I through VI. In the paragraphs that follow some supplemental information and operational comments appear for each table. Only those landmarks which were covered by more than one monitor excursion have been shown, because one-time passes at a location are meaningless unless detailed charts or other people's observations are available for the comparison of data.

FREDERICK, MARYLAND - BEDFORD, PENNSYLVANIA

Table I contains observed data between Frederick, Maryland, and the tunnel on the Pennsylvania Turnpike about 20 miles west of Bedford. The upper time difference for each location was observed westward during the night of 9/10 August 1974. The lower time differences were noted on the eastbound trip ten days later.

Time differences for areas west of the tunnel were obtained westbound. However, on the return trip, the receiver/processor was unable to acquire the Dana signal. Attempts continued from approximately 0930 to noon (20 August 1974) when acquisition finally was successful. The operator concluded that Dana had been off the air. A check with the Coast Guard on 21 August 1974 confirmed that the Dana transmitter was shut down for over two hours in the morning of 20 August.

The last readings on Table I show the time differences entering the tunnel westbound and eastbound. Approximately 90 seconds are spent in the tunnel. On the westbound trip, total acquisition (complete restart) had to be executed after the tunnel was cleared. On the eastbound trip, emergence from the tunnel resulted in the lost signal indication disappearing, but the wrong cycle alarm continued to be displayed. In this case, no search procedure was carried out, only re-cycle identification.

It is noted that the driver did not read the tenth's digit as he was preoccupied with executing a satisfactory insertion into the tunnel.

FREDERICK, MARYLAND - WASHINGTON, D. C., BELTWAY

Table II observations were made on Interstate 70 between Frederick, Maryland, and the Washington, D. C., Beltway (I-495). The upper numbers were obtained northbound in thundershowers approximately 11 p.m., 9 August 1974. The lower numbers were obtained southbound in fair weather during the afternoon of 20 August 1974.

McLEAN - RICHMOND - McLEAN (VIRGINIA)

On 5 September 1974 a roundtrip between McLean and Richmond was made. Shortly after departure, the B slave (Dana) was lost but reacquired within a few minutes. The data appears on Table III. The upper numbers were obtained on the southbound trip, and the lower numbers northbound.

TABLE I

9/10 AUGUST AND 20 AUGUST 1974

FREDERICK, MARYLAND TO BEDFORD, PENNSYLVANIA

<u>Location</u>	<u>Exit</u>	<u>TDA</u>	<u>TDB</u>
70W Int. and 70S		52779.6 52780.1	69468.4 69468.6
Middletown Myersville Road Crossing 70W	42	52772.3 52773.0	69388.1 69388.2
Boonesborough/Smithburg St. Hwy. 66 Crossing 70W	35	52748.8 52749.2	69331.5 69331.5
US40 Crossing 70W (Near Hagerstown)	32B	52753.6 52755.2	69314.1 69314.6
Int. Md. Rt.65 where it crosses 70W near Hagerstown, near Antietam Battlefield. Sharpsburg Exit		52763.1 52764.8	69299.5 69299.4
Int. of Interstate 81 & 70W Chambersburg & Martinsburg Exit		52774.5 52774.3	69278.3 69278.3
Md. Rt. 63 and 70W Exit to Williamsport		52774.6 52775.1	69266.8 69266.2
Clear Spring Exit		52795.9 52799.0	69225.5 69225.4
Int. of Md. 56 and Rt. 70 Indian Springs Exit/Big Pool		52832.2 52833.0	69207.5 69208.3
Pa. & Md. Border on 70		52833.7 52831.8	69120.8 69121.3

Table I, continued

<u>Location</u>	<u>Exit</u>	<u>TDA</u>	<u>TDB</u>
70W, Warfordsburg, North of Hancock, US 522 Crossing 70W	33	52816.9 52817.2	69105.8 69106.1
Pa. 6 Crossing 70W (Townhill Area)	31	52771.9 52772.1	69039.3 69038.9
Pa. 915, Crystal Spring	30	52738.4 52938.9	69017.7 69019.3
At Ticket Gate Breezewood Exit		52725.7 52725.9	68996.4 68996.9
Pa. TPKE US220, Bedford	11	52765.3 52765.7	68893.7 68894.0
Entering Tunnel on Pa. TPKE		52823. 52821	68823. 68822



TABLE II

I-70 Frederick	
52779.6	69468.6
52780.1	69468.4
MD80	Buckeystown
52796.5	69514.3
52797.0	69515.6
MD109	Barnesville
52807.7	69541.5
52810.8	69543.6
MD121	Clarksburg
52822.4	69572.2
52822.3	69571.8
M118	(AEC) Germantown
52837.0	69600.1
52837.1	69599.0
Gaithersburg	(B of S) Darnestown
52845.1	69625.3
52844.1	69624.6
Shady	Grove
52855.0	69647.8
52855.1	69646.4
MD28	Rockville
52863.6	69661.1
52863.2	69661.3
Montrose	Road
52873.3	69679.2
52873.0	69680.3

I70S

LORAN-C OPERATIONS IN
A VEHICLE ENVIRONMENT

Monitor Platform - Pickup truck with 60" antenna and Telcom Loran-C processor.

Readings taken by driver and dictated on magnetic tape.

Upper number observed on 9 August 1974 (apx. 2300) northbound in rain squalls.

Lower number observed on 20 August 1974 (apx. 1600) southbound in fair weather.

Time Difference Gradients

Apx. 56 feet per 0.1 micro-second for "5200" number.

Apx. 69 feet per 0.1 micro-second for "69000" number.

TABLE 111

5 SEPTEMBER 1974

MCLEAN - RICHMOND - MCLEAN TRIP

<u>Location</u>	<u>TDA</u>	<u>TDB</u>	<u>Location</u>	<u>TDA</u>	<u>TDB</u>
Rt. 66 & I495	52983.1 52985.1	69935.8 69737.0	Rest Area	53146.0 53146.8	69833.4 69834.0
Rt. 50 & I495	52992.5 52993.0	B Lost 69745.0	Weigh Station	53164.2 53164.4	69839.8 69839.5
Gallows Rd. & I495	52998.6 52999.7	B Lost 69750.9	Dumfries/Manassas (234)	53174.9 53175.5	69845.2 69845.2
Rt. 236 & I495 (Annandale)	53008.5 53008.8	B Lost 69759.0	Triangle/Quantico (619)	53197.1 53197.9	69853.3 69853.4
Braddock Rd. & I495	53020.7 53021.0	69768.9 69769.9	Marine Base Quantico	53219.9 53220.1	69858.6 69859.1
The rest of the time differences are all on I-95. The location indicates the intersection with I-95.			Aquia (610)	53261.5 53262.0	69874.7 69875.2
Keene Mill Springfield, Va.	53026.8 53027.0	69792.6 69792.7	Stafford (630)	53289.6 53290.0	69890.7 69891.1
Ft. Belvoir/ Newington	53050.1 53050.9	69808.0 69807.4	Potomac Creek	53322.2 53322.0	69901.4 69901.7
Woodbridge U.S. 1	53095.1 53095.5	69823.7 69824.0	Falmouth	53353.6 53353.9	69910.4 99910.3
Occoquan (123)	53104.4 53103.2	69822.7 69822.6	Rappahannock River	53364.0 53364.5	69914.5 69914.4
Dale City	53139.4 53140.2	69830.1 69830.8	Fredericksburg/ Culpeper (3)	53381.4 53381.0	69927.2 69927.9

Table III, continued

<u>Location</u>	<u>TDA</u>	<u>TDB</u>	<u>Location</u>	<u>TDA</u>	<u>TDB</u>
Masaponax (US 1)	53411.9 53412.0	69955.9 69955.7	Atlee (656)	53722.4 53722.4	70241.9 70241.1
Ni River	53454.0 53453.8	69987.8 69987.8	Rest Area	53727.7 53727.8	70248.1 70247.8
Thornburg (606)	53474.3 53475.0	70002.3 70002.2	Parham Road (73)	53749.8 53750.1	70265.1 70264.9
Matta River	53486.1 53485.8	70009.0 70008.3	Exit 17 (Richmond)	53761.9 53762.8	70277.8 70277.9
Ladysmith (639)	53534.1 53534.7	70058.5 70058.9	Exit 15A (Richmond)	53782.2 53782.6	70284.0 70283.8
Rest Area	53553.4 53554.1	70078.3 70078.1	Exit 14 (Richmond)	53787.6 53787.8	70291.5 70292.6
Carmel Church (207)	53573.2 53573.4	70105.6 70105.9	Toll Gate	53795.1 53795.1	70305.5 70305.4
North Anna River	53595.8 53596.0	70130.6 70127.8	James River Bridge/Richmond	53805.7 53806.6	70323.2 70323.6
Doswell/West Point (30)	53619.7 53619.7	70153.1 70153.1			
South Anna River	53641.2 53641.4	70167.8 70167.7			
Ashland/Hanover (54)	53670.6 53671.0	70192.8 70192.9			
Lewiston Road (802)	53699.5 53700.0	70223.6 70223.4			

DOWNTOWN RICHMOND, VIRGINIA

For a test in the downtown area of Richmond, Broad Street was selected. From its intersection with Interstate 95, Broad Street runs westward through Richmond. Table IV displays the observed time differences. The top numbers were obtained while driving westward - the lower set while eastbound.

An inspection of the TDA values (Nantucket Leg) shows that Broad Street roughly parallels the Nantucket Loran lines.

The test run was made at midday on 5 September 1974, and traffic conditions prevented stopping at each intersection. The numbers were taken "on the fly." At the western end of the test run, the automobile was parked under the transmitting tower of WTVR (Channel 6). The car radio received considerable "hash" both on AM and FM in this area, but Loran-C operations were normal. The apparent down-shift in TDA within a block of the tower may possibly have been caused by the structure.

Based on the data in Table IV, it appears that a fix resolution of one-quarter city block is possible on Broad Street in Richmond.

WASHINGTON, D. C.

Initial testing in Telcom's local area was done on the Capital Beltway (I-495). The observations have not been included in this paper because performance on the Beltway is the same as for the open road areas presented in Tables I, II, and III. There was one opportunity to compare under and on the Woodrow Wilson Bridge crossing the Potomac River. The readings are:

	<u>TDA</u>	<u>TDB</u>
Vehicle	52976.4	69821.6
Vehicle	52976.1	69821.1
Houseboat	52976.5	69821.7

Early in its road test effort, Telcom was advised by two government sources that:

1. There is a "dead zone" in the 14th Street Bridge area, and
2. Loran-C operation on Constitution Avenue is "impossible."

TABLE IV

5 SEPTEMBER 1974

E BROAD STREET - RICHMOND, VIRGINIA

<u>Location</u>	<u>TDA</u>	<u>TDB</u>	<u>Location</u>	<u>TDA</u>	<u>TDB</u>
12	53800.4 53800.4	70318.5 70317.6	Foushee	53799.2 53799.2	70311.8 70311.7
11	53800.4 53800.0	70317.6 70317.0	Adams	53799.1 53799.1	70311.3 70311.0
10	53800.0 53800.0	70316.9 70316.0	Jefferson	53799.1 53799.1	70310.9 70310.4
9	53800.1 53999.9	70316.2 70315.9	Madison	53799.3 53799.1	70310.2 70310.1
8	53800.1 53799.7	70315.6 70315.3	Monroe	53798.9 53799.0	70309.8 70309.9
7	53799.9 53799.7	70315.3 70314.9	Henry	53799.1 53799.1	70309.3 70309.3
6	53799.9 53799.7	70314.9 70314.6	Smith	53798.9 53799.0	70308.9 70308.8
5	53799.7 53799.7	70314.1 70313.9	Gilmer	53798.8	70308.1
4	53799.7 53799.6	70313.8 70313.5	Hancock	53798.6 53798.5	70306.6 70306.6
3	53799.7 53799.3	70313.6 70313.2	Harrison	53798.4 53798.3	70305.9 70305.7
2	53799.5 53799.4	70312.8 70312.6	Rylan	53798.3 53798.4	70305.2 70305.4
1	53799.5 53799.4	70312.6 70311.9	Bowe	53798.4	70304.8

Table IV, continued

<u>Location</u>	<u>TDA</u>	<u>TDB</u>	<u>Location</u>	<u>TDA</u>	<u>TDB</u>
Lombardi	53798.1	70304.0			
	53798.1	70303.9			
Allen	53798.0	70302.5			
	53798.1	70302.6			
Lodge	53797.9	70302.2			
Meadow	53798.0	70301.9			
Allison	53797.7	70300.6			
	53797.6	70300.5			
Davis	53797.4	70298.3			
	53797.4	70298.5			
Terminal Pl.	53797.2	70297.1			
	53797.3	70297.4			
Boulevard	53797.0	70296.1			
	53797.2	70296.2			
Shepard	53797.0	70296.0			
	53797.1	70295.0			
Summit	53796.4	70294.0			
	53796.4	70294.6			
Cleveland	53796.4	70293.8			

These two information bits took the form of a challenge and planned downtown operations included the two areas. While traveling through the downtown business district, the vehicle was driven over a route that provided as much interference as possible on the car radio.

Table V displays the observations made on Constitution Avenue and Northwest Washington. From the time differences it is concluded that Loran-C fixes are possible on Constitution Avenue with a resolution of one-third to one-quarter of a block. The Northwest Washington observations are one-pass values. Similarly, Table VI lists the one-pass observations for the Southwest section of Washington including the DOT Building - home of Coast Guard Headquarters. A street chartlet showing the time differences at Coast Guard Headquarters appears on Figure 2.

With the information contained on Tables V and VI, it is possible to conduct a very interesting exercise. Using any two locations, four Loran-C lines can be drawn (two TDA lines and two TDB lines), and each line is assigned its observed value. Using a straight edge and a pair of dividers, it is possible to predict the time differences for any intersection. This was done using the Constitution Avenue intersections at 17th and 23rd Streets. The lines were drawn on a Washington, D. C., tourist map distributed by one of the major oil companies. The "predicted" values from this exercise when compared to actual observations agreed within several tenths of a microsecond.

With respect to the 14th Street Bridge "dead zone," the aforementioned exercise was carried out and the "predicted" readings for the northbound span were estimated. The comparison with actual observations are:

	<u>TDA</u>	<u>TDB</u>
"Predicted"	52933.9	69783.8
<u>Observed</u>		
Northbound Span	52934.2	69785.2
Southbound Span	52933.6	69784.1

The reported "dead zone" could not be confirmed.

OPERATOR OBSERVATIONS

The data listed in the foregoing charts were obtained during daylight and darkness in periods of fair and foul weather.

TABLE V

16 JULY 1974

CONSTITUTION AVENUENW WASHINGTON

	<u>TDA</u>	<u>TDB</u>		<u>TDA</u>	<u>TDB</u>
John Marshall Place	52917.6	69783.0	22 & C	52926.6	69774.0
National Art Gallery	52918.3	69782.5	23 & C	52927.1	69774.7
	52918.5	69782.1	Penn. & 6th	52918.0	69782.1
Intersection, E. of Archives	52919.1	69782.2	C & 6th	52917.7	69781.8
Archives Entrance	52919.4	69781.6	6th & Indiana	52917.4	69781.4
Int. West of Archives	52919.3	99782.0	6th & E	52916.4	69780.4
9th	52919.6	69781.6	6th & F	52915.6	69780.4
	52919.8	99781.4	7th & F	52916.3	69779.6
10th	52920.2	69781.2	8th & F	52916.7	69779.4
	52920.4	69781.0	9th & F	52916.9	69779.2
11th	52920.9	69780.4	10th & F	52917.6	69779.0
12th	52921.3	69780.4	11th & F	52917.9	69778.8
Hist. & Technology	52921.6	69780.1	11th & E	52918.7	69779.1
Museum Entrance	52921.8	69779.9	Penn. & 11th	52919.1	69779.8
14th	52922.1	69779.7	Penn. & 12th	52919.5	69779.3
	52922.2	69779.4	Penn. & 13th & E	52919.8	69778.6
15th	52922.5	69779.4	(CG HQ)		
	52922.8	69779.1	14th & E	52920.4	69777.9
	52922.5	69779.1			
16th (Monument Entrance)	52923.3	69778.7			
	52923.7	69778.3			
Eisenhower Sword	52923.9	69777.9			
	52924.1	69778.1			

Table V, continued

<u>CONSTITUTION AVENUE</u>			<u>NW WASHINGTON</u>		
	<u>TDA</u>	<u>TDB</u>		<u>TDA</u>	<u>TDB</u>
17th	52924.4	69777.7	15th & E	52920.9	69777.7
	52924.5	69777.7			
18th	52925.2	69777.2	Information	52923.3	69780.0
	52925.3	69777.3	Booth		
			(Wash. Monument)		
19th	52925.7	69776.7	15th & Indep.	52924.8	69781.0
	52926.0	69776.8	(CG R.)		
20th	52926.0	69776.4	Bureau of Eng.	52925.8	69781.9
	52926.2	69776.7	West Entrance		
21st	52926.5	69776.1			
	52926.7	69776.1			
22nd	52927.3	69775.1			
	52927.5	69775.4			
23rd & Constitution	52927.7	69775.4			
Constitution and Bacon Dr. (Lincoln Memorial)	52927.4	69775.9			

TABLE VI
SOUTHWEST WASHINGTON

16 JULY 1974

	<u>TDA</u>	<u>TDB</u>		<u>TDA</u>	<u>TDB</u>
(On Expressway)	52928.0	69784.6	6th & C SW	52921.8	69785.1
Mid-Bridge					
Main Ave. Waterway			6th & Maryland	52921.3	69785.0
			(Aeronautics & Space)		
Main Avenue Ramp	52926.2	69785.6			
and Expressway			Maryland & Independence	52920.4	69784.9
G & 9th SW	52925.1	69786.1			
			4th & Independence	52920.1	69785.2
G & 7th SW	52924.6	69786.5			
			Maryland & 3rd	52919.2	69785.0
81 Overpass on G	52924.2	69786.2			
Near DOT			3rd & Adams	52918.3	69784.7
DOT Building (G)	52923.7	69785.9	Penn. Avenue & 3rd	52917.5	69784.0
DOT/Church	52923.5	69786.2	Bridge at Tidal Basin	52927.1	69783.2
(Middle of Block)			(Approach to I-95)		
			(Near Jeff. Memorial)		
DOT 6th & F	52923.1	69786.2			
School Street Int.	52922.5	69786.0			
DOT Mail Ramp	52922.3	69785.7			
6th & D	52922.4	69786.5			
(Under RR Track)					

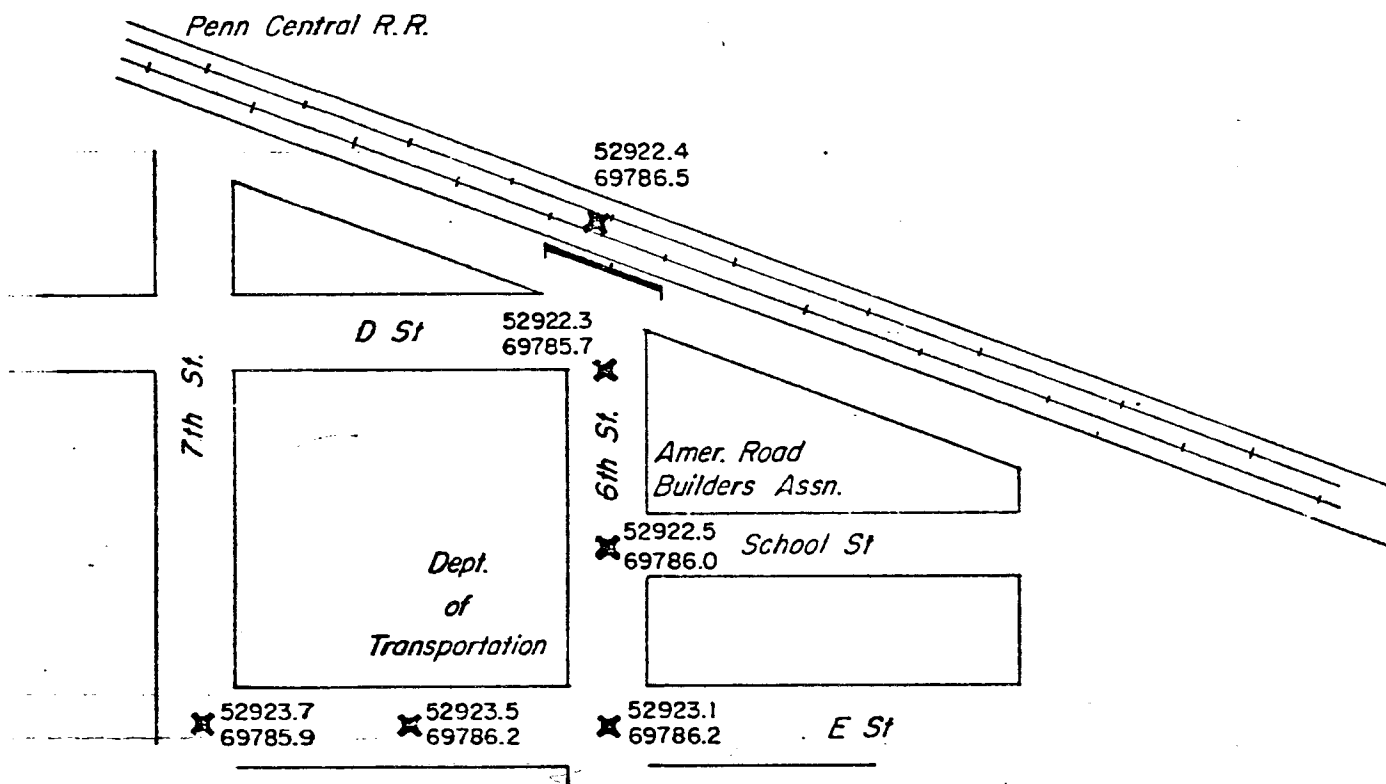


FIGURE 2
USCG HQ LORAN C CHART

No apparent difference in operation was noted for the different conditions.

Since no elaborate test equipment, such as an oscilloscope, was available in the vehicle, the only means of monitoring man-made interference was the car radio. Man-made interference, such as industrial and ignition noise from sources close to the automobile were easily recognized. Such man-made interference did not appear to bother Loran-C operations.

The Virginia section of the Capital Beltway is undergoing extensive construction work, and on every test run in this area, clogged traffic conditions were encountered. Sandwiched between semi-trucks, both laterally and fore/aft, appeared to have no effect on the receiver/processor operation. In downtown city traffic, congested traffic and local industrial noise conditions did not result in deteriorated operation. Similarly in areas such as highway cuts through hills with steep rock banks on each side of the vehicle did not appear to hamper tracking capabilities. Such areas were encountered in the Appalachian area of the Pennsylvania Turnpike.

Heavy power lines crossing or parallel to the highway also seemed to have no adverse effect on a moving vehicle. No efforts were made to park under a power line. However, if stopping under a power line proves to be a nemesis, it will have to be handled in the same manner as moving and standing under highway overpasses.

AREAS OF ADDITIONAL INVESTIGATION AND TESTING

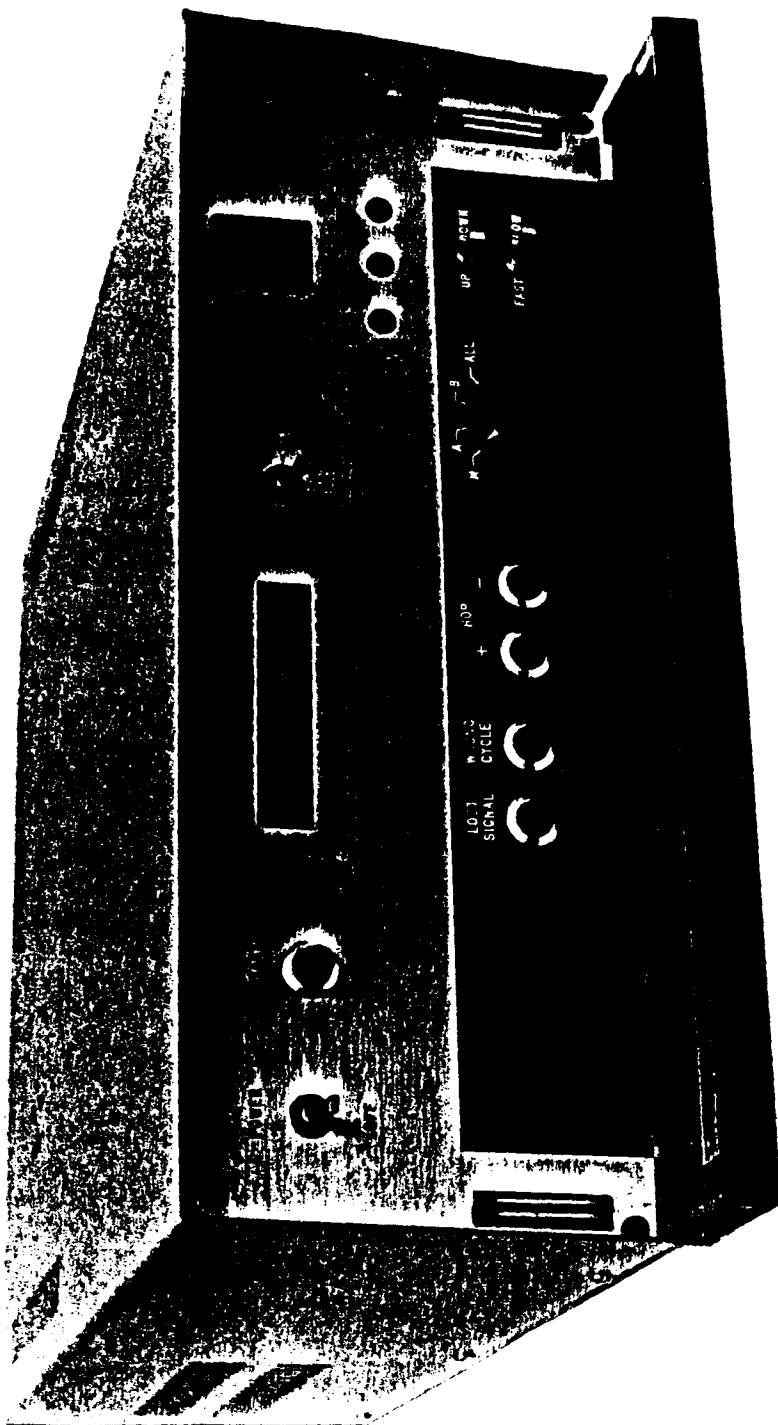
Combining the indicated desires of potential users listed earlier in the paper with the experience obtained in real-world testing, some areas of investigation and testing can now be defined.

The principal problem for land vehicle operation is the delivery of adequate signals for proper receiver operation. In order to provide adequate signal and still satisfy the users' wish for a minimum antenna installation, an effort to develop an RF front end specifically designed for vehicle applications may be necessary.

The most frequently observed malfunction is cycle slippage on the received signals. An improved RF section may help to overcome this problem. Another solution is the mechanization of the signal tracking loops in such a manner that high land speeds can be tolerated, and temporary loss of signal preserves the "status quo" in the timing circuitry. Investigation in this area is continuing at Telcom.

Because lost signal conditions and cycle slippages are a fact of life when traveling through tunnels and other extended no-signal areas, quick and automatic reacquisition and cycle selection is mandatory. A hazard exists in this area. If the processor acts immediately, then it may try to re-initialize during periods of temporary loss such as slow progress through a series of underpasses. On the other hand, if the machine is too patient, the automatic correction of a fault may be delayed excessively. The answer to this problem depends somewhat on the particular application of the user.

From the foregoing it appears that a vehicle Loran-C installation must be tailored to the specific demands and requirement of the user. But whatever these requirements may be, the Loran-C processor is a vital part of the installation. This paper only intended to show that a Loran-C receiver/processor can operate in a vehicle and provide accurate positional data. The manner in which position information is used remains to be defined. Perhaps it would be well for a spokesman of the potential user community to define their specific requirements and applications.



TELCOM LORAN-C RECEIVER

LORAN C AVM URBAN REPEATABILITY

by

R. S. Stapleton and F. J. Chambers
Teledyne Systems Company
Northridge, California

WGA - 1974 (3rd)

I. INTRODUCTION

A number of LORAN C AVM accuracy test demonstrations have been conducted in the past with various degrees of success. Those conducted in hi-rise urban areas have for the most part been significantly less successful than similar tests in lo-rise areas.

A summary of the results of all test demonstrations run to date is shown in Table I.

Table I. AVM Test Summary

Test Date	Test Location	Type of Test	Signal Coverage	Measured Radial Error	
				Mean	95%
October 1971	Philadelphia	Absolute Location	66%	346'	898'
January 1974	Philadelphia	Absolute Location	86%	303'	721'
June 1974	Las Vegas	Repeatable Accuracy	99%	91'	162' (90%)

LORAN D

This paper will discuss the results from previous urban tests and the reasons behind the results. The concept of repeatability is then discussed and a test plan presented which will measure LORAN C repeatability at an urban site. Finally the results from such a test are presented with cursory analysis.

II. BACKGROUND

The test method used in demonstrations for the Department of Transportation, Urban Mass Transit Administration in Philadelphia will provide an ideal model of the typical test method. In this method, a computer generated X-Y grid is superimposed on the test area. Coordinates in the X-Y system are then calculated for each test checkpoint and each calibration point. Calibration consists of making time difference measurements at each calibration point and storing this data along in the X-Y grid coordinates in the computer.

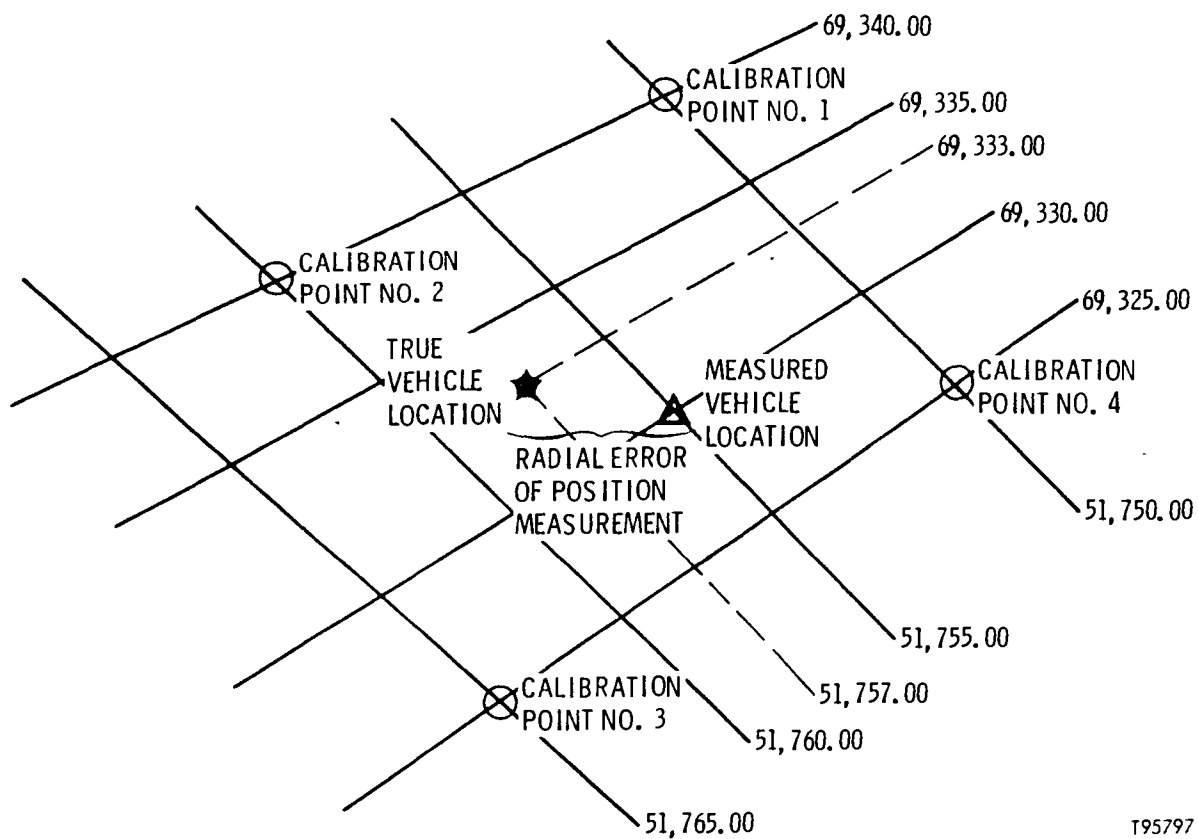
The demonstration, then, consists of driving a predetermined route which encompasses all the checkpoints. As the vehicle passes each specified checkpoint, the receiver time difference display is frozen and the measurement recorded. At the conclusion of the data taking process all the time difference readings are submitted to a computer program which selects a set of calibration points from the previously inputted calibration data for each checkpoint measurement and solves for the X-Y location of the checkpoint measurement. The difference, in feet, between this apparent X-Y location and the actual one is the radial error for each measurement.

This method is scientifically sound and will provide a true index of measurement error so long as the LORAN time difference grid is regular and continuous over the test area. This, of course, is the case at altitude and over water which are the two primary applications of LORAN navigation. For the most part, it is also the case in a low rise or residential urban area but it is definitely not typical of a dense hi rise area. Shielding by large buildings and concentrated electrical and electromagnetic fields combine to distort the LORAN lines of position, sometimes to a drastic extent. The test method previously described has no mechanism for dealing with this characteristic other than by increasing the resolution of the calibration points. Even this will probably not yield the true LORAN accuracy potential due to software difficulties.

Two examples of the types of errors that result from this test method are shown in Figures 1, 2, and 3.

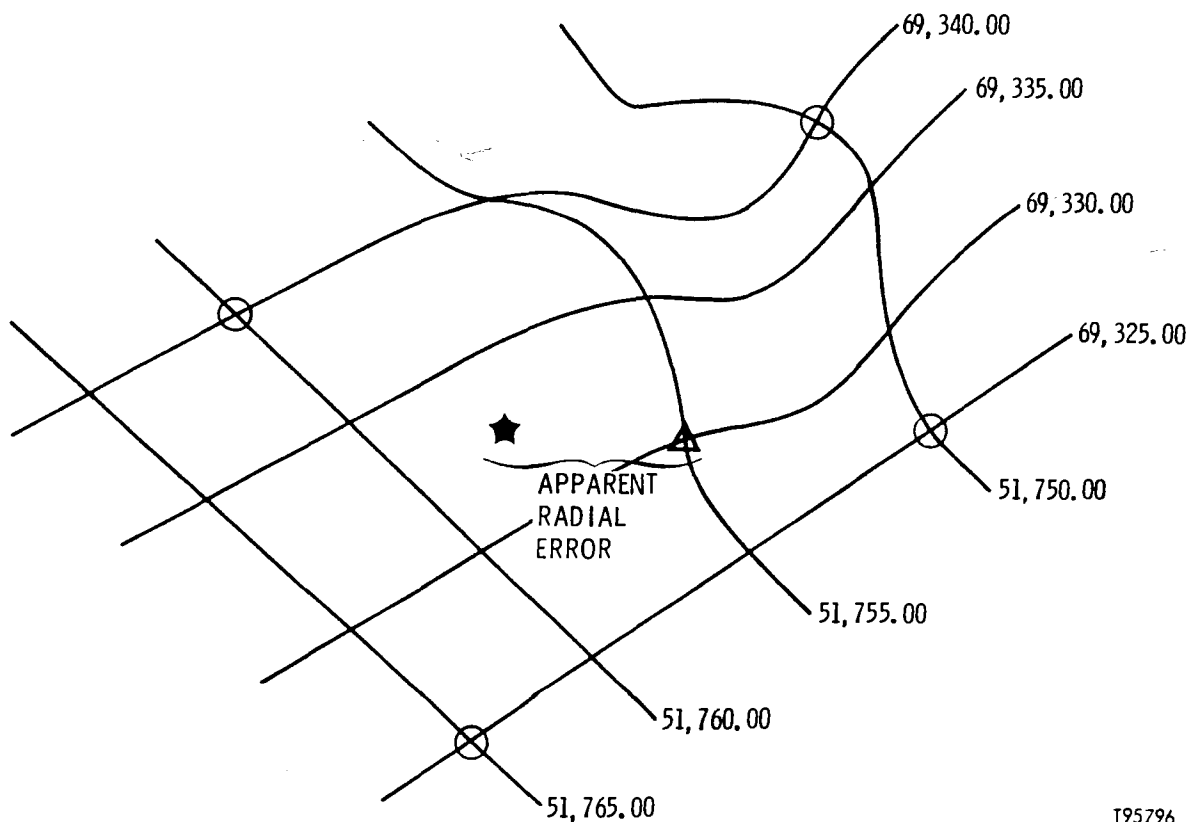
Figure 1 shows a theoretically perfect grid with four calibration points denoted and a checkpoint. The apparent vehicle location as computed from the measured time differences contain an error of about 200 feet. In Figure 2, the results of grid distortion at one of the calibration points produces a larger error while Figure 3 shows the effects of distortion at the checkpoint. Of course a severe case will include distortion at all locations (not an uncommon occurrence).

Grid distortion of this magnitude has been measured in the Philadelphia hi-rise test area. Attempts to deal with this problem by increasing the density of the calibration points and modifying the dynamic characteristics of the AVM receiver have shown only moderate improvement in accuracy results. In 1971 a test in the Philadelphia hi rise showed an error at the 95th percentile of 898 feet with coverage over 66% of the area. In 1974, a repeat of the high rise test run gave 95% figure of 671 feet, a mean of 303 feet, and 86% coverage. In order to score well at the 95th percentile, all but 5% of the measurements must be under the target accuracy number. With severe grid distortion over most of the area the task becomes very difficult. Also coverage of less than 100% of the test area is not acceptable.



T95797

Figure 1. Theoretically Perfect LORAN Grid



T95796

Figure 2. Grid Distortion at a Calibration Point

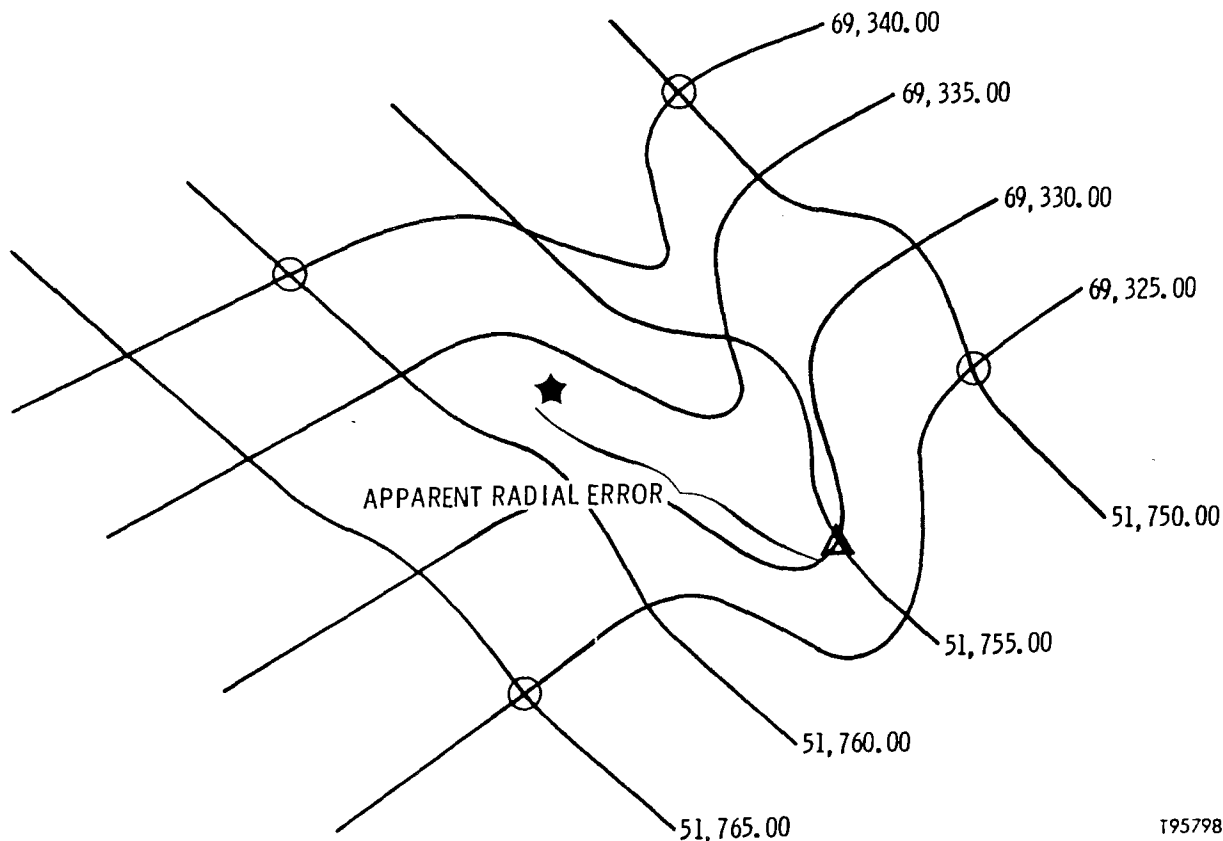


Figure 3. Grid Distortion at a Checkpoint

III. TEST METHOD

LORAN proponents have always realized that the ability of a receiver to repeat time difference measurements at a particular location is much better than the absolute accuracy of any single measurement. With this objective in mind, another AVM test demonstration was structured which would highlight this capability.

The test area selected was Las Vegas, Nevada due to its good LORAN signal coverage from the Southern Triad of the Air Force tactical LORAN D net. Station used were at Glendale, Nevada, Middlegate, Nevada, and Palmdale, California. Since the intent of the test was to show the repeatable accuracy of a typical AVM user such as an urban transit company, data was taken at each checkpoint with the vehicle stopped. Automatic time difference averaging was installed in the receiver and 10 averaged measurements were recorded at each checkpoint.

For this type of test, calibration consists of making repeated runs through all checkpoints, recording time difference measurements at each one. Figure 4 shows all the checkpoints measured throughout the test area. The route was run about 8 times during the two week interval prior to the demonstration. For convenience, the route was then divided into three approximately equal test routes. These routes are shown in Figures 5, 6 and 7. Each test route included some thirty of the checkpoints calibrated earlier. The three routes were then run over a two day period and the time differences recorded for comparison with the predicted coordinates.

The error was converted from microseconds to feet by multiplying the difference between each predicted and measured TD by the appropriate nominal gradient. Location of each measurement was then plotted.

IV. TEST RESULTS

The summary table of test results is shown in Table II.

Table II. Summary Test Results

	No. of Checkpoints	Mean Location Error	Radial Error at 90th Percentile
Route 1	34	71 Feet	148 Feet
Route 2	38	90 Feet	173 Feet
Route 3	27	117 Feet	169 Feet
Composite	99	91 Feet	162 Feet

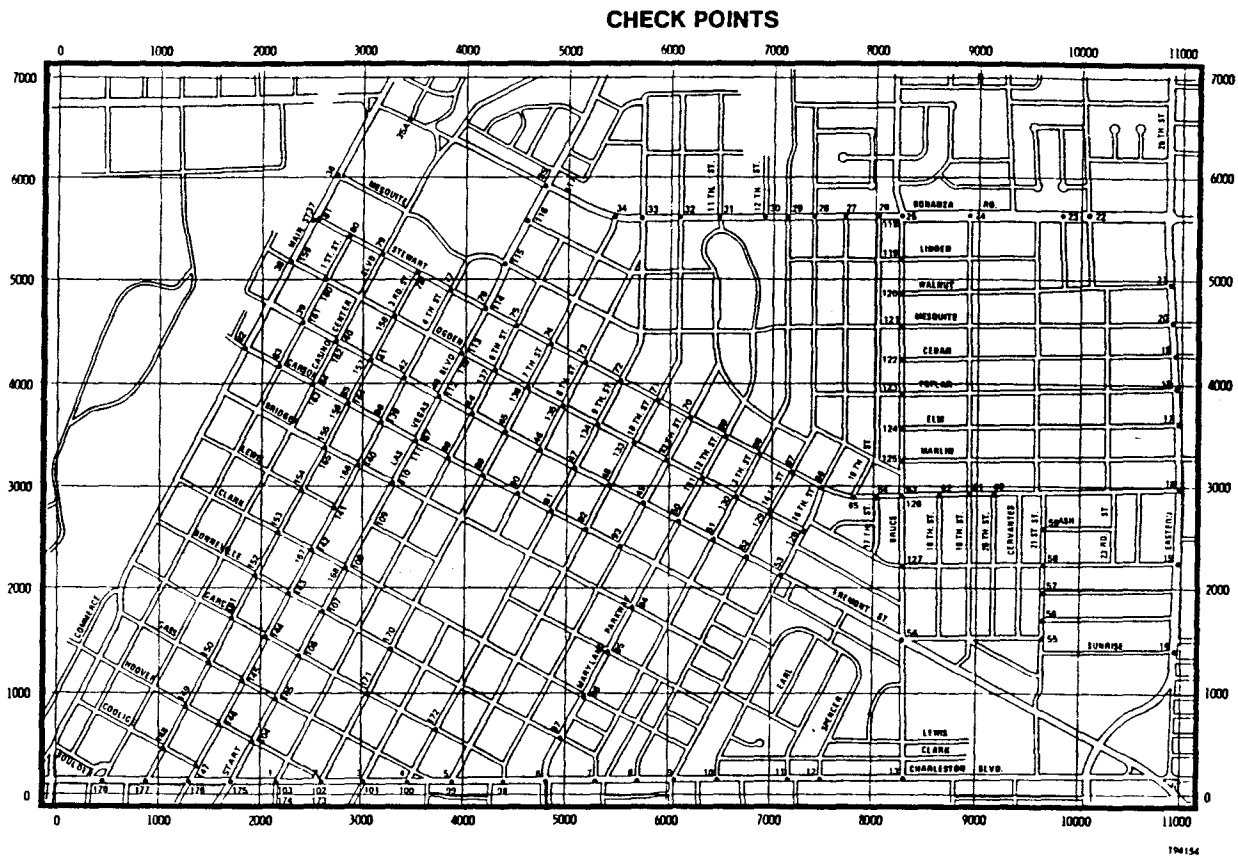


Figure 4. All Checkpoints Map

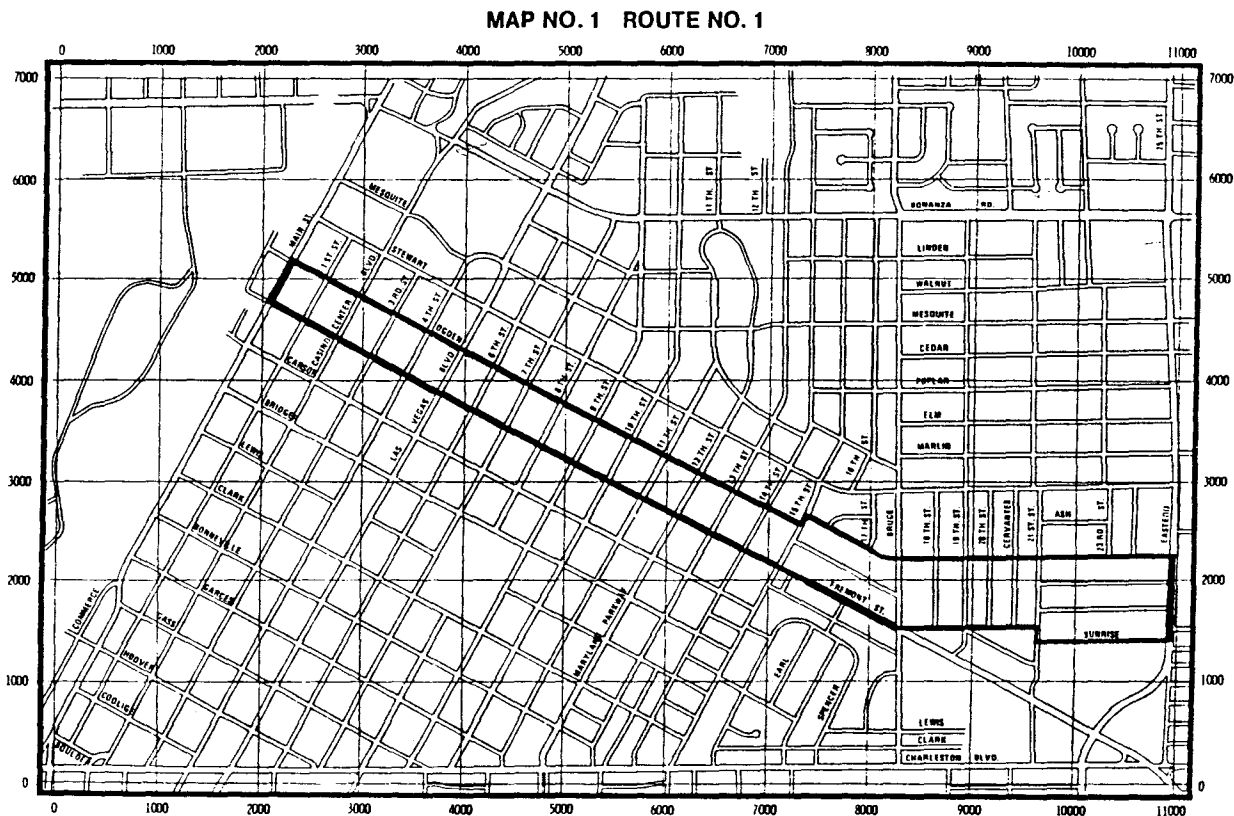


Figure 5. Route 1 Map

It should be noted that the results shown are based on the raw data taken during the demonstration only. No ancillary data reduction techniques were utilized. In spite of the fact that the tests were highly successful in every respect it is important to remember that this was a brief demonstration of the capability of the sensor only. No attempt was made to utilize available software or data transmission equipment. Indeed, a practical AVM system implementation will not only benefit from a highly sophisticated base station computer and automatic data transmission but may realize a significant position error reduction resulting from optimized LORAN transmitter geometry. For example, these results were obtained using a relatively low powered slave station located 250 miles from the test area.

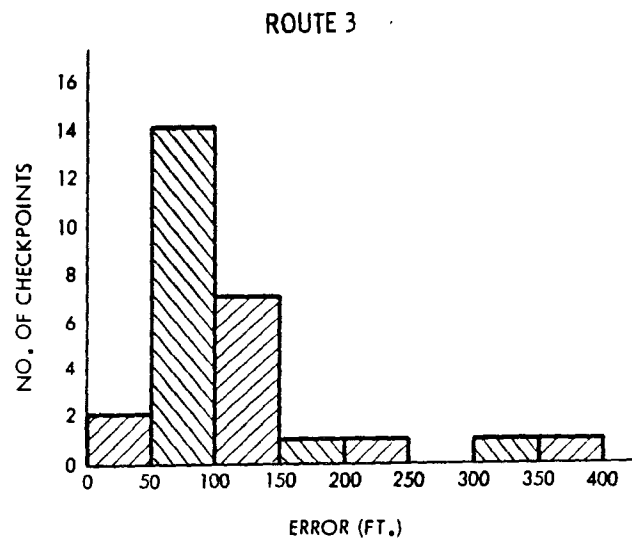
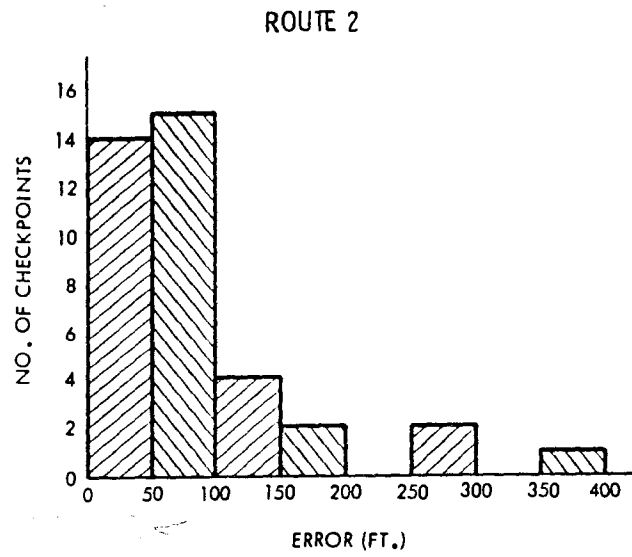
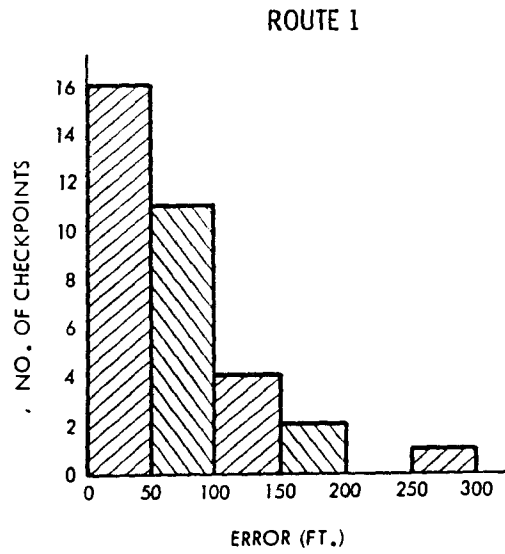
In addition, the crossing angle of the LORAN lines of position was approximately 46° which is considerably less than optimum. In no instance was any attempt made to reconcile the error components due to these practical limitations. The data is presented just as it was recorded.

Histograms of radial error is presented in Figures 8 and 9. Figure 8 shows the error using the average of 10 readings at each checkpoint. A separate histogram for each route is included. Figure 9 is a histogram of the error using each of the 973 readings made during the test. Readings from all routes are combined. Table III is a listing of the average and worst case error at each checkpoint.

Location plots for three of the points are presented here to show representative accuracy obtained. A plot of the largest error recorded (checkpoint 106) is shown in Figure 10 while the smallest (checkpoint 53) is Figure 11. A plot typical of the test is shown in Figure 12, checkpoint 124.

The results obtained support the claim that LORAN repeatability is indeed better than absolute accuracy in the city. The next step will be to perform a test similar to the one run in Las Vegas in the Philadelphia high rise. The results of this test will determine to what extent the encouraging results obtained by this method may be subscribed to a truly hostile (to LORAN) environment as presented by a major urban center.

LORAN system proponent remain confident that the repeatability of the system will prove to be more than adequate to make the LORAN navigation system a formidable contender in the lucrative although highly competitive Automatic Vehicle Monitoring field.



T94072

Figure 8. Histograms of Average Error

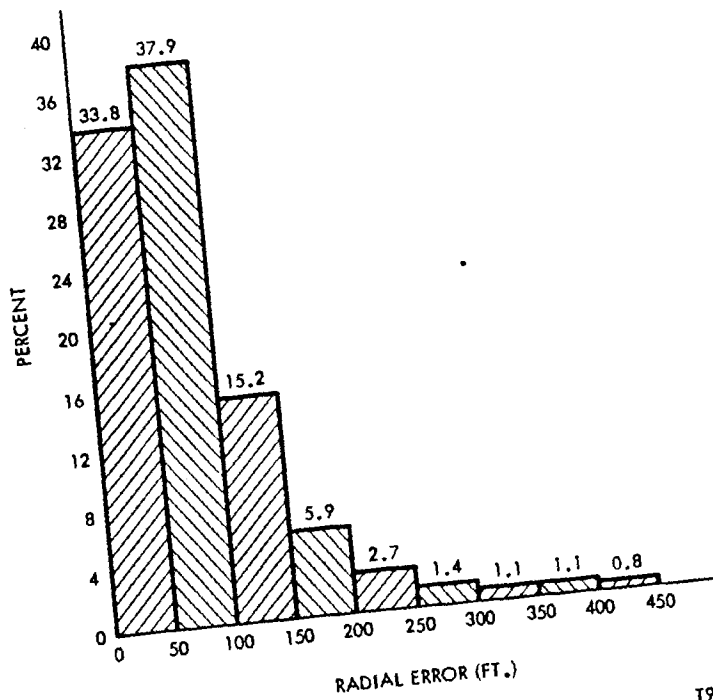
Table III. Average and Worst Case Errors

Checkpoint	TDA (ns)	Average Error TDB (ns)	Radial (Ft.)	Worst Point Radial Error (Ft.)
<u>Route 1</u>				
38	+ 46	+ 41	29	38
160	- 5	+ 71	71	83
79A	- 22	+ 1	14	35
158	+ 65	+ 85	62	82
77A	- 19	+ 48	55	67
113	- 2	+ 83	81	106
137	- 14	+ 15	21	35
136	+ 16	+ 33	26	35
135	+ 73	+166	133	160
134	- 49	+ 26	51	65
133	+ 10	+ 47	41	54
132	+ 12	+107	98	115
131	+ 11	+ 67	60	77
130	- 13	+ 35	40	82
128	+101	+239	193	250
127	+104	+151	111	127
62A	+ 47	- 18	43	55
61A	+ 81	+113	83	119
60A	+ 39	- 13	34	41
15	-231	+140	257	277
14	+ 48	- 2	31	39
54	- 81	-135	102	138
53	+ 42	+ 18	19	28
51	+ 21	- 19	29	35
50	+ 63	+ 36	30	39
49	+ 63	+ 33	29	42
48	+ 39	- 13	34	50
47	+134	+133	93	130
46	+180	+208	148	166
45	+ 89	+ 50	42	46
44	+ 94	+ 66	49	94
43	+154	- 82	162	234
42	+122	+ 39	58	69
40	No Signal			
39	+ 87	+113	82	107
<u>Route 2</u>				
Average Error (Using Run 1 as Calibration)				
82	+ 13	- 45	49	68
83	+ 21	- 38	47	63
84	+ 14	- 67	71	100
85	+ 81	- 41	83	127
86	+ 21	- 51	59	87
87	+ 19	- 52	59	96
88	+125	+ 29	63	71
89	+ 40	- 20	41	68
90	+ 42	- 22	44	68
91	- 26	- 60	48	60
92	- 42	-197	173	200
93	- 19	-128	116	171
7A	+ 9	-406	396	438
8A	-387	-365	256	321
9A	- 49	- 92	71	112
54	- 84	-115	84	131
63	- 63	-128	100	144
125	- 8	-189	179	234
124	+ 37	- 67	82	91
123	+ 66	- 61	92	120
122	+ 39	+ 42	30	56
121	+194	+113	92	129
120	+ 31	- 25	40	63
119	+ 59	- 9	43	70
25	-266	-144	123	153
26	-547	-276	251	392
27	-261	- 84	123	135

Table III. Average and Worst Case Errors (Continued)

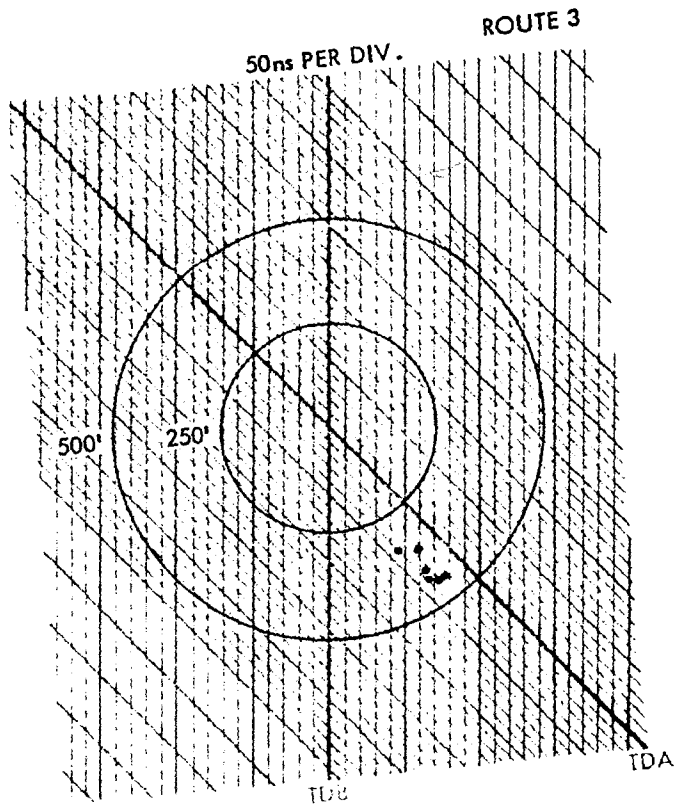
Checkpoint	TDA (ns)	Average Error TDB (ns)	Radial (Ft.)	Worst Point Radial Error (Ft.)
<u>Route 2 (Cont'd)</u>	<u>Average Error (Using Run 1 as Calibration)</u>			
28	-211	- 99	96	107
29	-173	-123	90	113
30	- 71	- 69	48	64
31	+ 1	- 23	23	60
32	+ 20	- 2	14	41
33	- 76	- 69	48	80
35	+ 16	- 10	18	39
35A	- 61	-107	82	106
36	+157	+ 50	74	77
37	- 82	-120	89	119
38	+ 14	- 25	31	62
<u>Route 3</u>				
39	+286	+195	145	166
40	No Signal			
41	+ 31	+150	132	179
42	+ 35	+ 5	19	39
43	+105	+ 71	53	200
111	- 23	+129	135	174
110	- 20	+ 90	96	110
109	+ 1	+ 80	77	101
108	- 28	+ 50	62	107
107	-201	-144	105	108
106	-156	+328	390	432
105	+153	+410	337	372
104	+ 19	+110	98	125
175	-160	+ 18	113	158
176	+ 80	+190	153	153
177	+ 51	+ 97	75	110
148	+ 4	+177	169	183
149	+214	+279	202	243
150	- 81	+ 89	126	177
151	+ 3	+ 89	85	106
152	- 2	+ 81	79	106
153	- 34	+ 60	74	97
154	+ 58	+112	87	97
155	+ 74	+108	80	107
85	+ 38	+110	91	100
84	-111	- 1	69	45
83	- 20	+ 46	54	72
82	+ 79	+ 66	47	63

HISTOGRAM OF ERROR FOR ALL READINGS



T94083

Figure 9. Histogram for 973 Readings



CHECKPOINT NO. 106

	TDA	TDB
MEASURED	130XX.XX	262XX.XX
1	39.26	83.83
2	39.19	84.16
3	39.06	84.06
4	39.09	84.15
5	39.09	84.16
6	39.07	84.17
7	39.10	84.19
8	39.08	84.16
9	39.12	84.21
10	39.10	84.20
TOTAL	39.104	84.158
GRADIENT	445'/H SEC	700'/H SEC
WRT/E	125°	87°
SLAVE LOCATION	PALMDALE CALIFORNIA	MIDDLEGATE NEVADA

Figure 10. Checkpoint 106

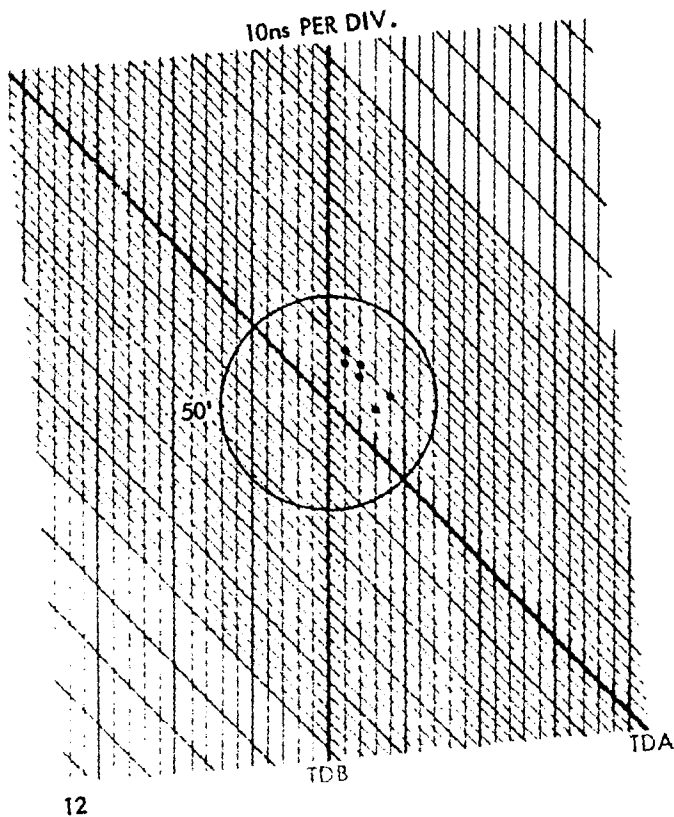


Figure 11. Checkpoint 53

CHECKPOINT NO. 53

	TDA	TDB
	130XX.XX	262XX.XY
MEASURED	48.08	91.04
1	48.13	91.08
2	48.13	91.06
3	48.12	91.06
4	48.12	91.05
5	48.13	91.05
6	48.13	91.05
7	48.12	91.06
8	48.12	91.05
9	48.11	91.05
10	48.11	91.07
TOTAL	48.122	91.058
GRADIENT	445'/μSEC	700'/μSEC
WRT/E	125°	87°
SLAVE LOCATION	PALMDALE CALIFORNIA	MIDDLEGATE NEVADA

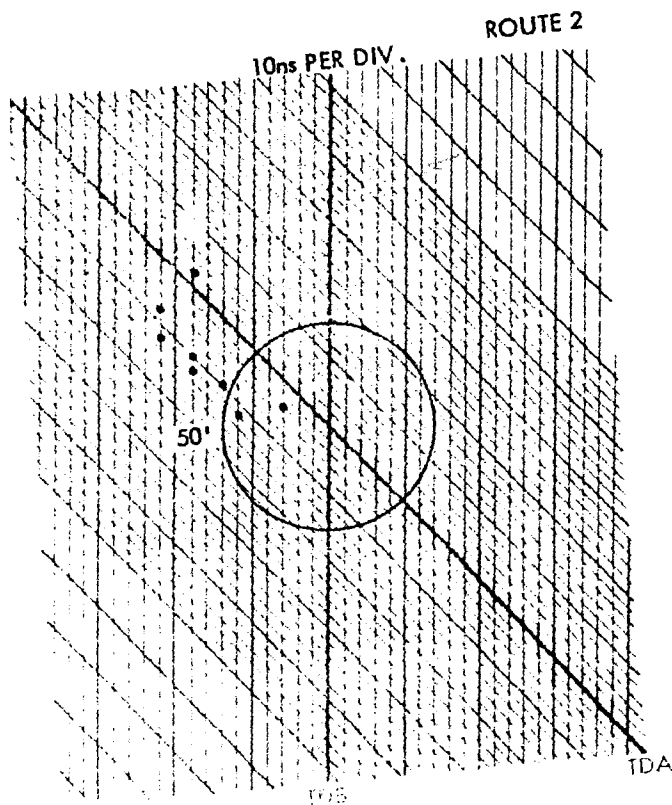


Figure 12. Checkpoint 124

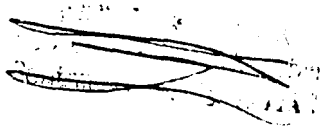
CHECKPOINT NO. 124

	TDA	TDB
	130XX.XX	262XX.XY
MEASURED	51.40	92.44
1	52.16	92.52
2	51.41	92.35
3	51.35	92.35
4	51.35	92.35
5	51.35	92.37
6	51.34	92.33
7	51.34	92.35
8	51.38	92.41
9	51.36	92.33
10	51.34	92.38
TOTAL	51.438	92.373
GRADIENT	445'/μSEC	700'/μSEC
WRT/E	125°	87°
SLAVE LOCATION	PALMDALE CALIFORNIA	MIDDLEGATE NEVADA

5

#5 - Can 3.

Frank



FILE COPY

3-5

LOW COST NAVIGATION PROCESSING FOR LORAN-C AND OMEGA

by

James F. DeLorme and Arthur R. Tuppen
ITT Avionics Division
390 Washington Avenue
Nutley, New Jersey 07110

*note discrepancy in spelling of names in
NPA 3rd convention program.*

(15 printed pages)

Presented at:

The Institute of Navigation
Thirtieth Annual Meeting
June 25 to 27, 1974

and (?)

very similar { 3rd Annual Convention (1974)
Wild Boar Assn
Great Gun NJ Oct 1974

under skin
Frank

40 pages

*Ref 586
PAPER 3-5*

ABSTRACT

Investigations and development of a Loran feasibility model, which were conducted to determine the impact of microcomputer concepts on performance and cost of radio navigation equipment, have demonstrated that the performance requirements for both austere and sophisticated Loran-C or Omega users can be satisfied within the economic value to these users. Continuing development of MOS/LSI semiconductor technology has provided microcomputer sets, central processor units and compatible semiconductor memories whose architecture is in accordance with the requirements for radio navigation processing. The result of this feasibility demonstration was a microprocessor configuration which served as a base for consideration of a low cost Omega navigator and a combined Loran/Omega navigator. The resultant configurations for these navigations has the potential to satisfy user cost objectives for either Loran-C or Omega navigation equipment, and a combined Loran/Omega navigator. Further, it is clearly demonstrated that mechanization of navigator functions such as conversion to latitude and longitude, and steering can be provided at minimal cost to the user.

INTRODUCTION

Use of radio navigation for aviation has been restricted due to limited coverage and the high cost of navigational processors required to provide automatic and continuous position-fixing in earth's coordinates or to provide guidance information.

The National Plan for Navigation specifies implementation of Loran-C for the Coastal Confluence Region, Omega for global coverage, and application of differential Loran-C as the river and harbor aid to navigation system. This implementation will provide radio navigation coverage throughout the world as well as high accuracy coverage throughout most of North America.

The high cost of radio navigators can be attributed to wide variations in user requirements, previous low production quantities, and the high cost of resultant general-purpose, programmable processors. Advances in MOS/LSI technology provide microcomputer sets which can be used to implement user equipments within the economic limitations of most applications.

This paper presents the results of a developmental program for a Loran feasibility model which provides automatic and continuous navigation and offers the potential of low cost user equipment. As configured, the radio navigator provides a modular approach to satisfy the low cost austere user, and also, permits expansion to incorporate additional functions as required by the sophisticated user.

The result of the developmental program is a relatively mature microprocessor configuration which serves as a base for discussion of a low cost Omega navigator.

The first section of this paper summarizes pertinent microprocessor considerations. The subsequent section discusses the design approach for the Loran model and the results obtained. The third section provides considerations on a design approach for Omega which is followed by a discussion on a combined Loran/Omega. The final section demonstrates the impact of this technology on the cost of a radio navigation set and the additional cost to provide a completely automatic set.

BACKGROUND

An important stated objective for radio navigation development programs is to seek designs which, in addition to improving performance, will reduce duplication by effectively serving both multi-user and multi-purpose requirements. More specifically, future developments of user equipments must offer more cost-effective designs; this objective should be realized through a design approach which has the flexibility to incorporate additional functions on a modular basis. In consonance with this objective, the general requirements for air and marine radio navigation ⁽¹⁾ have been reviewed to enable performance of a functional analysis and formulation of a design approach which would provide the required flexibility and modularity to satisfy both the simple and more complex requirements.

Local, regional, and global navigation areas were considered; therefore, the analysis performed is in accordance with the stated requirements for a river and harbor aid to navigation system, the U.S. Coastal Confluence Region (CCR), and global navigation. For example, the man-portable unit to be carried aboard an international ship as it enters the river and harbor control sector for automatic remote processing, or to provide guidance and automatic position reporting for unmanned vehicles is included. At the other end of the spectrum is the user equipment which includes a control indicator with latitude and longitude readouts, navigation system coordinates, or guidance information including cross-track-error (CTE) and along-track-distance (ATD). Furthermore, the global navigator will differ greatly in computational complexity from that of the local area navigator.

Economic limitations have been stated in the referenced literature and these costs range from \$3,000 for the austere surveillance application to \$15,000 for a complete airborne navigator. The general requirements for user equipments can be summarized as follows: the most austere user operating in a very limited area does not require a display or a conversion to geodetic coordinates and may only require limited processing to be compatible with the communications channel; from this starting point the next step would be a sensor processor for position-fixing which would require a display and a processor to provide position information in either hyperbolic or circular coordinates; finally a complete navigator requires both sensor and navigational processors to provide a general solution to the transformation from circular or hyperbolic coordinates to geodetic coordinates and a control indicator to accommodate the guidance problem.

The advent of monolithic microelectronic integrated circuitry, referred to as small scale integration (SSI) in the early 1960's provided the potential for significant reduction

in the cost of radio navigation equipment, as well as in size, weight, and power by at least a factor of four, accompanied by markedly improved reliability and maintainability. However, these cost reductions did not bring the cost of a navigator within the allowable economics for many users and, in particular, the austere user.

Developmental efforts increased the digital circuitry which could be placed on a monolithic chip, medium scale integration (MSI). As a further extension, these random logic chips were organized and interconnected into special-purpose hybrid packages to perform the arithmetic and logic functions required for processing navigation information. The next step in this evolution was to design monolithic chips, large scale integration (LSI), to replace the special-purpose hybrid packages.

Monolithic LSI attracted considerable attention as a low cost design approach; however, this was limited to the high volume user. Several factors make it difficult to employ monolithic LSI in low-production-quantity and quick-turnaround programs including high non-recurring cost, long design-cycle, high production costs for the LSI chips, and inflexibility to modification. Earlier designs (special-purpose hybrid and monolithic LSI) reduced size and weight; however, the cost objectives were not realized. To date, equipments have not been available within the allowable economics for most users, and the available equipments do not have the flexibility for multi-purpose applications or for multi-users.

Microcomputer concepts represent a new class of MOS/LSI circuits which will have an impact on user equipment developments in the 1970's similar to that of the microelectronic integrated circuitry of the 1960's. MOS/LSI monolithic chips required to implement a navigational microprocessor are available in standard units, and these units are in high volume production. As previously stated, large production quantities are required to realize a low unit cost and to amortize the high development costs of LSI. Due to the general utility of the chips, the required high volume production is projected. A disadvantage cited for MOS/LSI chips has been the slow speed as compared to bipolar chips. This point must be examined in the context of the requirements of a navigation processor. A design study and the development of a Loran feasibility model has clearly demonstrated that the computational rates and input operation required for this processing are compatible with the real-time operation of the MOS/LSI chips.

The previous paragraph described why microcomputer sets can provide low cost navigational processing. The question of flexibility must be considered to demonstrate that multipurpose applications and the benefits to multi-users can be accommodated. With the recent increased availability of high speed, high density semiconductor memories microprogramming has become a realistic approach; hence, this approach can be used to implement the microcomputer functions by replacing the fixed conventional control logic with ROM semiconductor memory.

The characteristics of a navigational processor using the microprogramming approach are determined by the processor configuration and the microprograms. Because these

processors will be used for particular applications or users, the programs for each application are firmed by storing them in ROM. As a result, the characteristics of the processors are easily altered by changing the ROM program (assuming that the microprocessor configuration can accommodate the changed program). This permits a wide variety of user equipments to be implemented using the basic microprocessor configuration. Only the ROM's and possibly the interface circuits will differ from one user equipment to another. Modifications and custom features can be added to the basic configuration by changing the ROM program; this feature provides the desired flexibility to accommodate multi-users and multi-purpose applications.

Microprocessors are available in MOS/LSI chip sets (1) with architecture similar to general-purpose computers. Figure 1 illustrates a microprocessor configured with Intel's 2nd generation 8080 CPU (5), a single-chip MOS 8-bit parallel central processor. The microcomputer set is formed when the CPU is interfaced with semiconductor memories (ROM and RAM) and peripheral devices using random logic. The internal organization of the CPU is centered around an 8-bit interval bidirectional data bus. All communications within the processor and with external elements occurs on this data bus in the form of 8-bit bytes of data.

This particular CPU is associated with a basic instruction set, which provides a means to mechanize algorithmic and logical processes. The basic microcomputer set operation is controlled by the sequence of microinstructions in the microprogram. At each program count, the CPU addresses the ROM to read the next instruction; this instruction is read into the instruction decode and control (figure 1) where it is decoded; the instruction decode and control function then controls execution of this instruction by the ALU; following execution of the instruction, the control increments the program counter to prepare for start of the next instruction. The process is repeated to sequence through the complete microprogram.

As delineated, the architecture of a microcomputer set permits continuous and cyclic use of a minimum of hardware to perform arithmetic, logic, and control operations. To illustrate the operation of the microprocessor, a sequential synchronous computer system was assumed, and the complicating and obscure aspects of the processing requirements for a radio navigator were ignored. The important issues not discussed thus far were how the functional requirements for a navigator could be mechanized into microprograms, and could the real-time processing requirements be satisfied? A Loran model has been developed and the mechanization is described in the following sections.

DESIGN CONSIDERATIONS FOR LORAN MICROPROCESSOR

The design configuration of the Loran-C feasibility model was primarily determined by the lower processing speed of the first generation 8008 CPU. The real-time requirements of a Loran receiver prevented the use of one CPU to perform all the processing functions, (data collection, servo algorithms, etc). This condition led to the use of one CPU for each signal (Master, Slave A, and Slave B) to be tracked. Associated with each CPU are the

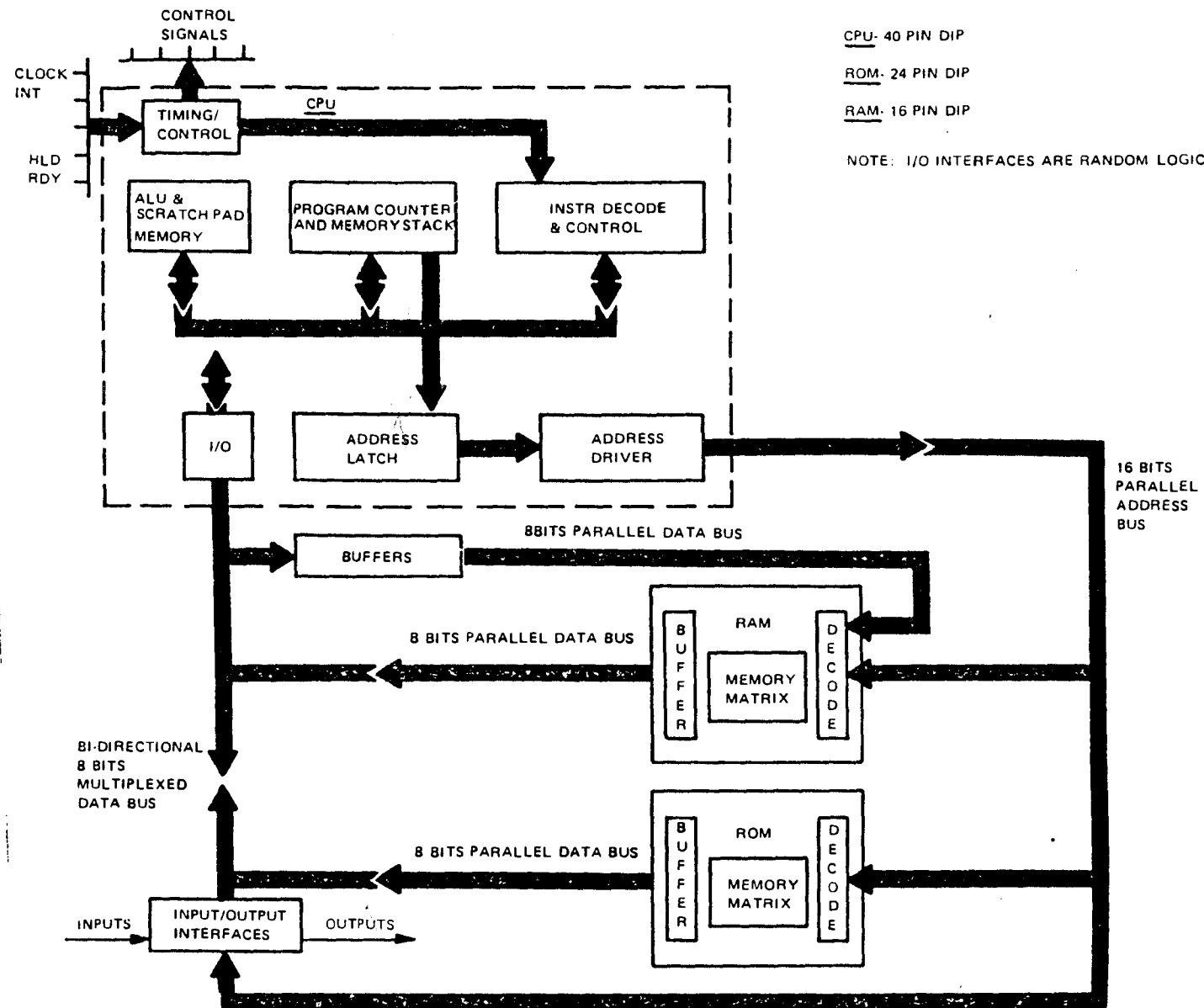


Figure 1. Navigation Microprocessor Set

read-only memories (ROM's) program chips, and the random access memories (RAM's), which are the working registers for the CPU. It is planned to convert the first generation 8008 CPU's to one second generation 8080 CPU.

The ROM's are the control elements of the processors. In addition to containing the servo algorithms for the Loran tracking functions, they control the input/output (I/O) functions, the Loran timing information, and the interrupt control functions. Each ROM contains 256 eight-bit words of instruction/data for the processor.

The RAM's serve as working registers, data storage, and control registers for the Loran functions. Each CPU has access to 256 eight-bit words of RAM. The RAM is common to all phases of the Loran processing (search, settle, and track). The RAM was limited to 256 eight-bit words because a RAM chip is organized on a 256 one-bit word basis. The use of eight RAM chips provides uniform word length (8 bits) when compared to the ROM chips and the CPU. For the Loran tracking functions, the RAM size is more than adequate, thereby encouraging maximum use of digital processing for the Loran track functions. This factor, combined with the availability of linear integrated circuits (sample/hold, analog multiplexers, etc) and the advantage of linear sampling technique over hard-limited sampling in certain signal environments, led to the selection of a linear sampling technique for the phase, envelope, and AGC tracking functions.

Hard limiting is used in the automatic search and settle processes which are described in subsequent sections.

LORAN MICROPROCESSOR

The Loran microprocessor receiver (figures 2 and 2A) is a fully automatic receiver (search, settle, track) combining both hard limit and linear processing. Hard limit processing is used for search and settle, while linear processing is used for track (phase, AGC, and envelope).

The front panel operator controls are rate information, slave search time difference, (A and B), start master search, and power on-off.

There are nine front panel status indicators, indicating the basic functions of search, coarse settling, and envelope settling, for Master, Slave A, and Slave B.

BASIC LORAN FUNCTIONS

Search consists of two stages, Master search followed by Slave A and Slave B search. Both are a hard limit process where a hard limited RF is synchronously sampled at certain time intervals for a prescribed time period. The result of sampling is binary, that is, a '1' when the signal is +5 volts and a '0' when the signal is at 0 volts. Since sampling is on a synchronous basis, the result of summing a particular sample over a period of time is an indication of the presence or absence of a signal at that point in time. By correlating the data from time positions spaced by 1000 microseconds (according to the proper phase

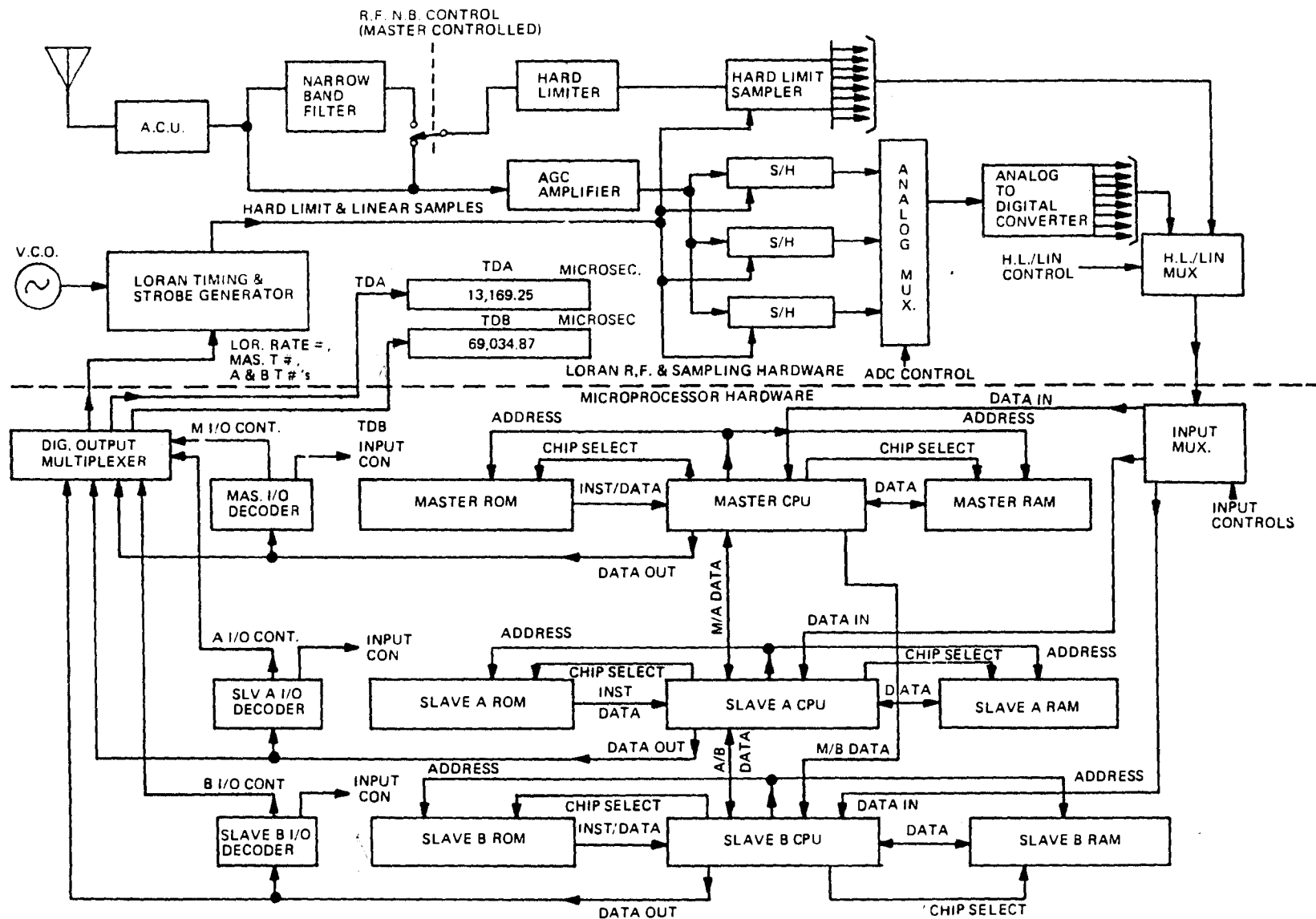


Figure 2. Loran Microprocessor Receiver

*NOTE PROPOSED
SIMPLIFICATION TO ONE
CPU — pg 6 & 22*

and 22
 BUT SEE Page 6 for
 simplification

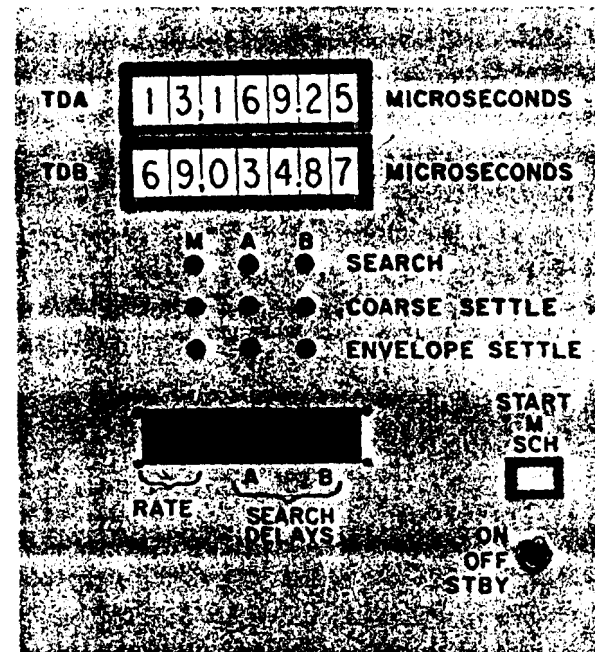
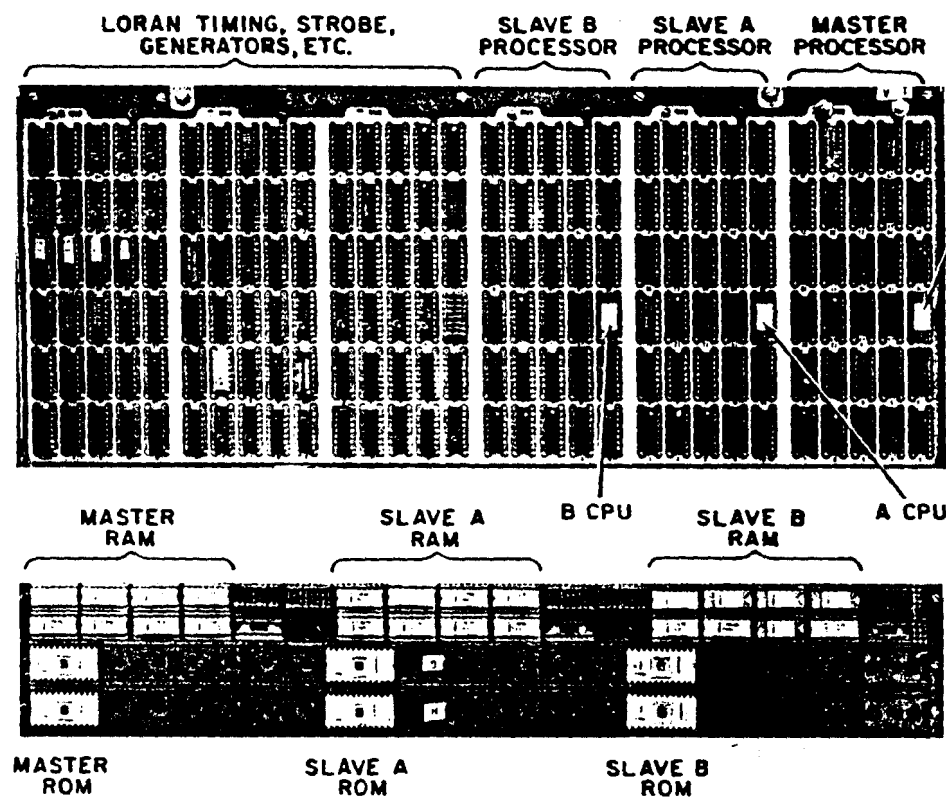
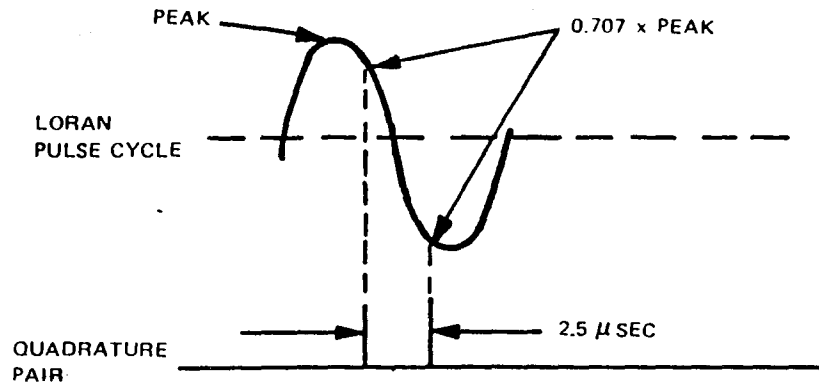


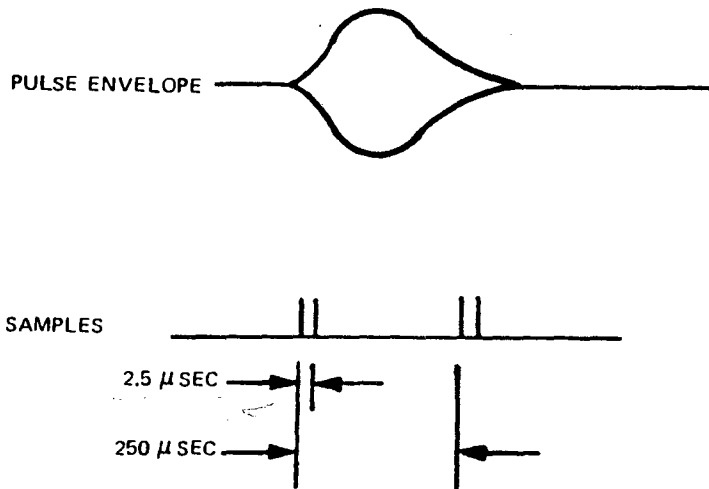
Figure 2A. Loran Microprocessor

code) a determination of whether the correct signal is present at that time position is made. The generation of a sampling pattern is based upon the following:

1. Quadrature sampling (2.5 usec pairs) to guarantee signal energy no less than 0.707 of signal peak at that time.

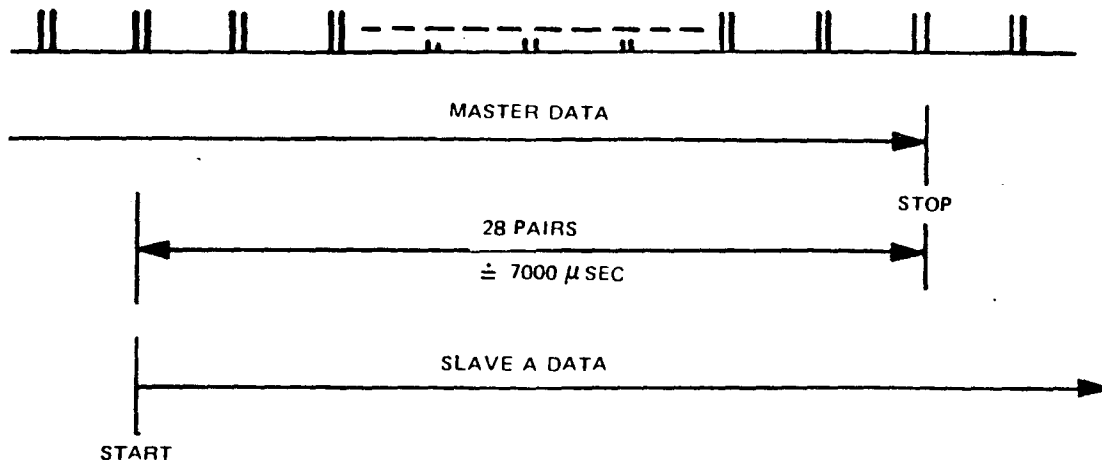


2. Sampling interval of 250 usec to guarantee sampling of Loran pulse.

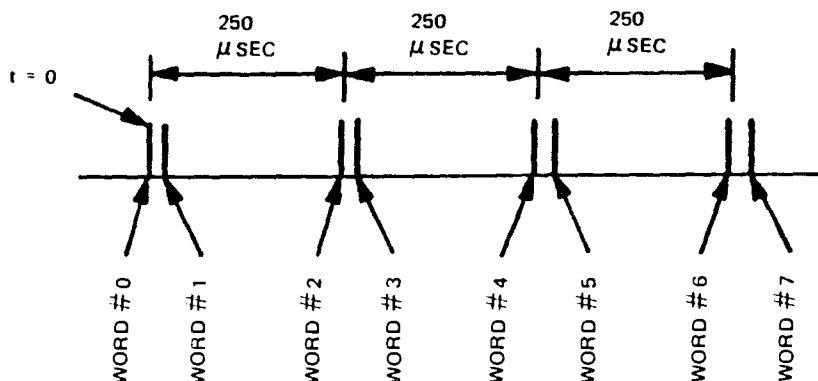


Due to lengthening of the pulse envelope by the narrowband filter, 250 μsec spacing is more than adequate. In addition, 250 μsec spacing is a common factor for Loran-C ($250 \times 4 = 1000 \mu\text{sec}$) Loran-D ($250 \times 2 = 500 \mu\text{sec}$) transmissions, permitting the strobe generator hardware to be common. Therefore, the only change necessary to perform Loran C or D search would be a software change.

3. RAM memory restricts the quantity of samples which can be taken at one time. Since each CPU has access to 256 eight-bit words, it is feasible that $3 \times 256 = 768$ separate samples can be stored and integrated. The use of RAM memory for program control slightly decreases the available amount of RAM to 224 words per CPU. Overlap in the samples for each CPU was made to permit independent correlation per CPU as follows:



As demonstrated in figure 3, the final configuration permits a time window of $27,750 \mu\text{sec}$. This requires up to five separate data collection routines to scan the entire Loran interval ($100,000 \mu\text{sec}$) at the Loran rate SS-0. Once data is taken, the results are correlated and compared to a search threshold. Any time position where the search threshold is exceeded is recorded in a RAM location, by storing the RAM location which was the start of the correlation process. For example, if a correlation started with RAM word No. 4 and the threshold was exceeded, the No. 4 would be recorded, thereby representing $4/2 \times 250 \mu\text{sec}$. If the word was odd (for example, 5), this would represent $\frac{5-1}{2} \times 250 \mu\text{sec}$. On a time scale, words 4 and 5 represent:



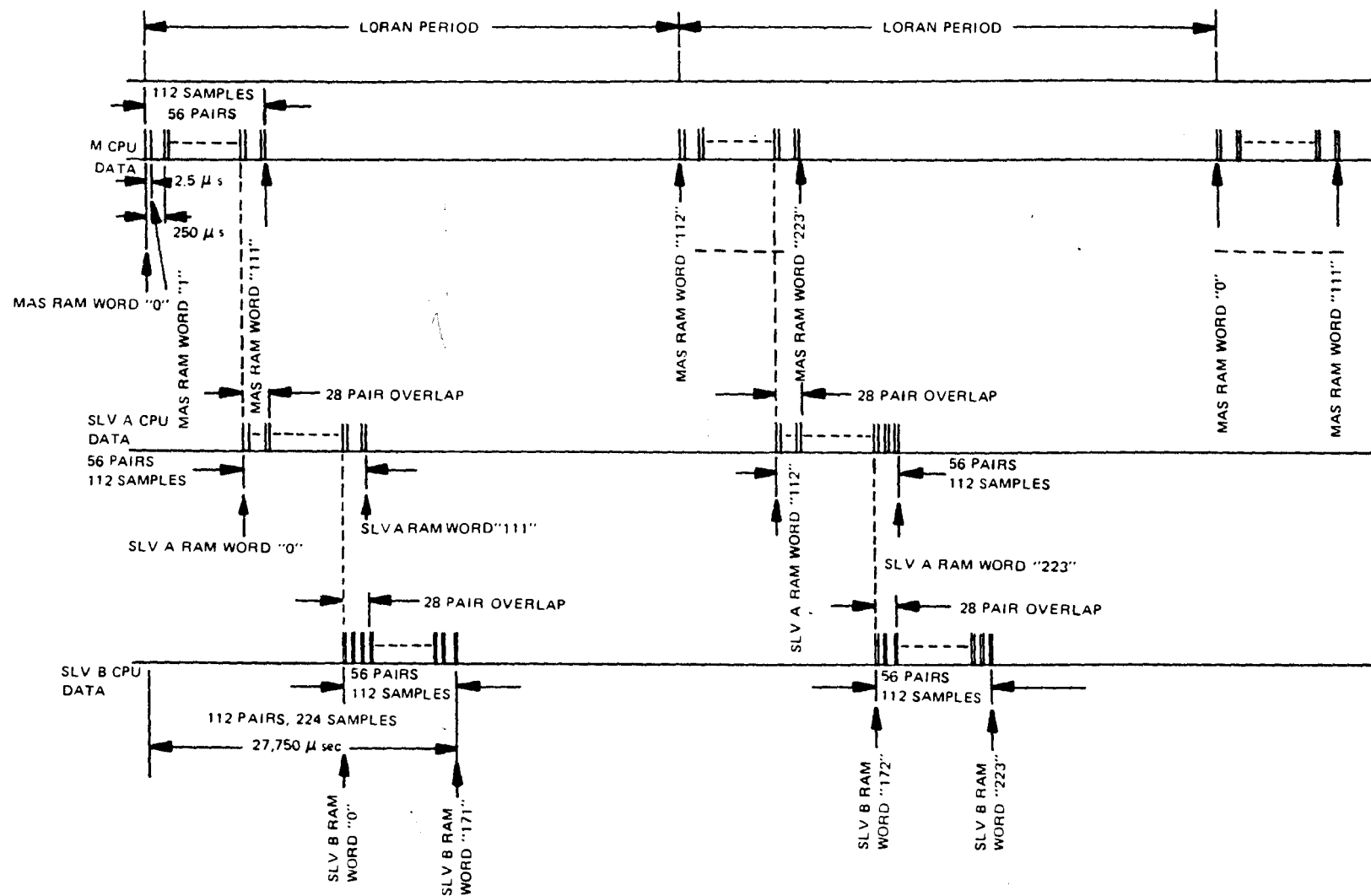


Figure 3. Search Strobe Pattern

approximately 500 μ sec after $t = 0$. When the proper correlation is determined, the frequency divider reset time is determined by whichever RAM word number initiated the correlation. The correlation routine is the sum of 16 memory locations according to two different phase codes ($M1 + M2$, or $M2 + M1$). As an example: $M1 + M2$ would be

$$\begin{aligned} M1 &\rightarrow 1 + 9 + \overline{17} + \overline{25} + 33 + \overline{41} + 49 + \overline{57} \\ &+ \\ M2 &\rightarrow 113 + \overline{121} + \overline{129} + 137 + 145 + 153 + 161 + 169 \end{aligned}$$

where the time between words 1 and 113 is equivalent to one Loran period. The sum of $M2$ and $M1$ would be:

$$\begin{aligned} M2 &\rightarrow 1 + 9 + \overline{17} + 25 + 33 + 41 + 49 + 57 \\ &+ \\ M1 &\rightarrow 113 + 121 + \overline{129} + \overline{137} + 145 + \overline{153} + 161 + \overline{169} \end{aligned}$$

Once the master signal has been located, and the timing circuits are synchronized, the slave search routine begins. Slave search consists of the hard limit sampling of a time window where the slave signal is estimated to be. The sampling intervals are similar to the MASTER SEARCH intervals of quadrature pairs each 250 μ sec. The time window covered is 13,000 μ sec, meaning that the slave time difference must be predicted to within 6,000 μ sec (13,000 - 7,000) since the group length is 7000 μ sec. Since the master has already been synchronized, correlation according to an S1 and S2 phase code pattern is performed, using samples with the same timing pattern of a master correlation (word No. 1 and word No. 9 to word No. 169). Once the Slave A transmission is identified and the Slave A time number is updated, the same procedure is performed for the Slave B transmission. Once Slave B data is correlated and the slave B time number is updated, all three CPU's enter the settling mode.

SETTLING

Settling is the process of positioning the track strobes within +20 microseconds of the desired crossover. This is accomplished by sampling at a number of different points ahead of the time position determined during search. If signal energy is detected, a timing jump is made. The magnitude of the jump is determined the number of points which detect signal energy. This process is repeated until only the last pair detect energy indicating that the last pair is somewhere on the leading edge of the groundwave. The settling strobe pattern is illustrated in figure 4.

The data input and storage routines are essentially the same as those used for the search process. Longer integration times are required to increase the signal to noise improvement factor, simply because the settling system is attempting to detect lower signal levels than search. A typical integration time is 150 Loran periods for a narrowband (4 KHz) RF, and 600 Loran periods for a wideband (25 KHz) RF signal. Since the integration times are significant, the signal must be phase tracked to eliminate any oscillator

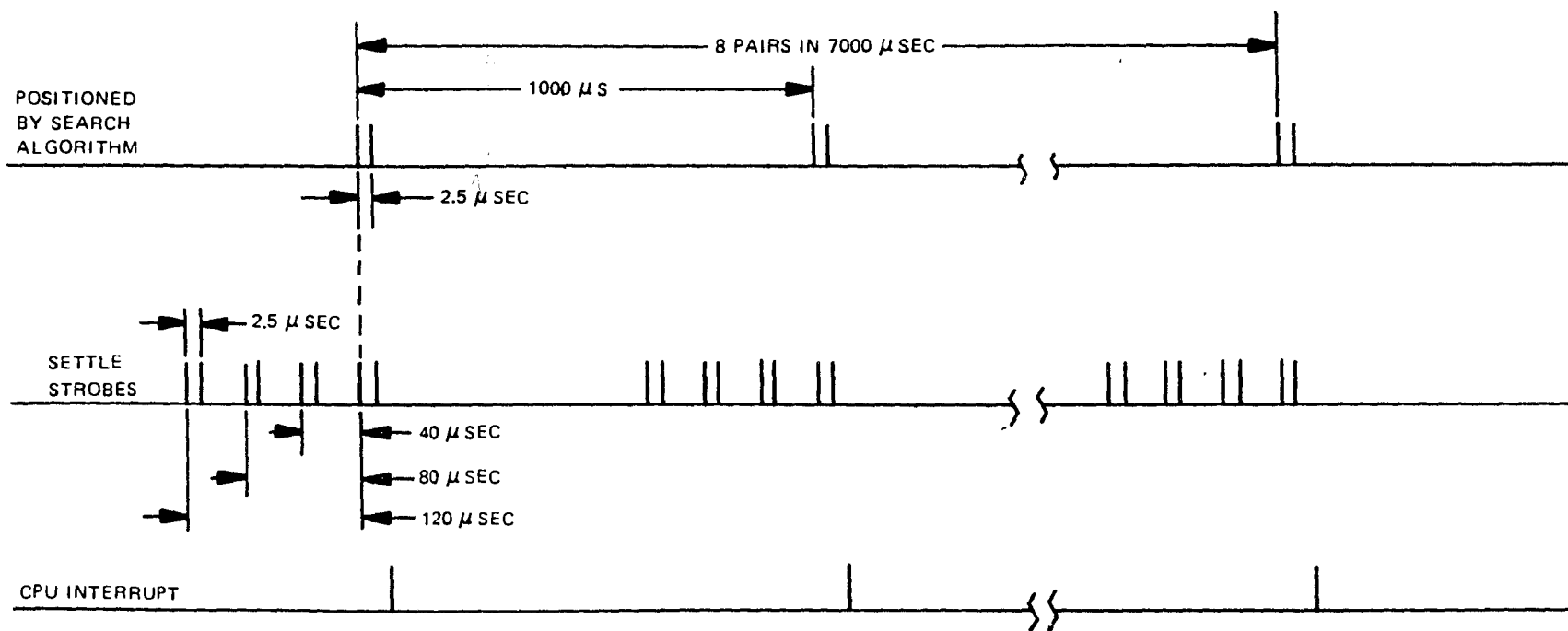


Figure 4. Settling Strobe Pattern

drift or Doppler shift due to velocity of the vehicle. Phase tracking is accomplished by using one of the last samples to detect the phase crossover. In the case of a linear system, an AGC sample, in quadrature with the phase sample is required for RF gain control for the linear phase loop.

Due to the slow speed of the processor, alternate sampling of hard limit and linear data is required. This is performed by sampling hard limit settle data for two Loran periods and then sampling ϕ and AGC for two Loran periods with the linear system. Timing and flow diagrams (figures 5 and 6) illustrates the settling hard limit/linear sample configuration.

TRACK

The track process basically consists of three different servo loops for each of the three received signals, Master, Slave A, and Slave B. The three different servo loops are:

1. Phase Track
2. Envelope Track or Cycle Select
3. Automatic Gain Control (AGC)

The track strobe pattern shown in figure 7 is generated for the Master and two slave transmissions, depending upon the master and slave time numbers. The strobe pattern for each Loran pulse is configured to sample the 100 KHz carrier at three points in time, each separated by 2.5 μ sec or 90 degrees of phase.

PHASE TRACK

Phase tracking is the continuous detection and fine measurement of the zero-crossing of a particular cycle of the received Loran pulse. To accomplish this in a linear fashion, a voltage measurement of the signal is made by a sample (ϕ) and hold circuit, the voltage is converted to a digital format (ADC), and processed by the computer as an error input (E) to a phase tracking servo. The end result of the servo is a time position number which determines the time position of the sample, and is used in the calculation of time difference.

ENVELOPE TRACK

To calculate the correct time difference from the phase track time numbers, each received signal must be tracked at the same relative zero crossing. The envelope track positions the phase samples at that zero crossing by measuring the amplitudes of the adjacent signal peaks (e_1 and e_2) to the zero crossing and determining the ratio between these

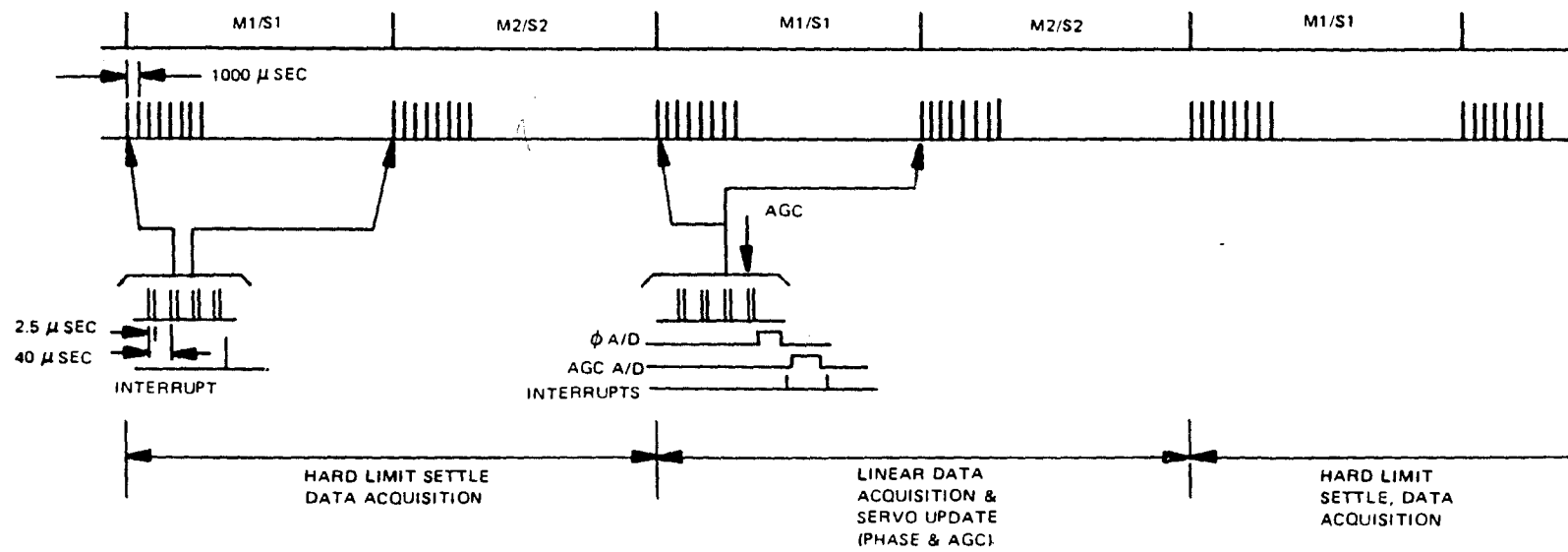


Figure 5. Hard Limit/Linear Strobe Configuration

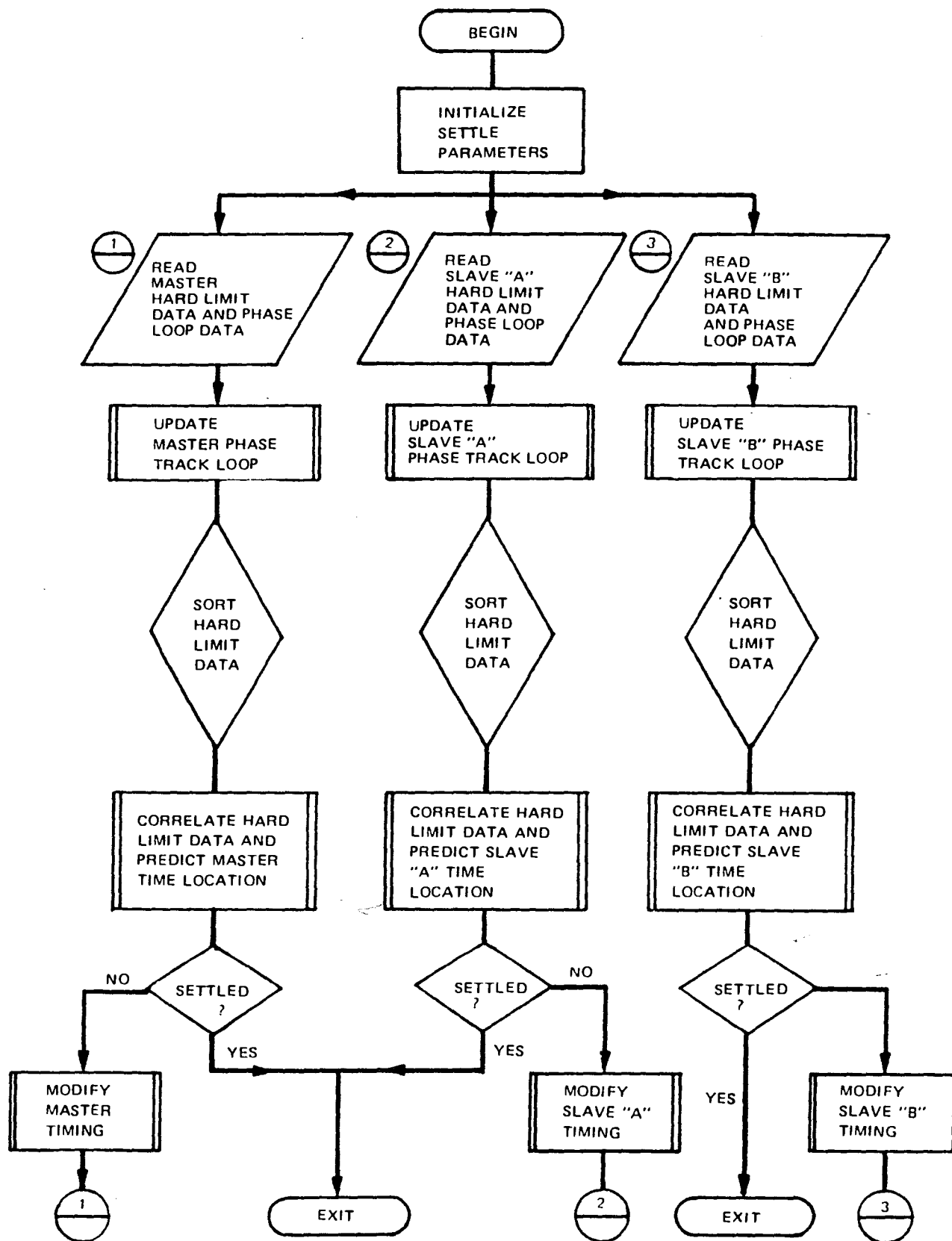
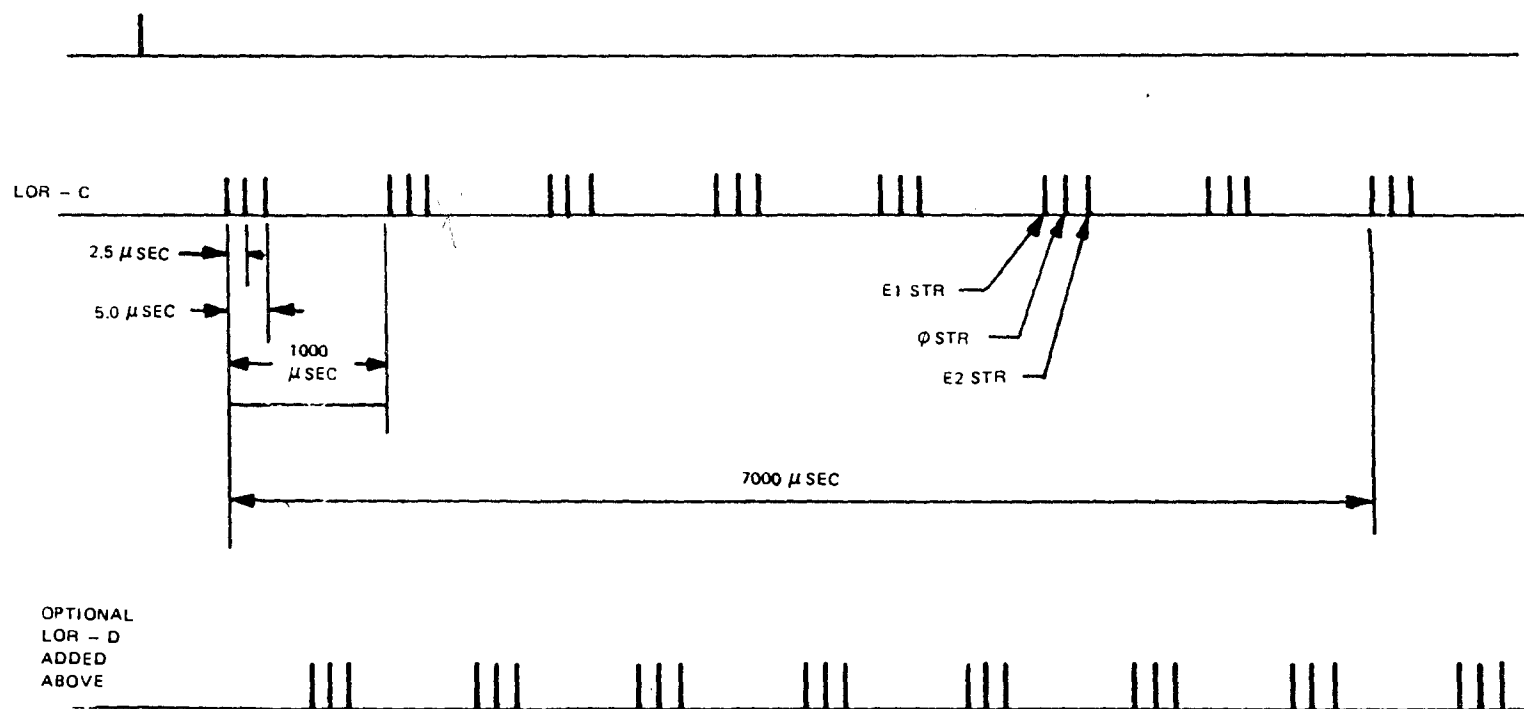


Figure 6. Settle, Flow Diagram



*SAME PATTERN FOR SLAVES

Figure 7. Track Strobe Pattern

two peak magnitudes. The fact that the leading edge of the pulse is monitored and controlled by monitor ground stations, enables the system to distinguish between adjacent crossovers on the leading edge, thereby selecting the proper crossover.

The outputs of the sample and holds which measure the peak magnitudes are multiplexed and converted to digital signals through the same ADC. The digital signals are processed and a ± 10 sec modification of the time number is made, if necessary.

AGC

To normalize the amplitude of the sampled RF signals, an automatic gain control (AGC) loop is required. This is accomplished by digitally comparing the magnitude of the peak following the phase zero crossing with an AGC reference word. The gain of the RF amplifier (which is processor controlled) is either increased or decreased depending if the peak magnitude is less or greater than the reference, respectively. Normalization of the signal amplitudes is necessary since the phase and envelope system performance is directly related to the signal amplitude.

A block diagram and flow diagram of the tracking system are presented in figures 8 and 9.

PERFORMANCE SUMMARY

With the design configuration specified in the previous paragraphs the end result is a fully automatic Loran-C receiver possessing the following performance figures with signal-to-noise ratios of $\geq 1/3$. (≥ -10 dB)

Search (Maximum Time):	< 30 seconds
COARSE SETTLE (Maximum Time):	90 seconds
ENVELOPE SETTLE (Maximum Time):	200 seconds (SNR worst case)
TIME DIFFERENCE RESOLUTION:	0.025 microsecond

DESIGN CRITERIA

In developing the feasibility model, it was the intention of the designer to provide sufficient flexibility so that the equipment would function reliably in almost any environment. This is made possible by the software configuration and the ease with which it may be changed. Since the read-only memories (ROM) may be either mask programmed (fixed), or electrically reprogrammable (PROM), the software is assembled so that the factors which determine system performance are contained within one ROM. This would enable the user to select a standard performance model by using the fixed ROM, or a custom PROM

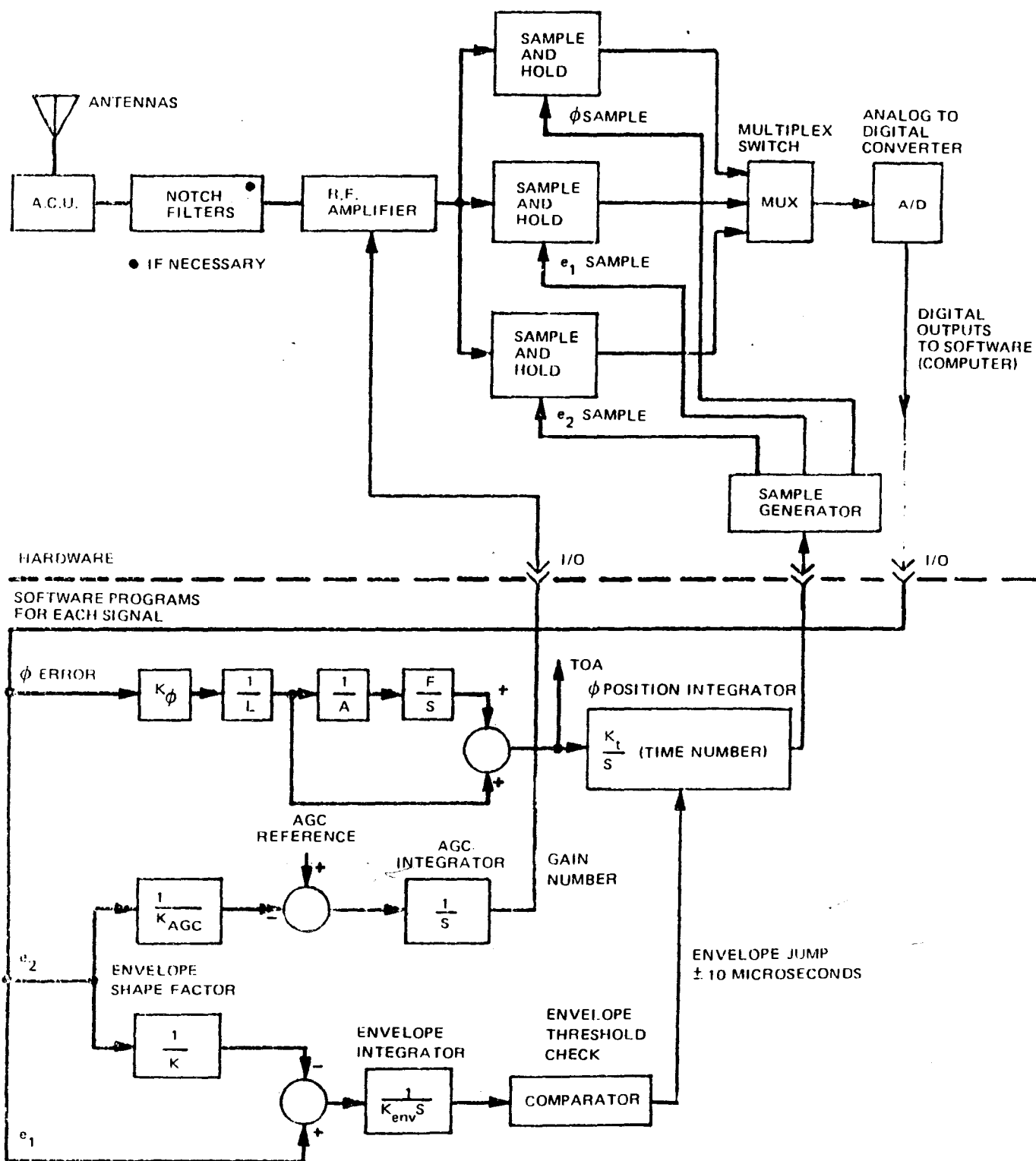


Figure 8. Receiver Tracking Loops Block Diagram

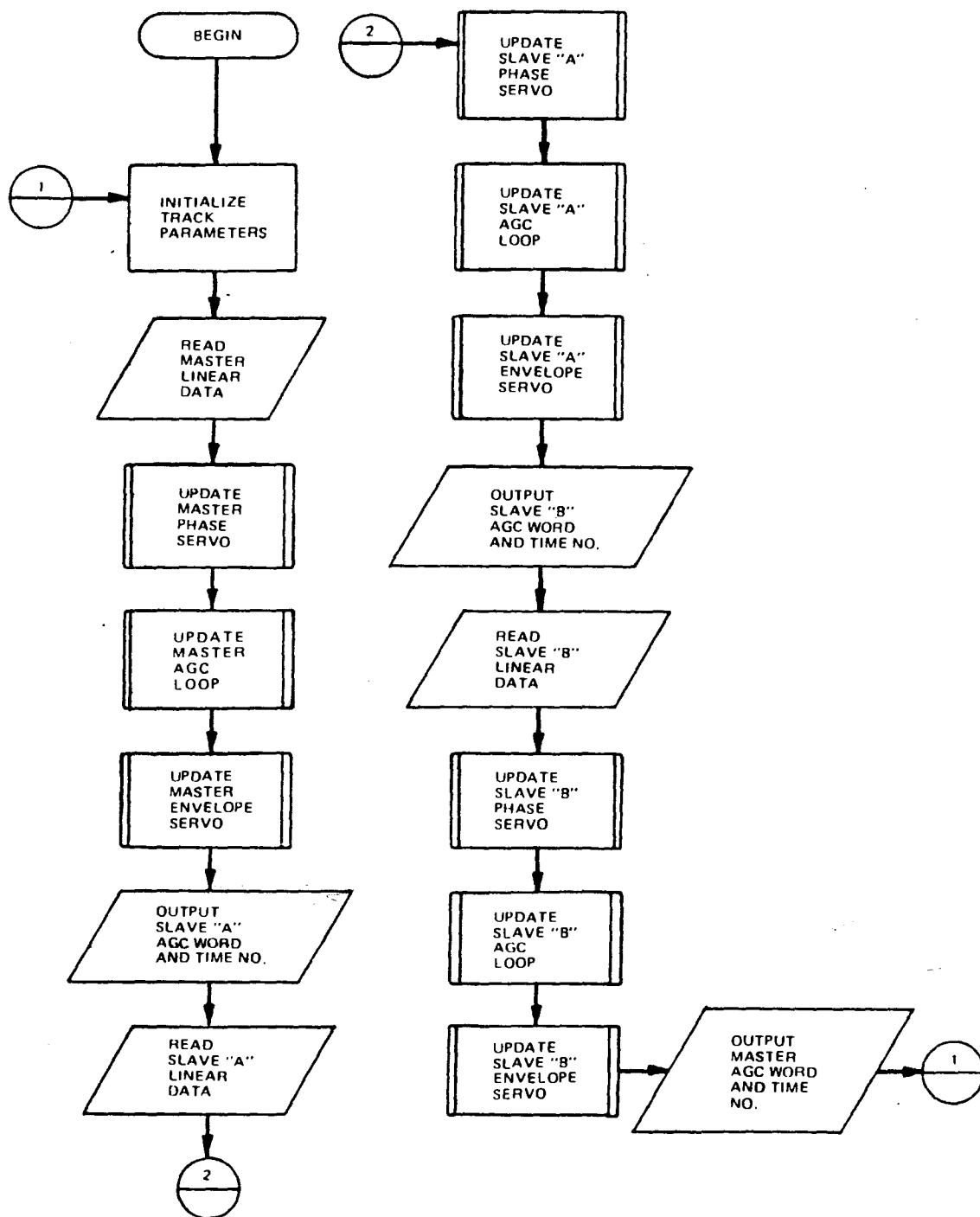


Figure 9. Track Flow Diagram

to achieve any desired performance. This feature enables extreme flexibility by storing groups of constants. The group of constants being selected would be determined by the operating conditions, thereby allowing the implementation of a number of desirable functions. This is accomplished by the software selecting a particular group of constants when a specific condition is satisfied. If the operating condition changes, the program will select a different group constants which would provide improved performance under the new operating conditions.

DESIRABLE FUNCTIONS

Software flexibility allows the system designer to consider a number of different features including:

- **ADAPTIVE PHASE LOCKED LOOP (PLL):** To make a PLL adaptive, a method of selecting the loop time constant (or bandwidth) as a function of the signal to noise ratio must be implemented. By taking a digital sample of the hard limited signal with the E2 (or AGC) sample, a statistical measure can be made of the SNR. The measurement then determines the smoothing counter parameters (L, A, KAGC, KENV) in the servo tracking loops (Phase, envelope, and AGC) (figure 8).

A set of parameters is selected by accessing a specified portion of ROM, where the parameter values are stored. Each time the tracking algorithms are exercised, a decision is made, determining which set of parameters are utilized.

- **NOISE CENSORING:** Noise censoring is the process of censoring a sample if the magnitude of the sample exceeds a threshold, determined by a signal-to-noise ratio measurement. This threshold can be part of the sets of parameters discussed previously. Since atmospheric noise is spiky in character, a significant improvement in servo noise performance can be achieved when the noise spikes above a certain level are censored.
- **SYNCHRONOUS INTERFERENCE REJECTION:** Protection against errors introduced by synchronous frequencies can be obtained through selective sampling techniques. Since sampling is performed on a pulse-by-pulse basis, the storage of data can be arranged on an odd pulse sum and an even pulse sum. It follows that detection of most synchronous frequencies is a relatively simple process, and once detected, the appropriate samples (odd or even) can be rejected.
- **ALL RATE LORAN:** The technique of combining real time inputs UTS, etc., with the track information from a tracking receiver to produce a synchronized signal for a second Loran chain is referred to as 'all-rate Loran'. The use of null ephemeris tables issued by the USNO to determine real time are vital to the use of this feature.

- SKYWAVE TRACKING: It is possible to extend the operational range of a Loran chain by tracking the skywave from a station or stations. Based upon measured time difference, a correction factor would be applied which would make the corrected time difference compatible with a Loran map. The correction factors could be stored in a ROM chip and could easily be applied to a skywave fixed time difference.

SIZING OF LORAN NAVIGATION

The introduction of second-generation microprocessors significantly changes the concept of the three processor approach used in the feasibility model. The size of both the hardware and software is greatly reduced. The two major factors leading to this reduction are:

1. Higher processing speed
2. Larger CPU package

HIGHER PROCESSING SPEED:

The higher speed (two-microsecond instruction cycle) permits sufficient time to perform the necessary processing for the master and slave signals within one Loran period. The duplication of the hardware and software necessary in the three processor approach is eliminated, allowing for the timesharing of common hardware and software. A reduction of three to one is realisable in software, and approximately two to one in hardware. The two-to-one figure is due to the common circuitry needed for Loran timing and strobe generation circuitry.

LARGER PACKAGE

The larger package enables the separation of the address bus from the data bus. With the 8008 package, the common data/address bus is relatively inefficient and time consuming. The saving in hardware when using the 8080 processor is considerable.

MECHANIZATION OF AN OMEGA NAVIGATOR

The objective of a design study was to provide an Omega navigator for the airborne user which will furnish automatic and continuous operation throughout the world. The starting point was a review of the development of the Omega System and the development of Omega receiving sets at ITT Avionics Division over the period from 1960 through 1974. As part of this review, candidate designs were selected so that a comparative analysis could be performed based on the operational Omega System configuration and the

requirements of an airborne user. The evaluation criteria used in this comparative analysis, ordered in accordance with their weight, are:

- Selection of an Omega sensor processor that can provide continuous navigation information day or night, under all weather conditions anywhere on the globe with a daytime position accuracy of approximately one mile using the operational Omega System configurations.
- Provision of an airborne Omega navigator within the stated economic value to the user.
- Provision of a new man-machine interface that replaces old methods of fixed function switches, knobs, meters, and panel lights.

This section presents a design approach for satisfying the performance objectives and briefly discusses the man-machine interface. The final section of this paper demonstrates that the stated cost objectives can be met.

An eight-station operational configuration with relatively high power transmitters has been selected to radiate the Omega navigation signals and provide a global navigation grid with good geometry. The electromagnetic field intensities produced by the transmitters (10 kW radiated power) is adequate such that signals from at least four stations can be reliably extracted from the atmospheric noise.

Since the primary consideration in the reception of signals in the VLF spectrum is atmospheric noise (impulse type noise), and that KTB noise and CW interference are secondary, the early Omega receivers (such as the ITT Avionics Division AN/WRN-2 design) were broadband limiting type receivers which reduced the disturbing effect of impulse noise on a desired signal as follows: First, receive the desired signal plus impulse noise in a wide bandwidth linear receiver; wide bandwidth meaning, in the limit, wide enough to pass the impulse with negligible widening, and linear meaning this portion of the receiver is always gain controlled so that the desired signal is maintained at a standard level. Second, the combined signal plus impulse noise is then fed to either a hard limiter or a noise censor designed to hard limit or to delete samples at a level just above the desired signal standard level. Finally, the output of this limiter is injected into a narrow bandwidth filter, narrow bandwidth meaning, in the limit, just wide enough to pass the desired navigation signal. When the previously described procedure is used (compared to using the narrow band filter alone), the signal-to-noise ratio in the narrow band due to the impulses is improved by a factor proportional to the ratio of the wide bandwidth to the narrow bandwidth, and is a function of the amplitude distribution of the noise.

It is important to realize that the previous description in effect says that the way one obtains impulse noise reduction is to design a wide bandwidth receiver with zero dB dynamic range; however, if any CW type signals which are stronger than the desired signal exist within the bandpass of this zero dB dynamic range wideband receiver, these stronger signals will capture (desensitize) the receiver. Since there are the three basic Omega frequencies at 10.2, 11-1/3, and 13.6 KHz plus the possibility of sixteen additional frequencies between 11.55 and 13.15 KHz, plus transmissions in this band from other countries, which can be as much as 80 dB stronger than the desired signal at a given geographical location, obviously, a wideband, front-end with zero dB dynamic range is just not practical for a real-world Omega receiver. This consideration led to the design of narrow band receivers such as the AN/SRN-14.

To obtain the impulse noise improvement (experimentally it has been demonstrated to be greater than 10 dB) a linear dynamic range must be provided to prevent capture; however, to satisfy the global requirement would require a linear dynamic range greater than 100 dB. To satisfy this dynamic range requirement would require analog-to-digital converters which would not satisfy the cost objective; however, this does suggest a sampling system that can adapt to extreme differential signal conditions when they exist.

To examine all areas of the world in an attempt to quantitatively assess the signal conditions would be an insurmountable task; hence, it is suggested that the dynamic range problem can be bounded by considering the maximum signal condition, the minimum signal condition, and sampling six areas approximately equally spaced throughout the world. In this determination another question must be considered: Are there any other frequencies within the 10 to 14 KHz band that would interfere with reception of the Omega frequencies? At this time, the only known frequencies are the Russian Omega stations and they will be considered in the following discussion.

The first consideration is what atmospheric noise level can be expected and what are the characteristics of this noise. Atmospheric noise is produced mainly by lightning discharges in thunderstorms; therefore, the noise level is dependent on carrier frequency, time of day, weather, season, and geographical location. Subject to variations in local stormy areas, noise generally decreases with increasing latitude on the surface of the earth. It is particularly severe during the rainy seasons in areas such as the Caribbean, East Indies, equatorial Africa and Northern India. CCIR Report 322 gives the distribution of radio noise throughout the world. The results of this report are used to estimate noise levels at the areas considered in this discussion. It is further reported that the noise is impulsive in character.

To determine the maximum dynamic range requirements, the field intensities were considered in close proximity to the North Dakota transmitter. The near field due to the North Dakota transmissions are obtained from actual measurements, and field intensities for the distant station are derived from field intensity graphs presented in the report "Omega - A World-Wide

Navigational System," AD No. 630900. Figure 10 shows the results as a function of distance. The maximum dynamic range requirement established by the signal condition at ten nautical miles from the transmitter shows an 80 dB differential between the strongest and weakest signal. At a distance of 1000 nautical miles, this dynamic range requirement is reduced to 40 dB. In addition, the atmospheric noise in a 100 Hz bandwidth to be expected at this latitude is shown.

To summarize the dynamic range requirements as shown in figure 10:

- The most stringent requirement is at close proximity to an Omega transmitter (the 10 nmi condition) which imposes an 80 dB dynamic range requirement on the detection process.
- At a distance of 100 nmi from an Omega transmitter the requirement is reduced to 60 dB.
- The atmospheric noise level in a 100 Hz bandwidth at this latitude is expected to range between 26 to 40 dB above one $\mu\text{V}/\text{meter}$ and the KTB in a 100 Hz bandwidth suggested is less than 26 dB which demonstrates that the atmospheric noise and KTB are in a ratio greater than 1:1.

From these three facts the following inferences are drawn:

1. The receiver design should not be dictated by the 80 dB requirement since this is imposed by a very small percentage of the total coverage area. The 60 dB requirement should be the design criterion and a lower level of performance close to the transmitter should be accepted.
2. A zero dB RF amplifier (hard limiting) is not the optimum approach. The filters required to reduce the in-band CWI are physically realizable but a degradation in impulsive noise performance would result.
3. The spectral density of all in-band signals should be carefully examined so that a tradeoff can be performed between the extremes of the dynamic range requirements (the 0 dB at one extreme and 80 dB at the other extreme). To illustrate, a more optimum approach may be three bandpass filters at 10.2, 11.3, and 13.6 KHz that reduce adjacent interference to an acceptable dynamic range that can be accommodated by the detection process.

Figure 11 illustrates the estimated spectral intensity for all possible signals in the Omega band ten nautical miles from the North Dakota transmitter. This illustration includes the spectral lines for the Russian transmissions.

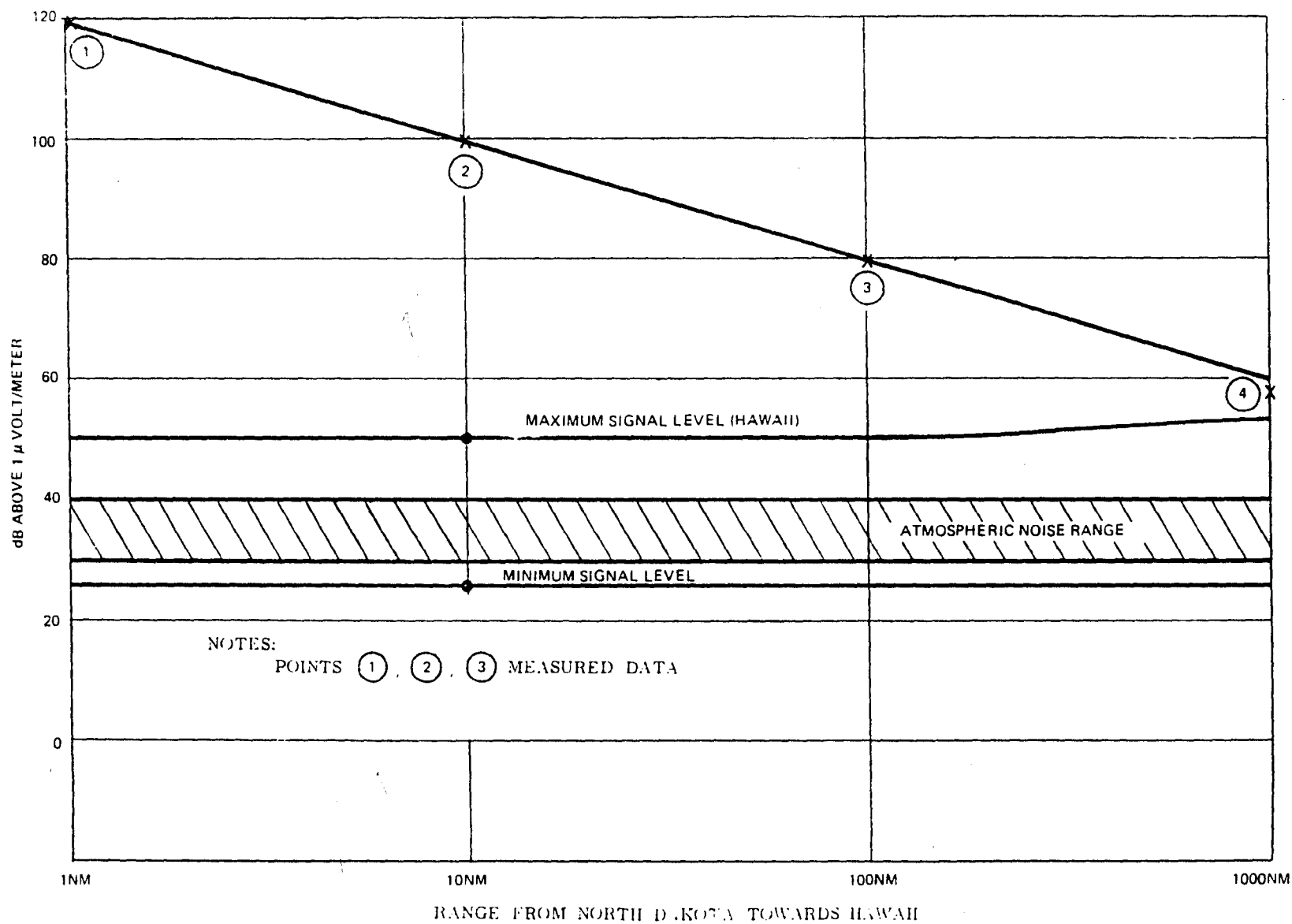


Figure 10. Field Strength Near North Dakota Transmitter

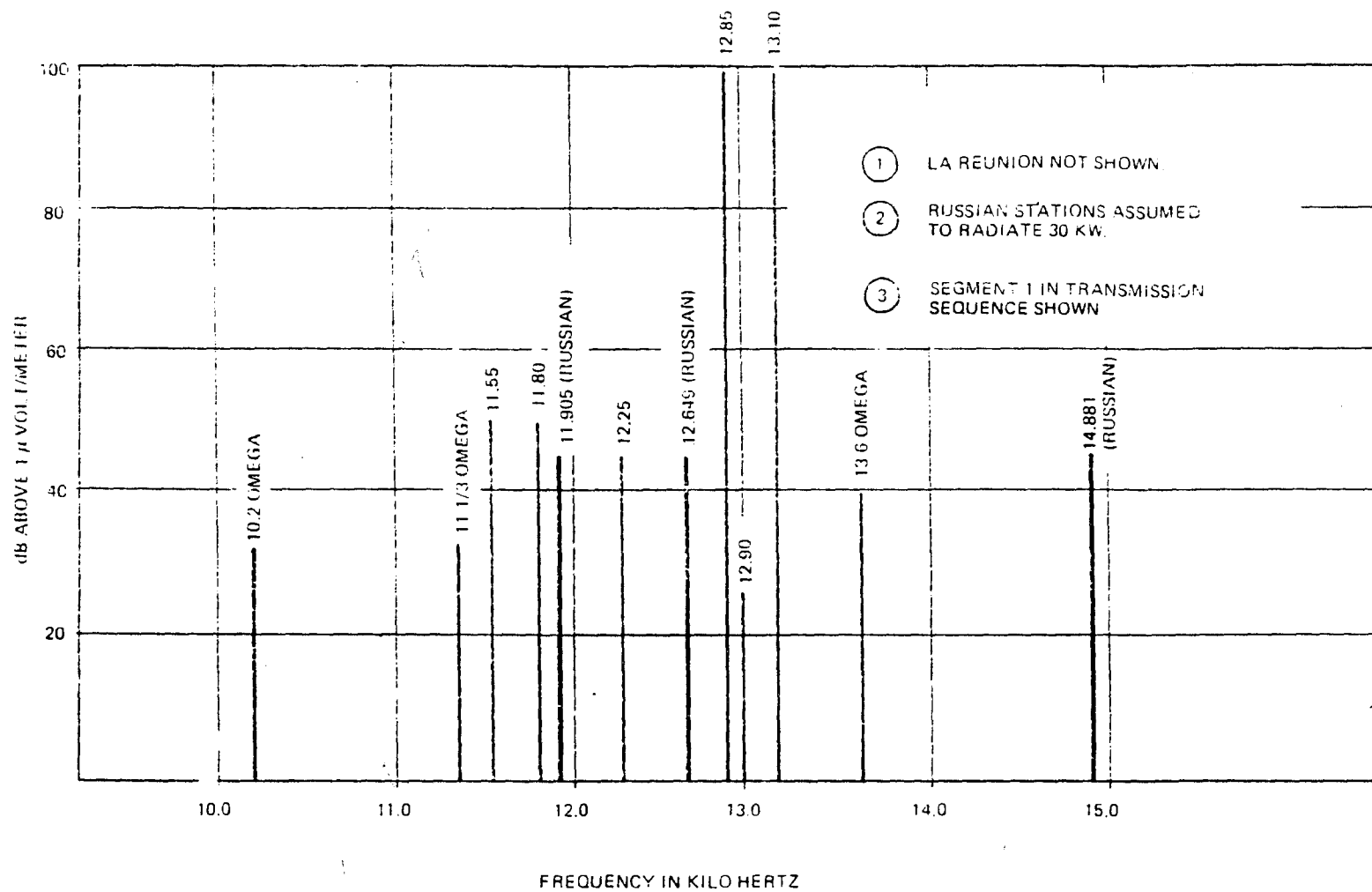


Figure 11. Power Spectral Density Near North Dakota Transmitter

These two illustrations provide the important parameters required for specification of a selective sampling technique and adaptive noise censoring. More specifically, a sampling scheme which takes advantages of the harmonic properties of the Omega frequencies can reduce the rejection requirements of the bandpass filters, and a noise censoring technique can be implemented to adjust the censoring level as a function of the range to each transmitter. These functions can be mechanized in software by software control of the sampling and using the range to a transmitter to adjust the censoring level.

The sampling scheme is based on the fact that in the period of time that includes $3/2$ periods of the 10.2 KHz signal, there are two periods of the 13.6 KHz signal. For detection of the 13.6 KHz signal, pairs of samples are taken over an even number of periods of the 13.6 KHz, and over the even number of samples the contribution of an interfering 10.2 KHz signal will be eliminated. This selective sampling technique is summarized in the following table.

$N \times T$ T in μsec	$3/2$	2	$5/2$	3	$9/2$	5
$T_{10.2}$	147				441	
$T_{13.6}$		147		220.5		
$T_{11.33}$			220.5			441

A similar method can be used to provide a phase measurement of the $11\frac{1}{3}$ KHz signal when there is an interfering 10.2 KHz signal; however, if the interfering signal is 13.6 KHz a differencing procedure would be mechanized. By software mechanization of these procedures the other Omega interfering signal can be reduced to the quantization level in the analog-to-digital converter. Further, for the other possible 16 additional frequencies between 11.55 and 13.15 KHz a weighted sampling technique would be employed.

To summarize these considerations, by implementing a linear RF receiver and software mechanization of selective sampling and adaptive noise censoring a signal-to-noise improvement of greater than 10 dB in an impulse noise environment will be attained at distances greater than approximately 100 nmi from a transmitter. For aircraft flying directly over a transmitter a DR mode will be used to prevent capture.

To determine the receiver sensitivity requirement the minimum expected field intensity was investigated. Indications are that this condition will be experienced in the Baffin Bay

Region in the Arctic due to the very high attenuation rate over the Greenland land mass. Measured data is available for this area and it is tabulated in table 1.

Three important parameters are derived from this tabulation:

1. Expected atmospheric noise level is 30 dB above 1 μ volt/meter in a 100-Hz bandwidth, this sets the sensitivity requirement for the RF section.
2. Tracking of Norway is required for good crossing angles.
3. Although transmitted at a greater power level than the U.S. signals, the Russian signal will not cause an interference problem in this region.

The previous considerations are used to determine the maximum and minimum signals conditions on the globe. In addition to these conditions, it is desirable to determine the expected number of usable Omega signals throughout the world. To obtain an estimate, six additional widely spaced areas are considered. The results are shown in table 2.

The selection of only eight areas makes this a gross estimate on a statistical basis and should be further investigated. The following indications are deduced from this tabulation:

- The minimum number of expected received stations is greater than four in the eight areas considered.
- In some areas all eight stations may be acceptable.
- At distances greater than 1000 nautical miles from all stations, the dynamic range requirements are not stringent (less than 40 dB).

The conclusions derived from these considerations are:

- An 80 dB dynamic range capability must be provided for in the linear amplification and this dynamic range should be shifted as a function of range.
- The Russian signal should not cause an interference problem except within 1000 nautical miles of these transmitters, based upon signal amplitude alone. Errors introduced due to coherence may occur at a lower level however.
- All eight stations will be available in some areas and provisions should be made to track all eight.
- The sensitivity of the RF section should be less than 30 dB above 1 μ volt/meter to prevent degraded operation in the Arctic region.
- Tracking of the Norway station in the Arctic region is required to obtain good crossing angles for the phase differences.

Table 1. Estimation of Signal Strength at Thule, Greenland

		dB above 1 volt/meter
Norway	Extrapolation from measured data, Canadian DOT	10 to 30
Trinidad*	Extrapolation from Balboa measurement	22 to 36
Hawaii*	Measured	28 to 40
No. Dakota	Extrapolation from Forestport measurement	28 to 38
La Reunion		
Argentina		
Australia		
Japan	Approximately same distance as Hawaii	28 to 38
Russian Signals		
<p><u>OBSERVATIONS</u></p> <ol style="list-style-type: none"> 1. Noise level 30 dB above 1 μvolt/meter (100 Hz BW) 2. Signal range 10 to 40 dB above 1 μvolt/meter 3. Possible to track up to 5 stations 4. Norway required for good crossing angles 		

*NELC Electromagnetic Field Strength Measurements at 10.2 kHz, NEL Report 1239

Table 2. Electromagnetic Field Intensity Distribution

TEST LOCATIONS								
Day Night	21° N 158° W	76° N 68° W	9° S 62° W	32° N 33° E	11° N 92° E	51° N 151° E	24° N 122° E	39° N 33° W
Norway A	32 42	10 30	29 34	48 50	32 40	39 45	33 41	50 52
Trinidad B	44 48	22 36	56 56	38 42	NA	18 34	30 36	51 52
Hawaii C	50 52	28 40	38 44	30 36	NA	34 42	26 34	34 40
N. Dakota D	100 100	28 38	36 42	42 46	8 22	36 42	12 32	48 50
La Reunion E	NA	NA	10 30	38 42	45 48	38 42	23 34	26 34
Argentina E	26 36	NA	52 53	20 34	NA	10 20	NA	28 38
Australia G	32 40	NA	32 40	NA	30 40	29 37	34 40	NA
Japan H	40 44	28 38	26 40	26 32	42 48	53 54	61 61	22 34

Notes:

1. Field intensities in dB above 1 μ volt/m.
2. Expected daytime to nighttime range indicated.
3. NA - estimated to be less than minimum.
4. Double cross means near-in exclusion.

- To accommodate the large range of expected signal-to-noise conditions over the world adaptive tracking loops must be mechanized for near optimal performance, particularly, to obtain continuous and reliable tracking of Norway in the Arctic region.
- This linear wide band system can provide a signal-to-noise ratio improvement of greater than 10 dB in an impulse noise environment.

The general functional requirements for an Omega navigator in accordance with the previous considerations are illustrated in figure 12. To illustrate a modular approach the functions are divided into two sets. The first set includes the required functions for position-fixing, and the second includes the additional functions for conversion to the geodetic or the generation of guidance signals. Further, these subroutines are considered on a modular basis to provide the flexibility for multi-user applications.

COMBINED LORAN AND OMEGA

Studies and implementations at ITT Avionics Division have established that a combined Loran and Omega navigator is feasible and can be provided without a large percentage increase in cost of either taken separately. The following conclusions were derived in these studies:

- A common loop antenna or whip antenna can be employed and an integrated antenna coupler can be provided which satisfies the sensitivity requirements of Loran or Omega with either antenna.
- Separate bandpass filters must be provided for Loran and Omega.
- For near optimal performance, linear amplification and detection is selected for Loran and Omega and a common amplifier can be implemented.
- A navigation microprocessor can be configured to mechanize either a Loran or an Omega navigator.

The configuration selected from these studies is shown in figure 13.

The correct design of low noise antenna couplers working from a reactive antenna (which includes all VLF and LF receiving antennas) is well enough understood at this time so that it is possible to state firmly the physical antenna size required to satisfy specified Loran and Omega sensitivities. The two basic types of antennas are electric (for example, whip) and magnetic (for example, loop) antennas.

With a vertically polarized electric field being received, airborne electric antennas are (of practical necessity) single ended, and the active member can be formed into any physical shape, with a vertical stick as one extreme and a flush flat plate as the other extreme.

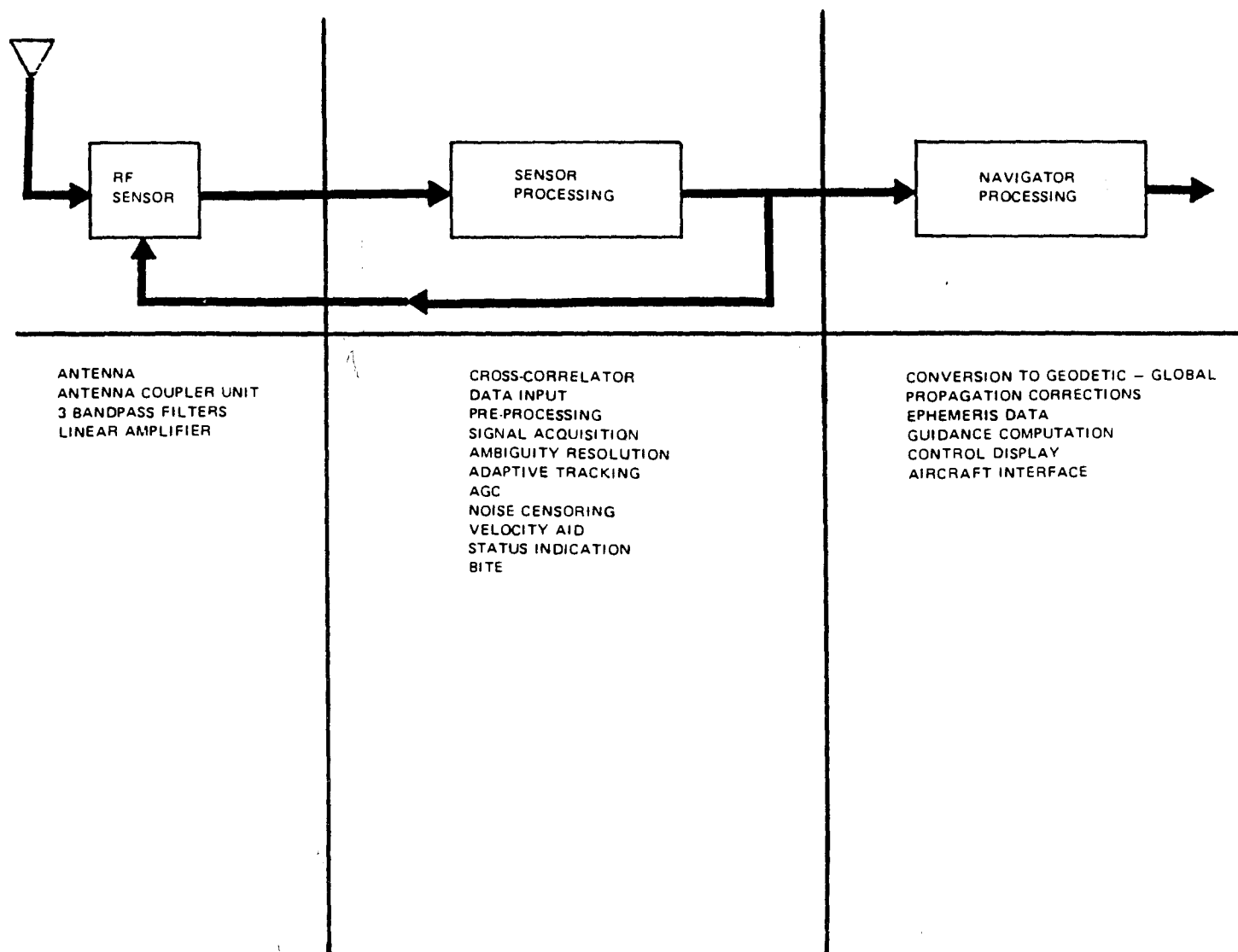


Figure 12. Omega User Equipment Functional Requirements

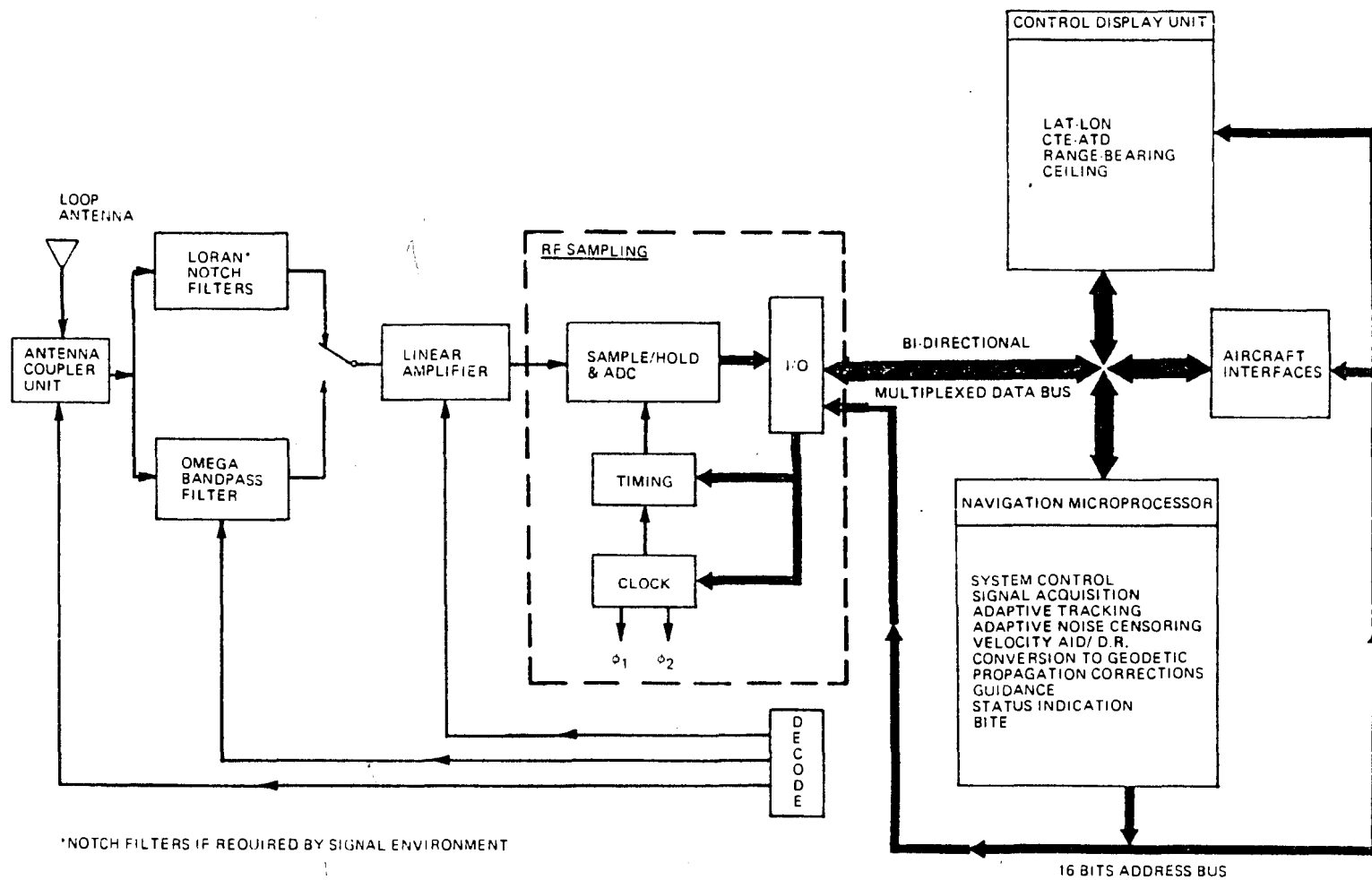


Figure 13. Combined Loran/Omega Navigational Set

With a vertically polarized electric field, loop antennas present the additional complication that two crossed loops must be used, and not only must properly timed loop switching between loops be generated, but properly timed polarity switching for each loop must also be generated. To accomplish this switching, relative heading and station bearing must be known. However, because of the firm statement made by many experimenters that loop antennas have given appreciably better performance than whip antennas in the presence of P-static, the loop antenna has been selected.

Using the best available low noise transistor and an antenna coupler input circuit which is simultaneously correctly optimized for signal-to-noise ratio and can also be switched between crossed loops with a resulting phase change of less than 1.5 degrees, it is found that for a Loran signal of $20\mu\text{v/m}$ to produce a 1:1 carrier-to-thermal-noise ratio in a 20 KHz bandwidth a surface mounted ferrite core loop antenna one inch high and seven inches square is required.

With a correctly designed Omega ACU this same ferrite loop will produce a 1:1 carrier-to-thermal-noise ratio in a 100 Hz bandwidth when receiving $10\mu\text{v/m}$ at any Omega frequency between 10.2 KHz and 13.6 KHz.

In the interest of cost reduction it is desirable to develop a single input circuit that optimally handles both Loran and Omega, and provides the previously stated sensitivities that were considered separately. This can be provided in a single doubly-resonant input circuit.

Because of the fundamental fact that VLF and LF receiving antennas are generators with reactive output impedances it is necessary to properly absorb this generator into the filter to achieve proper filtering with no resulting signal losses. For either antenna a single pole doubly-resonant filter which simultaneously resonates the reactive antenna at both Omega and Loran frequencies with single pole selectivity can be provided. Further, to obtain the previously stated carrier-to-noise ratio, the antenna circuitry must be transformed to present the correct equivalent generator impedance to the input low noise transistor. Implementation of this design approach will provide the previously stated sensitivities in accordance with the requirements of each system.

As delineated in the previous sections, the architecture of a microcomputer set permits continuous and cyclic use of a minimum of hardware to perform arithmetic, logic and control operations. The important issues not discussed thus far were how the functional requirements for a combined Loran/Omega navigator could be mechanized into microprograms, and could the real-time processing requirements be satisfied?

The functional requirements have been deduced for the combined system and to provide a navigator as configured in figure 13. A timing analysis has been performed and it has been

demonstrated that the selected micro computer set shown in figure 1 can provide the processing required for either a Loran or Omega navigator. The functional requirements have been sized and the memories requirements are delineated in table 3.

Table 3. Software Sizing for Intel 8080 (8 Bits/Word)

Function	ROM	RAM
Omega	2,000	500
Loran	4,000	800
Propagation Model	2,000	200
Coordinate Converter	3,000	200
Steering	400	50
Control/Display	2,500	100
Control and System Subroutines	3,000	—
Total	16,900	1,850

It has been demonstrated on the Loran feasibility model that the real-time processing requirements can be satisfied with off-the-shelf semiconductor technology.

The previous sizing demonstrates that the memory requirements can be provided with state-of-the-art semiconductor memories and it will be shown in the next section that the cost to provide a complete navigator is a small percentage of the total system cost.

COST ANALYSIS AND TECHNOLOGY TRENDS

Microprogramming of the selected configuration will provide a navigational processor with a most useful characteristic, that of enabling a system designer to adapt standard hardware to specific applications. The designer can also obtain high computing efficiencies with microprograms specifically mechanized for the application. The capability to adapt a standard set of hardware to the various levels of complexity required combines the cost advantage of high-volume chip production with the computing efficiency of microprograms mechanized for navigation processing.

In addition to the previously stated advantages which provide the potential for low-cost today, the trends in this MOS/LSI technology must be examined. Due to volume production,

a yearly price reduction can be projected. Coupled with this price decrease, is the placement of more processing power, more read-only-memory, and more random access memory on a single semiconductor chip and within one IC package. From this second consideration, a further price reduction can be projected.

A measure of the performance of a CPU is the execution time for arithmetic operations. Consider the addition time for two 16-bit words; the access time for the two operands, the add time, and the time to return the sum to one of the original sources are included in this execution time. The performance projection for this addition time for two 16-bit words in the 1975 to 1976 time frame is 2 usec. The evolution to this 16-bit CPU is shown in figure 14.

Semiconductor memories are ideally suited to large-scale-integration onto monolithic MOS chips. Applications for these devices continue to expand which assures continued growth and high volume production. The repetitive structure of the memory element is well suited to automated design and manufacturing techniques and the extensive market allows a concentrated engineering effort to optimize chip design and to provide a highly reliable unit.

By combining performance of manufacturers of compatible chip sets for microcomputers, and considering the projected trends of the MOS technology, the bits per chip for semiconductor memories is projected in figure 14.

An important objective of our technology assessment study was to determine the impact of this technology on the cost of a combined Loran/Omega microprocessor navigator. Consequently, a complete radio navigator set was configured, partitioned into modules or printed circuit boards, and a recurring cost estimate and projection was made. The estimate was based on the following premises: space for the unit would not be at a premium; off-the-shelf MCS and random logic elements would be used; standard packaging techniques would be employed; automatic assembly and checkout would be used. The projected cost reduction was based on the benefits to be derived from the technology trend.

The results of this study demonstrate that, for the case considered the projected production recurring cost for a complete airborne Loran-C/Omega Navigator will be between \$8K and \$15K (Figure 14). It can be further projected that the cost of a navigator with worldwide capability will be less than \$10K before 1977.

Significant reduction in the non-recurring development cost of future radio navigation systems is also predicted due to the flexible modular nature of the software and hardware.

The cost of the navigator functions: latitude-longitude conversion, steering, control display, propagation corrections and dead-reckoning capability are also demonstrated. This projection clearly demonstrates that the cost of the navigator function using this semiconductor technology is a small percentage of the system cost, and further cost saving is most likely to be obtained by simplification and integration of the peripheral items.

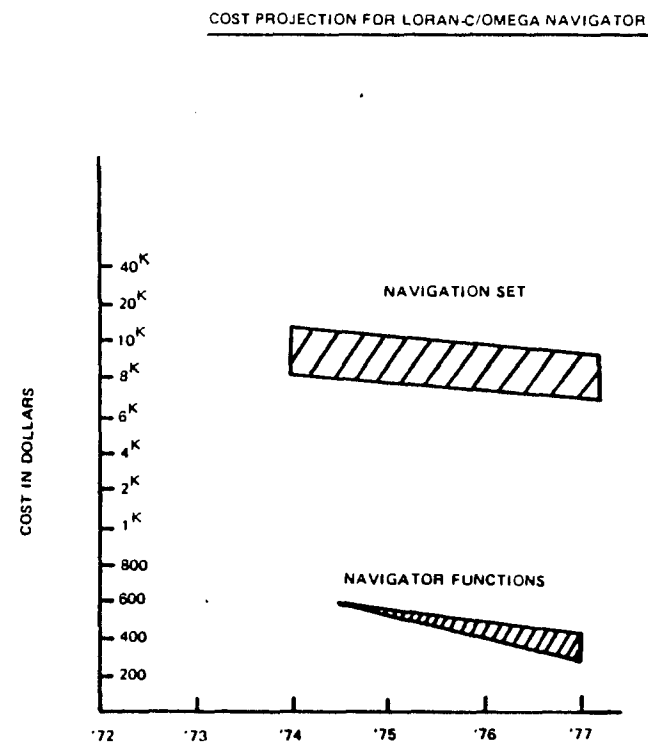
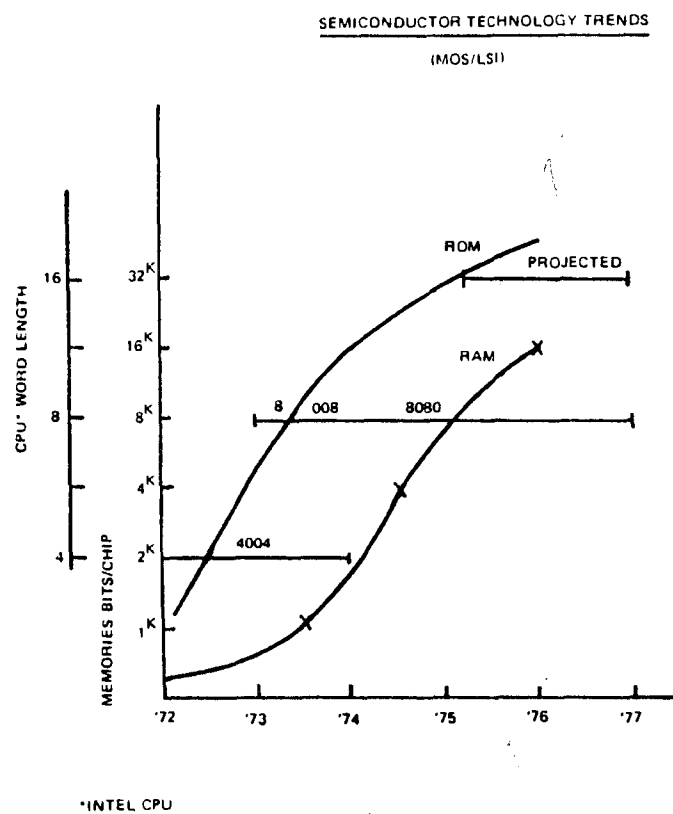


Figure 14. Technology and Cost Projections

In summary, figure 14 shows that the stated cost objectives for radio navigator can be achieved, and the projection further shows that advances in MOS/LSI semiconductor technology offers the potential for a continuing cost reduction.

ACKNOWLEDGEMENT

This paper summarizes a design study and development of a Loran feasibility model by ITT Avionics Division, Advanced Technology Navigation Microprocessor Department.

The authors would like to acknowledge the contributions of R. Apsel, D. Fredericks and D. Ott to development of the Loran model, and the contribution of M. Dishal and R. Reilly on combined Loran/Omega.

REFERENCES

1. John G. Busharis and Arthur R. Tuppen, "Low Cost Navigation Processing, Proceeding of the Radio Navigation Symposium", Sponsored by the Institute of Navigation, 13-15 Nov. 1973.
2. Robert A. Reilly, "Combined Loran-Omega Receiver," Proceedings of the Radio Navigation Symposium, Sponsored by the Institute of Navigation, 13-15 Nov. 1973.
3. James P. Van Etten, "Navigation Systems: Fundamentals of Low- and Very-Low-Frequencies Hyperbolic Techniques," ITT Avionic Division Technical Report, Sept. 1970.
4. Robert H. Cushman, "The Intel 8080: First of the Second-Generation Microprocessors," EDN MP Design Series, May 5, 1974.
5. MC8-8 Micro-Computer Set, Intel Publications, Intel Corp., Santa Clara, Calif., March 1973, 8008 Rev 3, and 8080 preliminary specification Rev 3.
6. "Omega - A World-Wide Navigation System," AD No. 630900.

FILE COPY

3-6

PREPRINT

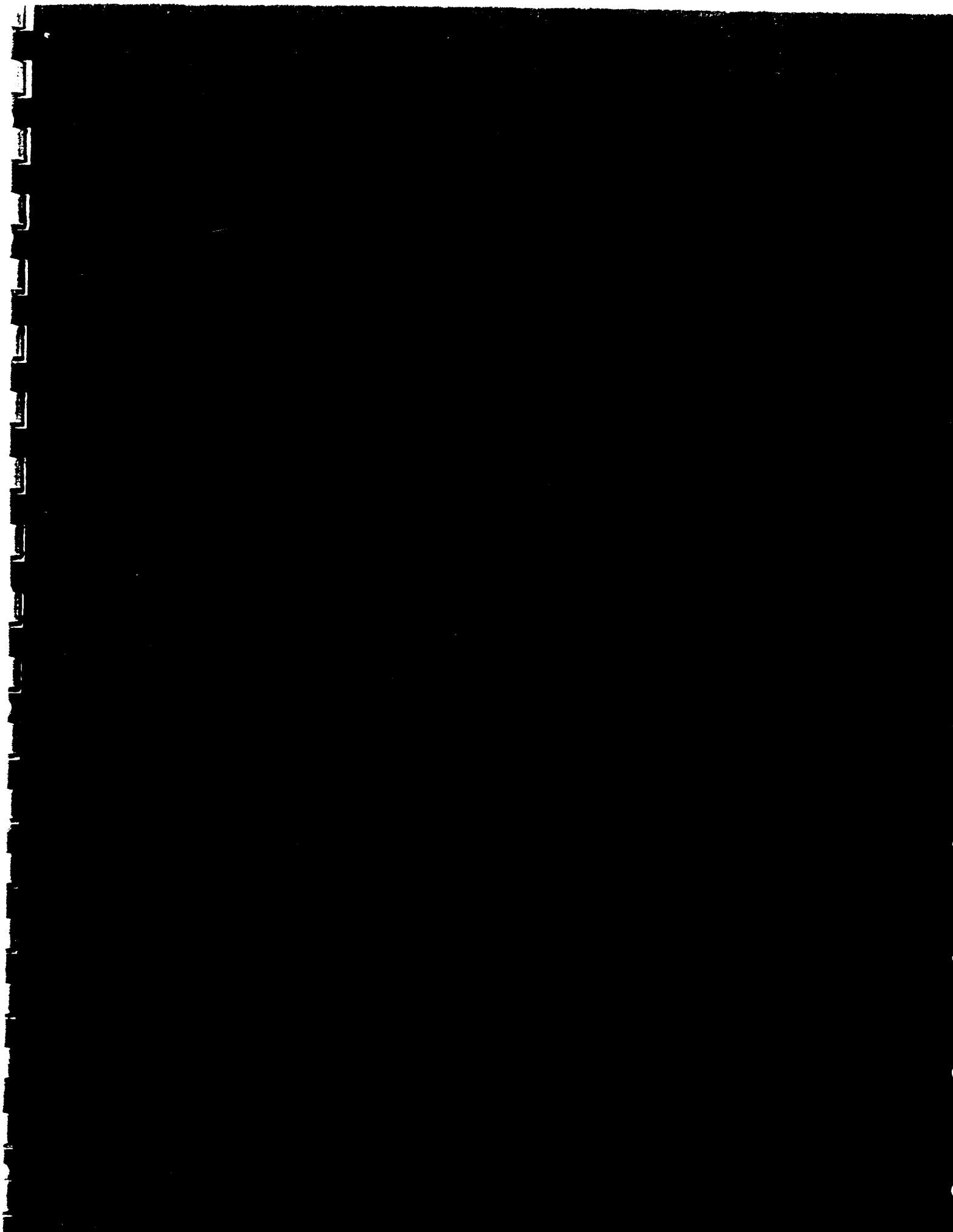
PREPARED FOR PRESENTATION
AT THE
THIRD ANNUAL CONVENTION
OF THE
WILD GOOSE ASSOCIATION
McAFEE, NEW JERSEY
2-4 OCTOBER 1974

REPORT ON GETTYSBURG WORKSHOP

BY

LEO F. FEHLNER

MEMBER, BOARD OF DIRECTORS
WILD GOOSE ASSOCIATION



INTRODUCTION

ON THE 14TH OF JANUARY THIS YEAR, A GROUP OF PEOPLE MET IN MY OFFICE AT THE APPLIED PHYSICS LABORATORY TO DISCUSS THE POTENTIAL OF LORAN-C AND PROBLEMS ATTENDANT ON THE EXPANSION OF LORAN-C RADIO NAVIGATION SERVICE. ONE OF THE PROBLEMS WHICH WE SURFACED FOR DISCUSSION WAS A COMMUNICATION GAP WHICH SEEMS TO EXIST BETWEEN USERS OF LORAN-C AND THE DESIGNERS AND PROVIDERS OF THE SERVICE. REAR ADMIRAL JAMES MOREAU, CHIEF OF THE OFFICE OF ENGINEERING OF THE COAST GUARD, DESCRIBED A PREVIOUS EXPERIENCE OF HIS, IN WHICH A THREE DAY WORKSHOP HAD BEEN USED EFFECTIVELY TO BRING EVERYBODY UP TO SPEED ON THE PROBLEMS OF BREAKING ICE WITH AN OIL TANKER. WE CONCURRED THAT SUCH A WORKSHOP COULD GO A LONG WAY TOWARD PLUGGING THE COMMUNICATIONS GAP IN THE LORAN COMMUNITY, AND IT WAS SUBSEQUENTLY DECIDED TO EXPLORE THE JOINT SPONSORSHIP OF A LORAN-C WORKSHOP BY THE COAST GUARD AND THE WILD GOOSE ASSOCIATION.

AT A MEETING OF YOUR BOARD OF DIRECTORS HELD ON GOVERNORS ISLAND ON 16 JANUARY 1974, JIM MOREAU BRIEFED THE BOARD ON HIS CONCEPT OF A LORAN-C WORKSHOP. YOUR BOARD THEN UNANIMOUSLY APPROVED A MOTION TO OFFER TO THE DEPARTMENT OF TRANSPORTATION THE COOPERATION OF THE WILD GOOSE ASSOCIATION IN CONDUCTING A LORAN-C WORKSHOP. PRESIDENT HIGGINBOTHAM APPOINTED ME CHAIRMAN OF A COMMITTEE TO IMPLEMENT THE MOTION, AND IN DUE COURSE I BECAME A MEMBER OF THE STEERING COMMITTEE FOR THE WORKSHOP.

REFERENCE
REF 597
PAPER 3-6
PP 13 + 1
2890412

OTHER MEMBERS OF THE STEERING COMMITTEE WERE JOHN BEUKERS, JAMES CULBERTSON, DAVID HAISLIP, WILLIAM POLHEMUS, WILLIAM ROLAND, AND JAMES WALKER. JIM MOREAU WAS THE WORKSHOP CHAIRMAN AND GABRIEL FRENKEL WAS THE TECHNICAL COORDINATOR.

THE WORKSHOP WAS HELD IN GETTYSBURG, PA. ON THE 5, 6, AND 7 OF JUNE 1974, AND THE REST OF THE STORY IS NOW HISTORY RECORDED IN THE PROCEEDINGS. THE PUBLISHED PROCEEDINGS MAY BE PURCHASED FROM YOUR ASSOCIATION IN THE LOBBY.

SUMMARY OF THE WORKSHOP

ONE HUNDRED AND TWO PERSONS ATTENDED THE WORKSHOP, FIFTEEN WERE FROM USER GROUPS, 31 WERE FROM THE ELECTRONIC INDUSTRY, 16 WERE FROM THE U.S. GOVERNMENT OTHER THAN THE DEPARTMENT OF TRANSPORTATION, 9 WERE FROM FOREIGN GOVERNMENTS, 8 FROM MISCELLANEOUS OTHER GROUPS, E.G., LABORATORIES, PRESS, CONSULTANTS, AND 23 WERE FROM THE DEPARTMENT OF TRANSPORTATION.

AFTER A BRIEF PERIOD OF OPENING CEREMONIES, THE ATTENDEES WERE DIVIDED INTO SIX WORKING GROUPS. GROUP 1 WAS ASSIGNED THE TOPIC "USER NEEDS AND OPERATING TECHNIQUES" AND WAS CHAIRED BY BILL POLHEMUS. GROUP 2 WAS ASSIGNED "RECEIVER DEVELOPMENTS" AND CHAIRED BY LEO FEHLNER. GROUP 3 WAS ASSIGNED "CHARTING AND INFORMATION TRANSFER" AND WAS CHAIRED BY JOHN HANNA. GROUP 4 WAS ASSIGNED "NATIONAL/INTERNATIONAL ASPECTS" AND WAS CHAIRED BY DAVE HAISLIP. GROUP 5 WAS ASSIGNED "HARBOR AND ESTUARY NAVIGATION USING LORAN-C" AND WAS CHAIRED BY BOB DOHERTY. GROUP 6 WAS ASSIGNED "ANCILLARY LORAN-C APPLICATIONS" AND WAS CHAIRED BY JOHN BEUKERS.

THE TANGIBLE RESULTS OF THE WORKSHOP ARE THE WORKING PAPERS SUBMITTED BY THE WORKING GROUPS. THESE, HOWEVER, BY NO MEANS REPRESENT THE ONLY BENEFITS. THERE WAS UNIVERSAL AGREEMENT THAT THE OPPORTUNITY FOR DIRECT CONTACT, DISCUSSIONS AND EXCHANGE OF IDEAS WAS AN EQUALLY IMPORTANT BENEFIT. THE WIDE VARIETY OF THE AFFILIATIONS AND INTERESTS OF THE PARTICIPANTS ALLOWED EVERYBODY A BETTER APPRECIATION OF THE POINT OF VIEW OF THOSE WITH A DIFFERENT INTEREST. TO GIVE ONLY TWO EXAMPLES: THE OPPORTUNITY TO RECEIVE A FIRSTHAND ACCOUNT OF THE PROBLEMS AND CONSTRAINTS UNDER WHICH A FISHERMAN OPERATES WAS INVALUABLE TO EQUIPMENT MANUFACTURERS AND TO THOSE INVOLVED IN SYSTEM PLANNING. THE WORKING GROUP ON NATIONAL/INTERNATIONAL ASPECTS, WITH REPRESENTATIVES FROM NORWAY, GREAT BRITAIN, ICELAND, DENMARK AND CANADA, OFFERED A FORUM IN WHICH THESE REPRESENTATIVES COULD BE ADVISED DIRECTLY OF U.S. PLANS AND, IN TURN THEY COULD EXPRESS THEIR OPINIONS AS TO THE IMPACT OF THESE PLANS ON THEIR OWN OPERATIONS.

PRINCIPAL RECOMMENDATIONS

THE FOLLOWING MAJOR RECOMMENDATIONS WERE FORMULATED BY THE VARIOUS WORKING GROUPS:

LORAN-A SHOULD BE EXTENDED BY 5 YEARS. CONCURRENT LORAN-A/LORAN-C OPERATION IS NEEDED FOR ORDERLY DATA CONVERSION BY USERS,

ORDERLY EQUIPMENT DEVELOPMENT AND TO MINIMIZE ECONOMIC HARDSHIP THROUGH FORCED OBSOLESCENCE.

A LORAN USERS ADMINISTRATIVE COUNCIL SHOULD BE ESTABLISHED FROM MEMBERS OF THE INDUSTRY, USERS AND THE COAST GUARD. ITS ROLE WOULD BE TO PROVIDE GUIDANCE REGARDING NEEDS, PROCEDURES AND POLICIES TO ALL AFFECTED PARTIES.

THE USCG SHOULD PREPARE A DETAILED STUDY OF THE COST IMPACT ON DOT OF THE CONTINUING OPERATION OF THE LORAN-A CHAINS.

DISCUSSIONS AND COORDINATION SHOULD BE HELD WITH THE CANADIAN AND MEXICAN GOVERNMENTS ON IMPLEMENTATION SCHEDULES AND THE LOCATION OF STATIONS. IN ADDITION, MODIFICATIONS TO THE PLANS FOR IMPLEMENTATION ARE SUGGESTED.

A SET OF MINIMUM STANDARDS FOR LORAN-C RECEIVERS SHOULD BE ESTABLISHED, TO SERVE THE INTERESTS AND REQUIREMENTS OF THE USER COMMUNITY.

THE COAST GUARD SHOULD ORGANIZE A LORAN-C RECEIVER SYMPOSIUM TO ASSIST THOSE LORAN-A MANUFACTURERS WHO WISH TO ADD LORAN-C TO THEIR CAPABILITY.

SKYWAVES SHOULD BE USED TO EXTEND COVERAGE. INTRACHAIN RATHER THAN INTRASTATION HYPERBOLIC LINES SHOULD BE USED FOR SKYWAVE NAVIGATION.

MANY CHARTS NOW HAVING LORAN-C CURVES, BUT LIMITED TO DEFENSE DEPARTMENT USE, SHOULD BE MADE AVAILABLE FOR GENERAL SALE AFTER REMOVAL OF CLASSIFIED INFORMATION.

THE INSTITUTE OF NAVIGATION SHOULD SPONSOR AN INTERNATIONAL MEETING EARLY IN 1975 AS A MEANS OF EDUCATING THE USER COMMUNITY ON THE POTENTIALS OF HYPERBOLIC NAVIGATION SYSTEMS.

LORAN-C SHOULD BE CONSIDERED A MANDATORY REQUIREMENT FOR VESSELS WHICH REPRESENT A SPECIAL RISK FROM OIL SPILLS OR DEVIATIONS FROM SEA LANES.

THE LORAN-C SYSTEM DESIGN SHOULD BE FROZEN WITH RESPECT TO LORAN PULSE SHAPE, TRANSMISSION FORMAT, MODULATION SCHEME (IF ANY) AND GROUP REPETITION INTERVALS. THE COAST GUARD SHOULD ISSUE A SPECIFICATION ON THE LORAN-C SYSTEM THAT WILL ENABLE MANUFACTURERS OF USER EQUIPMENT TO DESIGN TO THE SPECIFICATION WITHOUT FEAR OF BEING OBSOLETE BY SYSTEM CHANGES.

THE COAST GUARD SHOULD DEVELOP REGULATORY POLICIES IN THE FOLLOWING AREAS: MAKING NAVIGATION EQUIPMENT MANDATORY, DEVELOPING CRITERIA FOR DOING SO FOR VARIOUS VESSELS, SETTING UP EQUIPMENT PERFORMANCE STANDARDS, DEVELOPING MEASURES FOR INSPECTION AND COMPLIANCE ASSURANCE, INITIATING NOTIFICATIONS AND HEARINGS, AND COORDINATING THESE MEASURES WITH APPROPRIATE U.S. AND INTERNATIONAL ORGANIZATIONS.

IN ADDITION, THE FOLLOWING INDIVIDUAL RECOMMENDATIONS WERE SUBMITTED:

GOVERNMENT FUNDING SHOULD BE MADE AVAILABLE FOR THE DEVELOPMENT OF SOLID-STATE DEVICES NECESSARY TO PRODUCE LORAN-D RECEIVERS. DEVICES PRODUCED AS A RESULT OF SUCH FUNDING SHOULD BE MADE AVAILABLE TO MANUFACTURERS WISHING TO PURCHASE THEM.

THE EAST COAST CHAIN, ALASKAN CHAIN, HAWAIIAN CHAIN AND GULF CHAIN SHOULD BE ASSIGNED GROUP REPETITION INTERVALS FROM THE EXISTING STRUCTURE. THE WEST COAST AND GREAT LAKES CHAINS AND ADDITIONAL INLAND COVERAGE SHOULD BE ASSIGNED GRIs FROM THE NEW STRUCTURE.

THE FOLLOWING UNSIGNED RECOMMENDATIONS WERE SUBMITTED BY ONE AUTHOR ON HARBOR NAVIGATION:

LORAN-C SHOULD NOT BE INTEGRATED INTO THE VESSEL TRAFFIC SYSTEM EXCEPT WHEN REQUIRED.

LORAN-C RECEIVER MARKETTERS SHOULD BE REQUIRED TO FURNISH INSTRUCTIONS FOR SELF-CALIBRATION OF INDIVIDUAL HARBORS.

LOCALLY USED TIME DIFFERENCES SHOULD BE MONITORED BY THE COAST GUARD AT ONE CRITICAL POINT FOR EACH HARBOR AND OBSERVED CHANGES/ERRORS BROADCAST.

SUMMARY OF WORKING PAPERS

THE WORKING PAPERS GENERATED FALL INTO TWO BROAD CATEGORIES: THOSE AUTHORED BY THE ENTIRE WORKING GROUP OR A SUBSTANTIAL PART OF IT AND THOSE GENERATED BY A SUBGROUP OR AN INDIVIDUAL.

WORKING GROUP NO. 1 - USER NEEDS AND OPERATING TECHNIQUES

THE WORKING GROUP ADDRESSED AND GENERATED PAPERS ON SIX MAJOR TOPICS:

CHRONOLOGY OF COAST GUARD PLANS FOR LORAN-C SYSTEM PHASE-IN.

ITEMS DISCUSSED INCLUDED: THE IMPLEMENTATION SCHEDULE, COVERAGE AREAS OFFERED, NEAR-TERM SCHEDULE OF CHART PREPARATION, DEFINITION OF THE TERMINOLOGY FOR "ACTIVATION OR OPERATIONAL STATUS" AND DISCUSSION OF THE PROBLEM OF FISHING GEAR HANGUPS IN THE GULF OF MEXICO. ON THE LAST SUBJECT, SOME RECOMMENDATIONS WERE GENERATED: SPECIFICALLY, TO USE AVAILABLE BOTTOM SURVEY DATA (SHADOW GRAPHS) OR TO INITIATE ADDITIONAL SURVEYS AND THEREBY ESTABLISH THE GEOGRAPHICAL LOCATION OF HANGUPS.

USER REQUIREMENTS AND COMMENTS RELATIVE TO TRANSITION TO LORAN-C. ITEMS DISCUSSED INCLUDED THE PROBLEMS OF TRANSITION (TECHNICAL, OPERATIONAL AND ECONOMIC). IT WAS RECOMMENDED THAT USCG PREPARE A STUDY OF THE COST IMPACT OF LORAN-A SHUTDOWN. A REVIEW AND CRITIQUE OF THE PROPOSED COVERAGE AND IMPLEMENTATION PLAN WERE ALSO OFFERED.

CATEGORIZATION OF USERS AND THEIR REQUIREMENTS FROM THE USER POINT OF VIEW. ITEMS DISCUSSED INCLUDED A BREAKDOWN OF USERS BY CATEGORY AND THE LISTING OF THE KIND OF NAVIGATION NEEDED. THE OUTPUT FORMAT AND EQUIPMENT COST FOR EACH CATEGORY WERE ALSO INCLUDED.

DEFINE CATEGORIES OF LORAN RECEIVERS FROM THE USERS' POINT OF VIEW. ITEMS DISCUSSED INCLUDED A TUTORIAL DESCRIPTION OF THE VARIOUS TYPES OF RECEIVERS -- FOR EXAMPLE, ENVELOPE VERSUS CYCLE TRACKING -- AND A SUMMARY OF THE DIFFERENCES BETWEEN LORAN-A AND LORAN-C RECEIVERS.

EVALUATION OF SPECIAL CHARACTERISTICS OF LORAN-C FROM THE USERS' POINT OF VIEW. ITEMS DISCUSSED INCLUDED A SUMMARY OF THE PRINCIPAL CHARACTERISTICS OF LORAN-C FROM THE USERS' POINT OF VIEW, NAMELY THE REASONS FOR THE ACCURACY AND LACK OF AMBIGUITY. ALSO INCLUDED ARE A DESCRIPTION OF THE BASIC BUILDING BLOCKS OF A RECEIVER AND DISCUSSIONS OF THE OPERATION NEAR OBSTRUCTIONS (SUCH AS BRIDGES), THE TEMPORAL EFFECTS THAT CAUSE TIME DIFFERENCE VARIATIONS, AND THE DIFFERENCE BETWEEN A PHASE-LOCKING AND AN ENVELOPE-TRACKING RECEIVER. MANY USER QUESTIONS WERE ANTICIPATED AND ANSWERED. GENERATION OF A SET OF MINIMUM STANDARDS FOR LORAN-C RECEIVERS WAS RECOMMENDED.

FORMATION OF A LORAN USER ADMINISTRATIVE COUNCIL. ITEMS DISCUSSED INCLUDED A LORAN USERS' ADMINISTRATIVE COUNCIL TO BE FORMED FROM MEMBERS OF INDUSTRY, USERS AND DoT (USCG). ITS OBJECTIVE WOULD BE TO PROVIDE GUIDANCE TO ALL INTERESTED PARTIES ON USER NEEDS, PROCEDURES, POLICIES AND OTHER RELEVANT MATTERS.

WORKING GROUP NO. 2 - RECEIVER DEVELOPMENT

THE PRINCIPAL TOPICS DISCUSSED BY THIS GROUP RELATED TO THE CATEGORIZATION OF RECEIVERS AND THE IMPACT OF THE TRANSITION FROM LORAN-A TO LORAN-C, WITH THE FOLLOWING RESULTS:

THERE APPEARS TO BE NO WAY TO CATEGORIZE RECEIVERS WHICH IS BOTH DEFINITIVE AND USEFUL TO THE COMMUNITY. RECEIVERS OF ANY FUNCTIONAL SOPHISTICATION CAN BE BUILT.

BOTH THE SHORT- AND LONG-RANGE EQUIPMENT TRENDS IN PERFORMANCE AND COST WERE PROJECTED.

A SPECIFICATION IN PRECISE NUMERICAL TERMS WAS DEVELOPED FOR A MINIMUM PERFORMANCE, LOW-COST LORAN-C RECEIVER SUITABLE FOR THE SAME KIND OF USE TO WHICH MINIMAL LORAN-A RECEIVERS HAVE BEEN PUT. THIS OUTPUT PROMPTED TWO DISSENTS: THAT THE POTENTIAL OF LORAN-C IS DILUTED THEREBY, AND THAT MICROPROCESSOR TECHNOLOGY WITHIN A FEW YEARS WILL ALLOW A HIGHER PERFORMANCE AT LOW COST.

THE PROBLEM OF GROUP REPETITION INTERVAL MANAGEMENT FROM BOTH THE RECEIVER AND ASSIGNMENT POINT OF VIEW WAS DISCUSSED. A RECOMMENDATION WAS MADE THAT A 4-DIGIT CODE BE ADOPTED TO IDENTIFY THE GRI.

A RECOMMENDATION WAS MADE BY A NUMBER OF PARTICIPANTS TO EXTEND THE LORAN-A OPERATION TO 1985 TO REDUCE THE ECONOMIC IMPACT ON USERS.

A RECOMMENDATION WAS MADE FOR A LORAN-C RECEIVER TECHNICAL SYMPOSIUM TO BE ORGANIZED BY THE COAST GUARD.

WORKING GROUP No. 3 - CHARTING AND INFORMATION TRANSFER

AFTER REVIEWING PRESENT PRACTICES, THE GROUP DISCUSSED AT LENGTH THE VARIOUS ASPECTS OF CHARTING AND ISSUED A LENGTHY PAPER COVERING THE FOLLOWING TOPICS.

THE GENERAL NEED FOR LORAN-C CHARTS. ITEMS DISCUSSED INCLUDED: THE REASON FOR CHART REQUIREMENTS BY THE VARIOUS USER GROUPS, THE COVERAGE AND THE DETAILS TO BE ON THE CHARTS. CHARTS OF LIMITED DISTRIBUTION SHOULD BE MADE AVAILABLE TO THE GENERAL PUBLIC (AFTER APPROPRIATE EDITING). SPECIAL CHARTS WILL BE REQUIRED FOR A NUMBER OF APPLICATIONS, SUCH AS URBAN VEHICLES AND TRADITIONAL FISHING GROUNDS.

CHART SCALE AND DETAILED ACCURACY STANDARDS WERE PRESENTED IN NUMERICAL TERMS.

ADDITIONAL SECONDARY FACTOR CORRECTION SHOULD BE INCORPORATED INTO THE CHARTS. TECHNOLOGY PERMITS KEEPING THE CALIBRATION MEASUREMENTS TO A MINIMUM AND OBTAINING THE ASF CORRECTIONS THROUGH CALCULATIONS.

THE USE OF SKYWAVES IS USEFUL IN EXTENDING LORAN-C RANGE, AND SHOULD BE CONSIDERED. SKYWAVE LINES OF POSITION WITH SECONDARY PHASE CORRECTIONS SHOULD BE PRINTED ON CHARTS. ALSO LINES OF POSITION BETWEEN CHAINS SHOULD BE CONSIDERED.

THE ONLY VALID APPROACH TO CHART CONVERSION FROM LORAN-A TO LORAN-C IS THROUGH A POINT-BY-POINT COMPARISON BY THE FISHERMAN. THIS PROCEDURE WILL TAKE AT LEAST 5 YEARS, HENCE RETAINING LORAN-A FOR THIS PERIOD IS NECESSARY.

WORKING GROUP NO. 4 - NATIONAL/INTERNATIONAL ASPECTS

THE WORKING GROUP WAS SUBDIVIDED INTO THREE SUBGROUPS ON INTERNATIONAL USE, NATIONAL USE AND THE ORGANIZATION OF AN INTERNATIONAL MEETING. THE FOLLOWING TOPICS WERE COVERED:

NEED FOR COMMUNICATION. ON THE NATIONAL LEVEL, THE PUBLIC AWARENESS PROGRAM, BY PROMOTING BETTER UNDERSTANDING OF LORAN-C, EASES THE TRANSITION FROM LORAN-A. ADDITIONAL EFFORTS THROUGH THE TRADE JOURNALS WOULD ALSO BE BENEFICIAL. ON THE INTERNATIONAL LEVEL, IT WAS SUGGESTED THAT AN INTERNATIONAL MEETING BE SPONSORED BY THE INSTITUTE OF NAVIGATION IN EARLY 1975. THIS WILL BOTH EDUCATE THE USERS AND GIVE AN OPPORTUNITY TO DETERMINE THEIR NEEDS.

REGULATORY ASPECTS. IT WAS DISCUSSED WHICH CLASS OF VESSELS SHOULD BE REQUIRED TO CARRY LORAN-C EQUIPMENT, MINIMUM PERFORMANCE STANDARDS OF SUCH EQUIPMENT, INSPECTION AND COORDINATION THROUGH INTERNATIONAL BODIES.

INTERFERENCE AND FREQUENCY CONVERSION. SIGNAL FORMATS, SITE LOCATIONS AND CONTROL OF OTHER SERVICES SHOULD BE INTERNATIONALLY REGULATED. MINIMUM CRITERIA FOR LICENSING COMMERCIAL MINICHAINS WERE FORMULATED.

CONSIDERATIONS RELATING TO EQUIPMENT AND SYSTEM COMPATIBILITY. WITH THE PLANNED EXTENSION OF LORAN-C WORLDWIDE, COMPATIBILITY OF SYSTEMS AND EQUIPMENT MUST BE ESTABLISHED. COMPATIBILITY

CONSIDERATIONS SHOULD EXTEND TO SUPPLEMENTARY FEATURES, SUCH AS POLLING THROUGH A DATA LINK.

WORKING GROUP No. 5 - HARBOR AND ESTUARY NAVIGATION USING LORAN-C

THERE WERE A NUMBER OF INDIVIDUAL PAPERS DEVOTED TO VARIOUS ASPECTS OF THE PROBLEM; IN SOME INSTANCES MORE THAN ONE PAPER WAS GENERATED, SOMETIMES EXPRESSING CONFLICTING POINTS OF VIEW:

HARBOR AND ESTUARY NAVIGATION SYSTEM IMPLEMENTATION. FIVE PAPERS DEALT WITH VARIOUS ASPECTS OF THE PROBLEM, NAMELY THE USE FOR LORAN-C IN THE HARBOR AND ESTUARY ENVIRONMENT, DATA RETRANSMISSION FOR TRAFFIC CONTROL, SYSTEM FEATURES (DISPLAY, PROCESSING, CONTROLLER), TRAFFIC CONTROL ASPECTS AND THE NEEDS OF THE INDIVIDUAL PILOT.

INTERIM APPROACHES. A PORT-BY-PORT SOLUTION WAS INDICATED, WHICH SHOULD BE CARRIED OUT BY THE INDIVIDUAL PORT AUTHORITIES. RECEIVER MANUFACTURERS SHOULD FURNISH INSTRUCTIONS FOR SELF-CALIBRATION OF INDIVIDUAL HARBORS. THE U.S. COAST GUARD SHOULD MONITOR LOCALLY USED TIME DIFFERENCES AND BROADCAST CORRECTIONS.

CALIBRATION AND NAVAID POSITIONING. VARIOUS TECHNIQUES, SUCH AS LOCATION OF RANGE MARKERS AND GENERATION OF CORRECTED CHARTS THROUGH A TRACK PLOTTER, WERE DISCUSSED IN TWO PAPERS.

EXTENDED LORAN-C CONFIGURATIONS. DIFFERENTIAL LORAN-C AND SHORT BASELINE LORAN-C WERE DISCUSSED IN TWO PAPERS. FOR DIFFERENTIAL LORAN-C, EXPERIMENTAL RESULTS WERE GIVEN, PROVIDING PERFORMANCE PROJECTIONS AND A SCENARIO FOR THE USE OF SUCH A SYSTEM. CONTINUATION OF EXPERIMENTS TO OBTAIN ADDITIONAL RESULTS WAS PROPOSED.

WORKING GROUP No. 6 - ANCILLARY LORAN-C APPLICATIONS

IN ADDITION TO SUBMISSIONS IN FIVE SPECIFIC ANCILLARY AREAS (OTHER THAN ROUTINE NAVIGATION ON WATER) A PAPER WAS GENERATED ON SYSTEM ASPECTS OF LORAN-C.

SYSTEM ASPECTS OF LORAN-C. THE NEED FOR STANDARDIZATION AND FINALIZATION OF LORAN-C FORMAT IS STRESSED. THIS SHOULD INCLUDE: TRANSMISSION FORMAT AND GROUP REPETITION INTERVALS. OTHER SYSTEM ASPECTS TO BE CONSIDERED INCLUDE REDUCTION OF SYNCHRONOUS AND CROSSRATE INTERFERENCE, CLEARANCE OF OTHERS FROM THE LORAN-C BAND, AND ESTABLISHMENT OF TRANSMITTER LOCATIONS.

USE OF LORAN-C FOR COMMUNICATIONS. EXISTING LORAN-C COMMUNICATIONS SYSTEMS, BROADCASTING OF TIMING CORRECTIONS, GENERAL PURPOSE BROADCAST AND THE EFFECT OF MODULATION ON THE NAVIGATION FUNCTION ARE DISCUSSED.

AIRCRAFT NAVIGATION. GENERAL REQUIREMENTS, LORAN-C AS A SUBSTITUTE FOR VORTAC, ITS OPERATION IN NON-VORTAC AND NON-ILS AREAS, EXPECTED PERFORMANCE, USER EQUIPMENT REQUIREMENTS AND RECEIVER ENHANCEMENTS ARE DISCUSSED.

LAND USE. REQUIREMENTS FOR CENSUS TAKING, CARS AND TRAINS, AND SYSTEM ASPECTS, SUCH AS FREQUENCY ALLOCATIONS, GRID DISTORTIONS AND GRID CORRECTIONS AND SIGNAL ENHANCEMENTS THROUGH MINICHAINS, ARE DISCUSSED. RECOMMENDATIONS FOR CONSIDERING THE IMPACT OF LAND-BASED APPLICATIONS IN THE COAST GUARD PLANS ARE ALSO GIVEN.

LORAN-C RETRANSMISSION SYSTEMS. A LARGE NUMBER OF AREAS NECESSITATING FURTHER STUDY WERE IDENTIFIED. THESE INCLUDE THE USE OF SUPPLEMENTAL SIGNALS (E.G., OMEGA), DIFFERENTIAL SKYWAVE/GROUNDWAVE EFFECTS, TELEMETRY SYSTEM PROBLEMS AND SKYWAVE PREDICTION. ADVANTAGES AND DRAWBACKS OF LORAN-C FOR THIS APPLICATION ARE DISCUSSED.

SCIENTIFIC APPLICATIONS. TIMING, GEODESY AND RADIOWAVE PROPAGATION WERE DISCUSSED IN ONE PAPER. A SEPARATE PAPER DISCUSSED APPLICATIONS TO WEATHER MONITORING.

CONCLUSION

AT THIS POINT, YOU MUST AGREE THAT A RATHER IMPRESSIVE ARRAY OF TOPICS WERE CONSIDERED DURING THE WORKSHOP. WHEN I REFLECT ON THE WORKSHOP, I AM UTTERLY AMAZED THAT SO MANY TOPICS COULD BE TREATED IN CONSIDERABLE DEPTH IN THREE DAYS. IT CERTAINLY ATTESTS TO THE QUALITY OF THE EXPERTISE OF ALL 102 THAT WERE ASSEMBLED IN GETTYSBURG LAST SPRING. I FOUND THE WORKSHOP A VERY REWARDING EXPERIENCE, AND I'M SURE MANY OTHERS DID ALSO.

ON BEHALF OF THE WILD GOOSE ASSOCIATION, WE WISH TO EXPRESS OUR APPRECIATION FOR THE OPPORTUNITY TO COOPERATE WITH THE DEPARTMENT OF TRANSPORTATION IN THE SPONSORSHIP OF THE WORKSHOP. SPECIAL THANKS FROM ALL PARTICIPANTS ARE DUE ADMIRAL MOREAU. HIS WAS THE SPARK THAT SET THE WHOLE THING OFF.

PREPRINT

PREPARED FOR PRESENTATION

AT THE

THIRD ANNUAL CONVENTION

OF THE

WILD GOOSE ASSOCIATION

McAFEE, NEW JERSEY

2-4 OCTOBER 1974

REPORT ON GETTYSBURG WORKSHOP

BY

LEO F. FEHLNER

MEMBER, BOARD OF DIRECTORS

WILD GOOSE ASSOCIATION

LORAN-C SPECTRUM: NAVIGATION AND COMMUNICATIONS

by

Carl S. Mathews
Commander U.S.C.G. (Ret.)
Engineering Consultant
Annandale, Virginia

and

Harold E. Englert
Senior Staff Engineer
Hartman Systems
Division of A-T-O Inc.
Huntington Station, New York

Comm 3

1974

#7

Veo F.

FETNER
REF 598
PB 13+1=14
PAPER 3-7
289042

hs

LORAN-C SPECTRUM: NAVIGATION AND COMMUNICATIONS

INTRODUCTION

In the early days of Loran-C, operators, designers, managers, and users were somewhat like blind men perceiving an elephant. The man who felt the elephant's leg likened the animal to a tree. The man who grabbed the elephant's tail considered the animal somewhat like a snake. The man who was showered by a water blast from the elephant's trunk said that the animal was like a water hose. One thing was certain to all. This was that the elephant, properly prepared, could be packaged and shipped in a spectrum box cubed 10 feet on a side. Each went home to await delivery of his box and to make preparations on the basis of what he had perceived. Each used appropriate advance publicity to herald the arrival of the marvelous new animal at each home zoo. For some of us, some 25 years later, we marvel at this "elephant" - Loran-C - and wonder at how we could have arrived at our first conclusions.

In most areas, early promises of the system have been fulfilled. The process has required massive changes in concept and performance standards for ground stations and user equipment. Revolutionary advancements in development of high power solid state devices provide us with entire new concepts for transmitting equipment. Similar changes in the arts of LSI circuitry, digital processing, and computer technology have led us to user equipment which exceeds even the early dreams of Loran-C inventors and proponents.

Spectrum and time are two absolutes in any physical system which provide the basic definitions and boundaries of performance. Spectrum can be neither created nor destroyed. Time passes. We can only allocate spectrum occupation and schedule time use. Our comprehensiveness in concept and cleverness in process design can provide a basis for improved utilization of spectrum and time. As reasonable scientists, engineers, managers, and users of spectrum and time, we must continually ask ourselves:

1. What are we doing now?
2. Why are we doing it this way?
3. Is there a better way?
4. How can we be better custodians of our privilege in allocation of spectrum and time?

Initial definitions of Loran-C navigation system parameters were made on the basis of meeting short-term requirements with existing technology. This initial phase of Loran-C development must be considered an exploitation phase. Currently new uses for navigation and positioning functions as well as other services demand conservative utilization of both time and frequency by the Loran-C system. Consideration of these elements is essential for the short-term survival of the system and long-term viability of expansion plans.

NAVIGATION REQUIREMENTS

The ground wave mode of propagation is essential for the precision required of the system for navigation and positioning. In order to assure transmission and utilization of this mode, signals must reach a useable amplitude before sky waves contaminate the desired signal. In order to improve signal-to-noise ratio and

to reject interfering signals, receiver bandwidth should be as narrow as rise time for sky wave rejection allows.

To reduce requirements for spectrum space, multiple stations must operate in the same band of frequencies. Accordingly time-sharing is required. Experience with Loran-A led logically to repetition rate discrimination. Desirability for increasing average power and providing station identification led to group pulsing and phase coding.

Acceptable antenna size and realizable transmitter capabilities imposed limits on bandwidth to carrier ratios of between 4:1 and 7:1. Accordingly, a center frequency between 70 kHz and 130 kHz appeared to be the best compromise, with a bandwidth as wide as could be sold on both a national and international basis.

ARTIFICIAL BOUNDARY PARAMETERS

Fortunately the frequency band from 90 kHz to 110 kHz had been allocated early to that system of navigation which was accepted as the International Standard Long Distance Aid-to-Navigation. In Region I (Europe) allocation of this band was subject to non-interference to other services operating in the band. In Region II (North and South America) this allocation was recognized and accorded priority status. In early equipment development and system implementation, significant problems were encountered in radiating a controlled spectrum conforming to the defined requirements of international agreements. These requirements, briefly stated below,

are:

1. 99% of energy radiated shall be contained within the allocated band.
2. No more than 1/2 of 1% of the energy shall be below, or above the allocated band.
3. No harmful interference shall be caused to any service operating outside the band.

Early in the program an ideal pulse shape was defined to be:

$$f(t) = \left[t/T_e - \alpha t/T \right]^2$$

This pulse shape and its spectrum are illustrated in Figure 1.

The pulse shape, if radiated, conforms to the requirements defined by the International Telecommunications Union (I. T. U.) and is pleasing to observe on monitor oscilloscopes at transmitting stations. Therefore, for the period from 1957 to 1962, this pulse shape was written into all specifications for transmitter procurement.

In two generations of tube transmitters, the pulse shape parameters were never completely met. In the AN/FPN-39/42 equipments the "Ideal Pulse" rise was approached, but the "Decay" parameters could be anyone's guess.

Field experience showed "tail" behavior to be a minor operational consideration, and cosmetic benefits of shape-purity were found to be observable only very close to a station in very "clean signal" conditions.

Equipment design of the AN/FPN-44/45 vintage led to radiation of a pulse shape which was nearly ideal. Pulse shape and spectrum were less dependent on

experience and skill of individual stations operators. As with earlier equipment, the press notices for the new concept were not fully realized in the brutal environment of the "real world." Improved trailing edge behavior did not noticeably improve user equipment performance.

SURVIVAL MEASURES

During the 1960's Loran-C became involved in serious competition for funding. A philosophy was adopted to make Loran-C viable for services other than navigation. Civil Defense Alert, Timing, and Communications were some of the various areas considered for service expansion.

Compatible existence with DECCA services in the Norwegian Sea (Sylt), North Atlantic (Cape Race), and Southeast Asia (Con Son) required resolution of interference problems. Trailing edge manipulation as a technique for DECCAJECTION became a practical reality.

COMMUNICATIONS

Early Office of Civil Defense communications systems provided information by dropping odd numbered pulses within the pulse group. With this technique 1 kHz and 500 cycle tones resulted when received RF signals were detected in a simple linear detector. This technique, while acceptable for limited functions, provided only a very low information rate. Consideration of the Loran-C signal linear processing techniques then utilized led to the concept of Pulse-Position Modulation (PPM) of the Loran-C signal to provide a higher data rate.

The Coast Guard system of redundant PPM information transmission led to very high reliability of single station transmission. Another system of transmitting the same information from multiple stations led to redundancy improvement within a selected service area.

Both these systems affected the whole Loran pulse including the previously inviolate leading edge. The PPM systems garnered reactions from the "greatest thing since sex" to the "inevitable destruction of Loran-C as a navigation system".

POLYPHASE COMMUNICATIONS

The DECCAJECTION technique required the transmission of energy in the pulse ringdown which is out of phase with energy in the leading edge. This technique produces notches in the spectrum at the various DECCA frequencies and still allows power spectrums radiated to be within I. T. U. requirements. Further, the navigation pulse rise is undisturbed.

The Polyphase Modulation (PM) technique is only a short step away from the DECCA-JECTOR. The tail of each pulse is transmitted in a state selected from a number of phase relations relative to the navigation sampling point. Bits of information are related to the communications states of tail phase by a schedule or "truth" table. The number of phase relations which may be utilized are a function of the number which can be radiated with acceptable control and the number which can be identified by a communications receiver under "Real World" conditions of noise, interference, and sky wave contamination. The required number of identifiable states 'N', is determined

by

$$N = 2^n$$

Where N = number of states

and n = number of information bits per Loran pulse.

If all eight pulses in each group are utilized, the maximum bit rate is defined by $8n \times \text{GRR}$. With the old familiar basic rates (GRR), and $n = 2$:

<u>GRR</u>	<u>Bit Rate</u>
SS	160 bits/second
SL	200
SH	266.7
S	320

These maximum bit rates can be buffered and partitioned to be compatible with the conventional 50, 75, or 100 baud rates used in communications.

POLYPHASE FEASIBILITY EXPERIMENT

As with most "developments" in Loran-C, the Polyphase innovation is expected, like Minerva, to spring forth full-grown and in armor, from the head of Zeus! To accomplish this spectacle, a Communications Modulation Test Pulse Generator was built by Hartman Systems to conduct various tests with a four-state Polyphase system configuration. These tests were conducted between April and August, 1974 at the U. S. C. G. Electronic Engineering Center at Wildwood, New Jersey. The Loran Receiver Test Complex (LRTC) was employed to determine the effects of polyphase modulation on the performance of various receivers, and to perform information bit error-rate tests. Additionally, performance parameters and drive requirements

were explored for AN/FPN-39 and AN/FPN-44 transmitters operating with polyphase modulation. Figures 2 and 3 show the wave forms of the AN/FPN-44 radiated pulses, and Figure 4 shows the drive waveforms.

POLYPHASE TEST RESULTS

These tests showed:

1. Performance of various generic types of navigation receivers under likely operating conditions is unaffected by Polyphase Modulation.
2. Bit error rates obtained with simulated tracking closely follow predicted performance for communications.
3. Transmitter performance during the tests was within the "test envelope" established for the experiment.
4. Navigation drive of eight cycles (approximately amplitude controlled) followed by a four-cycle communications drive produced a satisfactory radiated pulse for navigation and communications.

HORIZONS

During the experiments with the AN/FPN-39, various combinations of navigation and communication drive were explored. The normal eight-cycle navigation drive was changed to four cycles, and a three-cycle communications drive was used that was delayed sixty microseconds from the start of the navigation drive. This composite drive also produced adequate tail swing, and the radiated signal up to about fifty microseconds after pulse beginning was unaffected. Communications

modulation was produced without significant change in plate performance of the output stages, and spectrum could be controlled within the I. T. U. limitations.

These sign posts point to development of techniques to produce satisfactory tail swing by transmitter drive manipulation. One must conclude that this manipulation can be achieved both with the older tube transmitters, and with the solid state transmitters about to be deployed. One must speculate that a variably tuned passive "tail swinger" could also produce the desired communications modulation with no requirement for additional transmitter power. Intuitively polyphase modulation can improve performance of the navigation system in:

1. Search Time
2. Crossing rate rejection
3. Pulse to pulse skywave rejection

These results may be postulated because polyphase modulation decreases the interval over which signals are coherent. Tests to determine the validity of these conclusions have not been proposed or undertaken.

Results of polyphase modulation monitoring reported by Willi Vogeler of Telcom, Inc. tend to support the speculation of improved search. This conclusion must, however, include the caveat of 'proper search logic'.

CONCLUSIONS

We have had PPM communications systems operational for several years. During this time, system parameters have been bent to accommodate effects seen in transmitter and receiver performance.

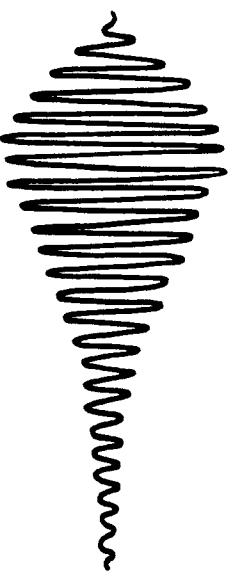
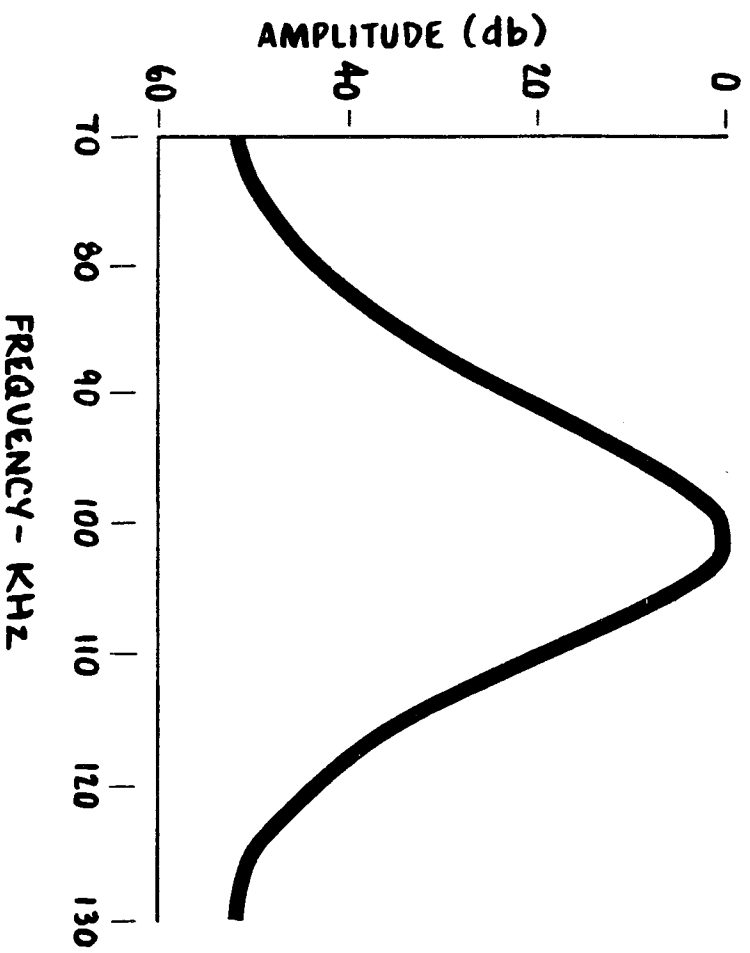
Tests with polyphase modulation have proven that parameters for compatibility of navigation and communications can be enlarged to encompass areas previously considered 'Forbidden territory'.

We have within our knowledge the theory and within our experimental results the tools to make a decision for expanded capability within the limitations of the Loran-C spectrum.

The Loran-C system, whether deployed on the U.S. East Coast or in Southeast Asia, has had a perennial problem of "talking to itself". In Southeast Asia the Coast Guard PPM system implemented the communications links necessary to provide the most precise Loran-C grid yet operational. The necessity for extreme reliability in interstation communications is obvious in defining the parameters for unmanned operation and control of stations and chains.

Information rates achievable with polyphase communications make capabilities available for special purpose use without limiting navigation parameters.

The development of processing techniques for fast Fourier and other orthogonal transforms in other applications offer us a 'view through the cracks' of areas for new approaches to Loran-C Navigation and Communications processing. Perhaps with our present perspective we are better off than the blindmen with the elephant.



$$f(t) = \left[\frac{t}{T} e^{-\alpha \frac{t}{T}} \right]^2 \sin(2\pi 10^5 t + \theta)$$

REQUIRED SPECTRUM

"IDEAL" SHAPE

Figure 1

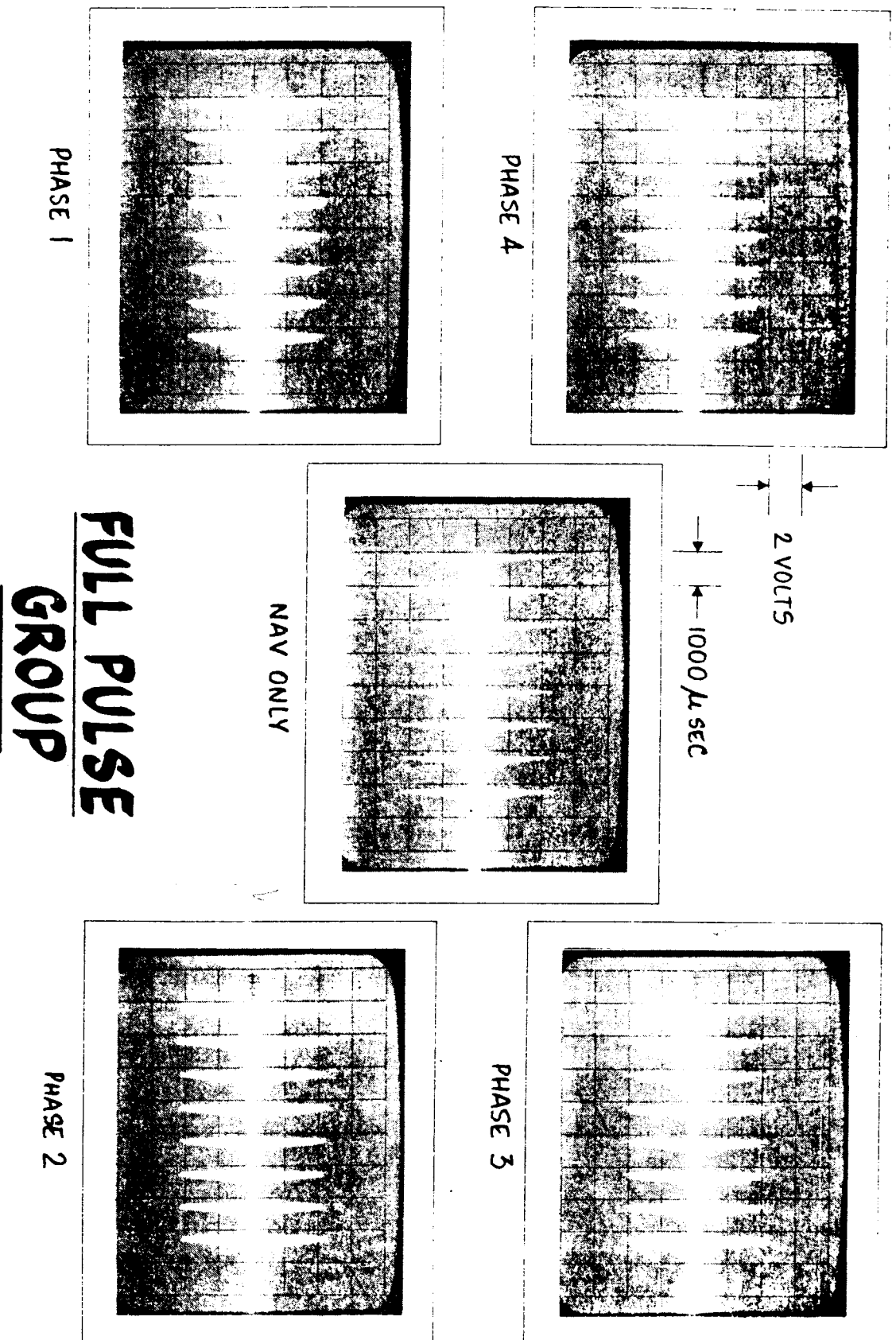


Figure 2

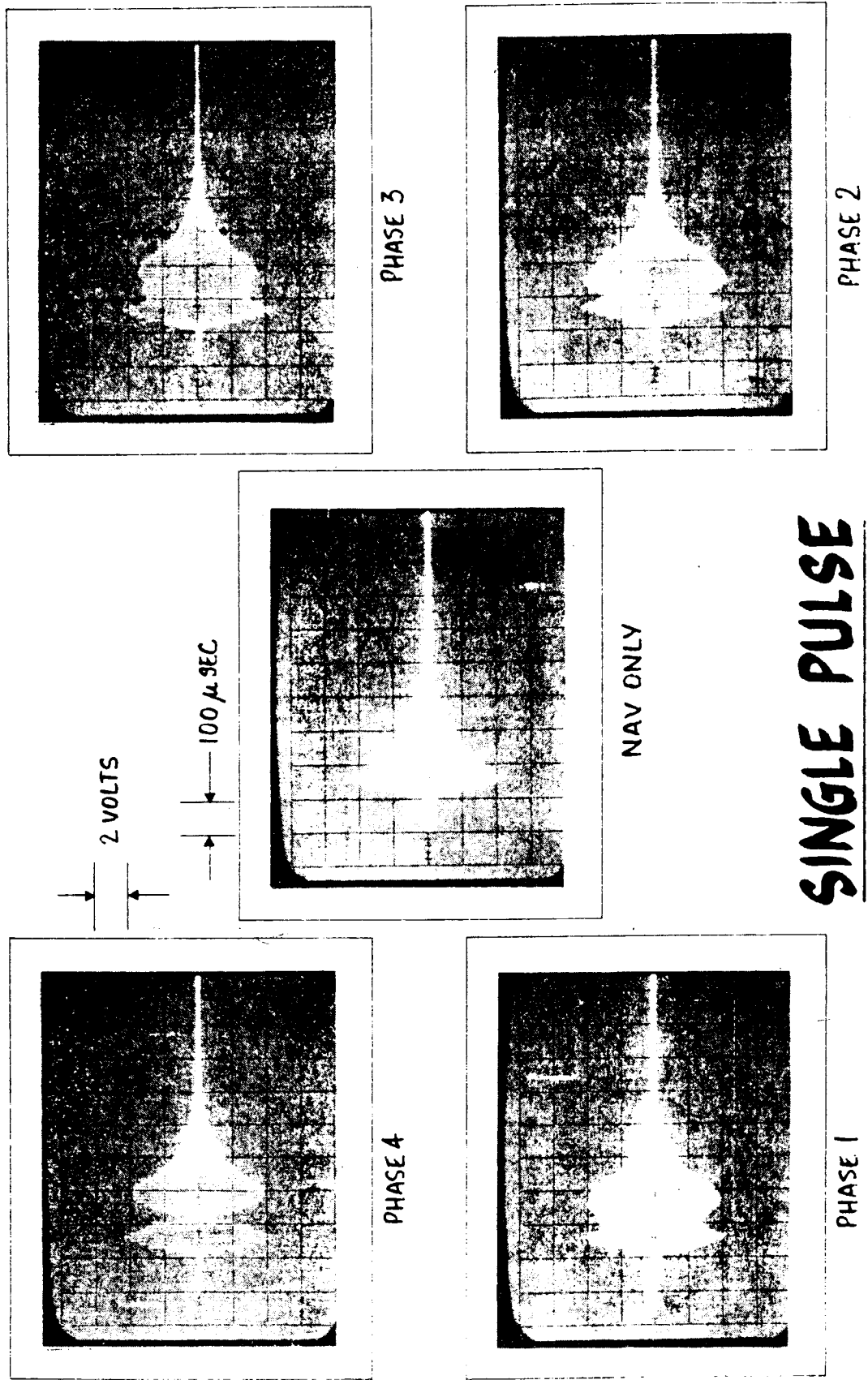


Figure 3

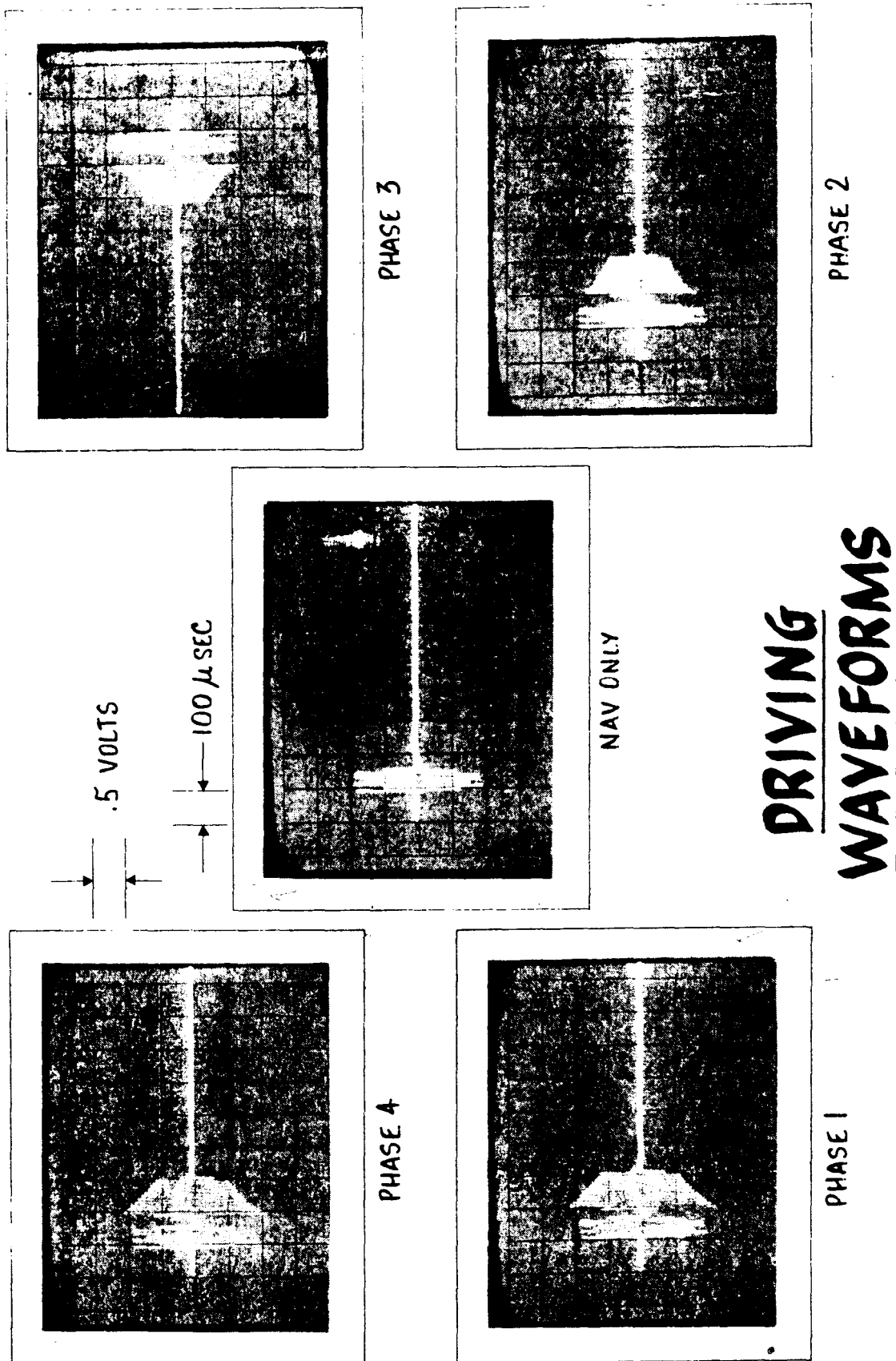


Figure 4

(8) ROBERT L. FRANK
~~16500 North Park Drive~~
~~Southfield, Mich. 48075~~

Revision (?) of WLA 3rd Conv Program

FILE COPY 3-8

ARM 111

RECENT ADVANCES IN ACCURATE AIRBORNE COMPUTATION OF SECONDARY PHASE FOR LORAN C RADIO-NAVIGATION

RONALD J. FREDRICKS, PH.D.
MICHAEL W. BIRD, PH.D.
KEITH A. WHEELER

PRESENTED AT THE
INSTITUTE OF NAVIGATION
WASHINGTON, DC
JUNE, 1975

ALGORITHM FOR LORAN SECONDARY PHASE COMPUTATION

LEAR SIEGLER, INC.



INSTRUMENT DIVISION

4141 EASTERN AVENUE, S. E.
GRAND RAPIDS, MICHIGAN 49508

condolatum
31 pages

12
11/11/75
1/24/76
10/1/76

RECENT ADVANCES IN
ACCURATE AIRBORNE COMPUTATION
OF SECONDARY PHASE
FOR LORAN C RADIO-NAVIGATION

Ronald J. Fredricks
Michael W. Bird
Keith A. Wheeler

ABSTRACT

This paper describes a simplified algorithm for improving the absolute accuracy of Loran C radio-navigation that is compatible with a small airborne data processor. The technique involves the use of a polynomial fit of loran secondary phase to the variables distance, altitude, vertical atmospheric lapse factor, ground index of refraction and effective wave impedance, Δ_E . The latter quantity was introduced by Johler of ITS to account for the fact that the propagation paths are, in general, over irregular inhomogeneous ground. A second set of polynomials maps Δ_E in terms of latitude and longitude for each station over a given area which may be 10,000 sq. mi. or larger. Some a-priori data points are required. These may be measured empirically as time differences vs. positions and/or calculated on a large digital computer using the wave integral equation and the known path topologies. Accurate calculation of the secondary phases using the above fitting polynomials in turn allows the subsequent loran-to-position coordinate conversion to be extremely accurate on an absolute basis. A demonstration of this technique in the Eglin Air Force Base vicinity using a-priori ground and airborne measurements indicated a prediction capability standard deviation of 0.25 μ s on either of the time differences. Comparison of recent flight test TD airborne data, obtained from the AN/ARN-101 Digital Modular Avionics System, with the values predicted using the preceding model, verified this capability in practice and are included herein.

The above authors are employed by
Lear Siegler, Inc./Instrument Division
4141 Eastern Avenue S. E.
Grand Rapids, Michigan 49508

INTRODUCTION

Frequently it is desirable to operate Loran C/D in other than a time difference or "repeatability" mode. For example, it may be necessary to know where one is located in the real world in terms of latitude, λ , and longitude, Λ , given a set of measured time differences or TD's, as they are called by loran specialists. Alternately, a destination may be given in one set of coordinates and the associated TD or (λ, Λ) required to be determined onboard the vehicle so that guidance commands can be computed. All of these examples require accurate conversion of TD's measured by the loran receiver into geodetic coordinates. For wide area navigation the general approach to coordinate conversion is some version of the well-known Sadano-Campbell method: given an assumed position, the expected time of arrivals (TOA's) are calculated for each of the three or more loran stations; then TD's are computed and compared with the observed quantities and position corrections obtained. For determination of TD's given position only, a single set of calculations need be performed; if given the TD's, several iterations may be necessary on the position estimate. The accurate calculation of the TOA's in the Sadano-Campbell method requires that the Loran secondary phase delay be properly modeled. Secondary phase is defined as the additional phase delay (or equivalently time delay) of the Loran groundwave signal carrier over a similar signal traveling the same geodetic distance through an air medium only. Calculation of secondary phase must take into account distance and terrain effects, receiver and/or transmitter elevation effects, and weather and other temporal effects on the received signal.

Until recently most Loran receivers assumed a simple all-seawater earth model. Since most Loran transmitters are located quite close to seacoasts, such a model is quite accurate for ship use at sea. However, use of such a model in an airborne receiver over land can result in 1-10 μ sec of time delay error at 1000 mi. from a transmitter. Sometimes these errors will cancel when TD's are taken, but rarely completely. Generally something like ± 1 μ sec of time delay error remains in the TD predictions over land which implies an aircraft position error of 1500 to 2000'. This is unacceptable for precise Loran navigation. Even ships can encounter such errors when they are in regions near land such as channels, harbors, etc. due to land-sea boundary reflections of the Loran wave.

During the period roughly from 1955 to 1965, Wait et al of the Institute of Telecommunications Sciences (ITS) at Boulder, Colorado did much theoretical analysis on propagation of low frequency groundwave over a spherical earth. Taking the basic works of Sommerfeld⁽¹⁾, Watson⁽²⁾, Norton⁽³⁾, Fock⁽⁴⁾, and Bremner⁽⁵⁾, he converted the residue series solution for the complex attenuation factor, F , over smooth homogeneous earth to integral equation form so that the mixed path or inhomogeneous smooth earth case could be analyzed⁽⁶⁾. The Loran secondary phase is, by definition, contained in the argument of F .

J. R. Johler, also of ITS, carried this work on from the late 1950's to the present. In particular, he and his co-workers extended the integral equation solution for F to account for irregular terrain effects such as due to mountains, land-sea boundaries, and scattering from points not on the geodesic between transmitter and receivers^{(7),(8)}. Towards the end of the last decade Johler introduced the concept of an effective wave impedance, Δ_E , as a means

to simplify calculations of the secondary phase. (9), (10), (11) While the relative boundary impedance, Δ , is independent of transmitter location and is the quantity used in the full integral equation solution for F , the effective wave impedance is defined to give the same value for $\arg(F)$ when inserted in the classical homogeneous earth residue series solution. Δ is a normalized quantity given by Johler as

$$\Delta = Z/Z_0 \quad (1)$$

where Z is the surface impedance (complex) at any point, in ohms, and Z_0 is the impedance of free space, ~ 377 ohms. Δ_E is a similar normalized quantity but it need not be the local wave impedance associated with the ground below the receiver. Rather, Δ_E is a function of transmitter and receiver locations and the inhomogeneous geodesic path between the two. It can be determined by a-priori TD or TOA measurements or theoretically using the integral equation approach.

Insertion of Δ_E along with receiver altitude, h_R , transmitter altitude, h_T , (if not at sea level) geodesic path length, ρ , ground index of refraction, n , and vertical lapse factor, α , into the classical residue theory allowed Johler to solve for both the magnitude and phase of F . Because of the definition of Δ_E , however, only the solution for $\arg(F)$ can be regarded as correct. Fortunately, for Loran radio-navigation we are primarily interested in the phase of F only as this represents the Loran secondary phase, ϕ_S . Even given that the classical theory can still be used via introduction of the effective wave impedance concept, the computer solution time and core requirements far exceed the capability of any practical airborne computer. Johler labeled his complete classical solution as computer program EGRWOO with the residue series calculation contained within as a subroutine, GROUND. At $\rho = 10$ km and h_R a few thousand meters, a single determination of ϕ_S may take a minute or so on an IBM 370. Even at large distances of 100 km or more, IBM 370 solution times are on the order of 1-5 sec and use around 50K of 32 bit word storage. Obviously one cannot use EGRWOO as it stands for on-board computations in most aircraft or even ship applications.

What the authors have accomplished at LSI is to develop a much simplified algorithm which closely approximates the EGRWOO solution time and which requires only 800 or so 16 bit words of computer storage. These techniques have been incorporated into the company's Loran-aided inertial navigation system for the U.S. Air Force AN/ARN-101 Navigation Set currently under flight test at Eglin AFB, Florida*. The complete algorithm includes not only the ϕ_S calculation itself but an efficient way of determining the Δ_E as a function of position using a-priori measurements and of storing a set of such impedance maps onboard.

In the following we shall describe this algorithm and give initial results of applying the technique to the Eglin Air Force Base area using a-priori TD measurements made on the ground and during straight and level airborne flight.

* The algorithm development and flight testing were performed under USAF Contract F19628-73-C-0292, A Digital Modular Avionics System AN/ARN-101(V).

Theoretical Secondary Phase Calculation

We may define the total signal phase of the received Loran signal in terms of the phase of a tagged point, emitted at time zero, on an equivalent 100 KHz sinusoid. With a receiver sampling point generally at or near the third r.f. cycle crossover, such an equivalent sinusoid interpretation is quite useful in the following. Calculation of the actual received pulse shape requires consideration of the emitted pulse shape and the different group velocities across the emitted spectrum. We shall not be concerned with such dispersion effects here, however.

Mathematically the total received signal phase, ϕ_R , of the equivalent sinusoid is given by

$$\phi_R = \phi_P + \phi_S + \phi_I \quad (1)$$

where ϕ_P is the primary received phase, ϕ_S is the secondary phase, and ϕ_I is an arbitrary initial phase angle present on the transmitted equivalent sinusoid. Without loss of generality we may set ϕ_I equal to zero and neglect it in the following. In equation (1) ϕ_P is in turn given by

$$\phi_P = \frac{\rho}{C} \eta (2\pi f) \quad (2)$$

where ρ is geodetic path length between transmitter and receiver, C is the vacuum speed of light*, η the air index of refraction along the ground, and f the carrier frequency (here 100 KHz).

While the calculation of ϕ_P is quite simple, as equation (2) shows, that for ϕ_S is very involved. For homogeneous smooth earth an attenuation function, F , is given very closely by the VanderPol-Bremmer residue series approximation to the original exact solution of Watson's.

$$F = [2\pi\alpha^{2/3}(k_1 a)^{1/3} \frac{\rho}{a}]^{1/2} \sum_i \frac{f_i(h_T) \cdot f_i(h_R) \exp\{-jX_i\}}{2\tau_i - 1/\delta^2} \quad (3)$$

with X_i given by

$$X_i = \tau_i \alpha^{2/3}(k_1 a)^{1/3} \frac{\rho}{a} + \frac{\pi}{4} \quad (4)$$

The τ_i are the roots of a Riccati equation:

$$\frac{d\delta}{d\tau_i} - 2\tau_i \delta^2 + 1 = 0 \quad (5)$$

* $C = 2.997925 \times 10^5$ km/sec will be assumed throughout.

and δ is defined in terms of the homogeneous wave impedance, Δ , by

$$\delta = \frac{-j \alpha^{1/3}}{(k_1 a)^{1/3} \Delta} \quad (6)$$

where Δ is given by

$$\Delta = \frac{k_1}{k_2} \left(1 - \frac{k_1^2}{k_2^2} \right)^{1/2} \quad (7)$$

In turn k_1 , the air propagation constant, is given by

$$k_1 = \frac{(2\pi f)}{C} \eta \quad (8)$$

and k_2 , the surface propagation constant, is expressed mathematically as

$$k_2 = \frac{(2\pi f)}{C} \sqrt{\epsilon_{2r} + \frac{i \sigma}{2\pi f \epsilon_0 \epsilon_{1r}}} \quad (9)$$

In the above equations, a is earth's radius, ϵ_0 is the permittivity of free space, ϵ_{1r} and ϵ_{2r} are the relative dielectric constants for air and for the earth's surface, respectively, σ is the local earth conductivity, and ρ , α , and η have already been defined. Finally, the altitude factors, $f_1(h)$, go to unity as $h \rightarrow 0$ but in general are ratios of Hankel functions of the second kind and order $1/3$ that are dependent upon τ_1 and h .

The corresponding expression for the received vertical electric field (TM mode propagation) of the equivalent sinusoid is then

$$E_z = 2 E_{\text{Primary}} \cdot F \quad (10)$$

where

$$E_{\text{Primary}} = A \cdot \exp\{j(-\phi_p + 2\pi ft)\} \quad (11)$$

and where ϕ_p is the product of k_1 and arc length, ρ , and where the amplitude, A , is inversely proportional to ρ . By definition we see then that ϕ_s is the argument of F (or more exactly the negative of $\arg F$ since, by convention, we assume a phase lag to be positive).

When the path is non-homogeneous the preceding classical solution may still be employed for the calculation of ϕ_S by replacing Δ in equation (6) by its effective value, Δ_E . Alternately we may solve the extremely complicated integral equation for F over the complete inhomogeneous path. It is the above classical set of equations that Johler included in subroutine GROUND for his program EGRWOO. Given ϕ_P and ϕ_S , the time of arrival, TOA, of a tagged point on the equivalent sinusoid may then be calculated by

$$\text{TOA} = \text{TOA}_P + T_S \quad (12)$$

where

$$\text{TOA}_P \stackrel{\Delta}{=} \frac{\phi_P}{2\pi f} \quad (13)$$

and

$$T_S \stackrel{\Delta}{=} \frac{\phi_S}{2\pi f} \quad (14)$$

With knowledge of the proper coding delays for a given master-slave pair the appropriate time difference, TD, may then be predicted.

Simplified Secondary Phase Calculation

Program EGRWOO was obtained from ITS and rewritten into a Fortran IV format compatible with LSI's IBM 370 computer. A table of $\arg \{\Delta\}$ vs $|\Delta|$ for $0.001055 \leq |\Delta| \leq 0.08$ was also obtained from ITS. A graphical presentation of this relationship appears on page 130 of Johler's report, TRER22. Johler observed that $\arg \{\Delta\}$ is uniquely related to $|\Delta|$, i.e., that Δ is a minimum phase function as it occurs in nature. The same also holds for $|\Delta_E|$ and $\arg \{\Delta_E\}$ by definition. Use of the classical residue series to calculate T_S or ϕ_S thus only requires the specification of $|\Delta_E|$ along with ρ , h_R , η and α . Program EGRWOO assumes $h_T=0$. If this is not the case, the quantity h may be substituted for h_R in EGRWOO where, to a first approximation

$$h \stackrel{\Delta}{=} h_R - h_T \quad (15)$$

It was decided to attempt a curve fit solution to the EGRWOO calculations of T_S . Such a curve fit, if it worked, would effect the much needed reduction in computation time and word size. It was desired that such an algorithm would allow T_S computations agreeing with EGRWOO within 0.1 μsec over the following ranges of the variable parameters:

$$10 \leq \rho \leq 2400 \text{ KM}$$

$$0 \leq h \leq 15,000 \text{ meters (3000 meters for } \rho < 50 \text{ KM)}$$

$$0.7 \leq \alpha \leq 1.0$$

$$1.0002 < \eta \leq 1.0005$$

$$0.001055 \leq |\Delta_E| \leq 0.08$$

Under 10 KM, a spherical earth solution using EGRWOO takes prohibitively long to solve on the IBM 370. The flat earth induction and static field contributions are easily calculated without EGRWOO anyway. Over 2400 KM, pulse dispersion begins to be noticeable and prevents one from simply calculating secondary phase based on a 100 KHz sine wave. For $h > 15,000$ meters, computational difficulties appeared in EGRWOO for distances over 50 KM. Also, for distances under 30 KM a similar lack of convergence appeared for altitudes above only 3000 meters. Such altitudes were, therefore, excluded from the curve fit data generation so as not to use up too much computer time.

Most temporal effects can be accounted for by use of an effective α somewhere in the range indicated. Furthermore, the secondary phase is only loosely dependent on η (not the primary phase, however, as equation (2) shows) and may be assigned the value 1.000338. Finally, ITS believes that all real world wave impedances that may be encountered at 100 KHz are bracketed by the limits on $|\Delta_E|$ shown.

The curve fit attempted for T_S was of the following form:

$$T_S = a_0 + a_1(\alpha - 0.85) + a_2h + a_3h^2 + \{b_0 + b_1(\alpha - 0.85) + b_2h + b_3h^2\} \rho \\ + \{c_0 + c_1(\alpha - 0.85) + c_2h + c_3h^2\} \rho^2 \text{ or } 1/\rho \quad (16)$$

It should be noted that $\alpha = 0.85$ is the nominal lapse factor for the index of refraction in the air. A separate fit was assumed for each Δ . The multiplier $1/\rho$ was used in the third term of the polynomial for distances under 500 KM and both ρ^2 and $1/\rho$ dependencies were tried out for larger distances.

A curve fitting program, program FIT, was developed by the authors to take EGRWOO outputs computed for a given wave impedance, h , α and η and fit this data to the preceding polynomial using error minimization in a least squares sense. Program FIT automatically checked for "unnecessary" coefficients (those contributing at most 0.05 μsec maximum to the T_S estimate) and regenerated the fit omitting such coefficients. In all cases the FIT predictions for T_S were compared with the EGRWOO calculated values.

Only a finite number of 9 wave impedances was assumed. This number was sufficient so that accurate linear interpolation on Δ or Δ_E , using T_S 's for the closest compiled Δ 's, could be performed. Similarly, only a finite number of altitudes and α values were used to generate each fitting polynomial.

For a given $|\Delta|$ at least two fits were generated, one valid for small and intermediate distances and the other for large distances out to 2400 KM. For large $|\Delta|$ the first fit itself was frequently broken into two range intervals in order to maintain the given desired fitting tolerance of 0.1 μsec or better. For the EGRWOO data, α values of 0.7, 0.85 and 1.0 were used. Radial distances were varied in steps of 2 KM from 10 to 48 KM inclusive, in steps of 25 KM from 50 to 525 KM and in steps of 100 KM from 500 to 2400 KM. Altitudes were varied in the following levels: 0, 1000, 2500, 5000, 7500, 10000, 12500, and 15000 meters for the latter two distance intervals and 0, 1000, 2000, and 3000 meters for the 10 to 48 KM interval.

The generation of the fitting coefficients took 7-10 hours on the 370. EGRWOO was run repeatedly to compute T_S vs ρ , α , and h for a given $|\Delta|$ and the complete set of data was stored on tape. Program FIT then automatically processed the stored data, generated the fits, tested for unnecessary coefficients, and printed out the error residuals. A new $|\Delta|$ was then chosen and the process repeated for nine different values of $|\Delta|$.

EGRWOO convergence itself was set to give 0.0001 μsec , or better, agreement with the VanderPol-Bremmer residue series solution for T_S . In turn, the VanderPol-Bremmer formula is accurate to 6 significant figures compared to the exact classical formula developed by Watson in 1919.

It can be noted from the algorithm equations that rate aiding signals to compensate for rapid changes in secondary phase due to large vertical or horizontal velocities may readily be calculated. One need only to take the appropriate radial or vertical derivatives of T_S and multiply by the corresponding velocity. Such rate aiding of a narrow band phase tracking receiver is required for a high performance aircraft in an area of large secondary phase variations where the Loran grid lines are highly "warped".

Program FIT automatically printed out the residual fitting error for each of the EGRWOO data points. Generally the number of required a's, b's, and c's was under 12 with as few as 7 sufficient for some fits. The following table (Table 1) shows typical results for three selected values of wave impedance.

Note that at the larger $|\Delta|$'s the RMS fitting error exceeded slightly the target RMS value of 0.1 μsec . However, the occurrence of such high values of $|\Delta|$ in nature appears very improbable. At such large values of $|\Delta|$ the error in calculating secondary phase using a simple all-seawater earth model is enormous (10 μsec or more at 1000 km) so even 0.2-0.3 μsec peak fitting errors seem small by comparison.

$ \Delta $	RANGE INTERVAL (KM)	# NON ZERO COEFFICIENTS	# EGRWOO DATA PTS	AV FITTING ERROR (μSEC)	RMS FITTING ERROR (μSEC)	$1/\rho$ OR ρ^2
0.001055	10-500	11	720	10^{-9}	0.027	$1/\rho$
0.001055	500-2400	7	480	-0.0051	0.055	ρ^2
0.04	10-500	11	720	10^{-9}	0.047	$1/\rho$
0.04	500-2400	7	480	-0.021	0.0678	ρ^2
0.08	10-50	9	240	0.01	0.07	$1/\rho$
0.08	50-500	11	480	0.0008	0.146	$1/\rho$
0.08	500-2400	8	720	0.018	0.134	ρ^2

Table 1 - Summary Of Typical Fitting Results

Table 2 compares actual EGRWOO calculations for T_S with the fit computed value of T_S . In particular, the error residual, T_E , is tabulated vs distance, where

$$T_E = T_S - \hat{T}_S \quad (17)$$

The fit being tested here is the first one in the preceding table, i.e., for $|\Delta| = 0.001055$ (seawater) and is for the range 10-500 km.

The distances, multiplies of 30 km, were intermediate to those used in generating the fit (every 25 km for $\rho \geq 50$ km and every 2 km for $10 \leq \rho < 50$ km). Also, an intermediate α of 0.93 was used along with an intermediate altitude of 3750 meters. Note that at 30 km the chosen altitude is really an extrapolation of the fitting polynomial rather than an interpolation of the polynomial because only altitudes up to 3000 meters were used to generate the fit under 50 km. Also note distances of 540, 570, and 600 km are really extrapolations as the fitting data cut off at 525 km. The overall RMS interpolation error was 0.026 sec, the same as the fitting error on the data points themselves.

Table 3 repeats the above interpolation test but in the range 500-2400 km using the seawater coefficients valid for $\rho > 500$ km. Here EGRWOO was run every 50 km beginning at 525 km and ending at 1975 km. Since the data used to generate the fitting polynomial was taken every 100 km beginning at 500 km, we are strictly interpolating on ρ . α was taken as 0.93 again but h was raised to 11,250 meters. These are intermediate values to those used to generate the fitting polynomial. The fitting polynomial is the second one listed in Table 1 and assumes a ρ^2 dependency. The interpolation error in the test was only 0.018 μ sec RMS and was largely a bias offset. Table 3 lists only 11 of the 30 points actually run. Errors on all the other points were also about 0.01 μ sec.

Table 4 depicts interpolation results on ρ , α and h for $|\Delta| = 0.08$. The test takes EGRWOO outputs for distance increment of 100 km starting at 550 km with $\alpha = 0.775$ and $h = 8750$ meters and compares these with the polynomial solution for T_S valid for $\rho > 500$ km. The RMS error was 0.038 μ sec, better than the fitting error on the data points themselves. Only 5 of the 20 test distances are tabulated in Table 4.

As mentioned, curve fits for only 9 different $|\Delta|$'s appeared to be sufficient to cover the range 0.001055 to 0.08 using linear interpolation on $|\Delta|$. Maximum error contribution due to the $|\Delta|$ interpolation appears to be 0.03 μ sec and that only for $|\Delta|$ near 0.08, $h=15,000$ meters, and $\rho = 2400$ km, about as worse a case as possible. Typical interpolation errors on $|\Delta|$ were only about 0.01 μ sec RMS. The 9 chosen values of $|\Delta|$ were

$$\begin{aligned} |\Delta| &= 0.001055 \text{ (seawater)} \\ &0.01 \\ &0.02 \\ &0.03 \\ &0.04 \\ &0.05 \\ &0.06 \\ &0.07 \\ &0.08 \end{aligned} \quad (18)$$

$\alpha = 0.93$, $|\Delta| = 0.001055$, $h = 3750 \text{ meters} \approx 12,303 \text{ ft}$

ρ (km)	$\eta, \text{ mui}$	T_S (EGRWOO) (μsec)	\hat{T}_S (μsec)	T_E (μsec)
30	14	0.8764	0.8758	0.0007
60	32	0.4930	0.4870	0.0060
90	49	0.3928	0.3962	-0.0034
120	65	0.3660	0.3799	-0.0140
150	81	0.3702	0.3935	-0.0232
180	97	0.3913	0.4219	-0.0306
210		0.4229	0.4588	-0.0359
240		0.4518	0.5010	-0.0393
270		0.5061	0.5468	-0.0408
300		0.5546	0.5951	-0.0405
330		0.6066	0.6452	-0.0386
360		0.6613	0.6967	-0.0354
390		0.7184	0.7491	-0.0308
420		0.7774	0.8024	-0.0250
450		0.8382	0.8564	-0.0182
480		0.9004	0.9109	-0.0105
510		0.9639	0.9658	-0.0019
540		1.0285	1.0211	0.0074
570		1.0940	1.0767	0.0173
600		1.1604	1.1326	0.0278

AV Error = -0.016 μsec

RMS Error = 0.026 μsec

Table 2 - EGRWOO Vs Fit Computations for T_S (Seawater) $10 \leq \rho \leq 500 \text{ km}$

$$\alpha = 0.93$$

$$|\Delta| = 0.001055$$

$$h = 11250 \text{ meters} = 36909 \text{ ft}$$

ρ (km)	T_S (EGRWOO) (μsec)	\hat{T}_S (μsec)	T_E (μsec)
525	1.8114	1.7617	0.0497
575	1.9113	1.8773	0.0340
625	2.0165	1.9930	0.0235
675	2.1257	2.1089	0.0168
725	2.2377	2.2250	0.0127
.	.	.	.
.	.	.	.
.	.	.	.
1025	2.9373	2.9246	0.0127
1075	3.0556	3.0417	0.0138
.	.	.	.
.	.	.	.
.	.	.	.
1525	4.1205	4.1032	0.0173
1575	4.2387	4.2219	0.0168
.	.	.	.
.	.	.	.
.	.	.	.
1925	5.0656	5.0574	0.0082
1975	5.1837	5.1774	0.0063

AV Error = 0.016 μsec

RMS Error = 0.018 μsec

Table 3 - EGRWOO vs Fit Computations for T_S (Seawater) $\rho \geq 500 \text{ km}$

$$\alpha = 0.78$$

$$|\Delta| = 0.08$$

$$h = 8750 \text{ meters} \approx 28707 \text{ ft}$$

ρ (km)	T_S (EGRWOO) (μsec)	\hat{T}_S (μsec)	T_E (μsec)
550	5.2321	5.2653	-0.0332
.	.	.	.
.	.	.	.
.	.	.	.
1050	8.6914	8.7393	-0.0479
.	.	.	.
.	.	.	.
.	.	.	.
1550	12.1649	12.2133	-0.0484
.	.	.	.
.	.	.	.
.	.	.	.
2050	15.6628	15.6874	-0.0245
.	.	.	.
.	.	.	.
.	.	.	.
2450	18.4675	18.4666	0.0009

AV Error = -0.035 μsec

RMS Error = 0.038 μsec

Table 4 - EGRWOO Vs Fit Computations for T_S ($|\Delta| = 0.08$)

The following table, Table 5, shows how linear interpolation works to predict T_S for $|\Delta| = 0.075$ given T_S at $|\Delta| = 0.07$ and $|\Delta| = 0.08$. To separate interpolation errors from fitting errors the interpolation was done using the EGRWOO calculated T_S 's rather than the fit calculated T_S 's.

ρ KM	T_S ($ \Delta =0.08$) μsec	T_S ($ \Delta =0.07$) μsec	T_S ($ \Delta =0.075$) μsec	\hat{T}_S ($ \Delta =0.075$) μsec	$ T_E $ μsec
50	8.0796	8.0338	8.0582	8.0567	0.0015
100	4.8095	4.7200	4.7646	4.7647	0.00010
300	4.1264	3.9124	4.0203	4.0194	0.00090
500	5.3609	5.0425	5.2053	5.2017	0.0036
1000	9.2552	8.6685	8.9741	8.9618	0.0123
2400	20.7942	19.3691	20.1158	20.0816	0.0342

$h = 15,000$ meters

$\alpha = 1.0$

Table 5 - Interpolation on $|\Delta|$

The total number of fits generated was 21. There were two fits for each of the first 6 wave impedances in equation (16) and 3 fits for each of the last three impedances. In the former case, the fits were from 10 to 500 km and from 500 to 2400 km radial distance while for the latter three impedances they were for 10-50 km, 50-500 km, and 500-2400 km radial distances. Program Fit determined there were 192 non-zero coefficients required for the 21 fits. A $1/\rho$ dependency was found best for $10 \leq \rho \leq 500$ km and a ρ^2 dependency best for $\rho \geq 500$ km in almost all cases. The 192 coefficients chosen are, therefore, valid for these dependencies. All rms fitting errors with respect to the EGRWOO data were under 0.1 μsec (typically 0.05 μsec) except for the last two fits ($\rho \geq 50$ km, $|\Delta| = 0.08$) where the errors were about 0.14 μsec rms with 0.2-0.3 μsec peaks. Tables 6, 7, and 8 list the derived coefficients for each of the 21 fits. In the tables an XX means the respective coefficient was determined to be non-sensitive and may be deleted.

Determination of the Various Wave Impedances

The simplified secondary phase polynomial solution requires a wave impedance map for the desired flight area(s) to be loaded onboard the loran receiver's computer in addition to the 21 polynomials. According to Johler, one may calculate the Δ_E 's using a-priori loran TD or TOA measurements actually taken in the area of interest or synthesized from digitized topographic and conductivity maps of the entire loran path using one of his integral equation programs.⁽¹²⁾ In general, however, one will use a combination of both measured TD's and computer synthesized theoretical TD's to calculate the Δ_E 's for the various Loran stations.

FIT #	$ \Delta $	RANGE INTERVAL (km)	# NON-ZERO CO-EFFICIENTS	# EGRWOO PTS USED IN FIT	AV FITTING ERROR (μSEC)	RMS FITTING ERROR (μSEC)	FIT #	$ \Delta $	RANGE INTERVAL (km)	# NON-ZERO CO-EFFICIENTS	# EGRWOO PTS USED IN FIT	AV FITTING ERROR (μSEC)	RMS FITTING ERROR (μSEC)
1	0.001055	10-500	11	720	10^{-9}	0.0272	2	0.001055	500-2400	7	480	-0.0051	0.055
$a_0 = -0.637216594$ 10^{-1}			$b_0 = 0.158704259$ 10^{-2}		$c_0 = 0.268655794$ 10^1		$a_0 = -0.311244445$ 10^0		$b_0 = 0.212634401$ 10^{-2}		$c_0 = 0.314479797$ 10^{-7}		
$a_1 = -0.351269284$ 10^{-1}			$b_1 = 0.218611643$ 10^{-2}		$c_1 = XX$		$a_1 = 0.107764443$ 10^0		$b_1 = 0.200863798$ 10^{-2}		$c_1 = XX$		
$a_2 = -0.631223038$ 10^{-5}			$b_2 = 0.361293015$ 10^{-7}		$c_2 = 0.283365291$ 10^{-3}		$a_2 = 0.899032798$ 10^{-5}		$b_2 = XX$		$c_2 = XX$		
$a_3 = 0.969404376$ 10^{-9}			$b_3 = 0.383672438$ 10^{-11}		$c_3 = 0.164050006$ 10^{-5}		$a_3 = 0.600223542$ 10^{-8}		$b_3 = XX$		$c_3 = XX$		
3	0.01	10-500	11	720	10^{-9}	0.0252	4	0.01	500-2400	7	480	-0.0051	0.0568
$a_0 = 0.941248793$ 10^{-1}			$b_0 = 0.255928505$ 10^{-2}		$c_0 = 0.158559233$ 10^1		$a_0 = -0.374701853$ 10^{-1}		$b_0 = 0.282373512$ 10^{-2}		$c_0 = 0.343133469$ 10^{-7}		
$a_1 = -0.473903805$ 10^{-1}			$b_1 = 0.230668550$ 10^{-2}		$c_1 = XX$		$a_1 = 0.165782838$ 10^{-1}		$b_1 = 0.227947381$ 10^{-2}		$c_1 = XX$		
$a_2 = -0.228000119$ 10^{-4}			$b_2 = 0.181737621$ 10^{-7}		$c_2 = 0.234371270$ 10^{-3}		$a_2 = -0.147378856$ 10^{-4}		$b_2 = XX$		$c_2 = XX$		
$a_3 = 0.146783625$ 10^{-8}			$b_3 = 0.369685660$ 10^{-11}		$c_3 = 0.164311900$ 10^{-5}		$a_3 = 0.639262077$ 10^{-8}		$b_3 = XX$		$c_3 = XX$		
5	0.02	10-500	10	720	-0.0049	0.0247	6	0.02	500-2400	7	480	-0.0118	0.059
$a_0 = 0.271748888$ 10^0			$b_0 = 0.362686206$ 10^{-2}		$c_0 = 0.342178520$ 10^0		$a_0 = 0.273490757$ 10^0		$b_0 = 0.357714856$ 10^{-2}		$c_0 = 0.368819582$ 10^{-7}		
-0.621005137 10^{-1}			$b_1 = 0.245222605$ 10^{-2}		$c_1 = XX$		$a_1 = -0.840137099$ 10^{-1}		$b_1 = 0.258932040$ 10^{-2}		$c_1 = XX$		
-0.423289562 10^{-4}			$b_2 = XX$		$c_2 = 0.186935062$ 10^{-3}		$a_2 = -0.431517526$ 10^{-4}		$b_2 = XX$		$c_2 = XX$		
$a_3 = 0.207261207$ 10^{-8}			$b_3 = 0.354059312$ 10^{-11}		$c_3 = 0.164706499$ 10^{-5}		$a_3 = 0.686710318$ 10^{-8}		$b_3 = XX$		$c_3 = XX$		
7	0.03	10-500	11	720	10^{-9}	0.036	8	0.03	500-2400	7	480	-0.016	0.062
$a_0 = 0.451469512$ 10^0			$b_0 = 0.465433802$ 10^{-2}		$c_0 = -0.927287938$ 10^0		$a_0 = 0.594881534$ 10^0		$b_0 = 0.427375024$ 10^{-2}		$c_0 = 0.390395897$ 10^{-7}		
$a_1 = -0.785371964$ 10^{-1}			$b_1 = 0.261091693$ 10^{-2}		$c_1 = XX$		$a_1 = -0.187931499$ 10^0		$b_1 = 0.291651551$ 10^{-2}		$c_1 = XX$		
$a_2 = -0.627405569$ 10^{-4}			$b_2 = -0.289245893$ 10^{-7}		$c_2 = 0.150301959$ 10^{-3}		$a_2 = -0.737430471$ 10^{-4}		$b_2 = XX$		$c_2 = XX$		
$a_3 = 0.274078889$ 10^{-8}			$b_3 = 0.340890806$ 10^{-11}		$c_3 = 0.164993587$ 10^{-5}		$a_3 = 0.740161850$ 10^{-8}		$b_3 = XX$		$c_3 = XX$		

Table 6 - T_S Fitting Coefficients for $|\Delta| \leq 0.03$

FIT #	Δ	RANGE INTERVAL (km)	# NON-ZERO CO-EFFICIENTS	# EGRWOO PTS USED IN FIT	AV FITTING ERROR (μSEC)	RMS FITTING ERROR (μSEC)	FIT #	Δ	RANGE INTERVAL (km)	# NON-ZERO CO-EFFICIENTS	# EGRWOO PTS USED IN FIT	AV FITTING ERROR (μSEC)	RMS FITTING ERROR (μSEC)
9	0.04	10-500	11	720	10 ⁻⁹	0.0468	10	0.04	500-2400	7	480	-0.021	0.0678
a ₀ = 0.636756317 10 ⁰			b ₀ = 0.571081273 10 ⁻²		c ₀ = -0.227641400 10 ¹		a ₀ = 0.943996301 10 ⁰			b ₀ = 0.495489663 10 ⁻²		c ₀ = 0.392006117 10 ⁻⁷	
a ₁ = -0.946254257 10 ⁻¹			b ₁ = 0.276691291 10 ⁻²		c ₁ = XX		a ₁ = -0.297966590 10 ⁰			b ₁ = 0.324968320 10 ⁻²		c ₁ = XX	
a ₂ = -0.819513480 10 ⁻⁴			b ₂ = -0.559741564 10 ⁻⁷		c ₂ = 0.125245265 10 ⁻³		a ₂ = -0.103900631 10 ⁻³			b ₂ = XX		c ₂ = XX	
a ₃ = 0.336675360 10 ⁻⁸			b ₃ = 0.319995014 10 ⁻¹¹		c ₃ = 0.164977429 10 ⁻⁵		a ₃ = 0.783991217 10 ⁻⁸			b ₃ = XX		c ₃ = XX	
11	0.05	10-500	11	720	10 ⁻¹⁰	0.059	12	0.05	500-2400	8	480	-0.006	0.063
a ₀ = 0.826251513 10 ⁰			b ₀ = 0.680981192 10 ⁻²		c ₀ = -0.369610810 10 ¹		a ₀ = 0.132483860 10 ¹			b ₀ = 0.562467127 10 ⁻²		c ₀ = 0.375861607 10 ⁻⁷	
a ₁ = 0.112354821 10 ⁰			b ₁ = 0.293250312 10 ⁻²		c ₁ = XX		a ₁ = -0.423778470 10 ⁰			b ₁ = 0.361596648 10 ⁻²		c ₁ = XX	
a ₂ = -0.100605942 10 ⁻³			b ₂ = -0.863011063 10 ⁻⁷		c ₂ = 0.108707152 10 ⁻³		a ₂ = -0.134923523 10 ⁻³			b ₂ = XX		c ₂ = XX	
a ₃ = +0.396581892 10 ⁻⁸			b ₃ = 0.292156567 10 ⁻¹¹		c ₃ = 0.164910518 10 ⁻⁵		a ₃ = 0.819899677 10 ⁻⁸			b ₃ = -0.219470477 10 ⁻¹²		c ₃ = XX	
13	0.06	10-50	8	240	-0.02	0.031	14	0.06	50-500	11	480	10 ⁻¹³	0.04
a ₀ = 0.617289977 10 ⁰			b ₀ = 0.140423259 10 ⁻¹		c ₀ = -0.324620764 10 ⁰		a ₀ = 0.15203497 10 ⁺¹			b ₀ = 0.683024252 10 ⁻²		c ₀ = -0.304708137 10 ⁺²	
a ₁ = 0.517689533 10 ⁻¹			b ₁ = XX		c ₁ = XX		a ₁ = -0.261156956 10 ⁰			b ₁ = 0.338378867 10 ⁻²		c ₁ = XX	
a ₂ = -0.122112739 10 ⁻³			b ₂ = XX		c ₂ = XX		a ₂ = -0.165432445 10 ⁻³			b ₂ = -0.108359234 10 ⁻⁷		c ₂ = 0.177077217 10 ⁻²	
a ₃ = -0.210464749 10 ⁻⁷			b ₃ = 0.311794559 10 ⁻⁹		c ₃ = 0.213441704 10 ⁻⁵		a ₃ = 0.509060740 10 ⁻⁸			b ₃ = 0.922295146 10 ⁻¹²		c ₃ = 0.167155693 10 ⁻⁵	
15	0.06	500-2400	8	480	-0.012	0.073							
a ₀ = 0.174927389 10 ¹			b ₀ = 0.627140425 10 ⁻²		c ₀ = 0.337591435 10 ⁻⁷								
a ₁ = -0.581550805 10 ⁰			b ₁ = 0.405168611 10 ⁻²		c ₁ = XX								
a ₂ = -0.167983892 10 ⁻³			b ₂ = XX		c ₂ = XX								
a ₃ = 0.848787838 10 ⁻⁸			b ₃ = -0.264920798 10 ⁻¹²		c ₃ = XX								

Table 7 - T_S Fitting Coefficients for $0.04 \leq |\Delta| \leq 0.06$

FIT #	$ \Delta $	RANGE INTERVAL (km)	# NON-ZERO CO-EFFICIENTS	# EGRNWO PTS USED IN FIT	AV FITTING ERROR (μ SEC)	RMS FITTING ERROR (μ SEC)	FIT #	$ \Delta $	RANGE INTERVAL (km)	# NON-ZERO CO-EFFICIENTS	# EGRNWO PTS USED IN FIT	AV FITTING ERROR (μ SEC)	RMS FITTING ERROR (μ SEC)
16	0.07	10-50	8	240	-0.024	0.035	17	0.07	50-500	11	480	-0.0057	0.049
$a_0 = 0.715936717$ 10^0			$b_0 = 0.165693691$ 10^{-1}			$c_0 = -0.695152495$ 10^0	$a_0 = 0.184882253$ 10^1			$b_0 = 0.779939919$ 10^{-2}			$c_0 = -0.390008994$ 10^2
$a_1 = 0.455158136$ 10^{-1}			$b_1 = XX$			$c_1 = XX$	$a_1 = -0.315035353$ 10^0			$b_1 = 0.365706558$ 10^{-2}			$c_1 = 0.115708745$ 10^2
$a_2 = -0.133051379$ 10^{-3}			$b_2 = XX$			$c_2 = XX$	$a_2 = -0.195483664$ 10^{-3}			$b_2 = -0.214642354$ 10^{-7}			$c_2 = 0.218168925$ 10^{-2}
$a_3 = -0.236541723$ 10^{-7}			$b_3 = 0.311467721$ 10^{-9}			$c_3 = 0.217287449$ 10^{-5}	$a_3 = 0.584725582$ 10^{-8}			$b_3 = XX$			$c_3 = 0.167687857$ 10^{-5}
18	0.07	500-2400	9	480	-0.0015	0.090	19	0.08	10-50	9	240	0.01	0.07
$a_0 = 0.224368055$ 10^1			$b_0 = 0.691268107$ 10^{-2}			$c_0 = 0.247223976$ 10^{-7}	$a_0 = 0.752930732$ 10^0			$b_0 = 0.211851495$ 10^{-1}			$c_0 = -0.881502303$ 10^0
$a_1 = -0.804753751$ 10^0			$b_1 = 0.461396300$ 10^{-2}			$c_1 = XX$	$a_1 = 0.233266434$ 10^0			$b_1 = -0.145882894$ 10^{-1}			$c_1 = XX$
$a_2 = -0.202979868$ 10^{-3}			$b_2 = -0.277887985$ 10^{-8}			$c_2 = XX$	$a_2 = -0.134783533$ 10^{-3}			$b_2 = XX$			$c_2 = -0.347040670$ 10^{-3}
$a_3 = 0.658580091$ 10^{-8}			$b_3 = -0.305728335$ 10^{-12}			$c_3 = XX$	$a_3 = -0.185075497$ 10^{-7}			$b_3 = XX$			$c_3 = 0.226539012$ 10^{-5}
20	0.08	50-500	11	480	.0008	0.146	21	0.08	500-2400	8	720	0.018	0.134
$a_0 = 0.246703897$ 10^1			$b_0 = 0.848916609$ 10^{-2}			$c_0 = -0.603953203$ 10^{-2}	$a_0 = 0.291092336$ 10^1			$b_0 = 0.740078603$ 10^{-2}			$c_0 = 0.143781406$ 10^{-7}
-0.198123745 10^1			$b_1 = 0.736414298$ 10^{-2}			$c_1 = 0.116512038$ 10^2	$a_1 = -0.112253482$ 10^1			$b_1 = 0.560487464$ 10^{-2}			$c_1 = XX$
$a_2 = -0.25936955$ 10^{-3}			$b_2 = XX$			$c_2 = 0.578435989$ 10^{-2}	$a_2 = -0.252488609$ 10^{-3}			$b_2 = -0.370230090$ 10^{-8}			$c_2 = XX$
$a_3 = 0.821357677$ 10^{-8}			$b_3 = -0.552734975$ 10^{-11}			$c_3 = 0.155433255$ 10^{-5}	$a_3 = 0.859508521$ 10^{-8}			$b_3 = XX$			$c_3 = XX$

Table 8 - T_S Fitting Coefficients for $|\Delta| = 0.07, 0.08$

R. Doherty, also of ITS, has developed a program called DATA MINS which will take TD data from one of more points and calculate least squares fitted Δ_E 's. (13), (14) These, when used in EGRWOO, will minimize the mean square error between predicted and measured TD's. With only a single data point (TD pair if a Loran triad is being mapped) it is obvious that a unique solution for Δ_E will not exist as the number of time differences is always one less than the number of paths. However, by assuming one of the Δ_E 's (generally the best behaved one) as known, the remaining Δ_E 's may be solved for uniquely. In the multipoint mode the same problem appears unless the data points are sufficiently close so that it may be assumed that the effective wave impedance of at least one of the stations remains constant. Nevertheless, in spite of this frequent lack of absolute uniqueness, Doherty's program is very useful for generating a best fit set of wave impedances with which one may accurately compute TD's even in the presence of irregular inhomogeneous terrain with land-sea boundaries, etc.

Of course, the Δ_E 's are not constant over the entire area an aircraft's or ship's mission might take it. At the very minimum then, this area should be broken up into several smaller subareas within which the wave impedances might be considered constant. For 0.3-0.5 μ sec accuracy, suitable for general navigation over most well-behaved areas, past experience by ITS has shown these subareas may have sizes from 10,000-100,000 sq. miles. For more precise navigation over land (0.1-0.3 μ sec accuracy) typical subarea sizes might be 2500-10,000 sq. miles for a well behaved area. When irregular terrain or a land-sea boundary lies inside or close to the navigational area of interest, it is better to use some form of power series solution of $|\Delta_E|$ in terms of local geodetic coordinates instead of reducing the subarea sizes further. This would require then the a-priori least squares fitting of a polynomial for $|\Delta_E|$ in terms, say, of (λ, Λ) to the DATA MINS calculations and then the subsequent loading of these polynomials on board the loran receiver in addition to the T_S polynomials already present.

Regardless of the number of subareas chosen the receiver processor must also include decision logic to decide in which subarea the craft is located. Furthermore, some form of hysteresis may be included so that the aircraft can fly along a subarea boundary without the loran coordinate converter constantly switching the set of selected wave impedances.

Finally, h , η , and α need to be supplied. h may be obtained by constantly differencing h_T from h_R as measured by baro-altimeter referenced to the transmitter elevation. If a radar altimeter is used the measured receiver altitude above ground must be corrected for the mean sea level elevation of the earth below. η and α may be determined by a combination of meteorological and loran monitor station measurements. As previously mentioned, η only loosely affects T_S and so it may be frequently assigned its nominal value of 1.000338 for the a-priori data calculations and in the airborne computer. α , however, is strongly weather dependent to which a recent paper by Doherty and Johler attests. (15) Its nominal value is about 0.85; however, an exact determination will require several loran monitor sites. In particular, monitors should be located near each transmitter so that clock drift, etc. is not confused with an α change. These, and only these, monitors should have control over the transmitters, if Loran C is to have high absolute accuracy over a large area. In turn, field monitors could then attribute any changes in the observed TD's to meteorological changes affecting α and, to some extent, η . The aircraft would then always use

the α (and η if necessary) of the day or hour appropriate for the given area of operation. All diurnal, annual, and random temporal effects could then be continuously compensated in this manner. Due to the rapid nature of some temporal variations, these quantities may also have to be updated every hour or so if very precise navigation is to be had (under 200' rms position error). In the absence of accurate α or η measurements the nominal values should be used and all temporal effects compensated for by slightly altering the assumed station emission delays loaded onboard the receiver computer.

Recent Results for Fitting Time Difference for Eglin AFB, Florida

To provide accurate Loran navigation and blind weapon delivery performance the simplified secondary phase algorithm has been implemented in the AN/ARN-101 Digital Modular Avionics System developed by Lear Siegler, Inc. In preparation for the AN/ARN-101 flight test at Eglin AFB, a-priori TD measurements were made. One hundred twenty (120) of these measurements were taken by the USCG during the winter of 1973-1974 at calibrated bench points on the ground using a mobile van and UPN-135 receivers over a 25x50 nmi area containing the Eglin reservation. Eighteen additional ground based data points were obtained from the loran data bank at ITS so as to increase the expanse for which data points were available to roughly a 40x72 sq nmi area extending in latitude from 30.3° to 31.0° and in longitude from -87.2° to -85.75°. These latter 18 points were taken between 1967 and 1973 by a variety of receivers and under non-controlled conditions. However, they were the only data available in their respective regions and so were used for this test of the algorithm.

The measured TD data used was "corrected" for temporal variations. This was done by noting the deviation of the two received TD's, TDA (Jupiter) and TDB (Dana), from the nominal yearly average values as measured by a monitor site located at the airbase itself. This monitor also controls Dana's emission delay and waveform and a second monitor, now at Bermuda, controls the Jupiter slave in a similar closed loop manner. As mentioned previously, it would be preferable to place such closed loop monitors much closer to their respective transmitters so that weather-induced effects on the loran signals could be clearly differentiated from transmitter phase or timing shifts. The simplified algorithm for secondary phase computation is still employable at Eglin, however, by fixing α at 0.85, η at 1.000338, and assuming that all shifts in the observed TD's at the monitor site are due to changes in the emission delays of the two slaves. The nominal values of these emission delays are 13695.719 μ sec for TDA and 68560.548 μ sec for TDB. Due to the active control on the Dana slave by the Eglin monitor, the apparent emission delay of that slave was always much closer to its nominal value than was the emission delay of the Jupiter slave. Since the measured USCG "data" was not raw TD's but was corrected for changes in the apparent coding delays, the fitting tests run on this data at Grand Rapids were initially performed with the emission delays set equal to their nominal values.

Use of DATA MINS in the multipoint mode on either of two sets of 60 points, each from the 120 USCG points, gave a set of three effective wave impedances for the entire area. Actually, only the slave wave impedances were assumed variable and the master wave impedance, Δ_{EM} , was fixed with $|\Delta_{EM}| = 0.045$ (with the phase uniquely determined as previously stated). These runs were made by ITS during March of 1974 and found $|\Delta_{EA}| = 0.028$ and $|\Delta_{EB}| = 0.040$ for either of the two sets of 60 data points, where Δ_{EA} is associated with the Jupiter slave and Δ_{EB}

with the Dana slave. Use of these effective wave impedances to predict back the 120 TD's gave zero mean errors but did give a 0.55 μ sec 1 σ variation on TDA and a 0.3 μ sec 1 σ variation on TDB. As expected, the variance on the Jupiter TD was larger because the path to Jupiter changes as one proceeds westward across the Eglin area from a predominately land path to a predominately sea path.

For precise navigation in the Eglin area, it was apparent that the wave impedances would have to be a function of position. Runs were made at both Grand Rapids and Boulder with DATA MINS in the "single point mode" where a wave impedance pair was calculated for each data point with Δ_{EM} assumed fixed at 0.045. Due to the large variations in $|\Delta_{EA}|$ or $|\Delta_{EB}|$ and since, in the Eglin area, a 10% change in either of the nominal $|\Delta_E|$'s would correspond to a change in predicted TOA of 0.2 μ sec, it was decided to use fitting polynomials on $|\Delta_{EA}|$ and $|\Delta_{EB}|$. Johler, Hyovalti, and Jones of ITS described a quartic fitting polynomial for $|\Delta_E|$ in a recent publication.⁽¹⁶⁾ These polynomials contain 15 coefficients which multiply various polynomials in λ , Λ through the fourth order. The polynomials are actually in terms of two variables u_1 , u_2 related to λ , Λ by

$$u_1 = \frac{2\lambda - (\lambda_I + \lambda_T)}{\lambda_T - \lambda_I} \quad (19)$$

$$u_2 = \frac{2\Lambda - (\Lambda_I + \Lambda_T)}{(\Lambda_T - \Lambda_I)} \quad (20)$$

where λ_I , Λ_I and λ_T , Λ_T are constants to be specified. The ITS program (called GENRAT), to determine the 15 coefficients, was run at Grand Rapids using 136 of the 138 available data points to generate the fit (two of the 120 recent measurements appeared to be anomalous, exhibiting wave impedances as calculated by DATA MINS considerably different from that for other data points only 1-2 miles away and so they were omitted). For the determination of u_1 or u_2 , λ_I was 30.3°, λ_T was 31.0°, and Λ_I and Λ_T were -87.2° and -85.75° respectively. These constants were also taken as defining the prime area within which quartic polynomials rather than constant solutions were permitted for effective wave impedances. All the 136 ground data points used to generate the $|\Delta_E|$ polynomials were within the boundaries of the prime area and were fairly well distributed throughout. Unfortunately, only the several year old data covered the extreme west, north, and east sections of the prime area. Maximum distances between any location in the prime area and one of the 136 data points were only a few miles except in the extreme north, west, and east sections where they were about 10 miles.

It should be mentioned that reasonably accurate navigation is permitted outside the prime area (3000 sq nmi) by the airborne algorithm adopted by LSI. In particular, computer storage is allocated for defining up to four additional areas, besides the prime area, with their own wave impedances and boundaries and including appropriate decision logic to determine what area should be selected in the algorithm. Furthermore, up to ten loran stations are assumed to be present for each area, comprising two chains - each with a master and

four slaves. Finally, the complete airborne algorithm allows storage for different α and η values for each station in each area although, if not specified, the nominal values of 0.85 and 1.000338 were automatically chosen.

By efficient coding it was possible to package the entire TD calculation algorithm within 792 16-bit words of a Lear Siegler airborne computer (an LS-52). The complete algorithm was called program PROP with PROP standing for "propagation" and included the twenty-one T_S polynomials as a subroutine called T_S . Included in the 792 words is a numerical calculation of $\frac{d}{dt}(TOA)$ useful for rate aiding a loran phase tracking loop. By definition, the rate of change of the time of arrival is

$$\frac{d(TOA)}{dt} = \frac{d(TOA_p)}{dt} + \frac{d(T_S)}{dt} \quad (21)$$

where

$$\frac{d(TOA_p)}{dt} = \frac{d(TOA_p)}{d\rho} \cdot V_\rho \quad (22)$$

and

$$\frac{d(T_S)}{dt} = \frac{\partial(T_S)}{\partial\rho} \cdot V_\rho + \frac{\partial(T_S)}{\partial h} \cdot V_h \quad (23)$$

with V_ρ the radial aircraft velocity and V_h the vertical aircraft velocity, both determined by some independent velocity sensor such as an inertial navigator. The radial and vertical partial derivatives in equation (23) may be calculated directly from the T_S polynomials in equation (16). Usually only $\frac{d}{dt}(TOA_p)$ is mechanized in a loran navigation system; however, in the AN/ARN-101 system $\frac{d}{dt}(T_S)$ is added to $\frac{d}{dt}(TOA_p)$ to provide a more accurate rate aid.

The complete algorithm was tested using the 136 original data points. The prime area effective impedance polynomials were used in PROP to predict back the measured TD's. Table 9 lists the coefficients for the two fitting polynomials used in the above test along with estimates for the fixed wave impedances, calculated via extrapolation, for the four (4) areas surrounding the prime area. Our results showed that for the 136 data points the mean discrepancies between original and predicted TD's were well under 0.001 μ sec for both TDA and TDB. Furthermore, the 1 σ prediction errors were both about 0.19 μ sec and peak errors were under 0.6 μ sec. These errors reflect a 2:1 to 3:1 improvement over the use of a single set of fixed wave impedances for the entire prime area.

Figure 1 shows the differences between the original and predicted TD's at 34 of the 136 data points, where the TD_A and TD_B differences are given in parentheses at each point with the TD_A difference appearing to the left. This figure displays the spatial variation in the fitting errors.

To further refine the impedance map, the apriori data was supplemented with airborne data collected during the first half of the AN/ARN-101 flight test. Using 148 sets of (TDA, TDB) vs (λ, Λ, h) measurements* as new data points along with 6 synthesized (Δ_{EA}, Δ_{EB}) points in the sparsely mapped northwest sector of the prime test area, the wave impedance maps were recomputed.

* These points were taken during straight and level flight at altitudes of 5, 10, and 15 thousand feet.

$ \Delta_{EA} $		$ \Delta_{EB} $
$0.33801220 \times 10^{-1}$	1	$0.39227348 \times 10^{-1}$
$0.16221799 \times 10^{-1}$	u_1	$0.14618851 \times 10^{-3}$
$0.71277805 \times 10^{-2}$	u_2	$0.71120672 \times 10^{-2}$
$-0.15815843 \times 10^{-1}$	$(u_1)^2$	$0.94893537 \times 10^{-2}$
$-0.44982925 \times 10^{-1}$	$u_1 u_2$	$0.12858086 \times 10^{-2}$
$0.16911747 \times 10^{-2}$	$(u_2)^2$	$-0.23696877 \times 10^{-2}$
$-0.16249973 \times 10^{-1}$	$(u_1)^3$	$-0.61056390 \times 10^{-2}$
$-0.54393224 \times 10^{-2}$	$(u_1)^2 u_2$	$-0.66968389 \times 10^{-2}$
$-0.67741945 \times 10^{-2}$	$u_1 (u_2)^2$	$0.81738196 \times 10^{-2}$
$0.32153202 \times 10^{-2}$	$(u_2)^3$	$-0.94769849 \times 10^{-3}$
$0.20129651 \times 10^{-1}$	$(u_1)^4$	$-0.62174872 \times 10^{-2}$
$0.46178937 \times 10^{-1}$	$(u_1)^3 u_2$	$0.24105937 \times 10^{-2}$
$-0.22996388 \times 10^{-1}$	$(u_1)^2 u_2^2$	$-0.15742116 \times 10^{-1}$
$0.26653439 \times 10^{-1}$	$u_1 (u_2)^3$	$0.19814842 \times 10^{-3}$
$0.21173048 \times 10^{-2}$	$(u_2)^4$	$0.35441120 \times 10^{-2}$

$$|\Delta_{EM}| \triangleq 0.045 \text{ (all areas)}$$

$$\lambda_I = 30.3^\circ, \lambda_F = 31.0^\circ, \Lambda_I = -87.2^\circ, \Lambda_F = -85.75^\circ$$

(a) Coefficients for Prime Test Area

Area	$ \Delta_{EA} $	$ \Delta_{EB} $
2	0.0226	0.0382
3	0.0316	0.0406
4	0.0361	0.0419
5	0.0336	0.0334

(b) Wave Impedances for Surrounding Areas

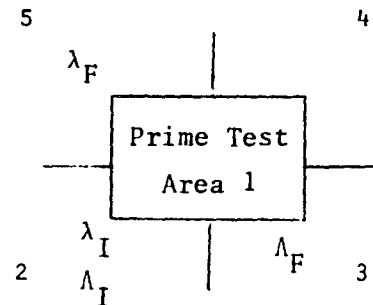
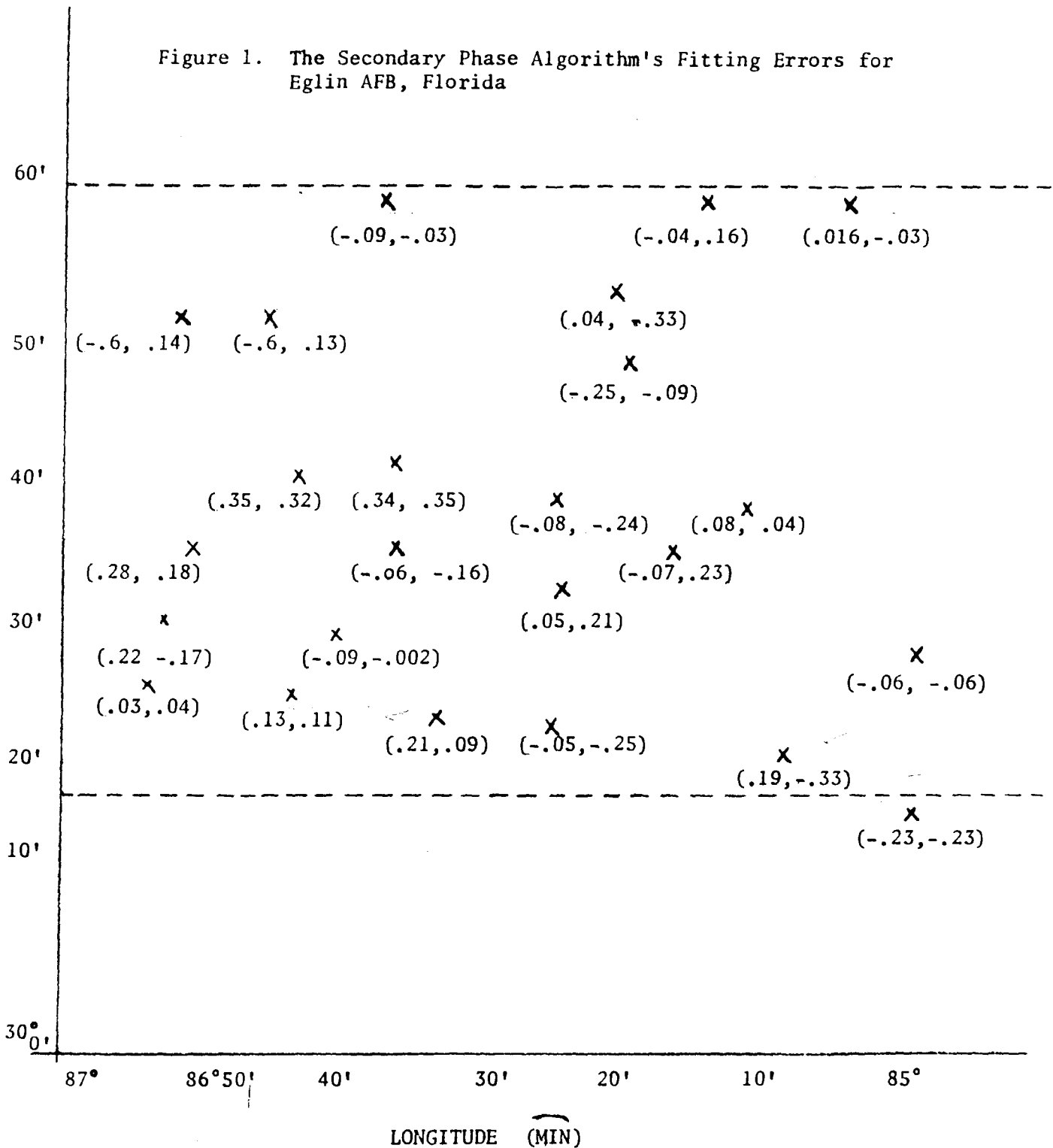


Table9 - $|\Delta_E|$ Maps for Eglin from Ground TD Measurements

Figure 1. The Secondary Phase Algorithm's Fitting Errors for
Eglin AFB, Florida



The slave A and slave B wave impedance maps corresponding to the recomputed fit described above are shown as contour plots in Figures 2 and 3. The predicted changes in TD_A and TD_B , at sea level, caused by the master and two slaves secondary phases are shown in Figures 4 and 5, respectively. Figure 4's (5's) contour plot shows the differences between slave A's (B's) predicted secondary phase and the master's predicted secondary phase. The apparent large gradients that appear at the boundaries in the plots do not exist in the airborne computer, but are merely a result of the calcomp plotter routine used to generate the plots.

The data set for these mappings also included 134 of the original ground measurements (2 more had been ruled suspect due to large, 10% or greater, deviations in wave impedance from neighboring points as calculated by DATA MINS). Thus there were 288 data points used to generate the modified fitting polynomials for the prime area. Testing out the 282 measured data points of the fit gave results depicted in Table 10. Use of the new impedance maps for subsequent flight tests over the prime area appears to give 1 σ TD errors almost as small as for the fitted data, namely 0.20-0.25 μ sec. Furthermore, the fixed wave impedances outside the prime area have been revised from the values listed in Table 9 to more nearly match the average values of $|\Delta_{EA}|$, $|\Delta_{EB}|$ near the periphery of the prime area as evaluated using the modified mapping polynomials.

The above results assumed the master wave impedance to be 0.045 in magnitude. Other secondary phase prediction fits were attempted for the prime area with $|\Delta_{EM}|$ varied between 0.04 and 0.055. As far as just the ground measurements were concerned, the fitting errors were about the same regardless of $|\Delta_{EM}|$. However, when fits of airborne data/ground data were attempted it was noted that altitude effect predictions were slightly more accurate using $|\Delta_{EM}| = 0.0504$. This value of $|\Delta_{EM}|$ will be assumed, therefore, in the following discussion on measured altitude effects.

Fits of $|\Delta_{EA}|$ $|\Delta_{EB}|$ to λ, Λ based upon 288 data points.

PRIME AREA

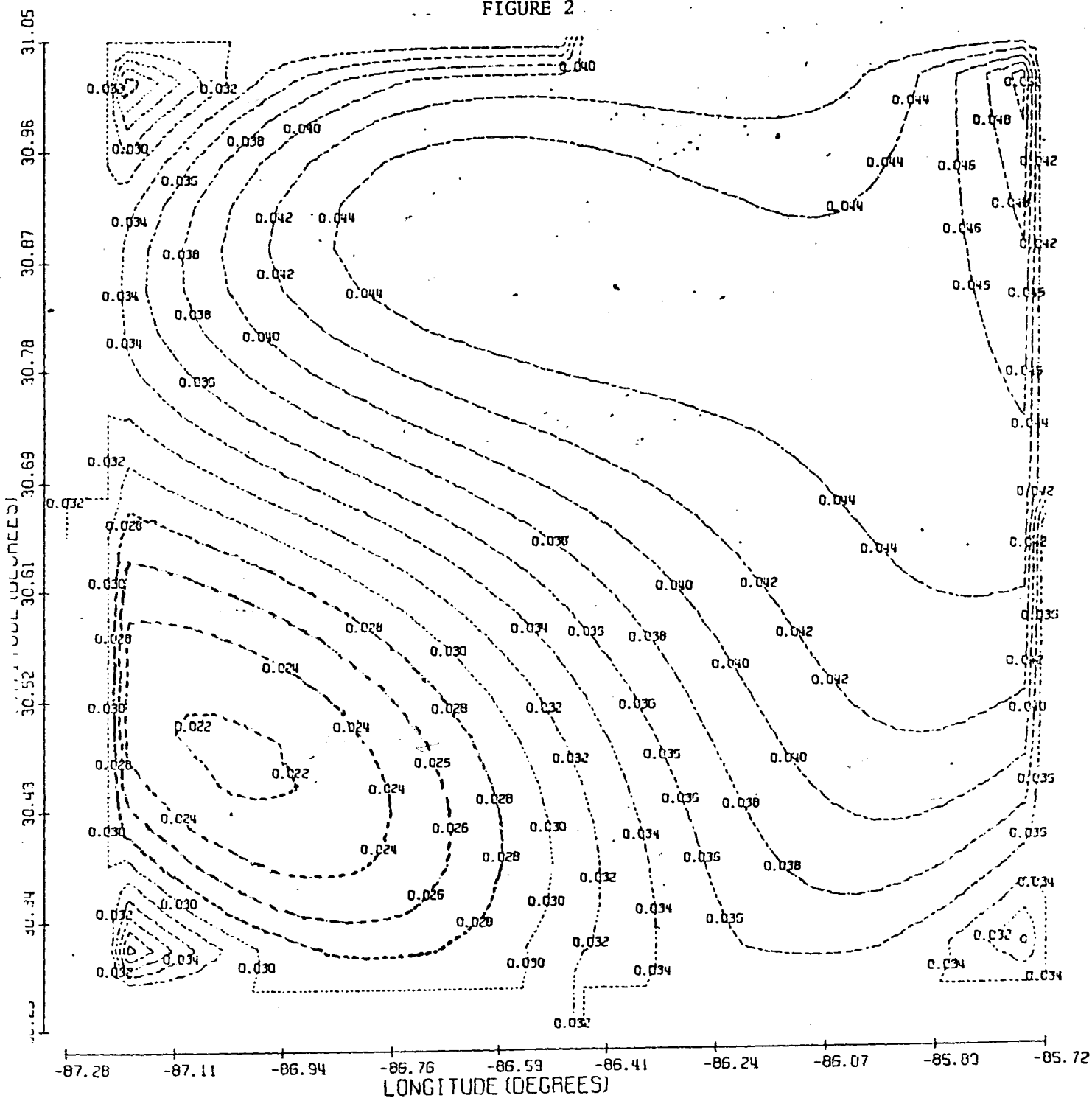
TDA MEAN	= 0.0173	TDB MEAN	= 0.0210
TDA VARIANCE	= 0.0477	TDB VARIANCE	= 0.0634
MAX TDA ERROR	= -0.5965	MAX TDB ERROR	= 0.7641
TDA STANDARD DEV.	= 0.2184	TDB STANDARD DEV.	= 0.2518

Table 10 - Goodness of Fit Test for 282 Actually Measured Data Points

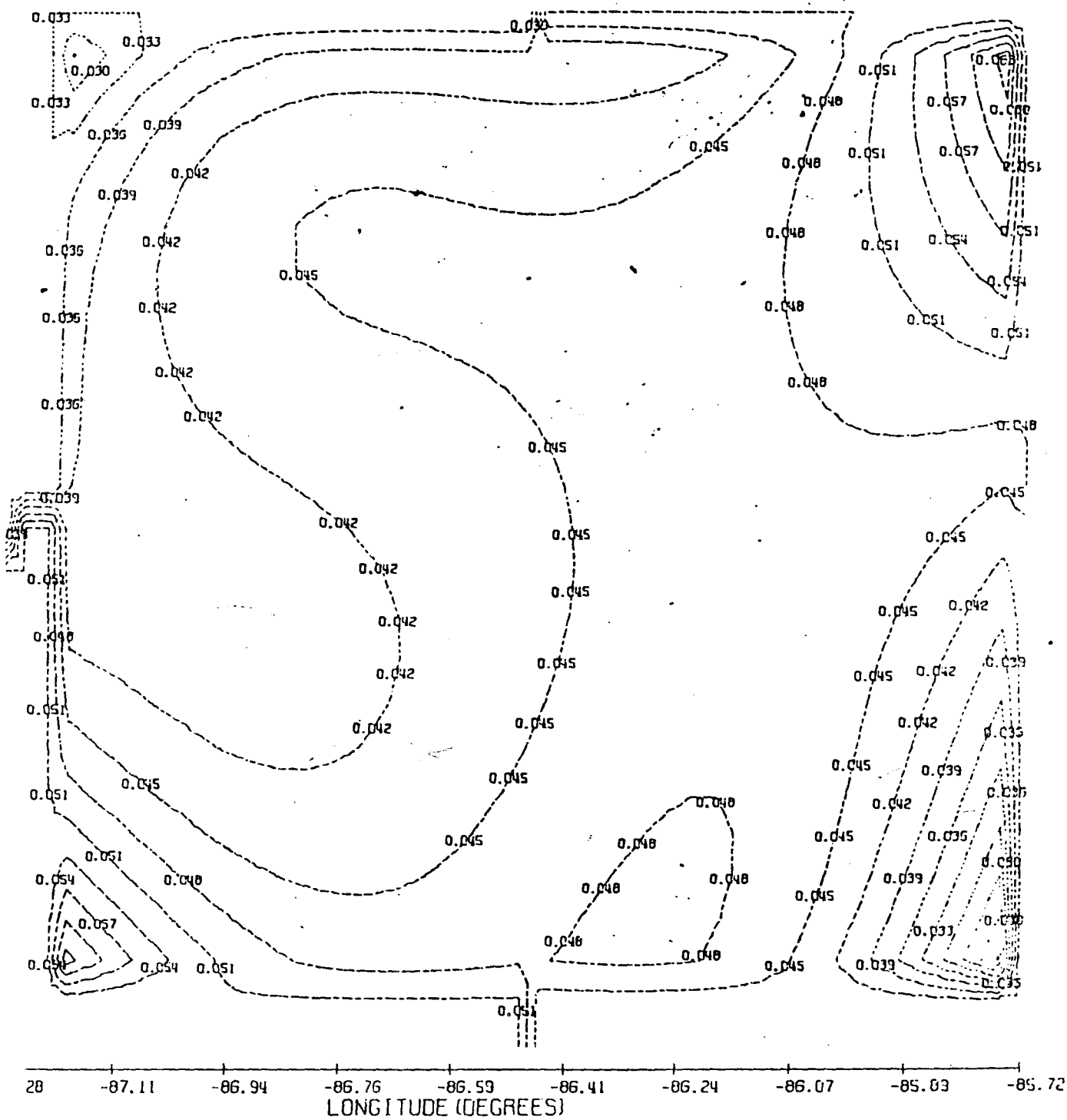
Emission Delay for TDA = 13695.473 μ sec

Emission Delay for TDB = 68560.673 μ sec

WAVE IMPEDANCE (TDA)
EGLIN AFB AREA
FIGURE 2

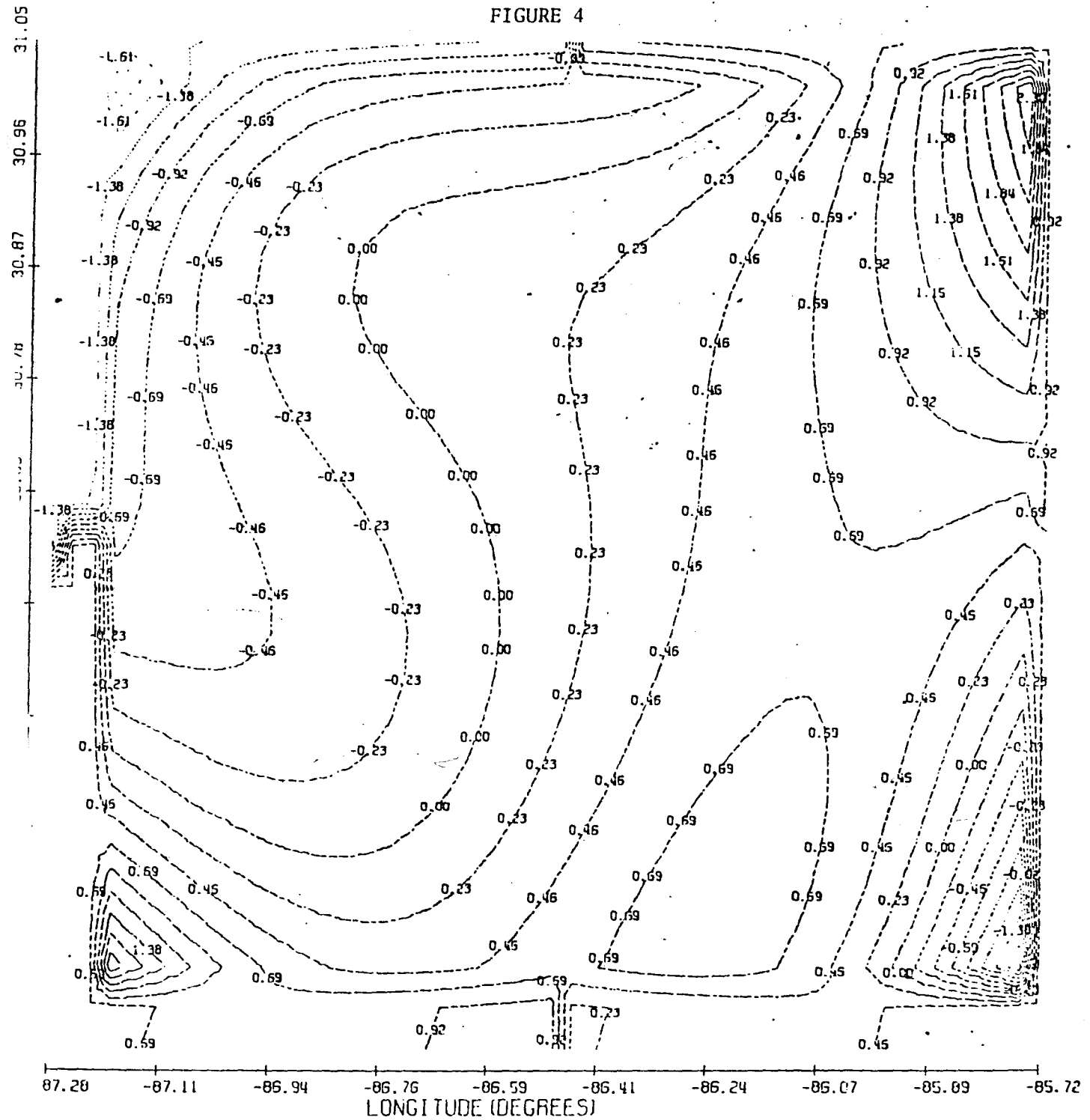


WAVE IMPEDANCE (TDB)
 EGLIN AFB AREA
 FIGURE 3

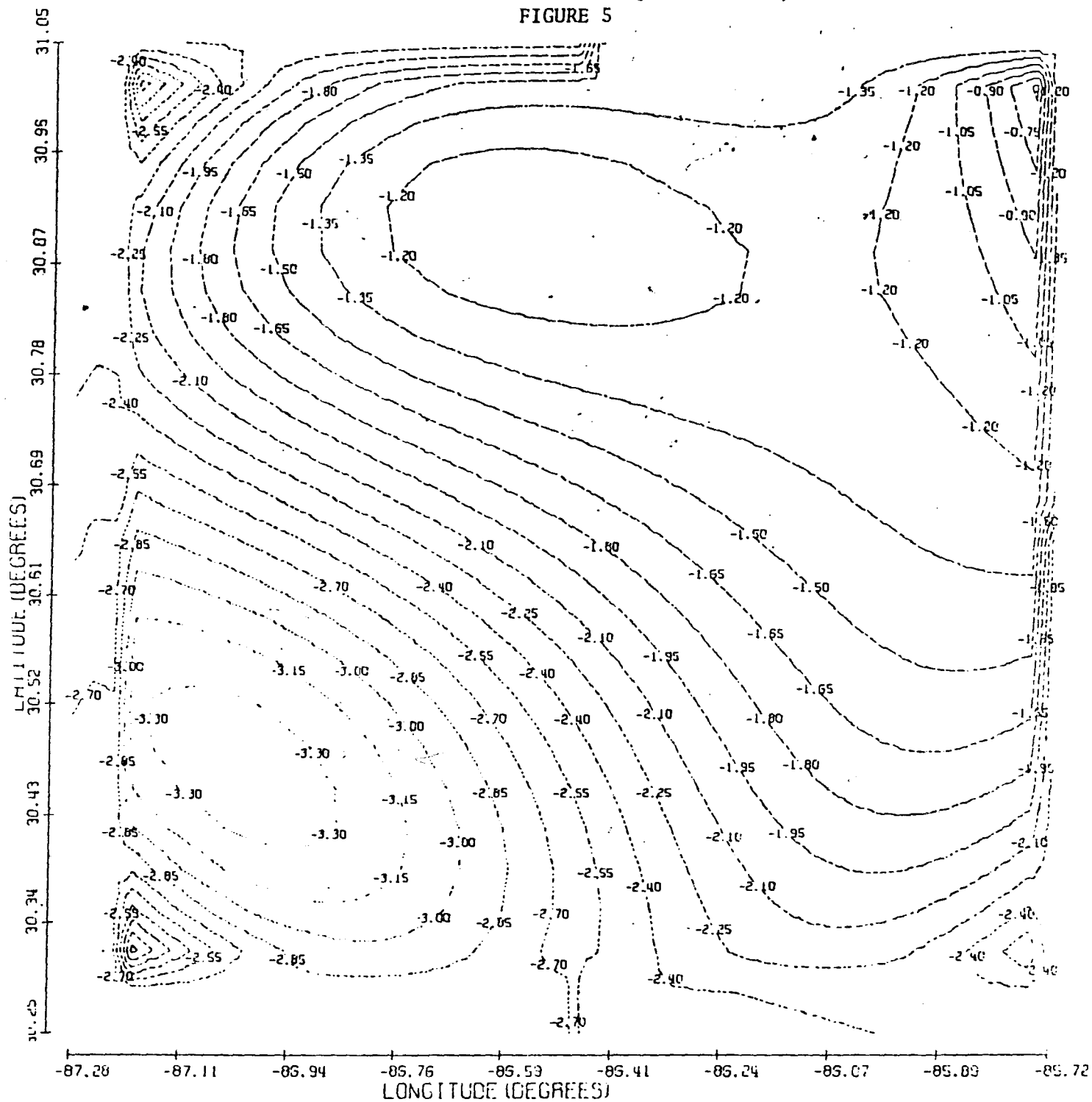


TDB SECONDARY PHASE
EGLIN AFB AREA
FIGURE 4

407



TDA SECONDARY PHASE
EGLIN AFB AREA
FIGURE 5



The absolute position errors exhibited by an airborne Loran navigation system using the secondary phase algorithm described in this paper were recorded during the flight test of the AN/ARN-101 Digital Modular Avionics System at Eglin AFB, Florida. The position errors were developed by differencing aircraft position information, obtained from tracking radars, with the position data computed by the AN/ARN-101 system. The dynamic position errors observed during flights over two of the Eglin AFB's ranges were found to be a function of the receiver's location, both its horizontal position and its altitude. The absolute position error's spatial dependency was expected because of the secondary phase algorithm's fitting characteristics shown in Figure 1. However, position error dependency on altitude raised the questions of how much the time differences vary with receiver altitude, and how effective is the secondary phase algorithm in compensating for the vertical variation in the TD's.

At a point on one of the Eglin ranges where the altitude effects are procured, data from a number of flights was processed and analyzed. Certain flights were partially devoted to the vertical effects investigation with the aircraft flying racetrack patterns at 5000, 10,000, 15,000 and 20,000 feet altitude. Table 11 shows the results of this investigation. The second and third columns show how the TD's vary, if a receiver's altitude above the test point increases. This data was developed by first extrapolating the TD's measured by the AN/ARN-101 receiver at points on the racetrack profiles over to the test point; next, for each altitude the TD's at the test point were averaged; and finally, the relative TD variations were obtained by subtracting the TD at 150 feet altitude.

The fourth and fifth columns of Table 11 show the TD's predicted by the AN/ARN-101 system for the test point using the secondary phase algorithm and the second wave impedance map described above. The predicted TD's for 150 feet altitude were subtracted to obtain the TD variations.

Table 11 shows that at the test point, TD_A increases 0.93 μsec in 20,000 feet with the secondary phase algorithms compensating for about one half of this change. The TD_B variation is less, 0.29 μsec in 20,000 feet, but again the algorithm only partially compensates for it. These results are for one test point on the Eglin AFB range where the altitude effect appears to be large when compared to data at other points.

TABLE 11
TIME DIFFERENCE VARIATIONS WITH ALTITUDE

ALT.	MEASURED (Δ 's)		101 PREDICTED (Δ 's)	
	TDA	TDB	TDA	TDB
150	0.0	0.02	0.0	0.0
5,000	.19	0.0	0.118	0.038
10,000	.22	.11	0.218	0.068
15,000	.70	.32	0.306	0.106
20,000	.93	.31	0.404	0.149

DISCUSSION

It is obvious from the preceding test that as the Loran absolute accuracy is made better, any incremental improvements require increasingly larger expenditures of computer processing time. We note the 0.20-0.25 μsec 1 σ TD errors achieved during the more recent flight tests using the 288 "measured" data points (134 ground, 148 airborne, 6 synthesized). This is quite remarkable for the Eglin area in view of past experience there and is certainly accurate for most loran navigational requirements. It should be borne in mind, however, that the ground TD measurements still used in the fit were subject to the effects of man-made local anomalies such as telephone and power lines, buildings, etc. Furthermore, 16 of the data points were taken years previous to the remainder with different receivers and probably using different measurement techniques. Indeed, most of the large residual TD errors in the fitted points were associated with these older ones, thus indicating that some shift in the chain may have occurred during the interim and hence that the various data are not really quite compatible.

Use of subroutine GROUND instead of the simple polynomial for T_S will have little effect on improving the accuracy at Eglin. The rms error between the polynomial solution and the residue solution at $\rho = 1000$ km and $|\Delta_E| = 0.02-0.03$ is under 0.05 μsec including all interpolation error. Use of the T_S polynomials here allowed TD prediction with a simple algorithm in an airborne computer with almost the same accuracy as obtainable on a large ground based computer.

The fact that the LSI/ITS algorithm does not completely track the changes of TDA or TDB with altitude over a given location on the ground may be explained as being due to local terrain effects. The effective wave impedance concept is an attempt to force the classical, homogeneous, earth theory to fit the real world situation with such non-homogeneous path occurrences as a land/sea boundary. One would have to program the Δ_E 's as functions of altitude as well as λ, Λ in order to reduce the altitude effect errors over a given point in the fitting area and yet keep the rms errors small over the entire area.

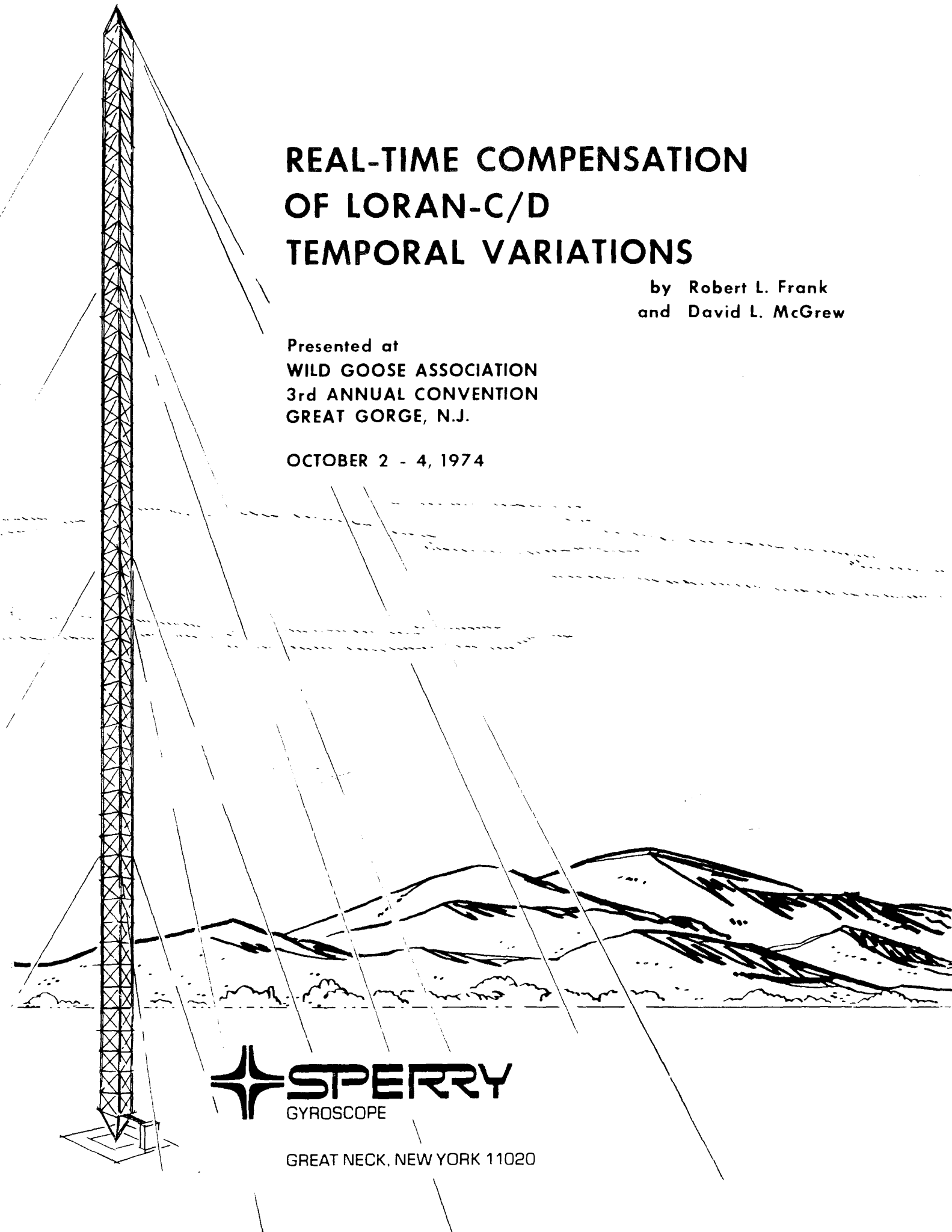
ACKNOWLEDGEMENTS

Thanks are due Dr. J. R. Johler of ITS, Boulder and Mr. Robert Doherty, also of ITS, for many fruitful discussions and for computer programs DATA MINS, EGRWOO, and GENRAT. DATA MINS earlier was converted by Mr. Doherty to use the author's T_S polynomial algorithm, instead of subroutine GROUND as EGRWOO does, so as to shorten its running time.

Thanks are also due Dr. Lee Strodtman of LSI for help in determining the T_S polynomials which fitted EGRWOO and for processing the Eglin data using DATA MINS and GENRAT.

REFERENCES

1. Sommerfeld, A. (1926), "Über die Ausbreitung der Wellen in der Drahtlosen Telegraphie", Ann. Phys. Lps., Vol. 81, p. 1135.
2. Watson, G. N. (1919), "The Transmission of Electric Waves Around the Earth", Proc. Royal Soc., Vol. A95, pp. 546-563.
3. Norton, K. A. (1936), "The Propagation of Radio Waves Over the Surface of the Earth and in the Upper Atmosphere", Proc. of the IRE, Vol. 24, and (1937) Vol. 25.
4. Fock, V. A. (1965), Electromagnetic Diffraction and Propagation Problems, Pergamon Press.
5. Bremmer, H. (1949), Terrestrial Radio Waves - Theory of Propagation, Elsevier Press.
6. Wait, J. R. (1964), "Electromagnetic Surface Waves", from Advances in Radio Research, Academic Press.
7. Johler, J. R. (1956), "Phase of the Low Frequency Ground Wave", N.B.S. Circular 573.
8. Johler, J. R. (1967), "Loran D Phase Corrections Over Inhomogeneous, Irregular Terrain", ESSA Tech. Rpt., IER 59-ITSA.
9. Johler, J. R. (1969), "Loran C, D Phase Corrections Over Irregular, Inhomogeneous Terrain - Simplified Computer Methods", ESSA Tech. Rpt., ERL 116 ITS83.
10. Johler, J. R., Hyovalti, D. C. (1970), "Radio Navigation Coordinate Corrections for Excess Phase Accumulation Over Irregular Inhomogeneous Terrain, ESSA Tech. Rpt., ERLTM-ITS220.
11. Johler, J. R. (1971), "Loran Radio Navigation Over Irregular Inhomogeneous Ground with Effective Ground Impedance Maps", U.S. Dept. of Commerce Rpt., OT/TRER22.
12. Johler, J. R. and Hyovalti, D. C. (1973), "Theoretical Computer Simulations for Loran C/D Radio Navigation System Predictions", U.S. Dept. of Commerce Rpt., OT-ITS 73-133.
13. Doherty, R. H. (1972), "A Loran-C Grid Calibration and Prediction Method", U.S. Dept. of Commerce Rpt., OT/TRER 25.
14. Doherty, R. H. (1972), "Fortran Programs and Descriptions for Use in a Loran C Grid Calibration and Prediction Method", U.S. Dept. of Commerce Rpt., OT TM-79.
15. Johler, J. R. and Doherty, R. H. (1973), "Meteorological Influences on Loran-C Ground Wave Propagation", Proceedings of the National Radio Navigation Symposium, 13-15 Nov., 1973, Washington, D.C. (sponsored by ION).
16. Johler, J. R., Hyovalti, D. C., Jones, W. B. (1973), "Impedance Maps to Predict the Effect of Irregular Inhomogeneous Ground on Loran C/D Radio Navigation Systems", U.S. Dept. of Commerce Rpt., OT-ITS 73-6.



REAL-TIME COMPENSATION OF LORAN-C/D TEMPORAL VARIATIONS

by Robert L. Frank
and David L. McGrew

Presented at
WILD GOOSE ASSOCIATION
3rd ANNUAL CONVENTION
GREAT GORGE, N.J.

OCTOBER 2 - 4, 1974

 **SPERRY**
GYROSCOPE

GREAT NECK, NEW YORK 11020

REAL-TIME COMPENSATION OF LORAN-C/D TEMPORAL VARIATIONS

Robert L. Frank
Consultant
16500 N. Park Dr., Southfield Mich. 48075

David L. McGrew
Senior Engineer
Sperry Gyroscope Div., Sperry Rand Corp.
Great Neck, N.Y. 11020

ABSTRACT

Data from Loran-C station monitoring is presented which shows diurnal and temporal variations attributed to weather. By an algorithm based on an assumption of uniform variation of propagation velocity over the service area, marked reductions in the variation in Loran measurements can be produced in desired portions of the service area. This accuracy improvement is achieved using Loran measurements made at the transmitters and minimizes the need for a separate monitor. An analysis of typical data is presented, showing error reduction which can be achieved and limitations of the method. Computer-controlled station operation is described which minimizes communication needs between stations.

1. INTRODUCTION

In its original deployment, Loran-C was aimed primarily at overwater coverage and variations in velocity of radio propagation were of only nominal concern. The first overland application in Southeast Asia was apparently in an area where overland propagation is quite stable. The next overland application, the installation of the Dana, Indiana, station in the eastern U.S. chain, gave indication of considerably larger variations, which have been the concern of several recent papers, which examined the phenomena from a meteorological viewpoint.

- - - - -
Robert L. Frank was formerly Sr. Research Section Supervisor (Advanced Radio Navigation) at Sperry Gyroscope Div., where he did the propagation analysis and suggested the compensation method.

David L. McGrew is presently responsible for portions of the computer system software specification and programming of the AN/TRN-35 Loran C/D Transmitters.

In the meantime, there have been three different Loran-D overland deployments which have not revealed any large propagation variations, but the Loran-D installations have so far employed modest 100 to 200 n. mile baselines with one 300 mile exception. Higher power Loran-D stations are now under construction with the objective of operating with 400 n. mile baselines and even longer with paralleled transmitter higher power configurations. That consideration was the impetus for the work reported here, but it may be noted that recent Loran-C proposals have also visualized in-land stations where the phenomena and techniques described here may be of importance.

In the present paper the emphasis is not upon meteorological explanations, but upon an understanding of the behavior of the Loran system. This understanding is then applied to a real time operating technique which minimizes the variations experienced in a desired portion of the service area. Since the new AN/TRN-35 Loran-C/D transmitter includes a general purpose minicomputer for digital signal processing and other station functions, this computer will be applied to minimize the operator's work load when compensating for propagation variations, and will also minimize inter-station communication requirements.

In the following sections, we first consider the effect of propagation variations on system behavior, then review some Loran station and monitor measurements which indicate the existence of propagation variations, next describe the compensation technique in principle and in computation detail, and lastly propose some further observations and analysis to improve our knowledge and to improve future system operation.

2. EFFECT OF PROPAGATION VARIATION

An elementary mathematical discussion of the effect of propagation errors follows. In diagram (a) of figure 1 the M-X (master-secondary) baseline is illustrated. The propagation time from M to X (or X to M) is represented as β . The coding delay at X is represented by CD. For illustrative purposes, a point α in the service area and midway between M and X is selected for examination. During a typical Loran interval, master transmissions, propagated down the baseline, are received at X, and after the specified coding delay, X transmissions are emitted. Initially, the time difference between M and X signals measured at M is:

$$TDM = \beta + CD + \beta = 2\beta + CD$$

at X, the time difference is

$$TDX = CD$$

and at α , if the propagation time from M to α is M_α , and the propagation time from X to α is X_α ,

$$TD_\alpha = |M_\alpha - [(\beta + CD) + X_\alpha]|$$

since $M_\alpha = X_\alpha$ (α is on a midpoint line between M and X)

$$TD_\alpha = |\beta + CD|$$

Now presume that the propagation velocity changes uniformly in the service area, and that the propagation time from M to X is different from the predicted value by $\Delta\beta$.

Then

$$TDM = \beta + \Delta\beta + CD + \beta + \Delta\beta = 2\beta + CD + 2\Delta\beta$$

and

$$\text{ERROR at M} = 2\Delta\beta$$

Since

$$TDX = CD \text{ (by definition)}$$

$$TD_\alpha = |M_\alpha - [(\beta + \Delta\beta + CD) + X_\alpha]| = |\beta + CD + \Delta\beta|$$

and

$$\text{ERROR at X} = \Delta\beta$$

which shows that the lines of position have been warped and the error is not uniform along the baseline.

If it is presumed that a service area monitor is located at position α , then a coding delay adjustment can be made at X which reduces the coding delay by $\Delta\beta$. Now,

$$TDM = \beta + \Delta\beta + CD - \Delta\beta + \beta + \Delta\beta = 2\beta + \Delta\beta + CD$$

$$\text{ERROR at M} = \Delta\beta$$

$$TDX = CD - \Delta\beta$$

$$\text{ERROR at X} = -\Delta\beta$$

$$TD_\alpha = \beta + CD$$

$$\text{ERROR at } \alpha = 0$$

If it is desired to minimize the error along any particular time difference line, a proportional correction can be made as discussed in detail later.

3. LORAN C/D PROPAGATION VARIATION EXPERIENCE

In the 1950's during the Cytac program, on the propagation path of the Northern portion of the installation with the master at Carolina Beach and the secondary at Forestport, New York, temporal fluctuations were observed comparable to those presently seen on the Carolina Beach-Dana path (Ref. 1, 2). Analysis made of that data indicated a very good correlation with weather conditions, although fluctuations were about 4 to 5 times as great as could be explained by simple calculations of expected changes in the index of refraction.

Analysis of the results of over-water operation of the East Coast Loran chain in 1959, found that propagation variations over water were very much smaller than those previously encountered over land, and could be fully explained by calculated variations in the index of refraction (Ref. 3, 4). A further analysis of over-water data from the East Coast chain, the Mediterranean chain, and the Alaskan chain in 1966 (Ref. 5) showed one to two tenths microsecond variations in propagation over 600 mile paths which could be fully explained by calculated variations in the index of refraction.

The original Cytac data was somewhat suspect because, for security reasons, the phase coding which would provide multi-hop skywave rejection between adjacent pulses in the Loran pulse group was not in operation when the extreme variations were measured. However, sufficient independent measurements were made in monitor stations near the master, near the secondary, and in the service area to rule out any other reasonable explanation. For instance, figure 2, a reproduction of the first open-literature Cytac description, illustrates precisely the behaviour to be expected from the simple analysis of propagation effects given above.

The south eastern Asia installation of Loran-C is shown in figure 3. The chain is controlled by a monitor at Udorn. One secondary station is located by Tan My, but for the purposes of this discussion, only the reception and monitoring of other stations of the chain at this location will be considered.

The eastern U.S. chain is shown in figure 4, with the exception of the secondary at Cape Race, Newfoundland, which will not enter the present discussion. Dana and Jupiter were controlled during the period to be considered here by a monitor

at Warner-Robins, Ga., and Nantucket is controlled by a monitor at Bermuda. The Warner-Robins monitor function was later moved to Eglin AFB, Fla. A number of other locations which will enter into the discussion are also shown.

Monthly averages of time differences for nearly one year for the Southeast Asia chain are shown in figure 5, and similar data extending for a period of three years is shown in figure 6 for the Southeast U.S. chain. In both of these situations the time difference readings are nearly constant at the control monitor, as would be expected, but at other locations, there are some fluctuations: on the order of $\pm 1/10$ microsecond in Southeast Asia and \pm one microsecond in Southeastern United States. Of particular significance is the fact that, although the readings are quite constant at the Udorn control monitor, there are in fact some fluctuations at Tan My, several hundred miles away: and similarly, although time difference readings are held constant at Warner Robbins control monitor, there are substantial fluctuations at Eglin Air Force Base, again several hundred miles away. An expanded detail of one week's data from the Southeast U.S. chain is shown in figure 7. These data present the moderately extreme case of a disturbed weather condition, but are not unique. In the U.S. chain, diurnal fluctuations on the round-trip Carolina Beach-Dana path (573 nmi one way) on the order of one microsecond are not uncommon in the winter, and one half microsecond are not uncommon in the summer. The difference between master and secondary readings represents this round trip propagation variation.

Measurements at other locations in the service area also gave indication of propagation temporal variations (Ref. 6), not always recognized as such (Ref. 7).

In the past, measurements of time difference or time of arrival at transmitting station sites have been mildly suspect because of several factors which could degrade accuracy:

- a) The local signal pickup is from the near field; the distant signal pickup is from the far field
- b) there might be reradiation from the transmitting antenna into the receiving antenna
- c) there is a huge signal unbalance, and the probability exists of extraneous pickup affecting the phase accuracy.

The senior author informally suggested that the facts could be more definitely resolved by the use of a technique which eliminates the above factors: using an idea first proposed for obtaining extreme accuracy in Loran survey applications, establish a monitor near each end of the transmitter baseline along the baseline sufficiently far from the transmitters to eliminate the above factors (at least 10 miles); then measure the time difference at each monitor and further take the difference between these two time differences--this is then independent of station synchronization (Ref. 3, 4). The USCG greatly elaborated this idea and implemented project DIPUTS, with monitors not only near each end of the Master-Dana baseline--Clarkton, N.C. and Cloverdale, Ind., but at two equispaced intermediate points--Mocksville N.C. and Paris, Ky. Furthermore, provisions were made to measure time of arrival against local cesium standards as well as time differences on several receivers (Ref. 8, 9, 10).

There is now as a result of the DIPUTS experiment little doubt that propagation variations do exist, and further that the measurements made at Loran-C stations are not grossly in error in showing these variations.

We will now interpret the measured variations in terms of a compensation technique.

4. COMPENSATION FOR PROPAGATION VARIATIONS

During the Cytac program, Sperry developed and demonstrated a "target area compensation" technique to reduce the effect of the variations presumed to be due to propagation: this involved only the use of time difference measurements made at the transmitting stations (Ref. 1). It should be emphasized that although the analysis showed a strong correlation with certain weather conditions, in particular with temperature, weather information was not used in the compensation. As presented here, the concept has been simplified over the original method and will in practice now be accomplished by digital computer in the AN/TRN-35 transmitter master station.

A clearer insight into the technique can be achieved by reference to figure 8. If the propagation variation is uniform over the service area between the master and the secondary, the time difference variation will be maximum at the master station when control is a fixed time difference at the secondary and maximum at the secondary if control is to a fixed time difference at the master; the variation will be zero at an intermediate point if control is such that the time difference variation is properly

proportional between the measurements made at the master and the measurements made at the secondary. In figure 8, the solid line shows the situation which would be expected if control were at the point along the baseline corresponding to the crossing of the baseline by the time difference line passing through Warner Robbins. Since the difference in distance is the same anywhere along this time difference line, this also represents what would be expected if control is at Warner Robbins. The Warner Robbins time difference is some 35% along the baseline between master and secondary. The solid curve shows, therefore, that the variation should be proportioned so that 35% of the variation occurs at the master and 65% occurs at the secondary. Inspection of figure 6 shows that in fact the variations measured were approximately in this ratio. Figure 8 further shows that, if the control were at Warner Robbins, approximately 10% of the total master-secondary variation would be expected at Eglin. Inspection of figure 6 shows that a variation of approximately this amplitude was indeed observed. A similar calculation makes the general trend of the variations in Southeast Asia, as shown in figure 5, also reasonable, although in this case the total variations were much smaller.

By inverting the above reasoning, it may be deduced from the actual measurements with ground monitor control as shown in figures 5, 6, and 7, what would happen if chain control held time differences constant at one of the transmitters rather than at the monitor; if control had held the time difference constant at the secondary station, the variation measured at the secondary would have appeared at the ground monitor location; if control had held the time difference constant at the master, the variation measured at the master would have appeared at the ground monitor location. Obviously, this is undesirable when there are appreciable variations due to propagation. Hence a more sophisticated tactical grid control technique is needed to proportion the variations when a ground monitor cannot be located near the target area.

Figure 9 compares the result of simulating the proportioning technique during one winter week of Southeast U.S. chain operation with actual operation. The heavy line represents variations measured at Carolina Beach minus 30% of the round-trip travel time variations and simulates the proportional control; the light-weight line is the actual ground monitor reading at Warner Robbins. In the preparation of figure 9, the data were visually averaged to simulate one hours monitoring. A bias between the sets of data has also been removed. (If the technique described is applied to a year's worth of data a summer-to-winter bias offset of approximately $2/10\mu S$ also remains.)

However, when the technique was applied to a week of summer data short-term results quite similar to figure 9 were obtained. The similar small variations ($\pm 0.1 \mu S$) of the simulated grid control without ground monitor and the actual ground monitor data illustrates the power of the proportioning technique.

The largest remaining jogs in the data are due to the rather coarse $0.1 \mu S$ timing corrections used by the chain monitor - smaller steps as used in S. E. A. would probably have resulted in smoother control had it been required.

The project DIPUTS data taken at the various monitor points nicely corroborates the assumptions used for the above compensation: at Mocksville, which has very near the same time difference as Warner Robins, the TD variations were substantially smaller than the variations at either Clarkton or at Paris, and the variations at Cloverdale were substantially larger than the variations at any of the other monitor stations (Ref. 11). Unfortunately, we do not have quantitative measures of the relative variations at this time.

Notwithstanding the above, there are several indications that the simplified uniform propagation assumption does not fit all situations. As a first example, the range of fluctuations along the Jupiter, Fla. to Dana path is approximately the same as along the Carolina Beach to Dana, path despite the fact that the Jupiter path is about 50 percent longer. Here the analysis is complicated by the presence of a partial overwater path.

Another counterexample is the 19-day observation period at Burlington described by Jeffery (Ref. 7). Figure 10 shows his data with the TD as measured at Dana by the USCG superimposed--with minor errors due to the reading of the USCG data from rather small-scale daily plots. The simple uniform velocity theory would have predicted variations at Burlington only 45 percent as large as at Dana--instead of variations equal to Dana as evidenced by the plots. A possible explanation is that the Dana signal traverses a flat path along the Great Lakes, whereas the Carolina Beach signal traverses the mountains. It is not surprising under the circumstances that Jeffery blames the monitor at Warner Robins for his variations!

That large variations related to propagation have not been observed in the Loran-D installations since much shorter baselines have been involved, and the installations have not been in the regions subject to the extreme index of refraction variations found in the eastern U.S. (Ref. 12).

5. IMPLEMENTATION OF PROPAGATION COMPENSATION TECHNIQUE

The compensation technique described is currently being implemented in the new AN/TRN-35 Loran transmitter, figure 11, being built by Sperry Gyroscope Division for Electronic Systems Division, Air Force Systems Command, USAF. The technique requires that time difference measurement be made at the transmitting stations. Hardware design techniques to insure that the time difference readings made at the stations are truly accurate and representative include:

- a) Reduction of extraneous pickup by careful component placement, shielding, grounding, RF line filters and non-electronic switching.
- b) Reduction of phase shift in local signal attenuation by use of wide band attenuator sections followed by a common signal path for local and remote signals.
- c) Use of the transmitting antenna as the receiving antenna to eliminate effects of receiving antenna offset. Electronic de-Qing (broad banding) the antenna to eliminate distortion of the received signal.
- d) Use of locally generated pilot pulse to calibrate out residual phase shifts.

The availability of accurate time difference measurements within the station digital control computer allows the compensation computations to be made automatically. In the conceptually simplest mode of operation, the master station instructs the secondary station to hold a commanded fixed time difference (coding delay). Since the time difference at the secondary station is fixed, the time difference reading made at the master includes any variations due to propagation on the round-trip baseline path. The master performs the linear proportioning calculation to ascertain the split of error between the master station and the secondary station. If the proportioning is not that desired, the master station commands a change in the coding delay at the secondary via a communication link and updates its own record of the secondary station coding delay.

This control loop is shown in more detail in figure 12, Most of the activity takes place at the master station. The master transmits its signal into the propagation medium. The secondary receives the master signal, waits its commanded coding delay and then transmits its own signal. The secondary signal is received back at the master

where the receiver measures the time difference. The master then uses this measured time difference together with its knowledge of the commanded coding delay and the fixed reference values of time difference, coding delay and one-way signal travel time to compute the normalized change in signal propagation time in units of microseconds of change per microsecond of travel time. This calculation is the second factor in the equation of figure 12. The first factor is the difference of the control point TD and the commanded coding delay. This factor represents actual signal travel time difference at the control point. The product of the two factors is the secondary station coding delay error. This error is filtered and then printed out to the master station operator as a required secondary coding delay adjustment (CDA). The master station operator communicates this CDA to the secondary station operator via HF or telephone communication link, in the same way that CDA's are often commanded from a monitor station in current Loran chains. The secondary station operator then enters the CDA into his equipment. When the master station operator is satisfied that the CDA has been executed at the secondary, he notifies his equipment of this fact and the master station record of the commanded coding delay is updated.

The foregoing discussion has described the control loop for one time difference line. In the AN/TRN-35 three such loops per chain are provided at the master station for control of up to three time difference lines in each of two possible Loran chains.

There are four optional modes of control (not including the standard modes of monitor station control). Operation in "closed chain/TD control" has been discussed. In "open chain/TD control" mode the secondary does not hold a fixed commanded coding delay but instead allows its Loran clock to free run and transmits at a fixed period in clock time without regard to the time of receipt of the master signal. For this mode the time difference measured at the master includes only the one-way baseline travel time changes and the equation of figure 12 is modified by removal of the 2 in the denominator. In "closed chain/TOA control" and "open chain/TOA control" modes additional computations are made at the master station to hold time-of-arrivals constant at the control point. These computations involve multiplying the change in signal propagation time by the master TOA at the control point and then filtering this product to generate CDA's for all stations in the chain including the master. The TOA modes will maintain the greatest accuracy in rho-rho or direct-ranging aircraft receiver applications in the presence of changes in Loran signal time-of-arrival. Examination of figure 7

indicates that there can be, at times, quite substantial rate of change of time-of-arrival variations, approaching 1/10 microsecond per hour.

The compensation technique has many benefits as described elsewhere in this paper. The costs of the technique are threefold: computer burden, communications system burden and operator burden. The computer burden is very slight. The AN/TRN-35 includes an AN/UYK-15 general purpose computer. The grid control program occupies less than 300 words and is executed once per 30 seconds requiring less than 0.01% of computer time. The communications system burden is little more than for conventional grid control from a monitor. Only coding delay adjustments and confirmation of their execution must be passed. To avoid accumulation of error, provision is made in the AN/TRN-35 for transmission to the secondary of the total commanded coding delay so that the operators may insure that proper records have been kept at both stations.

The burden on the secondary station operator is similar to that in a chain controlled by a monitor. He executes CDA's and confirms their execution to the master station operator. The master station operator has three tasks:

- a) Initialization data entry: Control mode and control point coordinates
- b) Communication: Coding delay adjustments and total coding delay to secondaries
- c) Operational data entry: Confirmation of CDA at secondary.

A number of possible additions to the AN/TRN-35 design are apparent:

- a) Loran pulse position modulation communication for CDA's and confirmation of CDA's.
- b) Use measurements at the secondaries and the monitor to obtain a more sophisticated propagation model such as a second order correction based on a uniform rate of change of propagation velocity as a function of space across the service area.
- c) Loran pulse position modulation communication to transmit propagation information to sophisticated aircraft receivers.
- d) Compensation for pulse envelope propagation distortion.

Perhaps some of these features can be added to the AN/TRN-35 system after experience with the basic grid control technique has been obtained. In any case, the implementation of the basic grid control described above will provide the AN/TRN-35 with the potential to minimize the Loran signal variations in a selected portion of the service area without the use of a monitor in that area. This additional capability is obtained with truly minimal burden on the station computers, the communication link and the operators.

6. IMPLICATIONS, SUGGESTIONS AND CONCLUSIONS.

The implementation of Loran-C and Loran-D systems in some portions of the world will require consideration of propagation variations to achieve the highest accuracy. The use of real time compensation schemes such as that described here gives promise of accuracy improvement without resorting to differential Loran operation.

Real time compensation might be used in conjunction with or as an alternative to predictions based on seasonal trends as suggested by Doherty and Johler (Ref. 8).

It is apparent that more information is needed to fully evaluate the implications of propagation variations on a world wide basis--to understand fully where and why variations do and don't occur.

An old suggestion is to obtain measurements at Loran-C stations in Alaska and Norway where the geography is such that one overland path and one overwater path exists from one Loran station pair to a third transmitter station site which can conveniently be used as a low cost monitor (Ref. 13). Figures 13 and 14 show these unique situations. In Alaska the X secondary can monitor the M-Z pair and/or the Z secondary can monitor the M-X pair. In either case one overland path is compared to one water path. Similarly in Norway, the W secondary can monitor the M-X pair and/or the X secondary can monitor the M-Z pair. In all cases the synchronization path is entirely overwater, eliminating synchronization as a variable, yet no new monitor locations are required for the tests.

Then, there is the possibility of more analysis of existing data from South East Asia Loran-C and Western U.S. Loran-D, to evaluate why apparently only small variations are encountered.

A final side-benefit of the understanding and analysis given here has been an actual improvement in the accuracy of Loran data reduction. In a significant number

of cases, unlikely-looking peaks and jogs in plots of monthly or daily averages of time-differences have been traced by referral to more original source data as certain human errors in transcription or plotting. A recognition on the part of station and chain operators that variations ascribed to propagation happen in generally understandable ways should also lead to quicker recognition of equipment malfunctions which otherwise might be dismissed as mere system quirks.

REFERENCES

- (1) W. Dean, R. Frank, et al., "Final Engineering Report - CYTAC Long Range Tactical Bombing System," Sperry Gyroscope Co., Report 5223-1307-14, March 1956, pgs. 188-210, 232-252, Figs. 124-130, 194-214. Contract No. AF 30 (602)-106.
- (2) W. Frantz, W. Dean, R. Frank, "A Precision Multipurpose Radio Navigation System," Part II (Propagation Considerations) (1957), IRE National Convention Record, Part 8, pgs. 79-98. (Summarizes data from Ref. 1)
- (3) W. Dean, P. Watts, "Application of Loran C to Intercontinental Surveying", Sperry Gyroscope Co. Report CA-4223-0032-1, December 1959, Contract No. AF CRC-TN-60-122.
- (4) W. Dean, R. Frank, P. Watts, "Use of Loran C for Intercontinental Survey", Supplement to International Hydrographic Review, Vol. 3, October 1962, pgs. 74-84. (Summarizes data from Ref. 3).
- (5) Final Report on Loran C Propagation Study, Sperry Systems Management Division, Pub. No. CJ 2232-1892, for U.S. Navy Strategic Systems Project Office Contract No. NObs 94323(FBM), April 1971.
- (6) R.H. Doherty, "A Loran C Grid Calibration and Prediction Method", Institute for Telecommunication Sciences, U.S. Dept. of Commerce, Boulder, Colorado, OT/TRER 25, U.S. Government Printing Office, Feb. 1972.
- (7) C.B. Jeffery, "Loran C on the Lower Great Lakes" 28th Annual Meeting of the Institute of Navigation West Point N.Y. 29 June 1972 (Also in Navigation Spring 1973).

- (8) R. Doherty and J.R. Johler, "Meterological Influences of Loran C Ground Wave Propagation" 2nd Annual Convention, Wild Goose Assn. Washington D.C. Sept 1973.
- (9) R. Doherty and J.R.Johler, "Unexploited Potentials of Loran C" Proc. of National Radio Navigation Symposium, Institute of Navigation, Washington D.C. Nov. 1973.
- (10) R.H. Doherty, "Spatial and Temporal Electrical Properties Derived From LF Pulse Ground Wave Propagation Measurements" AGARD Paper No. 30 Conference Proc. of XX Technical Meeting of Electromagnetic Wave Propagation Panel of AGARD-NATO Netherlands, March 1974.
- (11) J.R. Johler, Private Communication
- (12) R.L. Frank, "Current Developments in Loran D" Proc. of National Radio Navigation Symposium, Institute of Navigation Washington D.C. Nov. 1973. (Also to be published in Navigation 1974).
- (13) R.L. Frank, "Opportunities for Propagation Research in Operating Loran Systems", Loran Propagation Symposium, Inst. of Telecommunication Sciences, Boulder, Colorado, August 1972, (Verbal Presentation).

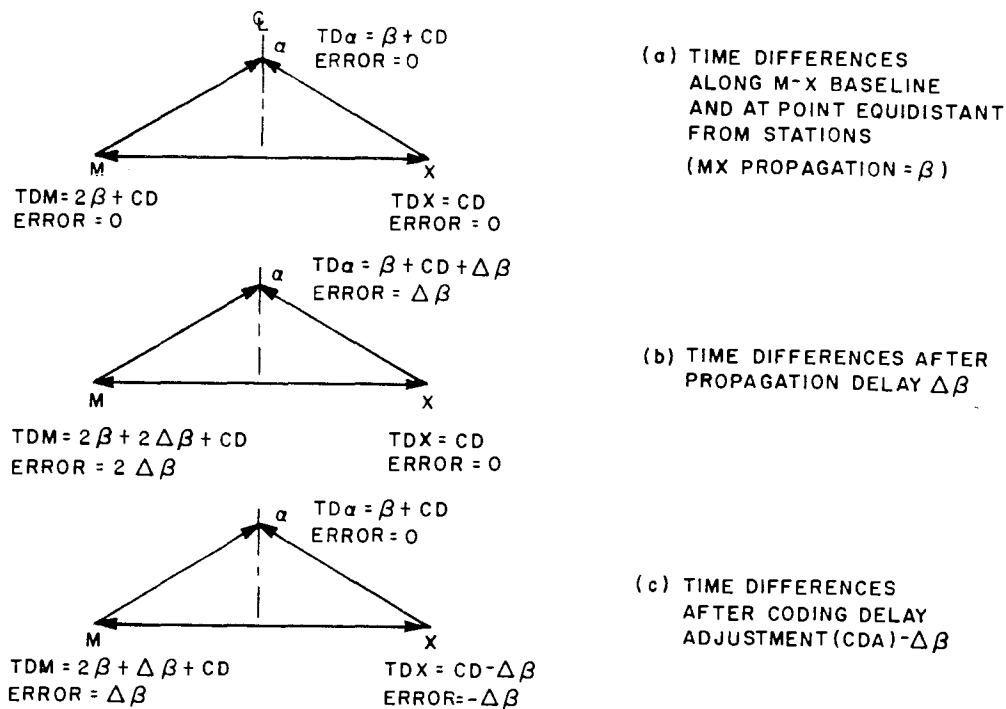


FIG. 1. TIME DIFFERENCES ON M-X BASELINE. PROPAGATION ERRORS CAN BE CORRECTED AT A SELECTED POINT IN THE SERVICE AREA.

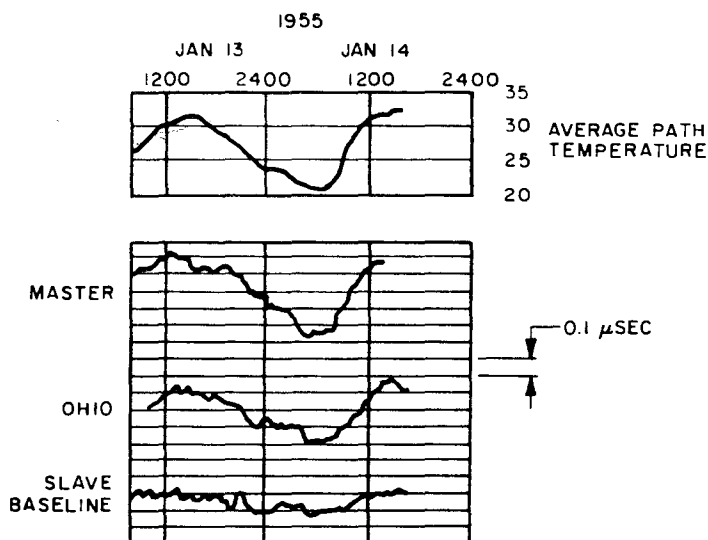


FIG. 2. CYTAC SYSTEM DATA ON CAROLINA BEACH NC - ROME NY STATION PAIR, SHOWING BEHAVIOR CHARACTERISTIC OF UNIFORM PROPAGATION VARIATION. (CODING DELAY HELD CONSTANT AT SLAVE.)

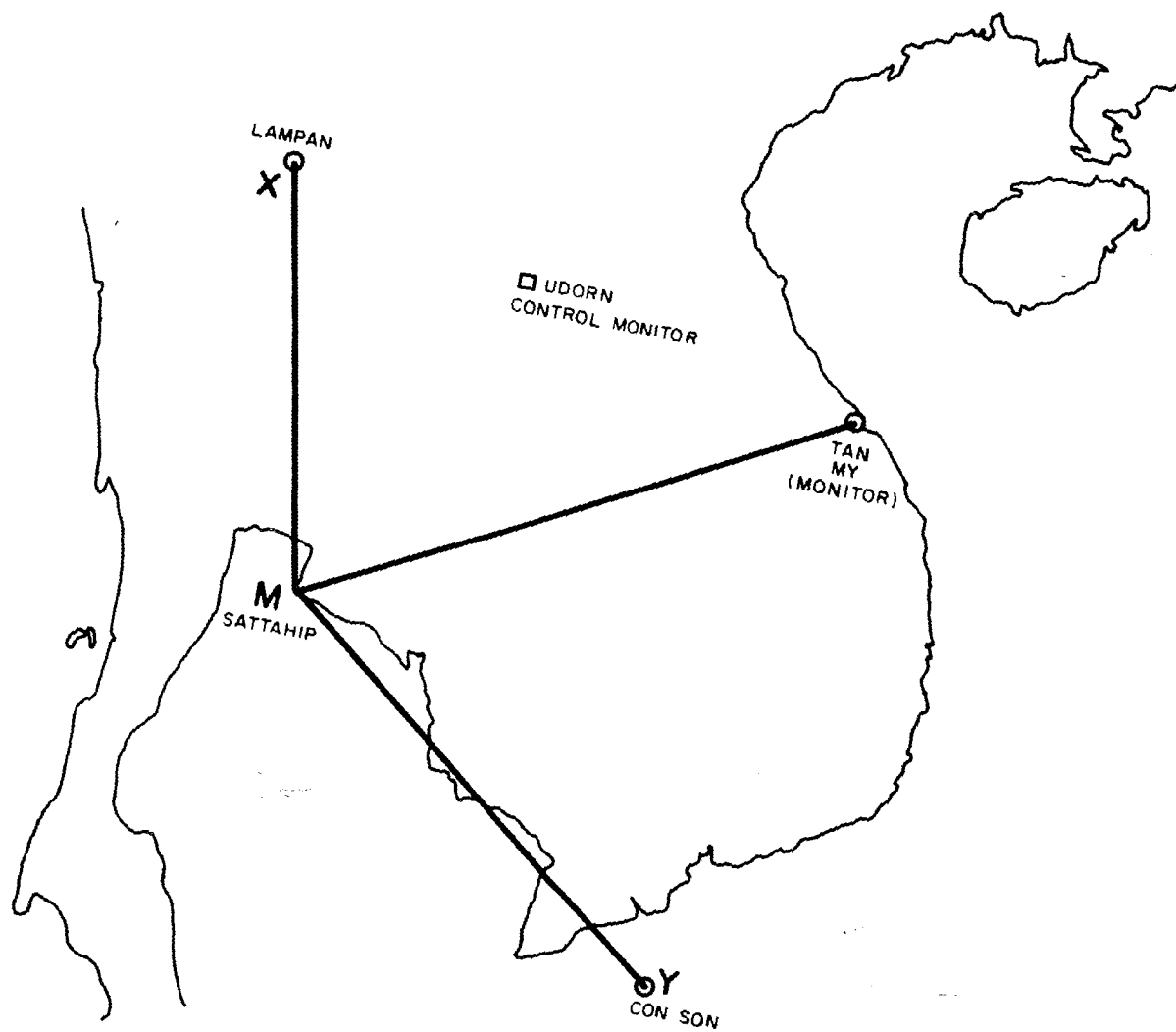


FIG. 3. SOUTHEAST ASIA LORAN CHAIN.

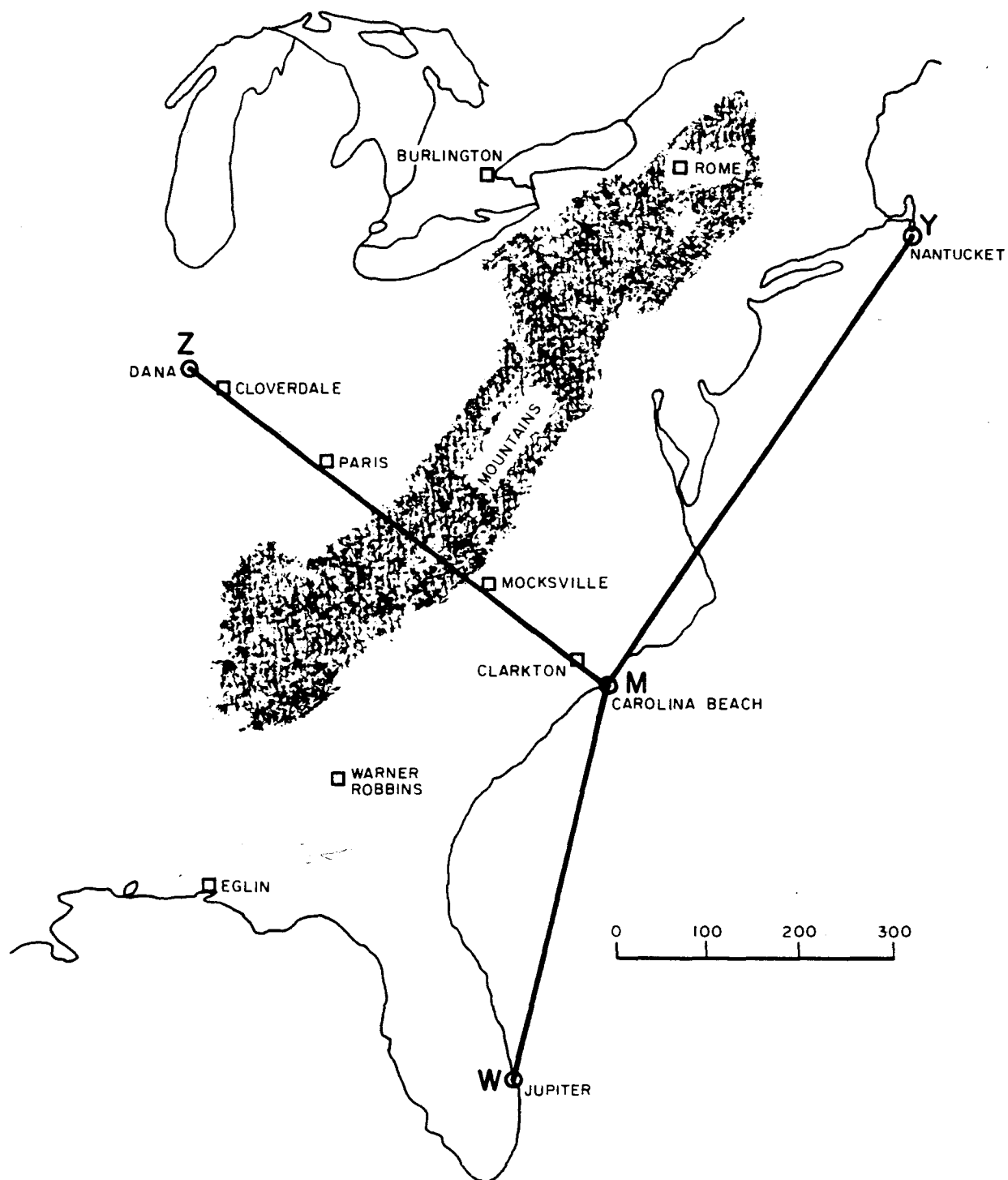


FIG. 4. EASTERN US LORAN-C CHAIN.

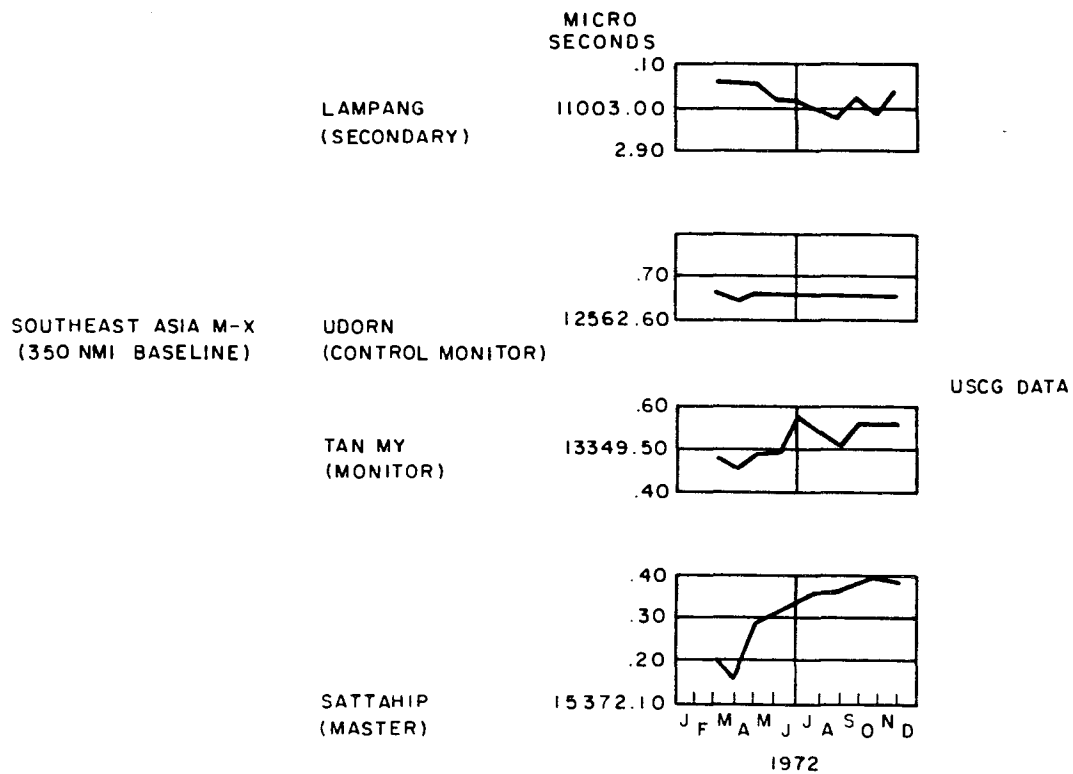


FIG. 5. TIME DIFFERENCE DATA. MONTHLY AVERAGES SHOW VARIATIONS ASCRIBED TO PROPAGATION VELOCITY.

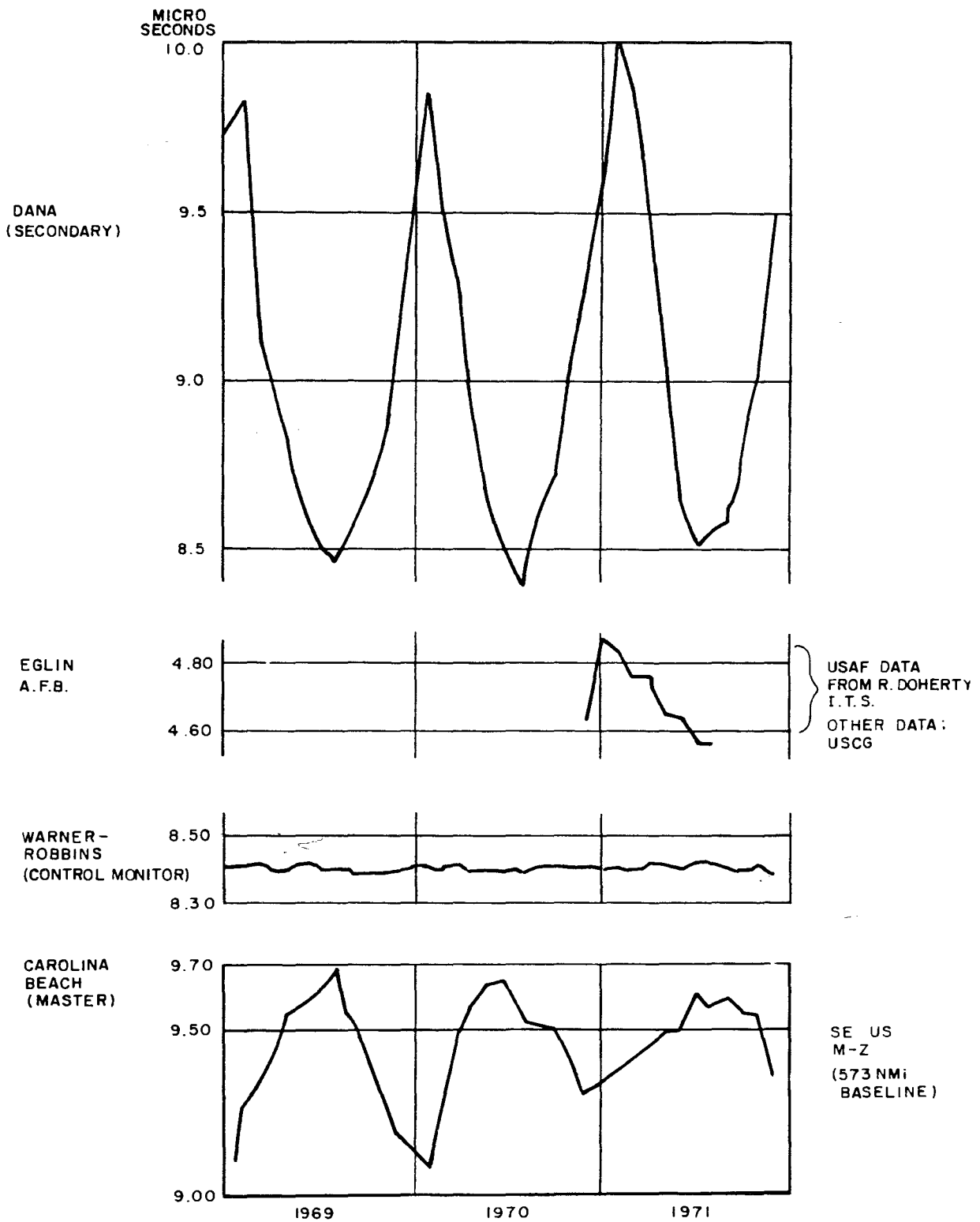


FIG. 6. TIME DIFFERENCE DATA. MONTHLY AVERAGES SHOW VARIATIONS ASCRIBED TO PROPAGATION OVER MOUNTAINS AND LARGE VARIATIONS IN REFRACTIVE INDEX.

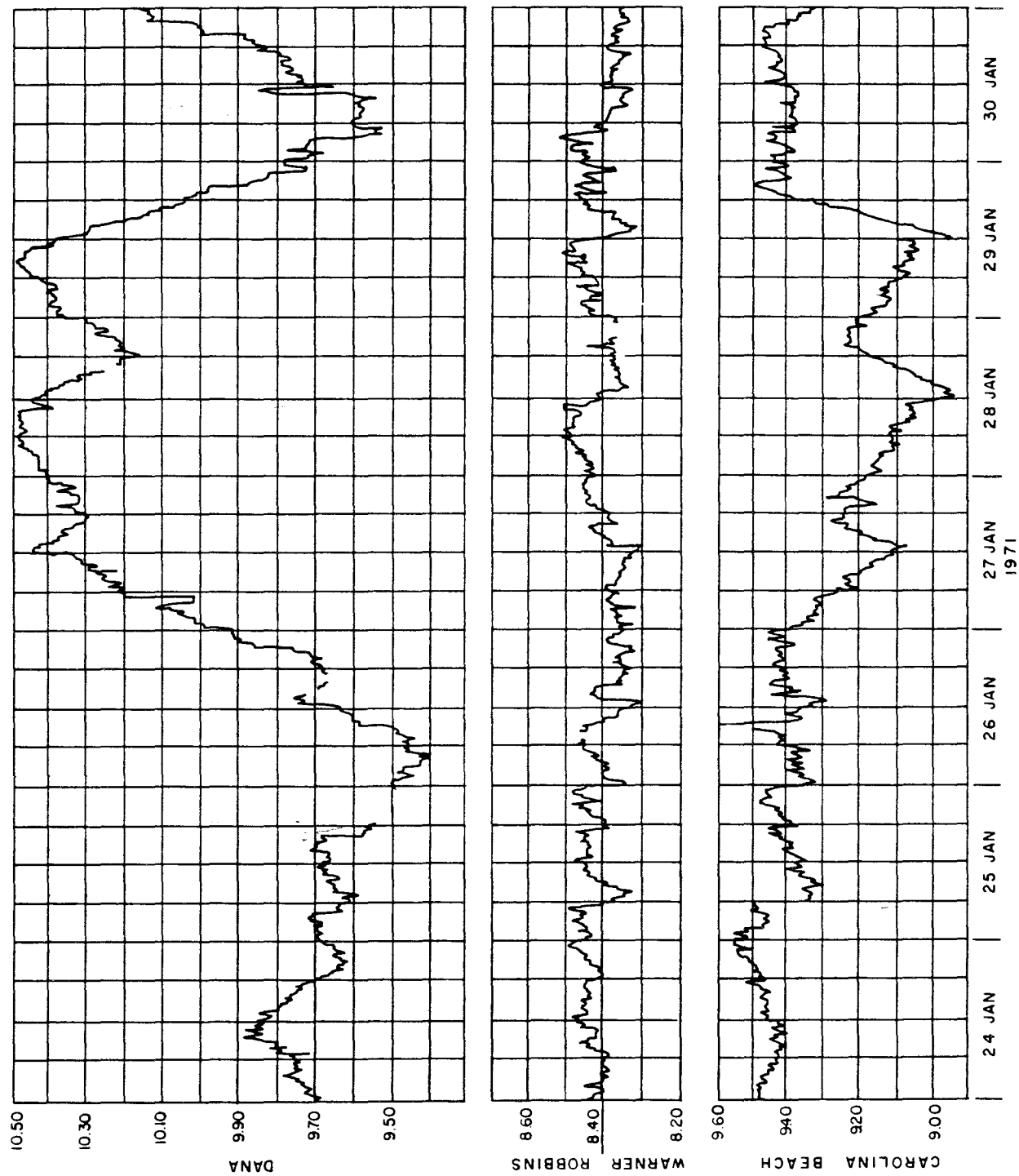


FIG. 7. TIME DIFFERENCE DATA. 15 MIN. AVERAGES SHOW DETAILED VARIATIONS DURING A DISTURBED WINTER WEATHER CONDITION. SE US 573 N.M. MZ BASELINE.

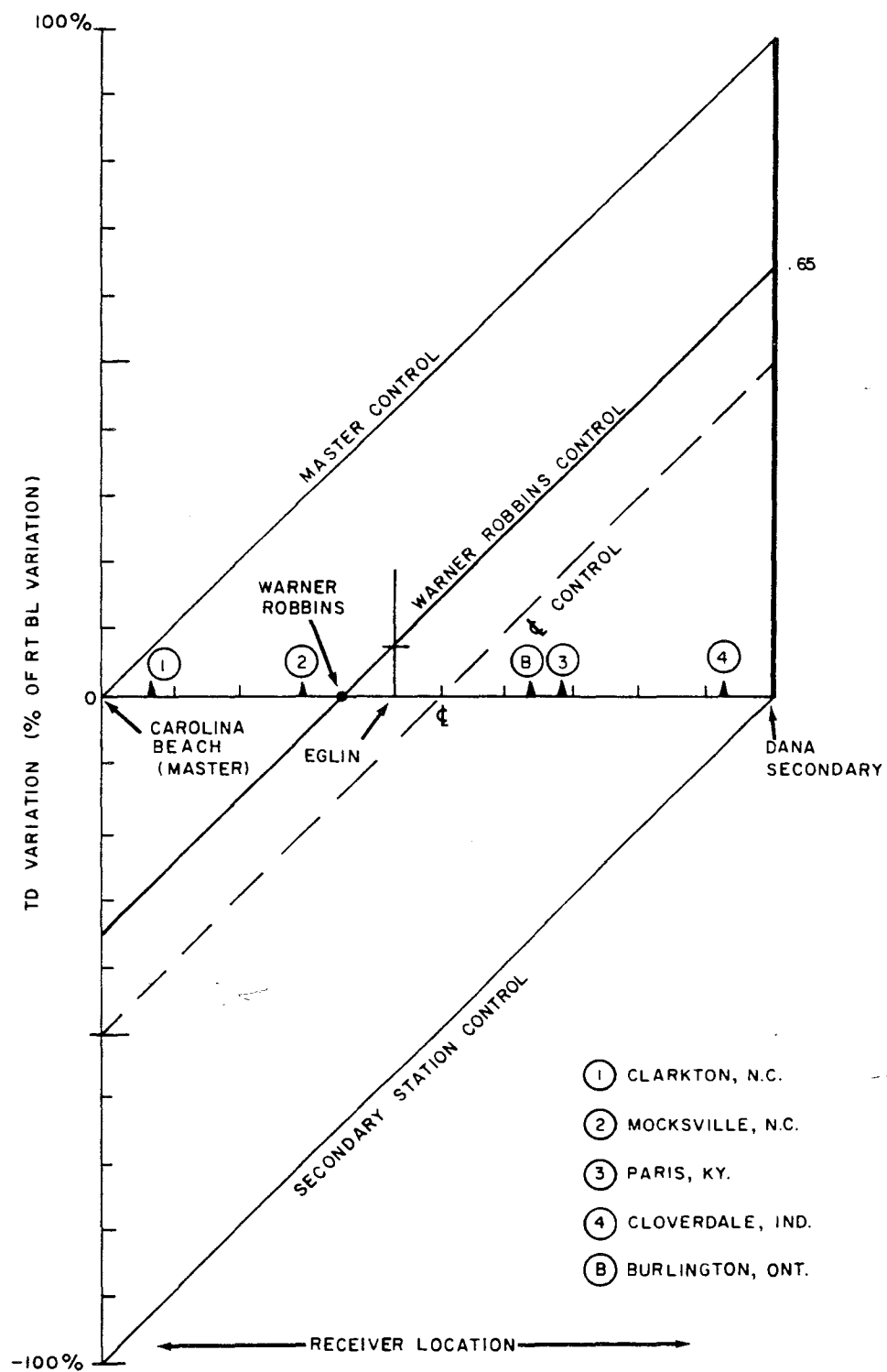


FIG. 8. UNIFORM PROPAGATION VARIATION EFFECT.

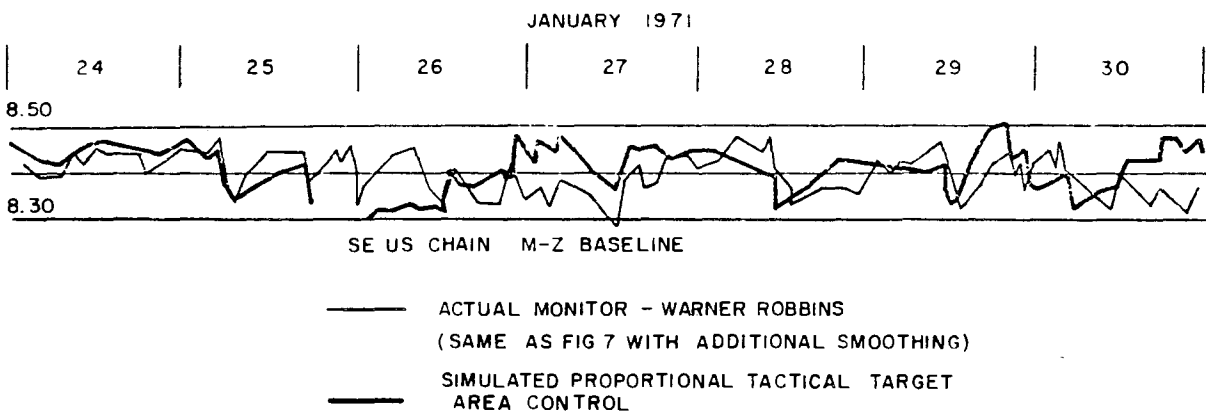


FIG. 9. STATION CONTROL WITHOUT MONITOR CAN APPROXIMATE MONITOR CONTROL FOR EXTENDED PERIODS.

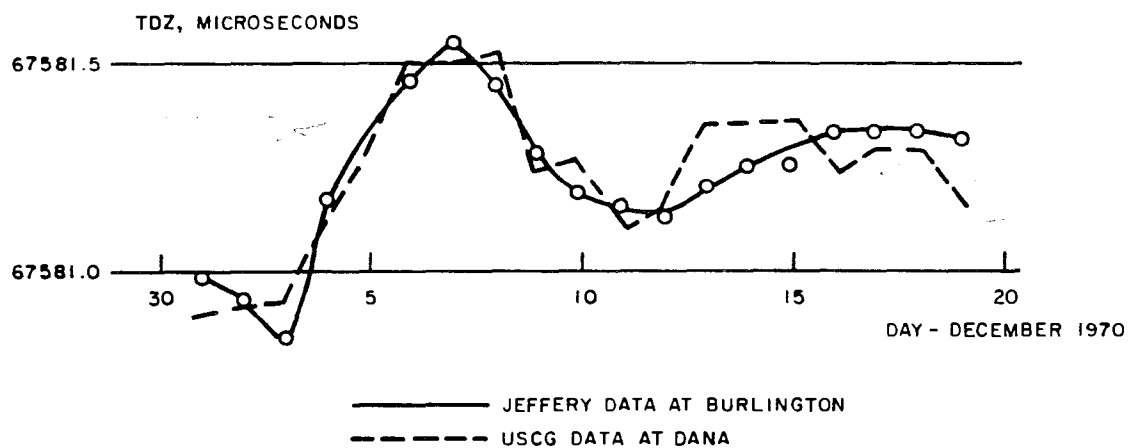


FIG. 10. VARIATION OF DAILY MEAN VALUES.

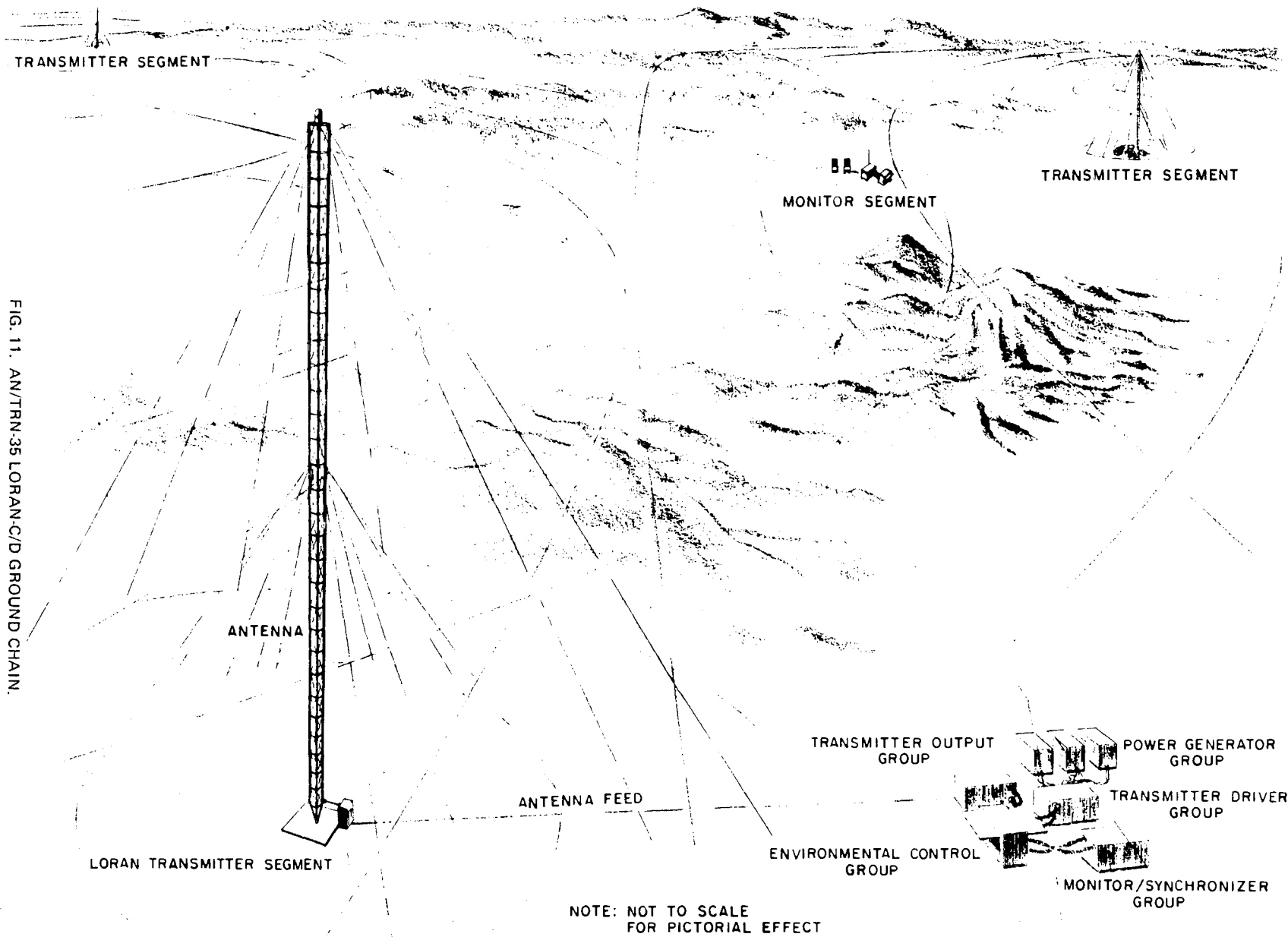
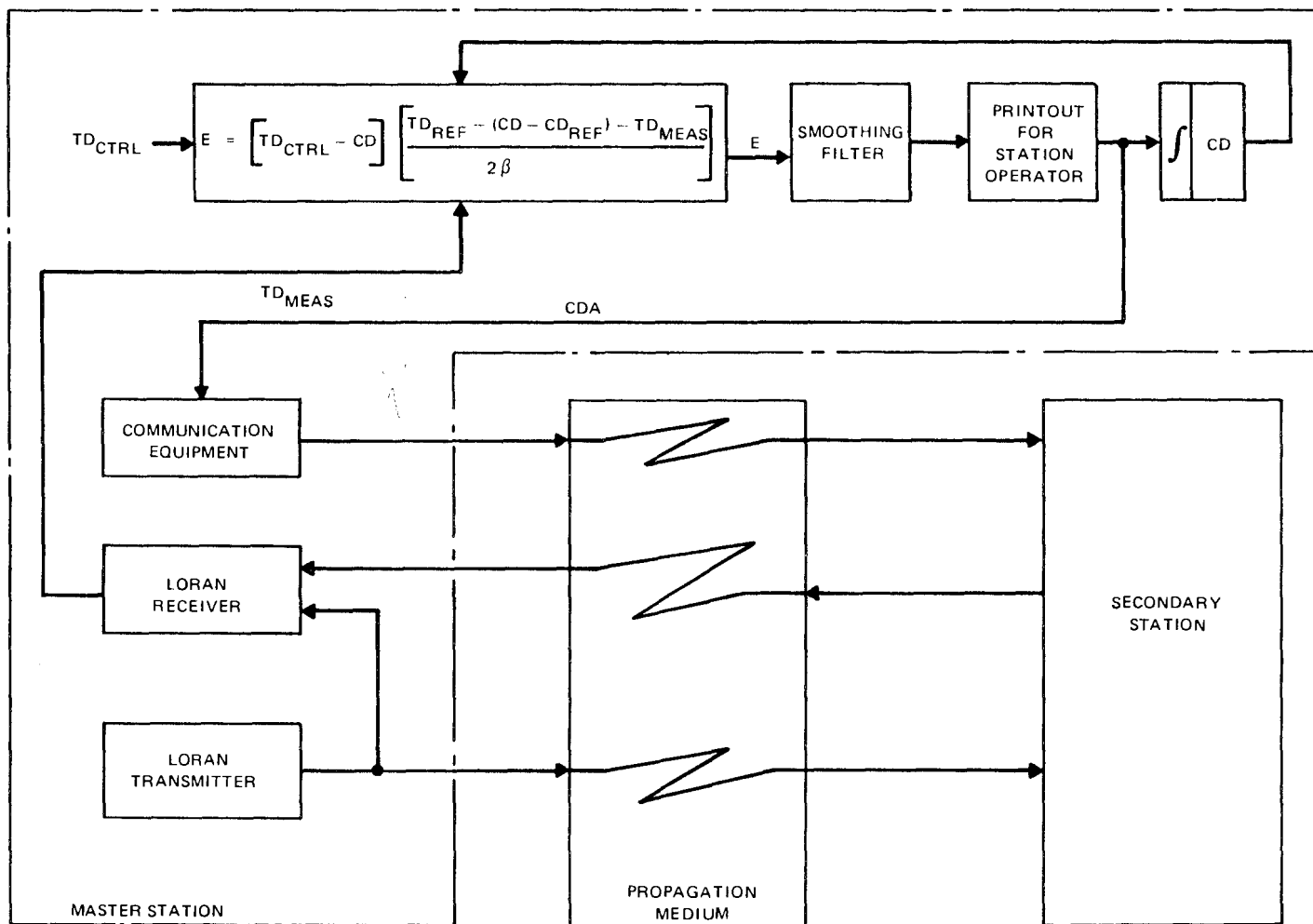


FIG. 11. AN/TRN-35 LORAN-C/D GROUND CHAIN.



SYMBOLS:

TD_{CTRL} - CONTROL POINT TIME DIFFERENCE
 TD_{MEAS} - TIME DIFFERENCE MEASURED AT THE MASTER
 CD - COMMANDED SECONDARY CODING DELAY
 CD_{REF} - REFERENCE SECONDARY CODING DELAY
 CDA - CODING DELAY ADJUSTMENT INSTRUCTION

TD_{REF} - REFERENCE SECONDARY TD AT MASTER
 β - NOMINAL ONE WAY BASELINE TRAVEL TIME
 E - CODING DELAY ERROR

FIG. 12. PROPAGATION CORRECTION CONTROL LOOP

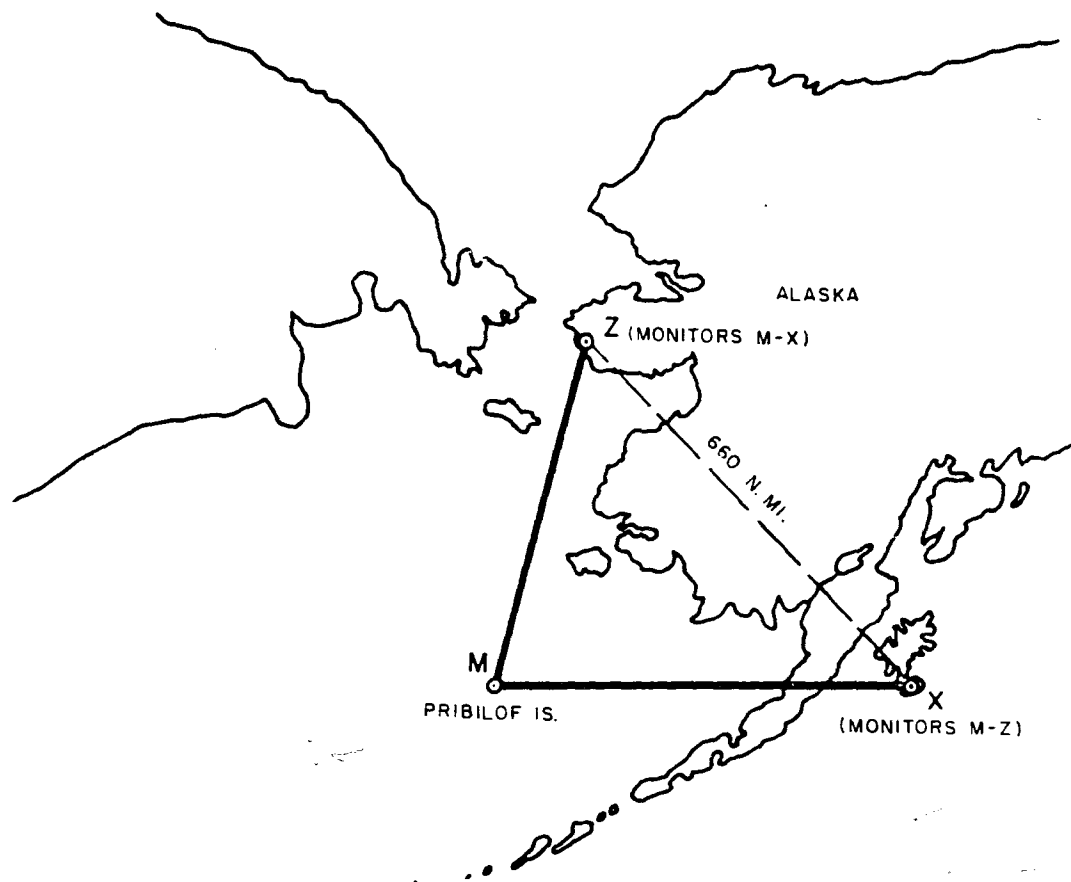


FIG. 13. LORAN C NORTH PACIFIC (AZIMUTHAL EQUIDISTANT POLAR PROJECTION).

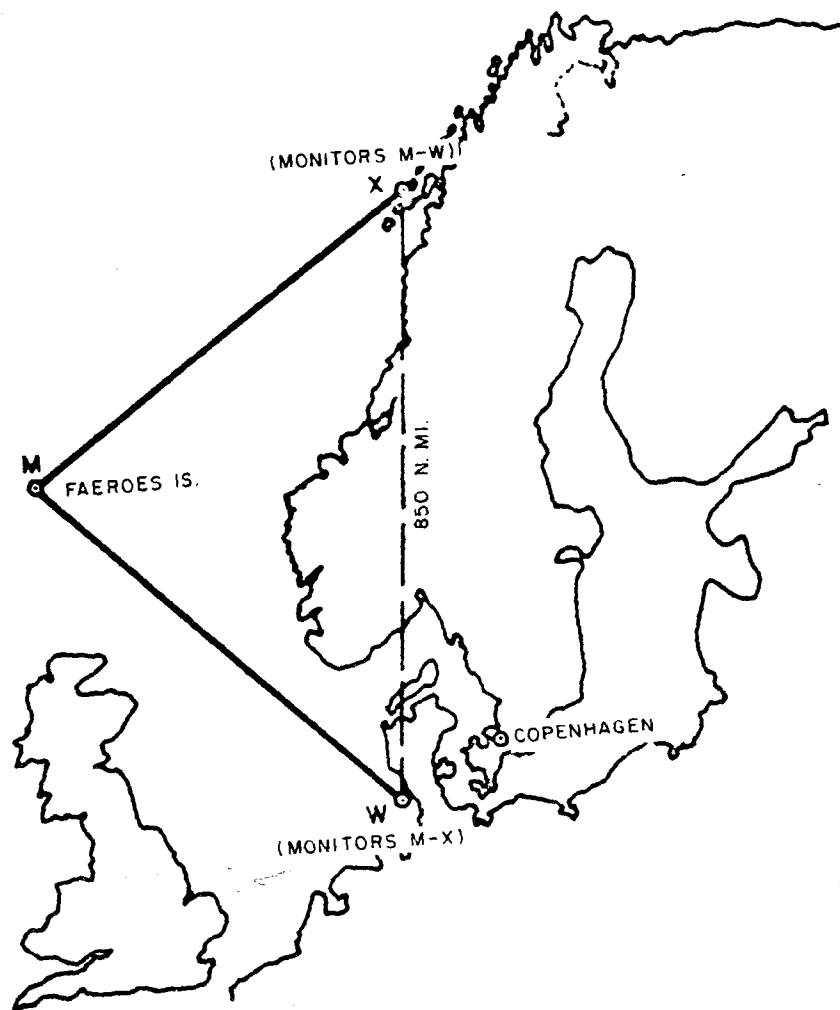
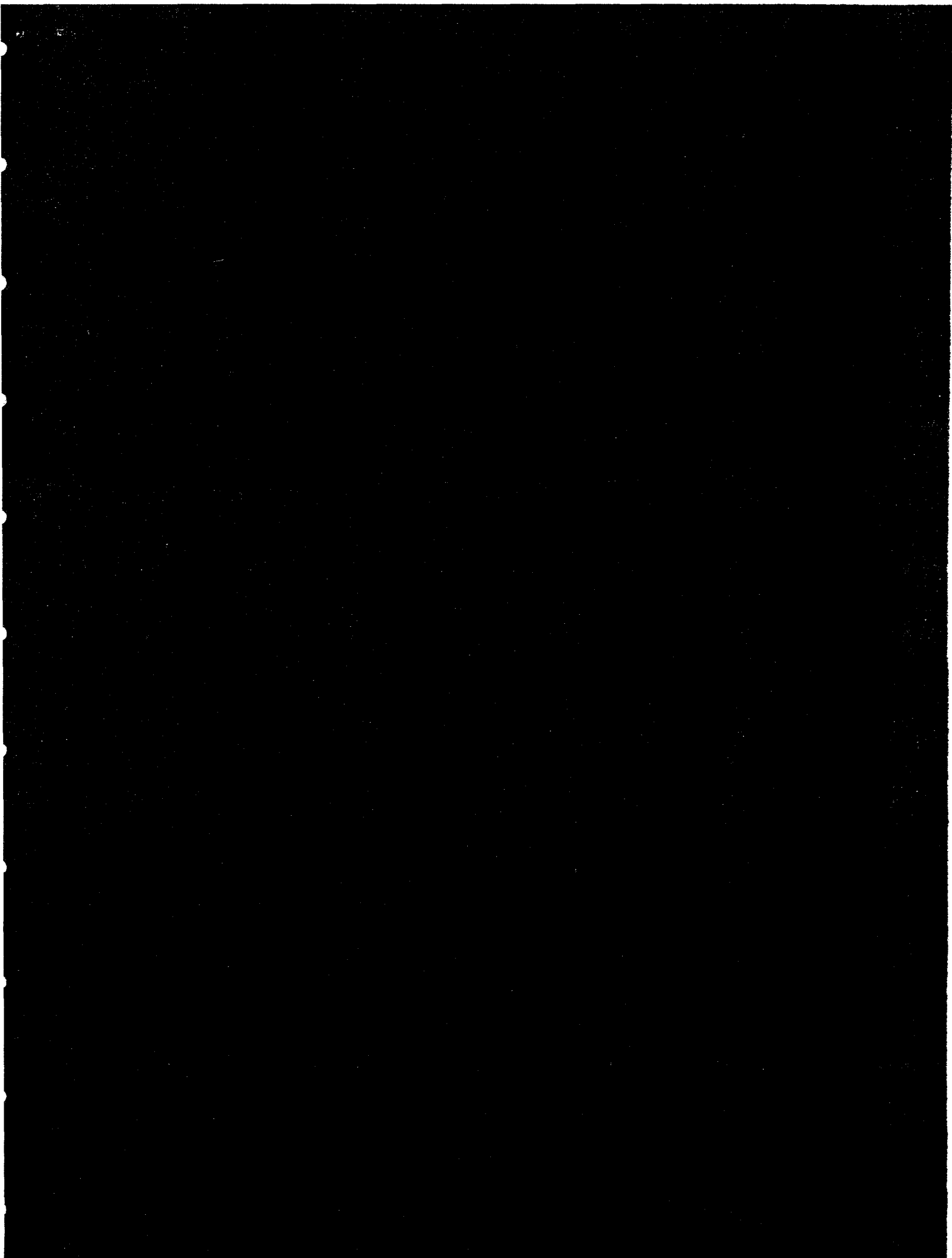


FIG. 14. LORAN-C NORWEGIAN SEA (AZIMUTHAL POLAR EQUIDISTANT PROJECTION).



FILE COPY

3-11

REF 635
PAPER 4-15
PP 17 85-161

LORAN-C PHASE CODE AND RATE MANIPULATION

FOR REDUCED CROSS CHAIN INTERFERENCE

by Commander William F. Roland
United States Coast GuardPUBLISHED
IN # 4

The Loran-C System is constrained by ITU regulation to ensure that 99% of all energy radiated from any station falls in the 90 to 110 kHz band. All stations radiate pulsed signals with a 100 kHz carrier frequency, and because a very wide band signal is transmitted, all signals have frequency spectra which overlap. Within a chain of stations, mutual interference is avoided by ensuring that each station's group of 8 pulses occur at a unique time such that there is no time overlap of signals, as shown in Figure 1. Between standard Loran-C chains, each operating with a different group repetition interval (GRI), mutual interference is controlled by selecting GRI's which minimize the effects of cross rate signals. Recent proposals for high accuracy limited coverage by Loran-C type stations either for harbor coverage or for privately owned radio location service, has brought out a need for discussion of the methods of assessing mutual interference between adjacent chains. This paper attempts to address that need, and provide the tools for assessing mutual interference.

Referring to Figure 1, a group of 8 pulses is transmitted from each station in a chain. Additionally, a ninth pulse is transmitted by the master station for visual identification of the master signal. The spacing of the pulses is 1000 usec, except the master ninth, at 2000 usec.

Each pulse has a non-symmetric envelope shape, rising to a peak in about 65 usec, and falling in less than 500 usec. Within the envelope, a positive going first half cycle of the carrier is defined as "zero" phase code, and a negative going first half cycle as 180° phase code. These are the only phases used in present codes. For simplicity, a (+) is used to designate zero phase code of a particular pulse, and a (-) to indicate 180° phase code of a particular pulse.

All carrier phase tracking Loran-C receivers operate on these signals by a process of cross correlation (1). Cross correlation is mathematically defined as:

$$C(\tau) = \frac{1}{T} \int_0^T s(t)r(t-\tau) dt$$

In this formula, $C(\tau)$ is the average value of the instantaneous product of the signal ($s(t)$), and the receiver's sampling waveform ($r(t-\tau)$) over the time period T . τ is the time error between the receiver's time reference and the signal time reference. In the receiver, 'T' is a long period of time and τ may vary during that period. However, since $s(t)$ and $r(t-\tau)$ are periodic in 2GRI, it is only necessary to look at the integral for that period. Also, τ will not vary significantly during that time.

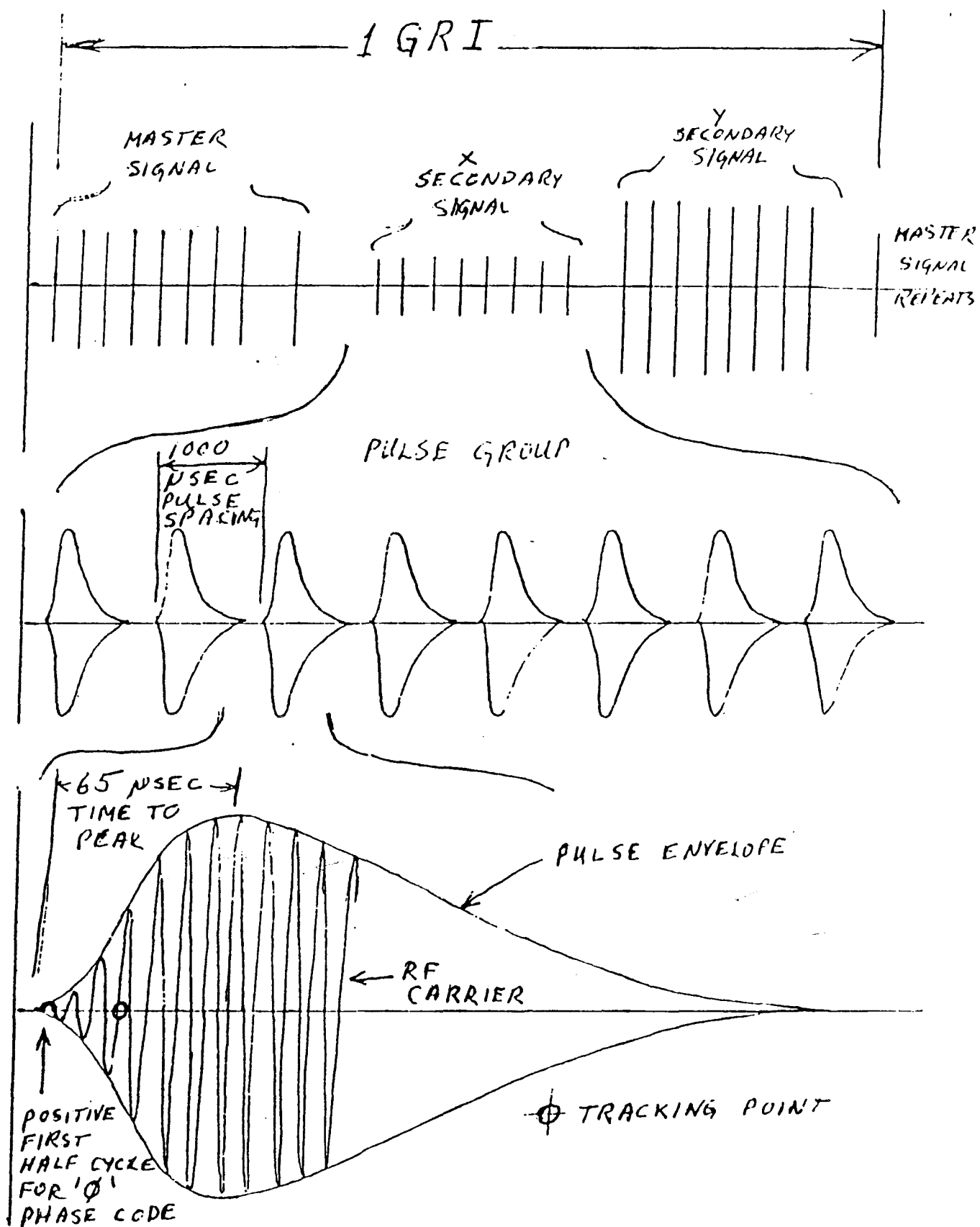


Figure 1. Loran-C signal format

The mechanization of $r(t)$ and the correlation processing may vary significantly from receiver to receiver, however the effect is the same. $s(t)$ and $r(t-\tau)$ contain a $\sin \omega t$ and a $\cos \omega(t-\tau)$ term respectively. Therefore, the product inside the integral can be rewritten:

$$\begin{aligned} s(t)r(t-\tau) &= A(t, t-\tau) \sin \omega t \cdot \cos \omega(t-\tau) \\ &= A(t, t-\tau) (\sin \omega(2t-\tau) + \sin \tau) \end{aligned}$$

The receiver circuits filter and discard the $2\omega t$ term and keep the $\sin \tau$ term. The $C(\tau)$ expression can then be written:

$$C(\tau) = \frac{\sin \tau}{T} \int_0^T A(t, t-\tau) dt$$

$C(\tau)$ is the error signal for a phase locked loop which drives $\sin \tau$ (hence τ and the receiver's clock reference error) to zero.

The following diagrams show pictorially the process. Figure 2 shows how the product of $s(t)$ and $r(t-\tau)$ varies with different τ and how the sampling is used to decode the pulse phase code. In 2a, the τ is zero, the $\sin \tau$, and therefore $C(\tau)$. In 2b, τ is 1.0 usec early and so the $C(\tau)$ is positive. In 2c, τ is 2.5 usec late and so $C(\tau)$ is negative. In 2d, the signal is phase coded (-) and so the carrier has the opposite polarity compared to 2c; but since the $r(t-\tau)$ is also phase coded, the product has the same sign as in 2c.

Extending this thought, Figure 3 shows how the eight pulses of a group are sampled and decoded, and that the samples are summed (integrated) to get $C(\tau)$. Note that one of the purposes of summing is to permit averaging to reduce the effects of noise.

Another very important concept is the handling of very large τ , such as occurs during search or in the presence of long delayed skywaves. Whenever all the signal phase code factors and the $r(t-\tau)$ sampling pulses have the same polarity, the $C(\tau)$ value for $T=2GRI$ equals 16 times any one sample. However, if some of the $r(t-\tau)$ phase code factors are of opposite polarity, $C(\tau)$ will be less. This occurs when the sampling pulses are aligned on the wrong pulses. Figure 4 illustrates the point. The Figure is identical to Figure 3, except that $r(t-\tau)$ is earlier in time than $s(t)$ by exactly 1000 usec.

Note that $C(\tau)$ equals the sum of the products of the phase code signs of $s(t)$ and $r(t-\tau)$ times the amplitude of a single sample. The sum of products of phase code signs is a measure of the correlation function of the signal and the receiver's sampling at a given value of τ . If the sum is zero, no matter what the magnitude of the individual samples, the net effect on the receiver will be zero. Since it is not desired to have the receiver track $s(t)$ except with τ very close to

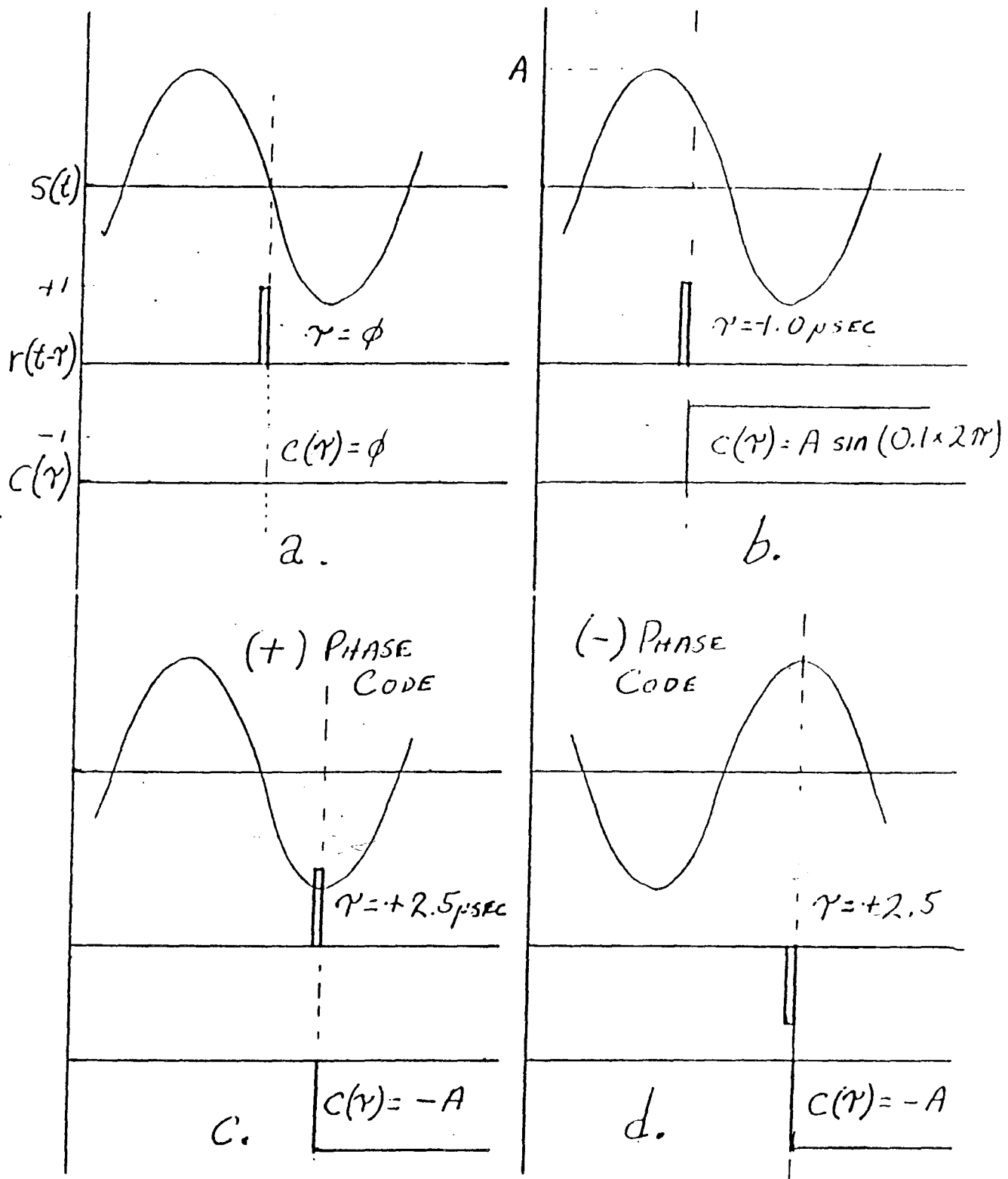


Figure 2. Instantaneous Product of $s(t)$ and $r(t-\gamma)$ for various γ . Only one cycle of $s(t)$ is shown, and $r(t-\gamma)$ is shown as a narrow sampling gate.

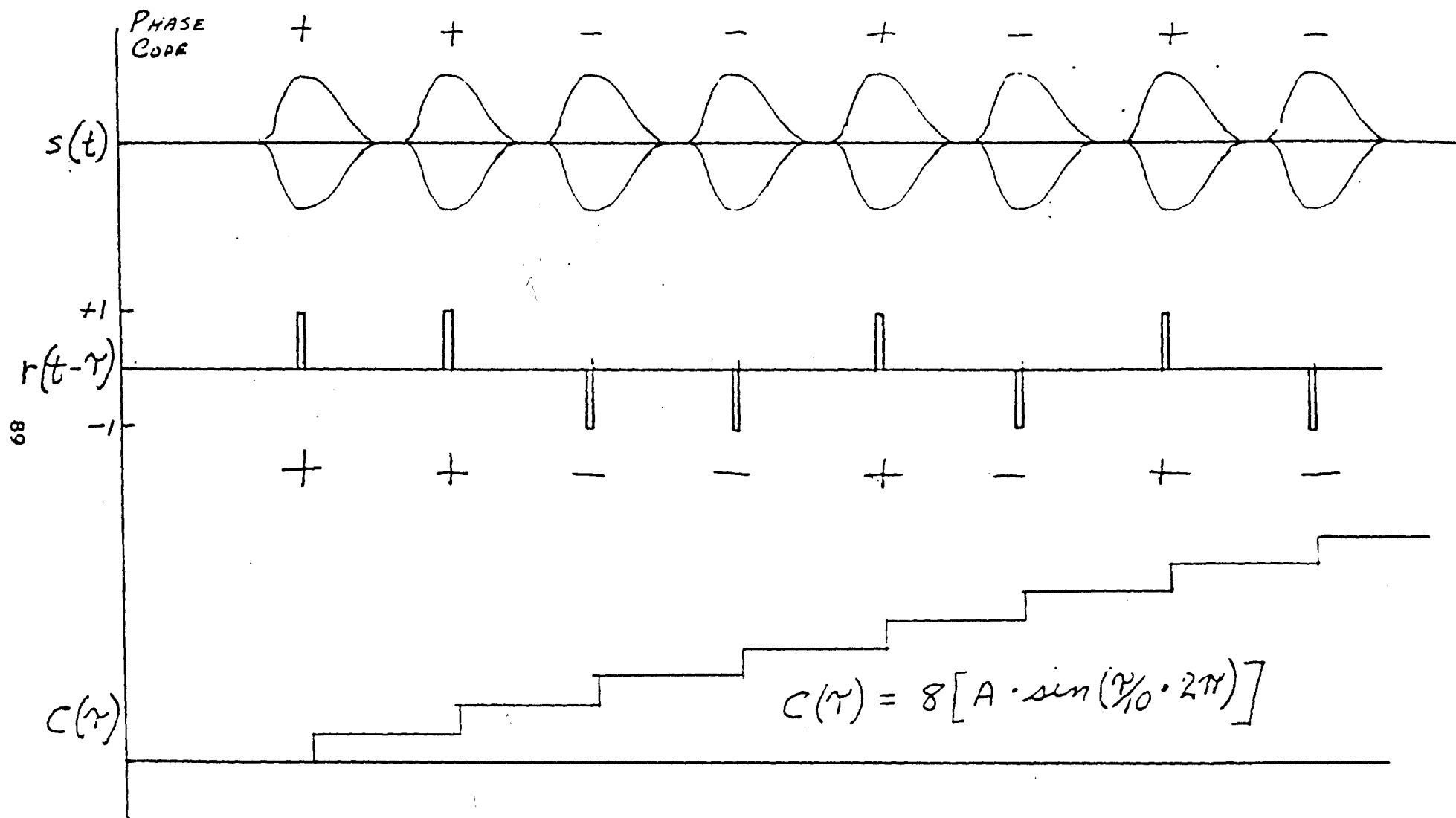


Figure 3. Correlation Integral during one interval of the Master Signal, $\tau = -2.5$ usec.

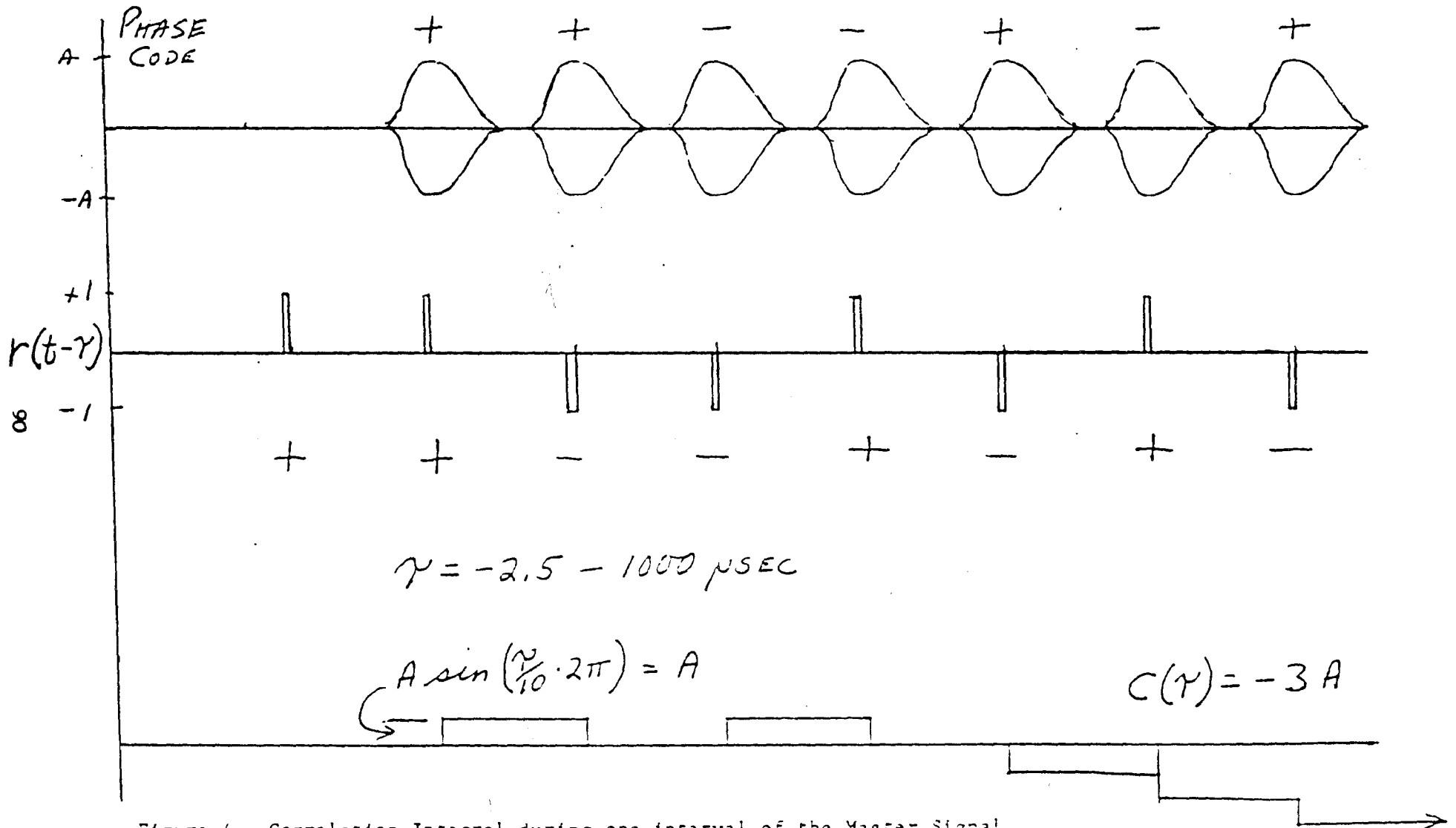


Figure 4. Correlation Integral during one interval of the Master Signal,
 $\gamma = -2.5 - 1000 \text{ usec.}$

zero, the sum of signs is used to make this not possible, by carefully designing the phase code. Table 1 below is a part of the set of possible mis-alignments by $N \times 1000$ usec of the master signal and the receiver master phase code, and the resultant sum of signs. Note that the individual amplitudes of the samples are not shown. Over a 2GRI time, $C(\tau)$ will sum to zero, because the sum of signs is zero, for τ values of -1000 usec, -2000 usec, -3000 usec, and -4000 usec.

	CODE IN RECEIVER INTERVAL A								CODE IN RECEIVER INTERVAL B								SUM OF PRODUCTS
RECEIVER CODE	+	+	-	-	+	-	+	-	+	-	-	+	+	+	+	+	
$S(t)$ @ $\tau = -1000$	0	+	+	-	-	+	-	+	0	+	-	-	+	+	+	+	
PRODUCT OF SIGNS	0	+	-	+	-	-	-	-	0	-	+	-	+	+	+	+	ϕ
$S(t)$ @ $\tau = -2000$	0	0	+	+	-	-	+	-	0	0	+	-	-	+	+	+	
PRODUCT OF SIGNS	0	0	-	-	-	+	+	+	0	0	-	-	-	+	+	+	ϕ
$S(t)$ @ $\tau = -3000$	0	0	0	+	+	-	-	+	0	0	0	+	-	-	+	+	
PRODUCT OF SIGNS	0	0	0	-	+	+	-	-	0	0	0	+	-	-	+	+	ϕ
$S(t)$ @ $\tau = -4000$	0	0	0	0	+	+	-	-	0	0	0	0	+	-	-	+	
PRODUCT OF SIGNS	0	0	0	0	+	-	-	+	0	0	0	0	+	-	-	+	ϕ

Table 1: Sum of the product of Signs for various τ , using the Master phase code in the receiver against the master signal.

It is obvious that a simple method of determining the sum of the products of signs would be helpful, when many different interfering situations are to be studied. It can be shown (or 'it is left as an exercise for the student') that if a table is made up as in Table 2, that the products of signs can be determined by entering in each column, the products indicated. The darkly outlined areas contain the products of signs. At the top of each area is the receiver code (earliest sample to the left), to the left is the signal code with the earliest pulse on the lower end. In this table, the receiver has master phase code, interval A, in the left hand outlined areas, and master phase code, interval B, to the right. In the upper areas, $s(t)$ has master phase code in the same interval as the receiver, i.e. $N \times 1000 = \tau$, which varies from -7000 usec to +7000 usec. In the lower areas, the $s(t)$ intervals and $r(t-\tau)$ intervals are reversed, i.e. $(15-N) \times 1000 \pm \text{GRI} = \tau$. To fill in the product of signs areas, each sign in the $s(t)$ column is visualized to move to the lower right, one column at a time. The sign is then entered as the product of its sign and the sign of $r(t-\tau)$ at the top of that column. Each column then is the $s(t)$ code from bottom to top, multiplied by the sign of $r(t-\tau)$ in that column. The sum of products is the algebraic sum of all the pluses and minuses in each row (but not including the $s(t)$ column).

Certain information can be deduced from the presentation of Table 2:

- a. When $N = 0, \pm 9, \pm 13$, $C(\gamma)$ may not be zero, depending only on $\sin \gamma$. If N equals some other value, $C(\gamma)$ is zero regardless of $\sin \gamma$, or the magnitude of $s(t)$.
- b. Therefore, in a receiver just turned on and beginning the search process, with no known initial value for γ , γ is varied until $|C(\gamma)| > 0$. The receiver must check for a false alignment on $N = 9$ or 13 . The receiver must not indicate proper synchronization until these checks are made.
- c. A long delayed skywave of the master is equivalent to a signal for which $N = +1, 2, 3$, etc. to 7 . If this occurs, $C(\gamma)$ for that skywave, when the receiver is tracking ground wave, is zero. Therefore long delayed skywaves will not cause an error in the receiver. Skywave delays for $N = \pm 8$ Through ± 15 are not possible, so these will not cause errors either.

A slight format change of Table 1 will permit removal of the middle $s(t)$ column, removing confusion when forming the sum of products. For reasons which will become clear later, it is convenient to form the sum of products in the center column. Table 3 is in the form I will use for the remainder of this paper. Step sum is explained later.

Table 3 looks at the effect of a secondary signal received during the receiver's master interval, such as might occur during master search. The following information can be derived from Table 3:

- a. $C(\gamma)$ is not zero for all γ and hence during master search, the receiver's search process must check to ensure against incorrectly detecting secondary signals and assuming that they are master signals.
- b. Long delayed secondary skywaves from a previous interval, equivalent to $N = +9, 11, 13$, could cause errors in the reception of the master signal. Therefore in the design of a chain, sufficient time must be allowed between the last secondary and the master signal to make this event unlikely.

Cross Rate Interference

Cross rate interference is the condition which exists when a receiver is receiving and operating on the signals from one Loran-C chain while signals from another chain are also being received. The 'other' chain is usually geographically adjacent to the one being received, and in fact the chains may share a 'dual-rated' station.

The Loran-C system rate structure (ie: the set of possible GRI's from which a chain rate may be selected) consists of GRI's which are multiples of 100 usec. If a receiver is operating on GRI'A', there are GRI'A' usec \div 100 possible time locations in GRI'A' in which the pulse group from a station in chain B could occur. (These time locations vary with geographic location and are the basis of cross-chain time differences.) If GRI'A' \div 100 and GRI'B' \div 100 are prime numbers or have no common prime factors, then the pulse groups from chain B will occur in all possible locations in GRI'A', but not necessarily sequentially. If there are common numbers between the A and B rate factors, then less than all locations will be used.

Table 2: Computation of $C(\gamma)$ for Master Signal received and Receiver set to Master Code.

STEP SUM

	INTERVAL A								RECEIVER SUM	CODE SUM		INTERVAL B							
N	+	+	-	-	+	-	+	-	A	SUM	B	+	-	-	+	+	+	+	
-7	-	+							+1	C	-1	-							
-6	-	-	+						0	C	0	-	+						
-5	+	-	-	-					-3	C	+3	+	+	+					
-4	+	+	-	+	-				0	C	0	+	-	+	-				
-3	+	+	+	+	+	+			+5	C	-5	-	-	-	-				
-2	+	+	+	-	+	-	-		0	C	0	+	+	-	+	-			
-1	+	+	+	-	-	+	+	-	+1	C	-1	-	-	+	+	-	-		
0		+	+	-	-	+	+	-	0	C	0	+	+	-	-	+	+	-	
+1			+	-	-	+	-	-	-1	C	+1	-	-	+	+	-	+	-	
2				-	-	+	-	+	0	C	0	-	-	-	+	-	+	+	
3					-	+	-	+	-1	C	+1	-	-	-	+	-	+	-	
4						+	-	+	0	C	0	-	-	-		+	-	+	
5						-	+	-	-1	C	+1	-	-	-			+	-	
6							+	-	0	C	0	-	-	-			+	-	
7							-	-	-1	C	+1	-	-	-				+	
8	-	-							-1	C	+1	+	-	-					
9	-	-	-						-2	C	-2	-	-	-					
10	+	+	-	+					+1	C	-1	-	+	-					
11	+	+	+	+	+				+4	C	+4	+	+	+	+				
12	-	-	+	-	+	-			-1	C	+1	+	-	+	-	+			
13	+	+	-	-	-	+			-2	C	-2	+	-	-	-	+			
14	-	-	+	+	-	+	+	-	+1	C	-1	+	-	-	+	-	-	+	
15	+	+	-	-	+	+	-	+	0	C	0	+	-	-	+	+	-	+	
16			+	+	-	-	+	+	+1	C	-1	-	-	-	+	+	-	-	
17				-	+	+	+	-	+2	C	+2	-	-	-	+	+	+	-	
18					-	-	-	-	-5	C	+5	-	-	-	+	+	+	+	
19						+	+	+	+4	C	+4	-	-	-		+	+	+	
20						-	-	-	-3	C	+3	-	-	-		+	+	+	
21							+	+	+2	C	+2	-	-	-			+	+	
22							-	-	-1	C	+1	-	-	-				+	

Σ = +16

Table 3. Computation of $C(\gamma)$ for Secondary Signal Received and Cross Correlated with Master Sampling.

During any single A interval, the eight pulses from the station on rate B will occur. If this coincides with the sampling of signals on rate A, the samples will be contaminated by the B signals. Since the pulses and sampling strobes on both rates are spaced at exactly 1000 usec, from one to eight samples could be contaminated.

We would like to evaluate the effect of this contamination using the sum of products table. If there is interference the magnitude of the sum of sums will not be zero, and the magnitude of this sum will be a relative indication of the magnitude of the effects. However, if the sum of sums is zero, we can say with confidence that interference will not occur.

To demonstrate this conclusion, refer to table 3, and suppose that the signal 'GRI, (GRI'B') is 1000 usec longer than 'A' (the rate set into the receiver), and that the receiver is tracking an A rate secondary as a B rate secondary signal begins to cross over. In the first interval that the signals overlap, condition 1 exists. In the next interval, the interfering signal is 1000 usec later and condition 2 exists. Then 3 and so on. During each of these intervals, the magnitude of the sample is the same, because B advanced exactly 1000 usec. The 'step sum' is the sum of the individual interval sums as the interfering signal steps through.

Note that the crossover could also have started on the right hand side of the upper section of the table, or on either side of the lower set of sums of products. There are a total of four possible crossing conditions, but only one has a step sum other than zero. During the cross over represented by this step sum, an offset would be put into the receiver's time reference for the signal being tracked. Therefore, cross rate interference exists in this example.

If all step sums, or simply the sum of all "sumA" and "sumB" entries, is zero, cross rate interference will not occur if both rate A and rate B have no common prime factors. Also the special case of rates different by exactly 1000 usec will not result in cross rate interference, if the step sums are zero.

Designing Rate and Phase Code Combinations for Minimum Interference:

In order that the step sums or the sum of sums is identically zero, the code for one of the two adjacent chains must have a balanced phase code. That is in order for there to be an equal number of pluses and minuses in each section of the products table one of the phase codes must be balanced (equal number of + and -). If in addition all step sums are zero and a rate difference of exactly 1000 usec is selected, then each crossing takes precisely 15 intervals and the net error contribution during that crossing is zero. A 15 interval crossing will take less than 1.5 sec. Since this is less than the typical receiver time constant, it is quite possible to not only make the net offset zero, but to also not significantly increase the standard deviation of receivers subjected to this cross rate signal.

There are seventy possible balanced phase codes for each interval of a two interval code, and therefore 4900 possible two interval codes. Half are complementary and half of those have reversed intervals, leaving 1225 codes. In order to select codes, a scheme is needed to minimize that list. Generally speaking it is convenient for the hardware to have the second interval code related to the first by some logic constant. For example in the present Loran-C codes, the B interval of both the master and secondary codes is the same as the A interval but with the even numbered pulses inverted (phase code sign changed). This same scheme will work for balanced codes only if an equal number of even numbered pulses are + and -. This cuts the available set of codes to 48! It is now only necessary to form them and test. Reading References 2, 3, and 4 will help.

Once a code is found, and I'll throw one out for fun:

+ + + - - - - + + + - + - - + -

we need to test the code to see if it is useful and then select a GRI to minimize cross rate interference. (Note that the scheme between the first and second intervals of the above code was to invert even numbered pairs of pulses.) It may also be necessary to come up with an alternative code for secondary stations.

First it is necessary to test the cross correlation of the code with itself, Table 4, and find that:

- a. The search scheme in a receiver must guard against correlations at $N = +/-4, +/-10, +/-12$, and $+/-14$
- b. There is protection from long delayed skywaves only through $N = +3$.

From this we conclude that a receiver for this code would have a search algorithm modified from that in a standard Loran-C receiver, and that the chain would probably best be used only when short base lines preclude the possibility of long delayed skywaves becoming significant.

Tables 5 and 6 show the sum of products for the cross correlation of the special code and the master and secondary codes used in the Loran-C system. Inspecting the step sums for a GRI difference of $+/-1000$ usec, it can be seen that there will not be cross rate interference. To emphasize this, the plots of Figure 4 represent the step sums of the four possible crossing situations of Table 5, and show the instantaneous relative value of $C(\tau)$ during each crossing. Similar plots could be made for Table 6. These plots show that the $C(\tau)$ for the interfering signal never becomes as great as the $C(\tau)$ for the desired signal sampled over only one interval.

Further inspection of the step sums of Tables 5 and 6 shows that a GRI difference of $+/-2000$ usec will also produce step sums equal to zero. What's more a check of the step sums for Table 4 indicates that 2 chains, both using the special code, but with a GRI difference of $+/-1000$ usec or $+/-2000$ usec would not cause interference to each other. This says that not only is this an acceptable code from the standpoint of interference to a Loran-C chain, but that the code could be used on two chains adjacent to a Loran-C chain and to each other. One chain would operate at the Loran-C GRI - 100 usec and the other at the Loran-C GRI - 2000 usec.

STEP Sum

N	SIG	RECEIVER INTERVAL A	SUM A		SUM B	RECEIVER INTERVAL B													
	+	+	+	+	-	-	-	+	①		②	+	+	-	+	-	-	+	-
-7	-	+							+12	0	-1	-							
-6	-	-	+						0	0	0	+	-						
-5	-	-	-	+					-1	0	+1	-	+	+					
-4	-	-	-	-					-4	-8	-4	-	-	-					
-3	+	-	-	-	+	-			-3	0	+3	+	-	+	+	+			
-2	+	+	-	-	+	+	-		0	0	0	-	+	+	-	-	+		
-1	+	+	+	-	+	+	+	-	+3	0	-3	+	-	-	-	+	-		
0		+	+	+	+	+	+	+	+8	+16	+8	+	+	+	+	+	+	+	+
1	↑	+	+	-	+	+	+	-	+3	0	-3	+	-	-	-	+	-		
2	↑	+	-	-	+	+	-		0	0	0		-	+	+	-	-	+	
3	↑			-	-	-	+	-	-3	0	+3			+	-	+	+		
4	↑				-	-	-		-4	-8	-4			-	-	-			
5	↑					-	+		-1	0	+1				-	+	+		
6						-	+		0	0	0						+	+	
7						+			+1	0	-1							+	
	-										=0								
8	+	-							-1	0	+1	+							
9	-	+	-						0	0	0	-	+						
10	-	-	+	-					-1	-4	-3	-	-	-					
11	+	-	-	+	+				0	0	0	-	-	+	+				
12	-	+	-	-	-	+			-1	-4	-3	-	-	+	-	-			
13	+	-	+	-	+	-	+		0	0	0	+	-	+	-	+	-		
14	+	+	-	+	+	+	-	+	+3	+8	+5	+	+	+	-	+	+	+	+
±15		+	+	-	-	+	+	-	0	0	0	+	+	-	-	+	+	-	-
-14	↑	+	+	+	-	+	+	+	+3	+8	+3	+	-	+	+	+	-	+	
-13	↑	+	-	+	-	+	-		0	0	0		-	+	-	+	-	+	
-12	↑			-	-	+	-		-3	-4	-1		+	-	-	-	+		
-11	↑				-	-	+	+	0	0	0			-	-	+	+		
-10	↑					-	-		-3	-4	-1				-	+	-		
-9						-	+		0	0	0						+	-	
-8						+			+1	0	-1							-	

Table 4. Special Code, cross correlation with Receiver on the same code.

Step Sum b

N	Sig	RECEIVER INTERVAL A								SUM A	SUM B	RECEIVER INTERVAL B							
	+	+	+	-	-	+	-	+	-			+	-	-	+	+	+	+	+
-7	-	+								+1	-1	-							
-6	-	-	+							0	+2	+	+						
-5	-	-	-							-3	-1	-	-	+					
-4	-	-	-	+	-					-2	-2	-	+	-	-				
-3	+	-	-	+	+	+				+1	+3	+	+	+	+	-			
-2	+	+	-	+	+	-	-			0	-2	-	-	+	-	+	-		
-1	+	+	+	+	+	-	+	+		+3	-1	+	+	-	-	+	+	-	
0	-	+	+	-	+	-	+	-	-	0	0	+	-	+	+	-	-	+	-
1	-	+		-	-	+	-	+		-1	-3	-	-	-	+	-	-	+	-
2	-			-	-	+	+	-	+	0	-2			-	+	-	+	-	-
3	-				-	+	-	-	+	-1	+1			+	+	-	+	-	-
4	-					+	-	+	+	+2	+2				+	+	+	-	+
5	-						+	-		-1	+1					+	+	+	-
6	-						+	-		0	+2						+	+	+
7	-							-		-1	+1							+	+
	-									$\sum = 0$									
8	+	-								-1	+1	+							
9	-	+	-							0	-2	-	-						
10	-	-	+	+						+1	-1	-	+	-					
11	+	-	-	-	+					-2	+2	-	+	+	+				
12	-	+	-	+	-	-				-1	+1	-	+	+	-	+			
13	+	-	+	+	+	+	+			+4	+2	+	+	+	-	-	+		
14	+	+	-	-	+	-	-	-		-3	-1	+	-	+	-	-	-	+	-
15		+	+	+	-	-	+	+	+	+4	-4	+	-	-	-	-	-	-	+
-14		+	-	+	+	+	-	-		+1	-5		-	-	+	-	-	-	-
-13				-	-	-	-	+		-4	-2			-	+	+	-	-	-
-12					+	+	+	+		+3	+1			+	+	+	-	-	-
-11					+	-	-	-		-2	+2				+	+	+	-	-
-10						+	+			+1	+3					+	+	+	+
-9						+	-			0	+2						+	+	+
-8							-			-1	+1							+	+

Table 5. Special code, cross correlation with receiver on Loran-C master code.

N	SIG	RECEIVER INTERVAL A								SUM A		SUM B	RECEIVER INTERVAL B							
		+	+	-	+	-	+	+	-				+	+	+	+	+	-	-	+
-7	-	+								+1		-1	-							
-6	-	-	-							-2		0	+	-						
-5	-	-	+	+						+1		-1	-	+	-					
-4	-	-	+	-	-					-2		-2	-	-	+	-				
-3	+	-	+	-	+	+				+1		-1	+	-	-	+	-			
-2	+	+	+	-	+	-	+			+2		0	-	+	-	-	+	+		
-1	+	+	-	-	+	-	-	-		-3		-1	+	-	+	-	-	-	+	
0		+	-	+	+	-	-	+	-	0		0	+	+	-	+	-	+	-	
1			-	+	-	-	-	+	+	-1		+5		+	+	-	+	+	+	
2				+	-	+	-	+	+	+2		0			+	+	-	-	+	-
3					-	+	+	+	+	+3		+1				+	+	+	-	-
4						+	+	-	+	+2		+2					+	-	+	+
5							+	-	-	-1		-3						-	-	-
6								-	-	-2		0							-	+
7								-		-1		+1								+
-	-																			
8	+	-								-1		+1	+							
9	-	+	+							+2		0	-	+						
10	-	-	-	-						-3		-1	-	-	+					
11	+	-	+	+	+					+2		-2	-	-	-	+				
12	-	+	+	-	-	-				-1		-3	-	-	-	-	+			
13	+	-	-	-	+	+	-			-2		-4	+	-	-	-	-			
14	+	+	+	+	+	-	+	+		+5		-1	+	+	-	-	-	+	-	
15		+	-	-	-	-	-	-	-	-6		+4	+	+	+	-	-	+	+	+
-16			-	+	+	+	-	+	+	+3		+3		+	+	+	-	+	+	-
-13				+	-	-	+	+	-	0		+4			+	+	+	+	+	-
-12					-	+	-	-	-	-3		+1				+	+	-	+	-
-11						+	+	+	+	+4		-2				+	-	-	-	
-10							+	-	-	-1		-1						-	-	+
-9								-	+	0		0							-	+
-8									+	+1		+1								+

Table 6. Special code, cross correlation with receiver on Lorqn-C secondary code.

It is appropriate to point out here that the receiver processing is presumed to maintain its designed linearity during the signal crossings. If, for example, the crossing rate signal is so strong that the antenna preamplifier saturates, then this analysis may not apply. The analysis does however apply to a hard limited receiver, so long as no nonlinearities occur in linear portions of the receiver.

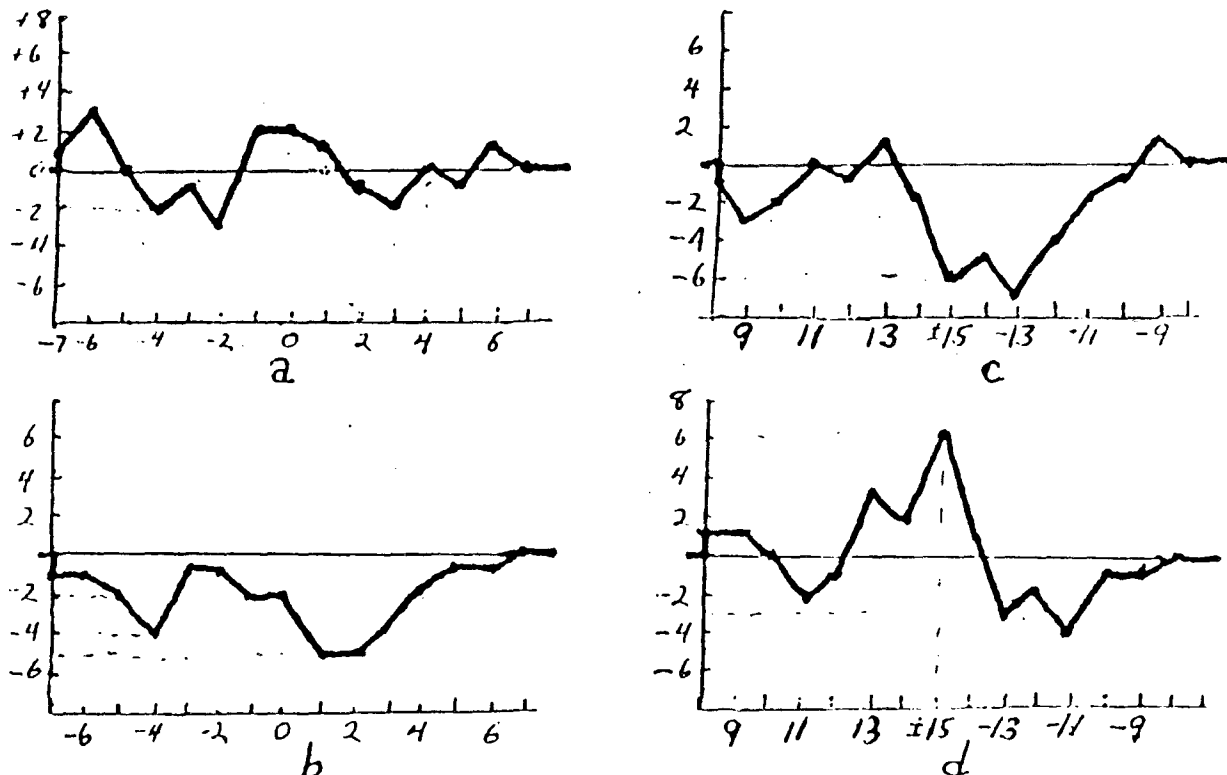


Figure 4. Plot of step sum vs N for the four possible crossing situations of Table 5.

The next step is the design of a second code for the secondary stations. This must be checked for:

- search correlations
- skywave correlations
- correlations with the first special code
- correlations and step sums against the Loran-C master code
- correlations and step sums against the Loran-C secondary code.

A possible code is: + - + + - + - - + - - - + + +

This code has properties similar to the first special code, and has been checked under all the same conditions.

Recommendation:

That codes and GRI's such as these, tested as described herein, be required for use in small Loran-C chains erected within or adjacent to standard Loran-C chains.

Bibliography:

- (1) Schwartz, M. "Information Transmission, Modulation, and Noise" McGraw Hill 1959.
- (2) Sperry Gyroscope Co. "Cross Chain Interference Study, Final Report", Sperry Report No. HB 9222-0055, April 1964.
- (3) Collins Radio Co. "Final Engineering Report for Cross-Chain Interference Study" Collins Report No. 523-0556247-00183M, 17 July 1964.
- (4) ITT Federal Laboratories "Final Engineering Report Cross-Rate Interference Study" ITT Report No. TD-63-313, November 1963.

112

ROBERT L. FRANK
~~16500 North Park Drive~~
~~Southfield, Mich. 48075~~

ROBERT L. FRANK
~~16500 North Park Drive~~
~~Southfield, Mich. 48075~~

SPATIAL AND TEMPORAL ELECTRICAL PROPERTIES DERIVED
FROM LF PULSE GROUND WAVE PROPAGATION MEASUREMENTS

ROBERT H. DOHERTY
U. S. Department of Commerce
OFFICE OF TELECOMMUNICATIONS
Institute for Telecommunication Sciences
Boulder, Colorado 80302

FILE COPY
3-12

For
Advisory Group For Aerospace Research
and Development

of

NATO

AGARD PAPER NO. 30

(AGARD CONF. PROCEEDINGS #114)

Conference Proceedings
Electromagnetic Wave Propagation Involving
Irregular Surfaces and Inhomogeneous Media
XX Technical Meeting of the Electromagnetic
Wave Propagation Panel of AGARD-NATO

Netherlands, March 1974

cancel ed
30 pages

Also presented at Wild Goose Assn
3rd Annual Convention Oct 1974

FRANK
REF 603
12 2011-21
GWSJH

Key Words

Low Frequency propagation, Weather effects, terrain effects,
refractive index lapse rate.

Spatial and Temporal Electrical Properties Derived
from LF Pulse Ground Wave Propagation Measurements

by

Robert H. Doherty
U. S. Department of Commerce
Office of Telecommunications
Institute for Telecommunication Sciences
Boulder, Colorado 80302

SUMMARY

Low frequency ground wave phase measurements made on two loran (100 kHz pulse transmissions) paths have been analyzed for spatial variations. One Loran-D path in Nevada and California passes over Death Valley producing a so called "Death Valley Anomaly". The other 1000 km Loran-C baseline path between Carolina Beach, N. C. and Dana, Indiana was measured in detail during the spring of 1970. Four locations in addition to the transmitter locations were monitored, one near Carolina Beach (the master), one just east of the Appalachian Mountains, one just west of the Appalachian Mountains and one near Dana, Indiana (the Z slave station). Effective surface impedance values were deduced for each segment of the propagation path.

In addition to these spatial evaluations of the phase, temporal variations of the phase over the Eastern path were approximately one microsecond even though synchronization accuracies were better than .1 microseconds. Changes in the surface impedance values as a function time are clearly indicated.

Analysis of data taken between February 11 and February 22, 1970 from five monitoring stations is presented. Four stations measured loran phase variations, and three stations recorded weather parameters. Since the phase variations are at least an order of

magnitude greater than can be explained by the primary wave propagation time of $\frac{\eta_1 d}{c}$ (where η_1 is the surface index of refraction and c is the velocity of light in a vacuum and d is the distance in meters), the correlation obtained is explained in terms of the α factor. The α factor is related to the rate of change of the refraction index of the earth's atmosphere with altitude, and these low frequency measurements appear to be a sensitive means for detecting changes in this lapse rate. Thus the α -factor is the theoretical parameter that relates ground wave propagation to weather changes in the earth's atmosphere.

In the particular case of a warm front, a phase change is predicted to occur before the passage of the front at the surface of the ground. On the other hand the passage of a cold front would predict a phase change after the passage of the front at the surface of the ground. Both of these phenomena were observed and recorded.

Temporal and spatial phase and amplitude variations of these low frequency signals are correlated with inhomogeneous media. Quantitative information on the magnitude of temporal variations in phase must be separated from the spatial variations in phase to interpret observations of irregular terrain effects.

1. INTRODUCTION

Loran-C and Loran-D are highly accurate operational positioning systems available today. This is true because the systems operate on low frequency ground waves which are unaffected by the ionosphere, a comparatively unstable propagation medium. However, small variations of these ground wave signals may be used to evaluate the variations in the electrical properties of the earth's surface over which these signals propagate. A pure ground wave measurement is quite possible, because the transmitted signal is a rapidly rising pulse waveform, and the received signal is measured at a point in time before the arrival time of the first ionospheric wave reflection (Johler, J. R., and Horowitz, S., 1973).

The electrical properties of the earth's surface include the impedance or conductivity of the ground, the roughness or terrain variations of the surface, the refractive index of the atmosphere at the surface, and the lapse rate or rate of change of refractive index with height above the surface. Effects of the inhomogeneities and irregularities are discussed by Johler, J. R. 1971a, whereas the refractive index and lapse rate effects were treated by Johler, J. R., et al. 1956.

Spatial variations of the transmitted signal are primarily influenced by the inhomogeneities of the surface impedance and by the variations in the terrain. Temporal effects may be produced by time changes in these spatial features, but are more easily influenced by the surface refractive index and the lapse rate of the refractive index of the earth's atmosphere, which are known to change diurnally and with changing weather conditions.

The Loran ground wave measurements discussed in this paper were obtained in two locations in the United States. A Loran-D chain has recently been installed in the western states. Phase time of arrival measurements were made along a path between the master station near Glendale, Nevada and the monitor station at China Lake, California. Measurements in the immediate vicinity of Death Valley, over which this propagation path crosses, are used to compare the predicted and observed spatial variations. This path is about 200 km long.

The East Coast Loran-C chain has one inland slave at Dana, Indiana. Along the all land path from the master at Carolina Beach, North Carolina to the Z slave at Dana, Indiana, four locations were monitored during February and March of 1970 (see figure 1). Temporal variations over this approximately 1000 km path will be discussed in terms of theoretical expectations, but not complete predictions. On this

path, phase propagation time, or time of arrival (TOA) measurements were made on both the master and the Z-slave signals at Cloverdale, Indiana, approximately 60 km from the Dana slave. At the other three sites, Paris, Kentucky; Mocksville, North Carolina and Clarkton, North Carolina, only Slave-Master time difference (TD) measurements were made.

It should be noted that both of these paths are land paths, one involving very rugged terrain and the other involving mountains, freezing temperatures and extremely variable weather conditions. These are the type of paths that have extreme variations in the surface electrical properties. Most world wide Loran-C paths are over sea water. In these instances the surface properties of impedance, terrain, refractive index and lapse rate are normally very constant. Over such paths 0.1 to 0.2 microseconds synchronization and positioning accuracies are common place. However on the Dana to Carolina Beach propagation path we have found apparently anomalous spatial and temporal variations in the propagation.

2. COMPARISON OF MEASURED DATE WITH THEORETICAL PREDICTIONS IN THE VICINITY OF DEATH VALLEY

For the Loran-D West master to monitor path (Glendale, Nevada to China Lake, California) the impedance and terrain were scaled from geological and topographic maps for use in a theoretical prediction model (Johler, J. R. and Horowitz, S. 1974). The terrain variations with distance from the transmitter which are used directly in the propagation theory to predict secondary phase corrections are shown in figure 2. Along this path Death Valley occurs at 200 km from the master station. Figure 3 shows the secondary phase correction calculated for this path. A large (approximately 2 microseconds) secondary phase increase is associated with the drop into Death Valley.

Direct phase measurements of the master signal were made in a mobile van using a cesium standard and a timing receiver. Figure 4 shows a schematic representation of measurements made in the vicinity of Death Valley and close to the master to monitor path. It was necessary to make the measurements along roads with the available TOA equipment, and roads could not follow the rugged master to monitor path. Thus, the measurements made at points 1 through 9 followed a much more gradual decent into Death Valley. The lines in figure 4 indicate contour intervals. A point measured at Badwater (point D) was typical of the point at 200 km on the master to monitor path. Points E and F are very typical and nearly on the master to monitor path. Points 1, 2 and 3 or A, B and C are typical of either the master to monitor path ahead of the abrupt drop into Death Valley or the more gradual path into Death Valley represented by points 1 through 9. If points A, B, C, D, E and F are adjusted for distance to the master and plotted on the master to monitor path for comparison with the predictions, the fit is quite good as seen in figure 5. However, points 1 through 9 plotted on this figure at their actual distances from the master station do not fit the predictions at all. This is to be expected because the drop into Death Valley is gradual rather than abrupt. It is recognized that another path should be scaled and predicted running from the master and approximately through points 1 through 9. Severe limitations in funding and manpower for this analysis have precluded this effort.

✓ The perturbation in the prediction curve just after point F is not thought to be valid, but is a consequence of a scaling and incrementing problem in the input data. The valid and invalid perturbations can be distinguished by changing input data increments and determining which variations remain constant.

3. MEASUREMENTS OVER CAROLINA BEACH TO DANA PATH USED TO DERIVE VARIATIONS OF THE PATH ELECTRICAL PROPERTIES.

Data gathered during February and March 1970 from four stations between Dana, Indiana and Carolina Beach, North Carolina (see figure 1) were used to derive changes in the emission delay and effective impedances for various path segments. Direct phase measurements of both the Dana (Z-slave) transmissions and the Carolina Beach (master) transmissions were made at Cloverdale during the entire operation. Time difference measurements were made at the other three locations for two or three weeks at each location. Large variations such as occurred on the master phase TOA shown in figure 6 on February 25th and 26th were used to obtain extreme variations at each location. The phase values were obtained from each of the three data channels represented in figure 6, and these values were used to deduce effective path impedances and changes in slave station emission delays shown in table 1. The magnitude of the impedance over the 60 km path from Dana to Cloverdale was assumed to remain constant at .0250. There is no apparent reason why the surface impedance should change with time over a few hour period as suggested by Table 1, and therefore it is anticipated that the temporal variations of the loran signals are related to conditions above the surface of the ground, primarily refractive index and lapse rate of the refractive index.

Figure 7 shows daily average values plotted for a one year period. Three of the time periods shown in Table 1 are also shown on this plot. Due to instrumentation peculiarities, the variations seen at Dana are reversed from the actual changes that occur. This figure also illustrates that the area monitor at Warner Robins A.F.B. controlled the chain by introducing coding delay corrections at Dana. That is, the emission delay of the Z-slave transmission was changed to hold the time difference constant at Warner Robins.

The variations shown in figure 7 have been analyzed to determine the emission delay changes at the Z-slave. These changes are shown in figure 8. The changes shown in this figure are comparable to the emission delay changes reported in Table 1. The exact changes on the individual days shown are not identical because figure 8 represents daily averages, whereas figure 6 and Table 1 are taken from hourly averages.

Figure 9 shows deduced seasonal changes over the master to Z-slave path using the data from figure 7. A comparison of the change on February 26 as shown in figure 9 and figure 6 appears much different. In figure 6 the + symbols shown each day at 0000 hours are equivalent to the preceeding days average values. If these variations are compared with the changes shown in figure 9, much closer agreement occurs.

Data presented in figures 6 through 9 and Table 1 indicate that short term and long term temporal variations are comparable in magnitude. The large variations occur primarily during winter months when temperatures drop below freezing. The variations appear to be larger for paths which traverse the mountains.

4. THEORETICAL EXPLANATION OF TEMPORAL VARIATIONS

The phase of the low frequency radio signal can be expressed as

$$\varphi = (\omega / c) \eta_a d + \varphi_c \quad (1)$$

where $\omega = 2\pi f$, c is the velocity of light in a vacuum η_a is the surface refractive index, d is the distance and φ_c is secondary phase corrections caused by finite impedance and refractive index changes on either side of the surface boundary along which the signal propagates. The surface refractive index η_a can range from 1.000240 to 1.000400,

but normally changes by less than .0001 over short periods of time. Therefore over a 1000 km path phase changes of less than .3 micro-second would be the maximum changes that would be anticipated.

The secondary phase correction φ_c can be expressed as

$$\varphi_c \cong (k_1 a)^{1/3} \alpha^{2/3} \tau_0 d/a \quad (2)$$

where τ_0 is primarily influenced by the surface impedance and is derived from the boundary condition at the surface of the ground as the zero-th root of Ricatti's equation, a is the earth's radius, k_1 is the wave number and α is associated with the lapse rate of the refractive index (Johler, J. R. 1971a). It is α that is assumed to be producing the major temporal variations.

A formula for α considering the differential change of η with h is given by Eckersley, J. L. and Millington, G. 1939

$$\alpha = 1 + \frac{a}{\eta_a} \frac{d[\eta(a+h)]}{d(a+h)} \quad (3)$$

As can be seen, this formula relates α to the change of η with height. Johler, J. R. 1971b used this formulation to derive the formula

$$\alpha = 1 - \left(\frac{a}{h_b} \right) \left(1 - \frac{1}{\eta_a} \right) \left(1 - \frac{N_b}{N_a} \right) \quad (4)$$

where $N_a = (\eta_a - 1)10^6$, and $N_b = (\eta_{h_b} - 1)10^6$. and a and h_b are in meters. In this formula the N_a and N_b are the commonly referred to N values for defining refractive index (Bean, B.R. and Dutton, E.J., 1966) ranging from 240 to 400 at the surface. These values may be obtained from meteorological quantities from the formula

$$N = 77.6 \frac{P}{T} + 3.76 \cdot 10^5 \frac{e}{T^2} \quad (5)$$

where P is pressure in millibars, T is temperature in degrees centigrade, and e is the partial pressure of water vapor in millibars. Using these fundamental relations and the dynamical condition

$$\frac{d\rho}{dh} + \frac{de}{dh} = -10 \text{ ge} , \quad (6)$$

where g is the acceleration of gravity and ρ is the air density Bremmer, H., 1949 developed a meteorological relationship for the α

$$\alpha = 0.766 - (0.0681 + 0.00237e) \frac{dT}{dh} + 0.306 \frac{de}{dh} , \quad (7)$$

where 100 meters is chosen as a unit of length for h .

Now if formula 4 is evaluated for a typical value of $\eta_a = 1.000314$ and $h_b = 2000$ meters and $a = 6.36739 \times 10^6$ meters, we find that

$$\frac{a}{h_b} \left(1 - \frac{1}{\eta_a} \right) \cong 1 . \quad (8)$$

Therefore, under these condition

$$\alpha \cong \frac{N_b}{N_a} \quad \text{for } h_b = 2000 \text{ meters} \quad (9)$$

Since the wavelength of the 100 kHz signal is 3 km, the lower 2 km of the atmosphere is considered to be of prime importance for determining the propagation velocity.

The approximation in formula 9 emphasizes the greater effect N changes have on α than they do on η . The approximation also indicates that as the surface refractive index, N_a , increases α decreases as was suggested by Hefley, G. 1972. It is believed that this condition does occur during the summer when a normal temperature lapse rate of about 6.5° per kilometer exists. Also during the summer the humidity

is high and the second term in equation 5 tends to dominate the determination of N values. During a two week summer period of observations made at Greensboro, North Carolina the surface N value ranged from 298 to 375. The data shown in figures 7 and 9 suggests a stability better than would be anticipated by this range of N values assuming this range is typical. The summer data tends to support the inverse relation between the phase variations produced by changes in the surface N values and the phase variations produced by changes in the α values.

During a two week winter period of observations made at Greensboro, North Carolina the surface N value only ranged from 292 to 312. This small range of surface N value changes would predict practically no change in the phase velocity of the primary wave during winter. Figures 6, 7 and 9, however suggest large changes in the propagation velocity at this time. The large changes in propagation time are attributed to changes in α . For this propagation path and for the average impedance taken from Table 1, changing α from 1 to .71 will cause a decrease in the propagation time of approximately .75 microseconds. This is approximately the variation from summer to average winter conditions as seen in figure 9. A further change in α from .71 to .53 will cause a further decrease in the propagation time of approximately .75 microseconds. These values were obtained from a computer program utilizing the equations given by Johler, J. R. et. al. 1956. This is essentially equivalent to the change from average winter conditions to extreme winter conditions as shown in figure 6 or figure 9. Table 2 shows values that substituted into equation 7 can explain these results.

A justification for these parameters is primarily based on the low humidity in terms of the partial pressure of water vapor. Observations of weather records show that the wet term of the refractive index equation i.e., $3.76 \times 10^5 \frac{e}{T^2}$ is much smaller in the winter than in the summer. Observations of refractive index measurements made at Mocksville, North Carolina and at Fayetteville, North Carolina on

February 26 (see figure 6) showed very low wet term for the refractive index. When the dry term of the refractive index becomes the controlling term of the refractive index equation, and when the temperatures are low, temperature inversion layers near the surface are common. Temperature inversion layers near the surface will cause a low α value according to equation 7. Also if one looks at the dry term only in equation 5 and assumes temperature is increasing with height as pressure decreases logarithmically with height, it is easy to see that N is decreasing rapidly. A rapid decrease of N with height, produces small α values.

Changes in the α values are associated with changes in meteorological parameters at heights above the surface. When weather frontal systems pass a station the upper air changes precede the surface changes for a warm front and follow the surface changes for a cold front as seen in figure 10 (Bean, B. R. and Dutton, E. J., 1966). This would suggest that changes seen on the Loran-C signals that were associated with frontal movements would correlate with surface refractive index changes with a finite lead or lag time. Figure 11 shows that this is indeed the case. This figure also shows that a decrease in the propagation time or a decrease in the α parameter is associated with the passage of both a cold front and the passage of a warm front.

These results suggested that individual fronts might be located in the weather records which produced observable Loran-C changes. One case of a cold front passage and one case of a warm front passage were identified (Doherty, R. H. and Johler, J. R., 1973). A warm front passage was noted on refractive index records from Indianapolis, Indiana; Fayetteville, North Carolina and Bristol, Tennessee on March 17th. The Loran-C records showed a weather related phase perturbation on March 15th. A cold front passage was observed on the same three refractive index records on Feb. 25th. A weather

related Loran-C perturbation was observed on the Carolina Beach to Cloverdale path on February 26th.

Conclusions

The spatial and temporal changes in electrical properties of the propagation medium can be investigated by measurements of low frequency (100 kHz) pulse ground wave transmissions. Spatial changes are primarily related to surface impedance and terrain variations. Measurements made over carefully selected paths that have impedance variations and no terrain variations, and paths that have large terrain variations and no impedance variations would be useful to separate the magnitude of the two effects. A separation of the theoretical predictions on the path shown in figure 2 suggest that the terrain effects are much larger for this particular path (Johler, J.R. and Horowitz, S. 1974).

The temporal variations observed on these Loran-C measurements suggest that certain weather phenomena could be monitored using the Loran-C transmissions. For example the changes in the propagation time of the signals could be used to monitor the integrated surface humidity over the monitored path.

Further theoretical and experimental studies relating the measured changes to predicted changes using actually measured refractive index height profiles should be carried out. These studies would be directed towards determining a method for predicting a lapse rate profile that would be an effective integrated profile for the entire propagation path. These profiles used in conjunction with radiosonde measured height profiles would yield a more complete mapping of the refractive index height profiles.

Acknowledgements

The author wishes to thank the U. S. Coast Guard for making available the measurements between Carolina Beach, North Carolina and Dana, Indiana. He also wishes to thank the U. S. Air Force Loran Programs Office for making available the measurements from the Loran-D west chain.

References

- Bean, B. R. and E. J. Dutton (1966), Radio Meteorology, National Bureau of Standards Monograph 92, (Superintendent of Documents, U. S. Government Printing Office, Washington, D. C. 20402).
- Bremmer, H. (1949), Terrestrial Radio Waves--Theory of Propagation (Elsevier Pub. Co. Amsterdam-New York).
- Doherty, R. H. and J. R. Johler (1973), Meteorological Influences on Loran-C Ground Wave Propagation, Paper presented at 1973 Annual Wild Goose Convention (to be published).
- Eckersley, J. L. and G. Millington (1939), Application of the Phase Integral Method to the Analysis of the Diffraction and Refraction of Wireless Waves Round the Earth, Phil. Trans. Roy. Soc. 237, 237.
- Hefley, G., (1972), The Development of Loran-C Navigation and Timing, National Bureau of Standards Monograph 129, (Superintendent of Documents, U. S. Government Printing Office, Washington, D. C. 20402).
- Johler, J. R., W. J. Kellar and L. C. Walters (1956), Phase of the Low Radio Frequency Ground Wave, National Bureau of Standards Circular 573 (Superintendent of Documents, U. S. Government Printing Office, Washington, D. C. 20402).
- Johler, J. R. (1971a), Loran Radio Navigation Over Irregular, Inhomogeneous Ground with Effective Ground Impedance Maps, Telecommunications Research and Engineering Report OT/TRER 22 (Superintendent of Documents, U. S. Government Printing Office, Washington, D. C. 20402).

- Johler, J. R. (1971b), Loran-A Ground Wave Pulse Propagation, Telecommunications Research Report OT/ITS RR 10 (Superintendent of Documents, U. S. Government Printing Office, Washington, D. C. 20402).
- Johler, J. R., and Horowitz, S. (1973), Propagation of Loran-C Ground and Ionospheric Wave Pulses, Office of Telecommunications Report 73-26 (Superintendent of Documents, U. S. Government Printing Office, Washington, D. C. 20402).
- Johler, J. R., and S. Horowitz (1974), Propagation of a Loran Pulse Over Irregular, Inhomogeneous Ground; To be published in AGARD Conference Proceedings on Electromagnetic Wave Propagation Involving Irregular Surfaces and Inhomogeneous Media.

Table 1.

Assumed Magnitude of Impedance - Dana to Cloverdale .0250

Date	Time	Deduced Emission Delay (μsec)	Carolina Beach to Dana	Carolina Beach to Cloverdale	Carolina Beach to Van	Dana to Van
Constant No.		68560.	Magnitude of impedance			
Van at Clarkton, N.C.						
2/12/70	1200	.32	.0417	.0441	.0450	.0411
2/12/70	2400	.45	.0445	.0474	.0520	.0434
2/18/70	1500	.50	.0456	.0486	.0550	.0437
2/20/70	0600	.30	.0419	.0444	.0410	.0423
2/20/70	1200	.24	.0402	.0424	.0400	.0403
2/20/70	1800	.41	.0424	.0450	.0440	.0422
Van at Mocksville, N. C.						
2/25/70	0400	.54	.0471	.0504	.0530	.0439
2/26/70	0700	.53	.0421	.0446	.0465	.0400
2/26/70	1200	.46	.0402	.0424	.0430	.0384
Van at Paris, Ky.						
3/16/70	1200	.41	.0400	.0422	.0460	.0285
3/17/70	1000	.49	.0441	.0469	.0510	.0337

Table 2.

$\frac{dT}{dh}$	e	$\frac{de}{dh}$	α	associated
$^{\circ}C/100\text{ m}$	m bars	mbars/ 100 m	calculated	N_a

assumed summer conditions

- .65	20	.2	.90	375
-1.00	20	.1	.91	375
-1.00	20	.4	1.00	300

assumed winter conditions

average .25	4	-.1	.71	300
extreme 1	4	-.5	.53	300
" 2	4	-.25	.53	300

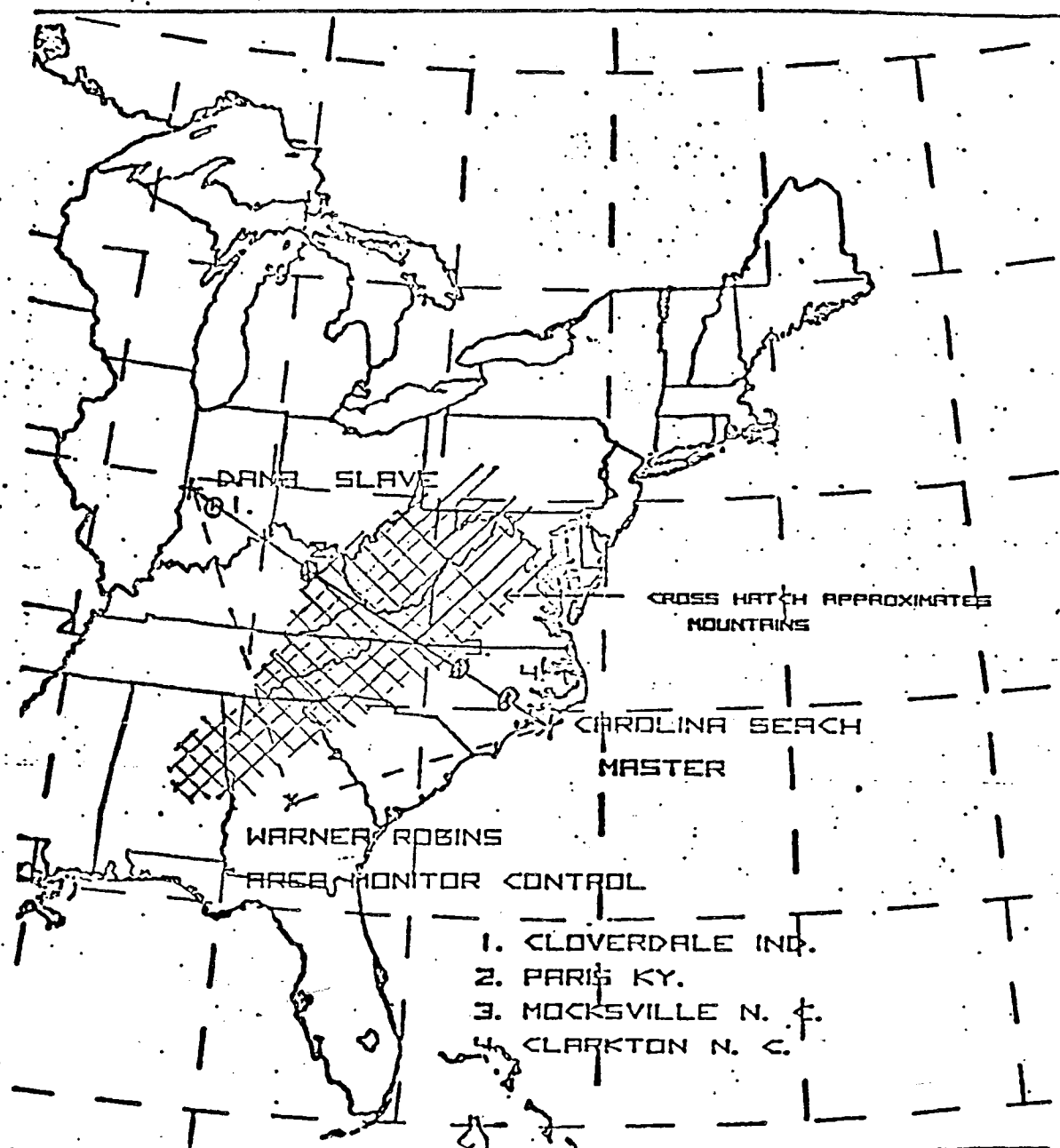


Figure 1. Configuration for monitoring temporal effects with Loran-C ground waves.

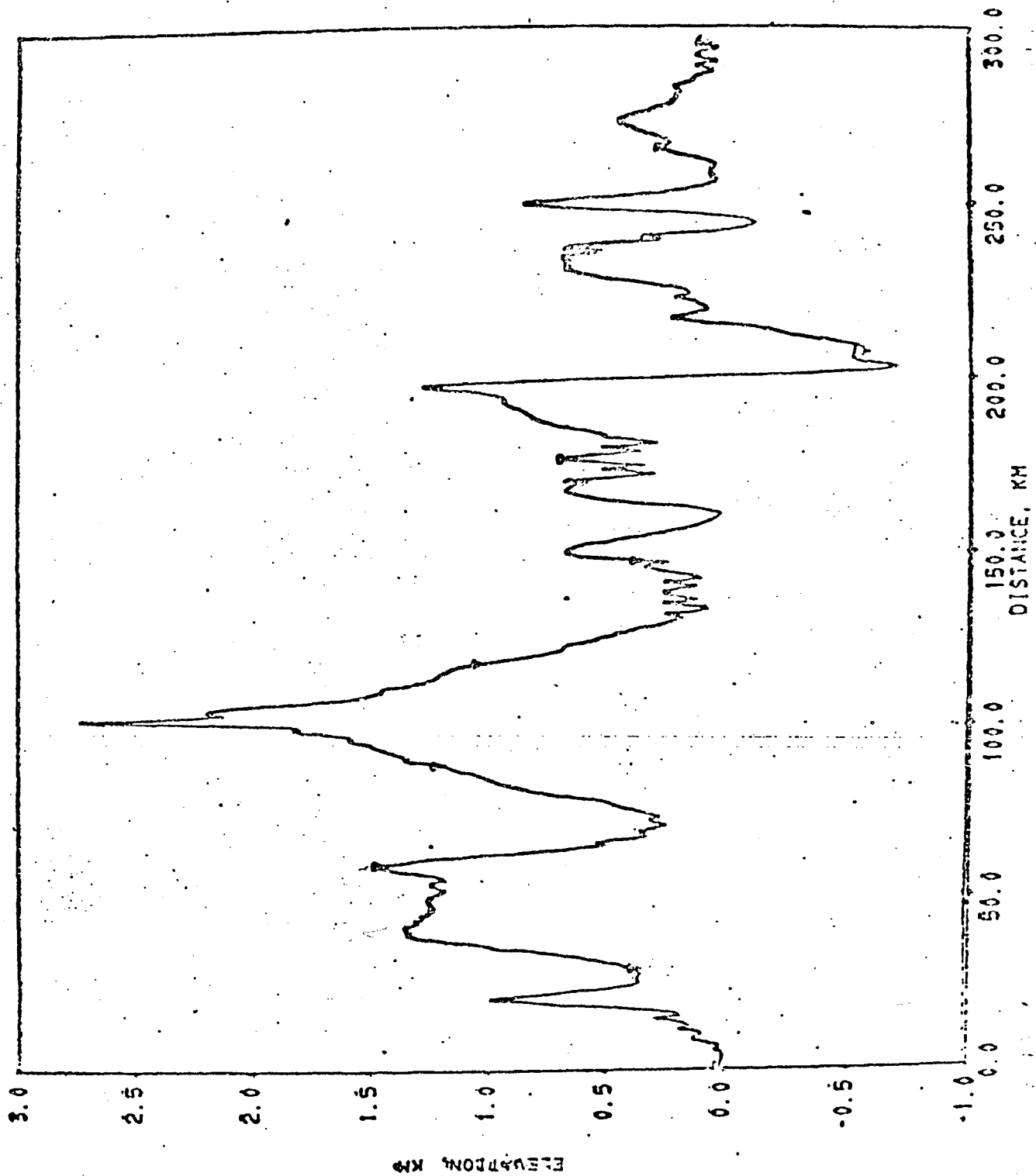


Figure 2. Terrain profile for Master-Monitor path Loran-D West.

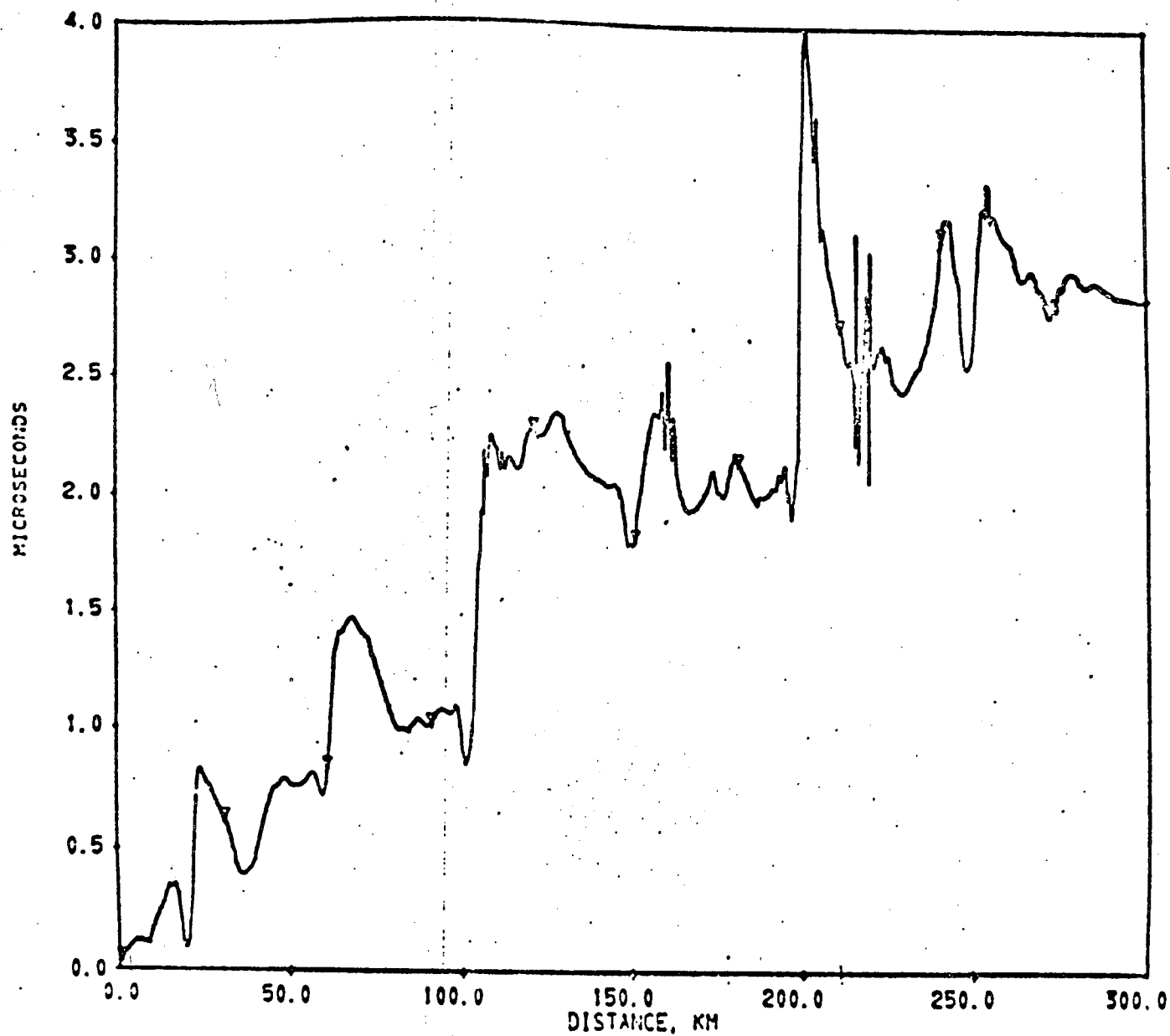


Figure 3. Secondary phase correction Master-Monitor path Loran-D West.

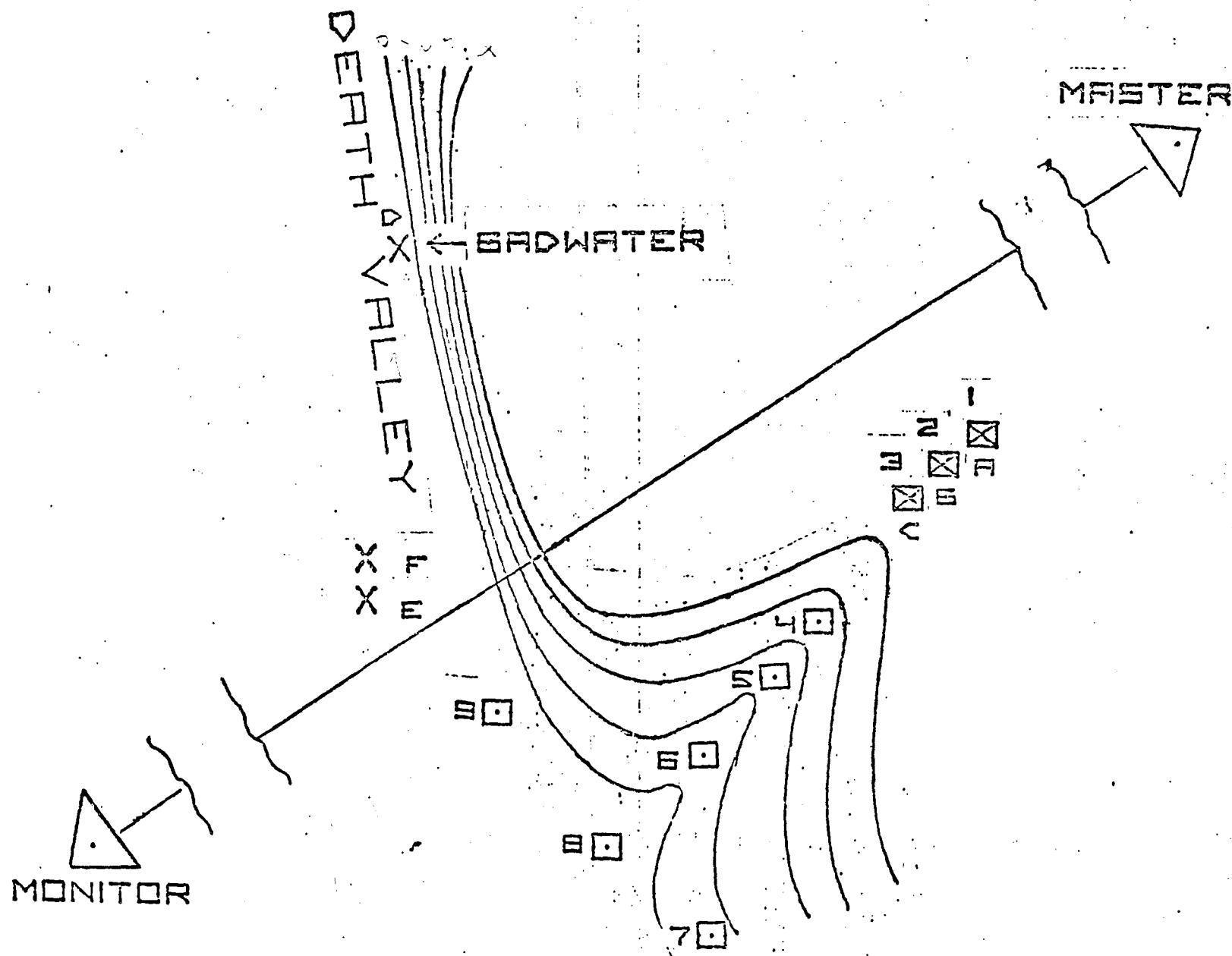


Figure 4. Loran-D West Measurement Locations for the Death Valley Anomaly on Master-Monitor Propagation Path.

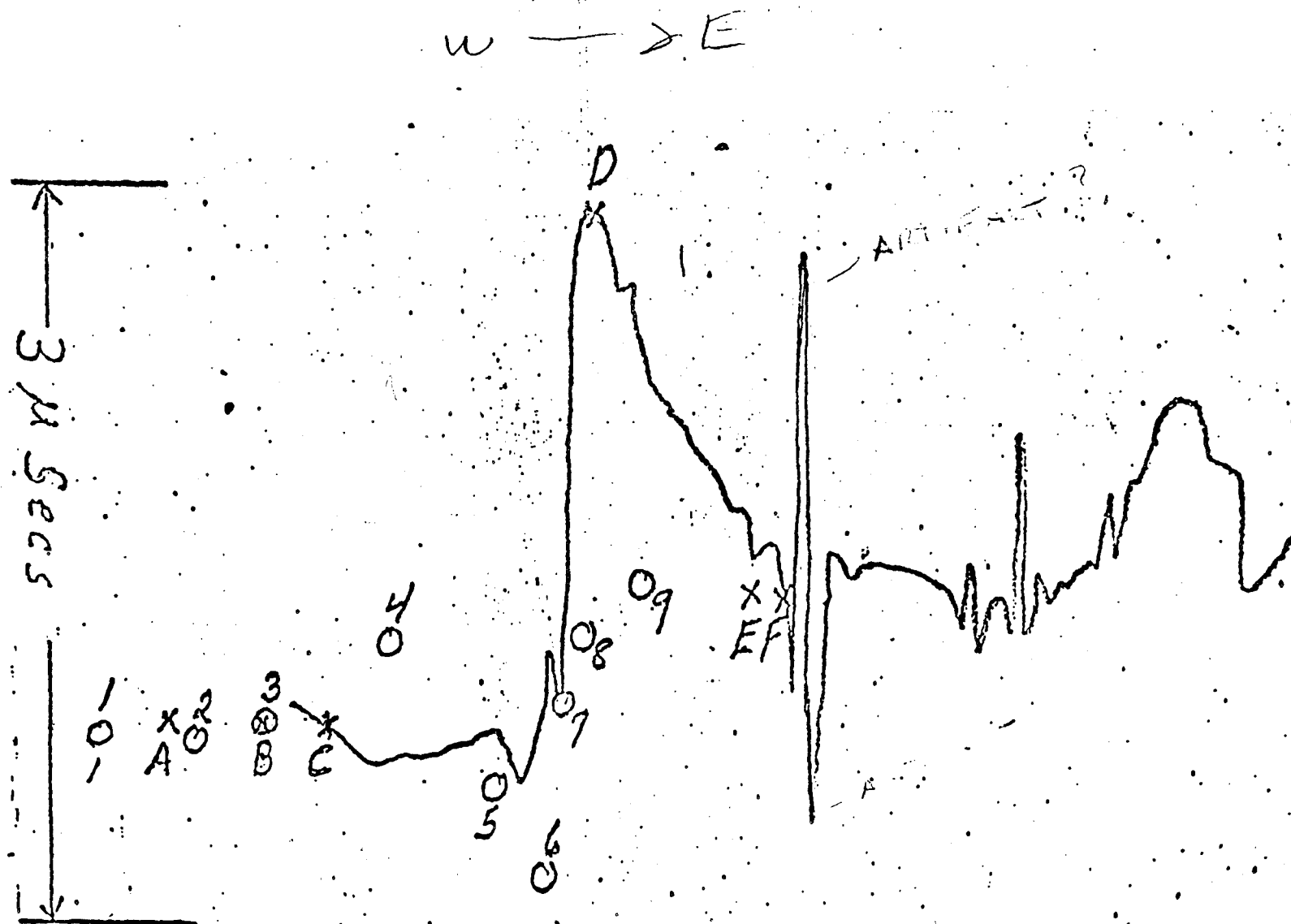


Figure 5. Comparison of Measurements with Theoretical Computer Software Predictions for the Death Valley Anomaly.

-23-

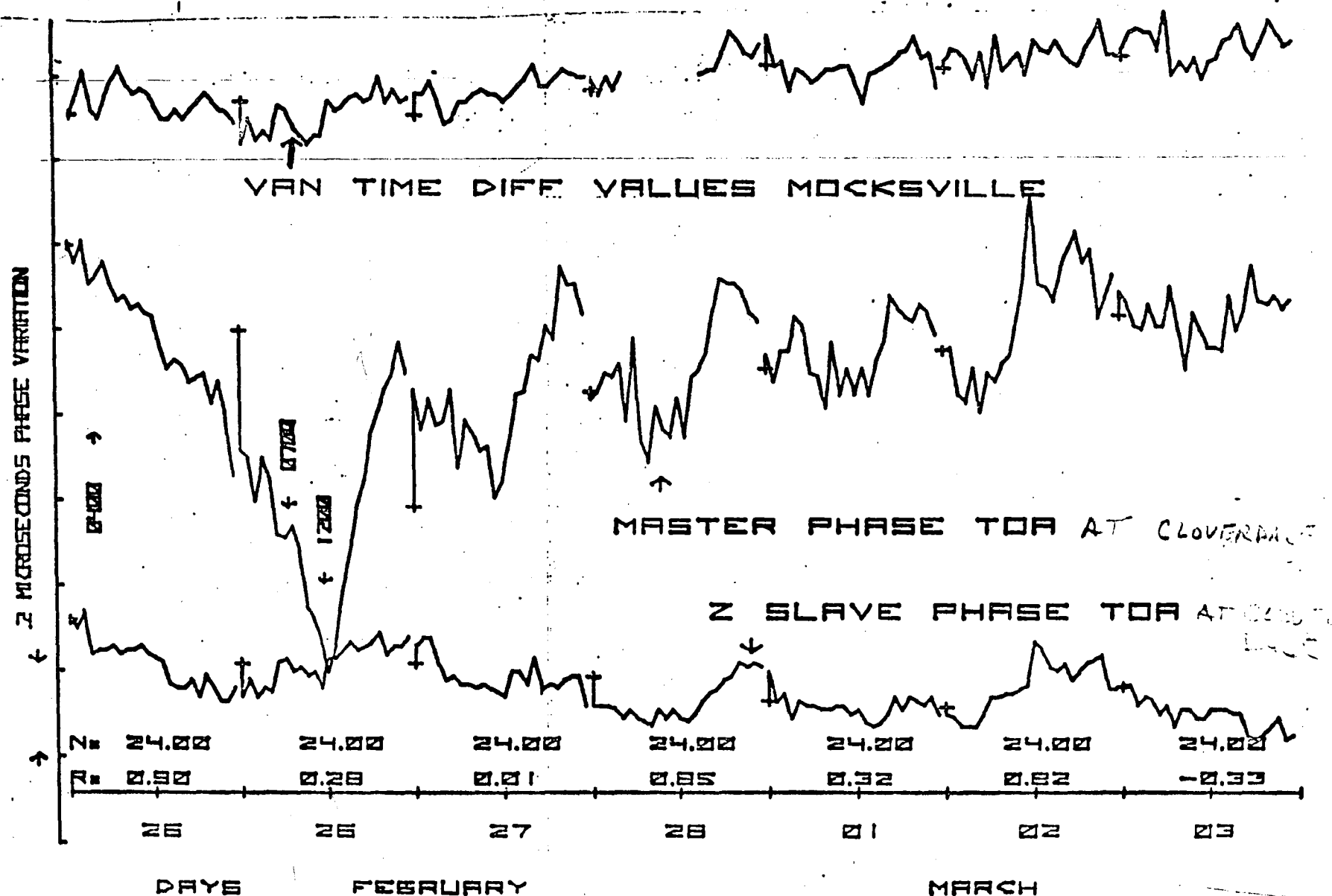


Figure 6. TD and TOA Measurements on Carolina Beach to Dana Path During February and March 1970.

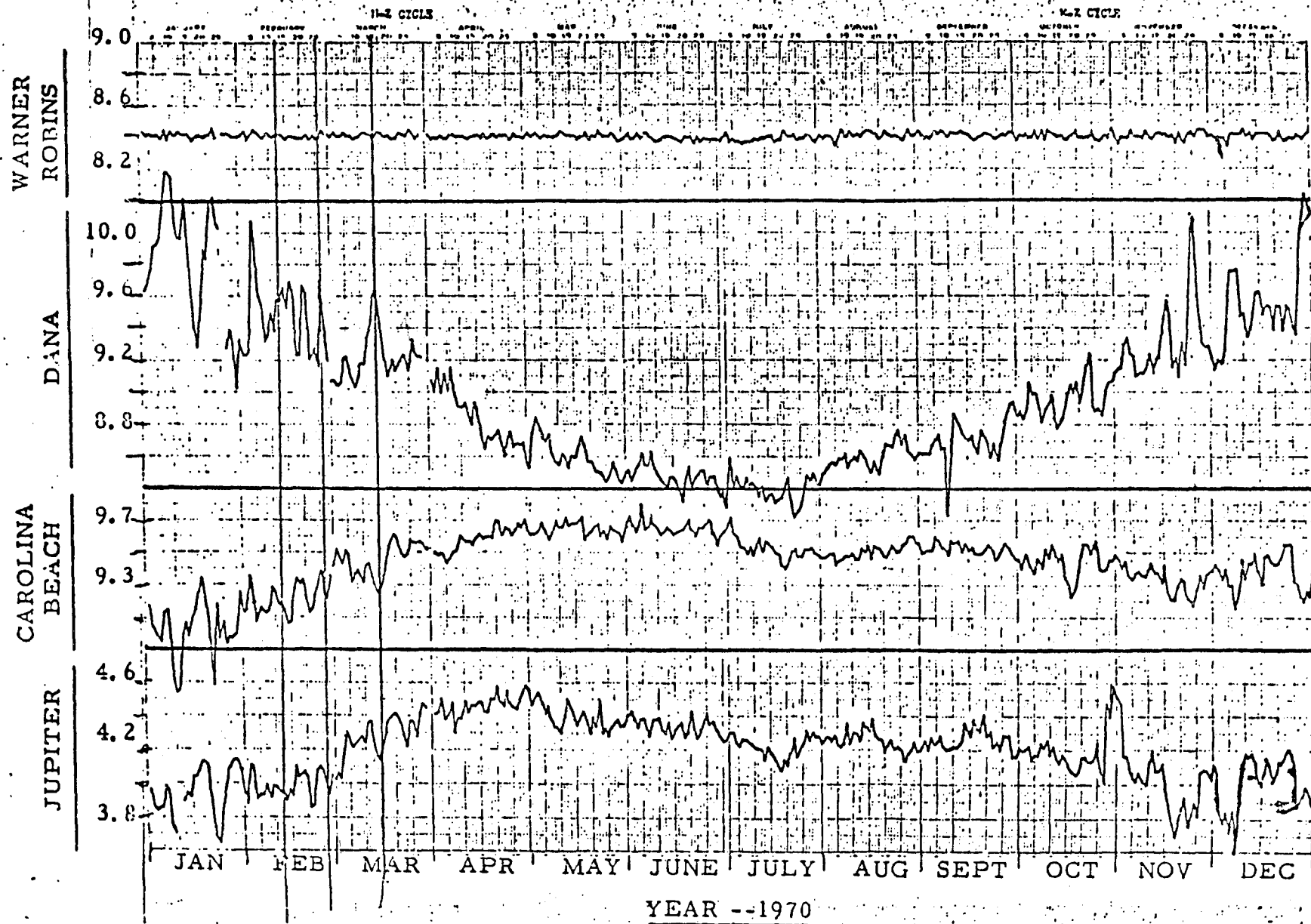


Figure 7. Z Cycle as Monitored at Station Indicated.

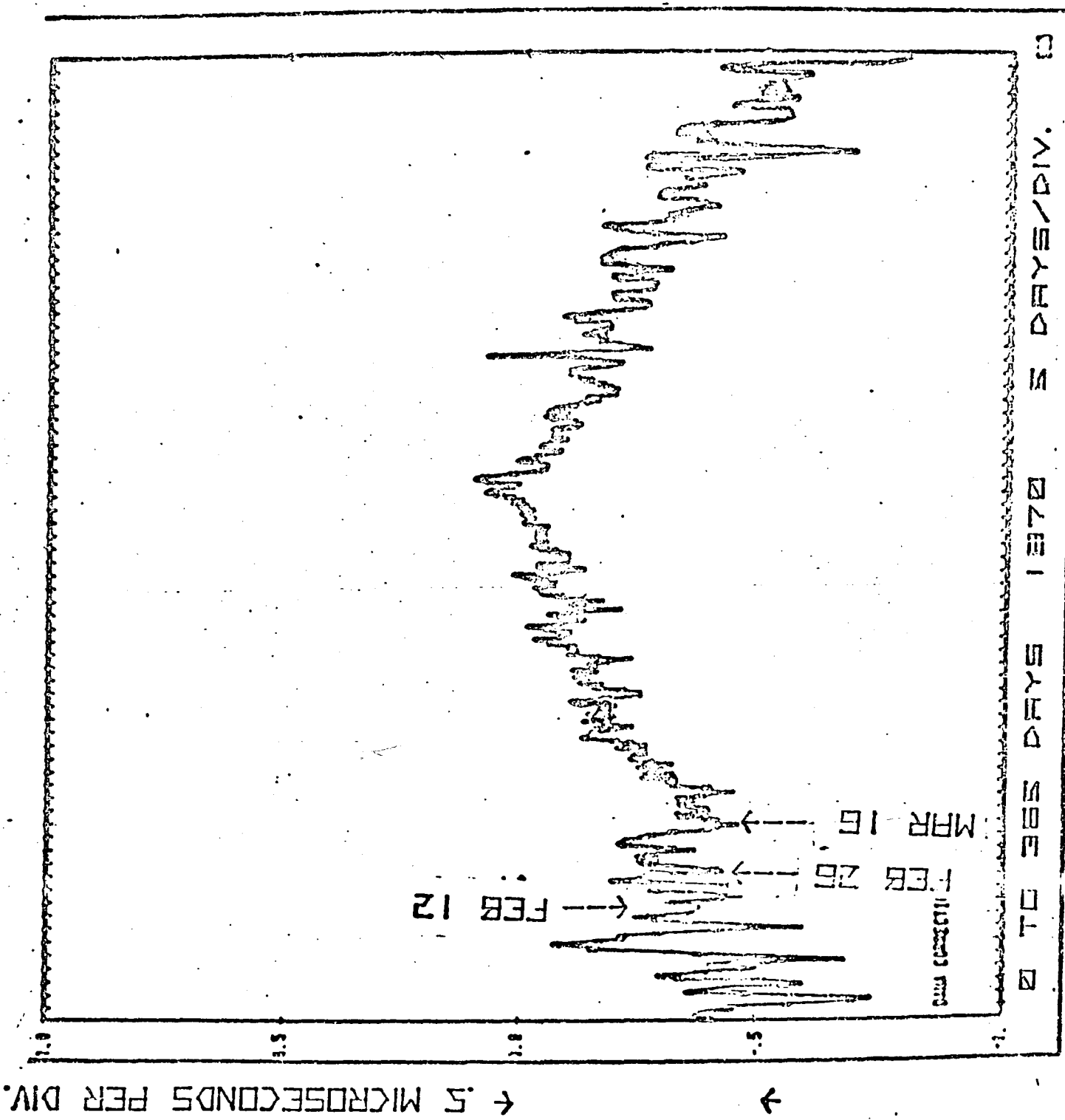
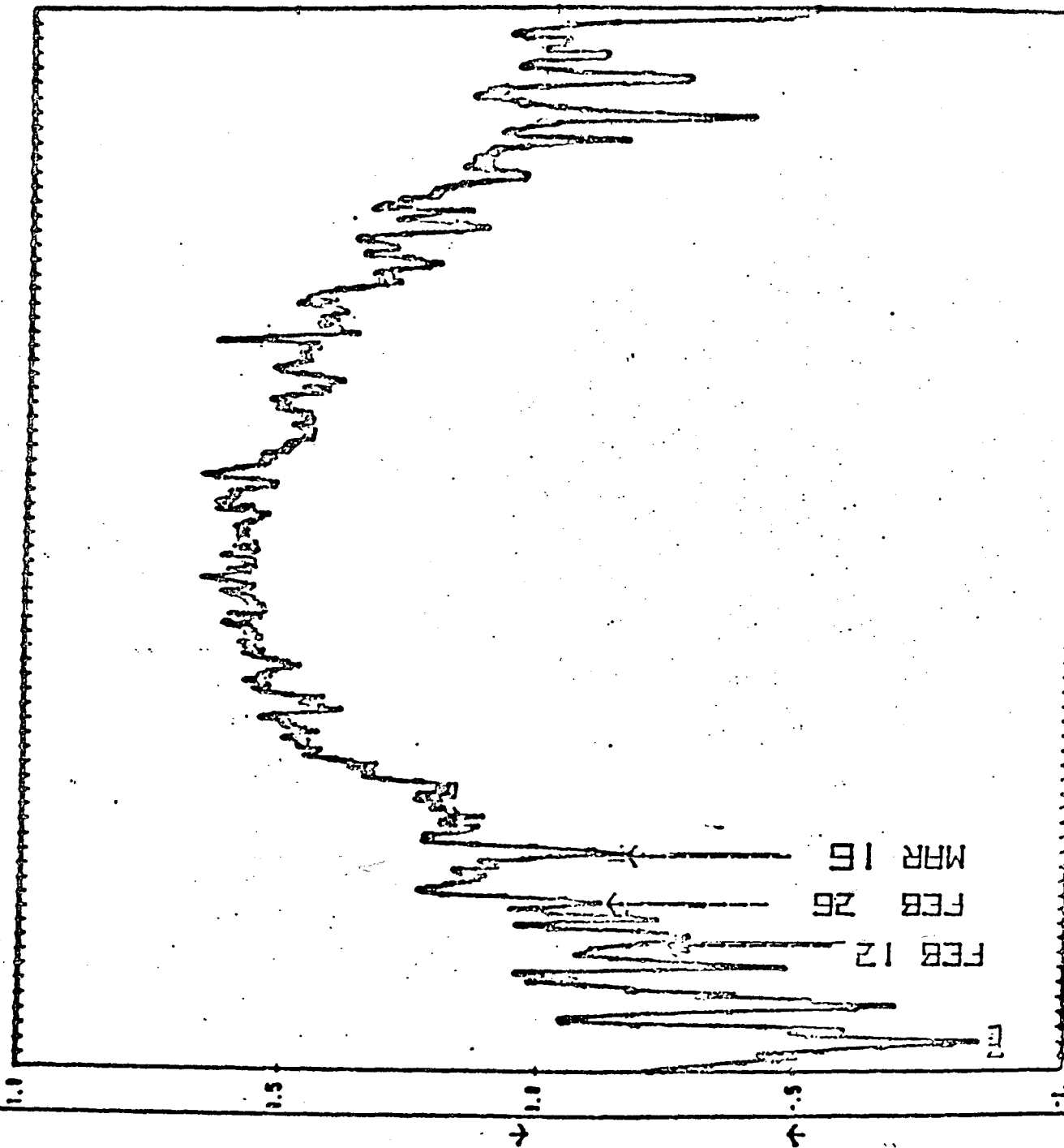


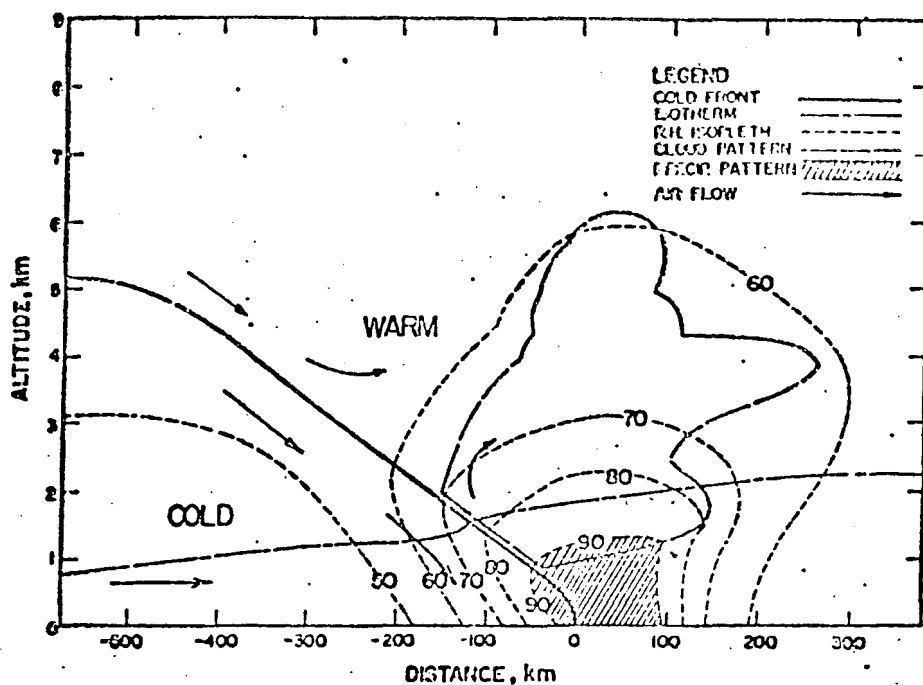
Figure 8. Changes in Z-Spectrum Emission Pulse from DAF-1A. Amplitude of Pulse in Divisions.

5 MICROSECOND PER DIV.

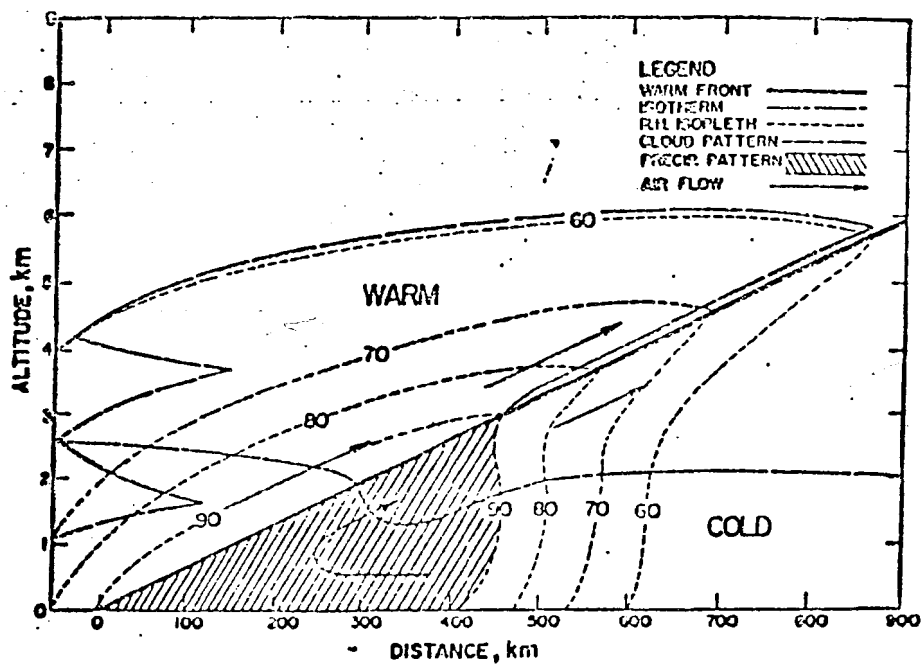
IN/SEEDS 1870 SEEDS OUT 2



REFRACTIVE INDEX PARAMETERS



Idealized diagram of a fast-moving cold front.



Idealized diagram of a warm front.

Figure 10. Warm and Cold Fronts Depicting Temporal Movement of Weather Systems.

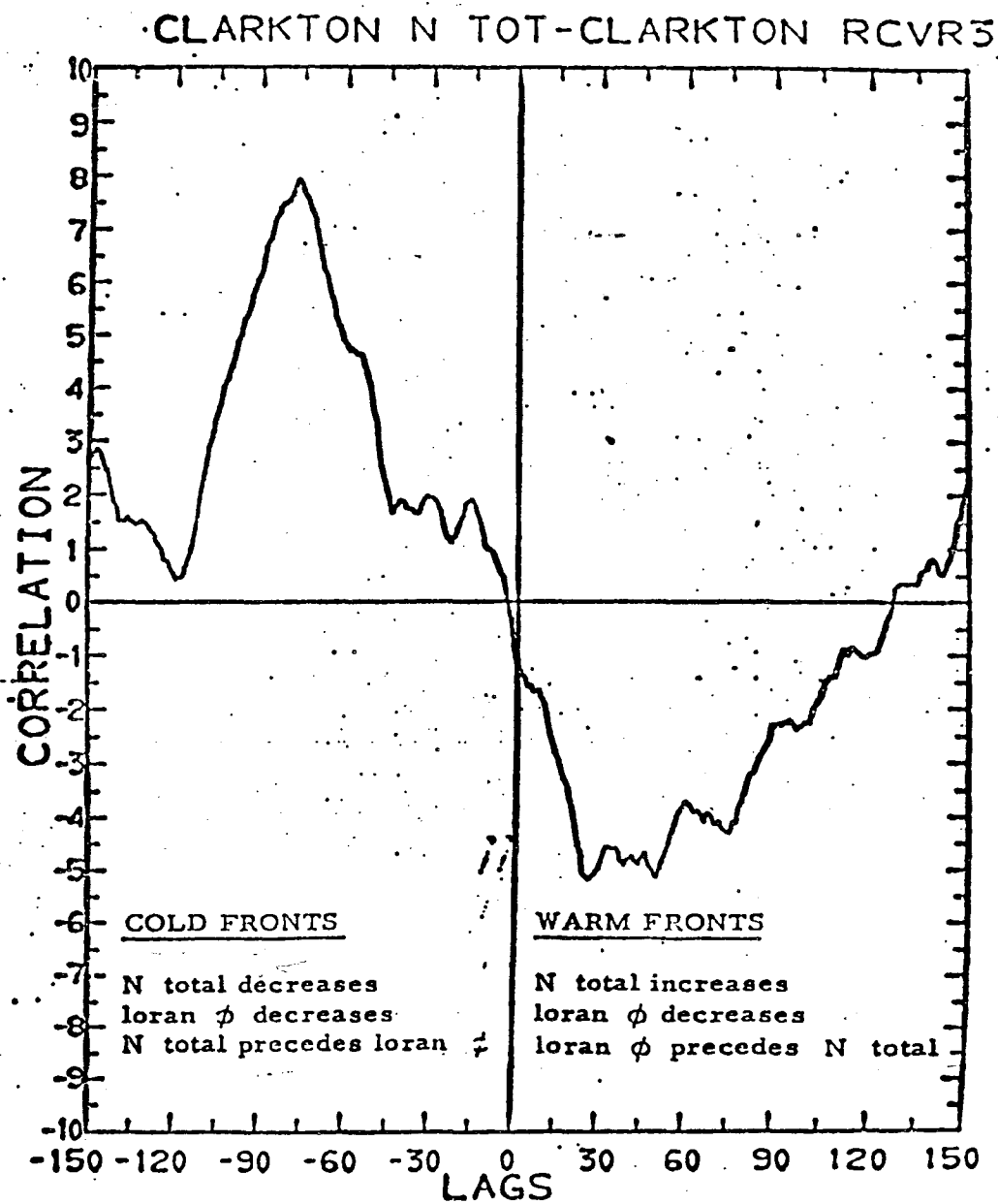


Figure 11. Lead, Lag Correlations Depicting Temporal Correlations with Weather Fronts.

List of Figures

- Figure 1. Configuration for Monitoring Temporal Effects with Loran-C Ground Waves.
- Figure 2. Terrain Profile for Master-Monitor Path Loran-D West.
- Figure 3. Secondary Phase Correction Master-Monitor Path Loran-D West.
- Figure 4. Loran-D West Measurement Locations for the Death Valley Anomaly on Master-Monitor Propagation Path.
- Figure 5. Comparison of Measurements with Theoretical Computer Software Predictions for the Death Valley Anomaly.
- Figure 6. TD and TOA Measurements on Carolina Beach to Dana Path During February and March 1970.
- Figure 7. Z Cycle as Monitored at Station Indicated.
- Figure 8. Changes in Z Slave Emission Delay from Daily Ave at Transmitters.
- Figure 9. Phase Variation Master to Z Slave from Daily Ave at Transmitters.
- Figure 10. Warm and Cold Fronts Depicting Temporal Movements of Weather Systems.
- Figure 11. Lead, Lag Correlations Depicting Temporal Correlations with Weather Fronts.

13

FILE COPY
3-13

ROBERT L. FRANK
16500 North Park Drive
Southfield, Mich. 48075

PROPAGATION OF A LORAN PULSE OVER
IRREGULAR, INHOMOGENEOUS GROUND

J. RALPH JOHLER
U. S. Department of Commerce
OFFICE OF TELECOMMUNICATIONS
Institute for Telecommunication Sciences
Boulder, Colorado 80302

and

SAMUEL HOROWITZ
Air Force Cambridge Research Laboratory
Bedford, Massachusetts 01730

For

Advisory Group For Aerospace Research
And Development

of

NATO

AGARD PAPER NO. 28

AGARD-CP-144

Conference Proceedings
Electromagnetic Wave Propagation Involving
Irregular Surfaces and Inhomogeneous Media
XX Technical Meeting of the Electromagnetic
Wave Propagation Panel of AGARD-NATO

Control sheet
14 pages

Netherlands, March 1974

(Also: 2d Annual Wild. Wave Connection
Great Gorge NJ Oct 1974)

REF 604
P. 41 + 1 = 15
1830421

START TYPING IMMEDIATELY BELOW THIS LINE

PROPAGATION OF A LORAN PULSE OVER IRREGULAR, INHOMOGENEOUS GROUND

J. Ralph Johler

U. S. Department of Commerce

OFFICE OF TELECOMMUNICATIONS

Institute for Telecommunication Sciences

Boulder, Colorado 80302

and

Samuel Horowitz

Air Force Cambridge Research Laboratory

Bedford, Massachusetts 01730

USE THIS AS
LEFT HAND MARGIN

SUMMARY

A numerical solution of an integral equation representation of the ground wave over irregular, inhomogeneous earth has been employed to calculate amplitude and phase of the propagated continuous wave as a function of frequency. A computer simulation again using numerical methods, transforms this result to the time domain yielding the impulse response. Then the impulse response is convolved with the Loran-C pulse function, that has been transformed from the time domain to the frequency domain. Our final result demonstrates the propagation of both pulse envelope and the cycles under the envelope in the presence of irregular, inhomogeneous ground. Although the Loran-C pulse propagation has been studied in detail, the method is applicable to the propagation of most any shape pulse over irregular, inhomogeneous ground. In the particular case of the Loran-C pulse, we conclude that the discrepancy or time difference between the pulse envelope and cycle is a unique function of the particular type of terrain over which the wave propagates, and it is, at the present state of the art, necessary to introduce such terrain into the propagation theory to give a unique prediction of the pulse propagation time.

1. INTRODUCTION

In a previously published paper (JOHLER, J. R., 1963), the true signal delay time, T_c , of a Loran-C pulse was studied theoretically for the special case of propagation over smooth, homogeneous, spherical ground. The delay time, T_c , (relative to the delay time of a signal traveling over the geodesic at the speed of light) was found by tagging a point in time on the pulse envelope, using a mathematical procedure that simulates actual time measurements used in Loran-C receivers when operating as a navigation system. The delay, t_c , of the cycle under the envelope, i.e., the carrier delay time, was also investigated. A discrepancy between the envelope and cycle delay, $T_c - t_c$, was found theoretically and has become known in practice (U.S. COAST GUARD, 1962) as the ECD (envelope to cycle discrepancy) in Loran-C radio navigation science. Over smooth, homogeneous, spherical ground the discrepancy near the third cycle of the Loran-C pulse was found to be primarily a function of distance, due perhaps to earth curvature and secondarily a function of the ground conductivity or impedance.

The physics of ground wave propagation can be completely described mathematically by the scalar quantity, y , that satisfies Maxwell's equations and the scalar wave equation,

$$(\nabla^2 + k^2) y = 0 \quad (1)$$

where k is the wave number and ∇^2 is the operator of Laplace. Components of the propagated field, such as the vertical electric, E_z , field can be obtained from y by differentiation. We employ, in the frequency domain, a harmonic function $\exp(i\omega t)$, where the frequency, $f = \omega/2\pi$ and t is the time. If r_0 is the geodesic distance connecting a transmitter and a particular receiving point O , it has been demonstrated previously (JOHLER, J. R., 1971; JOHLER, J. R. and BERRY, L.A., 1967; OTT, R. H. and BERRY, L. A., 1970; OTT, R. A., 1971) that the earth's surface, S , can be introduced into the calculation of y , with the aid of an integral equation,

$$y(O) = 2 f(r_0) + \frac{1}{2\pi} \int_S \left[y(Q) \frac{\partial}{\partial n} f(r_2) - f(r_2) \frac{\partial}{\partial n} y(Q) \right] ds \quad (2)$$

where,

$$f(r) = \exp(-i kr)/r \quad (3)$$

and n is the normal to the point, Q , on the surface, S . The geodesic distance, r_2 is the distance from Q to O . For a boundary condition at the surface of the ground (LEONTOVITCH, 1944) we use,

$$\frac{\partial y}{\partial n} = ik \Delta y \quad (4)$$

THE SURFACE IMPEDANCE

Here Δ is the surface impedance relative to free space, $\Delta = Z/Z_0$ where $Z_0 = 377$ ohms. If we distinguish the air medium above the ground by the wave number k_1 , and the ground medium itself by k_2 , we can write an impedance for vertical electric wave polarization:

LEFT HAND JARVIS

$$\Delta = \frac{k_1}{k_2} \sqrt{1 - \frac{k_1^2}{k_2^2}} \quad (5)$$

where,

$$k_1 = \frac{\omega}{c} \eta_1 \quad (6)$$

and

$$k_2 = \frac{\omega}{c} \sqrt{\epsilon_2 - i \frac{\sigma}{\omega}} \quad (7)$$

Here, η_1 is the surface index of refraction of air, ϵ_2 the dielectric constant of the ground, σ the ground conductivity, c the speed of light and ϵ_0 the permittivity of space.

The numerical techniques to solve the integral equation (2) as a function of frequency have been detailed in the references cited above. The principle feature of the special case calculated in this paper is the simplified use of a profile of terrain and ground impedance as a function of radial geodesic distance from the transmitter. This has been found to be capable of describing gross propagation time effects within the measuring resolution of Loran-C pulse equipment (JOHLER, J. R., 1971). Thus, "off path" and "back scatter" fields have been ignored because these effects have been found to be second order at LF, in the determination of propagation time of a pulse.

If,

$$W = \frac{Y}{f(r_0)} \quad (8)$$

the following algebraised form of the integral equation (2) has been obtained (JOHLER, J. R., 1971; JOHLER, J. R., and BERRY, L. A., 1967):

$$\begin{aligned} W[\Delta(x_1)] &= 1-B \sum_{k=1}^{i-1} p_k W[\Delta_2(x_k)] \\ &\times [F_1(x_1, x_k) \Delta(x_k) + F_2(x_1, x_k)] \\ &- B p_1 W[\Delta(x_1)] [F_1(x_1, x_1) \Delta(x_1) \\ &+ F_2(x_1, x_1)] \end{aligned} \quad (9)$$

where p_k is a weight assigned to the Gaussian quadrature formula, and,

$$B = \exp \left[i \frac{\pi}{4} \right] \frac{r_2}{x} \sqrt{\frac{k_1}{4\pi}} \quad (10)$$

$$F_1 = \sqrt{\frac{x_1}{x_k(x_1 - x_k)}} \quad (11)$$

$$F_2 = \left[1 + \frac{1}{ik_1 x_2} \right] \frac{\partial r_2}{\partial n} F_1 \quad (12)$$

and, x_1 and x_k are distances along the radial. The procedure for solving (9) has been described previously (JOHLER, J. R., 1971; JOHLER, J. R., and BERRY, L. A., 1967).

The terrain and ground impedance data enter the solution through $\frac{\partial r_2}{\partial n}$ and Δ respectively. These data must be supplied to the algebraic formula (9) to obtain a unique solution for the propagation time of a radio pulse.

2. THE SIGNAL PROPAGATION TIME

The complete theory for the propagation of the Loran-C pulse or any pulse of arbitrary shape has been summarized recently (JOHLER, J. R., and HOROWITZ, S., 1973). In this paper we have demonstrated how the ionospheric wave can be completely eliminated so that we can measure a true ground wave pulse. Thus, our discussion of a ground wave pulse over irregular, inhomogeneous ground in the time domain is a problem of great concern to Loran-C ground wave navigation.

The Loran-C pulse is synthesized from an analytic source function, $F_g(t)$, such that the "real part of" $F_g(t)$ is given by:

$$\begin{aligned} \operatorname{Re} F_g(t) &= \operatorname{Re} \exp[-\Gamma t] \\ &= \exp(-c_1 t) \cos \omega_c t \quad (0 < t < \infty) \\ &= 0 \quad (t < 0) \end{aligned} \quad (13)$$

In this equation,

$$\Gamma = c_1 + i\omega_c \quad (14)$$

where c_1 is a damping parameter, ω_c is the carrier frequency (radians per second) of the pulse. The pulse is broken or discontinuous at zero time according to equation (13), so that the logic of cause and effect will be clear after propagation to great distance. Thus, at a distance d from the source, the "time of arrival" of the signal (TOA) relative to a signal traveling at the speed of light is,

$$t' = t - \eta_1 \frac{d}{c} \quad (15)$$

The earliest time at which the signal can arrive is $t' = 0$. Negative values for t' would violate causality, if d is a geodesic and η_1 is a constant that accounts for a significant slowing up of the wave in air. Negative times are, however, of interest numerically as a precision check on the numerical computation (JOHLER, J. R., and HOROWITZ, S., 1973). The calculated field in the time domain $E(t', d)$, is found from:

$$E(t', d) = F^{-1} E(\omega, d) f_g(\omega) \quad (16)$$

In equation (16), F^{-1} designates the inverse Fourier transformation from the frequency domain to the time domain, and $f_g(\omega)$ is the Fourier transform of $F_g(t)$ in (13).

We synthesize the loran pulse from a sum of three damped sinusoids,

$$E(t', d) = \sum_{k=1}^3 A_k E(t', d, \Gamma_k) \quad (17)$$

where,

$$A_k = 1/2, -i/4, -i/4, \quad (k = 1, 2, 3) \quad (18)$$

$$\Gamma_k = c_k + i\omega_k \quad (19)$$

$$\omega_k = \begin{cases} \omega_c, & k = 1 \\ \omega_c + 2\omega_p, & k = 2 \\ \omega_c - 2\omega_p, & k = 3 \end{cases} \quad (20)$$

and where c_k is a damping constant, and ω_p is a modulation or envelope frequency. Using equations (16), (13), and noting that

$$E(t', d) = \frac{1}{2\pi} \int_{-\infty}^{\infty} \exp(i\omega t') E(\omega, d) \left\{ \int_0^{\infty} F_g(t) \exp(-i\omega t) dt \right\} d\omega, \quad (21)$$

we conclude that only a single type numerical integration of a fundamental formula for damped sinusoids need be used to get the total field $E(t', d)$ from $E_k(t', d)$.

$$\begin{aligned} E_k(t', d) &= \frac{1}{2\pi} \int_0^{\infty} |E_k(\omega, d)| \left\{ [\beta_1^{-1} \cos \alpha_1 \right. \\ &\quad \left. + \beta_2^{-1} \cos \alpha_2] + i [\beta_1^{-1} \sin \alpha_1 + \beta_2^{-1} \sin \alpha_2] \right\} d\omega \end{aligned} \quad (22)$$

where

$$\alpha_1 = \omega t' = \varphi'_c(\omega, d) + \tan^{-1} \left(\frac{(\omega_k + \omega)}{c_k} \right) \quad (23)$$

USE THIS AS
LEFT HAND MEMBER

$$\alpha_3 = -\omega t' + \varphi'_c(\omega, d) + \tan^{-1} \left(\frac{(\omega_k - \omega)}{c_k} \right) \quad (24)$$

$$\beta_1 = \sqrt{c_k^2 + (\omega_k + \omega)^2} \quad (25)$$

$$\beta_3 = \sqrt{c_k^2 + (\omega_k - \omega)^2} \quad (k = 1, 2, 3) \quad (26)$$

and

$$\varphi'_c = -\varphi_c - \frac{\pi}{2} = \arg [F(\omega, d)] \quad (27)$$

The ground wave cycle time can be represented by

$$t_c = \frac{\varphi_c}{\omega} \quad (28)$$

seconds.

The analytic field in the time domain, $E(t', d)$, can be written as,

$$E(t', d) = |E(t', d)| \exp [i \arg E(t', d)] \quad (29)$$

The modulus, $|E(t', d)|$, is the amplitude envelope of the pulse. The envelope of a pulse can be used to tag unambiguously a point in time on the pulse and indeed this point, when properly tagged represents the true signal propagation time. The cycles under the envelope are defined by "the real part of" the analytic function,

$$\operatorname{Re} E(t', d)$$

Precision Loran is basically a phase comparison device. But it is necessary to resolve cycle ambiguities of $\pm 2\pi n$ radians, $n = 1, 2, 3 \dots$. This type of ambiguity can be resolved by using envelope detection to tag a point in time, T_c , on the pulse. The vernier measurement of the true propagation time is then accomplished with phase detection of the cycle because this latter measurement is more precise than the envelope measurement at the current "state of the art". Thus, the envelope propagation time lag will be designated by T_c to distinguish it from the cycle time lag, t_c .

Mathematically, there are many methods for tagging a point in time on the pulse envelope. For purposes of this paper, the roots, $t' = T_c$ of the equation,

$$|E(t', d)| - C \frac{\partial}{\partial t} |E(t', d)| = 0 \quad (30)$$

will be employed. Here C is an arbitrary constant that moves the tagged point to the appropriate part of the pulse, such as the leading edge. The Loran-C pulse employed in this paper used the following constants:

$$c_1 = c_2 = c_3 = 25000; f_p = 2500 \text{ Hz}; f_c = 100 \text{ kHz}.$$

Figure 1 shows the pulse that has been propagated over irregular, inhomogeneous ground to a distance of 193.14 km. Both the envelope $|E(t', d)|$ and the cycles, $\operatorname{Re} E(t', d)$, are shown as a function of time, t' , between 0 and 200 μs (microseconds). The amplitude is normalized to unity maximum dipole (transmitter) current moment, $I_0 l = 1$.

3. PHYSIOGRAPHIC DATA

The data required by the computer simulation of ground wave pulse propagation consisted of terrain elevation relative to the transmitter and ground impedance as a function of geodesic distance from the transmitter. The particular propagation path simulated on the computer for purposes of this paper was located in a very rugged region of Nevada where the Loran-D system has recently been deployed. In particular, the Master to Area Monitor propagation path between $36^\circ \text{ N } 41'$ latitude, $114^\circ \text{ W } 39'$ longitude, and $35^\circ \text{ N } 41'$ latitude, $117^\circ \text{ W } 45'$ longitude was scaled for ground impedance and terrain elevation along a geodesic. The ground impedance was derived from geological resistivity maps (U.S. GEOLOGICAL SURVEY, 1932) and the terrain was scaled from topographic maps (U.S. GEOLOGICAL SURVEY, 1957). The terrain elevation as a function of distance from the transmitter is

104 mi. →

given in figure 2 and the ground impedance as a function of distance is given in Table 1.

TABLE 1

Ground Impedance As a Function of
Distance Along Propagation Path,
at 100 kHz

Distance, Km	$ \Delta $	$\arg \Delta$, radians
3.01	.021	.7710
3.03	.058	.9042
15.05	.021	.7710
27.09	.021	.7714
33.13	.041	.8153
45.15	.021	.7714
63.21	.052	.8736
72.24	.021	.7710
84.28	.041	.8153
93.33	.047	.8483
108.36	.052	.8736
114.38	.047	.8483
120.40	.041	.8153
129.43	.021	.7714
151.50	.052	.8736
162.53	.021	.7714
174.57	.031	.7688
180.59	.021	.7714
186.61	.047	.8483
195.64	.022	.7762
201.66	.021	.7714
213.70	.047	.8483
234.77	.064	.9344
243.80	.031	.7688
249.82	.047	.8483
267.87	.031	.7688
273.92	.021	.7714
328.08	.022	.7762

4. ENVELOPE TO CYCLE DISCREPANCY

We now present a set of theoretical deductions that we hope will stimulate careful measurements of propagation time of a loran pulse. Consequentially, we reserve comparisons with measured data for future papers. A preliminary comparison with observations has verified the existence of the predicted anomaly at a distance of 200 km from the transmitter in figure 2, (DOHERTY, R. H., 1974).

The secondary phase corrections, ϕ_c , as a function of distance from the transmitter is given in radians* in figure 2 for comparison with terrain elevation. The correlation of the phase perturbations with terrain is obvious. Thus, the effects of ground curvature changes predominate because, in figure 3, where we demonstrate the effect of removing the terrain and propagating the wave over smooth, but inhomogeneous ground defined by Table 1, the perturbations are found to be greatly diminished. The region of 200 km, figure 2, is of particular interest because here we note a quite severe perturbation as a result of elevation changes in the ground. We have employed the region, figure 2, from 193.14 km to 300.99 km to demonstrate the effects of terrain on pulse dispersion or envelope to cycle discrepancy (ECD) using the computer simulation.

To estimate the relative effects of inhomogeneities and terrain we have calculated three cases. The analytic function $E(t, d)$ was calculated for propagation over smooth, inhomogeneous ground with the impedance constant with frequency at its 100 kHz value. Using equation (5) it can be readily shown that

$$\Delta \approx \Delta_{100} \sqrt{\frac{f}{f_{100}}} \quad (30)$$

where Δ_{100} is the impedance at 100 kHz and Δ is the impedance at any other frequency f . This weak frequency dependence probably should be used for impedances deduced at 100 kHz, if the correct frequency dependence is to be introduced into the transient solution. However, the effect is small compared with the effect of irregular terrain or ground curvature changes. Thus, the second case calculated introduced the frequency dependence of equation (30). Finally, the third case introduces both inhomogeneous and irregular ground as data defined in figure 2 and Table 1, respectively.

*1.592 $\phi_c = t_c$ in μs at 100 kHz.

The tagged points in time on the pulse envelope, T_c , are given in Table 2, in microseconds for all cases. Various values of the constant, C , equation (29) are given as parameters. Thus $C = 3(10^{-6})$ tagged a point near the third carrier cycle of the 100 kHz pulse, or near 32.81 μs . Thus, for case 1 at a distance of 193.14 km, we find a true propagation time $t' = 32.81 \mu s$. The earliest time a signal could have arrived at this distance from the transmitter would have been $t' = 0$. Of course, figure 1, the pulse amplitude would be zero at $t' = 0$. Hence, we find it more convenient to tag a point at approximately one half the peak pulse amplitude. In practice, this point is quite appropriate for navigation on the ground wave (JOHLER, J. R., and HOROWITZ, S., 1973). Later times could be contaminated with skywaves and earlier times would give lower signal to noise levels.

TABLE 2
PROPAGATION CORRECTION FOR TAGGED POINT IN TIME ON PULSE ENVELOPE, MICROSECONDS

C	193.14	197.65	198.65	200.16	210.69	240.29	300.99	CASE
1.0(10 ⁻⁶)	22.07 21.47 22.36	22.09 21.48 21.19	22.09 21.48 22.23	22.10 21.48 22.02	22.06 21.47 22.79	22.35 21.46 22.58	22.99 21.72 22.67	1 2 3
2.0	24.23 23.60 24.46	24.27 23.62 23.26	24.24 23.63 24.37	24.23 23.62 24.24	24.24 23.65 24.75	24.49 23.61 24.76	24.63 23.88 24.79	1 2 3
3.0	26.02 25.20 25.98	26.03 25.20 25.84	26.03 25.21 26.00	26.03 25.20 25.95	26.79 25.20 26.52	26.01 25.42 26.26	26.20 25.44 26.35	1 2 3
4.0	28.08 27.16 27.97	28.06 27.24 27.97	28.06 27.23 27.98	28.03 27.27 27.94	28.78 27.24 27.94	28.01 27.39 27.94	28.10 27.47 27.95	1 2 3
5.0	29.23 28.44 29.31	29.23 28.40 29.23	29.23 28.43 29.41	29.23 28.43 29.45	29.18 28.40 29.77	29.40 28.79 29.49	29.45 28.86 29.75	1 2 3
6.0	30.78 30.10 30.93	30.78 30.21 30.93	30.78 30.16 30.93	30.78 30.18 30.93	30.78 30.16 30.94	30.99 30.31 30.94	30.14 30.40 30.94	1 2 3
7.0	32.10 31.50 32.00	32.10 31.50 32.00	32.10 31.50 32.00	32.10 31.50 32.00	32.10 31.50 32.00	32.10 31.50 32.00	32.10 31.50 32.00	1 2 3
8.0	33.10 32.50 33.00	33.10 32.50 33.00	33.10 32.50 33.00	33.10 32.50 33.00	33.10 32.50 33.00	33.10 32.50 33.00	33.10 32.50 33.00	1 2 3
9.0	34.10 33.50 34.00	34.10 33.50 34.00	34.10 33.50 34.00	34.10 33.50 34.00	34.10 33.50 34.00	34.10 33.50 34.00	34.10 33.50 34.00	1 2 3
10.0	35.10 34.50 35.00	35.10 34.50 35.00	35.10 34.50 35.00	35.10 34.50 35.00	35.10 34.50 35.00	35.10 34.50 35.00	35.10 34.50 35.00	1 2 3

CASE 1 - Smooth Inhomogeneous Ground (variable impedance with frequency)
 2 - Smooth Inhomogeneous Ground (constant impedance with frequency)
 3 - Irregular, Inhomogeneous Ground

TABLE 3
POSITIVE AND NEGATIVE CYCLE AXIS CROSSING TIME, MICROSECONDS
CASE 1

Distance, Km	193.14	197.65	198.65	200.16	210.69	240.29	300.99
	4.44	4.44	4.44	4.47	4.46	4.48	5.03
9.200	14.13	14.16	14.17	14.17	14.18	14.32	14.99
19.040	24.01	24.02	24.03	24.03	24.04	24.39	24.67
28.900	33.95	33.97	33.97	33.98	33.96	34.36	34.62
38.940	43.92	43.94	43.94	43.94	43.92	44.30	44.59
48.980	53.90	53.91	53.91	53.92	53.90	54.28	54.57
58.990	63.88	63.89	63.89	63.90	63.88	64.26	64.56
68.980	73.87	73.88	73.88	73.89	73.87	74.25	74.55
78.970	83.86	83.87	83.87	83.88	83.86	84.23	84.54
88.960	93.85	93.86	93.86	93.87	93.85	94.22	94.53
98.950	103.84	103.85	103.85	103.86	103.84	104.21	104.52
108.940	113.83	113.84	113.84	113.85	113.83	114.22	114.52
118.930	123.82	123.83	123.84	123.84	123.82	124.19	124.51
128.920	133.81	133.82	133.82	133.83	133.81	134.17	134.50
138.910	143.80	143.81	143.81	143.82	143.80	144.16	144.49
148.900	153.79	153.79	153.80	153.80	153.78	154.20	154.57
158.790	163.78	163.78	163.79	163.79	163.75	164.24	164.65
168.730	173.72	173.73	173.73	173.74	173.72	174.33	174.82
178.690	183.62	183.63	183.64	183.64	183.62	184.32	184.86
188.600	193.43	193.43	193.43	193.43	193.41	194.720	195.38
198.600	198.610	198.610	198.610	198.620	198.600		199.14

TABLE 4
POSITIVE AND NEGATIVE CYCLE AXIS CROSSING TIME, MICROSECONDS
CASE 1

Percentage	192.14	197.43	198.45	200.14	210.49	240.29	300.99
9.330	4.67	4.68	4.68	4.68	4.67	5.01	5.67
19.070	20.24	14.10	14.10	14.10	14.14	14.33	14.61
28.900	34.02	29.00	24.03	24.03	24.02	24.39	24.60
38.940	33.96	33.97	33.97	33.98	33.96	34.44	34.63
48.980	43.92	43.94	43.94	43.94	43.92	44.30	44.39
58.990	53.90	53.91	53.92	53.91	53.90	54.28	54.37
68.970	63.88	63.90	63.90	63.90	63.88	64.26	64.36
78.840	73.87	73.88	73.88	73.89	73.87	74.25	74.35
88.830	83.84	83.87	83.87	83.88	83.84	84.24	84.34
98.840	93.85	93.86	93.86	93.87	93.85	94.23	94.33
108.830	103.83	103.85	103.85	103.86	103.84	104.22	104.31
118.820	113.82	113.84	113.84	113.85	113.83	114.21	114.31
128.810	123.81	123.83	123.83	123.83	123.81	124.20	124.30
138.790	133.80	133.82	133.82	133.82	133.80	134.19	134.29
148.780	143.78	143.80	143.80	143.81	143.79	144.17	144.27
158.760	153.77	153.78	153.79	153.79	153.77	154.16	154.26
168.750	163.76	163.78	163.78	163.78	163.74	164.15	164.25
178.670	173.70	173.71	173.70	173.72	173.70	174.09	174.20
188.660	183.68	183.69	183.69	183.69	183.69	184.09	184.09
198.670	193.58	193.59	193.59	193.60	193.58	194.08	194.18
208.670	203.58	203.59	203.59	203.60	203.58	204.08	204.18

TABLE 3
POSITIVE AND NEGATIVE CYCLE AXIS CROSSING TIME, MICROSECONDS
CASE 3

Distances, Km	197.14	197.65	198.45	199.16	200.16	210.69	200.29	200.77
	8.33	3.72	5.81	7.81	6.59	5.25	5.04	
16.00	8.33	13.18	13.21	17.00	14.06	14.99	13.61	
16.00	14.92	10.09	20.10	21.86	20.96	19.90	20.50	
20.70	24.05	21.03	23.03	24.78	23.90	24.91	23.54	
20.70	24.76	31.90	29.93	34.96	30.07	29.90	30.32	
20.70	37.93	41.94	44.91	41.65	40.82	39.00	40.31	
40.73	44.76	47.93	49.90	51.61	46.43	49.00	44.07	
40.73	54.73	52.92	54.00	54.99	55.70	54.06	55.09	
40.73	57.93	62.90	64.06	64.56	65.70	64.08	65.00	
60.70	64.71	67.09	69.00	71.84	70.73	69.03	70.40	
60.70	74.70	72.09	74.06	74.53	75.73	74.08	75.00	
60.70	84.69	82.07	84.03	84.51	85.73	84.04	85.07	
60.70	94.68	92.06	94.02	94.49	95.72	94.04	95.07	
60.70	104.67	102.05	104.00	104.47	105.71	104.03	105.06	
60.70	114.67	112.04	114.79	114.45	115.70	114.03	115.06	
60.70	124.66	122.03	124.77	124.43	125.69	124.02	125.05	
60.70	134.65	132.02	134.76	134.40	135.67	134.02	135.05	
60.70	144.63	142.00	144.74	144.37	145.65	144.01	145.04	
60.70	154.63	152.79	154.72	154.36	155.64	154.00	155.03	
60.70	164.60	162.76	164.68	164.27	165.60	164.79	165.02	
60.70	174.67	172.72	174.63	174.23	175.56	174.78	175.01	
60.70	184.68	182.62	184.60	184.16	185.54	184.73	185.00	
60.70	194.68	192.60	194.27	193.82	195.29	194.67	195.13	
	197.60							

To understand the derivation of the envelope to cycle discrepancy (ECD) it is necessary to tag a point in time on both the envelope and the cycle. This is precisely the procedure used by Loran-C and Loran-D radio navigation systems. For convenience, we have used the zero axis crossings of the cycles to tag points in time on the cycle. These are listed in Tables 3, 4, and 5 for cases 1, 2 and 3 respectively.

Consider now the particular envelope tagged point in time, $T_c = 32.81 \mu s$, Table 2, where $C = 3.0(10^{-8})$ and the distance = 193.14 km. This is case 1. Using Table 3, at 193.14 km we find two columns of zero crossings of the cycle (depicted graphically in figure 1). The times $t_c = 9.30+$, $19.06+$, \dots , μs , represent the positive slope zero crossing in which the cycle increases from negative to positive across the abscissa. The times, $t_c = 4.64-$, $14.15-$, $24.01-$, \dots , μs , represent the negative slope cycle crossings. Since Loran measuring equipment can readily distinguish between positive and negative cycle crossings we can confine our discussion to one or the other columns of Table 3. Now our true signal propagation time, $T_c = 32.81 \mu s$ brings us close to the positive slope cycle crossing, $t_c = 28.98$. We can therefore use the positive slope cycles for the calculations of discrepancy assuming, as indeed it can, that the measuring equipment makes a phase comparison at this axis crossing. The only consequences of our arbitrary selection of tagged points in time is an arbitrary constant that is independent of distance, terrain and impedance of the ground. It is more a matter of convenience and instrumentation as far as practical measurements are concerned. We now calculate ECD,

$$ECD = T_c - t_c = 32.81 - 28.98$$

$$\text{or } ECD = +3.83 \mu s.$$

TABLE 6
ENVELOPE TO CYCLE DISCREPANCY

$$C = 3(10^{-8})$$

MICROSECONDS RELATIVE 193.14 Km

Distance, Km	CASE 1	CASE 2	CASE 3
193.14	0	0	0
197.65	+0.04	+0.04	+0.58
198.65	-0.02	+0.03	-0.32
200.16	-0.02	+0.07	-2.10
210.69	-0.03	+0.08	-0.64
240.29	-0.18	-0.27	+0.03
300.99	-0.09	-0.18	-0.48
* 193.14	+3.83	+3.20	+3.31

*without normalization

As a consequence of the arbitrary constant discussed above these results can be normalized to a distance of 193.14 km so that the change in ECD can be studied for cases 1, 2 and 3. Using, $C = 3(10^{-8})$ and using negative slope cycle crossings, in Tables 3, 4 and 5, we have derived the ECD as a function of distance for the propagation models defined by cases 1, 2 and 3. The comparison of cases 1 and 2 emphasizes the necessity of using equation (30), if impedances are employed along the propagation path that have been deduced for the 100 kHz carrier. It is quite apparent that inhomogeneous ground produces ECD changes of the order of several tenths of a microsecond. The extent of these changes depend upon the impedance contrast. However, as in the particular propagation path under consideration, the effects of terrain are much more severe. Thus, in case 3 we have found ECD changes of the order of several microseconds. These effects will of course completely dominate the effects depicted in cases 1 and 2. In fact, in the short distance of approximately 100 km described in Table 6, we have predicted ECD changes in excess of those predicted for smooth, homogeneous ground (Table 7) discussed in detail in a previous paper over distances of 1000 km! The important point to be noted here is the functional relationship between ECD and t_c or "time of arrival" (TOA) of the signal relative to a signal traveling at the speed of light. Over smooth, homogeneous ground we note in Table 7, that we have deduced the existence of a function of ECD. Suppose ECD takes on values $ECD = x_1, x_2, x_3, \dots$, then we have found that,

$$t_c = f_1(x_1) \quad (31)$$

TABLE 7

ECD OVER SMOOTH HOMOGENEOUS GROUND*

Distance,		$\sigma = .005$	$\sigma = 5$
Mi	Km	$T_c - t_c$	$T_c - t_c$
50	80	0	0
100	161	0.1	-0.1
200	322	0.2	-0.1
500	805	0.7	0.4
1000	1609	2.5	1.6
2000	3218	5.0	4.2

USE THIS A
LEFT HAND

*After Johler, J. R., 1963.

for $\sigma = 0.005$, $\Delta = .03336 \exp [i0.7765]$

$\sigma = 5$, $\Delta = .001055 \exp [i0.7854]$

if $f = 100$ kHz.

where f_1 is the smooth homogeneous ground propagation function. In cases 1 and 2 discussed above we can find t_c from:

$$t_c = f_2(x_2) \quad (32)$$

a model for smooth inhomogeneous ground that is quite different from smooth homogeneous ground. Finally, in case 3 we find

$$t_c = f_2(x_2) \quad (33)$$

a function that is drastically different from f_1 and f_2 if we desire to relate propagation time to pulse dispersion. Now, one could continue to derive functions $f_4, f_5 \dots$ for other propagation paths. It is apparent that $f_1, f_2, f_3 \dots$ are dependent upon the particular propagation path such that x_1 is associated with f_1, x_2 with f_2, \dots . We therefore conclude that some form of theory based upon Maxwell's equations and the boundary conditions at the surface of the ground is necessary to predict the propagation time of a pulse if a unique relationship between pulse dispersion and loran pulse TOA is to be established. Obviously, the greater the precision required, the greater the physiographic detail required in the propagation theory. We conclude that the current loran navigation accuracy of 0.1 μ s TOA determination can be achieved over irregular, inhomogeneous ground only if the terrain and ground impedance are modeled in sufficient detail as described in this paper. We also believe that ECD measurements while not providing a substitute for loran prediction, can provide a useful parameter for estimating approximate effects of curvature changes in the ground provided approximate theory is employed in the analysis to guarantee a unique value of t_c .

5. CONCLUSIONS

We conclude that the pulse envelope to cycle dispersion or discrepancy is a function of the particular propagation path to the transmitter. We conclude that a unique relationship between ECD and the propagation time, t_c , relative to a signal traveling at the speed of light can be determined by measurement of ECD provided some sort of propagation model based on Maxwell's equations and the boundary conditions at the surface of the ground are introduced to guarantee uniqueness.

6. REFERENCES

- DOHERTY R. H., 1974, Spatial and temporal electrical properties derived from LF pulse ground wave propagation measurements (AGARD Paper No. 30, XX Technical Meeting of EM Wave Propagation Panel of AGARD-NATO, March 1974).
- JOHLER, J. R., and HOROWITZ, S., 1973, Propagation of Loran-C ground and ionospheric wave pulses, Office of Telecommunications Report 73-20 (Superintendent of Documents, U. S. Government Printing Office, Washington, D. C. 20402).
- JOHLER, J. R., 1971, Loran radio navigation over irregular, inhomogeneous ground with effective ground impedance maps (Superintendent of Documents, U. S. Government Printing Office, Washington, D. C. 20402). *OT/TER 22*
- JOHLER, J. R., and BERRY, L. W., 1967, Loran-D phase corrections over inhomogeneous, irregular terrain, ESSA Tech. Rept. IER 59-ITSA 56 (Superintendent of Documents, U. S. Government Printing Office, Washington, D. C. 20402).

Handwritten signature

JOHLER, J. R., 1963, The propagation time of a radio pulse, IEEE Trans. on Ant. and Prop., AP-11, No. 6, 661-668.

KELLER, G. V., and FRISCHKNECHT, F. C., 1966, Electrical Methods in Geophysical Prospecting (Pergamon Press, New York, N.Y.).

LEONTOVITCH, M. A., 1944, On a method of solving the problem of electromagnetic waves near the earth's surface, Bull. del Acad. des Sci. de PURSS, Serie Physique, 8, 16-22.

OTT, R. H., and BERRY, L. A., 1970, An alternative integral equation for propagation over irregular terrain, Radio Science, 5, No. 5, 767-771.

OTT, R. H., 1971, An alternative integral equation for propagation over irregular terrain II, Radio Science, 6, No. 4, 429-435.

U. S. GEOLOGICAL SURVEY, 1932, Geologic map of the United States, 1:2500000 (U. S. Geological Survey, Denver, Colorado 80225).

U. S. GEOLOGICAL SURVEY, 1954, Western United States 1:2500000, topographic maps, see for example Death Valley California, Nevada (U. S. Geological Survey, Denver, Colorado 80225).

U. S. COAST GUARD, 1962, An analysis of the envelope-to-cycle discrepancy in the Loran-C system, Electronics Engineering Report No. L-31 (Electronics Engineering Division, U. S. Coast Guard Headquarters, Washington, D. C.).

7. ACKNOWLEDGEMENTS

This work was initiated by the author's participation in the Loran-D program of the U. S. Air Force, Tactical Loran SPO, L. G. Hanscom Field, Bedford, Mass. The investigation of the ECD in detail was prompted by a very interesting concept involving the application of measured ECD to deduce secondary phase correction, t_c , as proposed by T. W. Jerardi and R. W. Roll of the Applied Physics Laboratory of the Johns Hopkins University, Silver Spring, Maryland. A series of stimulating private communications in disagreement between the authors and L. F. Fehner, T. W. Jerardi and R. W. Roll of APL over the applicability of this concept led to a proposed experiment to compare measured ECD with theoretically calculated ECD. At this point in time the experiment has not been accomplished. We note that the concept is cited in: "How to harvest the full potential of Loran-C", by L. F. Fehner and T. A. McCarty, presented at 2nd Annual Convention of Wild Geese Association, 3-5 October 1973, in Washington, D. C.

USE SINGLE LINE SPACING

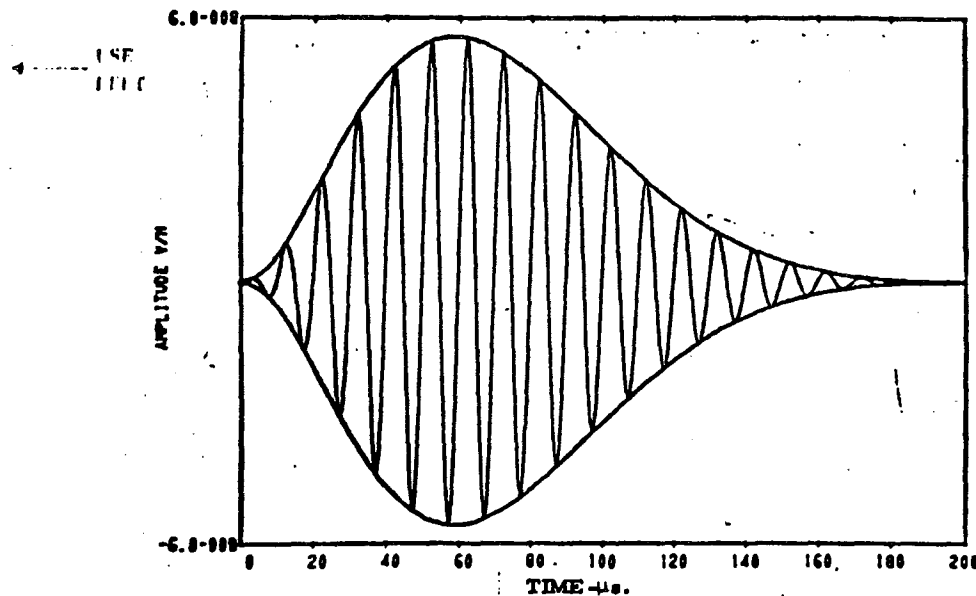


Figure 1. Amplitude $\pm |E(t', d)|$ and cycles, $Re E(t', d)$ of the computer simulated Loran-C pulse at a distance of 193.14 km from the transmitter over irregular, inhomogeneous ground.

USE SINGLE LINE SPACING.

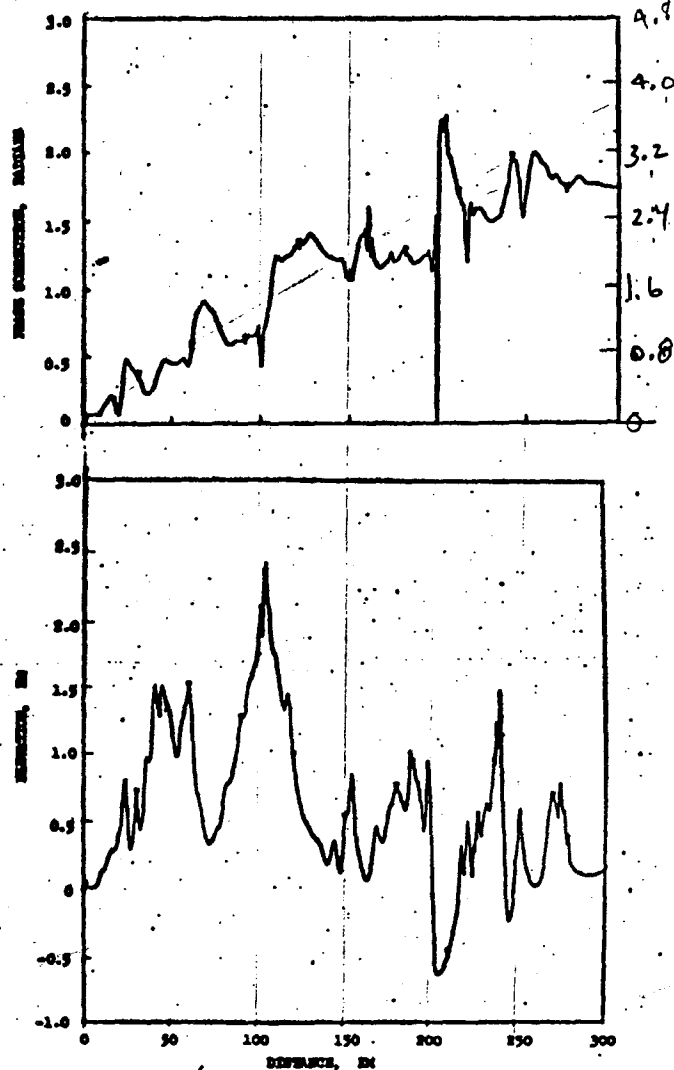


Figure 2. Elevation above transmitter as a function of distance from transmitter and corresponding phase lag, ϕ_c , radians relative to signal propagating at the speed of light, illustrating phase perturbations from irregular, inhomogeneous ground.

Case 3) -

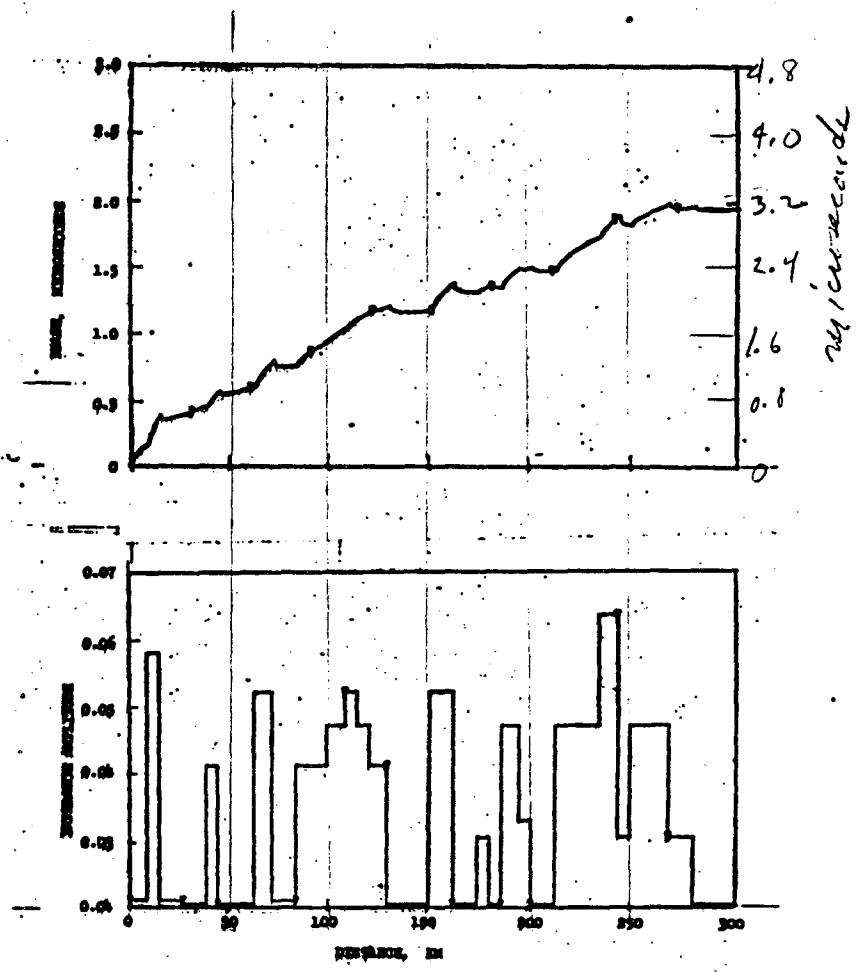


Figure 3. Ground impedance as a function of distance from the transmitter and corresponding phase lag, t_c , microseconds relative to signal propagating at the speed of light, illustrating phase perturbations from inhomogeneous ground.

(Line 2)

Figure 1. Amplitude $+ |E(t', d)|$ and cycles, $Re E(t', d)$ of the computer simulated Loran-C pulse at a distance of 193.14 km from the transmitter over irregular, inhomogeneous ground.

Figure 2. Elevation above transmitter as a function of distance from transmitter and corresponding phase lag, ϕ_c , radians relative to signal propagating at the speed of light, illustrating phase perturbations from irregular, inhomogeneous ground.

Figure 3. Ground impedance as a function of distance from the transmitter and corresponding phase lag, t_c , microseconds relative to signal propagating at the speed of light, illustrating phase perturbations from inhomogeneous ground.

USCARS - 121

USE THIS SPACE ONLY TO CLARIFY - DO NOT WRITE MATERIAL AND FIGURE

PERFORMANCE OPTIMIZATION OF LINEAR LORAN RECEIVERS OPERATING IN A NON-GAUSSIAN ATMOSPHERIC NOISE ENVIRONMENT

LARRY N. POSTEMA

PRESENTED AT THE
3rd ANNUAL CONVENTION OF THE
WILD GOOSE ASSOCIATION
GREAT GORGE, McAFEE, NEW JERSEY
OCTOBER, 1974

LEAR SIEGLER, INC.



INSTRUMENT DIVISION

4141 EASTERN AVENUE, S. E.
GRAND RAPIDS, MICHIGAN 49508

FEHNER
PP 19 + 2 = 21
REF 605-
PAPER 3-14
Aug 30 1974

Performance Optimization of Linear Loran
Receivers Operating In A Non-Gaussian
Atmospheric Noise Environment

By

Larry N. Postema
Lear Siegler, Incorporated
Instrument Division
Grand Rapids, Michigan

Abstract

This paper investigates the characteristics of non-gaussian atmospheric noise, and its effects on the performance of linear Loran receivers. The characteristics of atmospheric noise observed at Eglin AFB, Florida, during July of 1974, are presented. These are compared to the characteristics of atmospheric noise observed by another investigator on August 11, 1971 at Wildwood, New Jersey, just prior to the onset of a severe thunderstorm. The effects of observed atmospheric noise on receiver performance in both the Search and Synchronization, and Track modes is investigated. A scheme for improving the receiver track performance in atmospheric noise is presented along with the results of an IBM 370 digital simulation used to optimize the referenced scheme. Laboratory investigations were conducted to substantiate the results of simulation. These investigations used state-of-the-art AN/ARN-101 Loran receiver equipment, a dynamic Loran signal simulator, and an LSI built atmospheric noise source. The results of these investigations are presented. Finally, a means of reducing the effects of atmospheric noise on the receiver operation in the Search and Synchronization mode is presented along with the results of related laboratory investigations.

INTRODUCTION

A fundamental consideration in the design of any Loran receiver is the presence of atmospheric noise which serves to contaminate the Loran signals. The design approach generally used to account for the presence of atmospheric noise in the Loran frequency band is to assume that the noise component of the received signal is gaussian in nature. This assumption facilitates the use of well known analytical tools in the receiver design process. In the real world, however, atmospheric noise may or may not be gaussian in nature. In fact, under some conditions, atmospheric noise may bear almost no resemblance to gaussian noise. Once it is recognized that the receiver may be required to operate in a non-gaussian atmospheric noise environment, three questions come immediately to mind:

- What are the characteristics of non-gaussian atmospheric noise and how do they differ from gaussian noise?
- What effect will non-gaussian atmospheric noise have on the receiver performance?
- What can be done to optimize the receiver performance in the presence of non-gaussian atmospheric noise?

The remainder of this paper deals with answering these questions as they pertain to linear receivers.

Non-Gaussian Atmospheric Noise Characteristics

In general, the character of atmospheric noise will be determined by the following considerations:

- Time of day
- Season of year
- Geographic location
- Local weather conditions

As an example, atmospheric noise observed at night, under clear skies during the winter in the northern temperate zones could be expected to be nearly gaussian in nature. On the other hand, atmospheric noise observed during a day time summer thunderstorm in a tropical region could be expected to be very non-gaussian in nature. Investigation into the nature of atmospheric noise have been done by this writer, and others. This paper makes specific reference to investigations by Feldman (Reference 1). The investigations of this writer, and selected observations and results attributed to Feldman are discussed below.

Investigations Into Atmospheric Noise Performed By This Writer

On July 16, 17 and 18 of 1974, Loran band atmospheric noise amplitude data was taken at Eglin Air Force Base, Florida. The data taking process was facilitated thru the use of state-of-the-art AN/ARN-101 Loran receiver equipment (hereafter called the 101 receiver system) designed and built by Lear Siegler Incorporated under contract to the U. S. Air Force. The computer program in the 101 system was modified so as to provide for the

automatic taking and processing of noise data. The data taking process was structured so as to insure that no data elements would be contaminated by any of the Loran signals normally present in the Eglin area. Data was taken using an E-field antenna mounted on a ground plane located atop building 100 at Eglin Air Force Base. The local weather conditions that existed at the times data was taken were predominantly clear skies with little or no haze present. Data was taken at different times of day thru each of two bandpass filters. These filters are listed and described below.

- 101 Receiver System Wideband Filter - Two series 2-pole butterworth filters, each with a 35 KHZ bandwidth and a 100 KHZ center frequency. Taken together, these two filters are equivalent to a 3-pole 25 KHZ gaussian filter. In the 101 receiver system, the Loran signal tracking function is accomplished by processing data taken thru this filter.
- 101 Receiver System Narrowband Filter - A single 3-pole butterworth filter with a 6 KHZ bandwidth and a 100 KHZ center frequency. The frequency characteristic of this filter is steep skirted. In the 101 receiver system, the Loran search and synchronization function is accomplished by processing data taken thru this filter.

When observed on an oscilloscope during day time hours, and thru either of the bandpass filters described above, the atmospheric noise appeared non-gaussian and time-varying in nature. The noise appeared least intense during the morning hours and most intense during the late afternoon hours. A gradual transition between these two intensities would take place as each day wore on.

Cumulative Amplitude Probability Distribution (CAPD) curves of the data taken at Eglin are provided in Figures 1, 2 and 3, along with an indication as to date and time of day that data was taken. For purposes of comparison, the CAPD curve of gaussian noise is plotted in each figure. It is clear from Figures 1, 2 and 3 that the CAPD characteristics of the observed atmospheric noise are very non-gaussian in nature. Also, from Figure 3, it is seen that in late afternoon when atmospheric noise is most intense, its characteristics, as observed thru the wideband and narrowband filters, are nearly identical. This agrees with observations made by Feldman (Reference 1) that atmospheric noise characteristics do not vary significantly with the observation filter bandwidth so long as the bandwidth is greater than 1 KHZ. In Figures 1 and 2 it is seen that there is only a small amount of variation with filter bandwidth in the characteristics of atmospheric noise observed during the morning and mid-day hours. Figures 1, 2 and 3 indicate that the atmospheric noise observed at different times of day, though varying in intensity, are nonetheless similar in terms of their CAPD characteristics.

Selected Observations And Results Attributed To Feldman (Concerning Atmospheric Noise)-
On August 11, 1971, Feldman (Reference 1) accumulated atmospheric noise data at Wildwood, New Jersey just prior to the onset of a severe thunderstorm. Data was accumulated thru a bandpass filter with center frequency at 65 KHZ. The resultant CAPD characteristic was designated as representative of 'frontal' noise conditions. It is considered to be representative of the atmospheric noise that would have been observed if the bandpass filter center frequency had been 100 KHZ instead of 65 KHZ. This is because investigations by Feldman have indicated that low frequency noise characteristics are largely independent of the center frequency of the observation filter. The CAPD curve of the frontal noise observed by Feldman appears in the top of Figure 2-1, of Reference 1. This same curve appears in Figure 4 of this paper, except with the ordinate converted to a conventional log scale, and with the abscissa converted to represent noise amplitudes

normalized to their RMS value. Comparisons of Figures 1, 2 and 3 to Figure 4 indicates that the CAPD characteristics of the atmospheric noise observed at Eglin by this writer are very similar to those observed by Feldman on August 11, 1971 under frontal storm conditions.

In addition to accumulating noise data during frontal storm conditions in August of 1974, Feldman also accumulated noise data under weather conditions that were not severe in nature. Data was accumulated during day-time hours with the resultant CAPD curves designated as representative of 'tropical' noise. Data was also accumulated during night-time hours when two mild noise conditions were observed. The resultant CAPD curves are designated as representative of 'quiet' and 'quiet night' noise. The CAPD curves of tropical, quiet, and quiet night noise data are given in Figures 2-1 and 3-2 of Reference 1. CAPD curves of frontal, tropical and quiet night noise were derived by this writer from an IBM-370 digital simulation of the atmospheric noise model defined in Reference 1. These curves appear in Figure 5 of this paper. Comparison of the CAPD curves for frontal noise in Figures 4 and 5 indicates that the simulated frontal noise very closely approximates the frontal noise actually observed by Feldman. It is also observed from Figure 5 that in terms of its CAPD characteristics, quiet night noise is close to being gaussian in nature, whereas the tropical noise is closer to being frontal in nature. Feldman has indicated that frontal noise is representative of atypical temperate latitude noise behavior, but that it may be representative of more common noise conditions in equatorial regions. He also indicates that quiet noise conditions (nearly gaussian) are probably representative of most year around noise conditions in temperate latitudes, except that during the East Coast summer, for example, tropical noise conditions are more commonly experienced.

Investigations Into The Effects Of Non-Gaussian Atmospheric Noise On The Performance Of Linear Loran Receivers.

Linear receiver performance in both the 'search and synchronization' and 'track' modes has been investigated by this writer. These and other investigations discussed later were accomplished thru the use of a variety of digital simulation and laboratory tools. These tools are listed below.

- State-of-the-art AN/ARN-101 Loran receiver equipment (referenced earlier, and designated as 101 receiver system for short).
- Dynamic Loran Signal Simulator (LSS) capable of simulating RF Loran signals as they would appear to an aircraft flying any desired profile. The output of this simulator interfaces directly with the 101 receiver system.
- RF atmospheric noise generator designed and built by Lear Siegler, Inc. The output of this generator interfaces with the LSS (listed above) to provide a composite signal of Loran pulses plus atmospheric noise at the output of the LSS. The CAPD characteristics of the noise provided by this generator, as viewed thru the 101 receiver system bandpass filters, can be made to be anywhere between gaussian and frontal in nature.
- Actual off-air Loran signals.
- IBM-370 digital simulation of Loran C SSO signals.

- IBM-370 digital simulation of atmospheric noise per the model developed in Reference 1.
- IBM-370 digital simulation of pertinent 101 receiver system functions as listed below.
 - (1) Analog-to-digital (A/D) converter (including saturation and resolution characteristics).
 - (2) Loran signal tracking function (a second-order phase lock loop, or PLL).
 - (3) Automatic gain control (AGC) function.
 - (4) Noise estimation function.
 - (5) Loran track point signal strength estimation function.

The 101 receiver system functions listed in the last item indicated above constitute a simplified model of the overall 101 tracking function. The interrelationship of these functions is depicted in Figure 6. Investigations into the effects of atmospheric noise on the search and synchronization performance and on the tracking performance are discussed separately below.

Investigations Into the Effects of Non-Gaussian Atmospheric Noise on Search and Synchronization. During July of 1974 Loran search and synchronization tests were performed in later afternoon at Eglin AFB using off-air Loran C SS7 signals that were contaminated by atmospheric noise characterized by the CAPD curve shown in Figure 3. The Loran signals used were those generated by stations at Cape Fear, North Carolina (Master); Jupiter, Florida (Slave W); and Dana, Indiana (Slave Z). The signal-to-noise ratio of all three of these stations, observed at Eglin, was approximately 0 db (Air Force definition at track point) with Dana the weakest station. Tests were conducted using the 101 receiver system referenced earlier. In order for the test results to be meaningful to the reader, the following background information on the 101 receiver system search and synchronization process is provided: The computer program that performs the search and synchronization function in the 101 receiver system is designed such that the Master signals are located first. This is accomplished without distinguishing between Master long-delayed sky wave signals and Master ground wave signals. This process is called the Master search (MS) process. After the Master signals have been detected, appropriate time windows are established (based on the estimated present position) to bracket the ground wave signals of all three stations. These windows are then searched for the ground wave signals of all three stations. This process is called the ground wave search (GWS) process. The MS process is designed to look first for a strong Master signal. If a strong Master signal is not located, then the MS process proceeds to look for weaker Master signals. This design is accomplished by incorporating short, intermediate, and long integration times into the MS process. The GWS process, however, is designed always to look for weak signals. In order to accomplish this, the GWS process incorporates only a single, relatively long integration time. This insures detection of either strong or weak signals. Both the MS and GWS processes are designed such that the probability of false detections under conditions of gaussian noise is very low.

The results of search and synchronization tests at Eglin have shown that under conditions of atmospheric noise characterized by Figure 3, and with a Master signal-to-noise ratio of about 0 db at the track point, the MS process results in false detections about 44% of the time. The GWS process was found to be mostly unaffected by the presence of the non-gaussian atmospheric noise. The net effect of the large percentage of false Master searches experienced was to increase the mean time required to accomplish search and synchronization by about 80% (nearly double). It was observed that the MS process always detected at the short integration time. This was due to the relative signal strength of the Master signals in the Eglin area. Based on this observation, and noting that the GWS process employs only a single, long integration time, it was concluded that the effects of non-gaussian atmospheric noise on the search and synchronization process could be reduced thru the use of long time averaging of atmospheric noise brought about by a long integration time. This would seem to imply that the short and intermediate MS integration times should be deleted from the search and synchronization design in order to better accommodate non-gaussian atmospheric noise. However, this was deemed not to be a desirable approach, since then the advantage of quickly locating relatively strong Master signals would be lost. A better solution for the 101 receiver system application was to raise the detection thresholds associated with the MS short and intermediate integration times by 50%. This would result in only a 4 db loss in the effective levels of Master signal strength that could be quickly detected with a relatively high probability. This solution was prompted by the results of laboratory investigations using 101 receiver system equipment, Loran signal simulator equipment, and atmospheric noise generator equipment, all referenced earlier. These investigations showed that in the presence of simulated frontal noise, and with a Master signal-to-noise ratio of 0 db at the track point, the MS process resulted in false detections occurring 40% of the time with all detections occurring at the short integration time. By raising the MS short and intermediate integration detection thresholds by 25%, the occurrence of false MS detections was reduced to 10%. By raising these thresholds by 50%, the occurrence of false MS detections was reduced to virtually zero. All tests using the higher thresholds resulted in all MS detections still occurring at the short integration time. The proposed 50% increase in the MS short and intermediate integration detection thresholds was put to the test at Eglin under the same conditions (same time and day) that prevailed during those tests referenced earlier where false MS detections occurred 44% of the time. These tests resulted in false MS detections occurring a tolerable 17% of the time. This represented a 2.6 to 1 reduction in occurrence of false MS detections, which translates into a reduction in the increase in the mean time required to accomplish search and synchronization from approximately 80% with no increase in thresholds to only 20% when the MS short and intermediate integration detection thresholds are increased by 50%.

Investigations Into the Effects of Non-Gaussian Atmospheric Noise on the Tracking Process

These investigations were performed using an IBM-370 digital simulation of Loran C SSO signals, atmospheric noise, and all pertinent 101 receiver system functions as listed earlier. The effects of 4 types of simulated atmospheric noise on the receiver tracking performance were evaluated. The 4 noise types considered were

- Frontal noise
- Tropical noise
- Quiet night noise
- Gaussian noise

The CAPD characteristics of each of these noise types appears in Figure 5.

For each noise condition considered, the receiver tracking performance was evaluated by observing the resultant error variance of the simulated 2nd-order PLL (designated σ_e^2) when the bandwidth was fixed such that the loop time constant was equal to 10 seconds. This error variance was compared to the error variance that resulted under the same conditions described above, except without the effects of saturation attributable to the A/D converter. This error variance is designated $(\sigma_e^1)^2$. The improvement in receiver performance, then, is defined as follows for each noise condition considered.

$$IF = 10 \log_{10} \frac{(\sigma_e^1)^2}{\sigma_e^2} \text{ decibels}$$

where

IF = improvement factor

It is noted that the improvement factor computed as defined above also serves to represent the difference in tracking performance that results for a specific noise condition with power P as compared to that which would result with gaussian noise of equal power P.

For each noise condition, a key factor in the determination of σ_e^2 , and hence IF, will be the manner in which the automatic gain control (AGC) function^ε (referenced earlier) is defined. It is therefore useful at this point to provide the following background information on the AGC function: In the 101 receiver system, the AGC function is designed to adjust the analog signal level at the input to the A/D converter in a manner that, under gaussian noise conditions, insures that Loran signal plus noise at the track point stays within the range of the A/D converter. This is done to insure linear operation of the receiver under gaussian noise conditions, and is accomplished by requiring that the full scale (FS) level of the A/D converter be constrained such that

$$FS = \hat{S} + 3\hat{\sigma}_n$$

where

\hat{S} = the receiver's estimate of the Loran signal strength at the track point.

$\hat{\sigma}_n$ = the receiver's estimate of the noise standard deviation (square root of estimated noise power).

With this implementation of the AGC function, the A/D converter saturation level will have virtually no effect on the receiver performance under gaussian noise conditions.

Simulations were conducted using S/N levels (Air Force definition at track point) as listed below for the different noise types considered.

Frontal noise	-	S/N	=	-17.8db
Tropical noise	-	S/N	=	-12.1 db
Quiet night noise	-	S/N	=	-8.3 db
Gaussian noise	-	S/N	=	-8.3 db

For each noise condition, runs were made with and without the A/D converter saturation level in order to establish the tracking loop error variances needed to compute improvement factors. The results are tabulated below.

Table 1 - Receiver System Tracking Performance
For Different Noise Conditions.

Noise Type	S/N db	σ_{ϵ} μsec	σ_{ϵ}^1 μsec	IF db
Frontal	-17.8	0.097	0.427	12.9
Tropical	-12.1	0.057	0.202	11.0
Quiet Night	-8.3	0.105	0.146	2.9
Gaussian	-8.3	0.157	0.157	0

The results tabulated in Table 1 show that significant improvements in the receiver system tracking performance occur when the atmospheric noise is non-gaussian in nature. These improvements are directly attributable to the saturation characteristics of the A/D converter, and the manner in which the AGC function is defined. In specific terms, the saturation level of the A/D converter serves to clip those signal samples that have relatively large amplitudes due to contamination by unusually high amplitude noise spikes. This clipping action serves to improve the effective S/N as observed by the receiver at the output of the A/D converter. This, in turn, results in an improved tracking accuracy. In those simulation runs where the A/D converter saturation characteristic was included, the actual percentages of samples taken that were clipped was observed. These percentages are tabulated in Table 2 below.

Table 2 - Percentages of Samples Clipped By The
A/D Converter For the Different Noise
Conditions Considered.

Noise Type	S/N db	Noise (N) Samples Clipped %	Track Point Zero Crossing(c) Samples Clipped %	Track Point RF Peak(S) Samples Clipped %
Frontal	-17.8	3.5	3.3	4.0
Tropical	-12.1	1.9	2.7	2.9
Quiet Night	-8.3	1.4	1.4	1.6
Gaussian	-8.3	0	0	0.04

Investigations Into Means Of Optimizing The Tracking Performance Of Linear Loran Receiver
In the Presence of Non-Gaussian Atmospheric Noise.

In light of the results presented in the last section on receiver tracking performance, it would seem logical to assume that under conditions of non-gaussian atmospheric noise, further clipping of the tracking samples would serve to further improve the receiver tracking performance. Indeed, investigations attributed to Feldman (Reference 1) have indicated that this should be the case. Feldman investigated several schemes for

improving the receiver performance under non-gaussian atmospheric noise conditions. These included investigations into the schemes listed below.

- Hard-Limiter
- Clipper
- Hole-Puncher

Feldman concluded that a 15% clipper (clips 15% of all track samples) was the best all-around scheme to improve the receiver performance. Feldman found that the ability of the 15% clipper to provide near optimum performance was insensitive to both the range of input S/N as well as being relatively insensitive to the type of atmospheric noise that happened to be present.

Prompted by the results of Feldman discussed above, a modified version of the 15% clipper was devised, evaluated, and incorporated into the 101 receiver system. Recognizing that the 101 receiver system A/D converter saturation level was already providing a significant degree of tracking performance improvement under non-gaussian atmospheric noise conditions, it was determined that a near optimum tracking performance could be attained by incorporating a 'software' clipper that clipped sums of 4 of tracking zero-crossing (c) samples at a level defined by $3\hat{\sigma}_{nc}^*$. It was necessary to clip sums of 4 of c samples rather than individual c samples because of constraints that had previously been incorporated into the 101 receiver system hardware design, and which were not readily alterable.

Simulations were conducted under the same set of ground rules set down in the last section on investigations into the effects of non-gaussian atmospheric noise on the tracking process. These simulations were performed in order to evaluate the effectiveness of the combined A/D hardware clipper and $3\hat{\sigma}_{nc}$ software clipper, and compare it with the effectiveness of the near optimum 15% clipper (no hardware clipping) recommended by Feldman. The results of these simulations are shown in Table 3. It is seen from Table 3 that the $3\hat{\sigma}_{nc}$ software clipper on sums of 4 of c samples provides an additional 5.9 db improvement in the receiver tracking performance under frontal noise conditions to provide for a total improvement of 18.8 db. This is very close to the 18.3 db improvement provided by Feldman's 15% clipper, implying that the $3\hat{\sigma}_{nc}$ software clip level chosen is probably close to optimum. Table 3 also shows that the $3\hat{\sigma}_{nc}$ software clipper provides added performance improvement for noise conditions that are less severe as compared to frontal, except that under gaussian noise conditions, no improvement in performance is realized due to clipping.

In the 101 receiver system, the phase lock loops are designed to maintain a constant estimated PLL error variance under almost all conditions of noise when the loops are in a steady state condition (no aircraft dynamics). This is accomplished by adjusting the bandwidths of the loops as a function of estimated signal-to-noise ratio (S/N). Under conditions of aircraft dynamics these bandwidths are expanded, within limits, in order to better track the dynamics and hence insure that the loops remain locked onto the Loran signals. Since incorporation of the $3\hat{\sigma}_{nc}$ software clipper discussed earlier results in an improved receiver tracking accuracy under conditions of non-gaussian atmospheric noise, it follows that the loop bandwidth must be expanded in order to retain a constant error variance in the loop. The required expansion in bandwidth is accomplished by computing the bandwidth expansion as a function of estimated signal-to-clipped noise ratio (S/N_c) where the latter is computed from noise data that is subjected to the $3\hat{\sigma}_{nc}$ software clipper. All other receiver estimated quantities

* $\hat{\sigma}_{nc}$ is the receiver's estimate of the noise standard deviation computed on the basis of noise data that is subjected to the $3\hat{\sigma}_{nc}$ software clipper.

that are noise data dependent (except for $\hat{\sigma}$) are computed from noise data that is not subjected to the $3\hat{\sigma}_{nc}$ software clipper.^{nc} With this implementation of the $3\hat{\sigma}_{nc}$ software clipper, the net effect of the clipper is to improve the receiver tracking performance under dynamic conditions.

Improved receiver tracking performance under dynamic conditions was verified under laboratory conditions using the 101 receiver system in conjunction with a dynamic Loran Signal Simulator (LSS) and an RF atmospheric noise generator, all referenced earlier. The receiver was made to fly a profile shaped like a paperclip at a speed of 425 knots. The profile provided for the execution of 5 turns with g-levels, in order, as $\frac{1}{2}g$, $\frac{1}{2}g$, $1g$, $2g$, $3g$. All tests were performed using Loran C SS7 signals. The Loran signals were made to simulate the signals generated by the Cape Fear, Jupiter, and Dana stations as they would be observed in the Eglin Florida area. The atmospheric noise generator was made to generate frontal noise. The unclipped signal-to-noise level of all three stations (at the track point) was made to be -23db. Runs with and without the $3\hat{\sigma}_{nc}$ software clipper were made. The results of these simulations were recorded in terms of time difference (TD) error plots. These results are shown in Figures 7 and 8. A comparison of the error plots shown in Figures 7 and 8 clearly indicate the improved tracking performance of the receiver during dynamic turns when the $3\hat{\sigma}_{nc}$ software clipper is employed.

Table 3 - Receiver System Tracking Performance
For Different Clipping Schemes and Noise Conditions

Noise Type	Clipping Scheme Used	S/N	Track Point Zero-Crossing (c) Samples Clipped	σ_{ϵ}	IF (Total)	Δ IF (Amount Due To Software Clipper Only)
		db	%	μ sec	db	db
Frontal	Scheme A	-17.8	15.0	0.052	18.3	18.3
Frontal	Scheme B	-17.8	34.3	0.049	18.8	5.9
Tropical	Scheme B	-12.1	25.2	0.032	16.0	5.0
Quiet Night	Scheme B	- 8.3	27.7	0.091	4.1	1.2
Gaussian	Scheme B	- 8.3	25.0	0.154	0.1	0.1

Notes: (1) Scheme A = 15% Clip on Individual c samples (Feldman's Scheme).

(2) Scheme B = A/D Hardware Clip On All Samples Plus $3\sigma_{nc}$ Software Clip on Sums of 4 of c Samples.

Figure 1 - Cumulative Amplitude Probability
Distribution of Atmospheric Noise
Observed At Eglin Thru The 101
Receiver System Wideband and Narrowband Filters After Mid-Morning
(Reference Key)

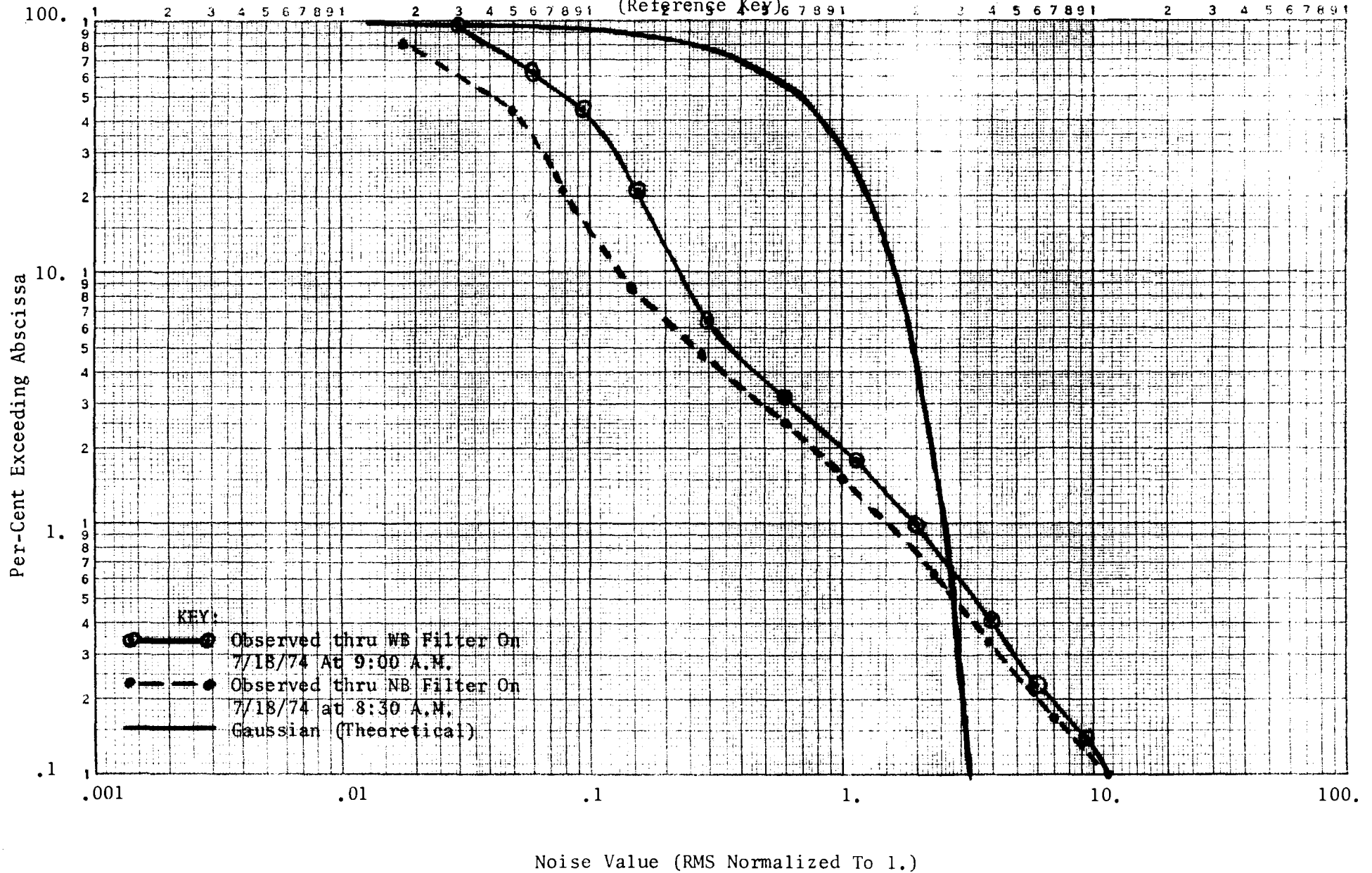


Figure 2 - Cumulative Amplitude Probability Distribution of Atmospheric Noise Observed at Eglin Thru The 101 Receiver System Wideband and Narrowband Filters At Mid-Day (Reference Key)

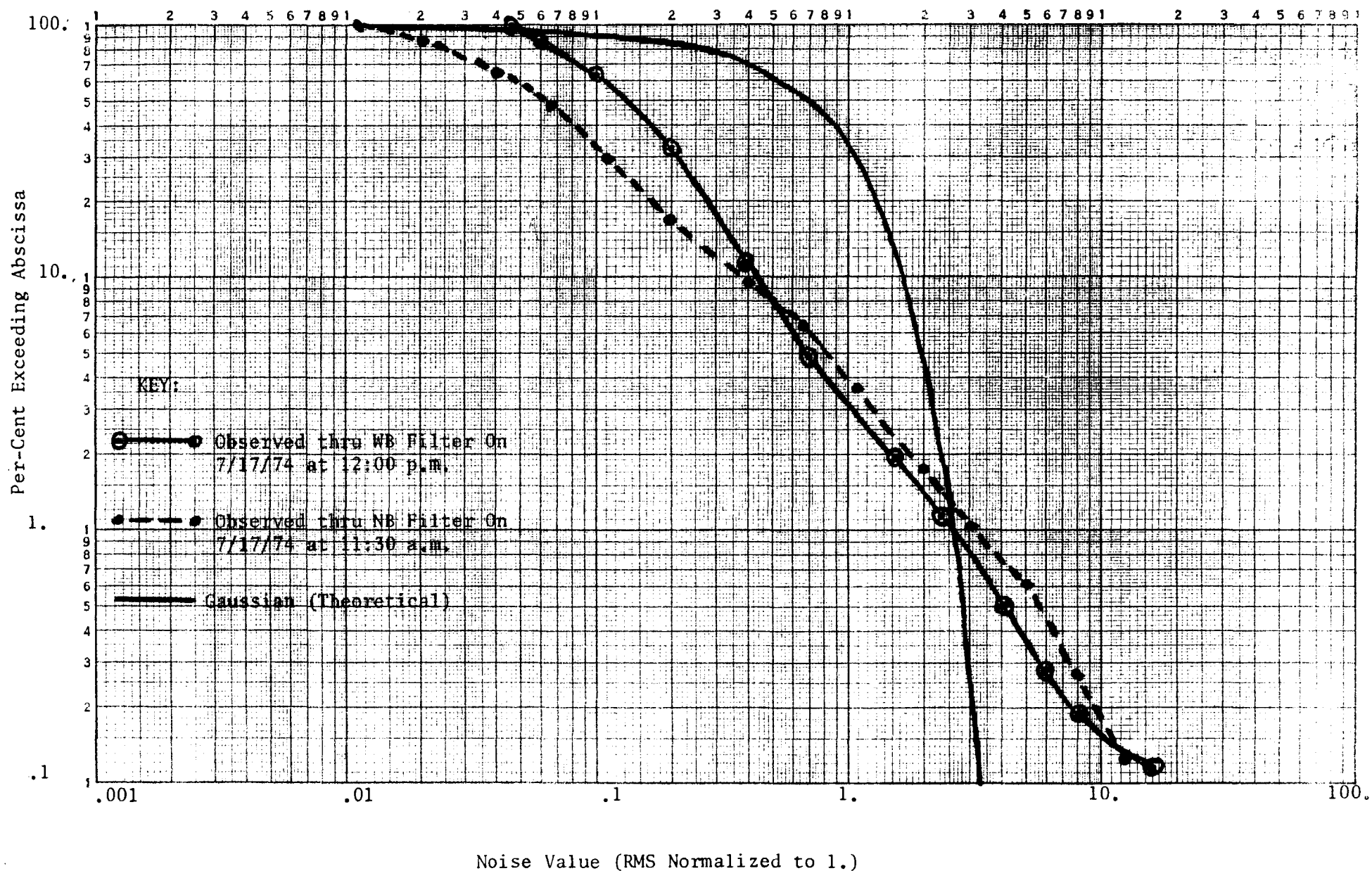


Figure 3 - Cumulative Amplitude Probability Distribution of Atmospheric Noise Observed at Eglin Thru the 101 Receiver System Wideband And Narrowband Filters In Late Afternoon (Reference Key)

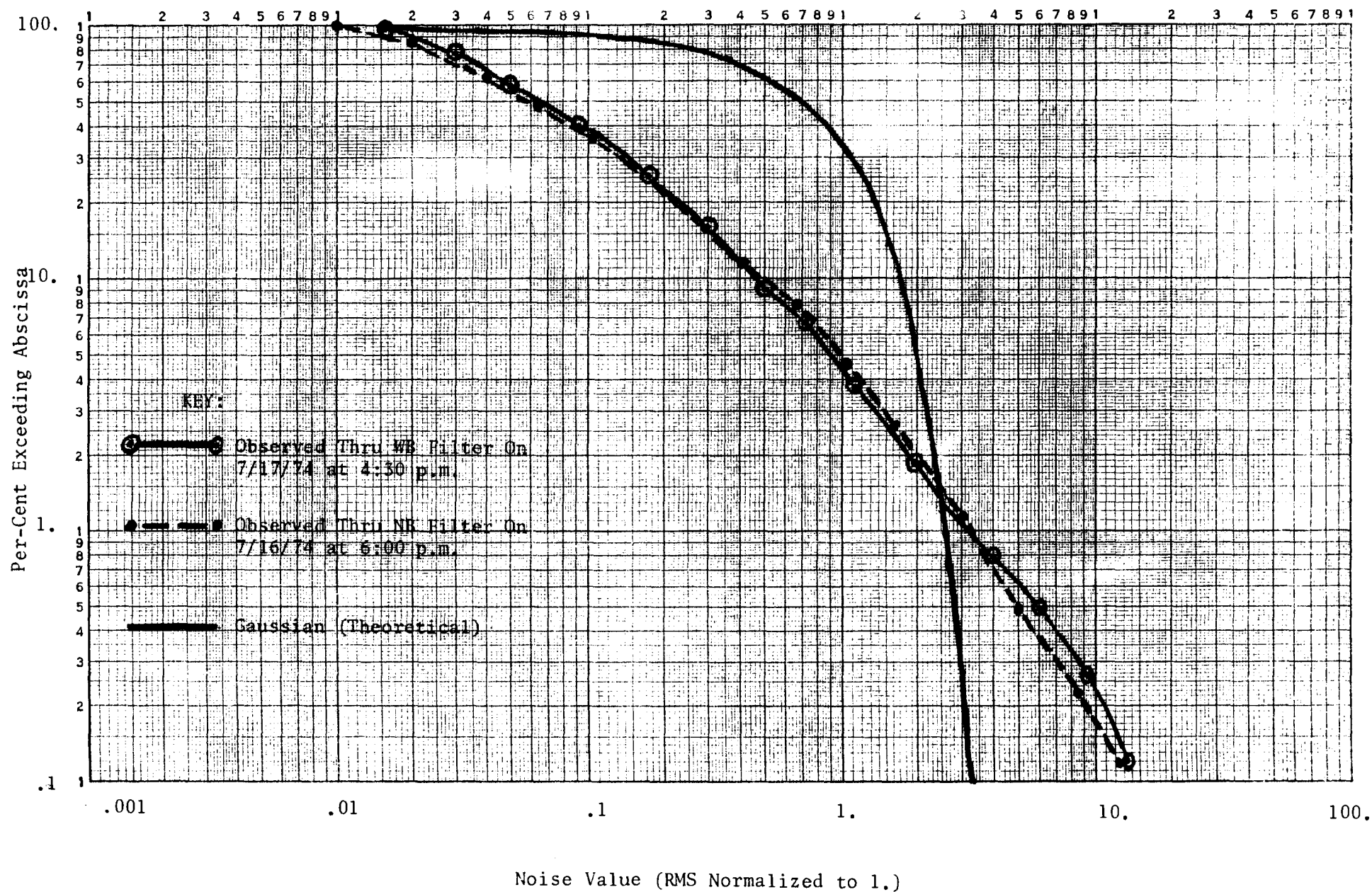


Figure 4 - Cumulative Amplitude Probability Distribution Of Frontal Atmospheric Noise Observed By Feldman on August 11, 1971 at Wildwood, Ner Jersey.

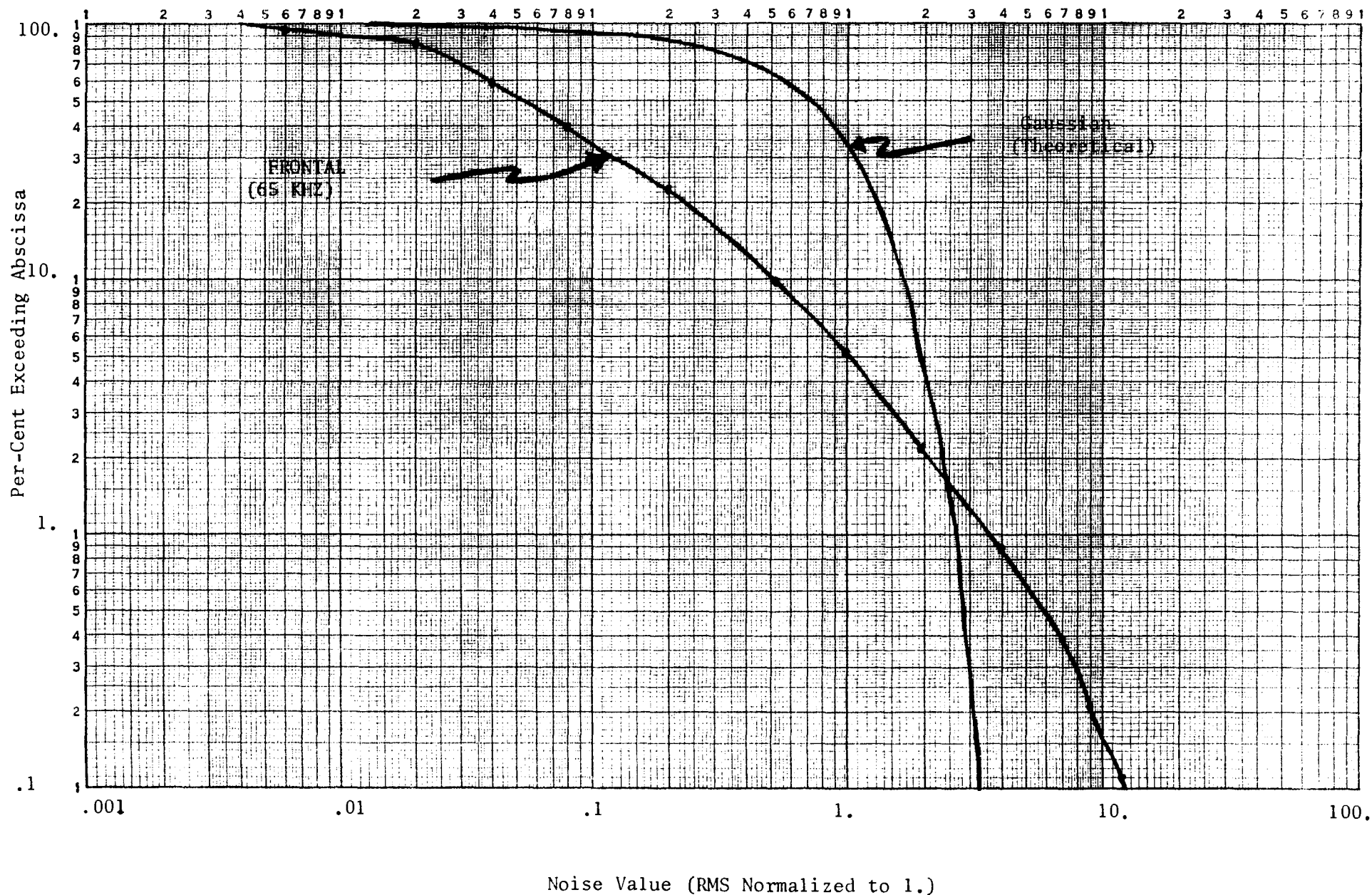


Figure 5 - Cumulative Amplitude Probability Distributions Of Different Types of Noise Data Derived Via Simulation From the Atmospheric Noise Model of Reference 1.

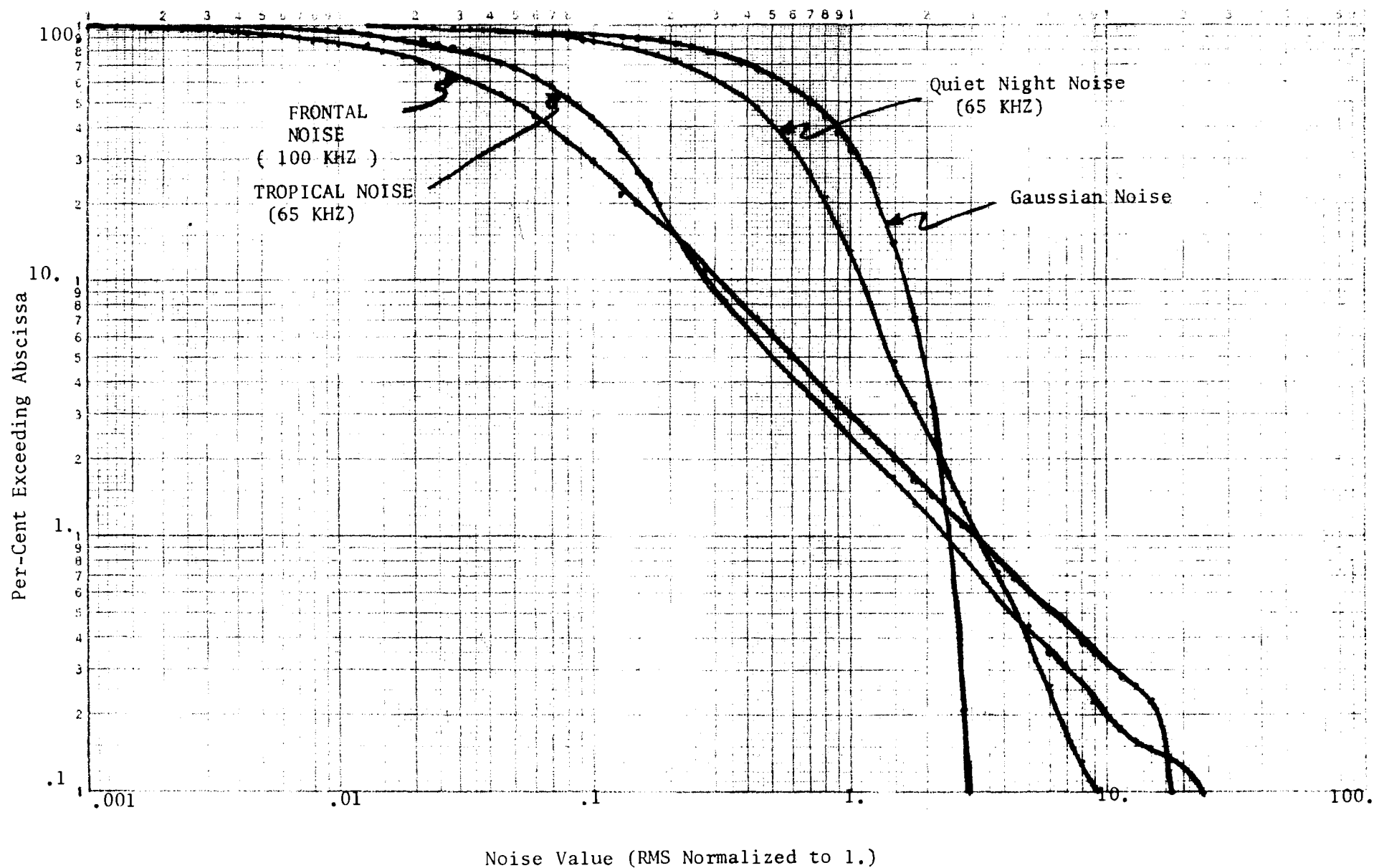
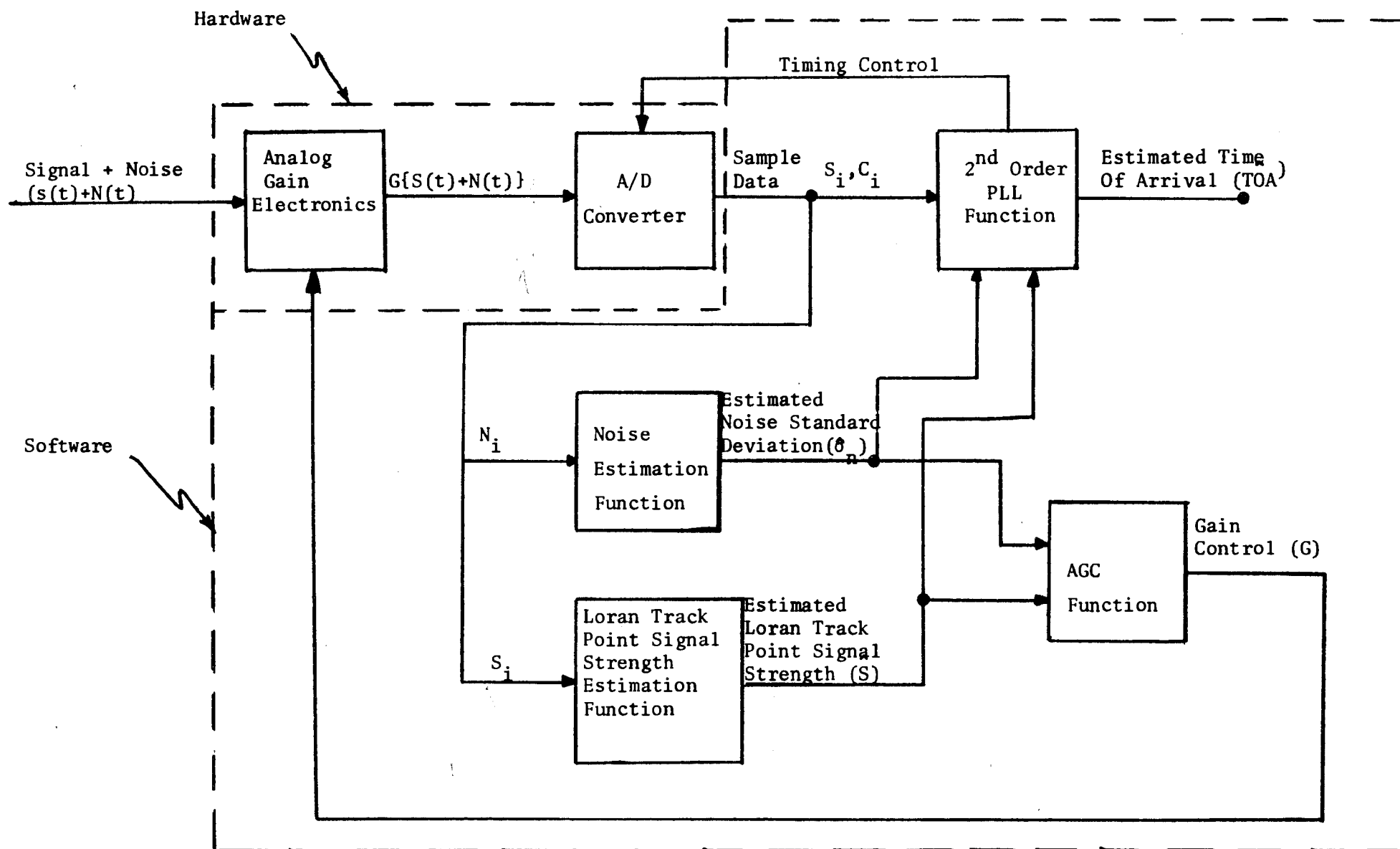


Figure 6 - Simplified Model Of The 101 Receiver System Tracking Function.



- NOTES:
- (1) N_i designates noise sample data
 - (2) C_i designates track point zero-crossing sample data
 - (3) S_i designates track point RF peak sample data

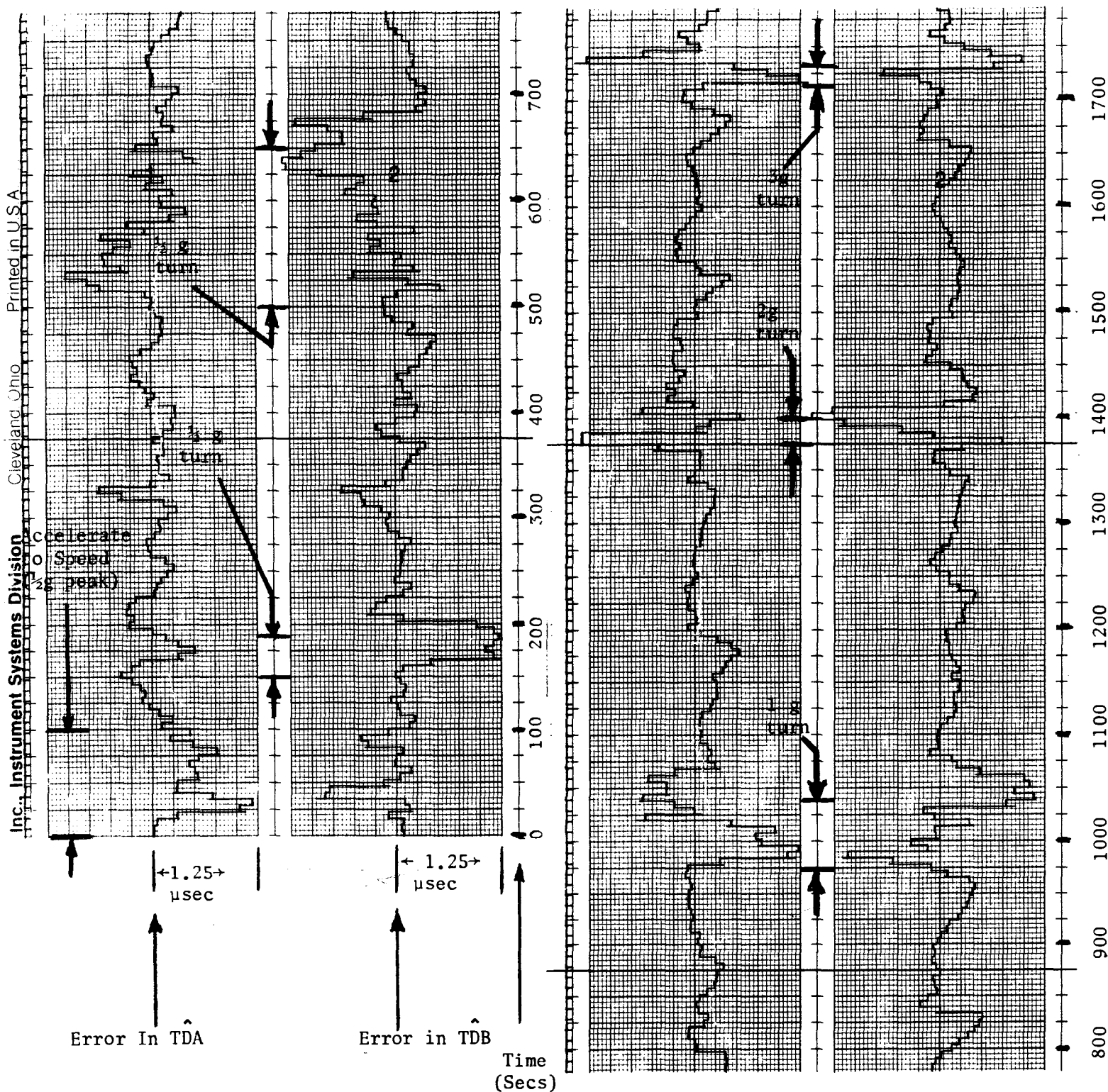


Figure 7 - Errors In the Receiver's Estimated Time Differences (TDB, TDB Under Dynamic Flight Conditions Without the 30_{nc} Software clipper. Track point S/N is -23 db. Noise type is frontal.

References

- (1) "An Atmospheric Noise Model With Application To Low Frequency Navigation Systems", Doctoral thesis by Donald A. Feldman performed at Massachusetts Institute of Technology and dated June, 1972.

FILE COPY
3-15

NOTES:

USCG LORAN-C
RECEIVER TESTING

NO F.
#15
1974 3RD

LCDR W. SCHORR
COMDT (C-EEE-4/63)
US COAST GUARD
Washington, DC 20590
202-426-1193

3 October 1974
GREAT GORGE, NJ
1973 Wild Goose
Annual Convention

FEHLNER
REF 606
PP 38
PAPER 315
7-840012

TEST PLAN DESCRIPTION

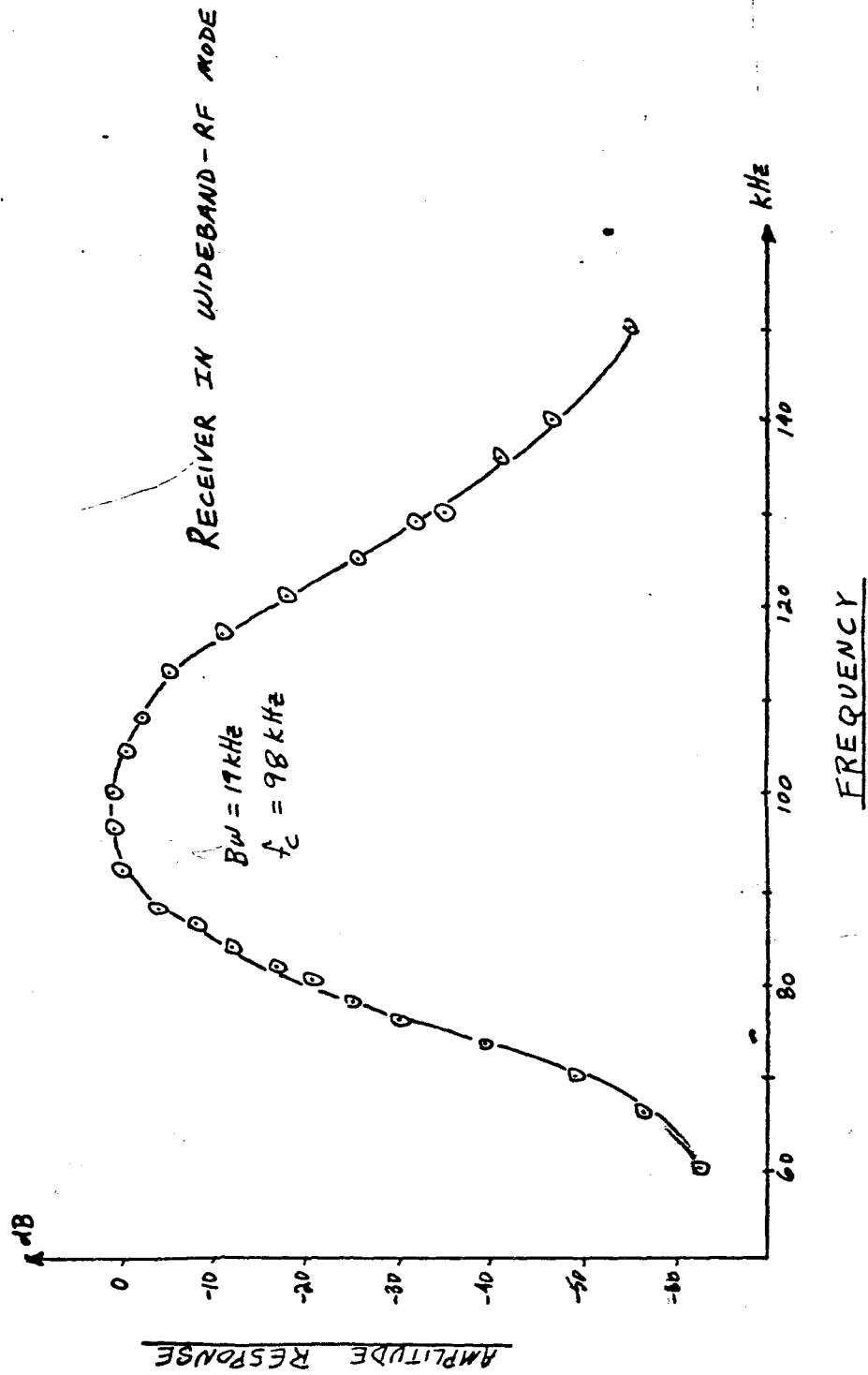
A. GENERAL PROCEDURES

1. Interfacing the receiver with the LRFC
2. DAS sample period considerations
3. Measurement of signals
4. Data reduction
5. Miscellaneous consideration

B. SPECIFIC TESTING PROCEDURES

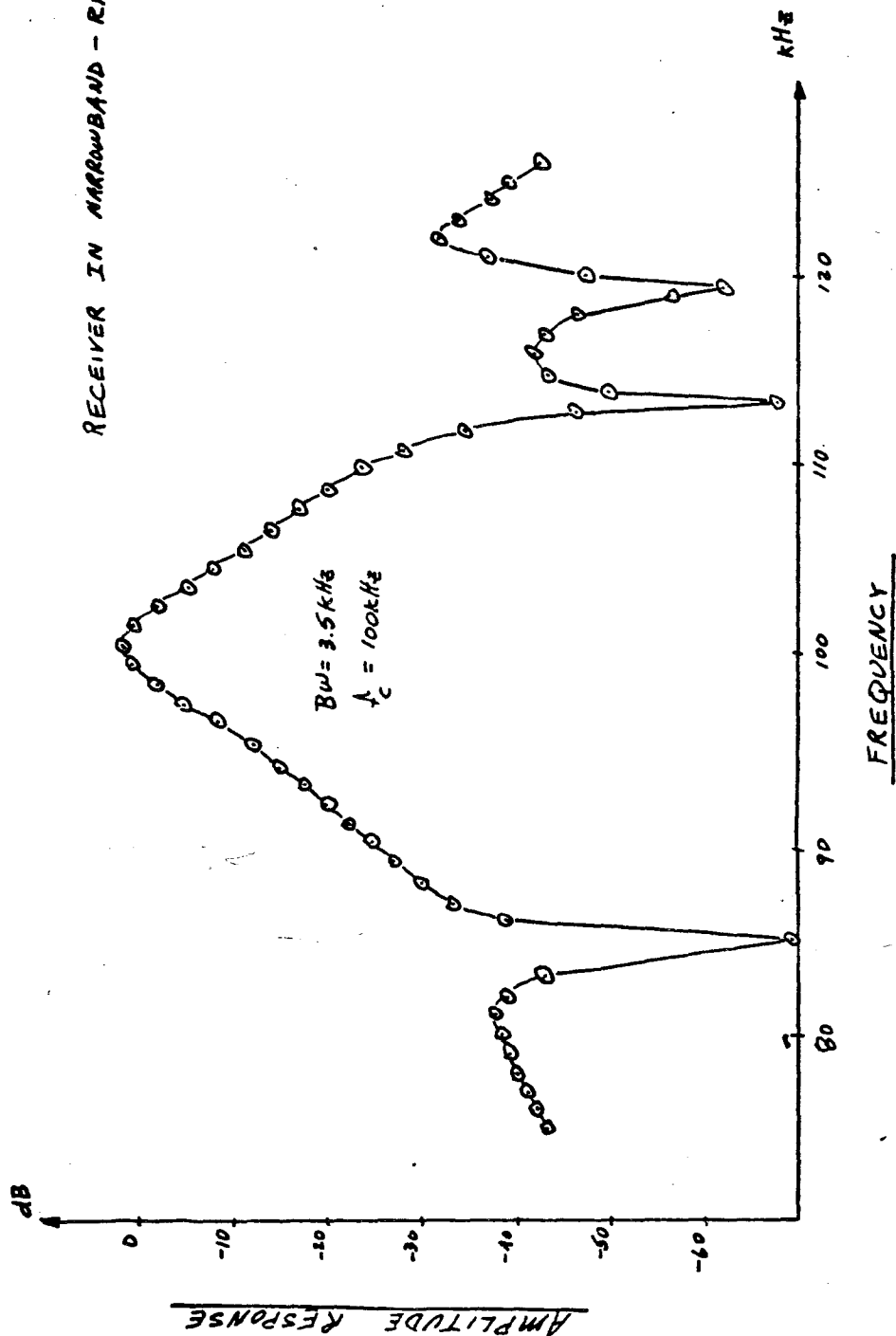
1. RF response
2. Notch filters
3. Lock-on as related to signal conditions
4. Envelope channel transfer characteristics
5. Servo loop bandwidth
6. Absolute signal level
7. Differential signal level
8. Noise performance
9. CW interference
10. Skywave contamination
11. Crossrate interference
12. Slow-rate test
13. On-air signal test
14. Alarm circuits
15. Receiver power supply
16. Reliability, maintainability, and repairability
17. Human engineering factors

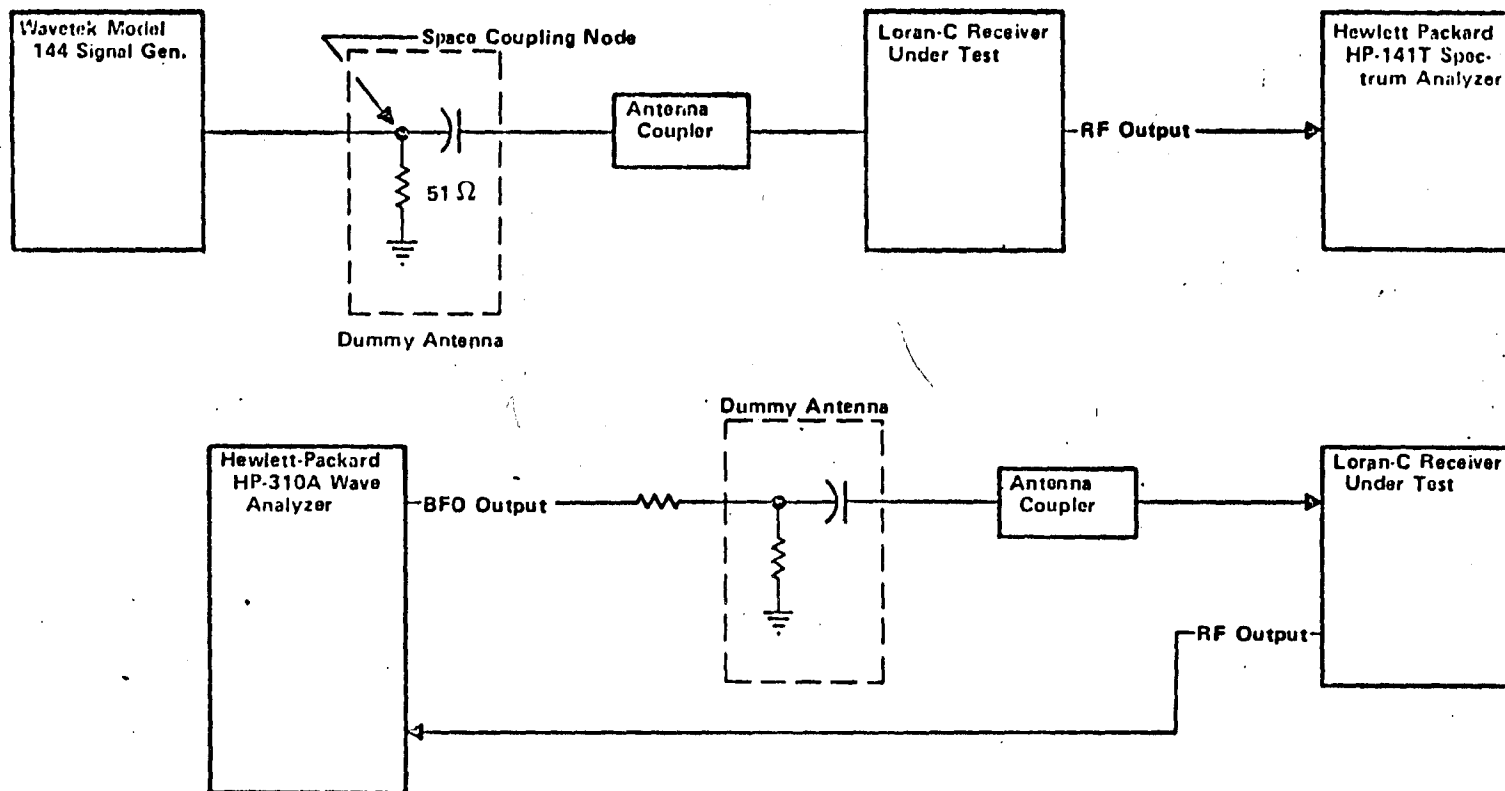
RF BANDPASS CHARACTERISTIC



RF BANDPASS CHARACTERISTIC

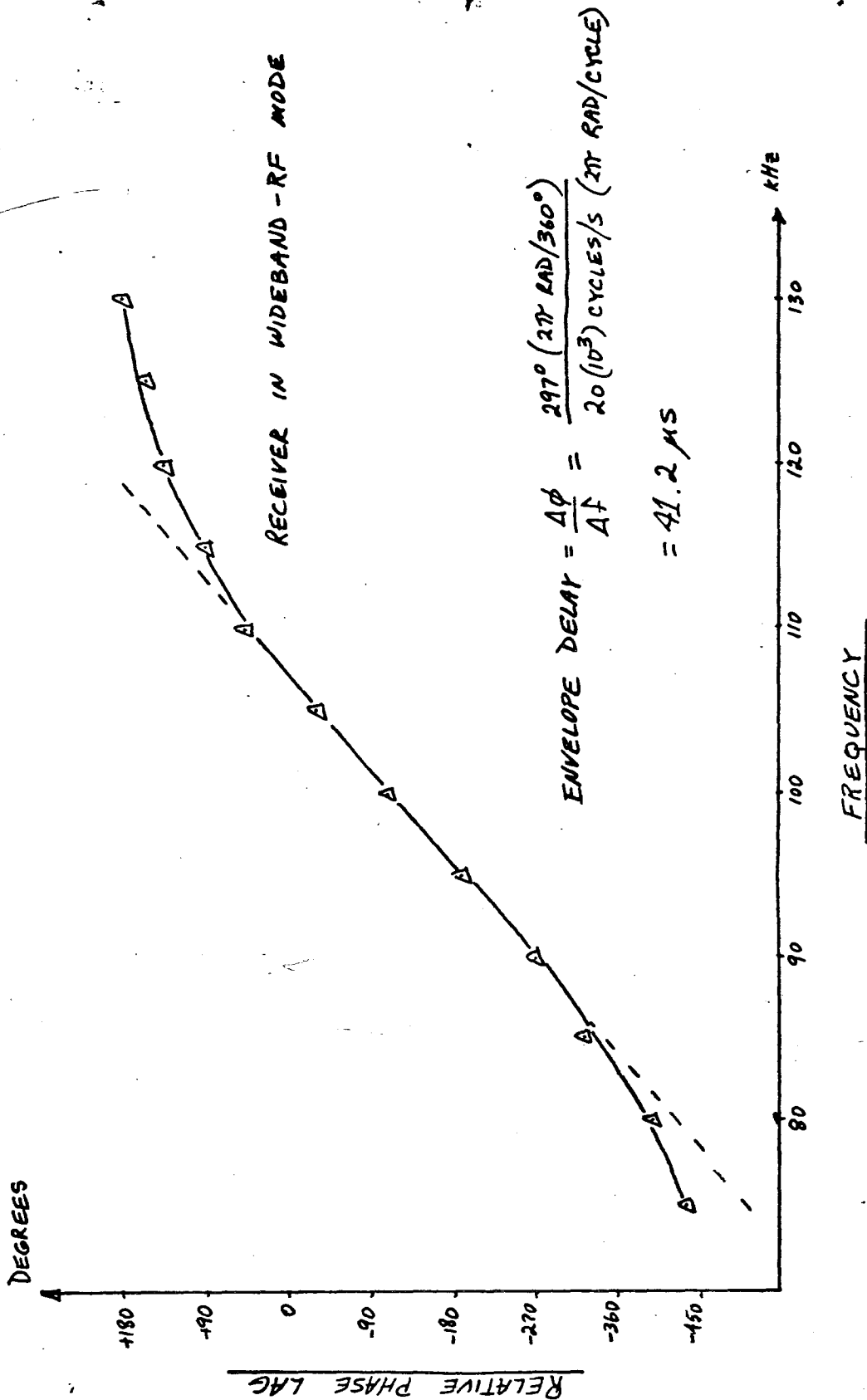
RECEIVER IN NARROWBAND - RF MODE

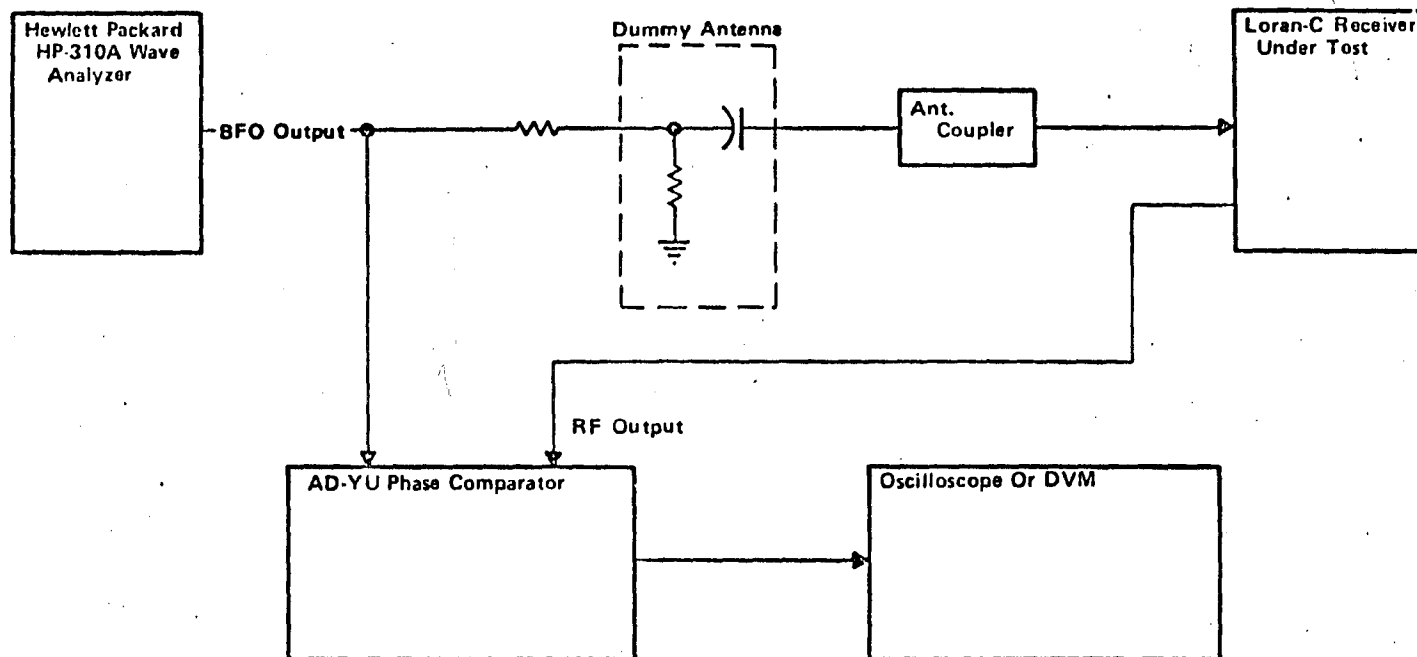




LRTC RF Bandwidth Test Setups

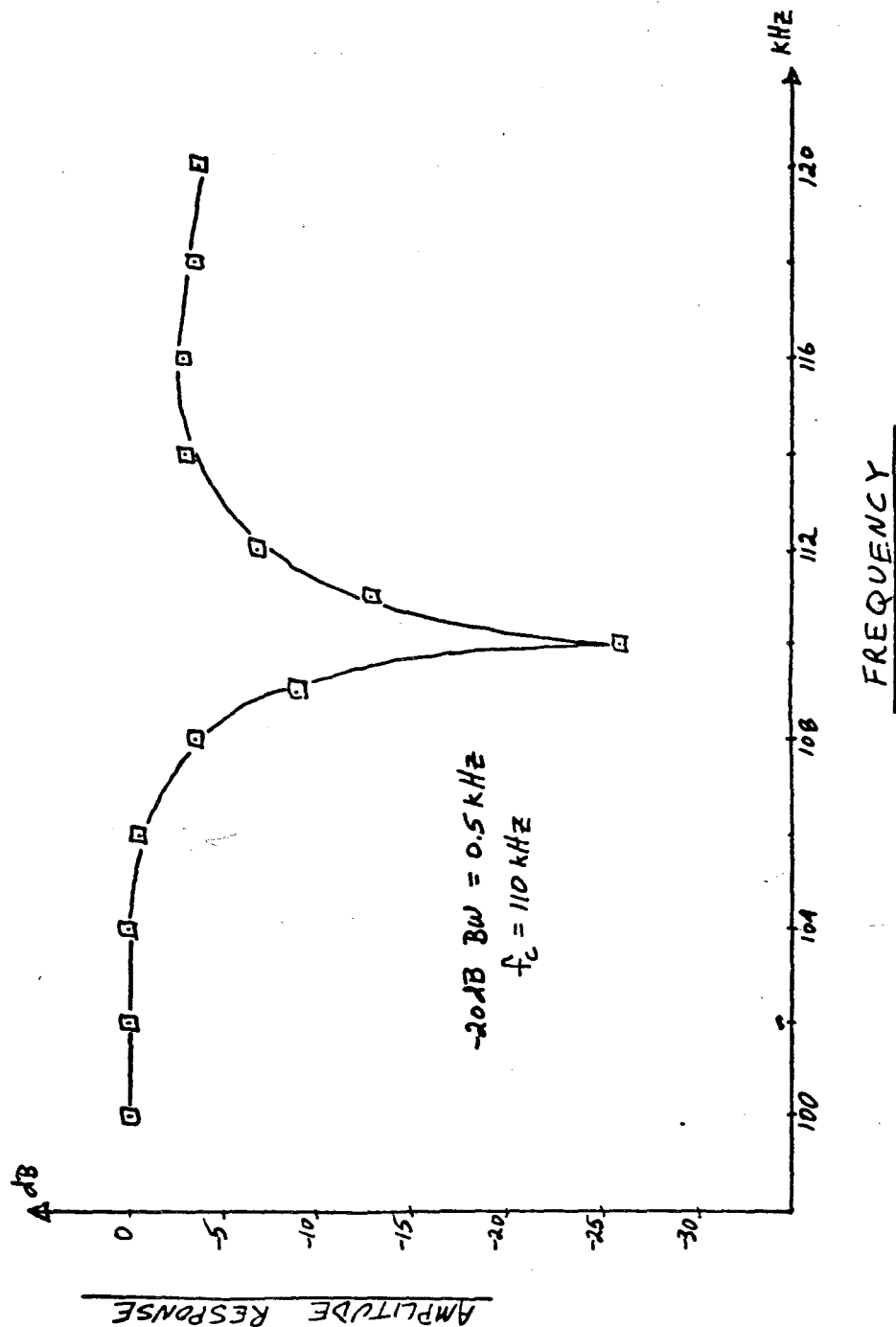
RF PHASE RESPONSE

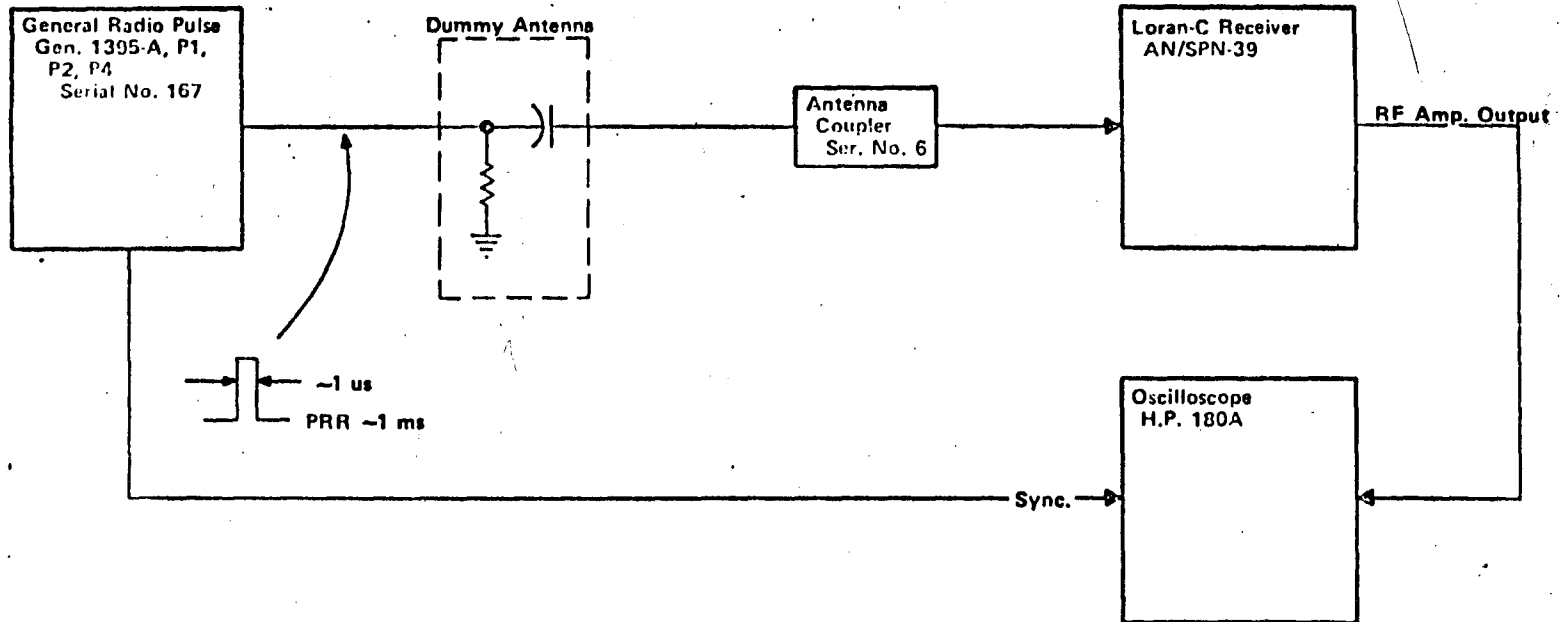




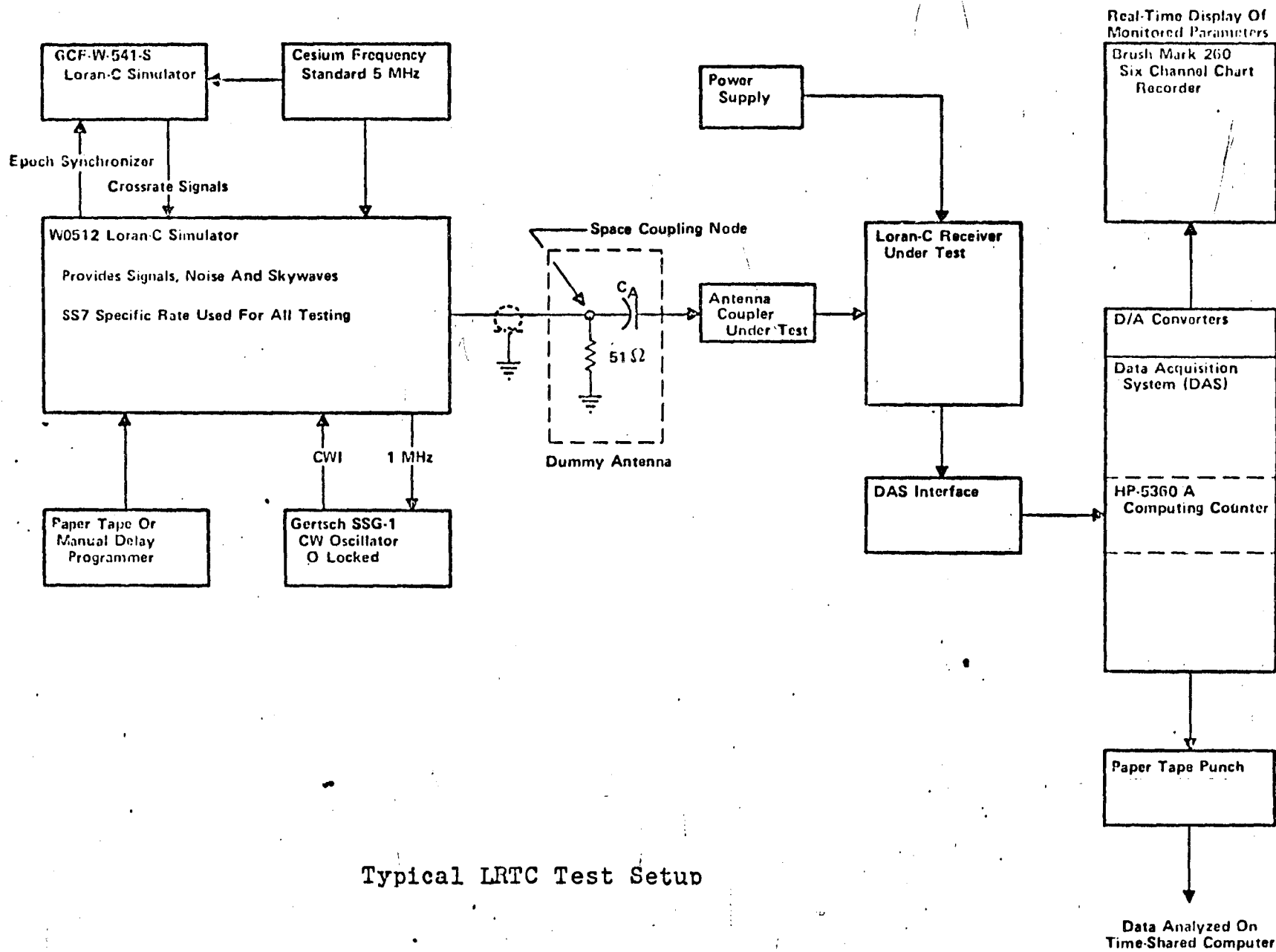
Typical LRTC Test Setup For RF Phase Response

NOTCH FILTER RESPONSE

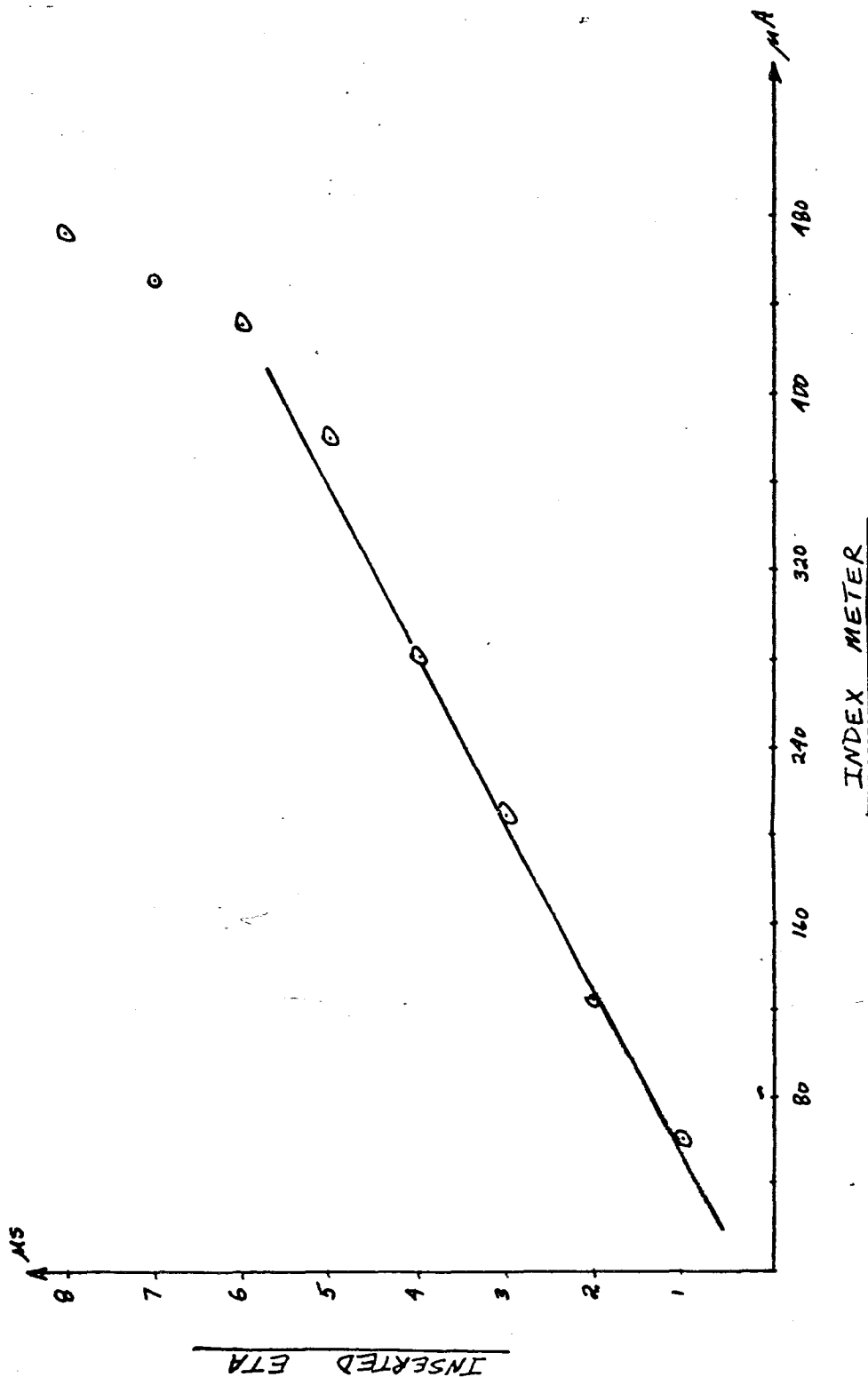




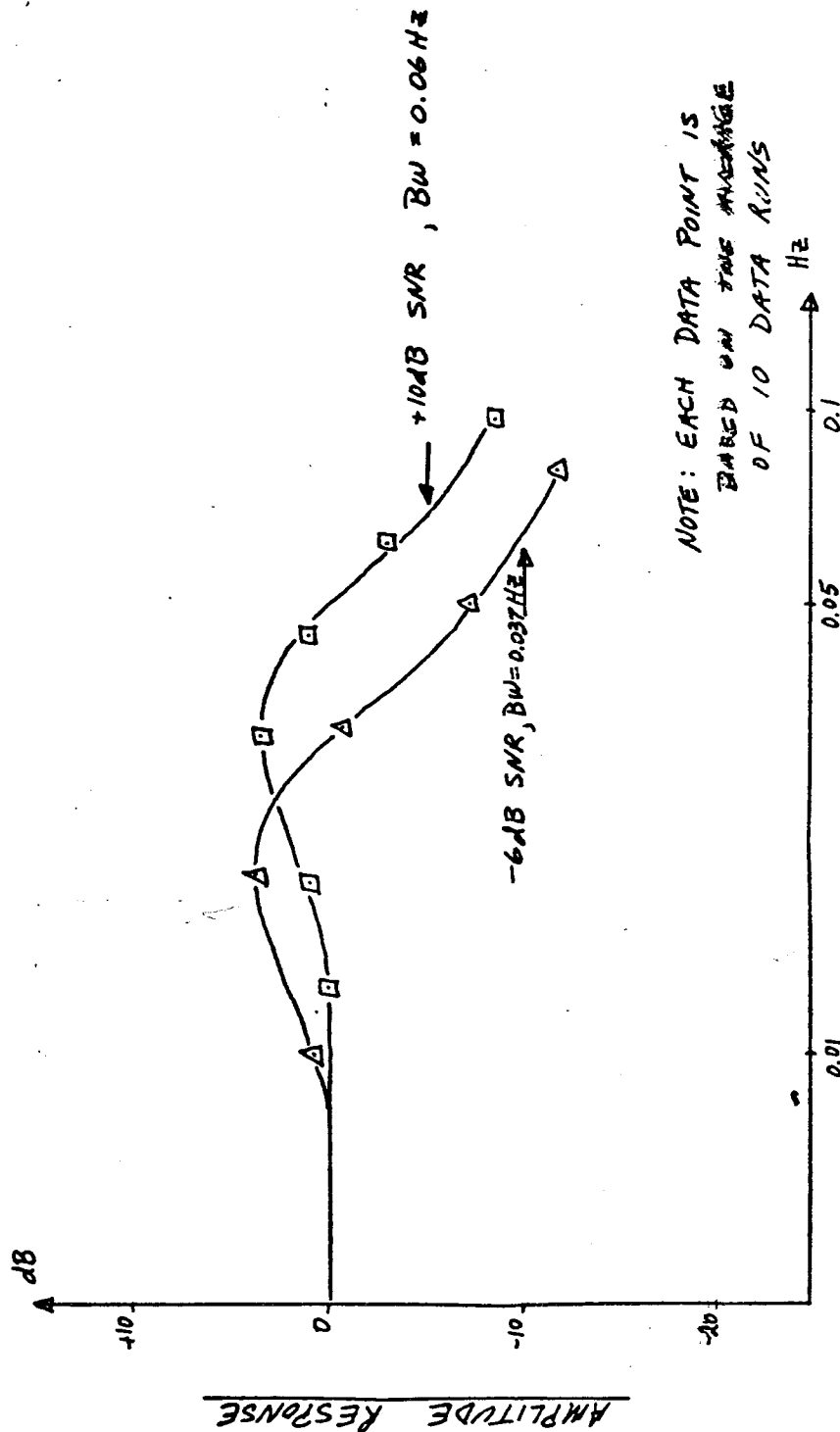
Impulse Response Test Setup



ENVELOPE CHANNEL TRANSFER CHARACTERISTICS



PHASE SERVO RESPONSE

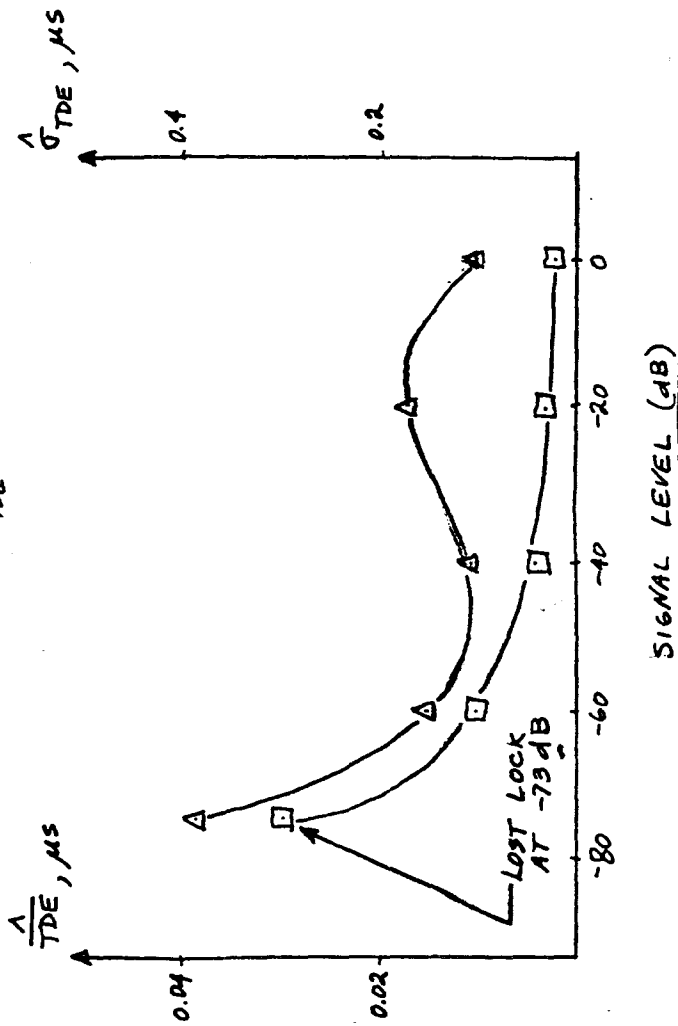


NOTE: EACH DATA POINT IS
BASED ON THE AVERAGE
OF 10 DATA RUNS

FREQUENCY

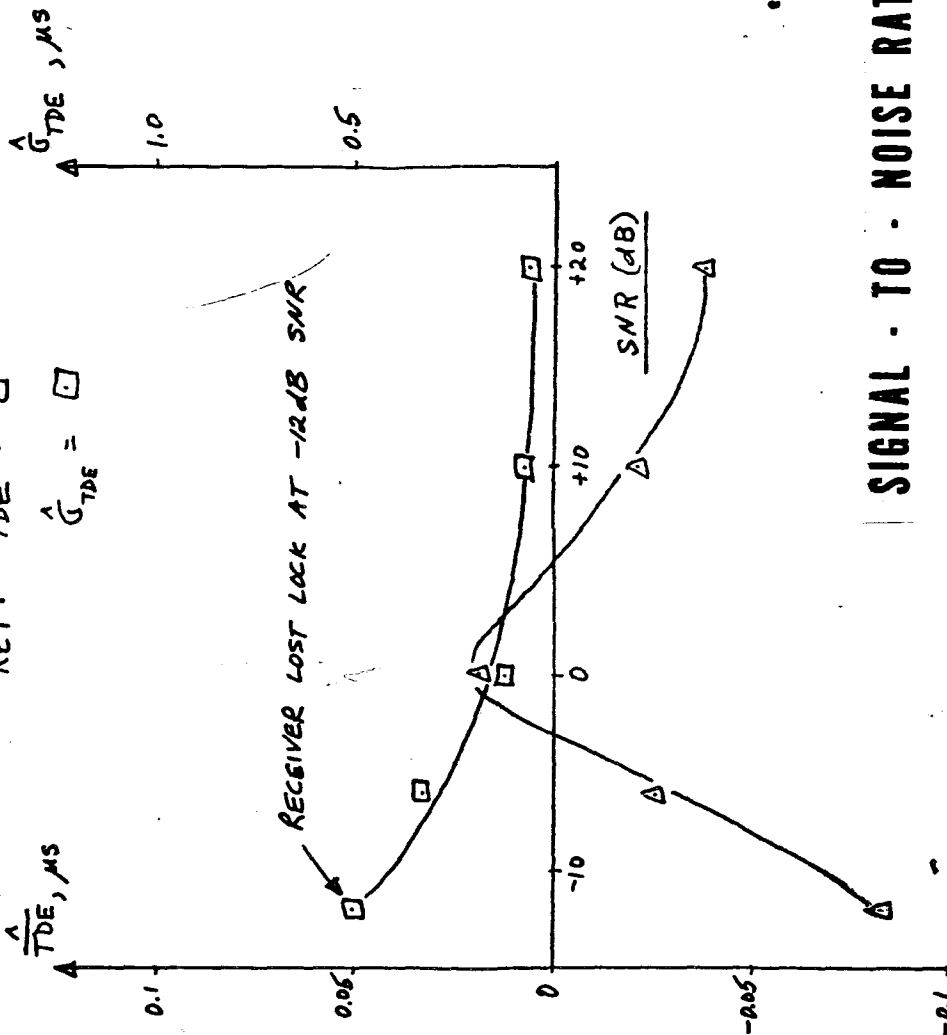
ABSOLUTE SIGNAL LEVEL TEST

KEY: $\frac{\lambda}{TDE} = \Delta$
 $\frac{\lambda}{G_{TDE}} = \square$



NOTES: (1) OdB = 25mVrms SSP
 (2) EACH DATA POINT IS BASED ON 50 STATISTICALLY INDEPENDENT SAMPLES.

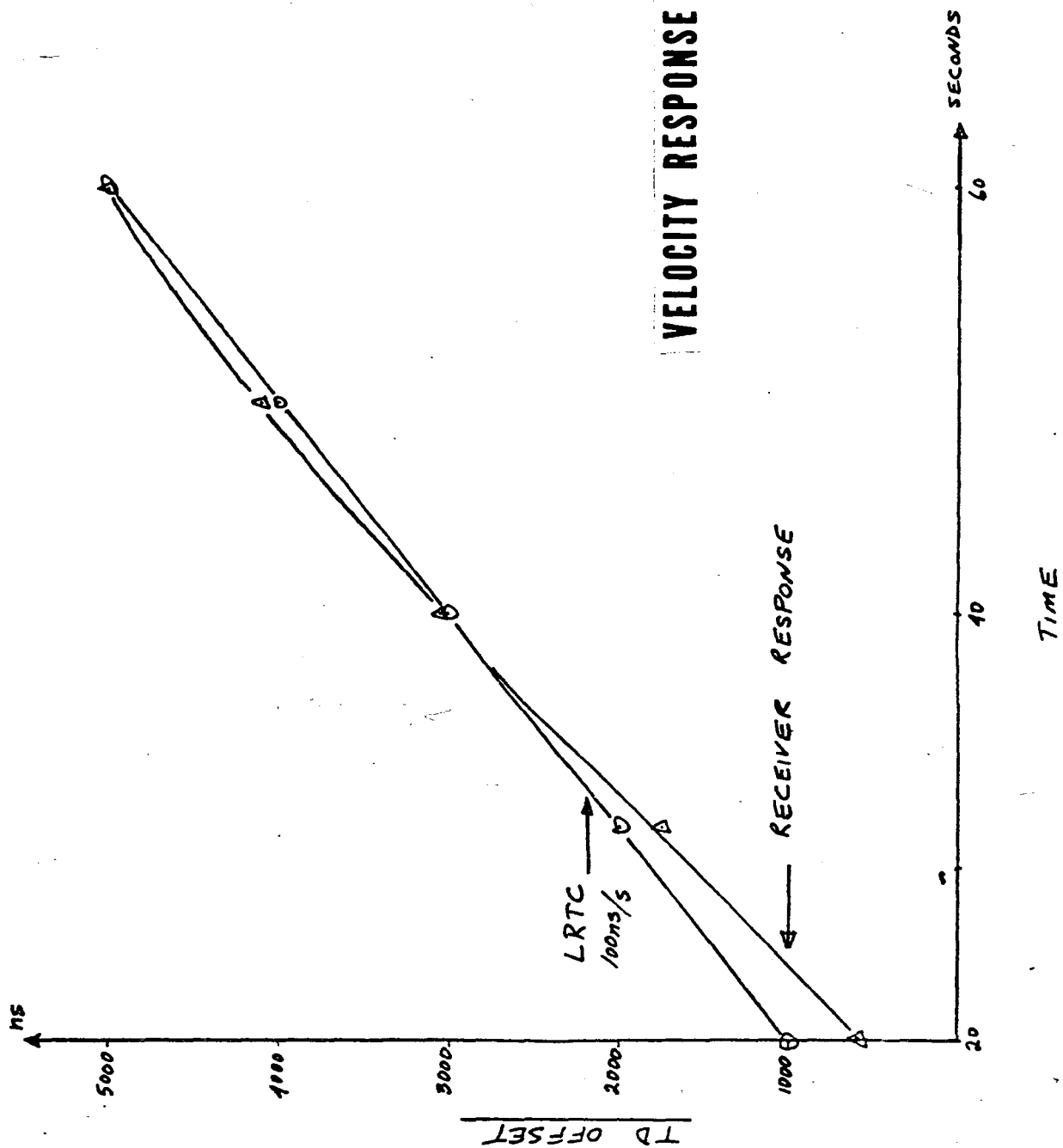
KEY: $\frac{A}{TDE} = \Delta$
 $\frac{A}{G_{TDE}} = \square$



NOTES: (1) SIGNAL LEVEL
 250mVrms SSP
 (2) EACH DATA POINT
 IS BASED ON 50
 STATISTICALLY INDEPENDENT
 SAMPLES.

SIGNAL - TO - NOISE RATIO TEST

VELOCITY RESPONSE TEST



I. Subj: 90% confidence intervals on σ for 50 independent samples.

$$L_{\sigma^2} = \frac{(n-1)s^2}{\chi^2_{[(1+\alpha)/2](n-1)}} = \frac{49 s^2}{\chi^2_{[(1+0.1)/2]49}}$$

$$U_{\sigma^2} = \frac{(n-1)s^2}{\chi^2_{[(1-\alpha)/2](n-1)}} = \frac{49 s^2}{\chi^2_{[(1-0.1)/2]49}}$$

$$L_{\sigma^2} = (0.8596 s)^2$$

$$U_{\sigma^2} = (1.2 s)^2$$

$$\Rightarrow \begin{array}{l} L_{\sigma} \approx 0.86 s \\ U_{\sigma} \approx 1.2 s \end{array}$$

II. Subj: 90% confidence interval on the mean for 50 independent samples.

$$L = \frac{\bar{A}}{\bar{X}} - t_{\alpha(n-1)} S_{\bar{X}}$$

$$U = \frac{\bar{A}}{\bar{X}} + t_{\alpha(n-1)} S_{\bar{X}}$$

$$\text{where } \alpha = (1+P)/2$$

$$P = \text{confidence level} = 0.9$$

$$\alpha = 0.95$$

$$S_{\bar{X}} = \frac{s}{\sqrt{n}}$$

$$t_{0.95(49)} = 1.677$$

90% confidence interval is then

$$\frac{\bar{A}}{\bar{X}} \pm \frac{1.677}{\sqrt{50}} s = \boxed{\frac{\bar{A}}{\bar{X}} \pm 0.237 s}$$

III References: (1) Oettle, Bernard. Statistics in Research. Iowa State University Press, Ames, Iowa: 1963, pp 70-100, 523-528.

(2) Crow, Edwin L., et al. Statistics Manual. Dover Publications, New York: 1960, p 242.

LIST OF ABBREVIATIONS

1. BCD: binary-coded decimal
2. BW: bandwidth (between -3 dB points of amplitude response for bandpass filters and DC to -3 dB point for lowpass filters)
3. CW: continuous wave
4. CWI: continuous-wave interference
5. DAC: digital-to-analog converter
6. DAS: Data Acquisition System
7. DFT: discrete Fourier transform
8. ECD: envelope-to-cycle difference
9. ETA: envelope timing adjustment
10. f_c : center frequency
11. FFT: fast Fourier transform
12. GRI: group repetition interval (e.g. for SS7, GRI = 99.3ms)
13. GRR: group repetition rate (GRR = 1/GRI)
14. LPA: local phase adjustment
15. LRTC: Loran Receiver Test Complex
16. MPT: multipulse Triggers
17. RF: radio frequency
18. rms: root-mean-square
19. ROF: Receiver Overhaul Facility, part of EECEN Navigation Receiver Repair Facility
20. s: standard error of the mean

LIST OF ABBREVIATIONS
(continued)

- 21. σ_{TDE} : standard deviation of time-difference error
- 22. SIR: signal-to-interference ratio
- 23. SNR: signal-to-noise ratio
- 24. SSP: standard sampling point
- 25. SW: skywave
- 26. TC: time constant (time for step response to go from zero to 63% of final value)
- 27. TD: time difference
- 28. TDE: time-difference error
- 29. \overline{TDE} : mean time-difference error
- 30. TOA: time of arrival

LIST OF DEFINITIONS

1.0 LORAN-C PULSE

Loran-C signals are transmitted in a band centered at a carrier frequency of 100 kHz with 99% of the spectral energy contained within the band of 90 to 110 kHz. The transmitted Loran-C signal is an electromagnetic signal having a pulse of the following form:

$$s(t) = A(t/t_p)^c \exp[c(1-t/t_p)] \sin(2\pi 10^5 t + \phi + \theta)$$

or $s(t) = f(t) \sin(2\pi 10^5 t + \phi + \theta),$

where $f(t) = A(t/t_p)^c \exp[c(1-t/t_p)]$ is the envelope shape between $t = 0$ and $t = t_p$

and A = function of distance from the radiating antenna and of propagation conditions

c = a constant, typically 1.5 to 2.0

t = time in seconds

t_p = time of the pulse peak, in seconds, typically 60 to 75 μ s

ϕ = the phase code, value = 0 or π

θ = the absolute ECD in radians, a function of transmitter settings and propagation path parameters.

For the W0512 LRTC Simulator, the pulse has the following form:

$$s(t) = A(t/65)^2 \exp(-2t/65) \sin(2\pi 10^5 t + \phi + \theta)$$

Each Loran-C transmitting station transmits a sequence of eight or nine pulses once each group repetition interval (GRI). In the sequence of eight or nine pulses, some pulses have 0° phase of the carrier, and others have 180° phase of the carrier. The pattern of 0° and 180° phase pulses (called the phase code) is dependent on whether the transmitting station is a master or secondary, and whether the particular GRI is designated an A or B interval. (A and B intervals alternate in time.) Pulses in a sequence of eight or nine

are separated by 1000 μ s except that the ninth pulse is 2000 μ s from the eighth and is used only to identify the master signal and to indicate master blink. Figure 1 gives the phase code for master and secondary in the A and B intervals.

Master Phase Code									
Interval	1	2	3	4	5	6	7	8	9
A	0	0	π	π	0	π	0	π	0
B	0	π	π	0	0	0	0	0	π
Secondary Phase Code									
Interval	1	2	3	4	5	6	7	8	
A	0	0	0	0	0	π	π	0	
B	0	π	0	π	0	0	π	π	

FIGURE 1

Loran-C Phase Coding

2.0 SIGNAL LEVEL OF A LORAN-C PULSE

The level of a Loran-C signal (a group of pulses from a single transmitting station) is the rms level of a CW signal having the same peak-to-peak amplitude as the Loran-C pulse envelope 25 μ s after the beginning of the pulse. The beginning of a pulse is the time at which the pulse envelope first exceeds 0.5% of the peak amplitude.

The level, when discussing electromagnetic fields, is expressed in decibels above one microvolt per meter (dB/1 microvolt/m). Otherwise, the level may be expressed in rms volts (V, mV, μ V) at the standard sampling point.

For example, a 25 mV rms CW signal has a peak-to-peak amplitude of 2.8×25 mV. Therefore, a 25 mV rms SSP Loran-C pulse would have a sampling point amplitude of 25 mV rms or a peak-to-peak amplitude of 71 mV. The amplitude of the pulse

(twice the sampling point amplitude for the LRTC W0512 Loran-C Simulator pulse) is then 142 mV peak-to-peak. The Loran-C pulse amplitude is defined at the standard sampling point, not at the peak of the pulse.

3.0 NOISE AND NOISE LEVEL

Simulated random noise will be considered to have a uniform power spectral density prior to filtering. After filtering by a single resonator L-C filter having a center frequency of 100 kHz and a bandwidth of 30 kHz, the noise level is the voltage generated across a 50 Ω resistive load, measured on a true rms voltmeter; this noise level is defined as the rms noise level, denoted by N. The filtered noise is then a bandlimited, jointly Gaussian random process.

4.0 LOCK-ON

Acquisition (or search) is the process which establishes the approximate location in time of the master and each of the selected secondaries and aligns the phase code. Acquisition, therefore, implies the action the receiver must take in order to determine the position of the master and selected secondaries relative to its internal timing. The accuracy with which this alignment is made is not critical in this mode. It is only necessary that the sampling strobes of the receiver be somewhere on the Loran-C pulse with the correct phase code alignment at the conclusion of the search mode. The settle process is defined as the procedure of identifying the correct cycle zero-crossing and establishing groundwave tracking. The receiver will be considered to be "locked on" when useful navigational information is available at the receiver outputs. $\text{Time to lock-on} = \text{time-to-search} + \text{time-to-settle} = \text{acquisition time} + \text{settle time}.$

5.0 ENVELOPE-TO-CYCLE DIFFERENCE (ECD)

Absolute ECD is the difference in μs between the envelope TOA and cycle TOA of a Loran-C pulse. Differential ECD is the difference between a secondary absolute ECD and master absolute ECD, or equivalently, differential ECD is equal to master-secondary envelope time difference minus master-secondary cycle time difference.

6.0 SIGNAL-TO-NOISE RATIO

The SNR is the ratio in dB of the Loran-C signal level, S, to the noise level, N.

7.0 SIGNAL-TO-INTERFERENCE RATIO

Interference may be considered as contamination resulting from CW, skywave, or cross-rate signals. Signal-to-interference ratios are defined as the ratio of the rms signal level of the Loran-C pulse to the rms level of the continuous interference or, in the case of cross-rate, to the defined SSP rms level. Note that the Loran-C pulse amplitude is defined at the sampling point, not at the peak of the pulse. All interference amplitudes are therefore referenced to the pulse sampling point. As an example, a 2.5 mV rms CW signal superimposed on a 25 mV rms SSP Loran-C pulse would yield a +20 dB signal-to-interference ratio, SIR.

8.0 UNITS FOR ENTRIES IN TEST TABLES

Most of the tests in this report have tables which list numerical values for all test parameters. The units of these numerical values are given in Table I.

9.0 SPACE COUPLING NODE

The space coupling node is the point of connection between the Loran-C simulator and the simulated antenna of a receiver. All signal, noise and interference levels are measured at this point.

10.0 LORAN-C SPECTRAL LINES

Periodic recurrence rates in the Loran-C transmission scheme give rise to discrete spectral lines which are distributed about the Loran-C carrier frequency of 100 kHz. The odd numbered pulses (1, 3, 5, 7) contribute spectral lines spaced one GRR apart (e.g., $SS7:GRR = 1.0/99.3 \text{ ms} \approx 10.0704 \text{ Hz}$) starting at 100 kHz and extending in both directions in the frequency domain. The even numbered pulses (2, 4, 6, 8) contribute spectral lines spaced one GRR apart starting at $100 \text{ kHz} + 1/2 \text{ GRR}$ and extending in both directions away from 100 kHz in the frequency domain. Thus, the even and odd spectral lines are interleaved with a spacing of $1/2 \text{ GRR}$ between each spectral line.

TABLE I

UNITS FOR TABULAR ENTRIES

TEST PARAMETER	TEST NUMBER											
	1	2	3	4	5	6	7	8	9	10	11	12
AIR TEMP	°C											
REL. HUMID.	%											
LINE VOLTAGE	VAC or VDC as appropriate											
GRI	ms											
M SIG. LEVEL		←										
M ECD	μs											
M SW LEVEL		←										
M SW DELAY	μs											
S _A SIG. LEVEL		←										
S _A ECD	μs											
S _A SW LEVEL		←	dB relative to 25 mV rms SSP									
S _A SW DELAY	μs											
S _B SIG. LEVEL		←										
S _B ECD	μs											
S _B SW LEVEL		←										
S _B SW DELAY	μs											
CRI LEVEL		←										
CRI GRI	ms											
NOISE LEVEL	dB/25 mV rms	(Gaussian noise, BW=30 kHz single resonator filter) centered @ 100 kHz										
I1 LEVEL		←										
F1	kHz											
I2 LEVEL		←										
F2	kHz											
I3 LEVEL		←	dB relative to 25 mV rms									
F3	kHz											
I4 LEVEL		←										
F4	kHz											
I5 LEVEL		←										
F5	kHz											
I6 LEVEL		←										
F6	kHz											
S _A TD	ms											
S _B TD	ms											
SAMPLE TIME	s											

APPENDIX A

SIGNAL INPUT TO THE RECEIVER UNDER TEST

A-1.0 SIGNAL INPUT TO THE RECEIVER UNDER TEST

Receiver acceptance test specification signal levels are usually given in terms of signal field strengths. However, the LRTC simulator output is a signal voltage at a 50 Ω output port, and is measured as a voltage signal level. It is not practical to generate a standardized field to couple to the antenna of the receiver under test for all the performance or acceptance tests. Therefore, an artifice is used to couple the simulator output directly to the antenna port of the receiver under test in a standard manner such that the simulator output voltage levels may be related directly to specified signal field strengths. The specified field strength (E_{sp}) is related to the voltage level at the simulator output port (space coupling node (SCN)) by the effective height (h_e) of the antenna,

$$e_{SCN} = h_e \times E_{sp}$$

The simulator output voltage, measured across a 50 Ω load, is adjusted accordingly. This is shown in Figure A-1.

The antenna capacitance to ground (C_A) may be measured using an RF bridge such as the General Radio Model 916-AL, or it may be specified by the manufacturer. It must be remembered that some receivers employ high-Q antenna couplers, and in these cases C_A must be within about ± 2 pF of the measured or specified value in order not to distort the bandpass characteristic of the antenna coupler.

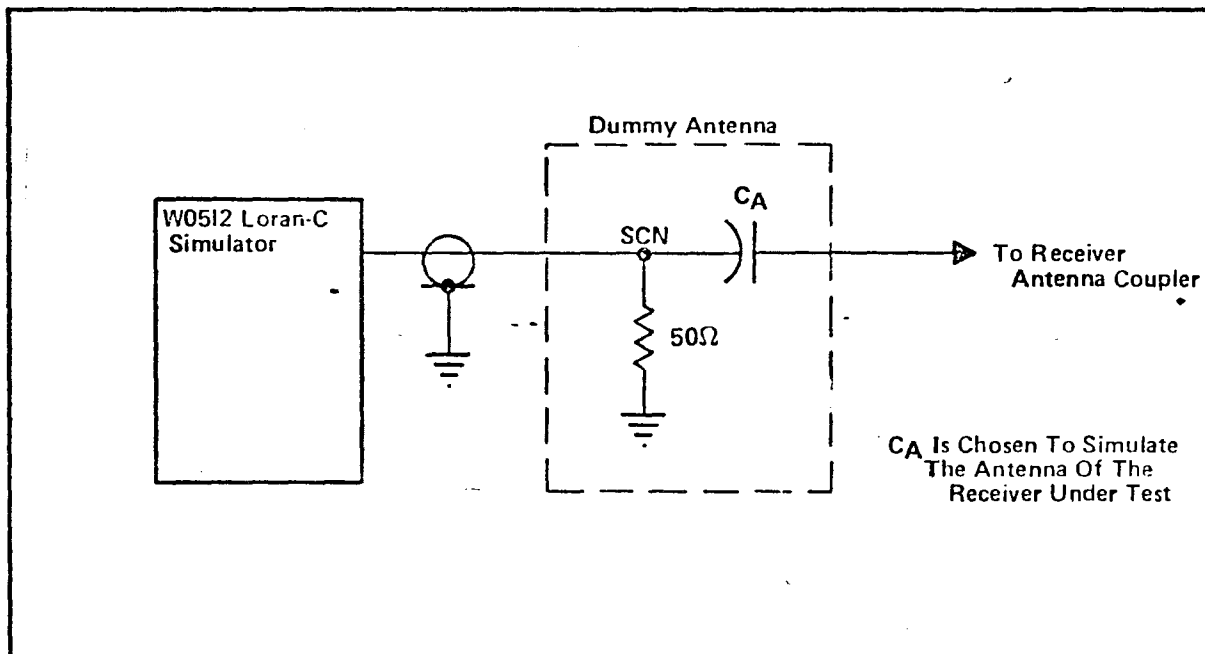


FIGURE A-1

LRTC Antenna Simulator
W0575 FINAL REPORT

APPENDIX B

DATA ACQUISITION INTERFACE REQUIREMENTS

B-1.0 DATA ACQUISITION INTERFACE REQUIREMENTS

The LRTC Data Acquisition System (DAS) accepts positive-logic, BCD, TTL-compatible data parallel by bit and parallel by character. Logic zero is 0 volts to +0.8 volts, logic one is +2.4 volts to +5.0 volts. The least significant four digits of the receiver-under-test BCD time-difference readout may be directly connected to the DAS input via a suitable connector (see Table B-I for cable type and pinouts). If the receiver TD outputs are binary, the DAS can be patched for octal or hexadecimal coding of the binary. Data in base 8 or base 16 can then be converted to base 10 and analyzed by computer. Alternatively, if BCD or binary outputs are not available, master and secondary sampling strobes can be buffered and connected via DAS relay contacts to an HP-5360A Computing Counter. The HP-5360A will measure the time-difference reading and present this information in BCD form to the DAS.

In addition to the 16 lines of data, a sample hold-off strobe must be generated to prevent DAS sampling during updating of receiver time-difference readouts. The sample hold-off line must be held at logic one until receiver updating is complete and the BCD readout of time-difference is once again steady. The sample hold-off line may not be held at logic one for more than 1 ms. Additionally, its duty cycle must be less than 5%.

Outputs from the receiver interface should be made with two, six-foot multiconductor cables, using the connector and pin positions specified in Table B-I. A schematic and associated timing diagram for a recent DAS interface is shown in Figure B-1.

TABLE B-I

LRTC DAS Inputs

Cinch Type 57-30240 Male Connector

<u>Pin #</u>	<u>Bit</u>		<u>Comments</u>
1	2^0	Least Significant Digit	Least Significant Bit, Least Significant Digit
2	2^1		
3	2^2		
4	2^3		
5	2^0	2nd Digit	Increasing Bit and Character Significance ↓
6	2^1		
7	2^2		
8	2^3		
9	2^0	3rd Digit	
10	2^1		
11	2^2		
12	2^3		
13	2^0	4th Digit	
14	2^1		
15	2^2		
16	2^3		
17			Sample Hold-Off Strobe
18			Do Not Use
19			Do Not Use
20			Do Not Use
21			Ground - Logic Return
22			VCC - +5.0 Volts
23			Do Not Use
24			Do Not Use

APPENDIX F

CALCULATIONS TO DETERMINE SERVO BANDWIDTH USING STEP RESPONSE DATA

F-1.0 CALCULATIONS TO DETERMINE SERVO BANDWIDTH USING STEP RESPONSE DATA

A. Assumption: That the servo system exhibits underdamped, two-pole dominant behavior. If this assumption is not applicable then this computation scheme is invalid.

B. Given: M_p = normalized maximum overshoot of step response (M_p greater than 0)

t_s = time in seconds required for the transient response to settle within 5% of its final value

C. Find: ζ = damping ratio (ζ less than 1)

f_n = natural frequency of the servo loop

f_B = -3 dB bandwidth of the servo loop

D. Procedure:

(1) Find ζ from

$$\zeta = \frac{\sqrt{\left(\frac{\log_e M_p}{\pi}\right)^2}}{1 + \left(\frac{\log_e M_p}{\pi}\right)^2}$$

(2) Find f_n from

$$f_n = \frac{3}{2\pi\zeta t_s}$$

(3) Find f_B from

$$f_B = f_n \sqrt{-(2\zeta^2 - 1) \pm \sqrt{0.995 + (2\zeta^2 - 1)^2}}$$

NOTE ON USE OF THE EECEN LORAN RECEIVER TESTING COMPLEX

1.0 GENERAL DESCRIPTION

As depicted in Figure 1, the Loran Receiver Testing Complex consists of two basic units, the Signal Simulator and the Data Acquisition System, (DAS). The Signal Simulator is further divided into the Analog Signal Unit (ASU) and the Digital Control Unit (DCU). The entire simulator is installed in a large, nonportable, three column rack. The DAS is mounted in one portable rack. The general functions of these units are described below, followed by descriptions of specific tests that can be performed with the equipment.

1.1 DIGITAL CONTROL UNIT (DCU)

The DCU generates Loran-C timing signals, for use by the ASU, from an external 5-MHz clock. The master and two secondary timing pulses are positionable in time to 0.02 μ s resolution with a time difference accuracy of better than 1 ns. The timing pulses for each signal may be independently controlled (in time) by manual input or automatic paper tape input. The paper tape input is used to control the frequency of slew commands to the unit (0.02 μ s/slew command) and hence controls the doppler, both sign and magnitude, for each master and secondary timing signal.

1.2 ANALOG SIGNAL UNIT (ASU)

The ASU is a modified AN/FPN-46 simulator with all of the digital circuits removed except the phase code logic. The ASU provides a master and two secondary pulses of 25 mV rms SSP (into 50 Ω) maximum amplitude. These signals are not passed through any frequency selective elements such as the original dummy antenna coupler. A skywave pulse or 25 mV rms SSP amplitude can be switched in with any master or secondary signal and positioned from 10 to 2,000 μ s behind the "groundwave." All pulse signals can be selectively attenuated from 0 to 60 dB in 1-dB steps. The master and secondary signals have independent ETA adjustments using circuits similar to those providing the ETA adjustment in the AN/FPN-44 transmitter. Thus, any absolute or differential envelope-to-cycle relationship may be entered on the ASU. Master, secondary and skywave triggers delivered to the "three-pole filter" (pulse forming network) are buffered to the front panel for use with an installed time interval counter to verify precise time relationships among the triggers. The ASU output signals are distributed to four 50-ohm unbalanced outputs via an A.R.I. Model AMC-8 Multicoupler.

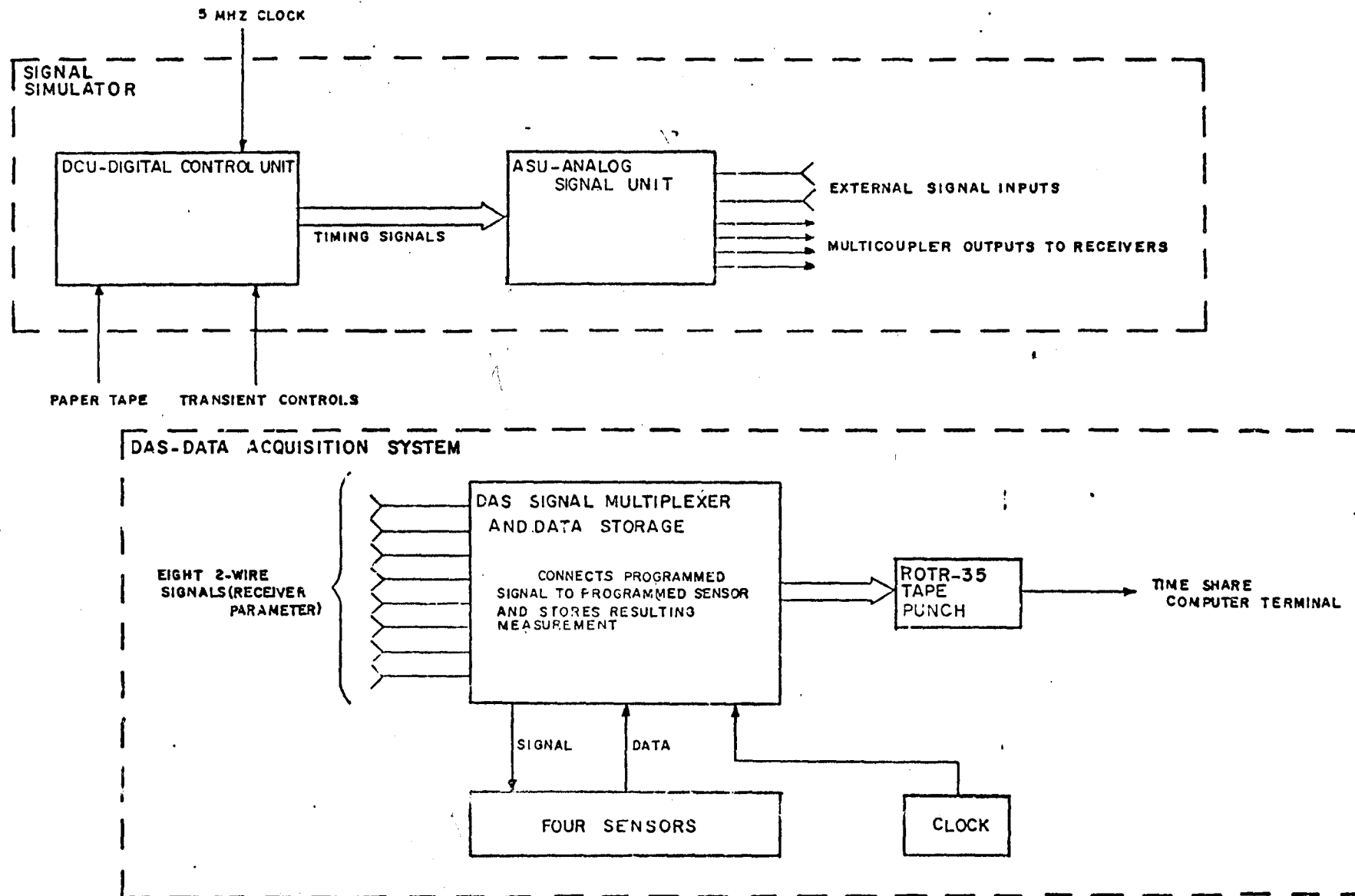


Figure 1
Block Diagram of LORAN Receiver Testing Complex
(LRTC)

1.3 DATA ACQUISITION SYSTEM (DAS)

The DAS consists of three basic parts; the signal multiplexer and data storage group, the four sensors or parameter measuring devices, and the data recording system. Eight, two-wire (common ground) independent signals of interest can be monitored on a time-shared basis. An external clock is used to establish and record time with other data. Any one of the sensors can be selected to measure any one signal or more than one signal provided the signal format for each is the same. The sensors provided are:

a. One HP5360A Computing Counter having 1 ns time-interval/period resolution. This counter is capable of measuring time, frequency, frequency deviation, etc. Its main advantage is its ability to perform mathematical operations on the "raw data" prior to computer processing. Some examples of the mathematical operations which may be performed are adding and subtracting of constants, multiplication by a scaling factor, etc.

b. Two CMC 901 Counters with 100-MHz time base.

c. Two Dana 4400 Digital Multimeters which can measure DC (to 10 μ V), AC (to 100 μ V), ohms (to 0.01 ohms) with four-decimal digit resolution and 20% overrange.

2.0 DETAILED DESCRIPTION

2.1 DIGITAL CONTROL UNIT (DCU)

The principle function of the DCU is to develop digital timing signals to generate the analog loran signals. In addition, the DCU provides the input point for stimulating the receiver via time-position modulation of the analog signals. This modulation is not communication modulation (introduced at the ASU) but rather represents off-line computer controlled modulation such as simulating platform movement or servo response testing.

2.1.1 TAPE READER

The tape reader is a 12 character, eight level, block reader manufactured by EECO. The reader uses light-sensitive diodes to detect the presence of a hole in the tape and provides a saturated transistor output whenever the hole is present. The tape used must be 95% opaque. The reader steps each block of 12 characters into the read position upon receipt of a positive going pulse (less than 10 μ s rise time) at the command input. Two front panel controls provide capability to reverse the direction of tape motion or slew the reader at its maximum rate of eight blocks per second. The data from the 12 character block is steady at the rear connector and ready for reading approximately 180 ms after the step command.

2.1.2 PROGRAM UNIT

The Program Unit accepts data from either the tape reader or front panel manual input digits, and outputs this data in proper format to control the Loran Timing Unit (LTU) digital phase shifters. The input data is in 9's complement form and represents the number of slew pulses to be delivered to the master or secondary phase shifter at that sample time. The slew pulses are emitted at 100-KHz clock rate and a total of 99,999 pulses may be programmed for any given sample time. The sample time base is front panel selectable as 0.2 second, 1 second, 2 second or 10 second, or manual pushbutton. Each sample pulse steps the tape reader, reads 9's complement data from either the reader or front panel and then outputs the indicated number of pulses. The sample rate is clocked off the system 5 MHz. Direction control is provided at the front panel or via the tape reader where the sign data is multiplexed onto the sixth level of the Least Significant Character of both the master and secondary data groups. This multiplexing produces alphabetic symbols in the Least Significant Character position of M and S control data.

2.1.3 PHASE TRANSIENT GENERATOR

The Phase Transient Generator provides periodic time position transients to the ASU via bursts of slew pulses and direction sense delivered to the LTU (in lieu of the program unit input). These pulses increment the LTU timing signals 1.28 or 2.54 μ s, hold them for a programmed time (either short to simulate an impulse, or long to simulate a step) and then return the timing signals to the original position. This transient recurs at a programmed rate up to maximum of once every 1600 seconds. The clock for both the periodicity and "width" of the transient is counted off M interval and hence the entire sequence is phase coherent with the Loran time base.

2.1.4 LORAN TIMING UNIT

The LTU is composed of three completely independent rate generators with 5-MHz inputs via independent 0.02- μ s resolution phase shifters. The master and two secondary signals are then recombined at the output to drive the ASU. The time delay of both secondary generators can be initially set to 1.0- μ s resolution (better than 7-ns accuracy). Incremental movement of each signal (so-called changes in the TOA of each signal) can then be controlled automatically as described above or manually by front panel pushbutton. All output waveforms

are available at a front panel jack for monitoring. In addition to the signals required for normal operation of the ASU, a time-shared and filtered 100-kHz signal is provided for use in the communication modulation circuits of the ASU.

2.1.5 OPERATION OF THE DCU

Operation of the DCU is straightforward as indicated by all front panel controls. Selection of certain parameters such as sample time increments for the tape reader are best considered within the context of the form of computer-aided analysis to be used with the resultant data. This is discussed in Section 3.0. The initial M-S time difference settings to be set in to the LTU should normally be an odd multiple of 5 μ s. This puts the resultant receiver reading in the middle of the DAS's character handling range.

2.2 ANALOG SIGNAL UNIT (ASU)

2.2.1 LORAN SIGNAL GENERATOR

2.2.1.1 The ASU is composed of a modified AN/FPN-46 simulator unit and various ancillary circuits. All vacuum tube power is supplied via an independent set of power supplies. The ASU generates three-groundwave signal groups from the time-shared MPT input signals. These triggers are re-locked to the communication modulated 100 kHz but are not re-locked to the normal 1 MHz. They pass from the modulation reclock directly to the "3-pole filter." The amplified output of the filter is sent to the time-shared attenuators for independent M/S amplitude control and then passed through the time-shared ETA circuit. This circuit shifts the phase of pulse carrier via a 10-turn gear reducer and front panel vernier control. Both secondary signals use one ETA setting, the master another. The signal is delivered from this unit to the multicoupler at a 50-ohm impedance level. Maximum signal amplitude is 25 mV rms SSP, minimum is 25 μ V rms SSP. Skywave signals can be generated in any or all intervals. The time delay of the signals is front panel controllable from 10 to 2,000 μ s. The delay is generated in analog fashion from the T/S MPT and hence follows any communication time-shift in these triggers. The phase code of the "originating" groundwave is maintained in the skywave by storing the sense of the phase code at the time of the groundwave MPT. The skywave pulse is generated by a COLAC pulse module at 25 mV rms SSP, passed through a 60-dB step attenuator and delivered to the multicoupler.

2.2.1.2 The original 30-kHz Gaussian noise source of the '46 simulator is retained intact in the ASU. The calibrated maximum output of this source is set to 250 mV rms at 50 ohms and delivered to the multicoupler (it is added to the simulator pulse signals at the multicoupler). The master and secondary interval waveforms are used to reclock the first MPT of each

signal as it is delivered to the three pole filter. This reclock signal is available at a front panel connector for monitoring the actual time delay of the signals generated by the three-pole filter. Similar monitoring of the skywave delay is also provided at the front panel.

2.2.2 ARI MULTICOUPLER

The multicoupler is an ARI Model AMC-8 which is modified to include a five-port passive summing junction (50 ohm) at the input. The multicoupler has -20 dB transfer from any input to any output, -44 dB transfer from any input to another input and -60 dB transfer from any output to another output. Three of the five input ports to the coupler are hardwired to the groundwave, skywave, and noise signal sources; the remaining two are available at the front panel. One of the front panel inputs can be operated as a continuous input or can be operated in a gated mode. The gate signal is the secondary interval waveform and is applied to a solid-state switch that connects the input port to the external source only during the interval. The port is grounded through a 50-ohm resistor at all other times. The signal present at the four output ports has a 25 mV rms SSP at 50 ohms. Assuming a typical 26-dB loss in a passive receiver coupler, the signal available at the receiver terminals can be varied over a 1.25 μ V to 1.25 mV range.

2.3 DATA ACQUISITION SYSTEM (DAS)

2.3.1 DESCRIPTION

The DAS is a self-contained instrument rack designed to acquire data on receiver performance via a number of sensors and store this data on a written and punched tape TTY record. A block diagram of the DAS is shown in Figure 1, Section 1.0. Eight independent parameters (time, voltage, current, resistance, frequency, time interval, period, events etc.) can be monitored on a cyclic basis and the data record generated from the samples taken. In effect these eight parameters can be viewed as time-slots; each slot may be used to monitor a given parameter. The basic sampling rate of the DAS is either one second per slot or 4 PRI per slot. Further provisions have been incorporated into the DAS to permit either of the basic sampling rates to be divided by any integer number up to sixteen. The digital result of such a parameter measurement can be stored in various registers; the register data can be displayed in real-time via D/A converters and the parallel array of register data from all such measurements can be scanned periodically by the data-intercoupler generating the TTY record. The periodic scan rate is determined via a front panel rotary switch and is variable from a maximum of once each sampling rate to a minimum of once per 100 samples.

2.3.2 OPERATING INSTRUCTIONS

a. Connection of analog signals (or pulses etc.) to the various sensors is done at the Program Unit front panel. Each time slot is defined there by a pair of contact closures connecting the IN jack to the OUT jack. Time slot 1 signal is connected to IN jack 1, time slot 2 to IN-2 etc.... The output jacks are then connected to the appropriate sensor in parallel if necessary (since all IN signals are isolated from one another by open contacts). The only precaution that must be observed here is that all signals delivered to a sensor must be in the same format, the Digital Multimeter for example cannot change operating mode between time slot 1 and 1+1.

b. The sensors must be programmed to sample in time slots consistent with their front panel signal connections. This sampling occurs 0.1 seconds after the time-slot is defined by front panel contact closure. Programming is done via patch cords on the matrix board Y. The time signals are present at the TIMING INPUT (e.g., time-1 is at G-H-18, 19, 20 of Y) points. These timing signals are connected up to SAMPLE COMMAND, connecting time slot 1 to sensor k as time slot 1 relay contacts are made on the front panel.

c. Four decimal characters worth of data (16 binary bits in 1-2-4-8 code) are brought down to matrix board W from each sensor and from the digital clock. This data is programmed to the eight, four character storage registers, with patch cords on W. Generally the four characters from each sensor are programmed into the register number corresponding to the time slot used to generate that sample. For example, if the HP 5360A was used in slots 1, 4 and 5 then patch cables would connect the HP data inputs to inputs to 4-character STORAGE REGISTERS, Reg 1, thence to Reg 4, thence 5.

d. The STORAGE COMMAND, overlapping matrices Y-Z, must be programmed by TIMING INPUTS to store the data patched to the corresponding storage register inputs in matrix W and X. This TIMING INPUT connected to STORAGE COMMAND causes the register to strobe the input data 0.2 seconds after the sensor was commanded to SAMPLE ((b) above). These connections must be consistent with the data patch done in (c) above.

e. The data stored in the various STORAGE REGISTERS may be displayed on chart recorders by programming OUTPUTS from 6 of the 8, 4-character STORAGE REGISTERS to the inputs of the 6, 2-character D/A converters. Six groups of data may be displayed, although only two characters from each group may be converted.

f. The data outputted to the TTY record is selected by programming the OUTPUTS FROM 4 CHARACTER STORAGE REGISTERS to 4 CHARACTER OUTPUT TO MUX in matrix Z. The data to the Data Inter coupler (MUX) can be arrayed in any order convenient for the record or subsequent computer analysis. Generally three decimal characters are programmed from each sensor's data group of four characters. This results in a data record of 24 characters per line. This length is consistent with TTY speed and the PRR sampling interval that generates an individual time-slot length of 0.4 second. A complete eight time-slot scan requires 3.2 seconds, within this time the TTY can print 32 characters, thus the 24 noted above, plus carriage return and line feed, allow a six character "saftey margin." This completes programming of the DAS.

2.3.3 DATA INTERCOUPLER (MUX)

The IRA^{Inc.} data intercoupler has a possible 40 character parallel data input capability. The MUX scans all input characters upon receipt of a command from the DAS Program Clock. This parallel input data is converted to serial ASCII format and a current drive line is connected to the TTY to record the data. The MUX must be internally programmed for the desired number of input characters and any additional characters such as sensor identifying labels, etc. Instructions for this program may be found in the IRA manual. To operate the unit the front panel switch is placed in RUN and the RESET button depressed.

3.0 COMPUTER CONTROLLED STIMULUS AND ANALYSIS

3.1 PROGRAMMING ROUTINES

There are 12 programming routines that are currently operational with the system;

a. /STATIST/ analyze input data from TTY punch tape record which is arrayed three characters per sensor, eight sensors across the page. The program is two-pass (thus not requiring statistical independence between samples) and computes, mean, variance and standard deviation of N points from the input record where N is specified by the operator.

b. /OSCILLATE/ generates numerical control tapes to stimulate the receiver via movement of the pulse TOA. Program generates equal amplitude harmonics at frequencies specified by the operator.

c. /TURNS/ generates numerical control tapes to simulate vehicle movement of the receiver. Maneuver is composed of two constant velocity (hence constant radius) turns where the angle of turn, acceleration and tangential velocity are specified by the operator. The resulting control tape also "stops" and "starts" the vehicle in constant acceleration maneuver.

d. /PROCESS/ re-formats standard three digit data from each sensor for use by a Fourier analysis routine (Cooley-Tukey algorithm). The number of points to be analyzed is specified by the operator.

e. /FTST/ Streamlined version of TYMSHARE's Fast Fourier Transform. Provides more efficient file structure, speeds execution and IN/OUT.

f. /DATAV/ Performs ergotic averaging of several synchronous data runs to enhance S/N information.

g. /FOURAVERAGE/ Provides averaging of Fourier Transform data for S/N enhancement.

h. /FOURSTAT/ Performs elementary statistical analysis similar to /STATIST/.

i. /REFORM/ Reformats DAS data for use with TYMSHARE's comprehensive statistical package.

j. /FOURTEST/ Translates DAS program tape to simulated Time Difference measurements compatible with Fourier Transform analysis. Used to calibrate DAS program tape without having to physically test it on the DAS.

k. /FASTPROCESS/ Performs same functions as /PROCESS/ except the eight DAS data channels are taken as sequential observations of a single parameter. Permits analyzation of data of a single parameter at eight times the normal sampling rate.

l. /LINEFIND/ Determines synchronous and non-synchronous interference frequencies for a given GRI.

3.2 OPERATING CONSIDERATION

The basic problem in using the simulation/analysis capabilities of the system lies in understanding basic analog-digital relationships. These are outlined briefly below:

a. Statistical analysis; the sampling period should be chosen long enough so that there is very little correlation, while it does not introduce biases in the sample statistics, does enlarge the confidence limits on a given statistic. For example, 100 independent samples with Gaussian distribution will allow one to estimate the mean of that distribution to within one dB of the true mean with 99% confidence. If every other sample has 0.5 correlation with the previous one, then the effective number of independent samples decreases to about 75 which raises the confidence limit to 1.5 dB. Sample correlation is a function of servo bandwidth generally one correlation time is one servo time constant.

b. Receiver stimulation via numerical control tapes; the Nyquist sampling criterion must be satisfied in this case. The sampling period of the tape reader defines some upper frequency ($1/2$ of $1/T$ tape sample) that can be reproduced by the TOA movement. The only errors in the numbers sampled and stored on the reader are quantization errors due to the $0.02\mu s$ discrete phase shifter interval. Thus sample aliasing is not a major problem and probably a sufficient rule of thumb is to insure that stimulation signals have all frequency components below $1/2$ of the upper Nyquist frequency defined above.

c. Receiver output sampling; when the receiver's response to various types of stimulation is being measured with the DAS care must be taken to insure that the Nyquist criterion is not violated and that the data record length is appropriate to the stimulation and analysis desired. For example the lowest Fourier fundamental obtainable from a data record of N points sampled every T time units is $1/N*T$ cycles per time unit. Non-redundant Fourier data points from such an analysis are provided up to $((N-2)/2)*1(N*T)$ cycles per time unit. If the receiver stimulus also contains wide-band noise, the Nyquist frequency of the DAS should be set well beyond the expected servo bandwidth to guard against sample aliasing of the noise. This guard band should probably be set at a factor of 4-5 times the servo bandwidth.

02 06

P. 10-11

SEP 1974



PROCESSED BY THE
FEDERAL BUREAU OF INVESTIGATION
U. S. DEPARTMENT OF JUSTICE

RECEIVED
SEP 19 1974

U. S. DEPARTMENT OF JUSTICE
FEDERAL BUREAU OF INVESTIGATION
WASHINGTON, D. C. 20535

100-101010-101
100-101010-102

Figure 3 - Cumulative Amplitude Probability Distribution of Atmospheric Noise Observed at Eglin Thru the 101 Receiver System Wideband And Narrowband Filters In Late Afternoon (Reference Key)

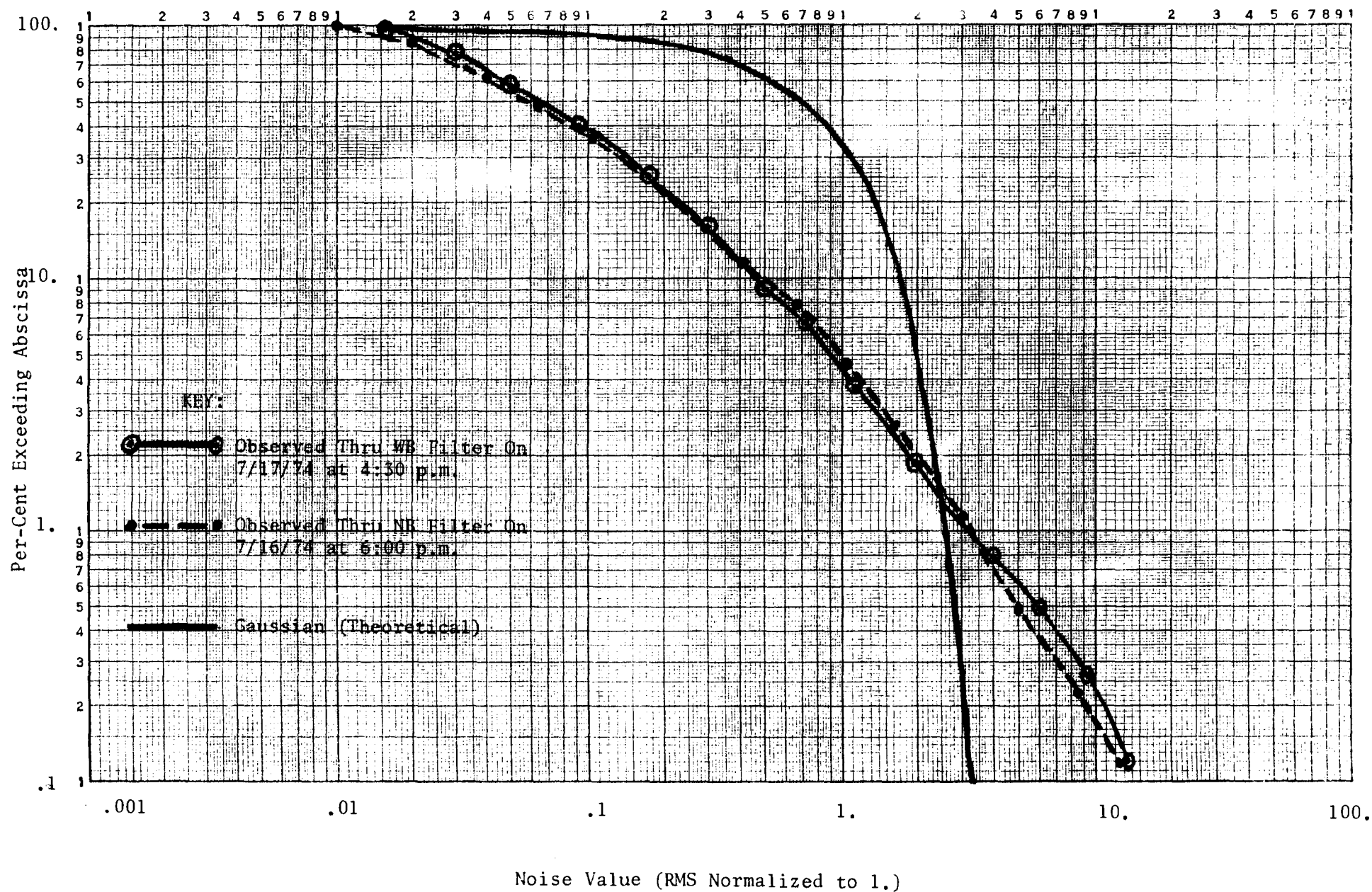


Figure 4 - Cumulative Amplitude Probability Distribution Of Frontal Atmospheric Noise Observed By Feldman on August 11, 1971 at Wildwood, Ner Jersey.

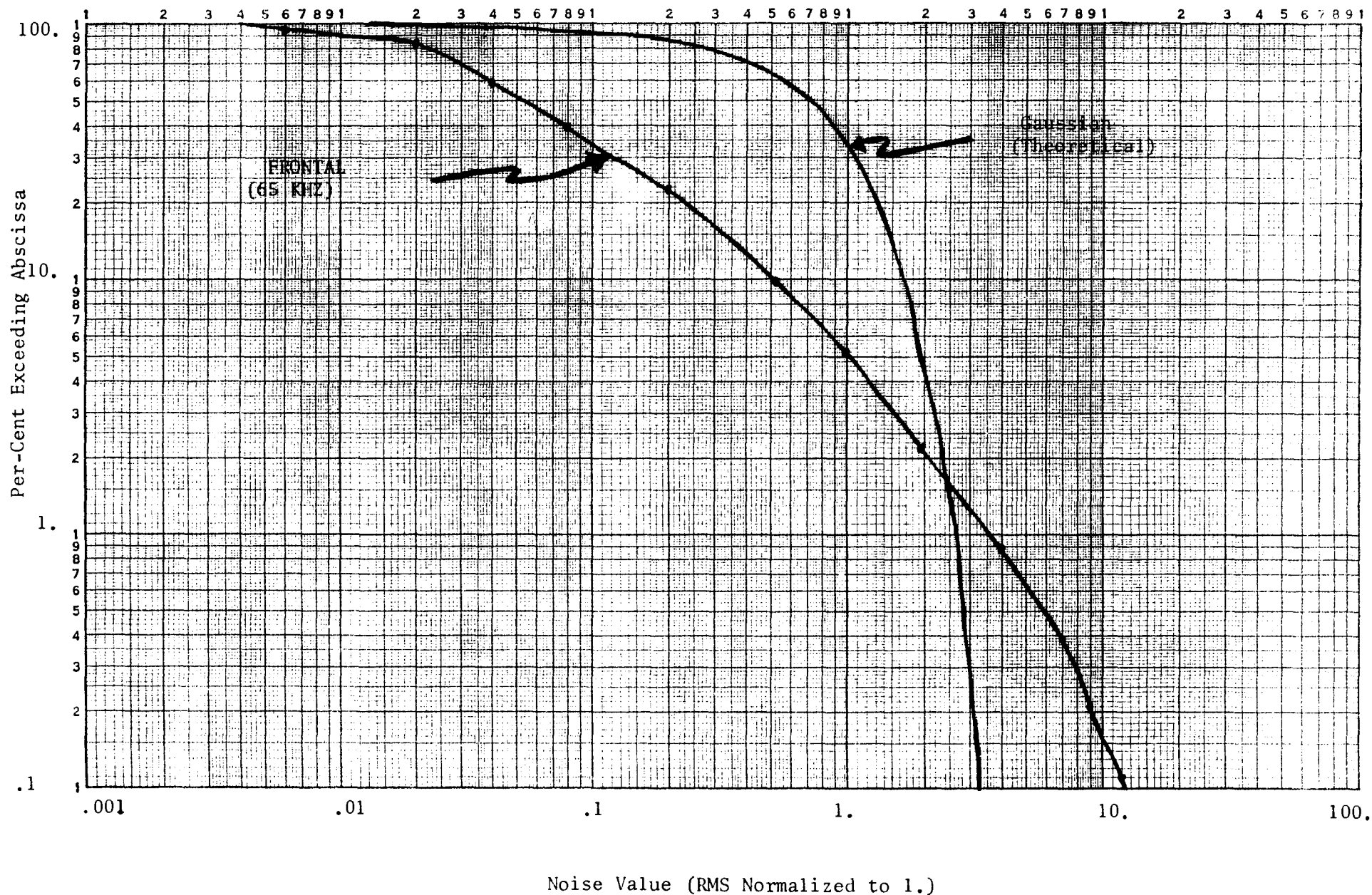


Figure 5 - Cumulative Amplitude Probability Distributions Of Different Types of Noise Data Derived Via Simulation From the Atmospheric Noise Model of Reference 1.

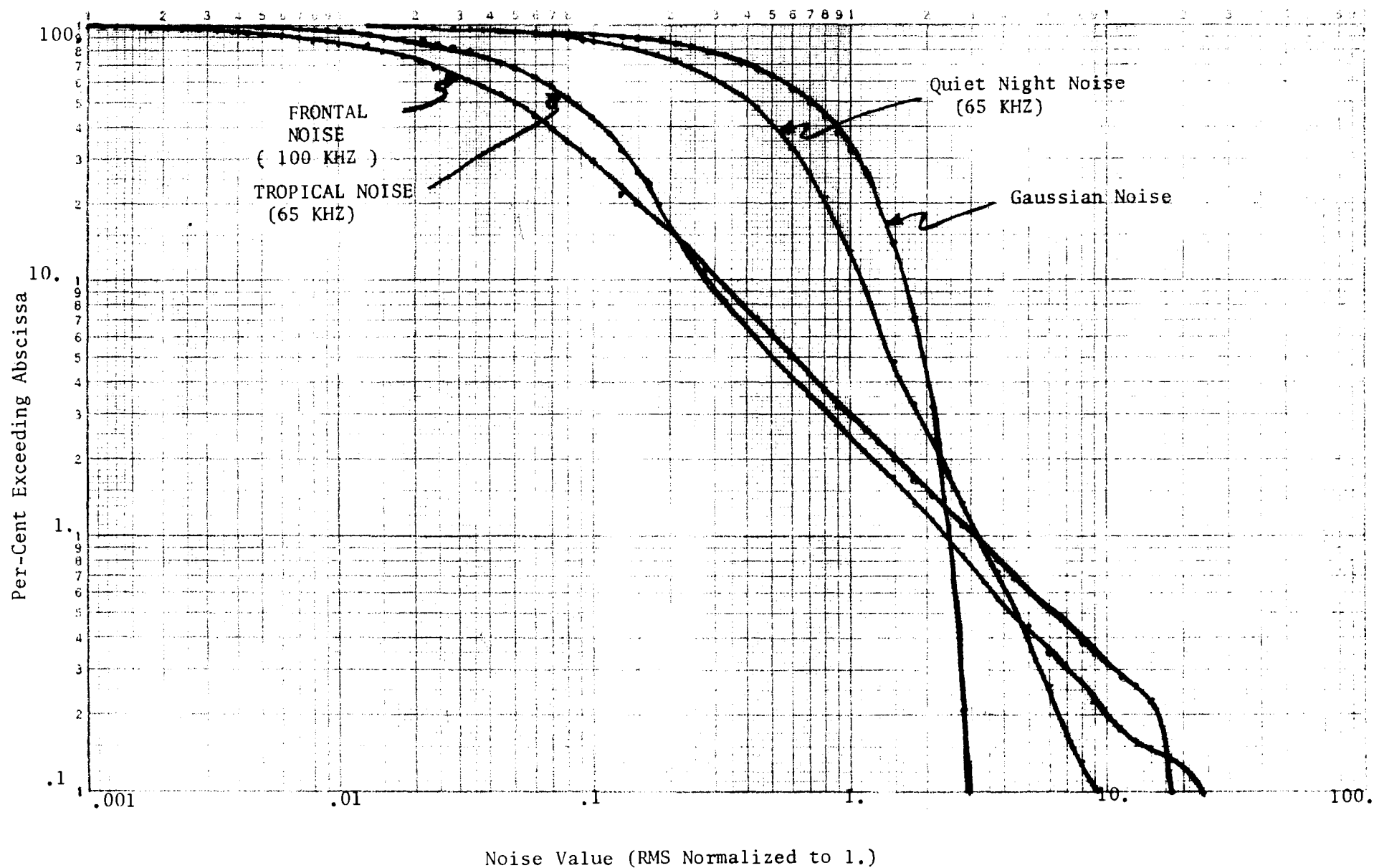
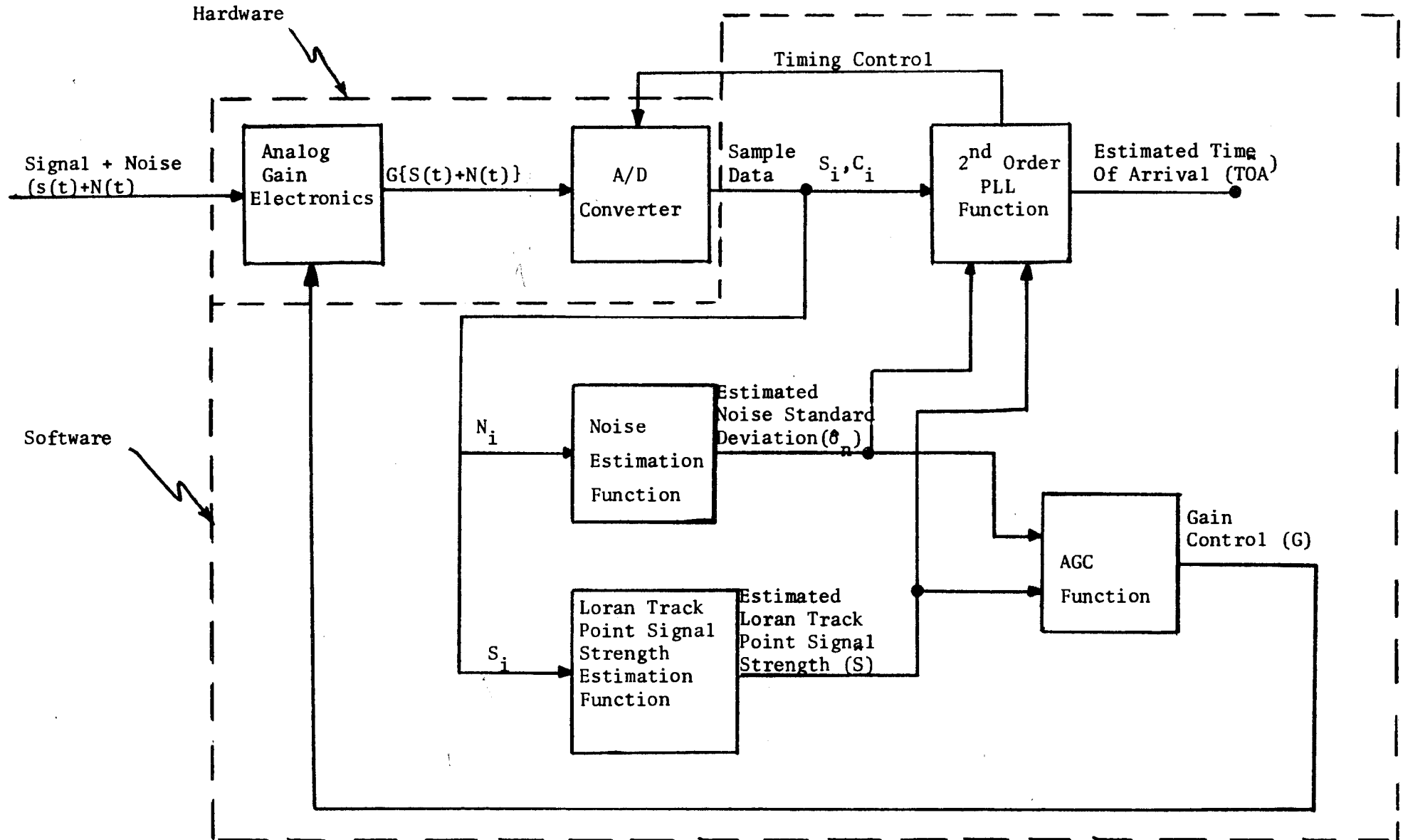


Figure 6 - Simplified Model Of The 101 Receiver System Tracking Function.



- NOTES:
- (1) N_i designates noise sample data
 - (2) C_i designates track point zero-crossing sample data
 - (3) S_i designates track point RF peak sample data

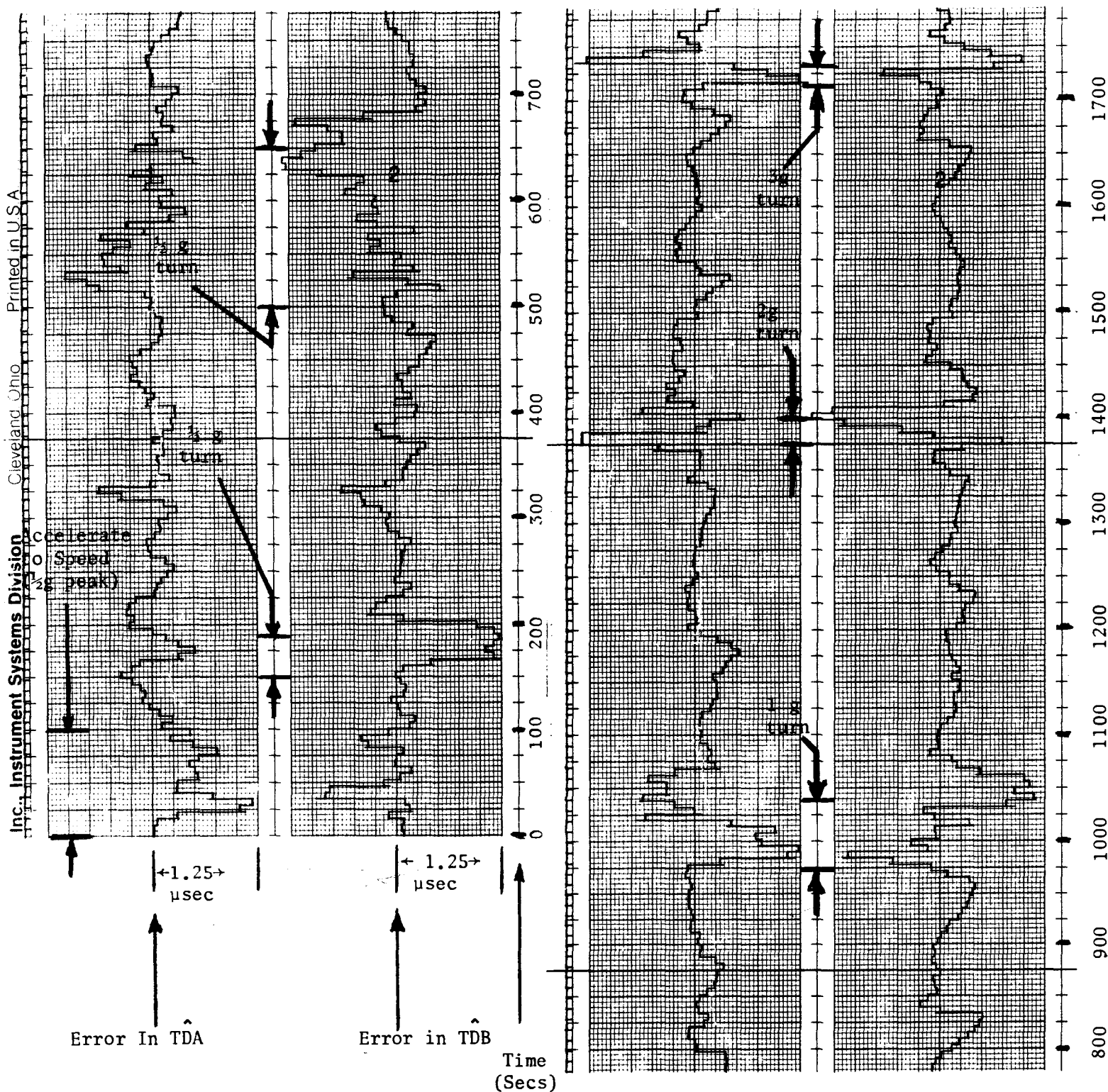


Figure 7 - Errors In the Receiver's Estimated Time Differences (TDB, TDB Under Dynamic Flight Conditions Without the 30_{nc} Software clipper. Track point S/N is -23 db. Noise type is frontal.

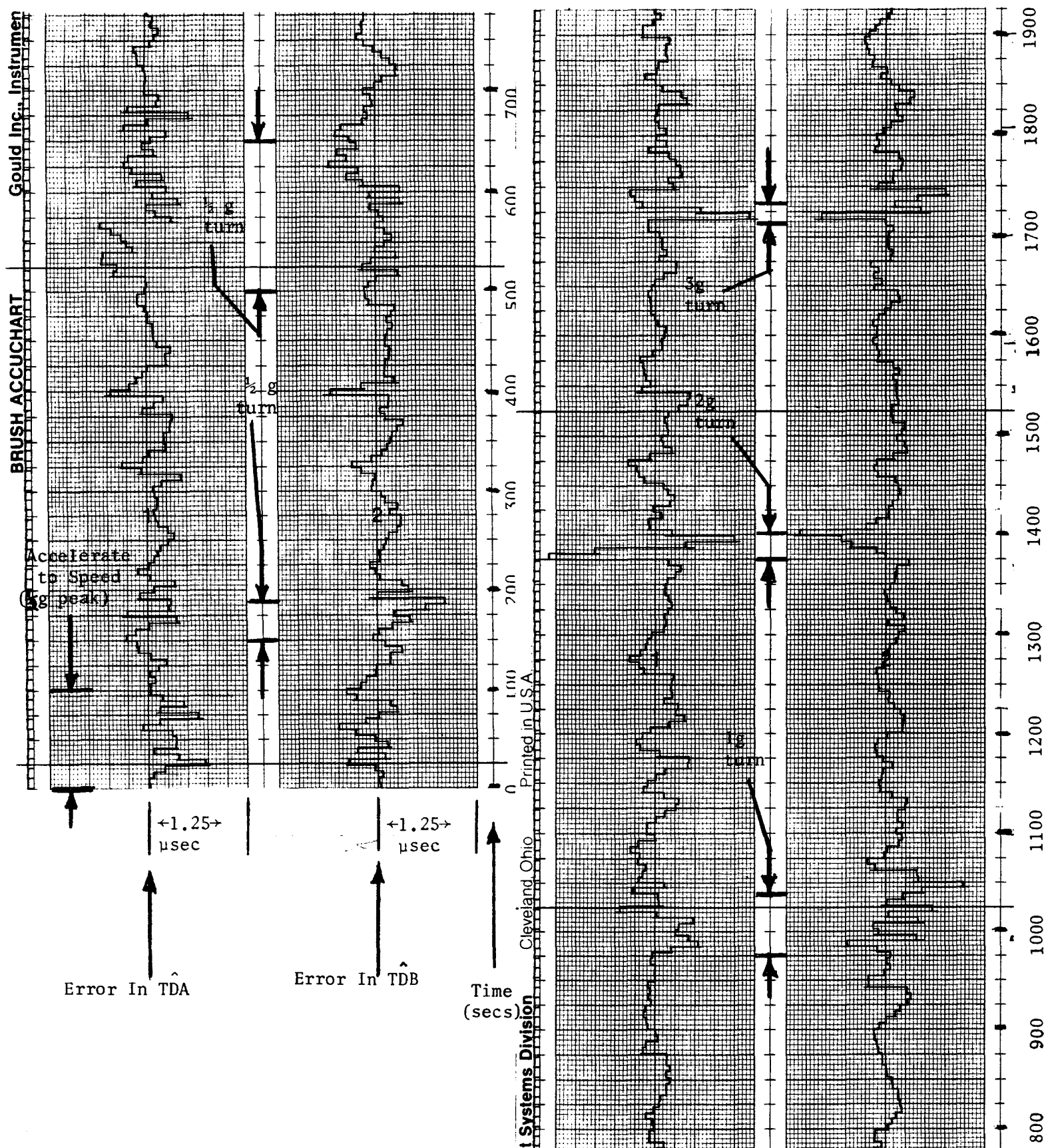


Figure 8 - Errors In The Receivers Estimated Time Differences (TDA, TDB) Under Dynamic Flight Conditions With The 30^{nc} Software Clipper. Track point S/N is -23 db. Noise type is frontal.

References

- (1) "An Atmospheric Noise Model With Application To Low Frequency Navigation Systems", Doctoral thesis by Donald A. Feldman performed at Massachusetts Institute of Technology and dated June, 1972.

FILE COPY
3-15

NOTES:

USCG LORAN-C
RECEIVER TESTING

NO F.
#15
1974 3RD

LCDR W. SCHORR
COMDT (C-EEE-4/63)
US COAST GUARD
Washington, DC 20590
202-426-1193

3 October 1974
GREY GORGE, NJ
1973 Wild Goose
Annual Convention

FEHLNER
REF 606
PP 38
PAPER 315
7-840012

TEST PLAN DESCRIPTION

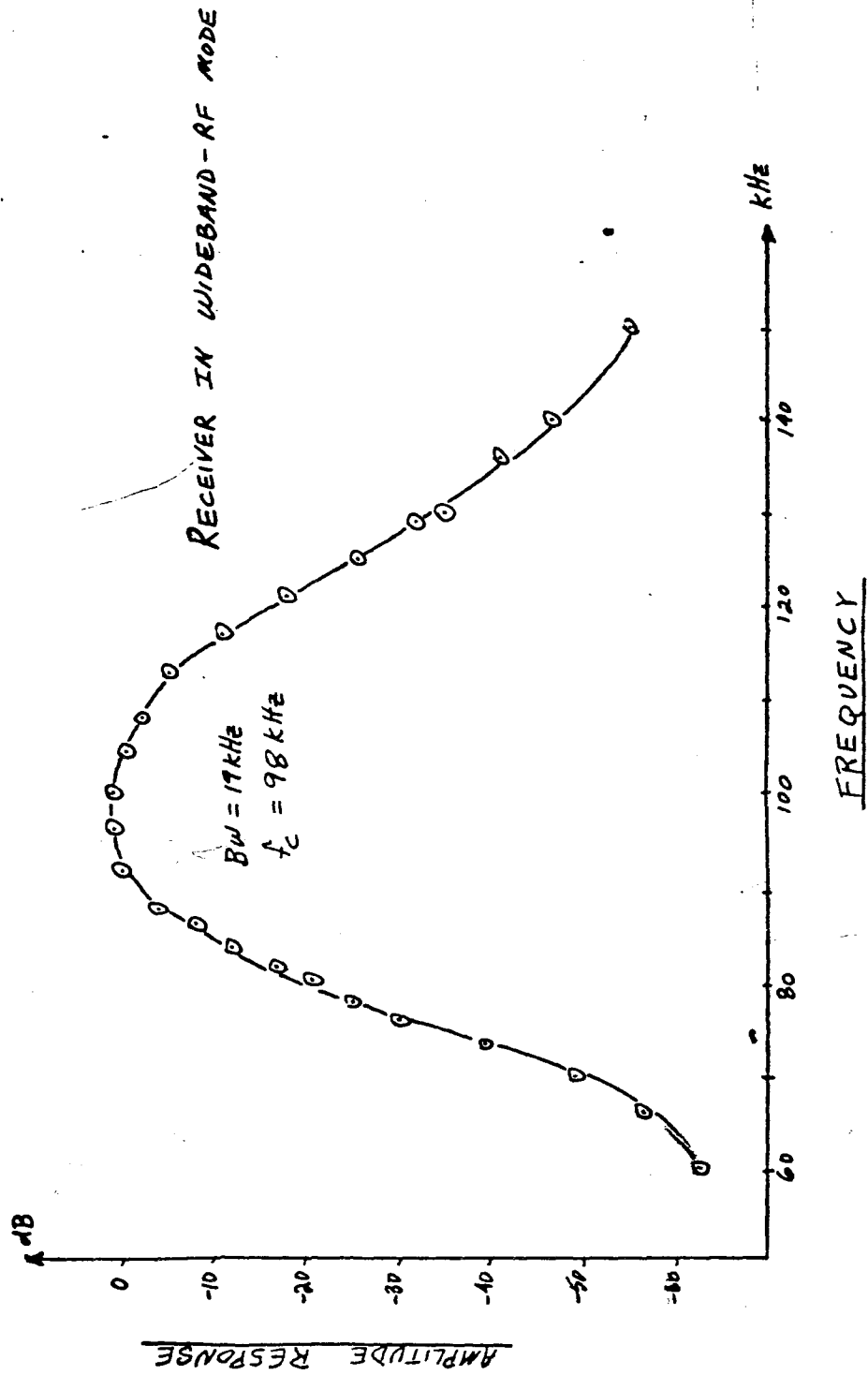
A. GENERAL PROCEDURES

1. Interfacing the receiver with the LRFC
2. DAS sample period considerations
3. Measurement of signals
4. Data reduction
5. Miscellaneous consideration

B. SPECIFIC TESTING PROCEDURES

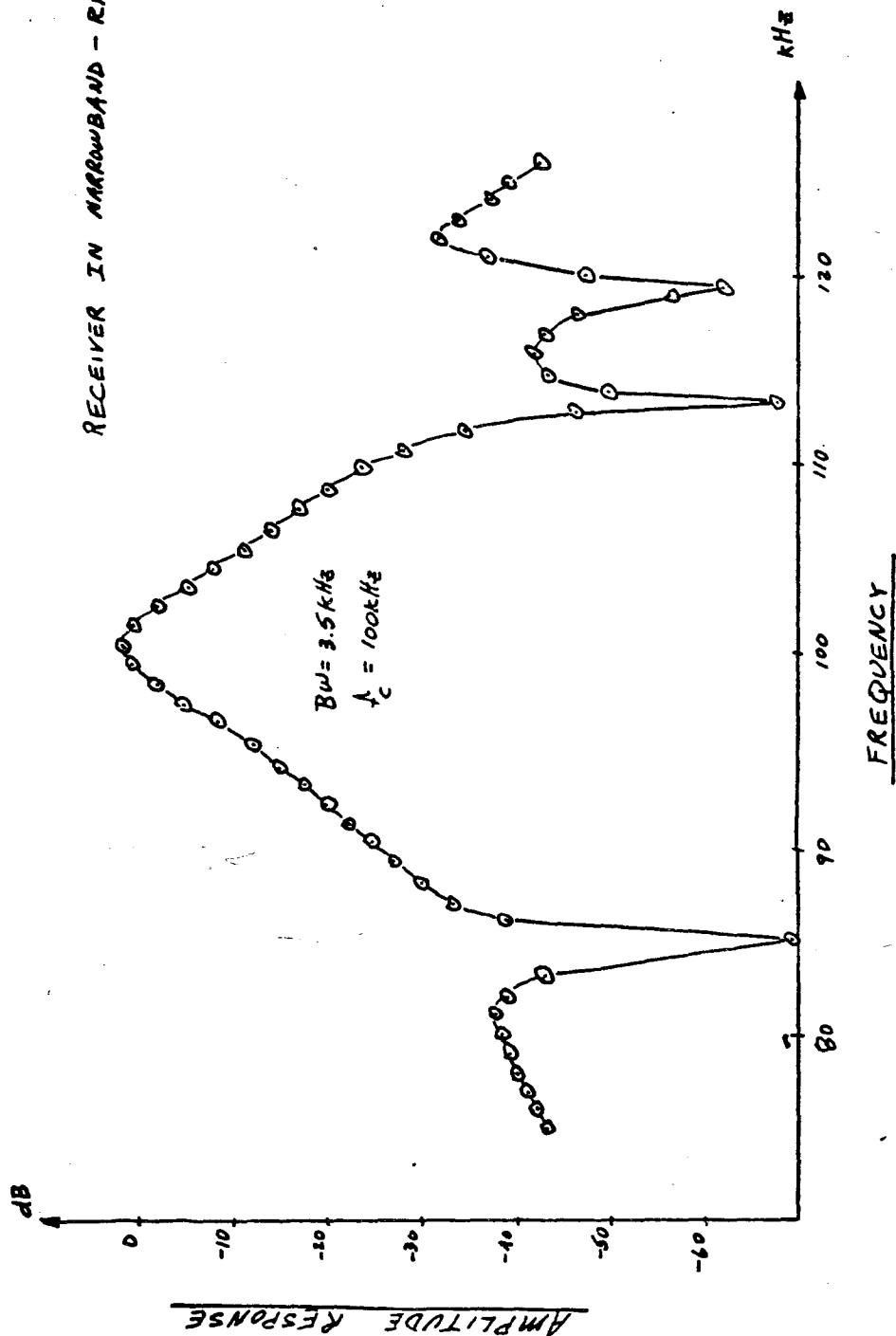
1. RF response
2. Notch filters
3. Lock-on as related to signal conditions
4. Envelope channel transfer characteristics
5. Servo loop bandwidth
6. Absolute signal level
7. Differential signal level
8. Noise performance
9. CW interference
10. Skywave contamination
11. Crossrate interference
12. Slow-rate test
13. On-air signal test
14. Alarm circuits
15. Receiver power supply
16. Reliability, maintainability, and repairability
17. Human engineering factors

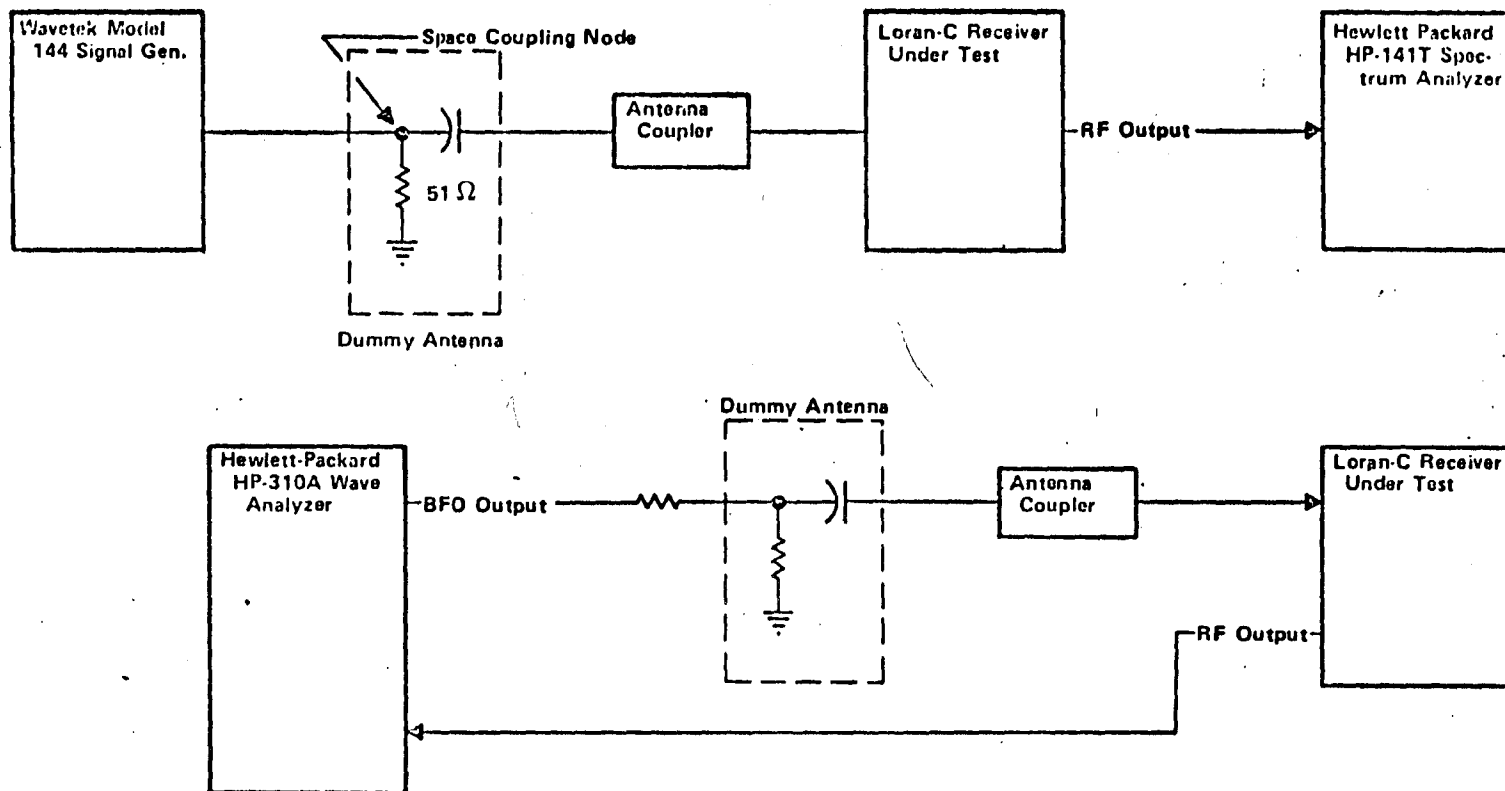
RF BANDPASS CHARACTERISTIC



RF BANDPASS CHARACTERISTIC

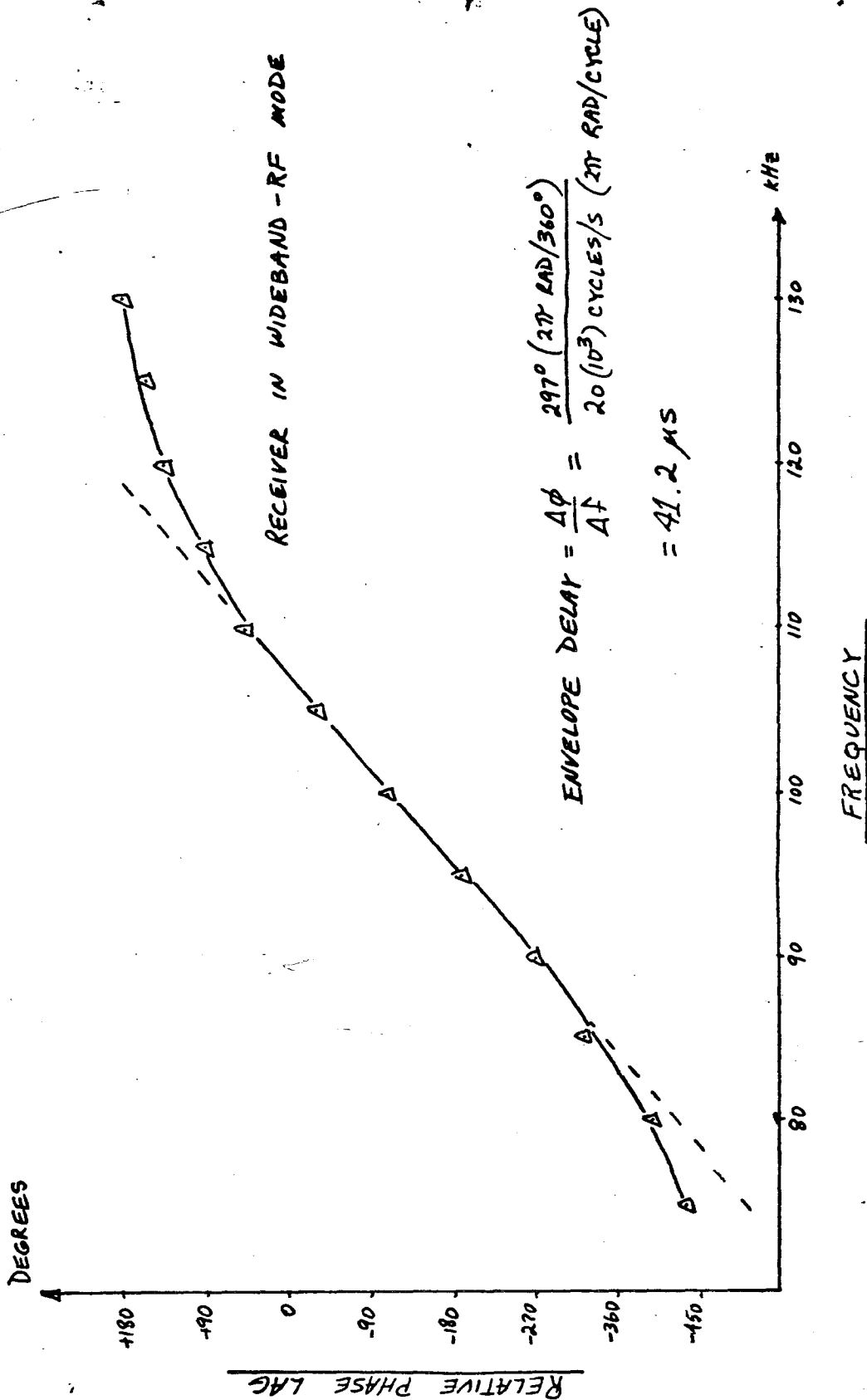
RECEIVER IN NARROWBAND - RF MODE

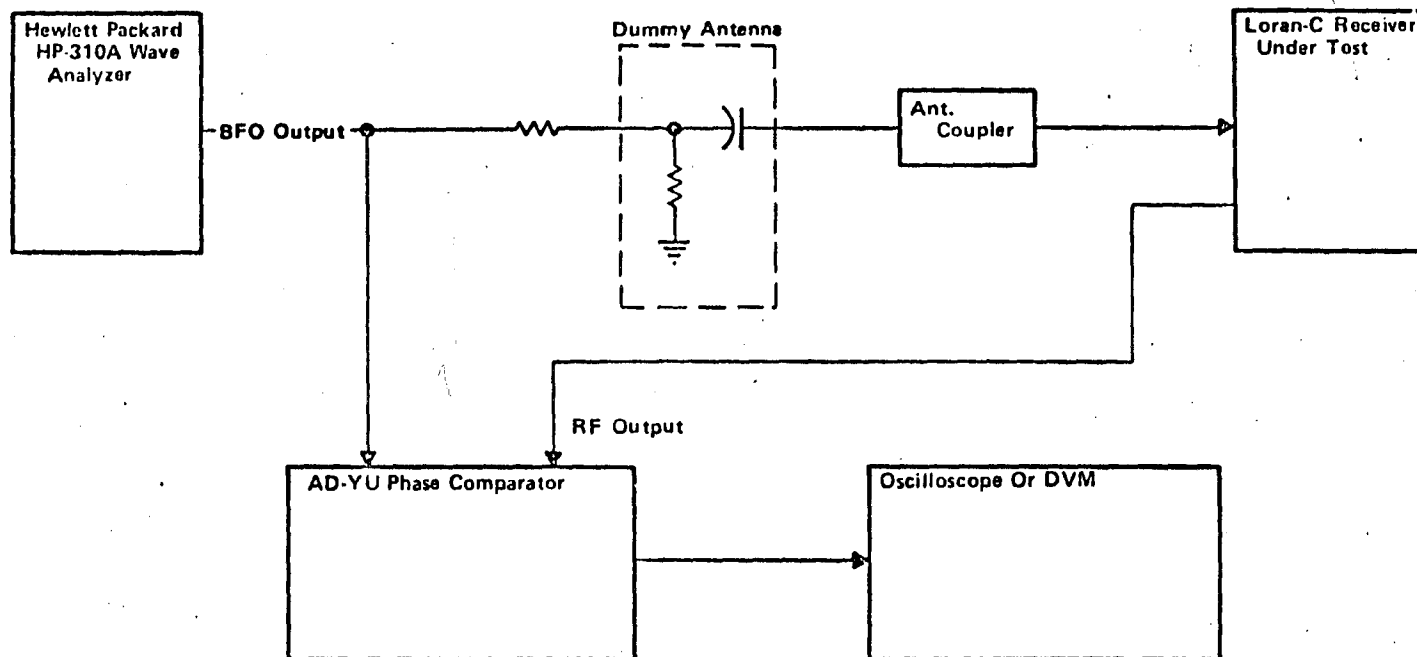




LRTC RF Bandwidth Test Setups

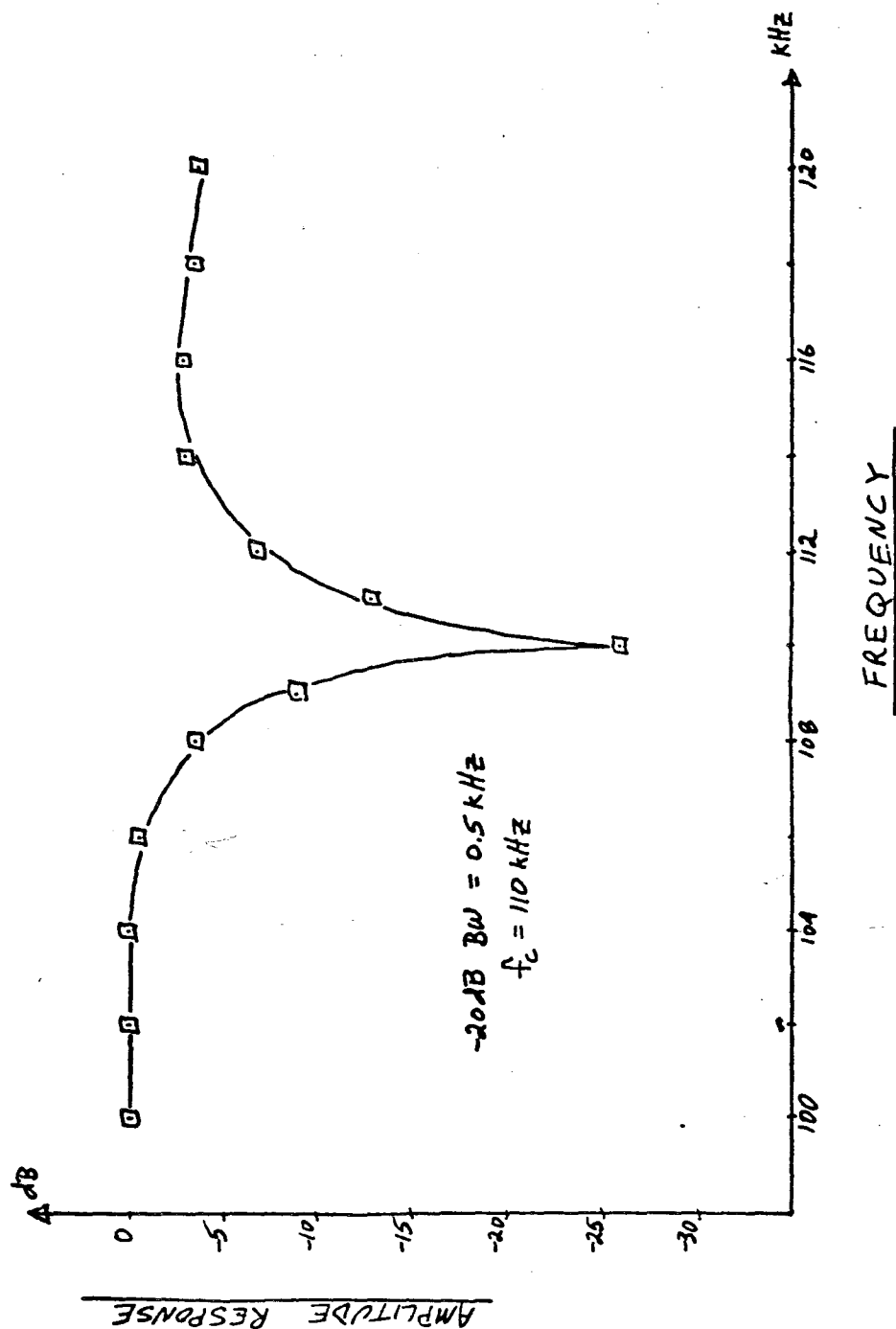
RF PHASE RESPONSE

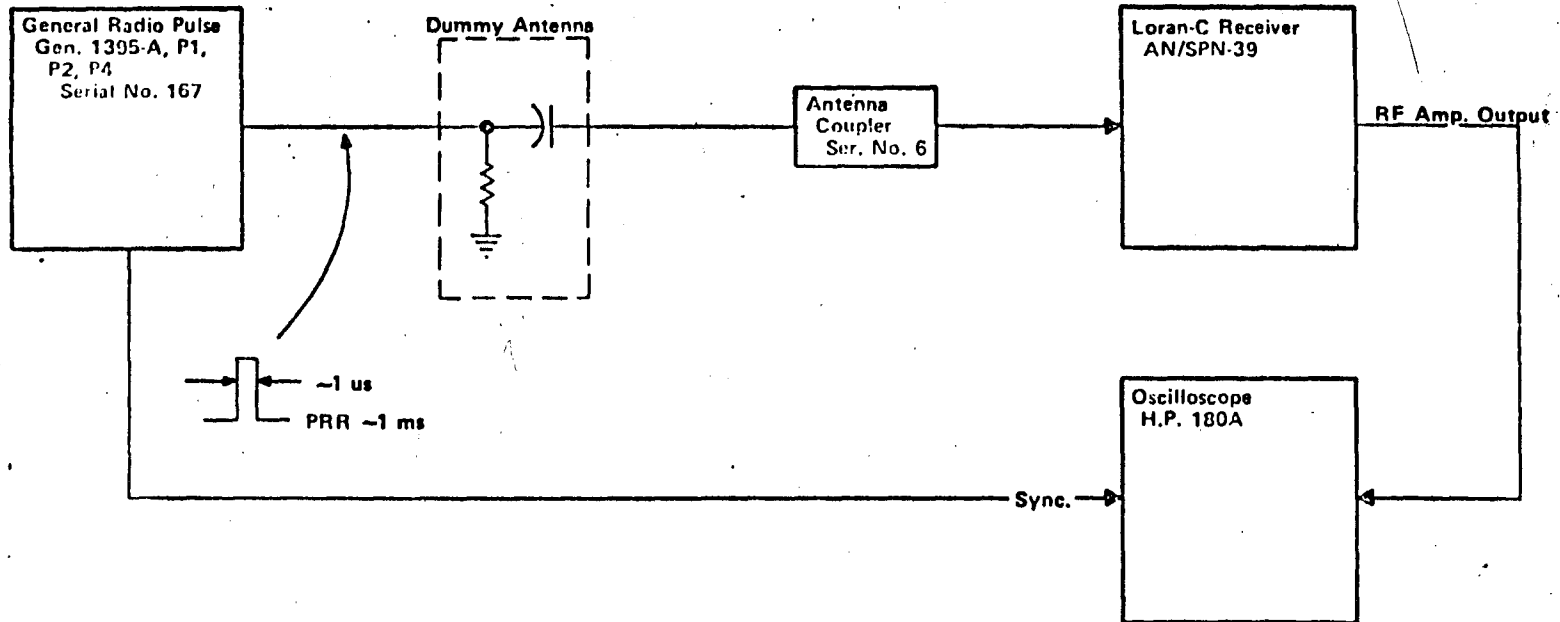




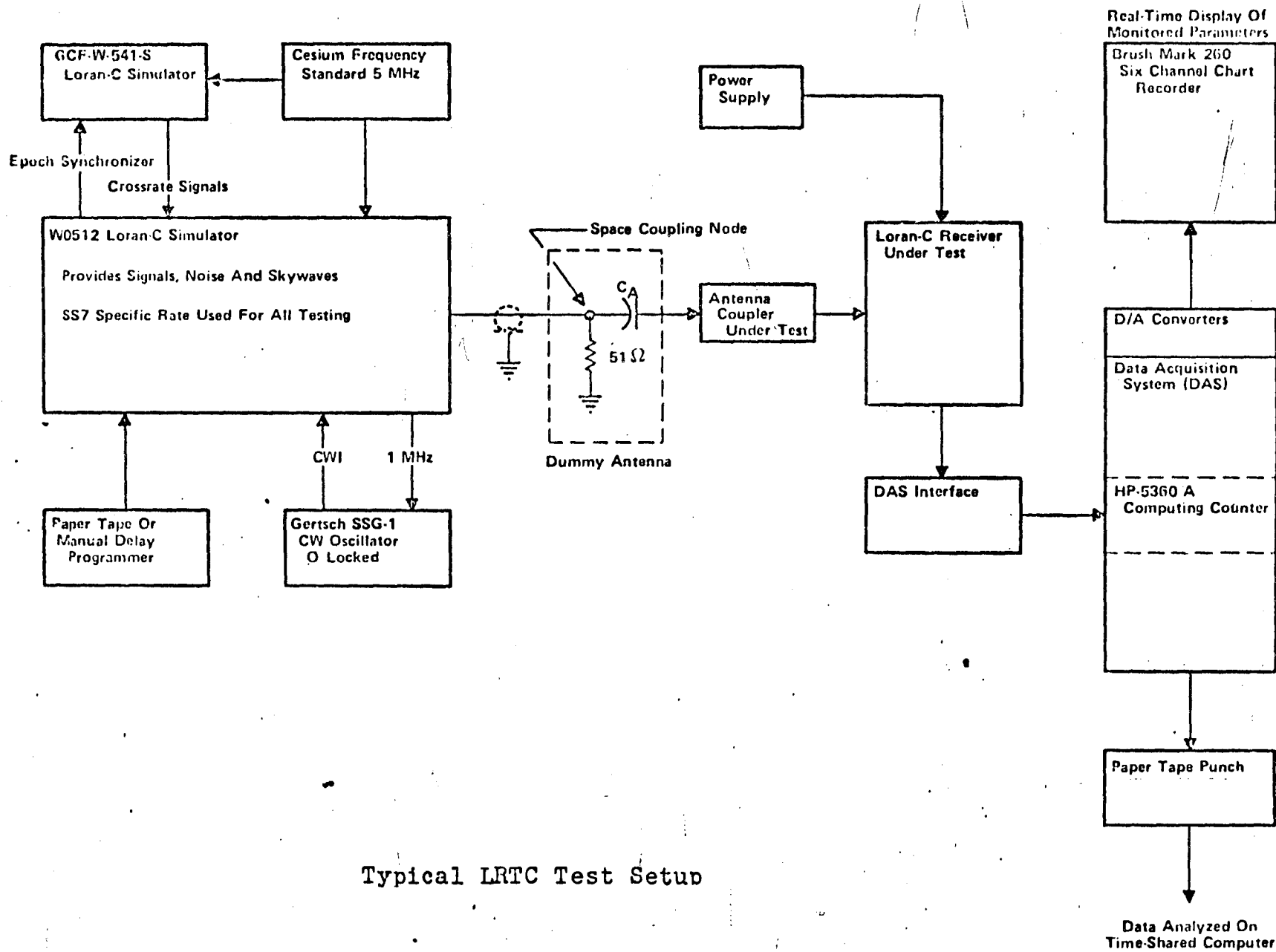
Typical LRTC Test Setup For RF Phase Response

NOTCH FILTER RESPONSE



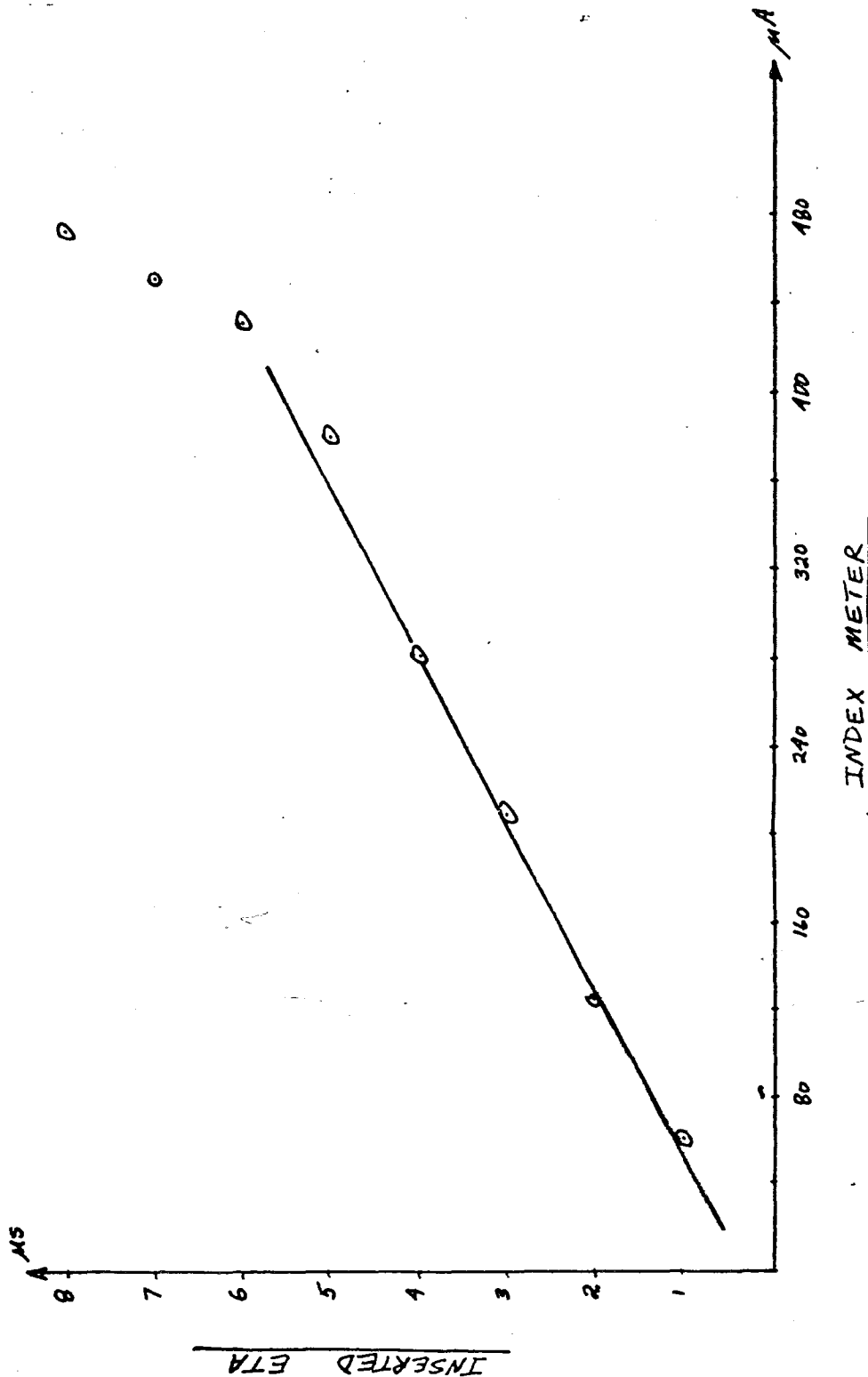


Impulse Response Test Setup

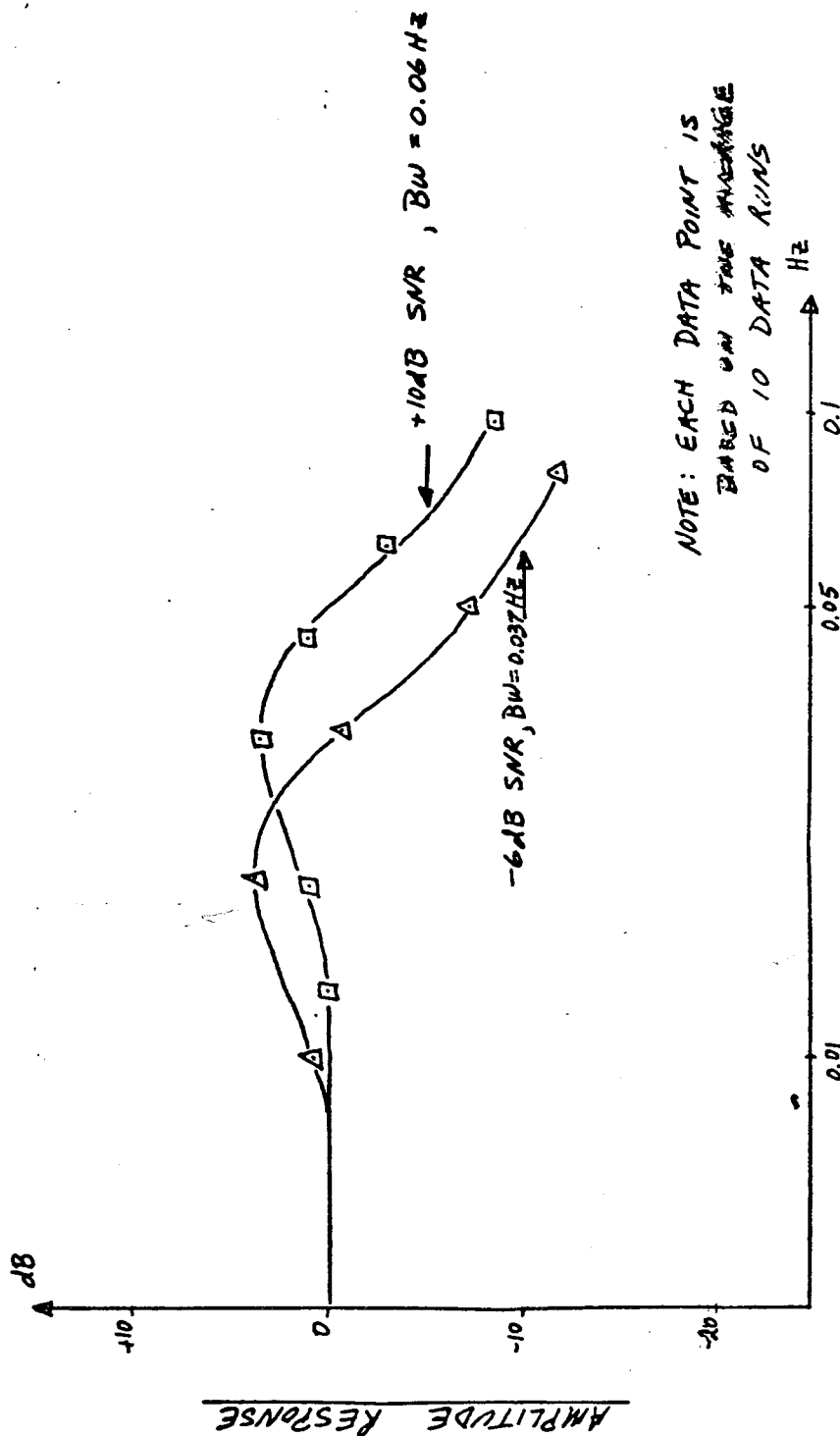


Typical LRTC Test Setup

ENVELOPE CHANNEL TRANSFER CHARACTERISTICS



PHASE SERVO RESPONSE

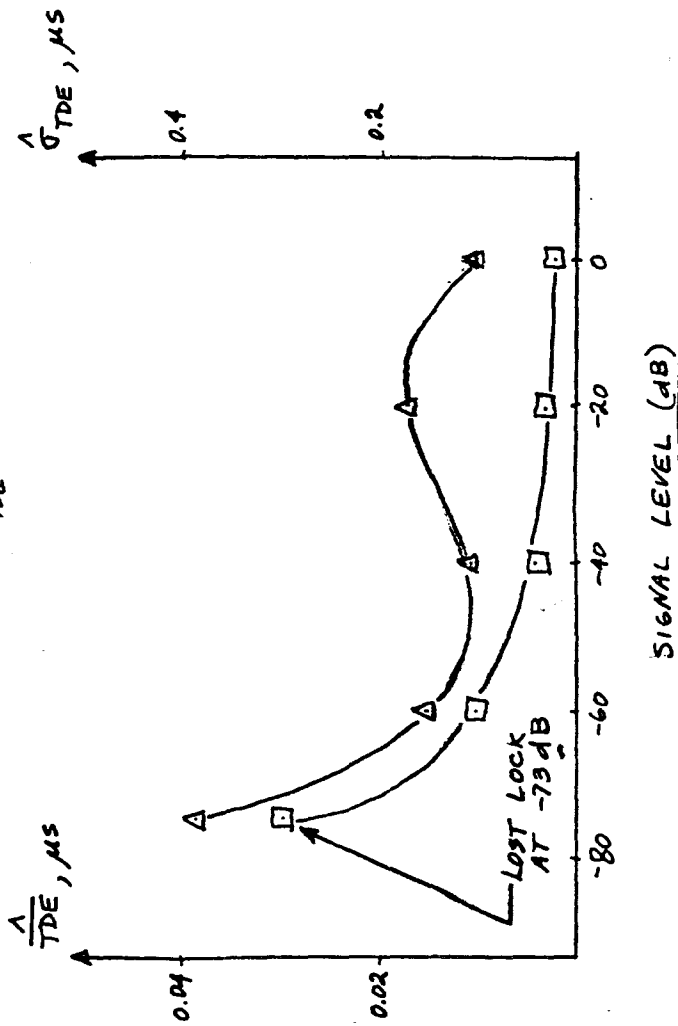


NOTE: EACH DATA POINT IS
BASED ON THE AVERAGE
OF 10 DATA RUNS

FREQUENCY

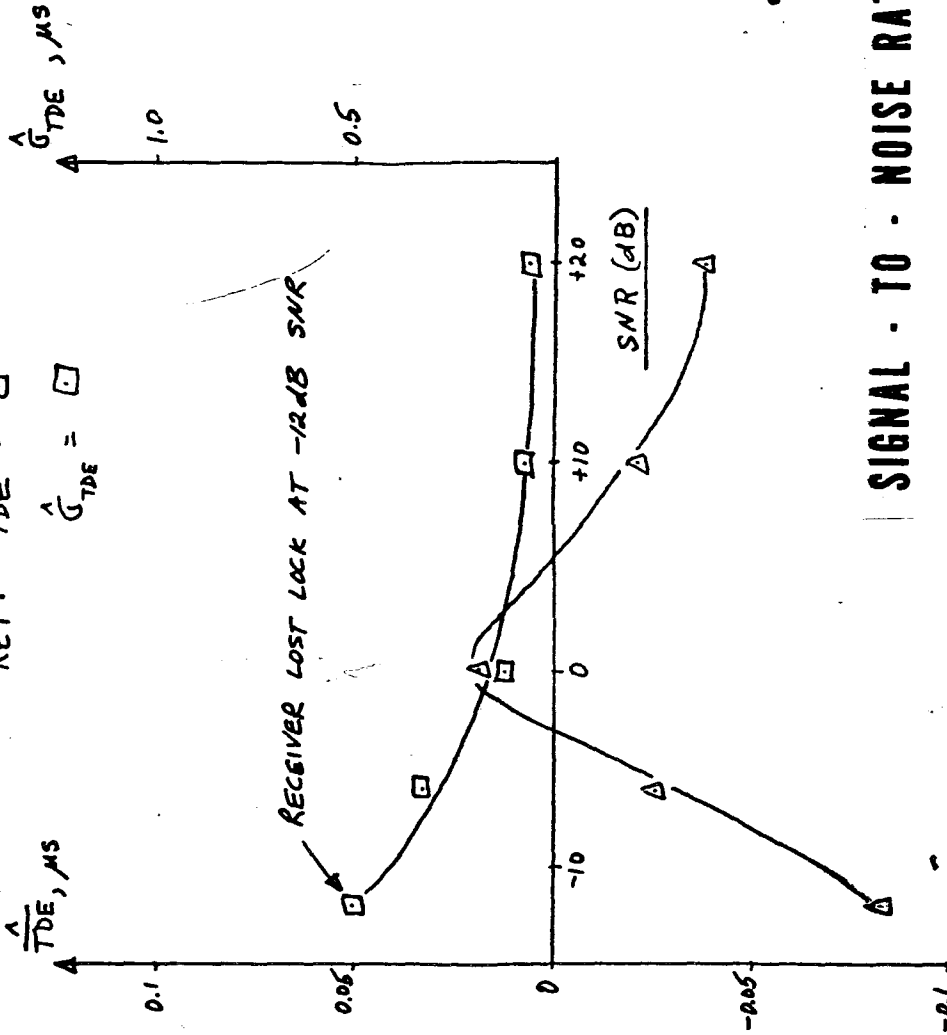
ABSOLUTE SIGNAL LEVEL TEST

KEY: $\frac{\lambda}{TDE} = \Delta$
 $\frac{\lambda}{G_{TDE}} = \square$



NOTES: (1) OdB = 25mVrms SSP
 (2) EACH DATA POINT IS BASED ON 50 STATISTICALLY INDEPENDENT SAMPLES.

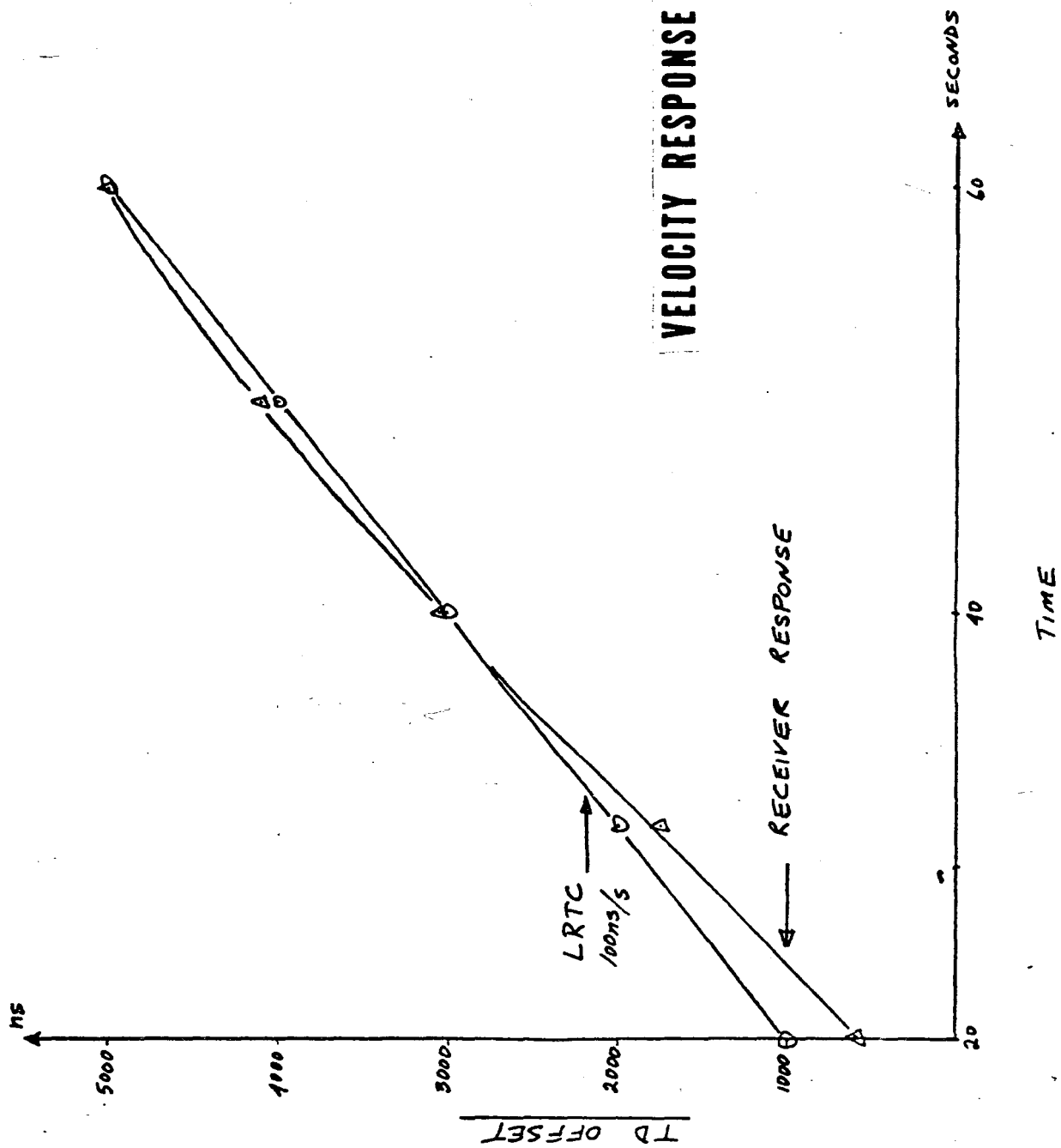
KEY: $\frac{A}{TDE} = \Delta$
 $\frac{A}{G_{TDE}} = \square$



NOTES: (1) SIGNAL LEVEL
 250mVrms SSP
 (2) EACH DATA POINT
 IS BASED ON 50
 STATISTICALLY INDEPENDENT
 SAMPLES.

SIGNAL - TO - NOISE RATIO TEST

VELOCITY RESPONSE TEST



I. Subj: 90% confidence intervals on σ for 50 independent samples.

$$L_{\sigma^2} = \frac{(n-1)s^2}{\chi^2_{[(1+\alpha)/2](n-1)}} = \frac{49 s^2}{\chi^2_{[(1+0.1)/2]49}}$$

$$U_{\sigma^2} = \frac{(n-1)s^2}{\chi^2_{[(1-\alpha)/2](n-1)}} = \frac{49 s^2}{\chi^2_{[(1-0.1)/2]49}}$$

$$L_{\sigma^2} = (0.8596 s)^2$$

$$U_{\sigma^2} = (1.2 s)^2$$

$$\Rightarrow \begin{array}{l} L_{\sigma} \approx 0.86 s \\ U_{\sigma} \approx 1.2 s \end{array}$$

II. Subj: 90% confidence interval on the mean for 50 independent samples.

$$L = \frac{\bar{A}}{\bar{X}} - t_{\alpha(n-1)} S_{\bar{X}}$$

$$U = \frac{\bar{A}}{\bar{X}} + t_{\alpha(n-1)} S_{\bar{X}}$$

$$\text{where } \alpha = (1+P)/2$$

$$P = \text{confidence level} = 0.9$$

$$\alpha = 0.95$$

$$S_{\bar{X}} = \frac{s}{\sqrt{n}}$$

$$t_{0.95(49)} = 1.677$$

90% confidence interval is then

$$\frac{\bar{A}}{\bar{X}} \pm \frac{1.677}{\sqrt{50}} s = \boxed{\frac{\bar{A}}{\bar{X}} \pm 0.237 s}$$

III References: (1) Oettle, Bernard. Statistics in Research. Iowa State University Press, Ames, Iowa: 1963, pp 70-100, 523-528.

(2) Crow, Edwin L., et al. Statistics Manual. Dover Publications, New York: 1960, p 242.

LIST OF ABBREVIATIONS

1. BCD: binary-coded decimal
2. BW: bandwidth (between -3 dB points of amplitude response for bandpass filters and DC to -3 dB point for lowpass filters)
3. CW: continuous wave
4. CWI: continuous-wave interference
5. DAC: digital-to-analog converter
6. DAS: Data Acquisition System
7. DFT: discrete Fourier transform
8. ECD: envelope-to-cycle difference
9. ETA: envelope timing adjustment
10. f_c : center frequency
11. FFT: fast Fourier transform
12. GRI: group repetition interval (e.g. for SS7, GRI = 99.3ms)
13. GRR: group repetition rate (GRR = 1/GRI)
14. LPA: local phase adjustment
15. LRTC: Loran Receiver Test Complex
16. MPT: multipulse Triggers
17. RF: radio frequency
18. rms: root-mean-square
19. ROF: Receiver Overhaul Facility, part of EECEN Navigation Receiver Repair Facility
20. s: standard error of the mean

LIST OF ABBREVIATIONS
(continued)

- 21. σ_{TDE} : standard deviation of time-difference error
- 22. SIR: signal-to-interference ratio
- 23. SNR: signal-to-noise ratio
- 24. SSP: standard sampling point
- 25. SW: skywave
- 26. TC: time constant (time for step response to go from zero to 63% of final value)
- 27. TD: time difference
- 28. TDE: time-difference error
- 29. \overline{TDE} : mean time-difference error
- 30. TOA: time of arrival

LIST OF DEFINITIONS

1.0 LORAN-C PULSE

Loran-C signals are transmitted in a band centered at a carrier frequency of 100 kHz with 99% of the spectral energy contained within the band of 90 to 110 kHz. The transmitted Loran-C signal is an electromagnetic signal having a pulse of the following form:

$$s(t) = A(t/t_p)^c \exp[c(1-t/t_p)] \sin(2\pi 10^5 t + \phi + \theta)$$

or $s(t) = f(t) \sin(2\pi 10^5 t + \phi + \theta),$

where $f(t) = A(t/t_p)^c \exp[c(1-t/t_p)]$ is the envelope shape between $t = 0$ and $t = t_p$

and A = function of distance from the radiating antenna and of propagation conditions

c = a constant, typically 1.5 to 2.0

t = time in seconds

t_p = time of the pulse peak, in seconds, typically 60 to 75 μ s

ϕ = the phase code, value = 0 or π

θ = the absolute ECD in radians, a function of transmitter settings and propagation path parameters.

For the W0512 LRTC Simulator, the pulse has the following form:

$$s(t) = A(t/65)^2 \exp(-2t/65) \sin(2\pi 10^5 t + \phi + \theta)$$

Each Loran-C transmitting station transmits a sequence of eight or nine pulses once each group repetition interval (GRI). In the sequence of eight or nine pulses, some pulses have 0° phase of the carrier, and others have 180° phase of the carrier. The pattern of 0° and 180° phase pulses (called the phase code) is dependent on whether the transmitting station is a master or secondary, and whether the particular GRI is designated an A or B interval. (A and B intervals alternate in time.) Pulses in a sequence of eight or nine

are separated by 1000 μ s except that the ninth pulse is 2000 μ s from the eighth and is used only to identify the master signal and to indicate master blink. Figure 1 gives the phase code for master and secondary in the A and B intervals.

Master Phase Code									
Interval	1	2	3	4	5	6	7	8	9
A	0	0	π	π	0	π	0	π	0
B	0	π	π	0	0	0	0	0	π
Secondary Phase Code									
Interval	1	2	3	4	5	6	7	8	
A	0	0	0	0	0	π	π	0	
B	0	π	0	π	0	0	π	π	

FIGURE 1

Loran-C Phase Coding

2.0 SIGNAL LEVEL OF A LORAN-C PULSE

The level of a Loran-C signal (a group of pulses from a single transmitting station) is the rms level of a CW signal having the same peak-to-peak amplitude as the Loran-C pulse envelope 25 μ s after the beginning of the pulse. The beginning of a pulse is the time at which the pulse envelope first exceeds 0.5% of the peak amplitude.

The level, when discussing electromagnetic fields, is expressed in decibels above one microvolt per meter (dB/1 microvolt/m). Otherwise, the level may be expressed in rms volts (V, mV, μ V) at the standard sampling point.

For example, a 25 mV rms CW signal has a peak-to-peak amplitude of 2.8×25 mV. Therefore, a 25 mV rms SSP Loran-C pulse would have a sampling point amplitude of 25 mV rms or a peak-to-peak amplitude of 71 mV. The amplitude of the pulse

(twice the sampling point amplitude for the LRTC W0512 Loran-C Simulator pulse) is then 142 mV peak-to-peak. The Loran-C pulse amplitude is defined at the standard sampling point, not at the peak of the pulse.

3.0 NOISE AND NOISE LEVEL

Simulated random noise will be considered to have a uniform power spectral density prior to filtering. After filtering by a single resonator L-C filter having a center frequency of 100 kHz and a bandwidth of 30 kHz, the noise level is the voltage generated across a 50 Ω resistive load, measured on a true rms voltmeter; this noise level is defined as the rms noise level, denoted by N. The filtered noise is then a bandlimited, jointly Gaussian random process.

4.0 LOCK-ON

Acquisition (or search) is the process which establishes the approximate location in time of the master and each of the selected secondaries and aligns the phase code. Acquisition, therefore, implies the action the receiver must take in order to determine the position of the master and selected secondaries relative to its internal timing. The accuracy with which this alignment is made is not critical in this mode. It is only necessary that the sampling strobes of the receiver be somewhere on the Loran-C pulse with the correct phase code alignment at the conclusion of the search mode. The settle process is defined as the procedure of identifying the correct cycle zero-crossing and establishing groundwave tracking. The receiver will be considered to be "locked on" when useful navigational information is available at the receiver outputs. Time to lock-on = time-to-search + time-to-settle = acquisition time + settle time.

5.0 ENVELOPE-TO-CYCLE DIFFERENCE (ECD)

Absolute ECD is the difference in μ s between the envelope TOA and cycle TOA of a Loran-C pulse. Differential ECD is the difference between a secondary absolute ECD and master absolute ECD, or equivalently, differential ECD is equal to master-secondary envelope time difference minus master-secondary cycle time difference.

6.0 SIGNAL-TO-NOISE RATIO

The SNR is the ratio in dB of the Loran-C signal level, S, to the noise level, N.

7.0 SIGNAL-TO-INTERFERENCE RATIO

Interference may be considered as contamination resulting from CW, skywave, or cross-rate signals. Signal-to-interference ratios are defined as the ratio of the rms signal level of the Loran-C pulse to the rms level of the continuous interference or, in the case of cross-rate, to the defined SSP rms level. Note that the Loran-C pulse amplitude is defined at the sampling point, not at the peak of the pulse. All interference amplitudes are therefore referenced to the pulse sampling point. As an example, a 2.5 mV rms CW signal superimposed on a 25 mV rms SSP Loran-C pulse would yield a +20 dB signal-to-interference ratio, SIR.

8.0 UNITS FOR ENTRIES IN TEST TABLES

Most of the tests in this report have tables which list numerical values for all test parameters. The units of these numerical values are given in Table I.

9.0 SPACE COUPLING NODE

The space coupling node is the point of connection between the Loran-C simulator and the simulated antenna of a receiver. All signal, noise and interference levels are measured at this point.

10.0 LORAN-C SPECTRAL LINES

Periodic recurrence rates in the Loran-C transmission scheme give rise to discrete spectral lines which are distributed about the Loran-C carrier frequency of 100 kHz. The odd numbered pulses (1, 3, 5, 7) contribute spectral lines spaced one GRR apart (e.g., $SS7:GRR = 1.0/99.3 \text{ ms} \approx 10.0704 \text{ Hz}$) starting at 100 kHz and extending in both directions in the frequency domain. The even numbered pulses (2, 4, 6, 8) contribute spectral lines spaced one GRR apart starting at $100 \text{ kHz} + 1/2 \text{ GRR}$ and extending in both directions away from 100 kHz in the frequency domain. Thus, the even and odd spectral lines are interleaved with a spacing of $1/2 \text{ GRR}$ between each spectral line.

TABLE I

UNITS FOR TABULAR ENTRIES

TEST PARAMETER	TEST NUMBER											
	1	2	3	4	5	6	7	8	9	10	11	12
AIR TEMP	°C											
REL. HUMID.	%											
LINE VOLTAGE	VAC or VDC as appropriate											
GRI	ms											
M SIG. LEVEL		←										
M ECD	μs											
M SW LEVEL		←										
M SW DELAY	μs											
S _A SIG. LEVEL		←										
S _A ECD	μs											
S _A SW LEVEL		←	dB relative to 25 mV rms SSP									
S _A SW DELAY	μs											
S _B SIG. LEVEL		←										
S _B ECD	μs											
S _B SW LEVEL		←										
S _B SW DELAY	μs											
CRI LEVEL		←										
CRI GRI	ms											
NOISE LEVEL	dB/25 mV rms	(Gaussian noise, BW=30 kHz single resonator filter) centered @ 100 kHz										
I1 LEVEL		←										
F1	kHz											
I2 LEVEL		←										
F2	kHz											
I3 LEVEL		←	dB relative to 25 mV rms									
F3	kHz											
I4 LEVEL		←										
F4	kHz											
I5 LEVEL		←										
F5	kHz											
I6 LEVEL		←										
F6	kHz											
S _A TD	ms											
S _B TD	ms											
SAMPLE TIME	s											

APPENDIX A

SIGNAL INPUT TO THE RECEIVER UNDER TEST

A-1.0 SIGNAL INPUT TO THE RECEIVER UNDER TEST

Receiver acceptance test specification signal levels are usually given in terms of signal field strengths. However, the LRTC simulator output is a signal voltage at a 50 Ω output port, and is measured as a voltage signal level. It is not practical to generate a standardized field to couple to the antenna of the receiver under test for all the performance or acceptance tests. Therefore, an artifice is used to couple the simulator output directly to the antenna port of the receiver under test in a standard manner such that the simulator output voltage levels may be related directly to specified signal field strengths. The specified field strength (E_{sp}) is related to the voltage level at the simulator output port (space coupling node (SCN)) by the effective height (h_e) of the antenna,

$$e_{SCN} = h_e \times E_{sp}$$

The simulator output voltage, measured across a 50 Ω load, is adjusted accordingly. This is shown in Figure A-1.

The antenna capacitance to ground (C_A) may be measured using an RF bridge such as the General Radio Model 916-AL, or it may be specified by the manufacturer. It must be remembered that some receivers employ high-Q antenna couplers, and in these cases C_A must be within about ± 2 pF of the measured or specified value in order not to distort the bandpass characteristic of the antenna coupler.

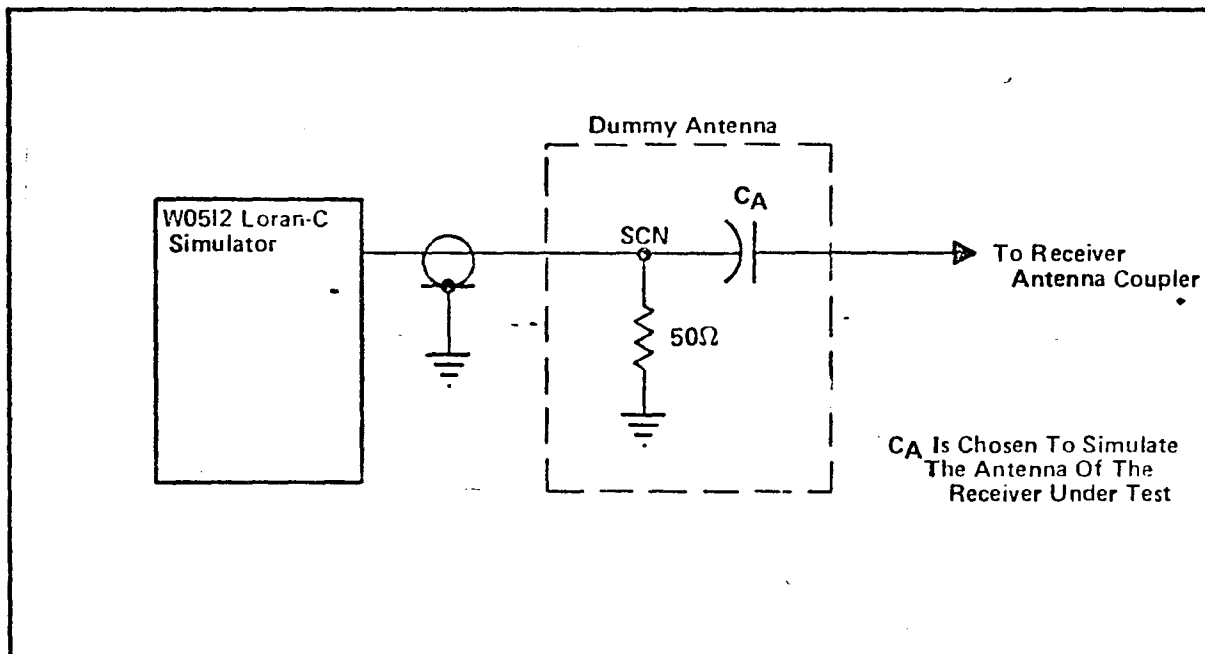


FIGURE A-1

LRTC Antenna Simulator
W0575 FINAL REPORT

APPENDIX B

DATA ACQUISITION INTERFACE REQUIREMENTS

B-1.0 DATA ACQUISITION INTERFACE REQUIREMENTS

The LRTC Data Acquisition System (DAS) accepts positive-logic, BCD, TTL-compatible data parallel by bit and parallel by character. Logic zero is 0 volts to +0.8 volts, logic one is +2.4 volts to +5.0 volts. The least significant four digits of the receiver-under-test BCD time-difference readout may be directly connected to the DAS input via a suitable connector (see Table B-I for cable type and pinouts). If the receiver TD outputs are binary, the DAS can be patched for octal or hexadecimal coding of the binary. Data in base 8 or base 16 can then be converted to base 10 and analyzed by computer. Alternatively, if BCD or binary outputs are not available, master and secondary sampling strobes can be buffered and connected via DAS relay contacts to an HP-5360A Computing Counter. The HP-5360A will measure the time-difference reading and present this information in BCD form to the DAS.

In addition to the 16 lines of data, a sample hold-off strobe must be generated to prevent DAS sampling during updating of receiver time-difference readouts. The sample hold-off line must be held at logic one until receiver updating is complete and the BCD readout of time-difference is once again steady. The sample hold-off line may not be held at logic one for more than 1 ms. Additionally, its duty cycle must be less than 5%.

Outputs from the receiver interface should be made with two, six-foot multiconductor cables, using the connector and pin positions specified in Table B-I. A schematic and associated timing diagram for a recent DAS interface is shown in Figure B-1.

TABLE B-I

LRTC DAS Inputs

Cinch Type 57-30240 Male Connector

<u>Pin #</u>	<u>Bit</u>		<u>Comments</u>
1	2^0	Least Significant Digit	Least Significant Bit, Least Significant Digit
2	2^1		
3	2^2		
4	2^3		
5	2^0	2nd Digit	Increasing Bit and Character Significance
6	2^1		
7	2^2		
8	2^3		
9	2^0	3rd Digit	
10	2^1		
11	2^2		
12	2^3		
13	2^0	4th Digit	
14	2^1		
15	2^2		
16	2^3		
17			Sample Hold-Off Strobe
18			Do Not Use
19			Do Not Use
20			Do Not Use
21			Ground - Logic Return
22			VCC - +5.0 Volts
23			Do Not Use
24			Do Not Use

APPENDIX F

CALCULATIONS TO DETERMINE SERVO BANDWIDTH USING STEP RESPONSE DATA

F-1.0 CALCULATIONS TO DETERMINE SERVO BANDWIDTH USING STEP RESPONSE DATA

A. Assumption: That the servo system exhibits underdamped, two-pole dominant behavior. If this assumption is not applicable then this computation scheme is invalid.

B. Given: M_p = normalized maximum overshoot of step response (M_p greater than 0)

t_s = time in seconds required for the transient response to settle within 5% of its final value

C. Find: ζ = damping ratio (ζ less than 1)

f_n = natural frequency of the servo loop

f_B = -3 dB bandwidth of the servo loop

D. Procedure:

(1) Find ζ from

$$\zeta = \frac{\sqrt{\left(\frac{\log_e M_p}{\pi}\right)^2}}{1 + \left(\frac{\log_e M_p}{\pi}\right)^2}$$

(2) Find f_n from

$$f_n = \frac{3}{2\pi\zeta t_s}$$

(3) Find f_B from

$$f_B = f_n \sqrt{-(2\zeta^2 - 1) \pm \sqrt{0.995 + (2\zeta^2 - 1)^2}}$$

NOTE ON USE OF THE EECEN LORAN RECEIVER TESTING COMPLEX

1.0 GENERAL DESCRIPTION

As depicted in Figure 1, the Loran Receiver Testing Complex consists of two basic units, the Signal Simulator and the Data Acquisition System, (DAS). The Signal Simulator is further divided into the Analog Signal Unit (ASU) and the Digital Control Unit (DCU). The entire simulator is installed in a large, nonportable, three column rack. The DAS is mounted in one portable rack. The general functions of these units are described below, followed by descriptions of specific tests that can be performed with the equipment.

1.1 DIGITAL CONTROL UNIT (DCU)

The DCU generates Loran-C timing signals, for use by the ASU, from an external 5-MHz clock. The master and two secondary timing pulses are positionable in time to 0.02 μ s resolution with a time difference accuracy of better than 1 ns. The timing pulses for each signal may be independently controlled (in time) by manual input or automatic paper tape input. The paper tape input is used to control the frequency of slew commands to the unit (0.02 μ s/slew command) and hence controls the doppler, both sign and magnitude, for each master and secondary timing signal.

1.2 ANALOG SIGNAL UNIT (ASU)

The ASU is a modified AN/FPN-46 simulator with all of the digital circuits removed except the phase code logic. The ASU provides a master and two secondary pulses of 25 mV rms SSP (into 50 Ω) maximum amplitude. These signals are not passed through any frequency selective elements such as the original dummy antenna coupler. A skywave pulse or 25 mV rms SSP amplitude can be switched in with any master or secondary signal and positioned from 10 to 2,000 μ s behind the "groundwave." All pulse signals can be selectively attenuated from 0 to 60 dB in 1-dB steps. The master and secondary signals have independent ETA adjustments using circuits similar to those providing the ETA adjustment in the AN/FPN-44 transmitter. Thus, any absolute or differential envelope-to-cycle relationship may be entered on the ASU. Master, secondary and skywave triggers delivered to the "three-pole filter" (pulse forming network) are buffered to the front panel for use with an installed time interval counter to verify precise time relationships among the triggers. The ASU output signals are distributed to four 50-ohm unbalanced outputs via an A.R.I. Model AMC-8 Multicoupler.

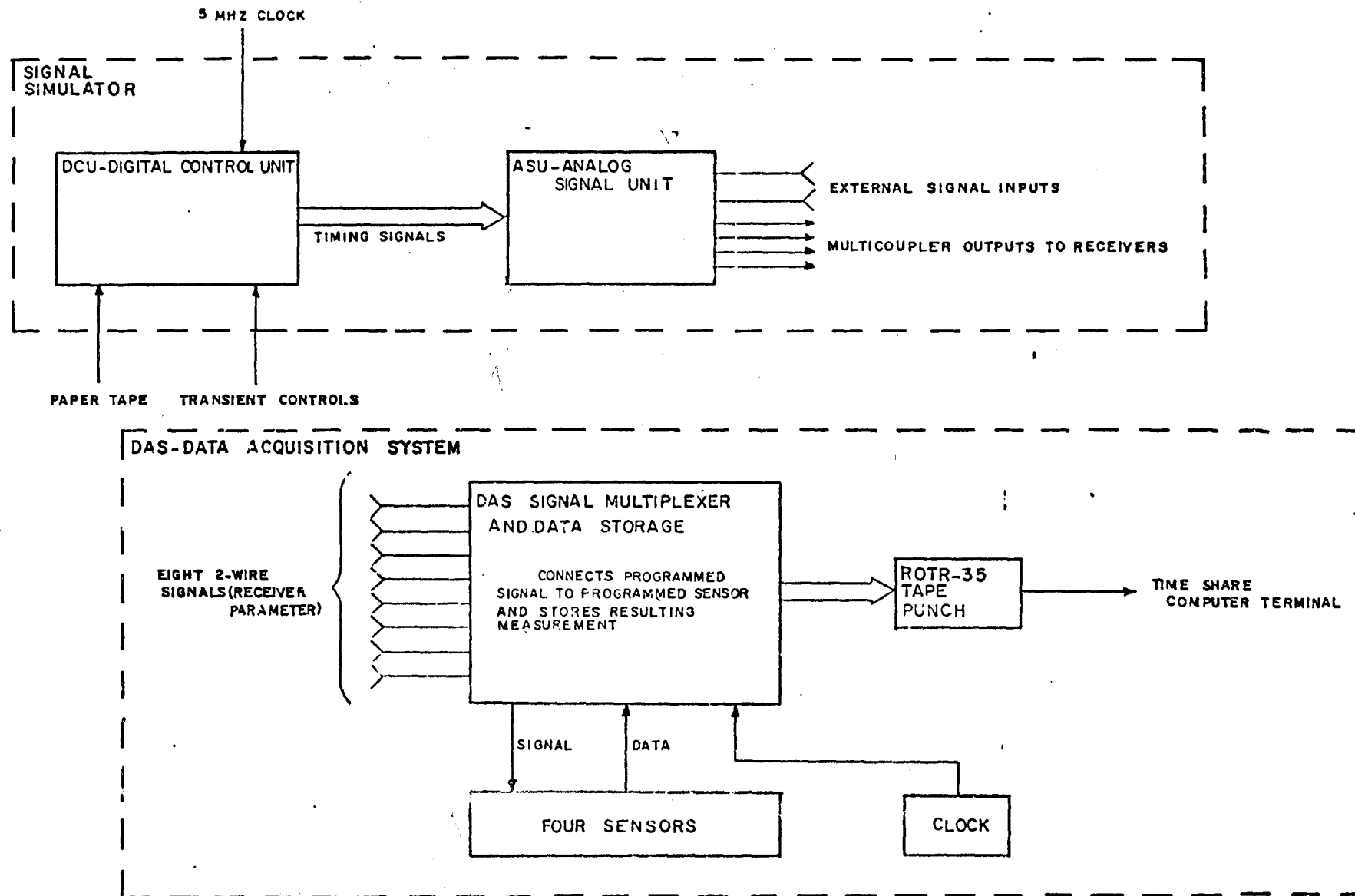


Figure 1
 Block Diagram of LORAN Receiver Testing Complex
 (LRTC)

1.3 DATA ACQUISITION SYSTEM (DAS)

The DAS consists of three basic parts; the signal multiplexer and data storage group, the four sensors or parameter measuring devices, and the data recording system. Eight, two-wire (common ground) independent signals of interest can be monitored on a time-shared basis. An external clock is used to establish and record time with other data. Any one of the sensors can be selected to measure any one signal or more than one signal provided the signal format for each is the same. The sensors provided are:

a. One HP5360A Computing Counter having 1 ns time-interval/period resolution. This counter is capable of measuring time, frequency, frequency deviation, etc. Its main advantage is its ability to perform mathematical operations on the "raw data" prior to computer processing. Some examples of the mathematical operations which may be performed are adding and subtracting of constants, multiplication by a scaling factor, etc.

b. Two CMC 901 Counters with 100-MHz time base.

c. Two Dana 4400 Digital Multimeters which can measure DC (to 10 μ V), AC (to 100 μ V), ohms (to 0.01 ohms) with four-decimal digit resolution and 20% overrange.

2.0 DETAILED DESCRIPTION

2.1 DIGITAL CONTROL UNIT (DCU)

The principle function of the DCU is to develop digital timing signals to generate the analog loran signals. In addition, the DCU provides the input point for stimulating the receiver via time-position modulation of the analog signals. This modulation is not communication modulation (introduced at the ASU) but rather represents off-line computer controlled modulation such as simulating platform movement or servo response testing.

2.1.1 TAPE READER

The tape reader is a 12 character, eight level, block reader manufactured by EECO. The reader uses light-sensitive diodes to detect the presence of a hole in the tape and provides a saturated transistor output whenever the hole is present. The tape used must be 95% opaque. The reader steps each block of 12 characters into the read position upon receipt of a positive going pulse (less than 10 μ s rise time) at the command input. Two front panel controls provide capability to reverse the direction of tape motion or slew the reader at its maximum rate of eight blocks per second. The data from the 12 character block is steady at the rear connector and ready for reading approximately 180 ms after the step command.

2.1.2 PROGRAM UNIT

The Program Unit accepts data from either the tape reader or front panel manual input digits, and outputs this data in proper format to control the Loran Timing Unit (LTU) digital phase shifters. The input data is in 9's complement form and represents the number of slew pulses to be delivered to the master or secondary phase shifter at that sample time. The slew pulses are emitted at 100-KHz clock rate and a total of 99,999 pulses may be programmed for any given sample time. The sample time base is front panel selectable as 0.2 second, 1 second, 2 second or 10 second, or manual pushbutton. Each sample pulse steps the tape reader, reads 9's complement data from either the reader or front panel and then outputs the indicated number of pulses. The sample rate is clocked off the system 5 MHz. Direction control is provided at the front panel or via the tape reader where the sign data is multiplexed onto the sixth level of the Least Significant Character of both the master and secondary data groups. This multiplexing produces alphabetic symbols in the Least Significant Character position of M and S control data.

2.1.3 PHASE TRANSIENT GENERATOR

The Phase Transient Generator provides periodic time position transients to the ASU via bursts of slew pulses and direction sense delivered to the LTU (in lieu of the program unit input). These pulses increment the LTU timing signals 1.28 or 2.54 μ s, hold them for a programmed time (either short to simulate an impulse, or long to simulate a step) and then return the timing signals to the original position. This transient recurs at a programmed rate up to maximum of once every 1600 seconds. The clock for both the periodicity and "width" of the transient is counted off M interval and hence the entire sequence is phase coherent with the Loran time base.

2.1.4 LORAN TIMING UNIT

The LTU is composed of three completely independent rate generators with 5-MHz inputs via independent 0.02- μ s resolution phase shifters. The master and two secondary signals are then recombined at the output to drive the ASU. The time delay of both secondary generators can be initially set to 1.0- μ s resolution (better than 7-ns accuracy). Incremental movement of each signal (so-called changes in the TOA of each signal) can then be controlled automatically as described above or manually by front panel pushbutton. All output waveforms

are available at a front panel jack for monitoring. In addition to the signals required for normal operation of the ASU, a time-shared and filtered 100-kHz signal is provided for use in the communication modulation circuits of the ASU.

2.1.5 OPERATION OF THE DCU

Operation of the DCU is straightforward as indicated by all front panel controls. Selection of certain parameters such as sample time increments for the tape reader are best considered within the context of the form of computer-aided analysis to be used with the resultant data. This is discussed in Section 3.0. The initial M-S time difference settings to be set in to the LTU should normally be an odd multiple of 5 μ s. This puts the resultant receiver reading in the middle of the DAS's character handling range.

2.2 ANALOG SIGNAL UNIT (ASU)

2.2.1 LORAN SIGNAL GENERATOR

2.2.1.1 The ASU is composed of a modified AN/FPN-46 simulator unit and various ancillary circuits. All vacuum tube power is supplied via an independent set of power supplies. The ASU generates three-groundwave signal groups from the time-shared MPT input signals. These triggers are relocked to the communication modulated 100 kHz but are not relocked to the normal 1 MHz. They pass from the modulation reclock directly to the "3-pole filter." The amplified output of the filter is sent to the time-shared attenuators for independent M/S amplitude control and then passed through the time-shared ETA circuit. This circuit shifts the phase of pulse carrier via a 10-turn gear reducer and front panel vernier control. Both secondary signals use one ETA setting, the master another. The signal is delivered from this unit to the multicoupler at a 50-ohm impedance level. Maximum signal amplitude is 25 mV rms SSP, minimum is 25 μ V rms SSP. Skywave signals can be generated in any or all intervals. The time delay of the signals is front panel controllable from 10 to 2,000 μ s. The delay is generated in analog fashion from the T/S MPT and hence follows any communication time-shift in these triggers. The phase code of the "originating" groundwave is maintained in the skywave by storing the sense of the phase code at the time of the groundwave MPT. The skywave pulse is generated by a COLAC pulse module at 25 mV rms SSP, passed through a 60-dB step attenuator and delivered to the multicoupler.

2.2.1.2 The original 30-kHz Gaussian noise source of the '46 simulator is retained intact in the ASU. The calibrated maximum output of this source is set to 250 mV rms at 50 ohms and delivered to the multicoupler (it is added to the simulator pulse signals at the multicoupler). The master and secondary interval waveforms are used to reclock the first MPT of each

signal as it is delivered to the three pole filter. This reclock signal is available at a front panel connector for monitoring the actual time delay of the signals generated by the three-pole filter. Similar monitoring of the skywave delay is also provided at the front panel.

2.2.2 ARI MULTICOUPLER

The multicoupler is an ARI Model AMC-8 which is modified to include a five-port passive summing junction (50 ohm) at the input. The multicoupler has -20 dB transfer from any input to any output, -44 dB transfer from any input to another input and -60 dB transfer from any output to another output. Three of the five input ports to the coupler are hardwired to the groundwave, skywave, and noise signal sources; the remaining two are available at the front panel. One of the front panel inputs can be operated as a continuous input or can be operated in a gated mode. The gate signal is the secondary interval waveform and is applied to a solid-state switch that connects the input port to the external source only during the interval. The port is grounded through a 50-ohm resistor at all other times. The signal present at the four output ports has a 25 mV rms SSP at 50 ohms. Assuming a typical 26-dB loss in a passive receiver coupler, the signal available at the receiver terminals can be varied over a 1.25 μ V to 1.25 mV range.

2.3 DATA ACQUISITION SYSTEM (DAS)

2.3.1 DESCRIPTION

The DAS is a self-contained instrument rack designed to acquire data on receiver performance via a number of sensors and store this data on a written and punched tape TTY record. A block diagram of the DAS is shown in Figure 1, Section 1.0. Eight independent parameters (time, voltage, current, resistance, frequency, time interval, period, events etc.) can be monitored on a cyclic basis and the data record generated from the samples taken. In effect these eight parameters can be viewed as time-slots; each slot may be used to monitor a given parameter. The basic sampling rate of the DAS is either one second per slot or 4 PRI per slot. Further provisions have been incorporated into the DAS to permit either of the basic sampling rates to be divided by any integer number up to sixteen. The digital result of such a parameter measurement can be stored in various registers; the register data can be displayed in real-time via D/A converters and the parallel array of register data from all such measurements can be scanned periodically by the data-intercoupler generating the TTY record. The periodic scan rate is determined via a front panel rotary switch and is variable from a maximum of once each sampling rate to a minimum of once per 100 samples.

2.3.2 OPERATING INSTRUCTIONS

a. Connection of analog signals (or pulses etc.) to the various sensors is done at the Program Unit front panel. Each time slot is defined there by a pair of contact closures connecting the IN jack to the OUT jack. Time slot 1 signal is connected to IN jack 1, time slot 2 to IN-2 etc.... The output jacks are then connected to the appropriate sensor in parallel if necessary (since all IN signals are isolated from one another by open contacts). The only precaution that must be observed here is that all signals delivered to a sensor must be in the same format, the Digital Multimeter for example cannot change operating mode between time slot 1 and 1+1.

b. The sensors must be programmed to sample in time slots consistent with their front panel signal connections. This sampling occurs 0.1 seconds after the time-slot is defined by front panel contact closure. Programming is done via patch cords on the matrix board Y. The time signals are present at the TIMING INPUT (e.g., time-1 is at G-H-18, 19, 20 of Y) points. These timing signals are connected up to SAMPLE COMMAND, connecting time slot 1 to sensor k as time slot 1 relay contacts are made on the front panel.

c. Four decimal characters worth of data (16 binary bits in 1-2-4-8 code) are brought down to matrix board W from each sensor and from the digital clock. This data is programmed to the eight, four character storage registers, with patch cords on W. Generally the four characters from each sensor are programmed into the register number corresponding to the time slot used to generate that sample. For example, if the HP 5360A was used in slots 1, 4 and 5 then patch cables would connect the HP data inputs to inputs to 4-character STORAGE REGISTERS, Reg 1, thence to Reg 4, thence 5.

d. The STORAGE COMMAND, overlapping matrices Y-Z, must be programmed by TIMING INPUTS to store the data patched to the corresponding storage register inputs in matrix W and X. This TIMING INPUT connected to STORAGE COMMAND causes the register to strobe the input data 0.2 seconds after the sensor was commanded to SAMPLE ((b) above). These connections must be consistent with the data patch done in (c) above.

e. The data stored in the various STORAGE REGISTERS may be displayed on chart recorders by programming OUTPUTS from 6 of the 8, 4-character STORAGE REGISTERS to the inputs of the 6, 2-character D/A converters. Six groups of data may be displayed, although only two characters from each group may be converted.

f. The data outputted to the TTY record is selected by programming the OUTPUTS FROM 4 CHARACTER STORAGE REGISTERS to 4 CHARACTER OUTPUT TO MUX in matrix Z. The data to the Data Inter coupler (MUX) can be arrayed in any order convenient for the record or subsequent computer analysis. Generally three decimal characters are programmed from each sensor's data group of four characters. This results in a data record of 24 characters per line. This length is consistent with TTY speed and the PRR sampling interval that generates an individual time-slot length of 0.4 second. A complete eight time-slot scan requires 3.2 seconds, within this time the TTY can print 32 characters, thus the 24 noted above, plus carriage return and line feed, allow a six character "saftey margin." This completes programming of the DAS.

2.3.3 DATA INTERCOUPLER (MUX)

The IRA^{Inc.} data intercoupler has a possible 40 character parallel data input capability. The MUX scans all input characters upon receipt of a command from the DAS Program Clock. This parallel input data is converted to serial ASCII format and a current drive line is connected to the TTY to record the data. The MUX must be internally programmed for the desired number of input characters and any additional characters such as sensor identifying labels, etc. Instructions for this program may be found in the IRA manual. To operate the unit the front panel switch is placed in RUN and the RESET button depressed.

3.0 COMPUTER CONTROLLED STIMULUS AND ANALYSIS

3.1 PROGRAMMING ROUTINES

There are 12 programming routines that are currently operational with the system;

a. /STATIST/ analyze input data from TTY punch tape record which is arrayed three characters per sensor, eight sensors across the page. The program is two-pass (thus not requiring statistical independence between samples) and computes, mean, variance and standard deviation of N points from the input record where N is specified by the operator.

b. /OSCILLATE/ generates numerical control tapes to stimulate the receiver via movement of the pulse TOA. Program generates equal amplitude harmonics at frequencies specified by the operator.

c. /TURNS/ generates numerical control tapes to simulate vehicle movement of the receiver. Maneuver is composed of two constant velocity (hence constant radius) turns where the angle of turn, acceleration and tangential velocity are specified by the operator. The resulting control tape also "stops" and "starts" the vehicle in constant acceleration maneuver.

d. /PROCESS/ re-formats standard three digit data from each sensor for use by a Fourier analysis routine (Cooley-Tukey algorithm). The number of points to be analyzed is specified by the operator.

e. /FTST/ Streamlined version of TYMSHARE's Fast Fourier Transform. Provides more efficient file structure, speeds execution and IN/OUT.

f. /DATAV/ Performs ergotic averaging of several synchronous data runs to enhance S/N information.

g. /FOURAVERAGE/ Provides averaging of Fourier Transform data for S/N enhancement.

h. /FOURSTAT/ Performs elementary statistical analysis similar to /STATIST/.

i. /REFORM/ Reformats DAS data for use with TYMSHARE's comprehensive statistical package.

j. /FOURTEST/ Translates DAS program tape to simulated Time Difference measurements compatible with Fourier Transform analysis. Used to calibrate DAS program tape without having to physically test it on the DAS.

k. /FASTPROCESS/ Performs same functions as /PROCESS/ except the eight DAS data channels are taken as sequential observations of a single parameter. Permits analyzation of data of a single parameter at eight times the normal sampling rate.

l. /LINEFIND/ Determines synchronous and non-synchronous interference frequencies for a given GRI.

3.2 OPERATING CONSIDERATION

The basic problem in using the simulation/analysis capabilities of the system lies in understanding basic analog-digital relationships. These are outlined briefly below:

a. Statistical analysis; the sampling period should be chosen long enough so that there is very little correlation, while it does not introduce biases in the sample statistics, does enlarge the confidence limits on a given statistic. For example, 100 independent samples with Gaussian distribution will allow one to estimate the mean of that distribution to within one dB of the true mean with 99% confidence. If every other sample has 0.5 correlation with the previous one, then the effective number of independent samples decreases to about 75 which raises the confidence limit to 1.5 dB. Sample correlation is a function of servo bandwidth generally one correlation time is one servo time constant.

b. Receiver stimulation via numerical control tapes; the Nyquist sampling criterion must be satisfied in this case. The sampling period of the tape reader defines some upper frequency ($1/2$ of $1/T$ tape sample) that can be reproduced by the TOA movement. The only errors in the numbers sampled and stored on the reader are quantization errors due to the $0.02\mu s$ discrete phase shifter interval. Thus sample aliasing is not a major problem and probably a sufficient rule of thumb is to insure that stimulation signals have all frequency components below $1/2$ of the upper Nyquist frequency defined above.

c. Receiver output sampling; when the receiver's response to various types of stimulation is being measured with the DAS care must be taken to insure that the Nyquist criterion is not violated and that the data record length is appropriate to the stimulation and analysis desired. For example the lowest Fourier fundamental obtainable from a data record of N points sampled every T time units is $1/N*T$ cycles per time unit. Non-redundant Fourier data points from such an analysis are provided up to $((N-2)/2)*1(N*T)$ cycles per time unit. If the receiver stimulus also contains wide-band noise, the Nyquist frequency of the DAS should be set well beyond the expected servo bandwidth to guard against sample aliasing of the noise. This guard band should probably be set at a factor of 4-5 times the servo bandwidth.

02 06

P. 10-11

SEP 1974



PROCESSED BY THE
FEDERAL BUREAU OF INVESTIGATION
U. S. DEPARTMENT OF JUSTICE

RECEIVED SEP 10 1974

U. S. DEPARTMENT OF JUSTICE
FEDERAL BUREAU OF INVESTIGATION

SEP 10 1974

Prepared for Presentation
at the
Third Annual Convention
of the
Wild Goose Association
McAfee, New Jersey
2-4 October 1974

Progress Report on the Group/Phase Test
by
James A. Perschy
and
Richard R. Smith

ABSTRACT

This paper reports the progress to date on implementation of the Group/Phase Test which was described in a paper read to the 2nd Annual WGA Convention. The test is designed to explore the hypothesis that accurate knowledge of the envelope-to-cycle difference, measured at the receiver, can be used to make real-time corrections for the secondary phase factor. Included are descriptions of the test instrumentation, the expected quality of the data and the format of data tapes.

INTRODUCTION

The Applied Physics Laboratory is conducting a test for the U.S. Air Force and the Defense Advanced Projects Agency to determine the validity of one facet of the theory of groundwave propagation at 100 kHz. The theory indicates that if proper account is taken of group and phase velocities in the propagation of pulses of the Loran-C radio navigation service, then geodetic position should be computable using the vacuum speed of light and the times of arrival of the pulse and the carrier. The test is being conducted in the eastern United States using the East Coast Loran-C chain and requires two identical sets of precision equipment, one in a mobile test van and the other at a fixed site at the U.S. Naval Observatory (NAVOBSY). The van will occupy at least ten field sites during the course of the test. The position of each site is being precisely surveyed using the Navy Navigation Satellite System. The recorded data include very accurate measurements of the Loran-C groundwave phase and envelope times of arrival, and absolute time.

APL is assisted in this test by NAVOBSY and the Defense Mapping Agency Topographic Center (DMATC). The test effort includes group/phase monitor system definition, assembly and check out of equipment, acquisition and analysis of field test data, and a final report documenting the test and incorporating pertinent test results.

TEST PLAN

A basic problem in using Loran is that analytical methods of predicting the effective velocity of LF propagation do not define the Loran grid with sufficient accuracy. In recent applications, extreme accuracy of navigation and position location has required extensive grid calibration before Loran systems could be employed to their best advantage. Recent work has led us to conclude that an accurately measured value of Envelope to Cycle Difference (ECD) could be used to make real time

corrections for the secondary phase factor. This conclusion is based on theory, analogy to propagation at higher frequency, and qualitative observations. The observations are that there is indeed an ECD which indicates that the medium in which the groundwave propagates is dispersive. Also wherever and whenever ECD is large, predictable accuracy is poor and vice versa. This implies a functional relationship between ECD and phase error, which, if it were known, could be used to correct the phase data. According to theory and experiment, different frequencies propagate at different speeds in a dispersive medium; and because of this, the pulse propagates at a different speed than the carrier, giving rise to ECD.

Due to the complexity of the Loran spectrum and the unknowns associated with the dispersive characteristics of the medium, the most direct and meaningful way to determine the desired function is by a test in the East Coast Loran-C chain. Highly accurate measurements of the time of arrival of the third cycle zero crossing, ECD and geodetic distance are required at various distances from transmitters along various ray paths. It was originally planned that two vans would be instrumented to achieve versatility in the choice of ray paths to be examined. However, it was learned that a van was immediately available for assignment to this project. In the interest of an early start, it was decided to instrument this van, and install the other instrumentation next to the Master Clock Ensemble at the Naval Observatory. This allows examination of the ray paths which pass through NAVOBSY from Carolina Beach, Dana, and Nantucket. The results obtained should be adequate to determine the validity of the group/phase concept and to assess the desirability of additional testing for which an additional van would be required.

The ten field sites at which data will be taken are shown in Fig. 1. The specific locations are near Danville, Indiana; Marietta, Ohio; Georgetown, Delaware; Wilmington, North Carolina; Emporia, Virginia; Towanda, Pennsylvania; Dexter, New York; Toms River, New Jersey; Grottoes, Virginia; and

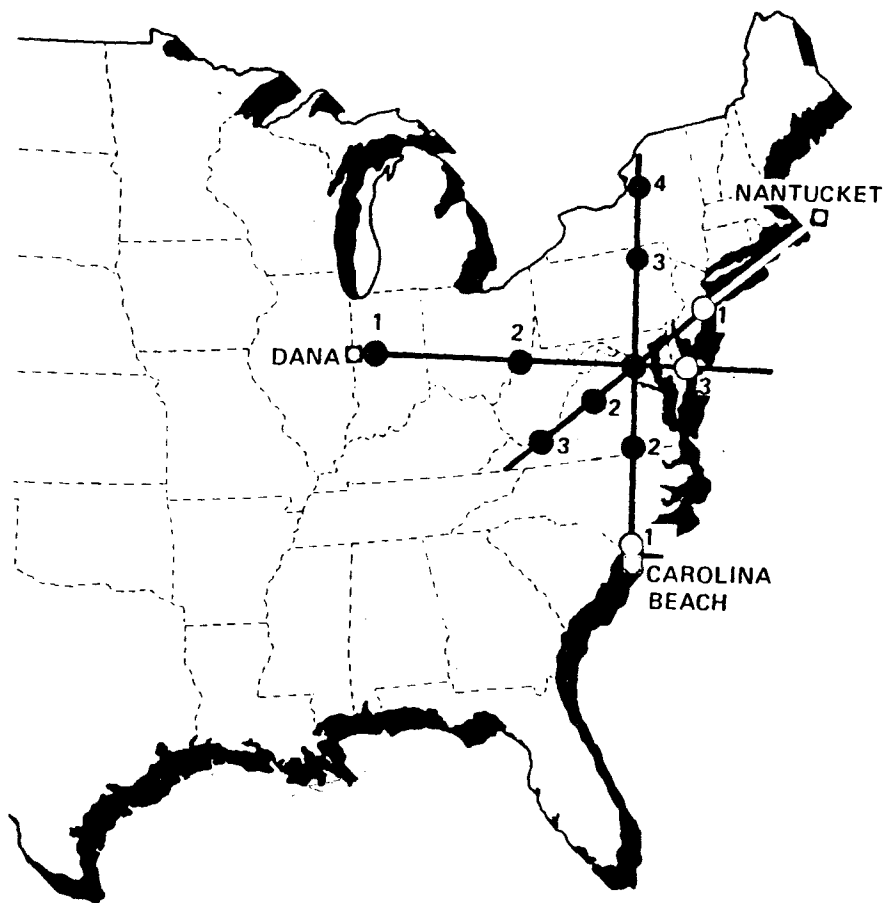


Fig. 1 LOCATIONS OF FIELD TEST SITES

Bluefield, West Virginia. Geociever station monuments exist at each of these sites. These monuments mark the exact location at which Loran-C data are to be taken. They are located within a corridor that diverges from a point source at the transmitting antenna to one quarter wave length, 2500 ft., on either side of the geociever station monument at the Naval Observatory. The corridor then remains constant at a 5000 ft. width for the usable remainder. Each of the monuments is being surveyed by Geociever Survey Teams of the Defense Mapping Agency under the direction of Philip M. Schwimmer of DMA and Charles B. Sharp of DMA Topographic Center. The geodetic data are being reduced at the Topographic Center under the direction of James W. Walker.

Each field site will record data from the transmitter associated with the ray path it is on, and the fixed site will concurrently record data from the same transmitter.

TEST INSTRUMENTATION

Figure 2 is the system functional block diagram for a single group/phase test station. Two identical systems are being designed and assembled for the test. Referring to Fig. 2, the Loran-C signal is inputted to a fixed gain tuned receiver via a wide-band variable attenuator. The purpose of the wide-band attenuator is to standardize the Loran-C pulse amplitude as seen by the tuned receiver without distorting the signal waveform or causing a phase shift which varies with signal strength. At least 10 dB of attenuation always remains in the attenuator to minimize mismatch effects between the antenna and the input to the tuned receiver. The output of the tuned receiver is adjusted by the wide-band attenuator to give a Loran-C pulse amplitude of ± 0.5 volt. The receiver output connects to an analog-to-digital converter, the purpose of which is to digitize wave samples using sample points on the Loran-C pulse. Sample triggers open a sample and hold circuit at the input of the analog-to-digital converter, and the converter then digitizes the analog voltage at the

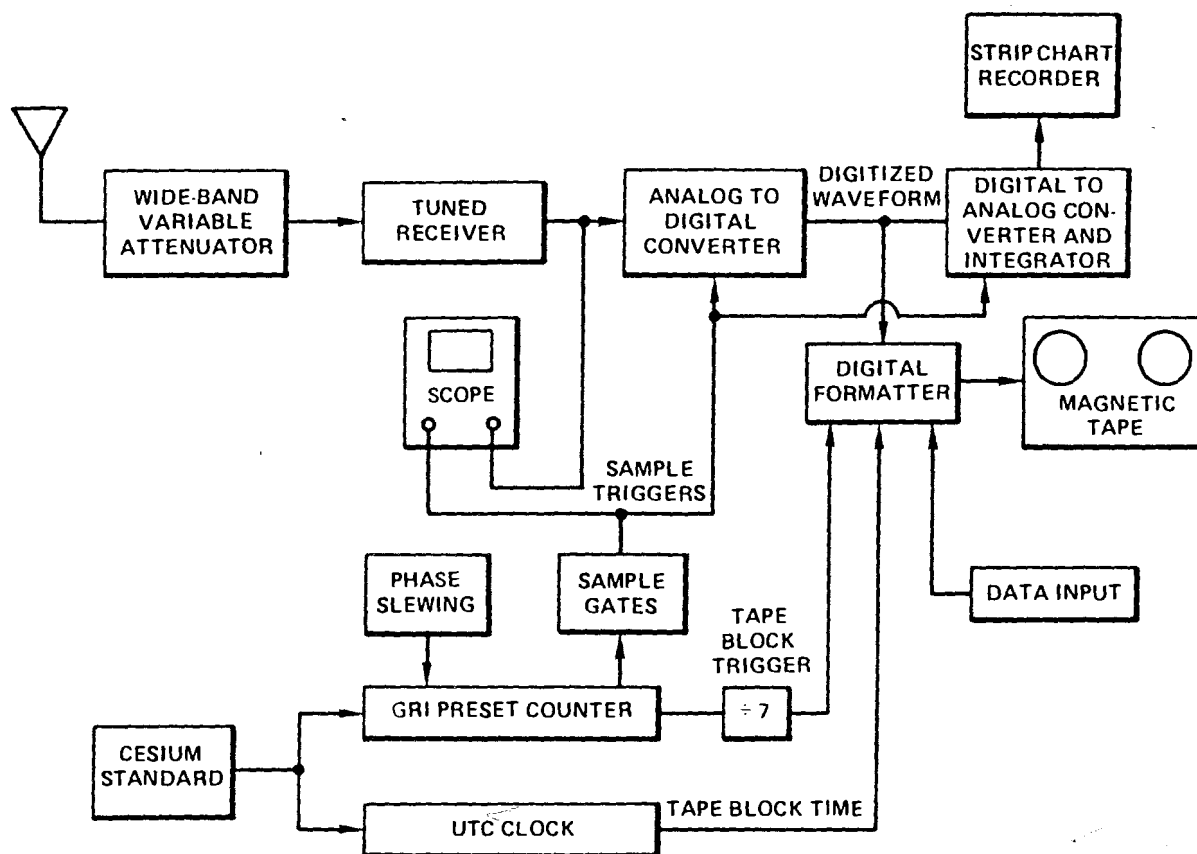


Fig. 2 GROUP/PHASE MEASUREMENT SYSTEM

output of the sample and hold circuit to 13 bits plus a sign bit. The sample triggers are generated by sample gates. Timing of the sample gates is derived from a group repetition interval (GRI) preset counter. The phase of the preset counter can be adjusted in plus or minus 0.1 μ s time intervals by phase slewing circuitry. The phase of the GRI counter is adjusted such that the sample triggers, displayed on one channel of an oscilloscope, most nearly match the desired sample points on the Loran-C pulse which is displayed on a second channel of the oscilloscope. The precision timing for the GRI preset counter, and also for a Universal Time Coordinated (UTC) clock, is derived from a low noise Cesium beam frequency standard in the van mounted system. In the fixed site system, the timing is derived from the Master Clock Ensemble at the Naval Observatory.

The digitized Loran-C pulse waveforms, along with a synchronous output from the UTC clock and fixed data input information stored in digiswitches, are formatted by a digital formatter and stored on computer-compatible digital magnetic tape. The tape block size, i.e., the number of eight-bit characters written in one continuous block, is 512. This number of characters allows for point values from seven Loran-C pulses, a UTC clock time, and the input information stored in the digiswitches to be stored on each tape block in a standardized format.

As an on-site test of slowly varying conditions in the RF signal environment and possible drifts in the tuned receiver, two sample points are continuously averaged and displayed on a strip chart recorder. This is accomplished by a sampling digital-to-analog converter. The converter changes one inphase and one inquadrature sample from each Loran-C pulse back to analog form, averages each pulse on a capacitor, and drives the strip chart recorder.

Figure 3 is a block diagram of the instrumentation used to compare the two Austron receivers. At the writing of this report, measurements using this test instrumentation are preliminary. Receiver

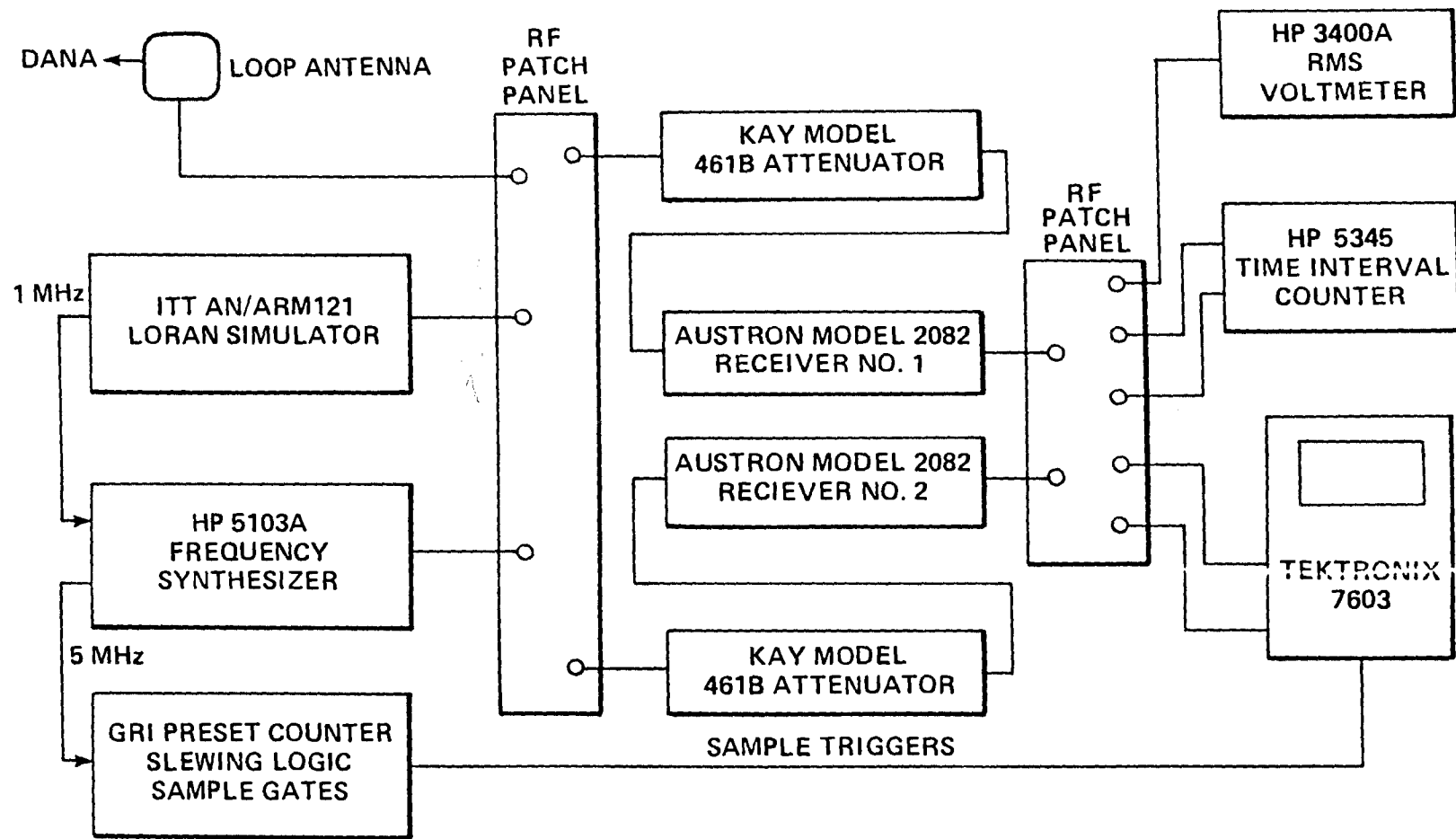


Fig. 3 PRELIMINARY RECEIVER COMPARISON TESTS

gain is measured by comparing the signal strength into the Kay attenuator to the output of the Austron Receiver with a RMS voltmeter. The HP5103A Frequency Synthesizer is used to measure receiver gain versus frequency and also for phase comparisons. The Tektronix type 7603 oscilloscope is used for coarse comparison of phase delays between the two receivers and to compare Loran pulse outputs either from the simulator or the loop antenna. The HP5345 Time Interval Counter is used as a phase meter comparing receiver delays versus frequency and temperature. The Time Interval Counter will eventually be used to measure the time difference between the field UTC clock and the traveling clock which will be used for time transfer as will be discussed below. The GRI Preset Counter Slewing Logic and sample gates are contained in one of the two digital units fabricated for a complete measurement system. When observing a Loran pulse, the Frequency Synthesizer is set to five MHz and used as a substitute for the Cesium standard which will eventually clock the GRI preset counter. Cable lengths for the instrumentation in Fig. 3 are matched to one quarter of an inch.

The maximum gain of both receivers was determined to be in excess of 130 dB. The attenuator pot was removed from both receivers and replaced with a fixed attenuator set for a gain of 106 dB. This gives sufficient gain to receive data at APL at two volts peak to peak output with 16 dB attenuation inserted at the antenna input. Receiver noise referenced to the input is 0.35 microvolt for receiver No. 1 and 0.45 microvolt for receiver No. 2. The frequency response curves of both receivers were measured and plotted. The phase delay through the receivers was measured to be 17.5 microseconds. A difference in phase delay of 0.5 microsecond at 100 kHz was removed by adding a 900 pf shunt capacitor at the fixed attenuator tap in the receiver with the phase lead.

Figure 4 contains plots of the gain versus frequency characteristics of the two Austron receivers. Two curves are shown for the two receivers before modification. The plotted points are for receiver No. 2 after the phase lag capacitor

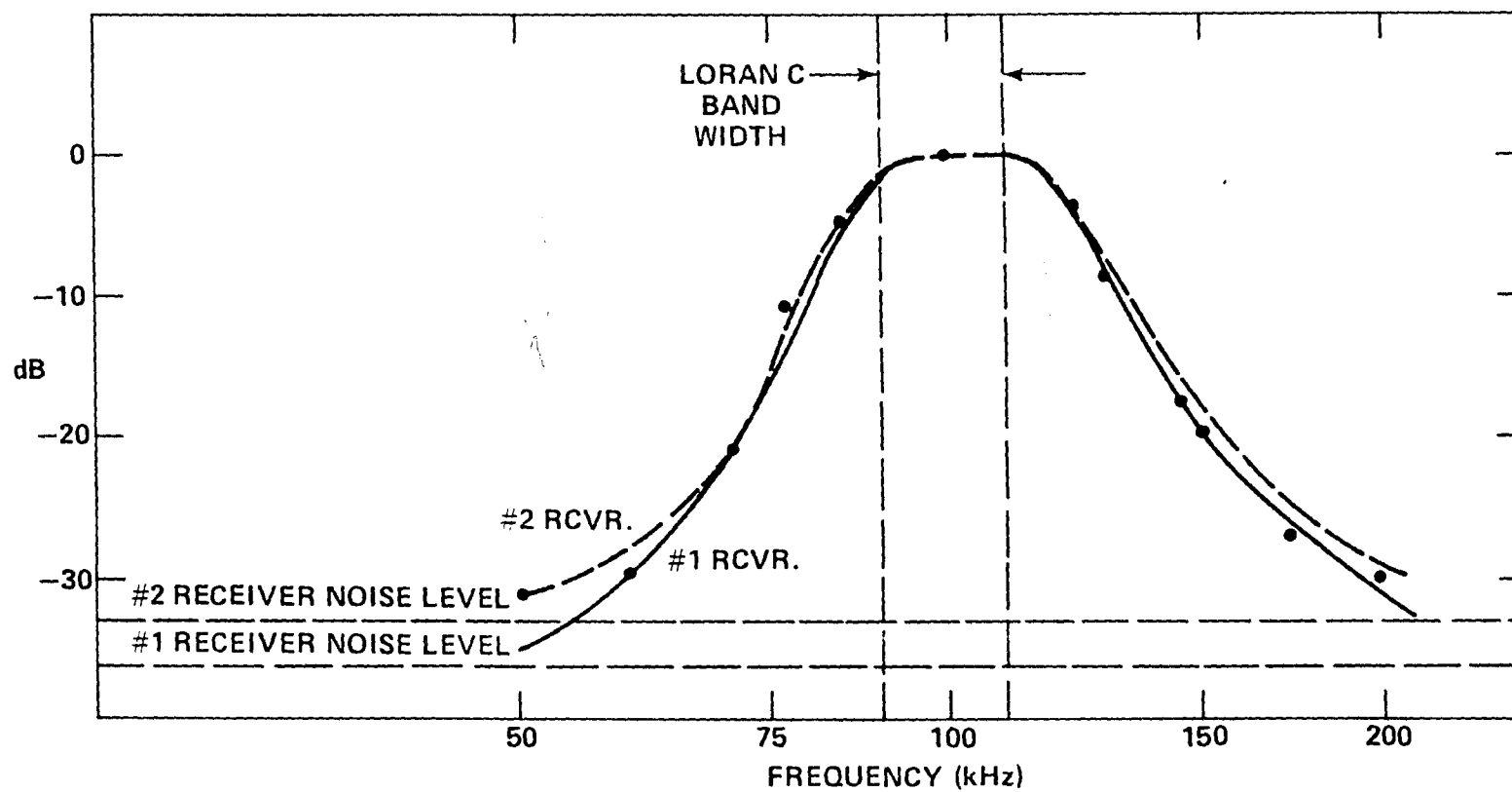


Fig. 4 GAIN VERSUS FREQUENCY PLOTS OF AUSTRON RECEIVERS

was added. As can be seen from the plots, frequency response is wide-band for a Loran pulse and biased slightly toward high-frequency response.

The HP5345 Time Interval Counter is used as a phase meter to compute receiver delays versus frequency and temperature. To accomplish this, the differences between the frequency synthesizer output zero crossings and the receiver output zero crossings are summed over one second giving less than one nanosecond deviation due to noise. The Interval Counter is set to the gating averaging start-stop counter mode. The positive going zero crossing of the synthesizer signal into the attenuator starts a measurement and the negative going zero crossing of the receiver stops a measurement.

To resolve cycle ambiguity, the delay was first observed using the Loran pulse simulator. This observation indicated that one and one-half cycles must be added to the average interval measurement of the start-stop counter for the correct answer. The measured delay through one receiver at 100 kHz is 17.476 microseconds. The frequency dispersion in the receiver, without using notch filters, in the Loran pulse frequency range, 97 to 103 kiloHertz, is +40 nanoseconds per kiloHertz, 242 nanoseconds total. Adding a notch filter at 88 kiloHertz decreases the measured delay through the receiver to 17.307 microseconds and increases the dispersion to 265 nanoseconds. Adding a notch filter at 122 kiloHertz increased the measured delay through the receiver by 65 nanoseconds. One receiver has been cycled from 65°F to 80°F in a Tenny thermal chamber. A center frequency drift in delay of five nanoseconds per degree Fahrenheit was observed.

Measurements of the differences in the two receivers' characteristics will be made. After both measurement systems are assembled, measurements of the differences in receiver characteristics will again be made by digitally processing identical sample points recorded on magnetic tapes. Preliminary measurements indicate that to achieve the desired accuracy of the group/phase measurements, the two receivers must be matched as closely as

possible and, in addition, on site measurements of the receiver 100 kiloHertz delay must be made. The delay will be measured by recording the Cesium standard 100 kiloHertz output first direct, and then through the receiver.

Figure 5 gives more detail on the timing portion of the group/phase monitor electronics. The 5 MHz signal is multiplied by two to give 10 MHz. The purpose of this multiplication is to derive a time interval that, when divided by an integer, gives the 2.5 microsecond sample interval required by the sample gates. The 10 MHz signal is divided by 25 to give time intervals of 2.5 microseconds. Further division of the signal frequency by 40 gives 100 microsecond intervals. Pulses at 100 microsecond intervals trigger a preset counter with a maximum division of 1,000. This preset counter is the GRI preset counter. The output of the GRI preset counter triggers a divide by seven counter which furnishes a tape block trigger signal to the digital formatter. The entire counter chain is synchronized, i.e., clocked from the 10 MHz signal.

The 10 MHz signal also triggers a divide by 10^7 counter in the UTC clock timing chain which is synchronized by a one pulse per second signal provided by the low-noise Cesium beam frequency standard. The output of this counter is used to furnish the needed 0.1 microsecond accuracy for recording the UTC clock on magnetic tape. The one pulse per second signal from the divide by 10^7 counter drives the slower time counters of the UTC clock. The entire UTC counting chain is synchronized with the 10 MHz signal and, as a result, with the GRI preset counter.

Figure 6 is a photograph of the measurement system which will be installed at the Naval Observatory in Washington, D.C.

Figure 7 is a photograph of the Loran pulse derived from the Loran-C signal simulator summed with sample triggers for the analog-to-digital converter.

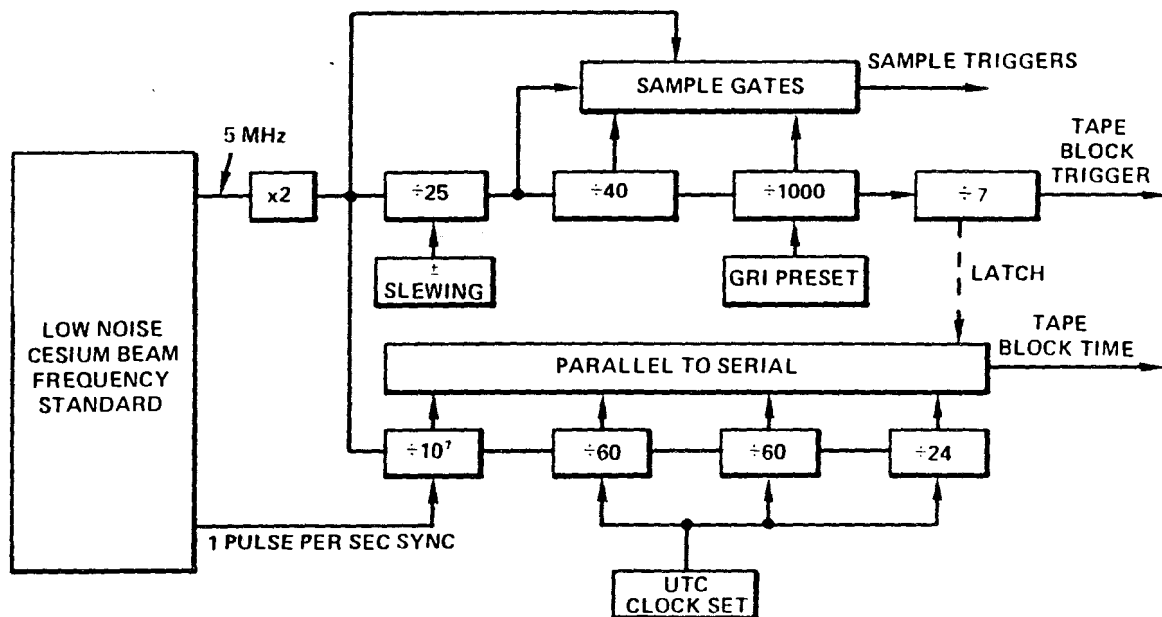


Fig. 5 GRI PRESET COUNTER AND UTC CLOCK

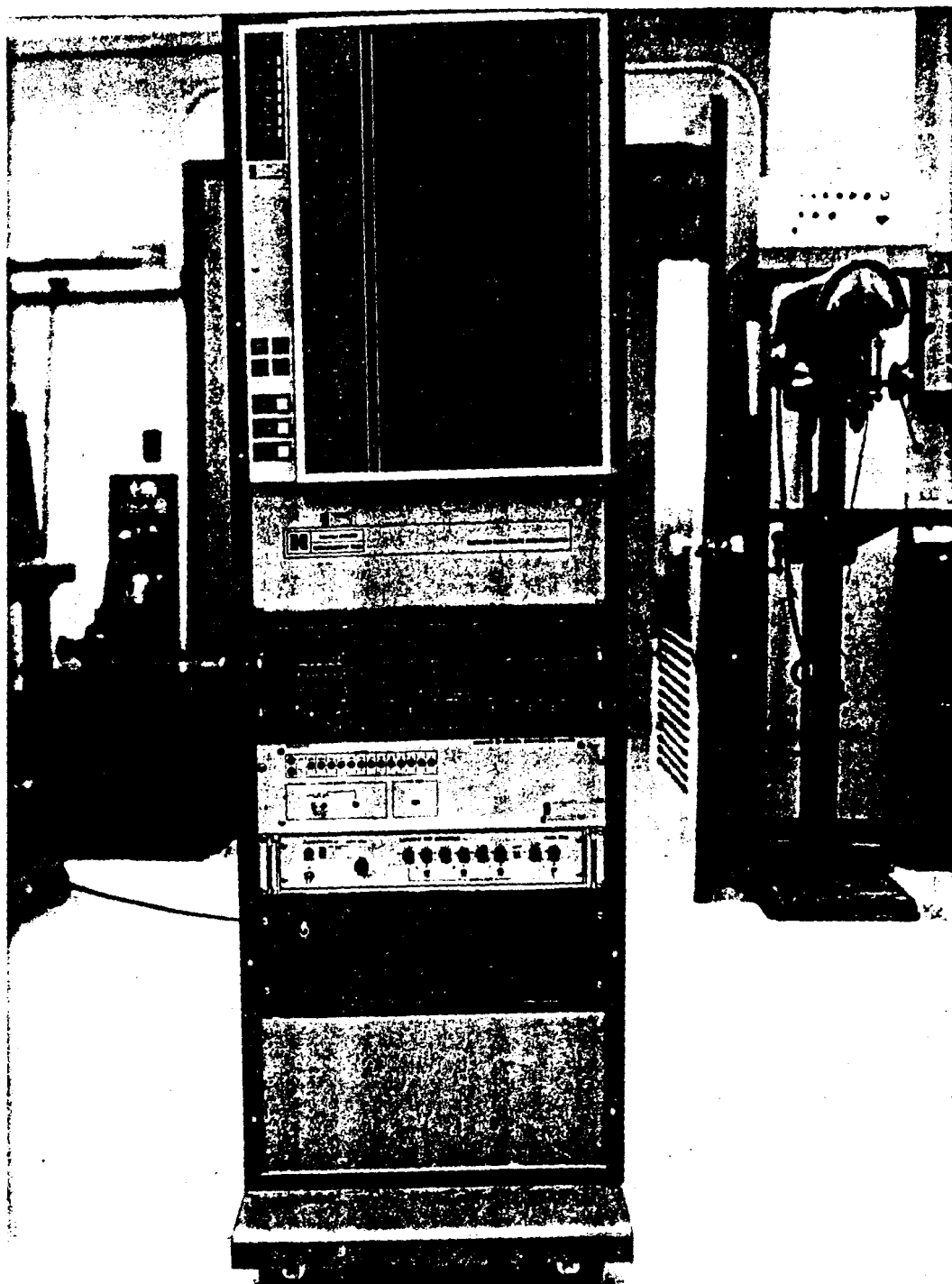


Fig. 6 PHOTOGRAPH OF FIXED SITE MEASUREMENT SYSTEM

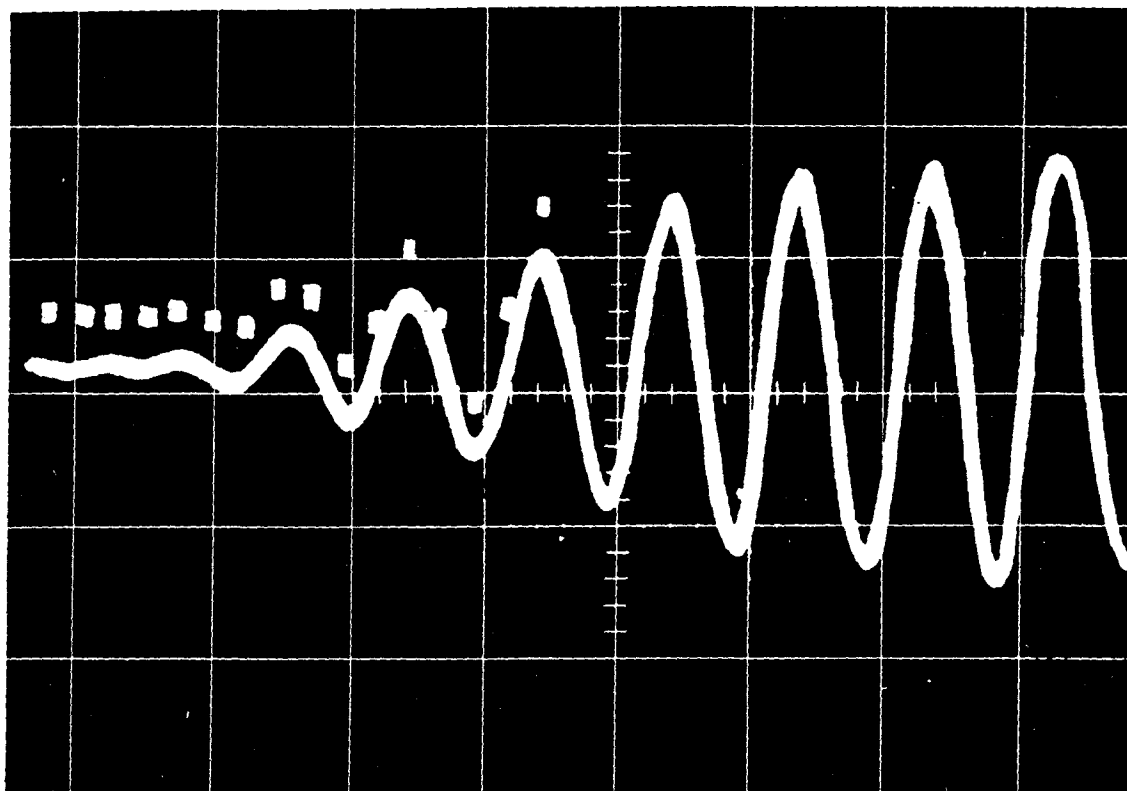


Fig. 7 PHOTOGRAPH OF LORAN PULSE SHOWING MEASUREMENT
TRIGGERS SUPERIMPOSED

CHARACTERISTICS OF THE RECORDED DATA

The types of data which will be recorded on each tape are identified in Table 1. This table also shows the resolution with which each type of data will be recorded.

Data sampling will be done as shown in Fig. 8. Only the first pulse of each group will be sampled and a total of 32 voltage measurements will be taken on each of these pulses. The first 16 will be at 2.5 microsecond intervals, and the second 16 will be at 7.5 microsecond intervals. It is the first set of 16 measurements that will be used for the Loran-C Group/Phase Test study since it can be expected that these measurements will be samples of the groundwave. The second set of 16 measurements will be recorded so that studies on skywave effects can be made at a later date. All the electrical data will be recorded against Universal Time Coordinated.

The 15th strobe point will be placed, as near as practicable, to the crossover point at the end of the third cycle, leaving two of the sampling points ahead of the first cycle. These two data samples might clearly be used as D.C. bias determination and/or total noise characteristic study.

Data will be recorded for a period of at least one hour at each location. The format of the data tape shown in Fig. 9 was determined, in part, by the buffer size of the 9000 series Kennedy nine-track tape recorder. Each data word carries 14 bit (13 bit plus sign) of significance. Two bytes (eight bits per byte) are assigned to each data word. There are 512 bytes in the buffer of the recorder-controller. This allows seven pulses, 224 data samples, or 448 bytes for data; seven bytes for time of the first sample to 100 nanoseconds, and the rest of the buffer is used for header information as indicated.

The new data tapes, both for the fixed and field sites, will be returned to APL/JHU by evening of the day they are recorded for quick-look

Table 1. Taped Data

<u>Parameter</u>	<u>Digits/Bits</u>	<u>Units</u>
In-Phase Volts, X	13 bits + sign	Volts
In-Quadrature Volts, Y	13 bits + sign	Volts
Gain	2 digits	-dB
Time	13 digits	Hr, Min, 10^{-7} sec
Day Number	3 digits	Day
Year	1 digit	Year
Group Repetition Interval	3 digits	10^{-4} sec
Transmitter	1 digit	1
Site	2 digits	1
Weather Code	2 digits	1
Atmospheric Pressure	5 digits	10^{-3} in. Hg
Wet Bulb Temperature	3 digits	10^{-1} deg cent.
Dry Bulb Temperature (outside)	3 digits	10^{-1} deg cent.
Dry Bulb Temperature (inside)	3 digits	10^{-1} deg cent.
Data Recording Mode	1 digit	1
Predicted Time Calibration	9 digits + sign	10^{-9} sec
Notes	1 digit	1
End of File		

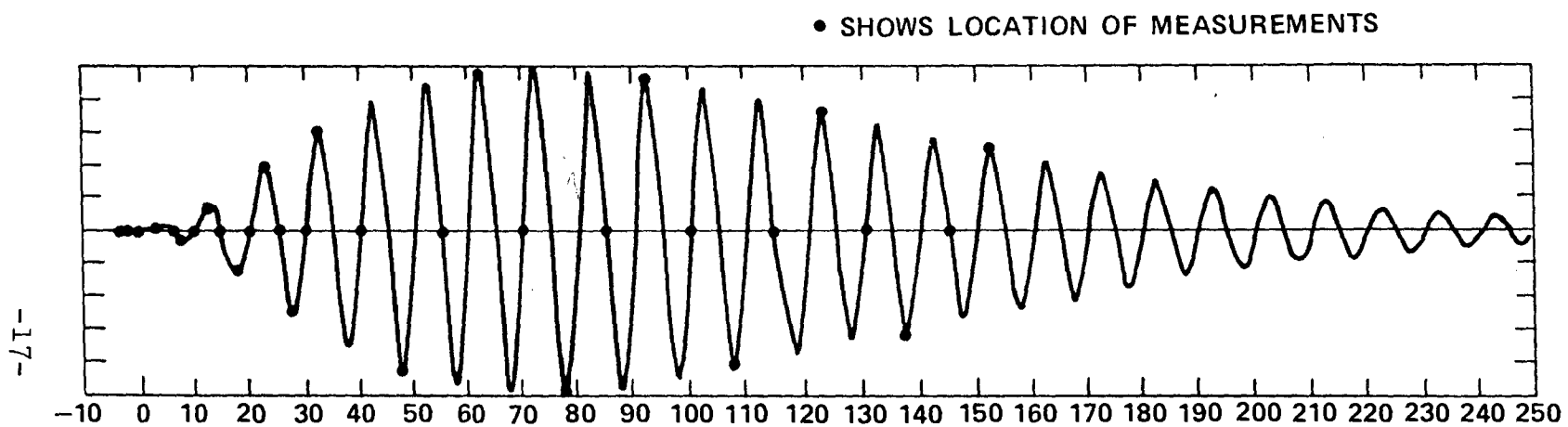
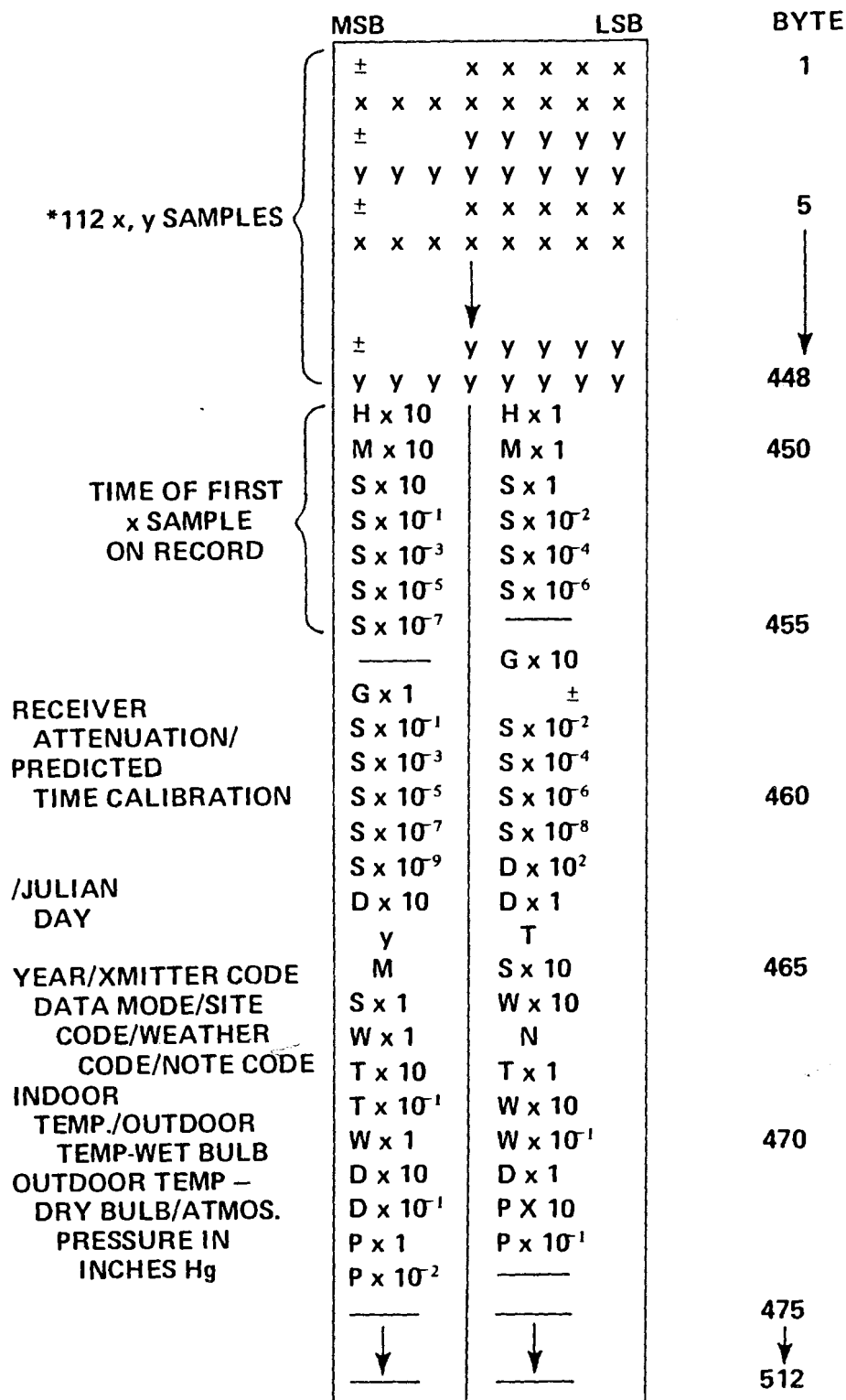


Fig. 8 VOLTAGE MEASUREMENTS ON LORAN PULSE



*x, y DATA IS IN 2's COMPLIMENTED BINARY
ALL OTHER DATA IS IN EBCDIC CHARACTER CODE

Fig. 9 RAW DATA TAPE FORMAT

preprocessing to examine the data quality and determine if the field site van should secure operations at that site and move to the next. If recording errors or unusually bad interference occurred, another attempt would be made within a day or two.

The quick-look preprocessor, as shown in Fig. 10, will reduce the data from each pair of fixed and field test sites independently. Mean and standard deviations about the mean are computed over 50 Group Repetition Intervals (GRI) (about five seconds). Examination of this reduced data should be adequate to determine a go or no-go data quality.

A new condensed data set will be generated during the preprocessor reduction. The first 16 data points of each pulse are stripped and carried forward to this new data set and written onto a standard IBM compatible nine-track binary magnetic tape. Each record will be blocked into samples from the 50 GRI groups used in the reduction. Each block will contain, in addition to the 16 samples per GRI, time at the first reading in the block, and the means and standard deviations over the 50 GRI span. A header record with information brought forward from the raw data tape will precede all data records on the tape.

These new condensed data sets, from the two sites, will then be used by an intermediate processing program which will perform data editing, time adjustments from the calibration data and, finally, merge the data onto a single data set containing all time correlated and edited data from both sites. This combined data set will then be used for all computations in the final analysis program where the desired relationship between the secondary phase factor and the pulse location on the carrier will be determined along with a statistical measure of its quality.

A low-noise Cesium frequency standard will be used to calibrate the field site low-noise Cesium standard making possible eventual data correlation and merging for further editing procedures and

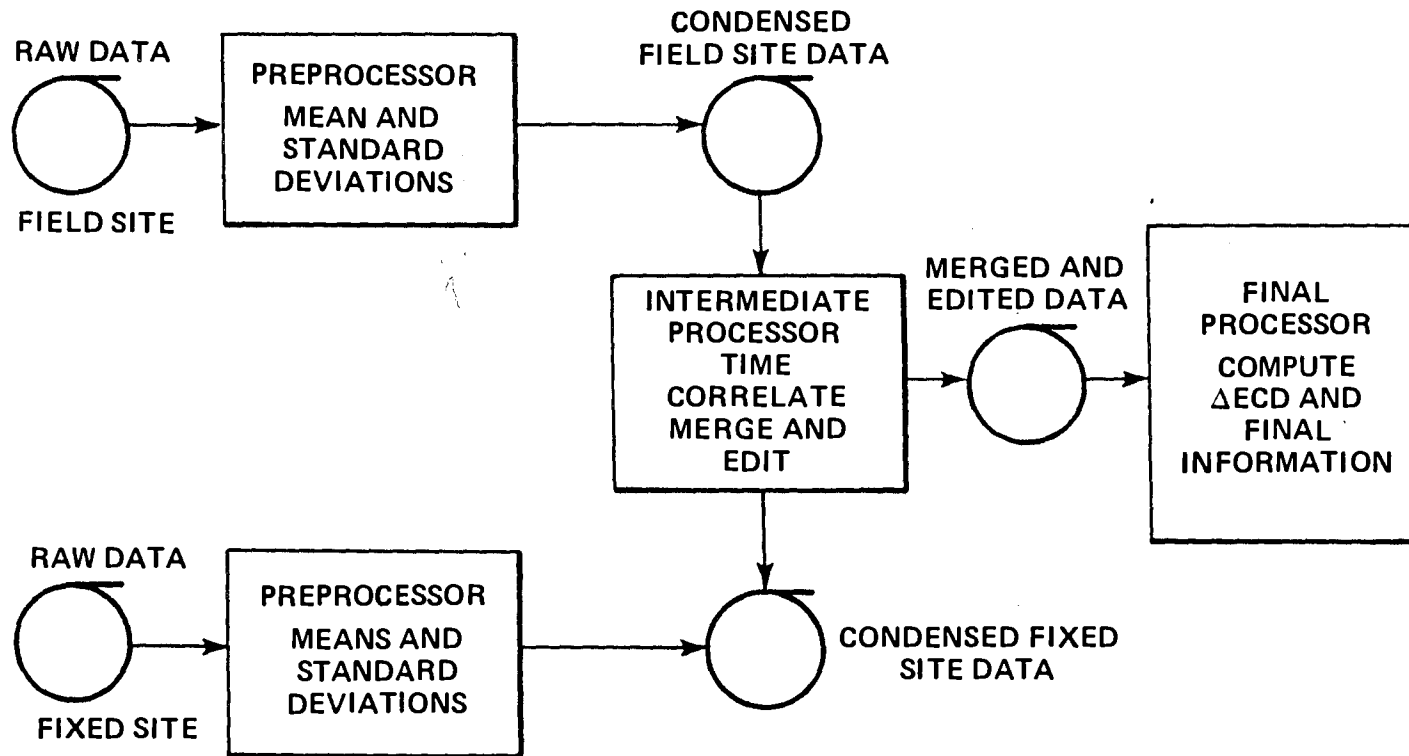


Fig. 10 PROCESSING DATA FLOW

processing; and, finally, achievement of the final results. The time transfers required for the calibration will be accomplished by personnel from the Naval Observatory under the direction of Dr. William Klepczynski. On the morning of the day Loran data are to be taken, a traveling clock supported by the low-noise Cesium standard will be calibrated against the Master Clock Ensemble at the Observatory. The traveling clock will then be carried to the field site where the field clock will be calibrated against the traveling clock. The traveling clock will then be returned the same day to the Observatory where it will again be calibrated against the Master Clock Ensemble. The resolution of these calibrations will be one nanosecond.

Estimates have been made of the fidelity with which the data describe the time history of voltage as a single Loran pulse passes the antenna. Although the geociever station monuments will be located with an RMS of 3 meters in a worldwide grid system, the geodetic distance between two monuments will be known with an RMS of 1/2 meter due to correlation of the errors in the measurements at each end as the distance becomes small. Table 2 shows these estimates. It is expected that each data point plotted to describe the desired relationship between ECD and the secondary phase factor will be determined within 17 nanoseconds RMS.

AVAILABILITY OF DATA

One of the principal purposes of this paper has been to disclose the nature of the data which will exist on magnetic tape. We believe that other investigators in the field of low frequency propagation may wish to use these data for their own purposes. Only copies of the raw data tapes will be used in subsequent data processing and analysis. The raw data tapes will not be available for loan. However, those who wish to use the data should contact the Loran Systems Program Office of the Air Force Electronic Systems Division.

<u>Type of Data</u>	<u>RMS Error</u>
Speed of Light, 299792456.2 m/sec	3 m/sec
Point Positioning	3 meters
Geodetic Distance	0.5 meter
Change in Time of Arrival of Phase	7 nanosec
Phase Time of Arrival (2)	3 nanosec
Clock Synchronization (1)	3 nanosec
Change in ECD, Δ ECD	15 nanosec
ECD (2)	10 nanosec
Clock Synchronization (1)	3 nanosec
Phase Time of Arrival (2)	3 nanosec
Change in Secondary Phase Factor, Δ SPF	7 nanosec
Plotted Datum, Δ SPF vs Δ ECD	17 nanosec

Note: Numbers in parenthesis are number of entries
in RSS

Table 2. Estimated Accuracy of Data

ACKNOWLEDGEMENTS

The authors wish to acknowledge the contribution of L. F. Fehlner who directs the Group/Phase Test Project, and to S. F. Oden in the design of the digital electronics.

